Enantioselective Fluorescent Sensors for Chiral Alpha-Hydroxycarboxylic Acids, Amino Acid derivatives and Diamines

Shanshan Yu
Dezhou, China

B. S., Wuhan University, China, 2008

A Dissertation presented to the Graduate Faculty
of the University of Virginia in Candidacy for the Degree of
Doctor of Philosophy

Department of Chemistry

University of Virginia
Aug, 2013 Degree **will be Conferred**

Abstract

A series of enantioselective fluorescent sensors based on chiral 1,1'-bi-2-naphathol (BINOL) was designed and developed for the recognition of chiral α-hydroxycarboxylic acids, amino acid derivatives and diamines.

A new concept with the use of a pseudoenantiomeric fluorescent sensor pair for enantioselective fluorescent sensing was introduced. A pseudoenantiomeric fluorescent sensor pair is composed of two fluorescent sensors that emit at different wavelengths and have the opposite enantioselectivity. When a 1:1 mixture of BINOL-based and H_8BINOL-based sensors are used to interact with mandelic acid, the sum and difference of the fluorescence intensity at the two different emission signals of the two sensors allow the determination of both the concentration and the enantiomeric composition of a mandelic acid sample by a single fluorescence measurement.

The fluorescent properties of a series of H_8BINOL-amine compounds were investigated. It is revealed that the intramolecular hydrogen bonds of these compounds can shift the emission of their H_8BINOL unit to a much longer wavelength. Binding with the acid suppressed its intramolecular hydrogen bonding and restores the short wavelength emission of the H_8BINOL unit, giving high sensitivity and good enantioselectivity.

A BINOL-amino alcohol enantiomeric pair is discovered to be able to conduct both enantioselective and diastereoselective fluorescent discrimination of the four stereoisomers of threonine derivatives. This is the first example that one enantiomeric sensor pair can be used to recognize four stereoisomers of chiral substrates containing

two chiral centers.

A BINOL-trifluoroacetyl compound is discovered to exhibit high sensitivity at one emission wavelength and high enantioselectivity at another when treated with a chiral diamine. By using this fluorescent sensor it was demonstrated for the first time that both the concentration and enantiomeric composition of a chiral substrate can be determined simultaneously with one fluorescent measurement.

These discoveries represent important progress in the field of enantioselective fluorescent sensors and have fundamental significance for the potential application of fluorescence in chiral catalyst screening.

Acknowledgements

I would like to thank Dr. Lin Pu for providing me the opportunity to pursue my graduate studies. My work on this project would not have been possible without his innovative ideas, critical thinking and careful guidance. He is more than just academic advisor for me. I benefit a lot from conversations with him when I encountered tough problems in my life. My gratitude also goes to my committee: Dr. Harman, Dr. Gunnoe and Dr. Chruma. I have learned much from them and appreciate their encouragement. I would also like to say thank you to Dr. Demas. For many times I interfered with him but he is always patient with my questions. I especially appreciate Dr. Li's willingness to serve as the outside member of my committee. I also appreciate Dr. Michal Sabat's help with crystals. I would also like to thank Dr. Guoqing Zhang for his help in my career.

I would like to thank my families for their enduring love and support through every step of my graduate school. Their understanding and support make me who I am. My gratitude also goes to Mark Turlington and Albert DeBerardinis. I am grateful for their training of me and their patient helpfulness with all of my questions, especially with my candidacy exam. Tiandong Liu, Lihong Zhou and Yang Yue helped me immensely with adjusting to the life in US and starting my work in the lab. I am also thankful for the many other great labmates that I have had the privilege of working with: Li Xiao, Yuhao Du, Wei Chen, Betrand Tran, Junliang Liu, Man Xu, Jun Ying, Chao Wang, Andrea Mulas, Winston Plunkett, Michael Kim, Abbey Pfister and Elaine Wu. Thank you guys for the invaluable friendship.

Table of Contents

List of Figures

List of Schemes

List of Tables

Chapter 1

Enantioselective Fluorescent Sensors

1. Introduction

Enantioselectivity is one of the essential research focuses for sensor science,[1-3] since the enantiomerically pure compounds have fundamental importance in pharmaceutical industry,[4] agrochemical area,[5] and food analysis.[6] Biological activity of drugs is tightly correlated with stereochemistry due to the inherent chiral environment in biological systems. Therefore, fast and easily performed method for acquiring enantiomerically pure compounds is in demand.

Asymmetric catalysis has been intensively investigated in the past two decades[7] because it can provide very convenient synthetic routes to chiral compounds, avoiding the labor-intensive and time-consuming separation of enantiomers. However, thousands of experiments need to be conducted in order to develop an efficient catalyst and a suitable reaction condition, which still requires tremendous investment in time and labor. The development of parallel synthesis and combinatorial chemistry provides fast, reliable methods for screening the properties of enormous number of chiral catalysts.[8, 9] However, the traditional analytical techniques, such as gas chromatography (GC) or high-performance liquid chromatography (HPLC), are not fast enough to determine the enantiomeric excess (*ee*) of products generated from combinatorial catalyst screening due to the serial and time-consuming nature of the chromatographic techniques. Therefore, high-throughput screening (HTS) techniques have become essentially important for the application of rapid chiral assay.

2. High-throughput screening techniques for *ee* determination

Researchers have been exploring in this area and some achievements have been made.[2, 3, 8, 10] A number of techniques are being developed for the high-thoughput ee screening of chiral compounds, such as UV/Vis,[11, 12] time resolved IR-thermographic method,[13, 14] electron spray mass spectrometry, capillary electrophoresis, circular dichroism and fluorescence.

2.1 UV/Vis-based systems

In 1997, Manfred T. Reetz, et al. established a rather crude UV/Vis-based screening system for the lipase-catalyzed kinetic resolution of chiral p-nitrophenol esters (Scheme 1-1).[12] The R and S esters were tested separated pairwise on a 96-well micro titer plate using a simple UV/Vis-based plate reader. The process of reactions was monitored by measuring the absorption of the *p*-nitrophenolate anion at 410 nm as a function of time.

Scheme 1-1. Kinetic resolution of ester catalysed by mutant lipases.

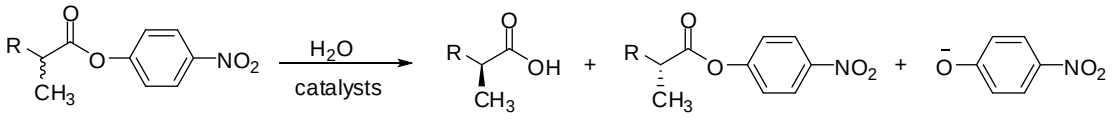

rac-**1-1**, R = *n*-C_8H_{17} (*S*)-**1-2** (R)-**1-1**

Another typical example is the use of enantioselective indicator displacement assays (eIDAs) by Eric V. Anslyn for the determination of *ee* of α-amino acids in 2008.[11] Chrome azurol S (**1-5**) was used as the indicator. Coordination of the indicator the

Cu(II) metal center of the Cu(II)-diamine complexes ([Cu(**1-3**)]$^{2+}$ and [Cu(**1-4**)]$^{2+}$) produced an absorbance band at 602 nm, while the free indicator showed absorption at 429 nm. When amino acids were added to the complex solution, the indicator was replaced and the absorption at 429 was increased differently for amino acids enantiomers. Then they applied this system to 96-well plate and demonstrated its ability to be used in an HT format.

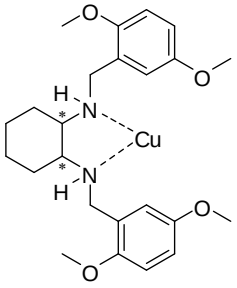

[Cu(**1-3**)]$^{2+}$

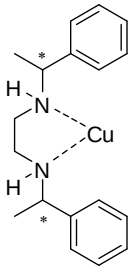

[Cu(**1-4**)]$^{2+}$

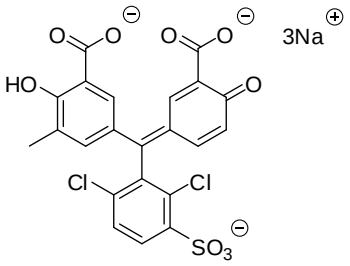

1-5

2.2 IR-thermographic assays

In 1998, Reetz et al. used an infrared camera to monitor the temperature change of the lipase-catalysed acylation of 1-phenylethanol (Scheme 1-2) on a special microtiter plate.[14] The results showed good spatial resolution and clearly identified the "hottest" reaction. They then applied this method to transition metal-catalyzed enantioselective ring-opening hydrolysis of epoxides and successfully demonstrated that time-resolved IR-thermographic method was feasible in the screening of enantioselectivity in catalytic reactions.

In 2002, Mahmoudian et al. tested the same lipase-catalysed acylation (Scheme 1-2)

on a 96-well plate and plotted a calibration curve to quantify *ee* from the temperature change.[13] Then they studied the screening of 96 racemic alcohols for acylation on a 96-well plate but only crude readout could be obtained, which suggested that with its limitations IRT can provide a crude but practical intitial method when screening large numbers of catalysts and/or substrates.

Scheme 1-2. Lipase-catalyzed enantioselective synthesis of (*R*)-**1-7** from *rac*-**1-6**.

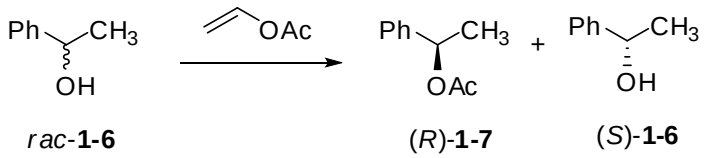

rac-**1-6** (*R*)-**1-7** (*S*)-**1-6**

2.3 Electron spray mass spectrometry

Since the R and S forms of a chiral compound show identical mass spectra, the basic principle to apply MS to the enantioselective catalysis is to create mass differences. In 1999, Reetz et al. utilized isotopically labeled substrates in the form of pseudo-enantiomers or pseudo-prochiral compounds (Scheme 1-3).[15] The kinetic resolution of racemates and the asymmetric transformation of prochiral substrates with enantiotopic groups could be monitored by detecting the relative amounts of reactants and/or products by ESI-MS.

Scheme 1-3. a) Asymmetric transformation of a mixture of pseudo-enantiomers involving cleavage of the functional groups FG and labeled functional groups FG*. b)

Asymmetric transformation of a mixture of pseudo-enantiomers involving either cleavage or bond formation at the functional group FG. c) Asymmetric transformation of a pseudo-meso substrate involving cleavage of the functional groups FG and labeled functional groups FG*. d) Asymmetric transformation of a pseudo-prochiral substrate involving cleavage of the functional groups FG and labeled functionalgroups FG*.

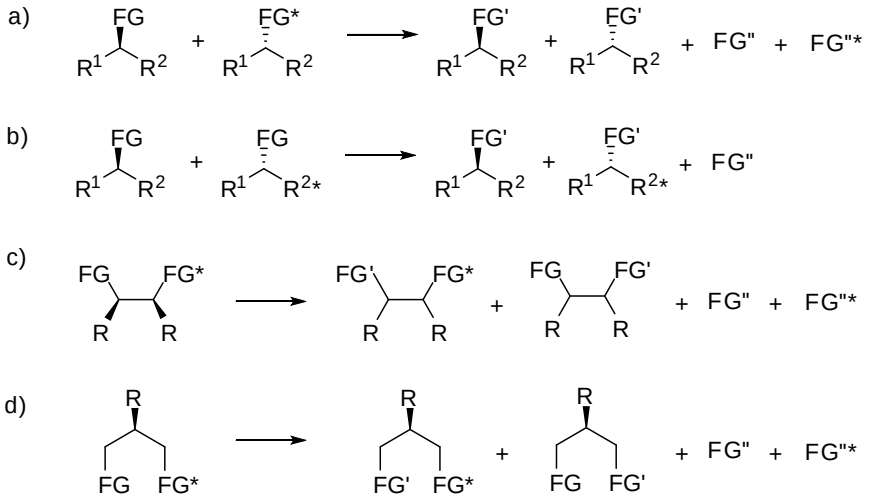

In the same year, Finn et al. employed a different approach, by using pseudo-enantiomeric "mass-tagged" chiral acylating agents **1-8** and **1-9** to determine ee values of chiral alcohols or amines (Sheme 1-4).[16] Nine secondary alcohols and five primary and secondary amines were tested with this method and the measured value fell within 10% *ee* of the true value.

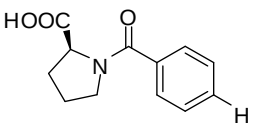

1-8

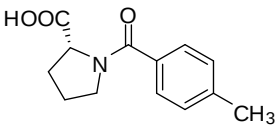

1-9

Scheme 1-4. Mass-spectrometric *ee* determination in the kinetic resolution of chiral alcohols.

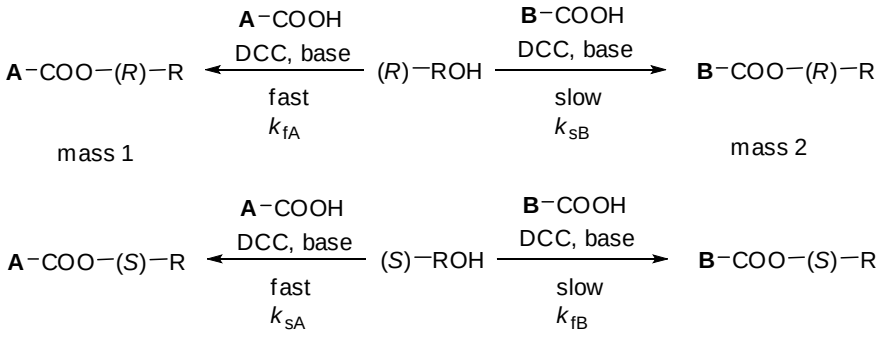

2.4 Capillary electrophoresis

The high-throughput ee-screening system based on capillary electrophoresis was developed by Reetz et al. by using the MegaBase system consisting of 6 bundles of 16 capillaries which spatially address standard 96-well microtiter plates.[17] Chiral amines **1-10** were derivatized with fluorescein isothiocyanate **1-11** for the parallel optical detection (Scheme 1-5). Soluble cyclodextrins derivatives were employed as chiral selectors to enable chiral separation. It was demonstrated that at least 7000 ee determinations could be performed per day, proving the ability of capillary electrophoresis in high-throughput manner.

Scheme 1-5. Derivatization of chiral amines for the determination of *ee*.

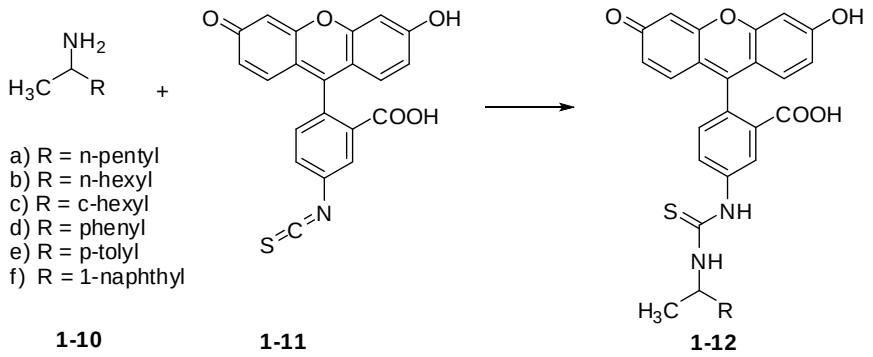

2.5 Circular dichroism (CD)

In 1999, Koichi Mikami et al. developed an HPLC-CD-based system[18], which allows the simultaneous detection of the CD signal $\Delta\varepsilon$, the absorption ε, and their ratio $g = \Delta\varepsilon/\varepsilon$. The dissymmetry factor g is independent of concentration and is linearly associated to the *ee* value. They applied this technique to the parallel asymmetric addition of diethylzinc to aldehydes in the presence of combinations of chiral diol ligands and nitrogen activators (Scheme 1-6).

Scheme 1-6. Asymmetric activation of diol-zinc catalysts by nitrogen ligands.

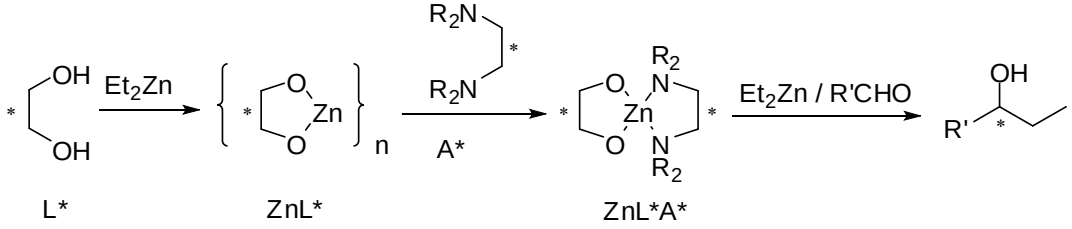

Anslyn et al. explored the use of the CD active metal-to-ligand charge transfer (MLCT) transitions in *ee* determination[19]. Metal complex [Cu(I)(BINAP)$(MeCN)_2$] PF_6 (**1-13**) was used to interact with enantiomers of four chiral diamines and it was

demonstrated that fingerprinting chemical identity, chirality and concentration could be achieved. Automation of a 96-well plate CD spectrophotometer made this system compatible with HTS.

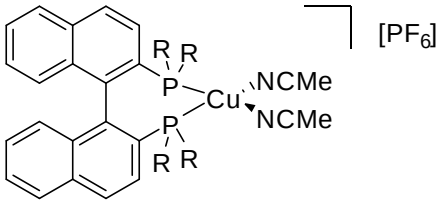

1-13

2.6 Fluorescence

In 1999, Scott J. Miller et al. employed a fluorescent acetic acid sensor (**1-14**) to examine the catalyst activity for the enantioselective acylation of trans-1,2-acetamidocyclohexanol **1-15** (Scheme 1-7).[20] They found that the most selective catalysts typically afforded the fastest reactions. The pH-sensitive fluorophore could monitor the evolution of acetic acid by turning on the fluorescence.

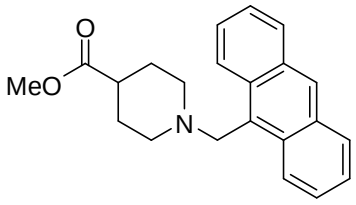

1-14

Scheme 1-7. Enantioselective catalytic acylation of trans-(+/-)-**1-15**.

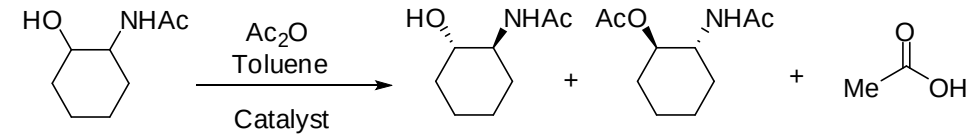

trans-(+/-)-**1-15**

In 2001, Mattew D. Shair et al. adapted the reaction mircoarray method for the high-throughput determination of ee.[21] Amino acids were attached to a glass surface and pseudoenantiomeric fluorescent probes **1-16** and **1-17** were coupled with amino acids. Parallel kinetic resolution during the amide coupling reaction converted the ee information of the sample into a ratio of fluorophores. With this technique approximately 75,000 samples can be arrayed onto a 25 mm x 75 mm glass slide and analysed in a comparable amount of time.

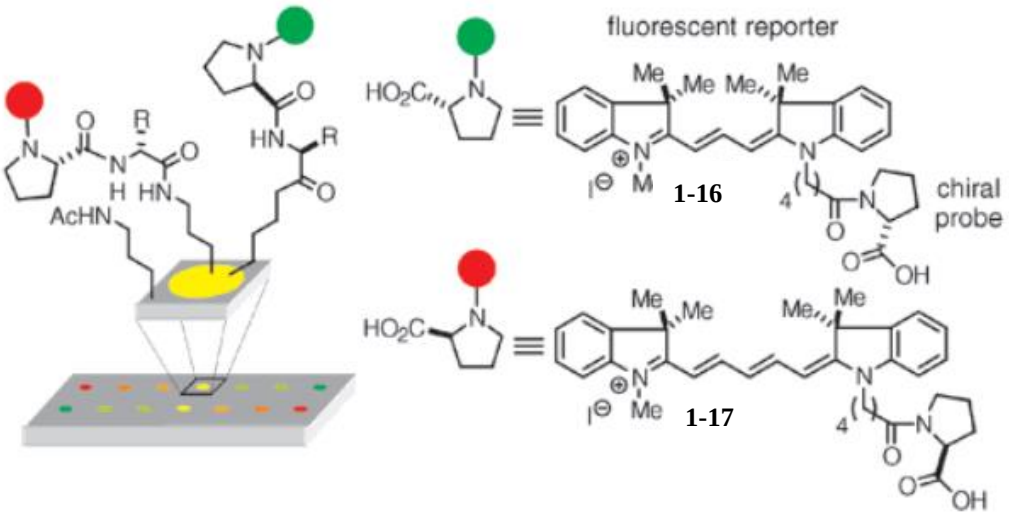

Among all the analytical methods mentioned above, the use of fluorescence has many incomparable advantages. Fluorescence spectrometers are of low cost and widely available. It has very high sensitivity, which is favorable for the small loading amount in high-throughput screening. It provides many different detection modes, such as intensity, wavelength and lifetime. Also, its ability to be used in real-time analysis is another attractive feature.

3. Enantioselective Fluorescent sensors

The two examples of use of fluorescence mentioned above are not straightforward for ee determination of chiral products, one through detection of the achiral product and the other through derivatization of the chiral compounds. In recent years, researchers have been exploring the direct enantioselective fluorescent sensors for the ee determination and a number of highly enantioselective fluorescent sensors for the recognition of chiral molecules such as carboxylic acids, amines, alcohols, amino alcohols and amino acid derivatives have been reported.

The three key components for the successful design of enantioselective fluorescent sensors are an appropriate fluorophore, binding sites and sensing mechanisms.[22] A fluorophore is the site for both photonic excitation and emission, which allows the detection of fluorescence. Binding sites are responsible for guest complexation and decomplexation and in enantioselective recognition must be selective for one enantiomer over the other. Common fluorescence recognition mechanisms are based on many structural features of molecules including π-π^* and n-π^* transitions, structural rigidity, noncovalent interactions (e.g., hydrogen bonds, π-π interactions, and hydrophilic and hydrophobic interactions), intra- or intermolecular energy transfer, and photoinduced electron transfers (PET). When a chiral fluorescent sensor interacts with enantiomers of chiral substrates, the chirality-matched enantiomer will form stronger interactions with the sensor than the chirality-mismatched enantiomer. This difference in interactions

leads to the different structural changes in fluorophore. As a result, different fluorescent responses can be observed. Some examples of the previously reported enantioslective fluorescent sensors are described below.

3.1 Hydrogen bonding

Our group has developed a series of 1,1'-bi-2-naphthol (BINOL) based enantioselective fluorescent sensors for the recognition of chiral α-hydroxycarboxylic acids.[2] BINOL is a very commonly used framework for the construction of enantioselective fluorescent sensors due to its fluorescent properties of naphthyl rings, hydrogen bonding ability of the hydroxyl group and chiral recognition ability caused by the hindered rotation of the two naphthyl rings.

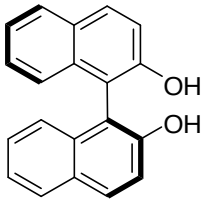

(*S*)-BINOL

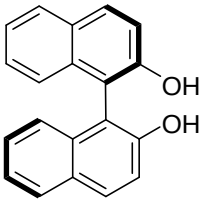

(*R*)-BINOL

The bisBINOL compound **1-18** was designed for the recognition of chiral mandelic acid (MA).[23] Structure **1-19** was a proposed complex between (*S, S*)-**1-18** and (S)-MA and features a binding site of three specific hydrogen bonds, which forms a more rigidified structure and enhances the fluorescence. Due to different binding constants of the sensor with two enantiomers of MA, different fluorescence enhancement was

achieved. Figure 1-1 gives the fluorescence response of (*S, S*)-**1-18** in the presence of (*R*)- or (*S*)-MA in benzene in which 2% of dimethoxyethane (DME) was added to improve the solubility of MA. (*S*)-MA (5×10^{-3} M) increases the fluorescence of (*S*)-**1-18** (9.5×10^{-5} M) more than (R)-MA with IS/I0 =2.87 and the enantiomeric fluorescence enhancement ratio ef was 2.49 [ef = $(I_S - I_0)/(I_R - I_0)$].

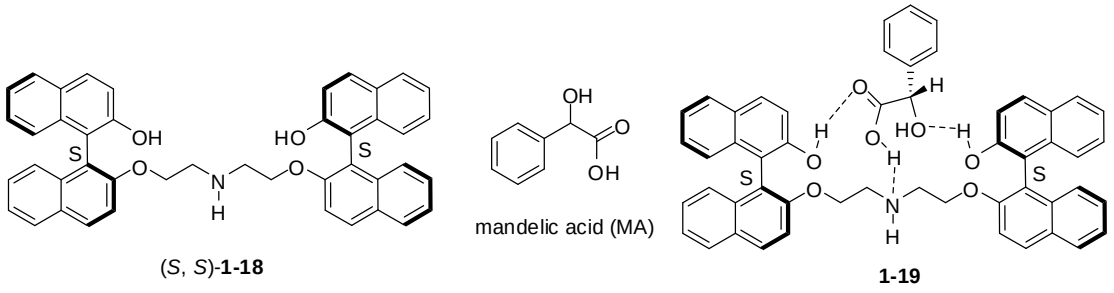

Figure 1-1. Fluorescence spectra of (*S, S*)-**1-18** (9.5×10^{-5} M in benzene/2% DME) with and without MA (5×10^{-3} M).

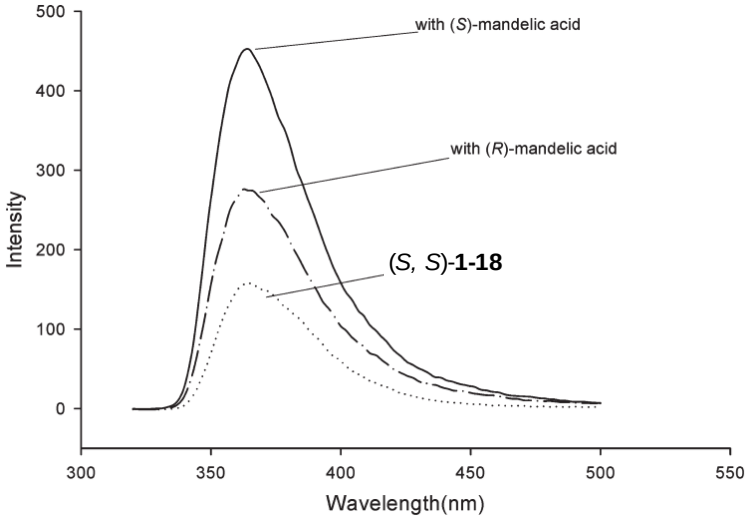

Compounds (*R*, *R*)-**1-20** and (*R*, *R*)-**1-21**, the dendritic derivatives of (*R*, *R*)-**1-18** with phenylene dendrons, were also synthesized.[24] By introducing dendritic branches to the

chiral receptor unit, the light-harvesting effect of the dendritic structure amplified the fluorescence signal of the receptors and greatly increased their sensitivity (Figure 1-2). The enantioselectivity of (*R, R*)-**1-20** was similar to that of the core (*R, R*)-**1-18** with an ef value of 2.05 and (*R, R*)-**1-21** was a little lower with an ef of 1.49.

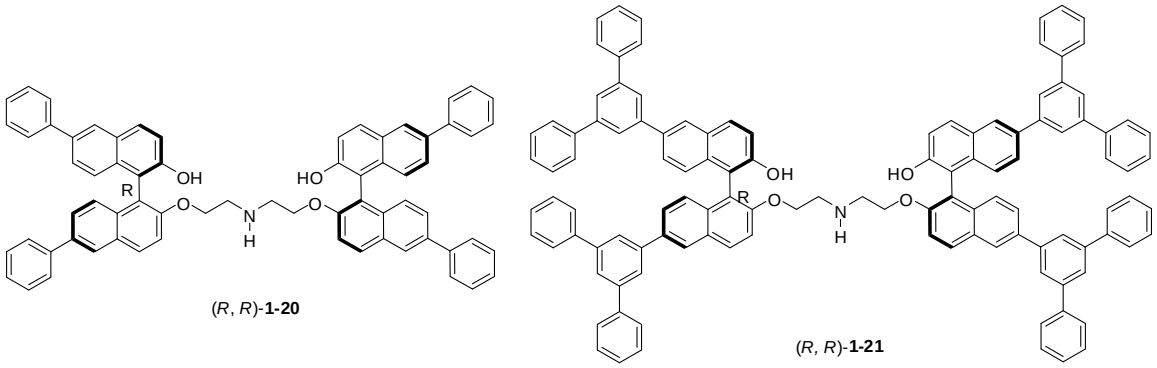

Figure 1-2. Fluorescence spectra of (*R, R*)-**1-18**, (*R, R*)-**1-20**, (*R, R*)-**1-21** (3.1×10^{-6} M, benzene/0.1% DME) with and without (R)-MA (1×10^{-3} M).

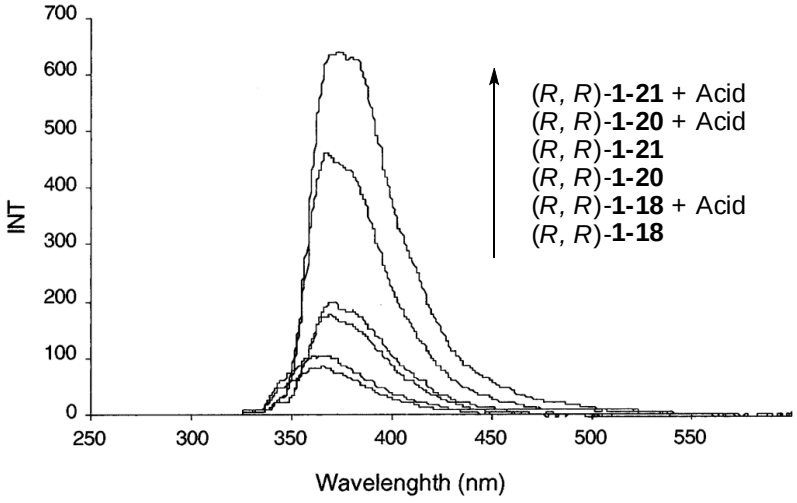

In order to improve the enantioselectivity, two bisBINOL-based macrocycles (*S*)-**1-22** and (*S*)-**1-23** were prepared.[25, 26] (*S*)-**1-22** show dual emissions at 365 nm and 424 nm, which were assigned to the monomer emission and excimer emission, respectively. As

shown in Figure 1-3, (*S*)-MA increased the fluorescence at 424 nm to 2.9 times of its original value and very high enantioselectivity with ef greater than 12 was obtained. The job plot indicated the formation of a 1:4 complex between the macrocycle and the acid. It is proposed that the interaction of the macrocycle nitrogen and the acidic proton of the substrate interferes with the intramolecular hydrogen bonding of the sensor and leads to the enhanced fluorescence.

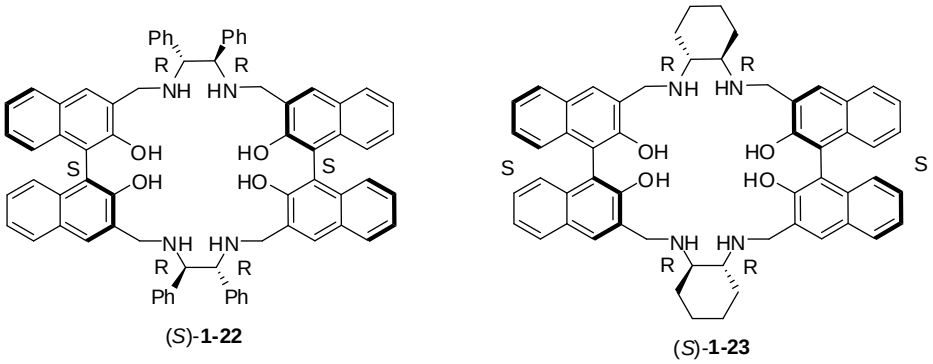

Figure 1-3. Fluorescence spectra of (*S*)-**1-22** (1×10^{-4} M, benzene/2% DME) with and without MA (2×10^{-2} M).

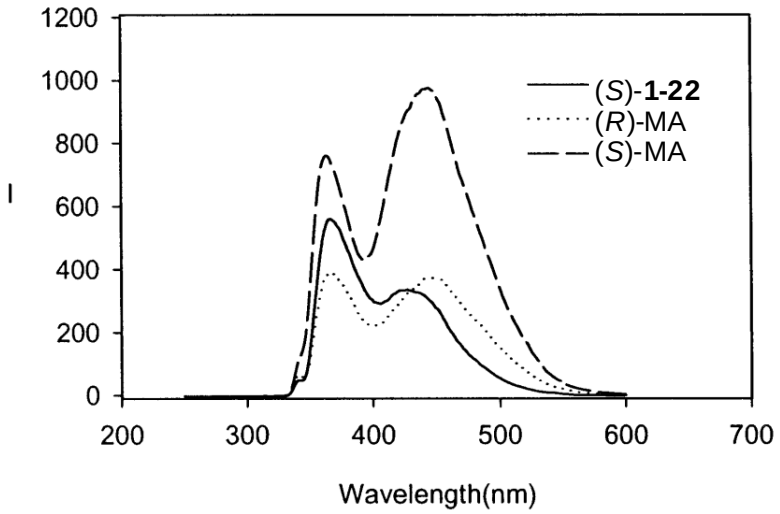

Its analogue (*S*)-**1-23**, prepared from (*1R, 2R*)-diaminocyclohexane, showed very different fluorescent properties.[26] The addition of (*S*)-MA increased its monomeric emission by over 20 folds while (*R*)-MA caused very little change (Figure 1-4). Therefore, it exhibited extraordinary high enantioselectivity for MA with ef = 46. A two-stage recognition process was proposed to account for the significant fluorescent enhancement: (*S*)-**1-23** formed a structurally rigid 1:1 complex with MA through the host-guest inclusion inside the chiral cavity; additional MA located outside the cavity interacted with the complex through multiple hydrogen bonds to further increase the fluorescence.

Figure 1-4. Fluorescence spectra of (*S*)-1-**23** (1×10^{-5} M, benzene/0.05% DME) with and without MA (5×10^{-4} M).

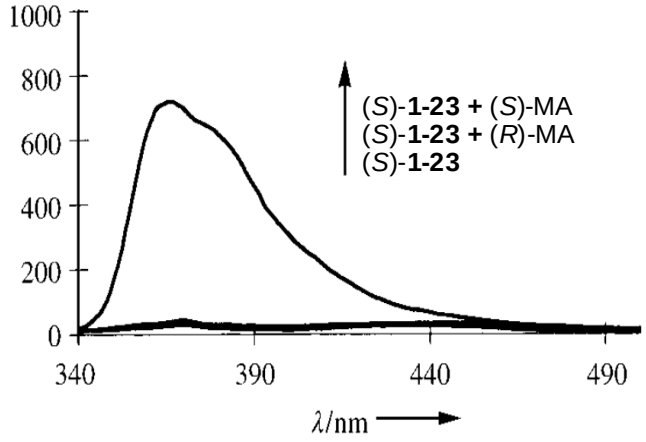

The acyclic BINOL-based amino alcohol (*S*)-**1-24** exhibited very special enantioselective precipitation with MA.[27] The clear solution of (*S*)-**1-24** immediately becomes a white suspension with addition of (*S*)-MA (>= 3 mM) while remains clear

with (*R*)-MA (3 mM – 8 mM) (Figure 1-5). Moreover, the observed enantioselective precipitation was associated with a dramatic (over 950-fold) solid-state fluorescence enhancement and ef was as high as 485 (Figure 1-6).

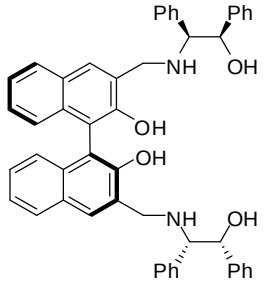

(*S*)-**1-24**

Figure 1-5. Photographs of (*S*)-**1-24** (5×10^{-4} M, benzene/0.4% DME) with (*R*)- and (*S*)-MA (4×10^{-3} M).

Figure 1-6. Fluorescence spectra of (*S*)-**1-24** (5×10^{-4} M, benzene/0.4% DME) with and without MA (4×10^{-3} M).

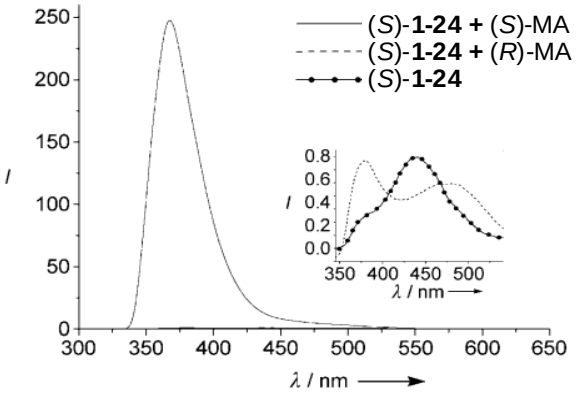

The compound (*S*)-**1-25**, which contains one more phenyl group than (*S*)-**1-24**, shows general enantioselectivity for structurally diverse α-hydroxyl carboxylic acids, including aromatic, aliphatic and tertiary α-hydroxyl carboxylic acids (Figure 1-7).[28] When (S)-**1-25** was treated with a chiral acid, one enantiomer of the acid greatly enhanced its monomer emission while the other quenched it (Figure 1-8). The I_R/I_S ratio was used to represent the enantioselectivity. The ^{1}H NMR study indicated the formation of 1:1 sensor/acid complex. The proposed structure of the complex is shown in Figure 1-9.

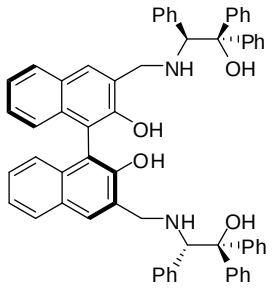

(*S*)-**1-25**

Figure 1-7. Fluorescent enantioselectivity of (*S*)-**1-25** toward various chiral α-hydroxycarboxylic acids.

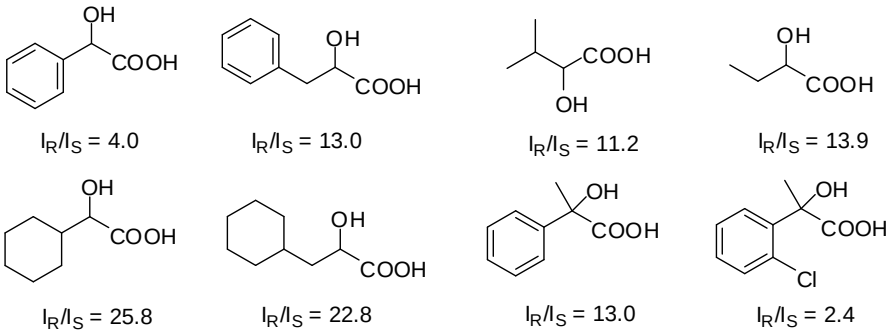

Figure 1-8. Fluorescence spectra of (*S*)-**1-25** (2×10^{-4} M, benzene/0.4% DME) with and without phenyllactic acid (5×10^{-3} M).

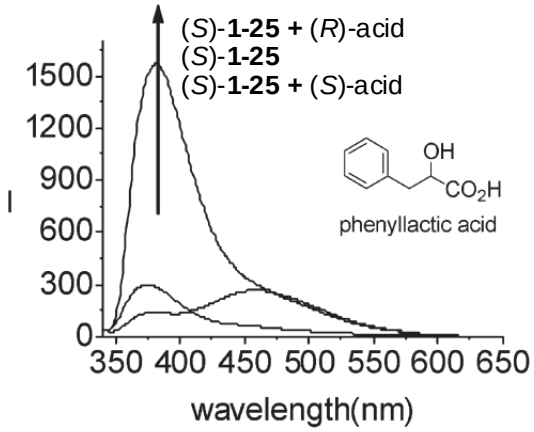

Figure 1-9. Calculated structure of the proposed 1:1 complex of (*S*)-**1-25** + (R)-phenyllatic acid.

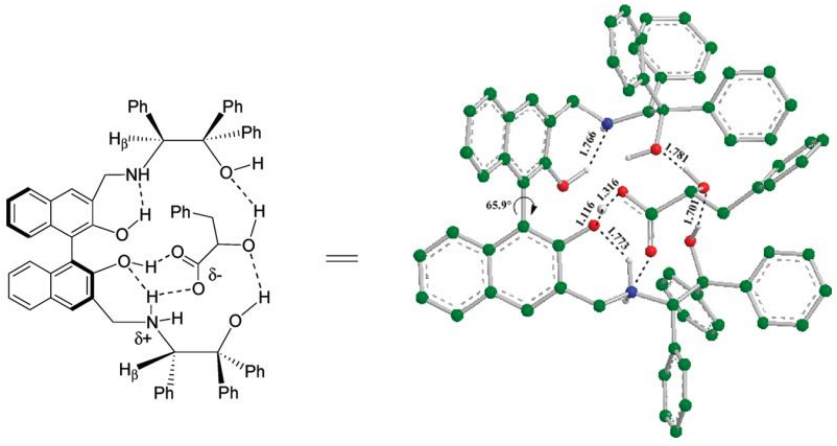

Crown ether is a commonly used binding unit in enantioselective recognition of organic ammonium salts due to the formation of tripod-like hydrogen binding complex **1-26**. Huszthy et al. designed acridino-crown ligand **1-27** for the enantioselective recognition of organic ammonium perchlorates **1-28** and **1-29**.[29] Besides the tripod-like hydrogen bonding, the extended aromatic ring system of the ligand can form strong π-π interaction with the substrates. When (*R*)- or (*S*)-**1-28** were added to a acetonitrile solution of **1-27**, the fluorescence intensity of naphthalene (λ_{em} = 330 nm) was almost completely quenched while the fluorescence of the acridine moiety (λ_{em} = 440 nm) underwent only partial quenching. The association constants exhibited big differences with 4.4 $\times 10^5$ M^{-1} for (*R*)-**1-28** and 2.3 $\times 10^6$ M^{-1} for (*S*)-**1-28**. This ligand also showed enantioselectivity for chiral ammonium **1-29** with association constant at 3.4 $\times 10^5$ M^{-1} for (*R*)-**1-29** and 1.7 $\times 10^6$ M^{-1} for (*S*)-**1-29**.

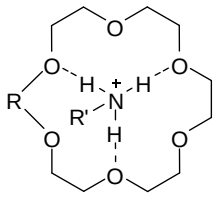

1-26

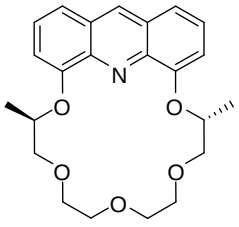

1-27

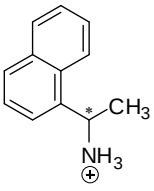

1-28

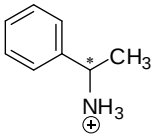

1-29

Karnik et al. developed a furo-fused BINOL based chiral crown **1-30** as an enantioselective chiral sensor for phenylethylamine **1-31** and ethyl ester of valine **1-32**.[30] Fluorescence enhancement was observed when **1-31** in chloroform was treated with perchlorate salts of **1-31** and **1-32**. The fluorescence was increased to 1.25 times with

(*R*)-**1-31** (1.64×10^{-6} M) but only 1.08 times with (*S*)-**1-31**, which gave ef value 2.97. It also exhibited enantioselective fluorescence enhancement for (*S*)-**1-32** and ef was 2.55. A linear relationship was observed for the concentration of **1-31** versus fluorescent intensity ratio, which indicated **1-30** is useful for the ee determination of the amine **1-31**.

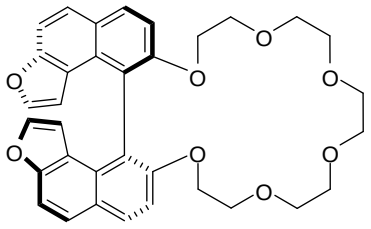

1-30

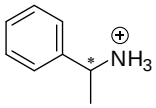

1-31

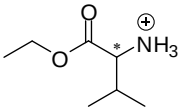

1-32

Wolf and coworkers have developed a series of C_2-symmetric 1,8-diacrydylnaphthalene fluorescent sensors for a range of chiral hydrogen bond donor analytes. Compound **1-33** was found to undergo enantioselective quenching (λ_{em} = 550 nm) in acetonitrile with a variety of chiral carboxylic acids **1-34** – **1-41**.[31] Among all these acids, camphanic acid **1-41** exhibited highest enantioselectivity with α (K^R_{SV}/K^S_{SV} or K^S_{SV}/K^R_{SV}) up to 4.5. Based on Stern-Volmer equation, compound **1-33** forms 1:1 complex with acids **1-34** – **1-37** and 1:2 complexes with acids **1-38** – **1-41**. It was proposed that the enantioselective fluorescence quenching was due to static quenching through nonradiative releaxation of the diastereomeric acid-base adducts.

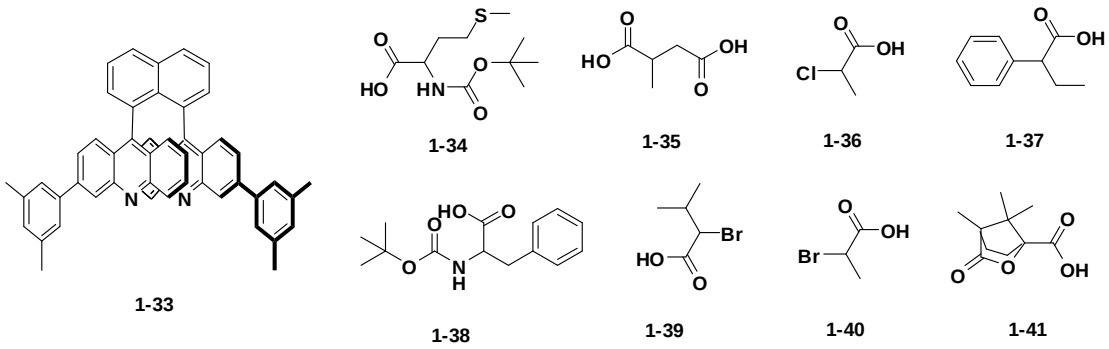

N,N'-dioxide **1-42** was also prepared and the twisting of the acrydyl rings can vary to accommodate analytes of varying size.[32] Enantioselective quenching can be observed when treated with chiral bidentate analytes **1-43** and **1-44**. The enantioselectivity factor α were 1.63 and 1.50, respectively.

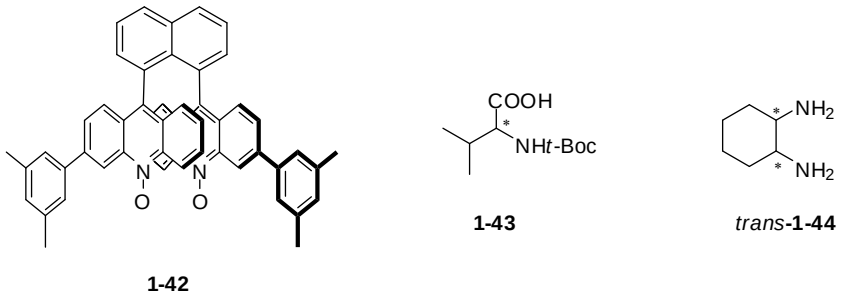

Similarly, compound **1-45** can enantioselectively recognize various carboxylic acids and amino acids.[33] Taking **1-36** and **1-39** as examples, the fluorescence of **1-45** was dramatically quenched when treated with (*S*)-enantiomer while only a little quenching could be observed with (*R*)-enantiomer (Figure 1-10). It was proved that the total concentration and ee of a chiral substrate **1-36** could be determined by using the racemic and enantiopure form of **1-45**. Six samples were tested and the results were within +/-2% of the actual concentration and +/-3% of the actual enantiopurity.

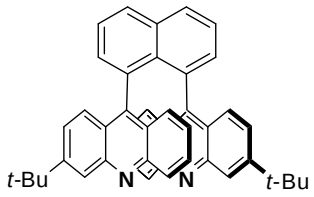

1-45

Figure 1-10. Stern-Volmer plots showing enantioselective fluorescence quenching of (-)-**1-45** in the presence of **1-36** and **1-39**.

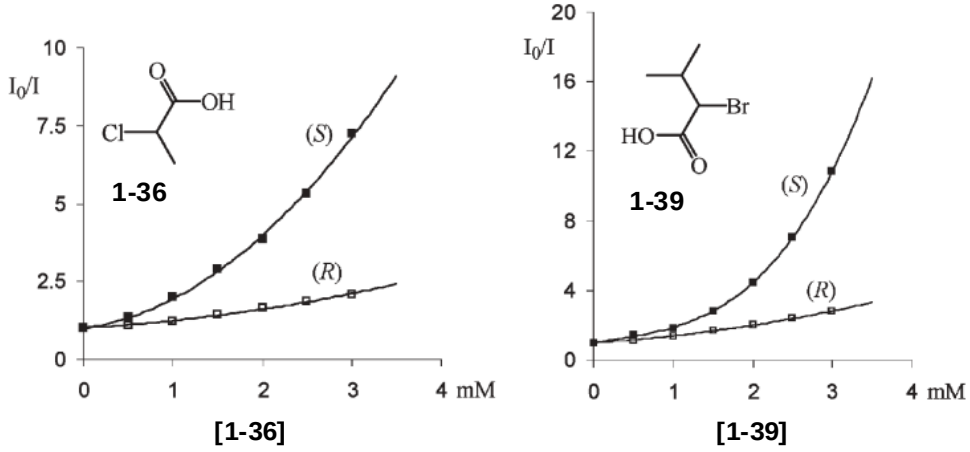

3.2 metal complexation

Transition metals, especially Cu (II), usually work as an efficient fluorescence quencher due to the formation of a metal-ligand charge transfer state. Treating a fluorophore with transition metals may turn off the fluorescence and produce a low background. If addition of guests to this complex can recover the fluorescence, a turn on fluorescent sensor with high sensitivity would be enabled.

Roberto Corradini and coworkers developed a series of monofunctionalized β-cyclodextrins bearing a copper (II) binding side arm and a dansyl group

(CD-NH-AA-CH2CH2NH-DNS) for the enantioselective sensing of unmodified α-amino acids. As shown in Figure 1-11, β-cyclodextrins was chosen as platform since it has the right size to include dansyl in its cavity to form rigid preorganized structure. The side arms and dansyl group provide an amino, an amide, and a sulfonamide group as binding sites for Cu(II). Chiral amino acid provides an additional chiral center to enhance enantioselectivity.

Figure 1-11. Structural elements considered in the design of enantioselective cyclodextrins.

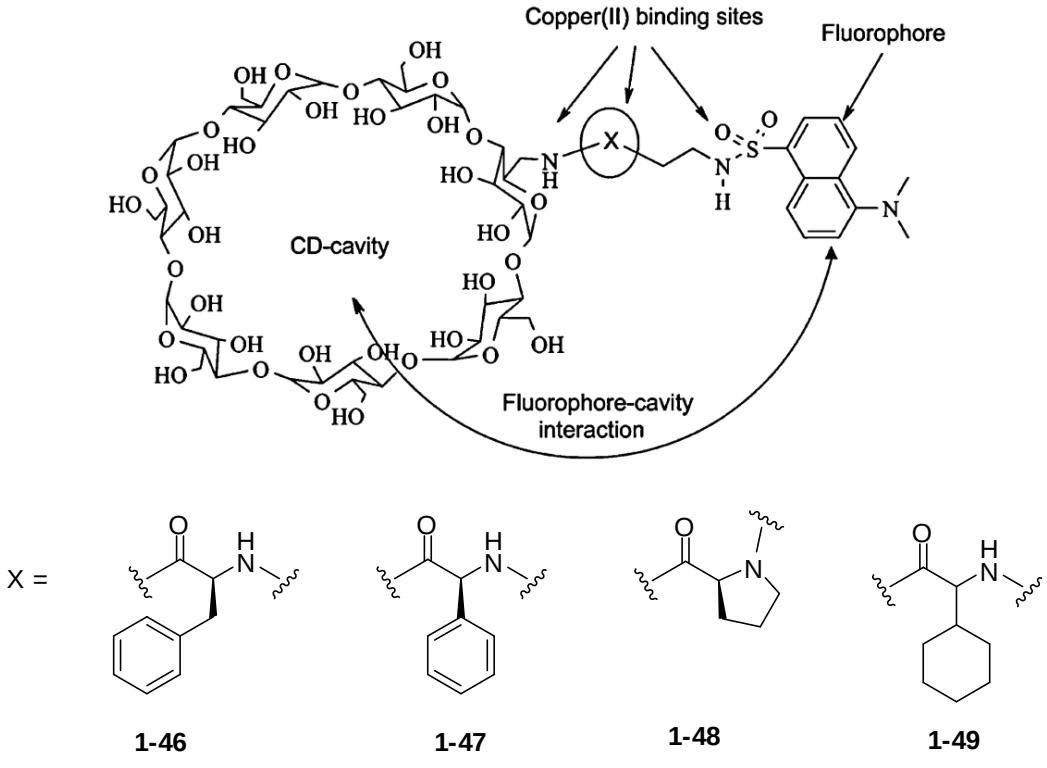

Compound **1-46** can form 1:1 complex with Cu(II) showing quenched fluorescence.[34] When equimolar amount of D- or L-amino acids were added to this complex solution (6

$\times 10^{-5}$ M) in 0.1 M tetraborate buffer (pH = 7.3), the fluorescence can be turned back on with enantioselectivity. This Cu complex showed good enantioselectivity for most of tested amino acids expect Ala, His and Asp (Table 1-1).[35] The mechanism of sensing can be attributed to the competition between the formation of the ternary Cu(II)/ligand/amino acid complex which is nonfluorescent and that of the binary Cu(II)/amino acid complex which is fluorescent because of displacement of the dansyl group.

Table 1-1. Enantioselectivity $\Delta F_D/\Delta F_L$ of Cu-**1-46** towards amino acids.

	Pro	Ala	Val	Leu	His	Asp	Lys	Ser	Phe	Phgly	Trp	Tyr
$\Delta F_D/\Delta F_L$	3.93	1.04	0.34	0.31	0.94	0.89	0.79	0.68	0.19	0.43	0.62	0.44

Another three cyclodextrins **1-47 – 1-49** were prepared and enantioselective fluorescence quenching was performed by adding Cu(II) complex of amino acid to a cyclodextrin ligand solution.[36] All four cyclodextrins showed significant enantioselectivity for both proline and valine. Calibration curves were obtained by using the fluorescence microplate reader to measure the interaction of cyclodextrins **1-46 – 1-48** with valine samples of different enantiomeric excess. Six samples were analyzed with the calibration curve and it shows an average error of 6%, which proved its accuracy and ability to be used for high-throughput screening.[37]

A BINOL-terpyridine-Cu(II) complex **1-51** was prepared by our group and its $CHCl_3$ suspension at 3.75% (w/v, g/mL) can form gel upon sonication.[38] The gel collapsed

when a $CHCl_3$ solution (0.1 mL) of (S)-phenylglycinol (0.1 equiv) was added while remained stable with (*R*)-phenylglycinol upon sonication. Complexation with Cu quenched the fluorescence of **1-50.** When the enantiomers of phenylglycinol were added to the solution of **1-51** (5.0 $\times 10^{-7}$ M in 2:3 CH_2Cl_2/n-hexane), it showed enantioselective fluorescence enhancement (Figure 1-12). This enantioselectivity can be attributed to the enantioselective displacement of the Cu(II) from **1-51** by the amino alcohol.

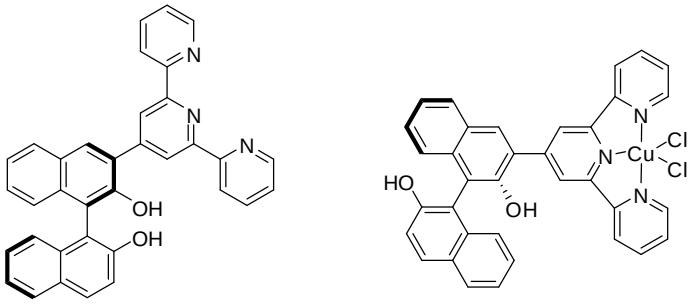

1-50 **1-51**

Figure 1-12. Fluorescence spectra of **1-51** (5.0 $\times 10^{-7}$ M) in CH_2Cl_2/n-hexane (2:3) in the presence of (R)- and (S)-phenylglycinol (5.0 $\times 10^{-4}$ M).

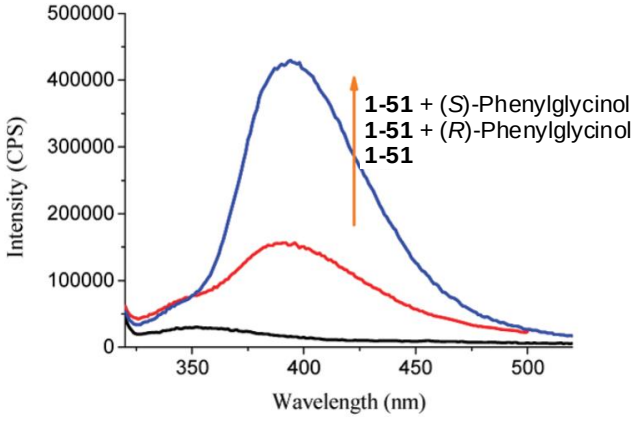

Zhu et al. synthesized a chiral perazamacrocyclic fluorescent sensor **1-52**.[39] Among the 14 tested metals, only Cu(II) could efficiently quench its fluorescence by forming a 1:1 complex. With excess amount of Cu(II), which is 2 eq, this ligand solution (1×10^{-5} M, in 1:1 methanol/water) exhibited remarkable enantioselective fluorescence enhancement toward unmodified amino acids **1-53** – **1-57**, in which **1-57** Phe showed the highest fluorescence enhancement with I_D/I_0 = 14.9 and highest enantioselectivity with $\Delta I/I_0$ = 4.9 (Figure 1-13).

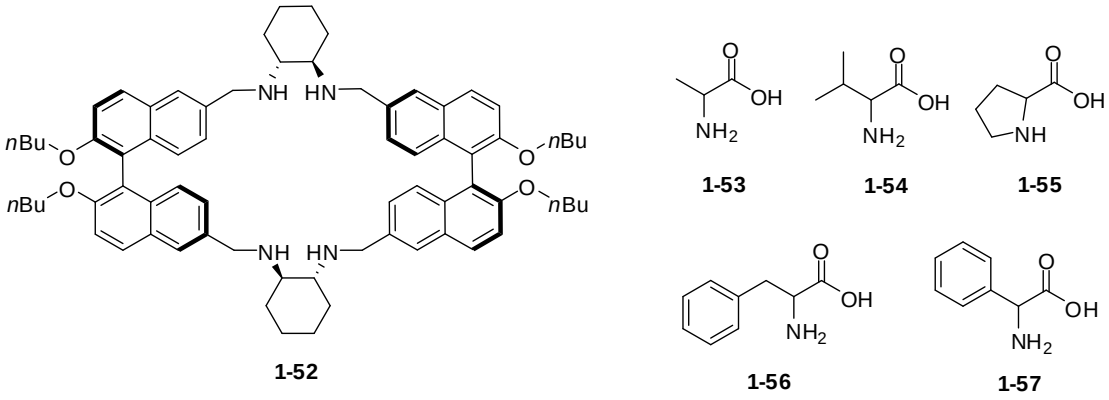

Figure 1-13. (a) Fluorescence spectra of **1-52**+Cu(II) (1×10^{-5} M + 2×10^{-5} M) with D- or L-Phe (1×10^{-4} M). (b) Plots of I/I_0 vs Phe concentration during titration.

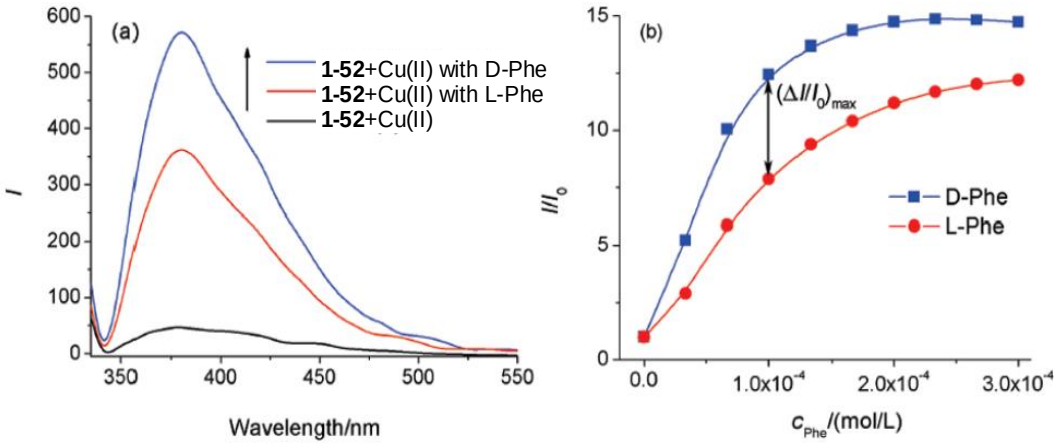

3.3 Reversible covalent interactions

The use of hydrogen bonding interactions has its limitations in protic solvents. Thus the fluorescent boronic acid based sensors have been extensively explored because they can covalently interact with diols in aqueous environment.[40]

Figure 1-14. Generic design of fluorescent PET sensors with the boronic acid recognition unit.

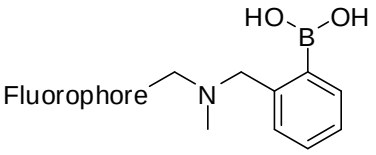

Figure 1-15. The effect of saccharide complexation and pH changes on the fluorescence of boronic acid.

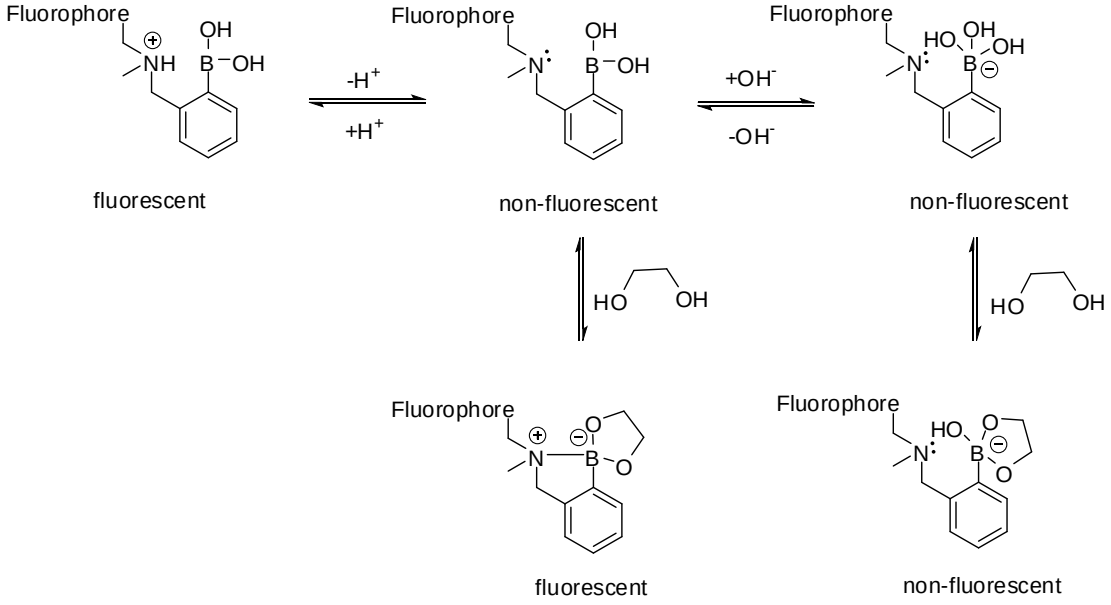

The design of these sensors follows fluorophore-amine base-boronic acid structure

(Figure 1-14). As shown in Figure 1-15, the amine base-boronic acid interaction lowers the pKa of the boronic acid and allows binding to occur at neutral pH. Also the lone pair of amine is available for photoinduced electron transfer (PET) to quench the fluorescence. Complexation with diols augments the N-B interaction and in turn distrupts PET, turning on the fluorescence. Seiji Shinkai, Tony D. James and Jianzhang Zhao have developed a series of enantioselective boronic acid sensors.

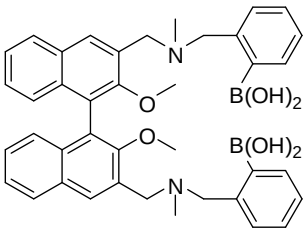

(R)-**1-58** and (*S*)-**1-58**

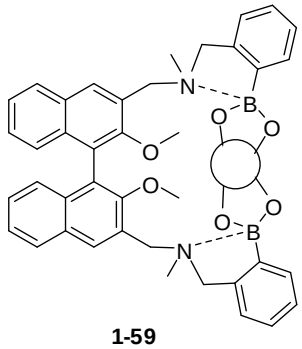

1-59

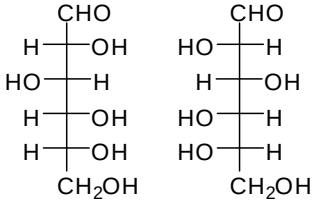

D-Glucose

L-Glucose

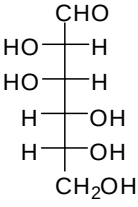

D-Mannose

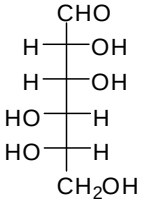

L-Mannose

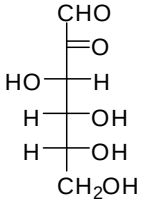

D-Fructose

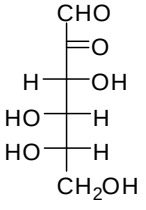

L-Fructose

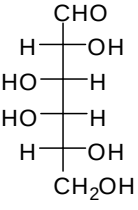

D-Galactose

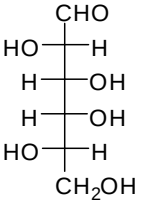

L-Galactose

The BINOL-bisboronic acid compound **1-58** was first designed for the chiral discrimination of D- and L-monosaccharides at pH 7.77 (phosphate 33.3% (w/w)

methanol buffer).[41] It formed 1:1 cyclic boronate ester **1-59** with guests and the fluorescence was enhanced due to suppressed PET. With (*R*)-**1-58** the complex stabilities of D-fructose, D-glucose, D-mannose and L-galactose are greater than those of L-fructose, L-glucose, L-mannose and D-galactose, respectively (Table 1-2). The stronger binding corresponds to the stronger fluorescence.

Table 1-2. Stability constants and fluorescence enhancements for saccharides with (*R*)-**1-58**.

Saccharide	D log K	L log K	D/L fluorescence ratio
Fructose	4.0	3.5	1.47
Glucose	3.3	3.1	1.93
Galactose	3.1	3.3	0.82
Mannose	<2.4	—	—

The same compound was then investigated for the interaction with a range of sugar acids over a range of pH values.[42] As shown in Figure 1-16, the recognition of D- and L-tartaric acid is strongly pH dependent. At pH 5.6 the fluorescence of (*R*)-**1-58** was enhanced by D-tartaric acid but diminished by L-tartaric acid. At pH 8.3 both D- and L-tartaric acid could enhance the fluorescence with much stronger fluorescence for D-tartaric acid. Gluconic acid showed similar responses.

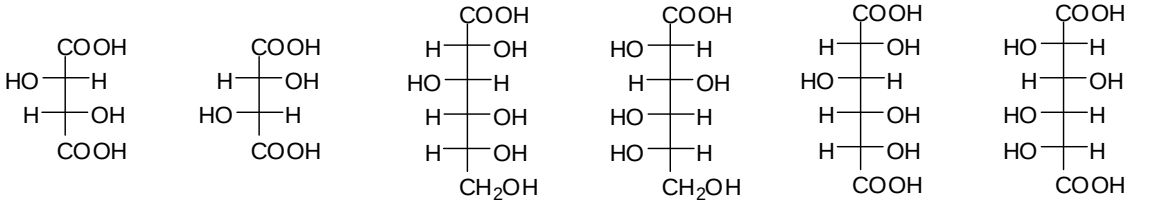

Figure 1-16. Fluorescence intensity-pH profiles for titrations of (*R*)- and (*S*)-**1-58** (5.0×10^{-6} M in 0.05 M NaCl solution (52.1% methanol in water)) with D- or L-tartaric acid (0.02 M).

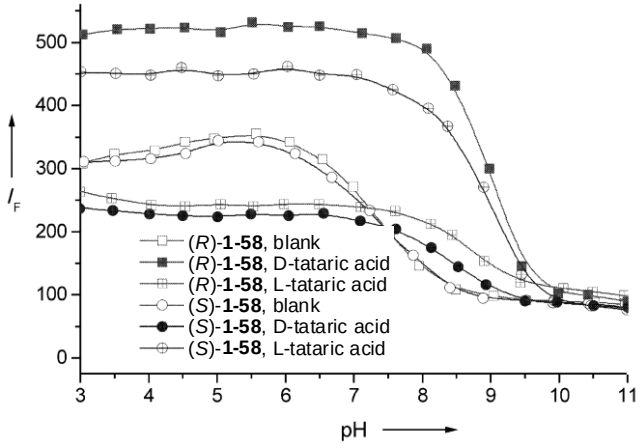

In order to make the chiral center in close proximity to the receptor's binding site, anthracene-bisboronic acid **1-60** was designed.[43] It exhibited significantly improved sensitivity and enantioselectivity toward sugar acids, such as tartaric acid, glucaric acid and gluconic acid. At pH 8.3, titration of (*S, S*)-**1-60** with L-tartaric acid caused a significant fluorescence enhancement (I/I_0 = 8.24), whereas only a small change (I/I_0 = 1.5) was observed with D-tartaric acid (Figure 1-17a). Calibration curve was generated and the ee of tartaric acid can be determined. Single-crystal X-ray data confirmed the 1:1 binding complex (Figure 1-18). It also exhibited significant enantioselectivity towards sugar alcohols. [44]

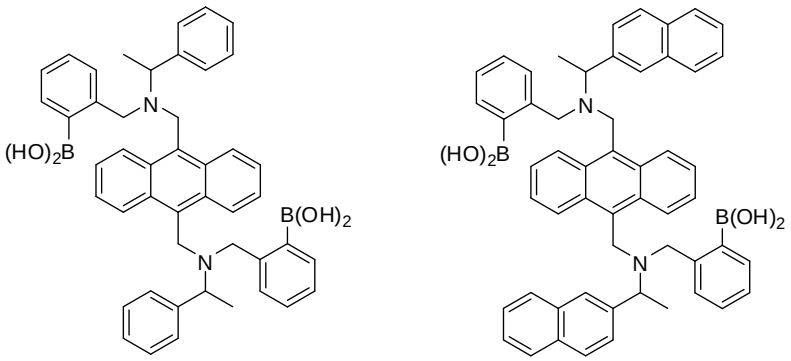

(*R*,*R*)-**1-60** and (*S*,*S*)-**1-60** (*R*,*R*)-**1-61** and (*S*,*S*)-**1-61**

Figure 1-17. Fluorescence intensity-pH profiles for titrations of (a) **1-60**, (b) (*R*, *R*)-**1-61** (3.0×10^{-6} M in 0.05 M NaCl solution (52.1% methanol in water)) with D- or L-tartaric acid (0.05 M).

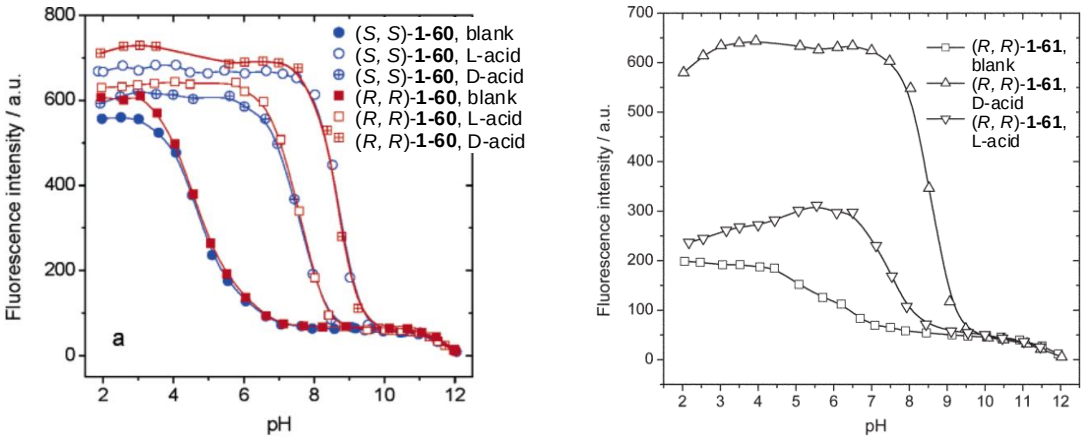

Figure 1-18. (a) Structure of (*R*, *R*)-**1-60**. (b) Structure of (*R*, *R*)-**1-60** complex with L-tartaric acid.

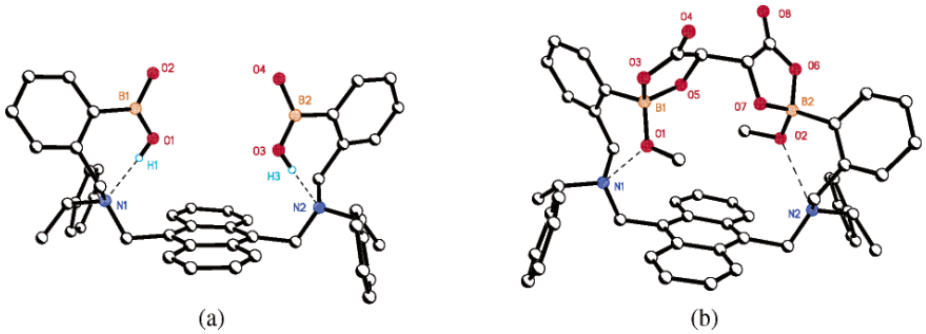

By introducing naphthalene a dual fluorophore boronic acid receptor **1-61** was prepared.[45] It displayed reduced fluorescence response compared to **1-60** due to close contact of the naphthalene and anthracene fluorophores. Addition of D-tartaric acid to (*R, R*)-**1-61** caused a large increase in fluorescence as a result of the formation of a rigid complex. Addition of L-tartaric acid only produced small changes in fluorescence.

The normal PET sensors, as described above, give stronger fluorescence at acidic conditions due to suppressed PET. The fluorophore acts as acceptor in PET process. However, the carbazole-bisboronic acid **1-62** displayed a reverse fluorescence intensity-pH relationship with diminished emission at acidic pH but enhanced emission at basic pH (Figure 1-19).[46] It is proposed that the reduced fluorescence is due to electron transfer from the cabazole moiety to the protonated amine and boronic acid moiety, which is called d-PET (fluorophore as donor). This theory was supported by DFT/TDDFT calculations. **1-62** exhibited fluorescence enhancement /diminishment selectivity toward the enantiomers of tartaric acid at neutral pH.

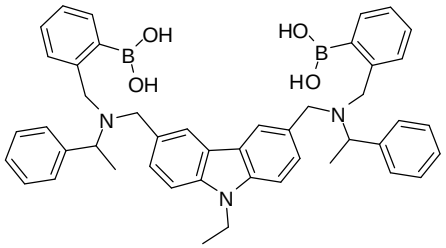

(*R*,*R*)-**1-62** and (*S*,*S*)-**1-62**

Figure 1-19. Fluorescence intensity-pH profiles of (*S, S*)-**1-62** (3.0×10^{-6} M in 0.05 M NaCl solution (52.1% methanol in water)) with D- or L-tartaric acid (0.05 M).

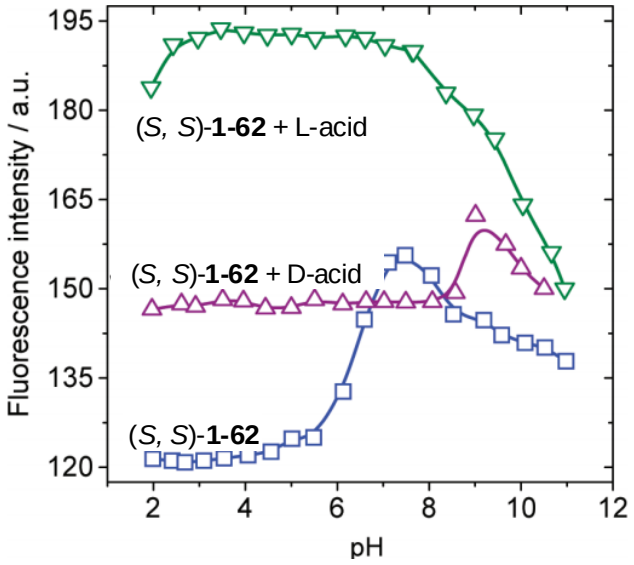

In order to extend the π-conjugation of the carbazole and to enhance the electron-donating ability of the fluorophore, thiophene was employed to acquire carbazole-thiophene-boronic acid sensor **1-63**.[47] Its emission maxima located at 413 nm, which is red shifted by 38 nm compare to sensor **1-62**. The d-PET contrast ratio is 3, which is 10-fold greater than **1-62**. Enantioselective recognition toward tartaric acid and mandelic acid was observed (Figure 1-20).

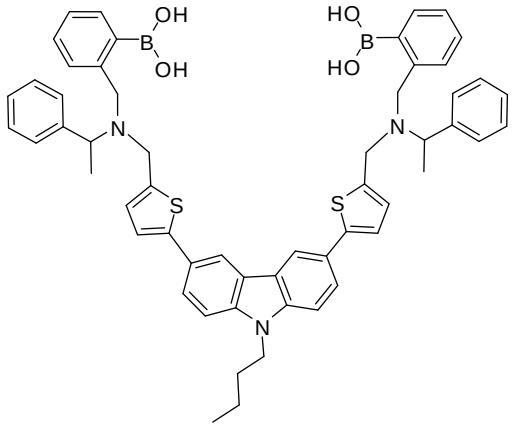

(*R*,*R*)-**1-63** and (*S*,*S*)-**1-63**

Figure 1-20. Fluorescence intensity-pH profiles of (*S*, *S*)-**1-63** (5.0×10^{-7} M in methanol/water 3:1) with (a) D- or L-tartaric acid (b) D- or L-mandelic acid (0.01 M).

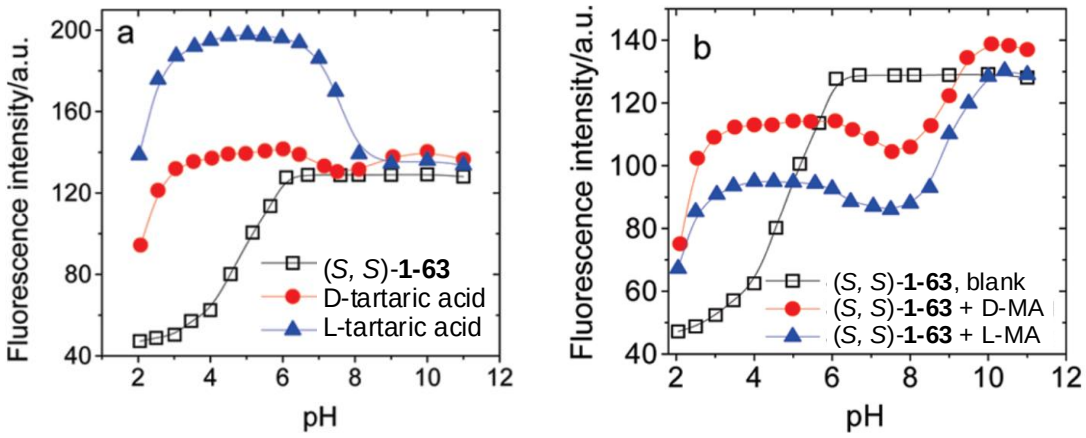

For all the boronic acid sensors mentioned above, the fluorophore, scaffold and chirogenic centers are integrated, limiting the design of boronic acid sensors. To solve this problem, modular chiral sensor **1-64** was deigned, in which the fluorophore (phenothiazine) and the chirogenic centers were modules and readily assembles onto a scaffold.[48] With this structural motif, any fluorophores that can be ethynylated are suitable for assembling a chiral sensor. The sensor **1-64** has emission maxima at 488 nm and the contrast ratio was about 6.0. It showed the fluorescence enhancement at acidic pH and diminishment at basic pH toward tartaric acids.

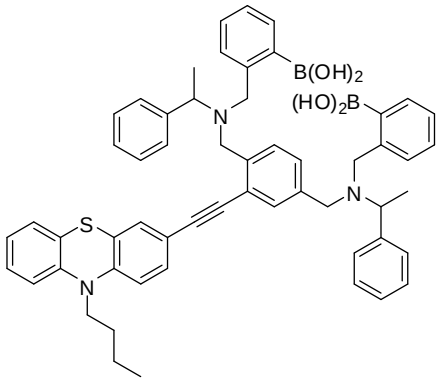

(*R*,*R*)-**1-64** and (*S*,*S*)-**1-64**

4. Conclusion

Although a large number of enantioselective fluorescent sensors for the recognition of chiral compounds have been developed, it is still a challenge to use them in the screening of chiral catalysts for asymmetric synthesis. Most of the fluorescent sensors with high enantioselectivity can be used to determine ee of substrates only at a certain concentration, which means a separate method for determining the total concentration is needed. This drawback significantly limits the application of fluorescent sensors in HTS of chiral catalysts.

Our lab has developed a series of BINOL-based chiral fluorescent sensors with very high enantioselectivity. The subject of this thesis is to further develop those sensors and explore methods for simultaneous determination of concentration and ee of chiral substrates, which will be a significant step toward the application of fluorescent sensor in the high-throughput screening of asymmetric catalysts.

References

1. Pu, L., *Chemical Reviews* **2004,** *104* (3), 1687-1716.
2. Pu, L., *Accounts of Chemical Research* **2012,** *45* (2), 150-163.
3. Leung, D.; Kang, S. O.; Anslyn, E. V., *Chemical Society Reviews* **2012,** *41* (1), 448-479.
4. Nunez, M. C.; Garcia-Rubino, M. E.; Conejo-Garcia, A.; Cruz-Lopez, O.; Kimatrai, M.; Gallo, M. A.; Espinosa, A.; Campos, J. M., *Current Medicinal Chemistry* **2009,** *16* (16), 2064-2074; Izake, E. L., *Journal of Pharmaceutical Sciences* **2007,** *96* (7), 1659-1676.
5. Natarajan, R.; Basak, S. C., *Current Topics in Medicinal Chemistry* **2011,** *11* (7), 771-787.
6. Simo, C.; Barbas, C.; Cifuentes, A., *Electrophoresis* **2003,** *24* (15), 2431-2441; Herrero, M.; Simo, C.; Garcia-Canas, V.; Fanali, S.; Cifuentes, A., *Electrophoresis* **2010,** *31* (13), 2106-2114.
7. Lin, G.-Q.; Li, Y.-M.; Chan, A. S. C., *Principles and Applications of Asymmetric Synthesis*. John Wiley & Sons: 2001; Christmann, M.; Bräse, S., *Asymmetric Synthesis: The Essentials*. 2007.
8. Reetz, M. T., *Angewandte Chemie-International Edition* **2001,** *40* (2), 284-310.
9. Maier, W. F.; Stowe, K.; Sieg, S., *Angewandte Chemie-International Edition* **2007,** *46* (32), 6016-6067; Jandeleit, B.; Schaefer, D. J.; Powers, T. S.; Turner, H. W.; Weinberg,

W. H., *Angewandte Chemie-International Edition* **1999,** *38* (17), 2495-2532.

10. Finn, M. G., *Chirality* **2002,** *14* (7), 534-540; Tsukamoto, M.; Kagan, H. B., *Advanced Synthesis & Catalysis* **2002,** *344* (5), 453-463; Traverse, J. F.; Snapper, M. L., *Drug Discovery Today* **2002,** *7* (19), 1002-1012.
11. Leung, D.; Folmer-Andersen, J. F.; Lynch, V. M.; Anslyn, E. V., *Journal of the American Chemical Society* **2008,** *130* (37), 12318-12327; Leung, D.; Anslyn, E. V., *Journal of the American Chemical Society* **2008,** *130* (37), 12328-12333.
12. Tielmann, P.; Boese, M.; Luft, M.; Reetz, M. T., *Chemistry-a European Journal* **2003,** *9* (16), 3882-3887; Reetz, M. T.; Jaeger, K. E., *Chemistry-a European Journal* **2000,** *6* (3), 407-412; Reetz, M. T., *Pure and Applied Chemistry* **2000,** *72* (9), 1615-1622; Reetz, M. T.; Zonta, A.; Schimossek, K.; Liebeton, K.; Jaeger, K. E., *Angewandte Chemie-International Edition* **1997,** *36* (24), 2830-2832.
13. Millot, N.; Borman, P.; Anson, M. S.; Campbell, I. B.; Macdonald, S. J. F.; Mahmoudian, M., *Organic Process Research & Development* **2002,** *6* (4), 463-470.
14. Reetz, M. T.; Becker, M. H.; Kuhling, K. M.; Holzwarth, A., *Angewandte Chemie-International Edition* **1998,** *37* (19), 2647-2650.
15. Reetz, M. T.; Becker, M. H.; Klein, H. W.; Stockigt, D., *Angewandte Chemie-International Edition* **1999,** *38* (12), 1758-1761.
16. Guo, J. H.; Wu, J. Y.; Siuzdak, G.; Finn, M. G., *Angewandte Chemie-International Edition* **1999,** *38* (12), 1755-1758.

17. Reetz, M. T.; Kuhling, K. M.; Deege, A.; Hinrichs, H.; Belder, D., *Angewandte Chemie-International Edition* **2000,** *39* (21), 3891-+.

18. Ding, K. L.; Ishii, A.; Mikami, K., *Angewandte Chemie-International Edition* **1999,** *38* (4), 497-501.

19. Nieto, S.; Lynch, V. M.; Anslyn, E. V.; Kim, H.; Chin, J., *Journal of the American Chemical Society* **2008,** *130* (29), 9232-+.

20. Copeland, G. T.; Miller, S. J., *Journal of the American Chemical Society* **1999,** *121* (17), 4306-4307.

21. Korbel, G. A.; Lalic, G.; Shair, M. D., *Journal of the American Chemical Society* **2001,** *123* (2), 361-362.

22. de Silva, A. P.; Gunaratne, H. Q. N.; Gunnlaugsson, T.; Huxley, A. J. M.; McCoy, C. P.; Rademacher, J. T.; Rice, T. E., *Chemical Reviews* **1997,** *97* (5), 1515-1566.

23. Lin, J.; Hu, Q. S.; Xu, M. H.; Pu, L., *Journal of the American Chemical Society* **2002,** *124* (10), 2088-2089.

24. Xu, M. H.; Lin, J.; Hu, Q. S.; Pu, L., *Journal of the American Chemical Society* **2002,** *124* (47), 14239-14246.

25. Lin, J.; Zhang, H. C.; Pu, L., *Organic Letters* **2002,** *4* (19), 3297-3300.

26. Li, Z. B.; Lin, J.; Pu, L., *Angewandte Chemie-International Edition* **2005,** *44* (11), 1690-1693.

27.Liu, H. L.; Hou, X. L.; Pu, L., *Angewandte Chemie-International Edition* **2009,** *48* (2),

382-385.

28. Liu, H. L.; Peng, Q.; Wu, Y. D.; Chen, D.; Hou, X. L.; Sabat, M.; Pu, L., *Angewandte Chemie-International Edition* **2010,** *49* (3), 602-606.
29. Prodi, L.; Bolletta, F.; Montalti, M.; Zaccheroni, N.; Huszthy, P.; Samu, E.; Vermes, B., *New Journal of Chemistry* **2000,** *24* (10), 781-785.
30. Upadhyay, S. P.; Pissurlenkar, R. R. S.; Coutinho, E. C.; Karnik, A. V., *Journal of Organic Chemistry* **2007,** *72* (15), 5709-5714.
31. Mei, X. F.; Wolf, C., *Journal of the American Chemical Society* **2004,** *126* (45), 14736-14737.
32. Mei, X. F.; Wolf, C., *Chemical Communications* **2004,** (18), 2078-2079.
33. Wolf, C.; Liu, S. L.; Reinhardt, B. C., *Chemical Communications* **2006,** (40), 4242-4244.
34. Pagliari, S.; Corradini, R.; Galaverna, G.; Sforza, S.; Dossena, A.; Marchelli, R., *Tetrahedron Letters* **2000,** *41* (19), 3691-3695.
35. Pagliari, S.; Corradini, R.; Galaverna, G.; Sforza, S.; Dossena, A.; Montalti, M.; Prodi, L.; Zaccheroni, N.; Marchelli, R., *Chemistry-a European Journal* **2004,** *10* (11), 2749-2758.
36. Corradini, R.; Paganuzzi, C.; Marchelli, R.; Pagliari, S.; Sforza, S.; Dossena, A.; Galaverna, G.; Duchateau, A., *Chirality* **2003,** *15*, S30-S39.
37. Corradini, R.; Paganuzzi, C.; Marchelli, R.; Pagliari, S.; Sforza, S.; Dossena, A.;

Galaverna, G.; Duchateau, A., *Journal of Materials Chemistry* **2005,** *15* (27-28), 2741-2746.

38. Chen, X.; Huang, Z.; Chen, S. Y.; Li, K.; Yu, X. Q.; Pu, L., *Journal of the American Chemical Society* **2010,** *132* (21), 7297-+.
39. Yang, X.; Liu, X. C.; Shen, K.; Zhu, C. J.; Cheng, Y. X., *Organic Letters* **2011,** *13* (13), 3510-3513.
40. James, T. D.; Shinkai, S., *Host-Guest Chemistry: Mimetic Approaches to Study Carbohydrate Recognition* **2002,** *218*, 159-200; James, T. D., *Creative Chemical Sensor Systems* **2007,** *277*, 107-152.
41. James, T. D.; Sandanayake, K.; Shinkai, S., *Nature* **1995,** *374* (6520), 345-347.
42. Zhao, J. Z.; Fyles, T. M.; James, T. D., *Angewandte Chemie-International Edition* **2004,** *43* (26), 3461-3464.
43. Zhao, J. Z.; Davidson, M. G.; Mahon, M. F.; Kociok-Kohn, G.; James, T. D., *Journal of the American Chemical Society* **2004,** *126* (49), 16179-16186.
44. Zhao, J. Z.; James, T. D., *Journal of Materials Chemistry* **2005,** *15* (27-28), 2896-2901.
45. Zhao, J. Z.; James, T. D., *Chemical Communications* **2005,** (14), 1889-1891.
46. Han, F.; Chi, L. N.; Liang, X. F.; Ji, S. M.; Liu, S. S.; Zhou, F. K.; Wu, Y. B.; Han, K. L.; Zhao, J. Z.; James, T. D., *Journal of Organic Chemistry* **2009,** *74* (3), 1333-1336.
47. Wu, Y. B.; Guo, H. M.; James, T. D.; Zhao, J. Z., *Journal of Organic Chemistry* **2011,**

76 (14), 5685-5695.

48. Wu, Y. B.; Guo, H. M.; Zhang, X.; James, T. D.; Zhao, J. Z., *Chemistry-a European Journal* **2011,** *17* (27), 7632-7644.

Chapter 2

Pseudoenantiomeric Fluorescent Sensors in a Chiral Assay

1. Introduction

In recent years, there have been growing interests in developing enantioselective fluorescent sensors because of their potential application as a rapid analytical tool in chiral assay.[1,2] A number of highly enantioselective fluorescent sensors have been reported for the recognition of chiral molecules such as carboxylic acids, amines, alcohols, amino alcohols and amino acid derivatives.[1-3] These sensors can be used to determine the enantiomeric composition of a chiral substrate at a given concentration. Because the fluorescence of a chiral sensor is strongly influenced by both the concentration and the enantiomeric composition of the substrate, these two parameters need to be determined separately.[1m] It would be highly advantageous if both the concentration and the enantiomeric composition of the substrate could be determined simultaneously by one fluorescence measurement. This should greatly simplify the analysis of the reaction products generated from high throughput screening experiments.

We propose to develop a novel strategy to simultaneously measure both the concentration and the enantiomeric composition of a chiral substrate by using pseudo-enantiomeric fluorescent sensor pairs. An enantiomeric fluorescent sensor pair is a racemic mixture which cannot be used for the desired chiral recognition. Whereas, in a pseudo-enantiomeric fluorescent sensor pair, the two sensors, e.g., (*S*)-A and (*R*)-B, will have opposite enantioselectivity and emit at two distinctively different wavelengths, e.g., λ_A and λ_B. When a mixture of the pseudo-enantiomeric sensor pair (*S*)-A and (*R*)-B

is treated with an enantiomeric mixture of a chiral substrate, we assume that one enantiomer of the substrate should enhance the fluorescence of (*S*)-A at λ_A giving a fluorescence intensity I_A, and the other enantiomer of the substrate should enhance the fluorescence of (*R*)-B at λ_B giving a fluorescence intensity I_B. It is proposed that the fluorescence intensity difference I_A-I_B could be used to determine the concentration difference of the two enantiomers of the substrate and the sum of the fluorescence intensity I_A+I_B could be used to determine the total concentration of the two enantiomers. That is, both the enantiomeric composition of the substrate and its concentration could be determined by one fluorescence measurement with the use of the pseudo-enantiomeric sensor pair.

2. Results and Discussion

2.1 Design and Synthesis of (*S*)-2-1 and (*R*)-2-2

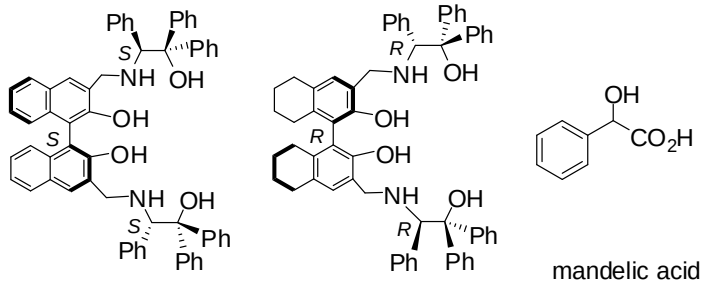

(*S*)-**2-1** (*R*)-**2-2**

We have conceived the use of the 1,1'-binaphthol (BINOL)-amino alcohol (*S*)-**2-1** and its analog (*R*)-**2-2** as a pseudo-enantiomeric sensor pair. These two compounds have the opposite chiral configuration at both the axially chiral biaryl centers and the

amino alcohol units. They are expected to exhibit emission at different wavelengths because of the much reduced conjugation of (*R*)-**2-2** versus (*S*)-**2-1**.

Scheme 2-1. Synthesis of BINOL-amino alcohol (*S*)-**2-1**.

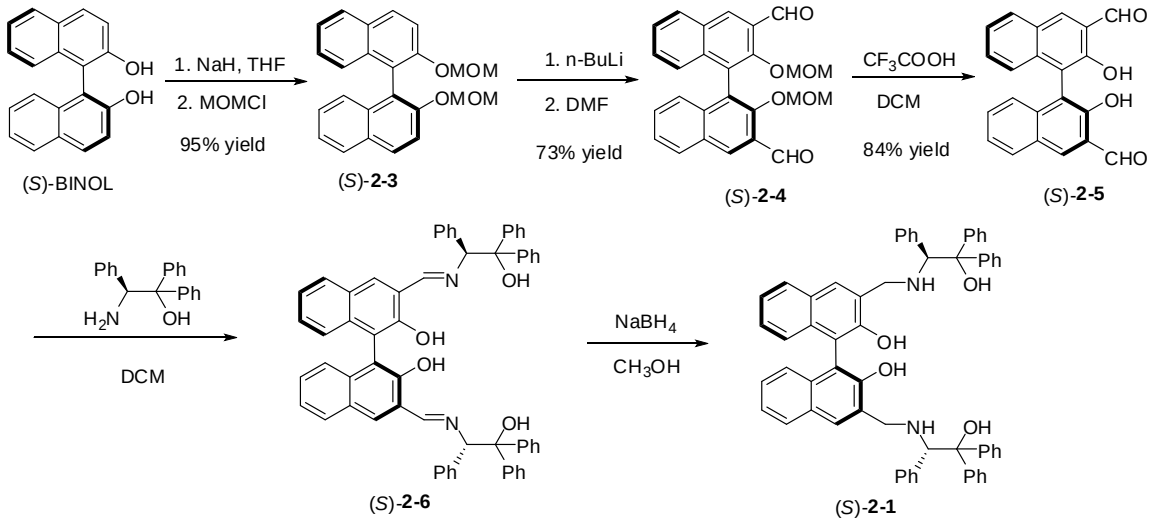

Scheme 2-2. Synthesis of H_8BINOL-amino alcohol (*R*)-**2-2**.

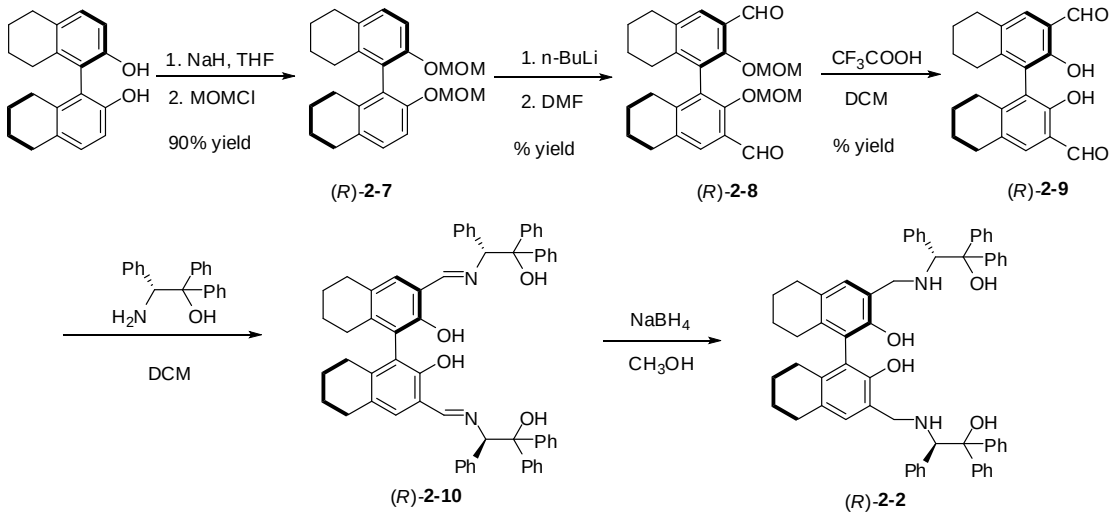

Compound (*S*)-**2-1** was readily prepared according to Scheme 2-1. Reaction of (*S*)-1,1'-bi-2-naphthol [(*S*)-BINOL] with NaH followed by treatment with MOMCl gave

the protected BINOL (*S*)-**2-3** in 95% yield. Ortho-lithiationg followed by addition of DMF and hydrolysis gave BINOL dialdehyde (*S*)-**2-5**. Condensation of (*S*)-**2-3** with the amino alcohol followed by reduction produced the BINOL-amino alcohol (*S*)-**2-1**. The H_8BINOL amino alcohol (*R*)-**2-2** was obtained following similar procedures starting with partially hydrogenated BINOL, (*R*)-H_8BINOL (Scheme 2-2).

2.2 Enantioselective Fluorescent Recognition of Chiral Acids.

(*S*)-**2-1** was reported as a generally enantioselective fluorescent sensor for α-hydroxycarboxylic acids in benzene solution.[3] Because of the reduced conjugation of (*R*)-**2-2** versus (*S*)-**2-1**, benzene interferes with the fluorescence spectrum of (*R*)-**2-2** and is not a suitable solvent for this pseudo-enantiomeric pair. We have thus examined the fluorescent response of (*S*)-**2-1** toward mandelic acid (MA) in CH_2Cl_2. Even though CH_2Cl_2 is a much more polar solvent, highly enantioselective fluorescent responses are still observed. As shown in Figure 2-1a, (*R*)-MA greatly enhances the fluorescence of (*S*)-**2-1** at λ_1 = 374 nm but (*S*)-MA only causes a very small fluorescence enhancement. It is found that I_R/I_0 = 11.4 and ef [enantioselective fluorescence enhancement ratio = $(I_R-I_0)/(I_S-I_0)$] = 26.0. Figure 2-1b gives the fluorescence responses of (*S*)-**2-1** at various concentrations of (*R*)- and (*S*)-MA.

Figure 2-1. (a) Fluorescence spectra of (*S*)-**2-1** (1.0×10^{-4} M, CH_2Cl_2) with/without MA (4.0×10^{-3} M). (b) Three independent measurements for the fluorescence enhancement of

(*S*)-**2-1** (1.0×10^{-4} M, CH_2Cl_2) at λ_1 = 374 nm with varying MA concentration. (λ_{exc} = 290 nm, slit = 4.0/4.0 nm).

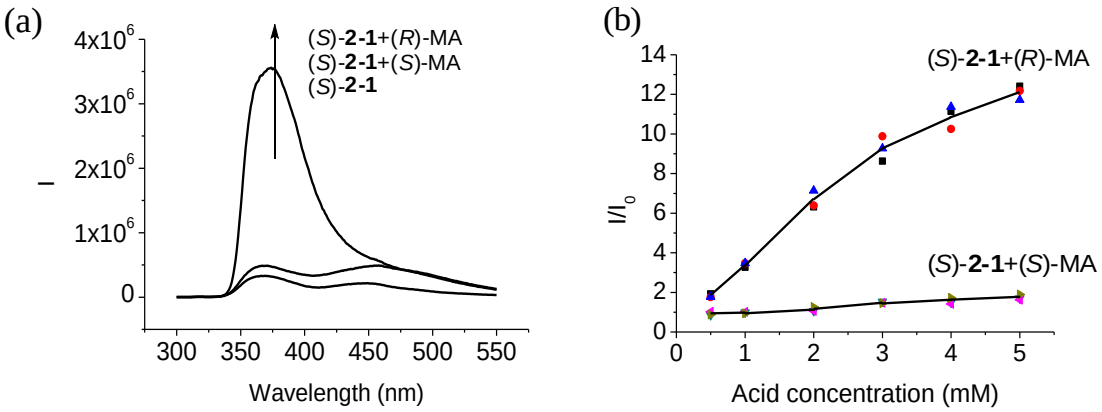

Figure 2-2. (a) Fluorescence spectra of (*R*)-**2-2** (1.0×10^{-4} M, CH_2Cl_2) with/without (*R*)- and (*S*)-MA (4.0×10^{-3} M). (b) Three independent measurements for the fluorescence enhancement of (*R*)-**2-2** (1.0×10^{-4} M, CH_2Cl_2) at λ_2 = 330 nm with varying MA concentration. (λ_{exc} = 290 nm, slit = 4.0/4.0 nm).

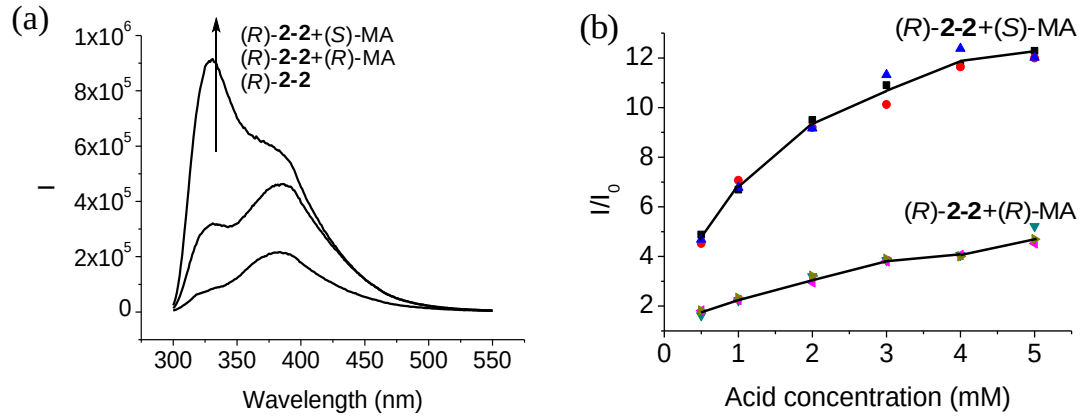

We studied the fluorescent response of (*R*)-**2-2** toward (*R*)- and (*S*)-MA in CH_2Cl_2. As show in Figure 2-2a, (*S*)-MA greatly enhances the fluorescence of (*R*)-**2-2** at λ_2 = 330 nm but (*R*)-MA causes a much smaller fluorescence enhancement. It is found that I_S/I_0

= 11.7 and ef = 3.6. Figure 2-2b gives the fluorescence responses of (*R*)-**2-2** at various concentrations of (*R*)- and (*S*)-MA.

The distinctively different fluorescent response wavelengths between (*S*)-**2-1** and (*R*)-**2-2** and their good and opposite enantioselectivity in the recognition of MA have encouraged us to study the use of this pseudo-enantiomeric sensor pair to interact with MA. A 1:1 mixture of (*S*)-**2-1** and (*R*)-**2-2** in CH_2Cl_2 is prepared in which each sensor's concentration is 1.0×10^{-4} M. This sensor pair solution is treated with MA of varying enantiomeric composition as well as total concentration. The fluorescence intensity at $\lambda_1 = 374$ nm is labeled as I_{10} without MA and I_1 with MA; and the fluorescence intensity at $\lambda_2 = 330$ nm is labeled as I_{20} without MA and I_2 with MA.

Figure 2-3a plots the fluorescence intensity difference at λ_1 and λ_2, $(I_1/I_{10}–I_2/I_{20})$, versus the enantiomeric purity of MA, [(*R*)-MA]%, with the total acid concentration varying from 2.0×10^{-4} M to 5.0×10^{-3} M. It shows that when pure (*R*)-MA, [(*R*)-MA]% = 1, is used, $I_1/I_{10} > I_2/I_{20}$ and when pure (*S*)-MA, [(*R*)-MA]% = 0, is used, $I_1/I_{10} < I_2/I_{20}$. As [(*R*)-MA]% increases, $(I_1/I_{10}–I_2/I_{20})$ changes from the negative region to the positive region. At the higher acid concentrations, there are greater fluorescence intensity differences, and as the acid concentration decreases, the fluorescence intensity difference decreases. Figure 2-3b plots the sum of the fluorescence intensity at λ_1 and λ_2, $(I_1/I_{10}+I_2/I_{20})$, versus the total acid concentration at varying [(*R*)-MA]%. It shows that as the acid concentration increases, $(I_1/I_{10}+I_2/I_{20})$ increases.

Figure 2-3. (a) Plot of (I_1/I_{10}–I_2/I_{20}) versus [(*R*)-MA]% at varying MA concentrations (mM). (b) Plot of (I_1/I_{10}+I_2/I_{20}) versus MA concentration at varying [(*R*)-MA]%. (λ_{exc} = 290 nm, slit = 4.0/4.0 nm).

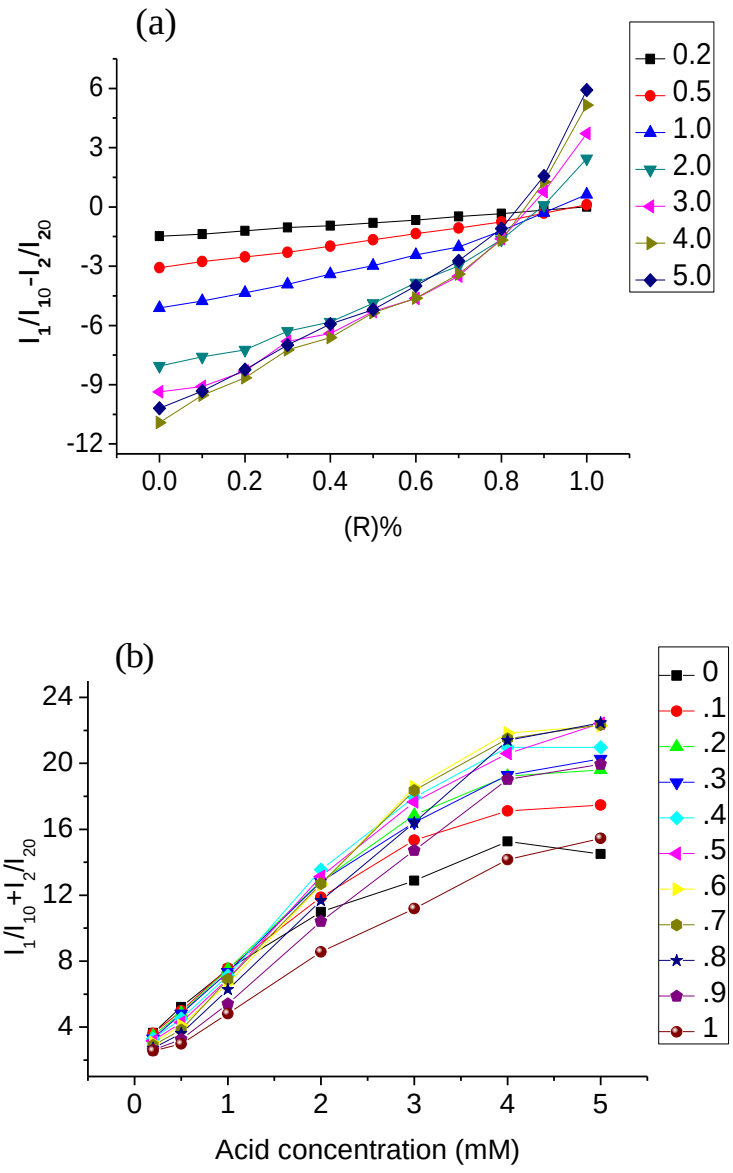

On the basis of Figure 2-3a,b, we have plotted (I_1/I_{10}–I_2/I_{20}) and (I_1/I_{10}+I_2/I_{20}) against the MA concentration and [(*R*)-MA]% respectively in Figure 2-4. In Figure 2-4a, both

3D and 2D graphs are used to show the relation of (I_1/I_{10}–I_2/I_{20}) and (I_1/I_{10}+I_2/I_{20}) with the MA concentration and the data are color-coded according to the MA concentration. These graphs show that in the concentration range of 0.5 mM to 4 mM, using (I_1/I_{10}–I_2/I_{20}) and (I_1/I_{10}+I_2/I_{20}) can determine the total concentration of MA. The points start to overlap outside this concentration range. In Figure 2-4b, both 3D and 2D graphs are used to show the relation of (I_1/I_{10}–I_2/I_{20}) and (I_1/I_{10}+I_2/I_{20}) with [(*R*)-MA]%, and the data are color-coded according to [(*R*)-MA]%. When (I_1/I_{10}+I_2/I_{20}) > 5, that is, the concentration of MA > 0.5 mM according to Figure 2-4a, the enantiomeric purity can be determined by using (I_1/I_{10}–I_2/I_{20}) and (I_1/I_{10}+I_2/I_{20}). Therefore, Figures 2-4a, b allow the direct determination of both the concentration and the enantiomeric concentration of MA by one fluorescence intensity measurement of the sensor-substrate sample.

Figure 2-4. (a) 3D and 2D plots of (I_1/I_{10} – I_2/I_{20}) and (I_1/I_{10} + I_2/I_{20}) with the MA concentration (mM). (b) 3D and 2D plots of (I_1/I_{10} – I_2/I_{20}) and (I_1/I_{10} + I_2/I_{20}) with [(*R*)-MA]%.

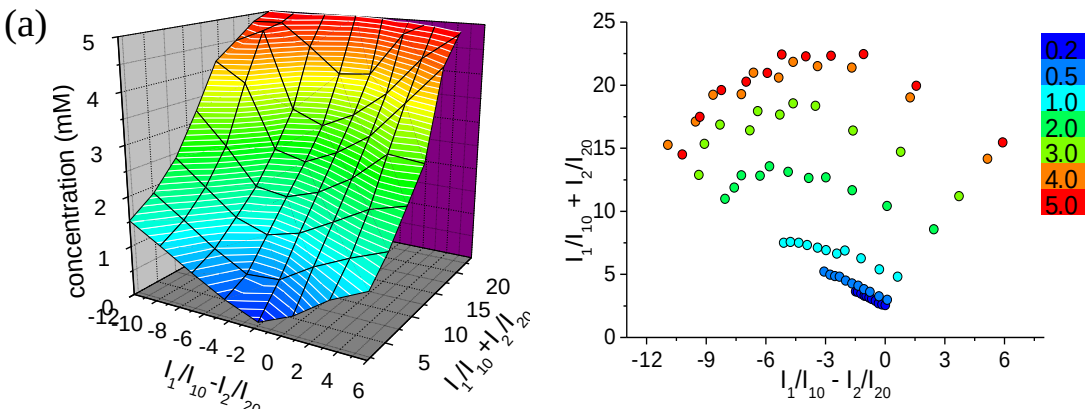

(b)

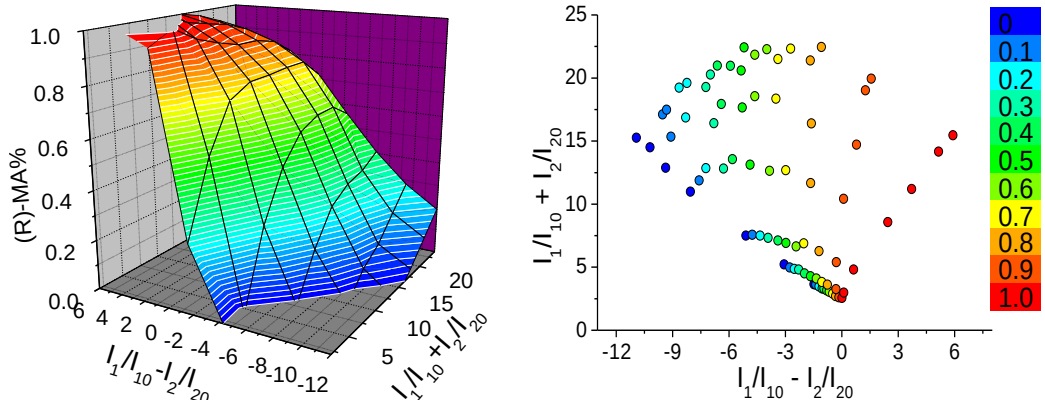

3. Conclusion

In conclusion, we have demonstrated that the pseudo-enantiomeric molecular pair (*S*)-**2-1** and (*R*)-**2-2** are highly enantioselective fluorescent sensors toward MA with distinctively different emission response wavelengths. Each molecule in this sensor pair recognizes the opposite enantiomer of MA. When a 1:1 mixture of (*S*)-**2-1** and (*R*)-**2-2** is used to interact with the chiral acid, in one fluorescence measurement, both the sum and the difference of the fluorescence intensity at the two emission wavelengths can be obtained to directly determine both the concentration and the enantiomeric composition of the chiral substrate. This new strategy is potentially useful for the analysis of the chiral substrate generated from the high throughput catalyst or reaction screening experiments which are expected to produce a great number of samples with varying concentrations and enantiomeric compositions.

4. Experimental Section

4.1 General Data

All reactions were carried out under nitrogen unless otherwise noted. All chemicals were purchased from Sigma Aldrich Chemical Co. or Alfa Aesar. THF was distilled over sodium and benzophenone under nitrogen atmosphere. Methylene chloride and diethyl ether were dried by passing through activated alumina columns under nitrogen. Solvents were stored over 4 Å molecular sieves.

Melting points were uncorrected and obtained on a Mel-Temp II capillary melting point apparatus. Optical rotations were measured on a Jasco P-2000 digital polarimeter. NMR spectra were recorded on a Varian-300 MHz or Bruker-600 MHz spectrometer. High resolution mass spectra were obtained from the University of Illinois at Urbana-Champaign (UIUC) Mass Spectrometry Facility. UV-Vis spectra were recorded on a Hewlett-Packard 8452A diode-array. Steady-state fluorescence emission spectra were recorded on a Horiba Fluorolog-3 Model FL3-22 spectrofluorometer (double-grating excitation and double-grating emission monochromators).

4.2 Preparation and Characterization of Compounds

Preparation and Characterization of (S)-2,2'-bis(methoxymethoxy)-1,1'-binaphthyl, (S)-2-3. Under nitrogen, (S)-1,1'-binaphthyl-2,2'-diol, (S)-BINOL (17.5 mmol, 5.0 g) was dissolved in THF (200 mL). The solution was cooled to 0 ℃, and NaH (43.75 mmol, 60% in mineral oil, 1.75 g) was added in small portions. The reaction mixture was stirred for 15 min and then chloromethyl methyl ether (43.75 mmol,

3.3 mL) was added slowly. The reaction mixture was allowed to warm to room temperature and stirred for 1 h. Water was added slowly to quench the reaction. The organic layer was separated, and the aqueous layer was extracted with ethyl acetate (three 30 mL aliquots). The combined organic extracts were washed with brine, and dried over Na_2SO_4. After evaporation of the solvent, the residue was purified by column chromatography on silica gel eluted with hexane/ethyl acetate (15/1) to afford compound (*S*)-**2-3** as a white solid in 95% yield (16.6 mmol, 6.22g). ^{1}H NMR (300 MHz, $CDCl_3$) δ 3.15 (s, 6H), 4.98 (d, J = 6.9 Hz, 2H), 5.09 (d, J = 6.6 Hz, 2H), 7.14-7.25 (m, 4H), 7.32-7.37 (m, 2H), 7.58 (d, J = 9.3 Hz, 2H), 7.88 (d, J = 8.1 Hz, 2H), 7.96 (d, J = 9.0 Hz, 2H).

Preparation and Characterization of (S)-2,2'-bis(methoxymethoxy)-1,1'-binaphthyl-3,3'-dicarbaldehyde, (S)-2-4. Under nitrogen, 2,2'-bis-methoxymethyl-1,1'-binaphthyl, (*S*)-**2-3** (3.0 mmol, 1.12 g) was dissolved in ether (33 mL). The solution was cooled to 0 ℃, and n-BuLi (10.5 mmol, 2.5 M in hexane, 4.2 mL) was added dropwise. The reaction mixture was stirred for 3 h at room temperature and cooled to 0 ^{0}C, and then anhydrous DMF (12.0 mmol, 1.3 mL) was added slowly. The reaction mixture was allowed to warm to room temperature and stirred for 2 h to afford a cream-like mixture. A saturated aqueous NH_4Cl solution was added to quench the reaction. The organic layer was separated, and the aqueous layer was extracted with ethyl acetate (three 20 mL aliquots). The combined organic extracts were washed with

brine, and dried over Na_2SO_4. After evaporation of the solvent, the residue was purified by column chromatography on silica gel eluted with hexane/ethyl acetate (4/1) to afford compound (*S*)-**2-4** as a yellow oil in 73% yield (2.2 mmol, 943 mg). ^{1}H NMR (300 MHz, $CDCl_3$) δ 2.88 (s, 6H), 4.76 (d, J= 1.2 Hz, 2H), 4.78 (d, J= 1.5 Hz, 2H), 7.27 (d, J = 8.4 Hz, 2H), 7.42 (t, J = 6.9 Hz, 2H), 7.53 (d, J = 6.9 Hz, 2H), 8.10 (d, J = 8.1 Hz, 2H), 8.67 (s, 2H), 10.59 (s, 2H).

Preparation and Characterization of (S)-2,2'-dihydroxy-1,1'-binaphthyl-3,3'-dicarbaldehyde, (S)-2-5. After compound (*S*)-**2-4** (1.1 mmol, 471mg) was dissolved in a minimum amount of CH_2Cl_2, trifluroacetic acid (1.0 mL) was added slowly, and the mixture was stirred at room temperature for 1 h. A saturated aqueous Na_2CO_3 solution was added to quench the reaction. The organic layer was separated, and the aqueous layer was extracted with CH_2Cl_2 (3 x 20 mL). The combined organic extracts were washed with brine, and dried over Na_2SO_4. After evaporation of the solvent, the residue was purified by recrystallization with CH_2Cl_2/ethanol to afford compound (*S*)-**2-5** as a yellow solid in 84% yield (0.92 mmol, 316 mg). ^{1}H NMR (300 MHz, $CDCl_3$) δ 7.19-7.22 (m, 2H), 7.38-7.43 (m, 4H), 7.98-8.02 (m, 2H), 8.35 (s, 2H), 10.19 (s, 2H), 10.59 (s, 2H).

Preparation and Characterization of (S)-3,3'-bis(((S)-2-hydroxy-1,2,2-triphenylethylamino)methyl)-1,1'-binaphthyl-2,2'-diol, (S)-2-1. Under nitrogen, to a 50 mL flask were added (S)-2-5 (224 mg, 0.65 mmol), (S)-2-amino-1,1,2-triphenylethanol (378 mg, 1.30 mmol) and methylene chloride (30 mL). The mixture

was heated at reflux for overnight, and monitored by 1H NMR spectroscopy. When the reaction was complete, the solution was cooled to room temperature and dried over Na_2SO_4. After filtration and evaporation, the resulting yellow imine product was dissolved in anhydrous methanol (25 mL), and NaBH4 (99 mg, 2.60 mmol) was added to the mixture at 0 ^oC. The reaction temperature was maintained at 0 ^oC until the solution became colorless and transparent. It was then allowed to proceed at room temperature for additional 30 min. Methanol was removed, and the residue was dissolved in ethyl acetate (50 mL) and washed with water (15 mL). The aqueous layer after separation was extracted with ethyl acetate (3×30 mL). The combined ethyl acetate layer was washed with brine (15 mL) and dried over anhydrous Na_2SO_4. After evaporation of the solvent, the residue was purified by flash column chromatography on silica gel eluted with ethyl acetate/petroleum ether (1/3) to afford (S)-2-1 as a white solid in 78% yield. ^1H NMR (300 MHz, $CDCl_3$) δ 3.62 (br s, 2H), 3.78 (d, J = 13.8 Hz, 2H), 4.16 (d, J = 13.8 Hz, 2H), 4,61 (s, 2H), 6.90-7.38 (m, 34H), 7.48 (d, J = 7.2 Hz, 4H), 7.77 (d, J = 6.6 Hz, 2H).

Preparation and Characterization of (R)-2,2'-bis(methoxymethoxy)-5,5',6,6',7,7',8,8'-octahydro-1,1'-binaphthyl, (R)-2-7. Under nitrogen, (R)-5,5',6,6',7,7',8,8'-octahydro-1,1'-binaphthyl-2,2'-diol (H_8BINOL), (25 mmol, 7.4 g) was dissolved in THF (300 mL). The solution was cooled to 0 ℃, and NaH (62.8 mmol, 60% in mineral oil, 2.52 g) was added in small portions. The reaction mixture was stirred for

30 min and then chloromethyl methyl ether (62.8 mmol, 4.8 mL) was added slowly. The reaction mixture was allowed to warm to room temperature and stirred for overnight. Water was added slowly to quench the reaction. The organic layer was separated, and the aqueous layer was extracted with ethyl acetate (three 30 mL aliquots). The combined organic extracts were washed with brine, and dried over Na_2SO_4. After evaporation of the solvent, the residue was purified by column chromatography on silica gel eluted with hexane/ethyl acetate (15/1) to afford compound (*R*)-**2-7** as a white solid in 90% yield (22.5 mmol, 8.6 g). ^{1}H NMR (300 MHz, $CDCl_3$) δ 1.65-1.76 (m, 8H), 2.07-2.17 (m, 2H), 2.27-2.37 (m, 2H), 2.78 (t, J = 6.0 Hz, 4H), 3.30 (s, 6H), 4.97 (d, J = 6.6 Hz, 2H), 5.03 (d, J = 6.6 Hz, 2H), 6.99 (d, J = 8.4 Hz, 2H), 7.05 (d, J = 8.4Hz, 2H).

Preparation and Characterization of (R)-2-8. Under nitrogen, (*R*)-**2-7** (15.5 mmol, 5.9 g) was dissolved in ether (180 mL). The solution was cooled to 0 ℃, and n-BuLi (62.5 mmol, 2.5 M in hexane, 25.0 mL) was added dropwise. The reaction mixture was stirred for 4 h at room temperature and cooled to 0 ^{0}C, and then anhydrous DMF (70.0 mmol, 5.4 mL) was added slowly. The reaction mixture was allowed to warm to room temperature and stirred for 2 h to afford a cream-like mixture. A saturated aqueous NH_4Cl solution was added to quench the reaction. The organic layer was separated, and the aqueous layer was extracted with ethyl acetate (three 40 mL aliquots). The combined organic extracts were washed with brine, and dried over Na_2SO_4. After evaporation of the solvent, the residue was purified by column

chromatography on silica gel eluted with hexane/ethyl acetate (4/1) to afford compound (*S*)-**2-8** as a light yellow oil in 58% yield. ^{1}H NMR (300 MHz, $CDCl_3$) δ 1.68-1.76 (m, 8H), 2.16-2.26 (m, 2H), 2.42-2.52 (m, 2H), 2.83 (t, J = 6.0 Hz, 4H), 2.98 (s, 6H), 4.78 (d, J = 6.6 Hz, 2H), 4.83 (d, J = 6.6 Hz, 2H), 7.62 (s, 2H), 10.22 (s, 2H).

Preparation and Characterization of (R)-2-9. After compound (*S*)-**2-8** (6.02 mmol, 2.64 g) was dissolved in a minimum amount of CH_2Cl_2, trifluroacetic acid (10 mmol, 1.4 mL) was added slowly, and the mixture was stirred at room temperature for overnight. A saturated aqueous Na_2CO_3 solution was added to quench the reaction. The organic layer was separated, and the aqueous layer was extracted with CH_2Cl_2 (3 x 20 mL). The combined organic extracts were washed with brine, and dried over Na_2SO_4. After evaporation of the solvent, the residue was purified by recrystallization with CH_2Cl_2/ethanol to afford compound (*S*)-**2-9** as a light yellow solid in 86% yield. ^{1}H NMR (300 MHz, $CDCl_3$) δ 1.64-1.82 (m, 8H), 2.16-2.26 (m, 2H), 2.44-2.55 (m, 2H), 2.83 (t, J = 6.0 Hz, 4H), 7.32 (s, 2H), 9.84 (s, 2H), 10.93 (s, 2H).

Preparation and Characterization of (R)-3,3'-bis(((R)-2-hydroxy-1,2,2-triphenylethylamino)methyl)-5,5',6,6',7,7',8,8'-octahydro-1,1'-binaphthyl-2,2'-diol, (R)-2-2. (R)-3,3'-DiformylH_8BINOL, (R)-2-9 (245 mg, 0.70 mmol) was dissolved in CH_2Cl_2 (22 mL) in the presence of 4 Å molecular sieves and combined with (R)-2-amino-1,1,2-triphenylenthanol (607 mg, 2.10 mmol). The reaction mixture was heated at reflux for 3 d, and monitored by using ^{1}H NMR spectroscopy. When the

reaction was complete, the solution was cooled to room temperature and dried over anhydrous Na_2SO_4. After filtration, the filtrate was concentrated under vacuum. The residue was passed through a silica gel column eluted with hexanes/ethyl acetate (8/1) to give the corresponding Schiff base. The Schiff base was dissolved in methanol (28 mL) and cooled down to 0 ℃. $NaBH_4$ (106 mg, 2.80 mmol) was added in small portions. The reaction temperature was maintained at 0 ℃ until the solution became colorless and transparent. Then, it was allowed to proceed at room temperature for additional 30 min. Methanol was removed by roto-evaporation, and the residue was dissolved in ethyl acetate (50 mL) and washed with water (15 mL). The aqueous layer after separation was extracted with ethyl acetate (3 x 30 mL). The combined organic layer was washed with brine (15 mL) and dried over anhydrous Na_2SO_4. After evaporation of the solvent, the residue was purified by flash column chromatography on silica gel eluted with hexanes/ethyl acetate (3/1) to afford (R)-**2-2** as a white solid in 73% yield. ^{1}H NMR (300 MHz, $CDCl_3$) δ 1.72 (m, 8H), 2.17 (m, 2H), 2.34 (m, 2H), 2.66 (m, 4H), 3.59 (d, J = 13.5 Hz, 2H), 3.77 (d, J = 13.5 Hz, 2H), 4.63 (s, 2H), 6.58 (s, 2H), 7.02-7.31 (m, 28H), 7.59 (d, J = 7.2 Hz, 2H). ^{13}C NMR (75 MHz, $CDCl_3$) δ 23.5, 23.6, 27.5, 29.5, 49.4, 69.0, 80.5, 121.8, 122.0, 126.4, 126.7, 126.9, 127.6, 127.7, 127.8, 127.9, 128.7, 128.8, 130.1, 130.4, 136.4, 137.4, 144.5, 145.4, 151.4. HRMS Calcd for $C_{62}H_{61}N_2O_4$ (MH^+): 897.4631. Found: 897.4623. m.p. 124-125 ^{0}C. $[\alpha]_D$ = 119.3 (c = 0.470, $CHCl_3$).

4.3 Preparation of Samples for Fluorescence Measurement.

Sensors were purified by column chromatography and then stored in a refrigerator. The enantiomers of mandelic acid were purchased from Aldrich and recrystallized from methanol. They were then passed through a short column of silica gel (eluted with diethyl ether) and dried under vacuum. All of the solvents were either HPLC or spectroscopic grade. The stock solutions of the sensors were freshly prepared for each measurement. A 0.01 M stock solution of mandelic acid in methylene chloride was freshly prepared. For the fluorescence enhancement study, a sensor solution was mixed with the mandelic acid solution at room temperature in a 5 mL volumetric flask and diluted to the desired concentration. The resulting solution was allowed to stand at room temperature for 2 - 3 h before the fluorescence measurement.

References

1. Selected references of enantioselective fluorescent sensors: (a) James, T. D.; Sadanayake, K. R. A. S.; Shinkai, S. *Nature* **1995**, *374*, 345-347. (b) Pugh, V.; Hu, Q. -S.; Pu, L. *Angew. Chem. Int. Ed.* **2000**, *39*, 3638-3641. (c) Reetz, M. T.; Sostmann, S. *Tetrahedron* **2001**, *57*, 2515-2520. (d) Korbel, G. A.; Lalic, G.; Shair, M. D. *J. Am. Chem. Soc.* **2001**, *123*, 361-362. (e) Jarvo, E. R.; Evans, C. A.; Copeland, G. T.; Miller, S. J. *J. Org. Chem*. **2001**, *66*, 5522-5527. (f) Wong, W.-L.; Huang, K.-H.; Teng, P.-F.; Lee, C.-S.; Kwong, H.-L. *Chem. Commun.* **2004**, 384-385. (g) Zhao, J.-Z.; Fyles, T. M.; James, T. D. *Angew. Chem., Int. Ed.* **2004**, *43*, 3461-3464. (h) Pagliari, S.; Corradini, R.; Galaverna, G.; Sforza, S.; Dossena, A.; Montalti, M.; Prodi, L.; Zaccheroni, N.; Marchelli, R. *Chem. Eur. J.* **2004**, *10*, 2749-2758. (i) Matsushita, H.; Yamamoto, N.; Meijler, M. M.; Wirsching, P.; Lerner, R.A.; Matsushita, M.; Janda, K. D. *Mol. Biosyst.* **2005**, *1*. 303-306. (j) Zhu, L.; Anslyn, E. V. *J. Am. Chem. Soc.* **2004**, *126*, 3676-3677. (k) Mei, X. F. ; Wolf, C. *J. Am. Chem. Soc.* **2004**, *126*, 14736-14737. (l) Li, Z.-B.; Lin, J.; Pu, L. *Angew. Chem., Int. Ed.* **2005**, *44*, 1690-1693. (m) Wolf, C.; Liu, S.; Reinhardt, B. C. *Chem. Commun.* **2006**, 4242-4244.

2. A review on enantioselective fluorescent sensing: Pu, L. *Chem. Rev.* **2004**, *104*, 1687-1716.

3. Liu, H. L.; Peng, Q.; Wu,Y. D.; Chen, D.; Hou, X. L.; Sabat, M.; Pu, L. *Angew. Chem.*,

Int. Ed. **2010**, *49*, 602-606.

Chapter 3

Study of the Fluorescent Properties of H_8BINOL-Amine Molecules: A New Window for the Enantioselective Fluorescent Recogniton

1. Introduction

Fluorescent chemical sensors have been applied to the detection of metal cations, pH, anions, proteins and DNAs.[1-3] Enantioselective fluorescent sensors are also receiving increasing attentions because they can provide real time analysis for the enantiomeric composition of chiral compounds and enhance the sensitivity in the detection of chiral substrates.[4,5] Among the enantioselective fluorescent sensors developed, those based on the chiral structure of 1,1'-bi-2-naphthol (BINOL) have been actively investigated and a few highly enantioselective fluorescent sensors have been discovered for the recognition of α-hydroxycarboxylic acids, amines, amino alcohols and amino acids.[6] H_8BINOL is a partially hydrogenated derivative of BINOL. The increased steric bulkiness of H_8BINOL because of the sp^3 carbons and the increased electron density on the aromatic rings make this compound both sterically and electronically quite different from BINOL. The use of H_8BINOL and its derivatives in asymmetric catalysis has been actively pursued and a number of efficient catalysts have been developed.[7] However, no study on using H_8BINOL to build enantioselective fluorescent sensor was reported before. In our laboratory, we have synthesized a series of H_8BINOL-amine compounds and have explored their application in the fluorescent recognition of mandelic acid (MA), a representative of α-hydroxycarboxylic acids. This investigation demonstrates that although the H_8BINOL-based compounds do not have the extended conjugation as those derived from BINOL, they still exhibit very interesting fluorescent properties and have

opened a new window in the fluorescence spectrum for the enantioselective fluorescent recognition. Herein, these results are reported.[8]

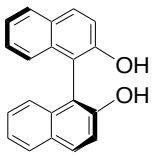

BINOL

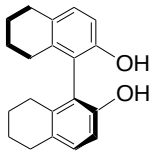

H_8BINOL

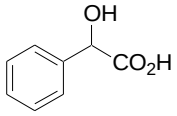

mandelic acid
(MA)

2. Results and Discussion

2.1 Synthesis of the H_8BINOL-Amine Molecules and Study of Their Fluorescent Properties

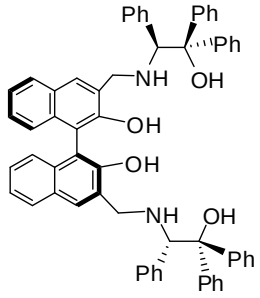

(*S*)-**3-1**

Recently, we reported that the BINOL-amino alcohol molecule (*S*)-**3-1** is a highly enantioselective fluorescent sensor for the structurally diverse α-hydroxycarboxylic acids.[9] In order to explore the application of H_8BINOL in fluorescent recognition, we have prepared a H_8BINOL analog of (*S*)-**3-1**. As shown in Scheme 3-1, protection of (*S*)-H_8BINOL with methoxymethyl (MOM) group gave (*S*)-**3-2**. Ortho-lithiation followed by addition of DMF and hydrolysis gave the H_8BINOL dialdehyde (*S*)-**3-3**.[10] Condensation of (*S*)-**3-3** with the amino alcohol (*S*)-**3-4** followed by reduction produced

the H_8BINOL-amino alcohol (*S*)-**3-5** in 71% yield.[11] The specific optical rotation of this compound is $[\alpha]_D$ = -119.9 (c = 0.865, $CHCl_3$), greater than that of (*S*)-**3-1** {$[\alpha]_D$ = -93.7 (c = 0.80, CH_2Cl_2)}. The ^{1}H NMR spectrum of (*S*)-**3-5** in $CDCl_3$ shows two doublets at δ 3.59 (d, J = 13.5 Hz, 2H) and 3.77 (d, J = 13.5 Hz, 2H) for the two diastereotopic protons (H_a) of the 3,3'-methylene substituents which are significantly more upfield than those observed for (*S*)-**3-1** at δ 3.78 (d, *J* = 13.8 Hz, 2H) and 4.16 (d, *J* = 13.8 Hz, 2H). This is consistent with the more electron rich aromatic rings of (*S*)-**3-5**.

Scheme 3-1. Synthesis of the H_8BINOL-Amino Alcohol (*S*)-**3-5**.

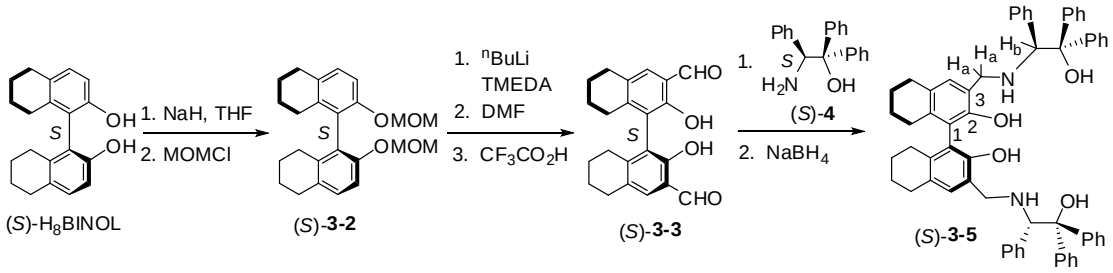

As shown in Figure 3-1, the UV spectrum of (*S*)-**3-5** in CH_2Cl_2 gives absorptions at $\lambda_{max}(\varepsilon)$ = 232 (2.6 x 10^4) and 290 (7.4 x 10^3) nm, without the long wavelength absorption of (*S*)-**3-1** at λ_{max} = 334 nm due to the reduced conjugation system in (*S*)-**3-5**. The peak position and shape of the absorption signals of (*S*)-**3-5** do not change while the concentration changes. The fluorescence spectra of (*S*)-**3-5** in CH_2Cl_2 at various concentrations are shown in Figure 3-2. Compound (*S*)-**3-5** gives a major emission at λ_{emi} = 390 nm whose shape and position also do not change with concentration. The major

emission wavelength of (*S*)-**3-5** is much longer than that observed for (*S*)-H_8BINOL at λ_{emi} = 323 nm as shown in Figure 3-3. Compound (*S*)-**3-5** only gives a very weak short wavelength emission signal at λ_{emi} = 318 nm. The concentration independence of both the absorption and emission of (*S*)-**3-5** indicates that the long wavelength fluorescence signal of (*S*)-**3-5** is not due to the formation of either excimer or ground state aggregate. The fluorescence spectrum of (*S*)-**3-5** is also very different from that of (*S*)-**3-1** which exhibits dual emission signals at λ_{emi} = 372 and 448 nm in CH_2Cl_2.[9] The fluorescence quantum yield of (*S*)-**3-5** is estimated to be 0.36% by using 2-aminopyridine as the standard.[12]

Figure 3-1. UV spectra of sensor (*S*)-**3-5** in methylene chloride at various concentrations.

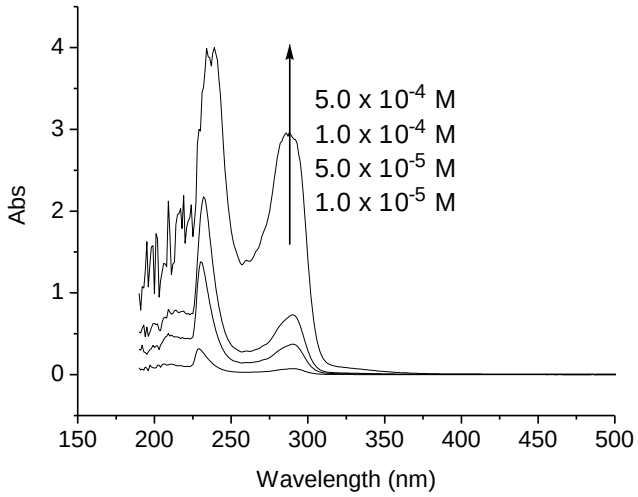

Figure 3-2. Fluorescence spectra of (*S*)-**3-5** in CH_2Cl_2 at various concentrations (λ_{exc} = 290 nm, slit = 3.0/3.0 nm).

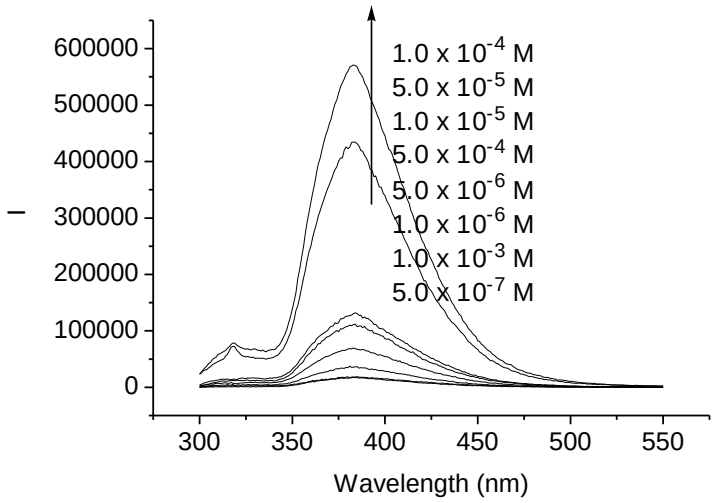

Figure 3-3. Fluorescence spectrum of (*S*)-H_8BINOL ($2.0x10^{-4}$ M in CH_2Cl_2) (λ_{exc} = 288 nm. slit = 4.0/4.0 nm).

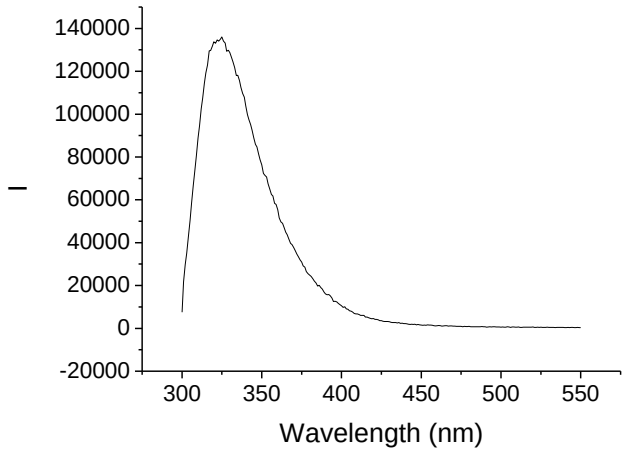

We have studied the solvent effect on the fluorescence property of (*S*)-**3-5**. Changing the solvent from CH_2Cl_2 to CH_3OH caused little change on the absorption as well as the fluorescence spectra of (*S*)-**3-5** at various concentrations (Figure 3-4). This indicates that the intermolecular hydrogen bonding interaction of (*S*)-**3-5** has little

influence on its electronic properties. Similarly, as shown in Figure 3-5, the use of acetonitrile as the solvent also maintains the absorption and fluorescence properties of (*S*)-**3-5**.

Figure 3-4. (a) UV and (b) fluorescence spectra of sensor (*S*)-**3-5** in methanol at various concentrations (λ_{exc} = 291 nm, slit = 4.0/4.0 nm).

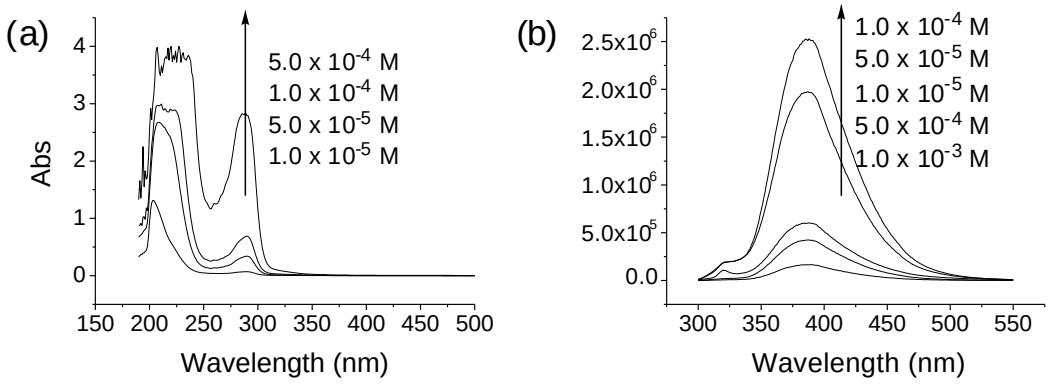

Figure 3-5. (a) UV and (b) fluorescence spectra of sensor (*S*)-**3-5** in CH_3CN at various concentrations (λ_{exc} = 291 nm, slit = 4.0/4.0 nm).

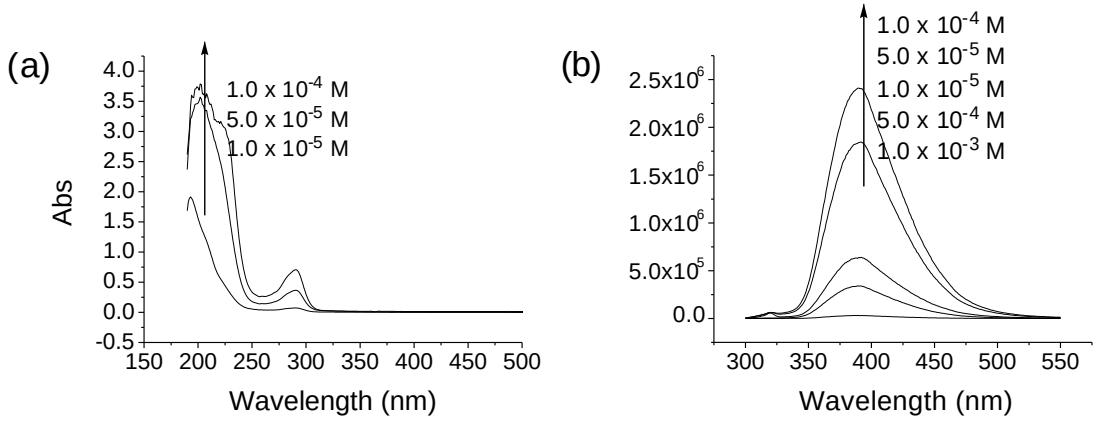

In order to gain further understanding on the fluorescent properties of (*S*)-**3-5**, we

have prepared the H_8BINOL-amine molecules (*S*)-**3-6** – (*S*)-**3-10** by using our recently developed one-step reaction of H_8BINOL with an in situ generated aminomethanol (Scheme 3-2).[13]

Scheme 3-2. Synthesis of the H_8BINOL-amine compounds (*S*)-**3-6** – (*S*)-**3-10**.

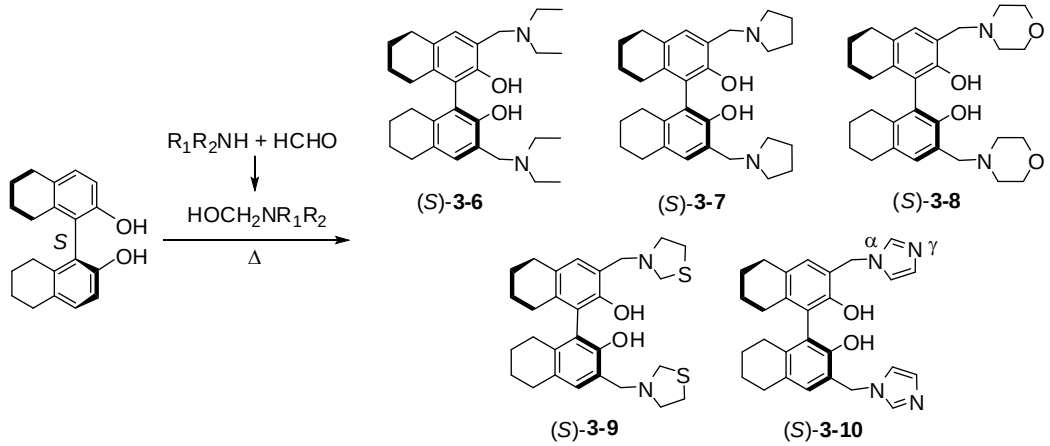

These H_8BINOL-amine compounds such as (*S*)-3-**7** and (*S*)-**3-8** have exhibited excellent enantioselectivity in the asymmetric arylzinc addition to aldehydes.[13] The fluorescence spectra of these compounds in CH_2Cl_2 (2.0×10^{-4} M) are obtained. As shown in Figure 3-6, compounds (*S*)-**3-6**, (*S*)-**3-7** and (*S*)-**3-8** show a major emission peak at about 380 nm, similar to (*S*)-**3-5**. However, compound (*S*)-**3-9** gives dual emissions as λ_{emi} = 329 and 370 (sh) nm, and compound (*S*)-3-**10** gives only a short wavelength emission at λ_{emi} = 324 nm. The fluorescence signal of (*S*)-3-**10** is very similar to that of (*S*)-H_8BINOL. No change in peak position and shape is observed when their concentration is varied (Figure 3-7).

Figure 3-6. Fluorescence spectra of compounds (*S*)-**3-6** – (*S*)-**3-10** [2.0 x 10^{-4} M in CH_2Cl_2. λ_{exc} = 292 nm for (*S*)-**3-6** – (*S*)-**3-9** and 291 nm for (*S*)-**3-10**. Slit: 5.0/5.0 nm for (*S*)-**3-6**, (*S*)-**3-7** and (*S*)-**3-9** and 4.0/4.0 nm for (*S*)-**3-8** and (*S*)-**3-10**].

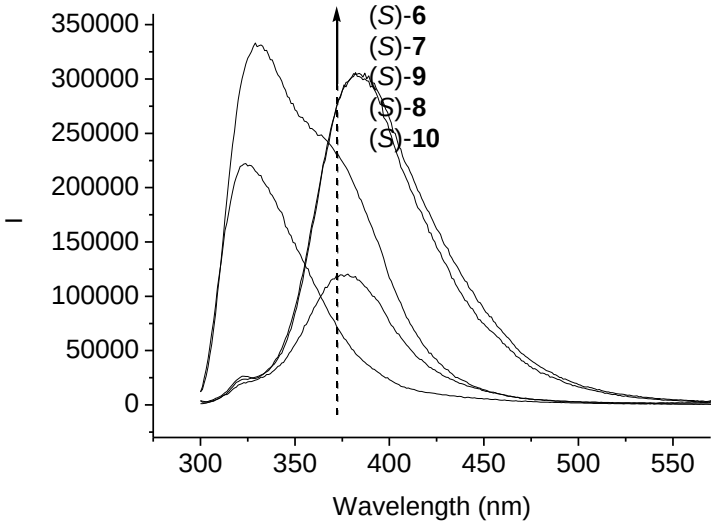

Figure 3-7. Fluorescence spectra of (a) (*S*)-3-**6** (b) (*S*)-3-**7** (c) (*S*)-3-**8** (d) (*S*)-3-**9** (e) (*S*)-3-**10** in CH_2Cl_2 at various concentrations (λ_{exc} = 290 nm, slit = 5.0/5.0 nm).

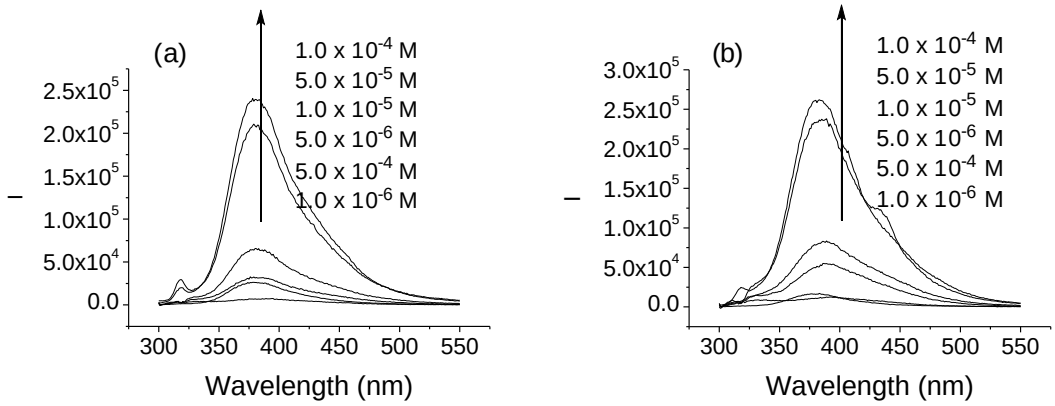

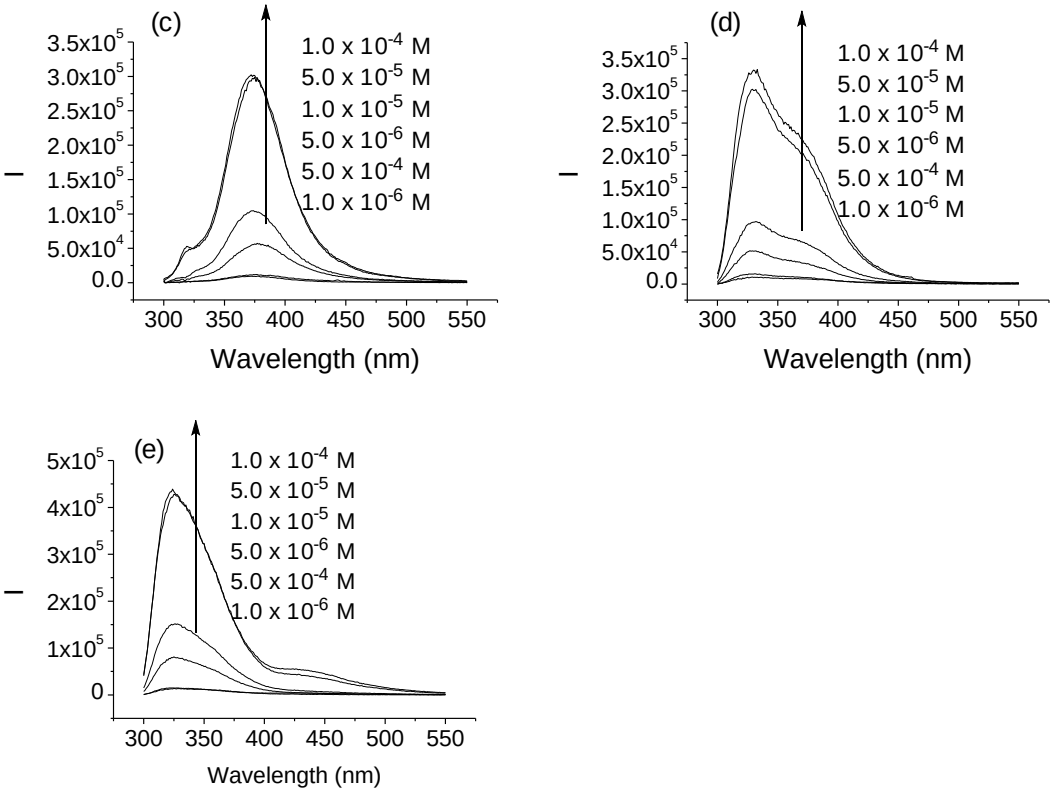

In the ^{1}H NMR spectra of compounds (*S*)-**3-6**, (*S*)-**3-7** and (*S*)-**3-8**, their H_8BINOL hydroxyl proton signals appeared at δ 11.13, 11.91, and 10.38, respectively.[13] These greatly downfield-shifted ^{1}H NMR signals indicate strong intramolecular hydrogen bonds between the hydroxyl protons and the basic nitrogen atoms. The chemical shift of the hydroxyl proton signal of (*S*)-**3-9** (δ 9.52) is about 2 ppm less downfield than that of (*S*)-**3-7**. This may imply a weaker hydrogen bond in (*S*)-**3-9** probably because of the reduced basicity of the nitrogen atom adjacent to the sulfur atom. The H_8BINOL hydroxyl proton signal of (*S*)-**3-10** is observed at δ 3.48, greatly upfield-shifted in comparison with those of (*S*)-**3-6** - (*S*)-**3-9**. This is attributed to the non-basic α nitrogen atoms of the imidazole rings of (*S*)-**3-10** which cannot form intramolecular hydrogen

bond with the H_8BINOL hydroxyl protons at all. The more basic γ nitrogen atom in each of the imidazole rings of (*S*)-**3-10** is not sterically feasible to form an intramolecular hydrogen bond.

On the basis of the above analysis, we propose that the difference between the fluorescence spectra of the H_8BINOL-amine compounds (*S*)-**3-6** – (*S*)-**3-10** could arise from the different capability of their nitrogen atoms to form intramolecular hydrogen bond. Compound (*S*)-**3-10** cannot form an intramolecular hydrogen bond and thus exhibits only the emission of its H_8BINOL unit. Compounds (*S*)-**3-6**, (*S*)-**3-7** and (*S*)-**3-8** have strong intramolecular hydrogen bonds and thus show emission of either the intramolecularly hydrogen bonded complex or its subsequent excited state proton transfer complex.[14] Compound (*S*)-**3-9** forms a weaker intramolecular hydrogen bond and it shows the emissions contributed by both the H_8BINOL unit and the intramolecularly hydrogen bonded complex.

The study of compounds (*S*)-**3-6** – (*S*)-**3-10** has revealed the nature of the emission of the H_8BINOL-amino alcohol (*S*)-**3-5** as a contribution from its intramolecularly hydrogen bonded complex. It explains why the fluorescence spectrum of (*S*)-**3-5** is very different from that of H_8BINOL. Unlike that observed in the ^{1}H NMR spectra of compounds (*S*)-**3-6** – (*S*)-**3-10**, the H_8BINOL hydroxyl proton signals of (*S*)-**5** are invisible probably because of fast exchange in solution.

2.2. Study of the Interaction of (*S*)-3-5 with Mandelic Acid

We have investigated the interaction of (*S*)-**3-5** with the enantiomers of MA. As shown in Figure 3-8a, when (*S*)-**3-5** ($1.0x10^{-4}$ in CH_2Cl_2) was treated with (*R*)-MA ($4.0 x 10^{-3}$), a large enhancement at the short wavelength emission (λ_{emi} = 330 nm) was observed with I_R/I_0 = 11.7. When (*S*)-MA was used under the same conditions, the enhancement at the short wavelength emission was much smaller. Thus, a good enantioselective fluorescent response was observed with ef = 3.5 [ef: enantioselective fluorescence enhancement ratio = $(I_R-I_0)/(I_S-I_0)$]. The fluorescence enhancement at the long wavelength emission of (*S*)-**3-5** is much smaller and also with little enantioselectivity. Figure 3-8b displays the results of three independent measurements for the fluorescence enhancement of (*S*)-**3-5** at the short wavelength emission while the concentration of the acid is varied. We have prepared (*R*)-**3-5**, the enantiomer of (*S*)-**3-5**, from (*R*)-H_8BINOL and (*R*)-**3-4**, and studied its interaction with (*R*)- and (*S*)-MA. It is found that (*S*)-MA causes much greater fluorescence enhancement for (*R*)-**3-5** at the short wavelength emission than (*R*)-MA. This confirms the enantioselective nature of the observed different fluorescence enhancements for the sensor in the presence of the two enantiomers of the acid.

Figure 3-8. (a) Fluorescence spectra of (*S*)-**3-5** ($1.0x10^{-4}$ M, CH_2Cl_2) with/without (*R*)- and (*S*)-MA ($4.0x10^{-3}$ M). (b) Three independent measurements of Fluorescence

enhancement of (*S*)-**3-5** ($1.0x10^{-4}$ M, CH_2Cl_2) at λ_{em} = 330 nm with varying acid concentration. (λ_{exc} = 290 nm, slit = 3.0/3.0 nm).

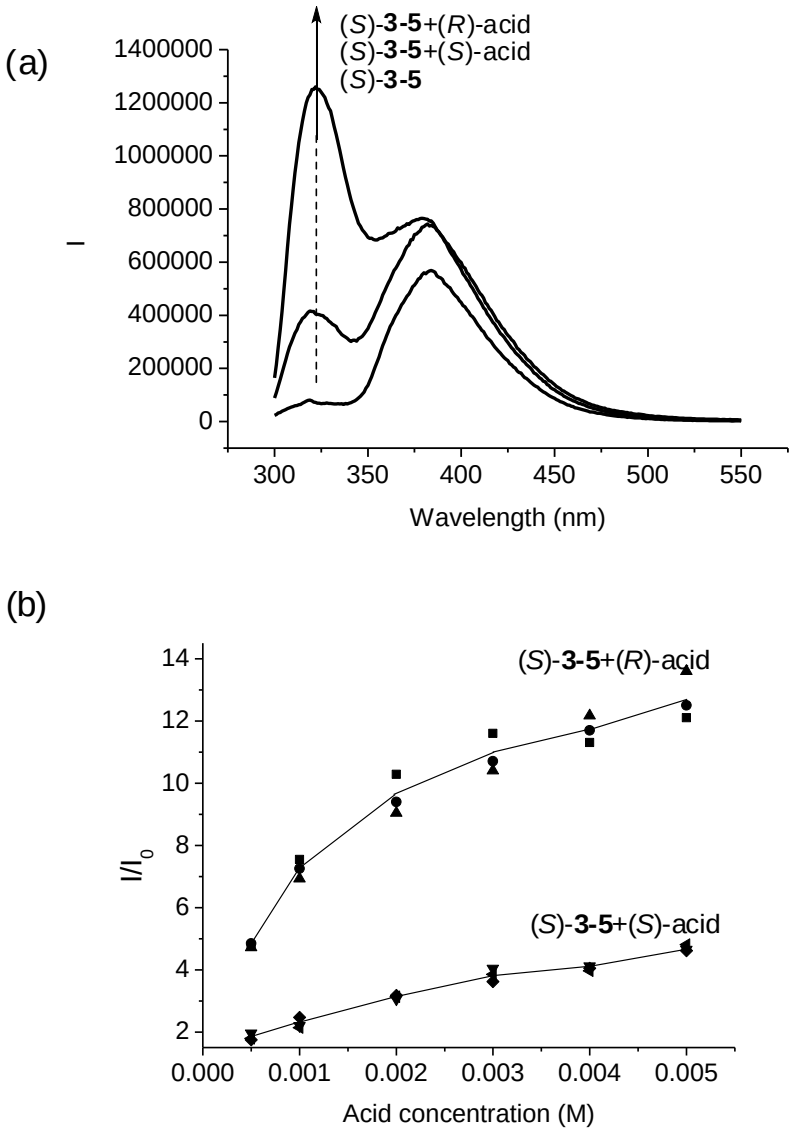

The greatly enhanced short wavelength emission of (*S*)-**3-5** in the presence of (*R*)-MA demonstrates that protonation of the nitrogen atoms of (*S*)-**3-5** by the acidic proton of (*R*)-MA should have suppressed the intramolecular hydrogen bonding between the

H_8BINOL hydroxyl protons of (*S*)-**3-5** and its amine nitrogens and restored the emission of the H_8BINOL unit. The overall fluorescence enhancement should be generated from the formation of the structurally more rigid intermolecular complex between (*S*)-**3-5** and (*R*)-MA.

When (*S*)-H_8BINOL is treated with (*R*)- or (*S*)-MA, there is almost no fluorescence enhancement and enantioselectivity (Figure 3-9). Thus, the intermolecular hydrogen bonding between the amino alcohol units of (*S*)-**3-5** and (*R*)-MA is important for the observed enantioselective fluorescent enhancement.

Figure 3-9. Fluorescence spectra of (*S*)-H_8BINOL (2.0×10^{-4} M in CH_2Cl_2) in the presence of (*R*)- and (*S*)-mandelic acid (4.0×10^{-3} M) [λ_{exc} = 288 nm. Slit = 4.0/4.0 nm].

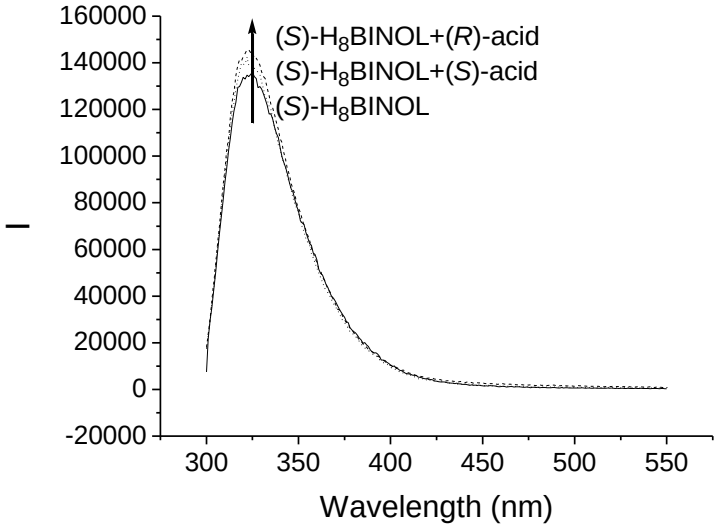

A ^{1}H NMR spectroscopic investigation on the interaction of (*S*)-**3-5** with (*R*)-MA in $CDCl_3$ was conducted while the total concentration was maintained at 6.0×10^{-3} M.

Addition of (S)-**3-5** to the solution of (R)-MA caused the α proton signal of (R)-MA to undergo upfield shift from δ 5.26 to δ 4.20 as the ratio of (*S*)-**3-5** relative (*R*)-MA reached 2:3. This large upfield shift indicates that the complexation between (*S*)-**3-5** and (*R*)-MA might have placed the α proton of the acid in the electronically shielded region of the sensor. Further increasing the ratio of (S)-**3-5** versus (R)-MA to 5:1 shifted the α proton signal of (R)-MA downfield to δ 4.53. Thus, the structure of the complex probably changes as the amount of (S)-**3-5** versus (R)-MA further increases. In the ^{1}H NMR spectrum, the two doublet signals of the diastereotopic protons H_a of (*S*)-**3-5** began to move toward each other with the addition of (*R*)-MA and then merged into a singlet at δ 3.74 when the ratio of (*R*)-MA relative to (*S*)-**3-5** reached 0.43:1 (= 1:2.3). However, when the amount of (*R*)-MA was further increased, the singlet split back into two doublets, which were then moving away from each other with increasing (*R*)-MA. When the ratio of (*R*)-MA relative to (*S*)-**3-5** reached 9:1, the H_a signals of (*S*)-**3-5** were observed at δ 4.24 (d, J = 12.3 Hz) and 3.63 (d, J = 12.0 Hz). We propose the following hypothesis to explain the above observed changes in the NMR signals of (*S*)-**3-5**. The intramolecular hydrogen bonds between the amine nitrogens and the core H_8BINOL hydroxyl protons in (*S*)-**3-5** should generate a rigid cyclic structure giving the two well-resolved diastereotopic proton signals for H_a. Addition of acid should protonate the amine group and allow free rotation of the 3,3'-substituents of (*S*)-**3-5**, resulting in the merged signal of the H_a protons. As the amount of (*R*)-MA increases, a structurally

rigid intermolecular complex between (*S*)-**3-5** and (*R*)-MA should be produced to give the well separated signals for the H_a protons.

On the basis of the above NMR study, the Job plots for the interaction of (*S*)-**3-5** with (*R*)-MA are produced.[15] Figure 3-10a is obtained by monitoring the change of the α proton signal of (*R*)-MA, and Figure 3-10b by monitoring the change of the H_b signal of (*S*)-**3-5**. Both plots indicate that (*S*)-**3-5** and (*R*)-MA form a 1:2 complex in the ground state. Because the fluorescence response of (*S*)-**3-5** toward (*R*)-MA at a constant total concentration of 1.0×10^{-4} M is very small, the Job plot could not be used to determine the excited state binding stoichiometry of (*S*)-**3-5** with (*R*)-MA.

Figure 3-10. Job plots of (*S*)-**3-5** with (*R*)-MA obtained by using the ^{1}H NMR signal change ($\Delta\delta = \delta_0 - \delta$) of (a) the H_α of (*R*)-MA {X = [acid]/([acid]+[sensor]}, and (b) the H_b of (S)-3-**5** {X = [sensor]/([sensor]+[acid])}.

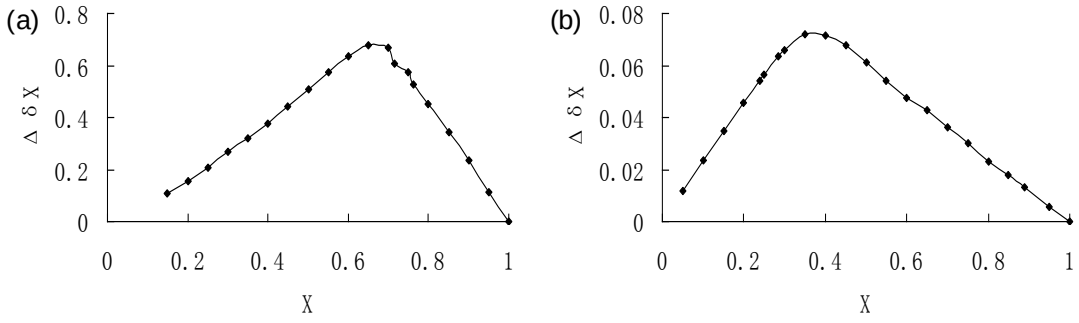

2.3 Interaction of the H_8BINOL-Amine Compounds (*S*)-3-6 - (*S*)-3-10 with MA

The fluorescent responses of the H_8BINOL-amine compounds (*S*)-**3-6** – (*S*)-**3-10** in

the presence of (*R*)- and (*S*)-MA are studied. As shown in Figure 3-11, when compounds (*S*)-**3-6**, (*S*)-**3-7** and (*S*)-**3-8** were treated with MA, large fluorescence enhancements at the short wavelength were observed similar to that observed for (*S*)-**3-5.** This is consistent with the suppressed intramolecular hydrogen bonding interaction of these compounds when their amine nitrogens are interacting with the carboxylic acid proton of the acid. However, almost no enantioselectivity was observed. When compound (*S*)-**3-9** was treated with MA, little fluorescence enhancement was observed. This indicates that the intermolecular interaction of (*S*)-**3-9** with MA should be much weaker than that of compounds (*S*)-**3-5** - (*S*)-**3-8** because of the weaker basicity of the nitrogens in (*S*)-**3-9**. Although the α nitrogen atoms of (*S*)-**3-10** are not basic at all, there is significant fluorescence enhancement in the presence of (*R*)-MA with $I_R/I_0 = 3.2$. It is proposed that the much more basic γ nitrogens of (*S*)-**3-10** should have participated in the complexation with (*R*)-MA to form a structurally more rigid fluorophore, leading to the observed fluorescence enhancement. When (*S*)-**3-10** was treated with the enantiomeric acid (*S*)-MA, the fluorescence enhancement was smaller, giving a good enantioselectivity of ef = 2.1. This indicates that (*S*)-**3-10** is a promising candidate for the enantioselective fluorescent recognition of MA.

Figure 3-11. Fluorescence spectra of (*S*)-3-**6** – (S)-3-**10** (2.0×10^{-4} M in CH_2Cl_2) in the presence of (*R*)- and (*S*)-MA (4.0×10^{-3} M) [λ_{exc} = 292 nm for (*S*)-3-**6** – (*S*)-3-**9** and 291

nm for (*S*)-3-**10**. Slit: 5.0/5.0 nm for (*S*)-3-**6**, (*S*)-3-**7** and (*S*)-3-**9** and 4.0/4.0 nm for (*S*)-3-**8** and (*S*)-3-**10**].

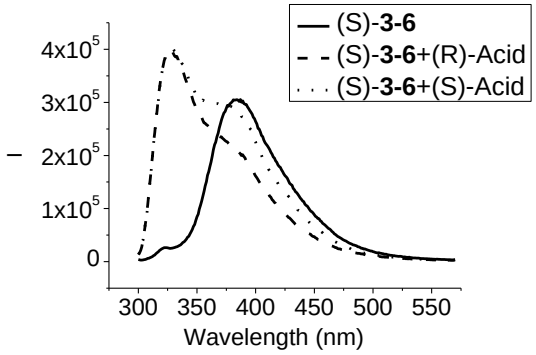

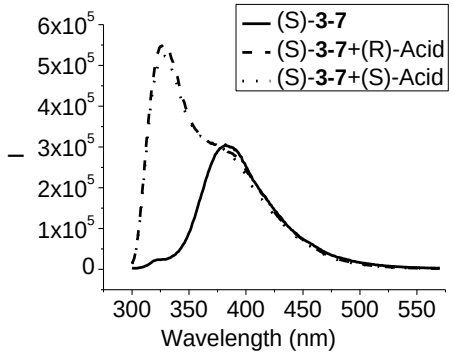

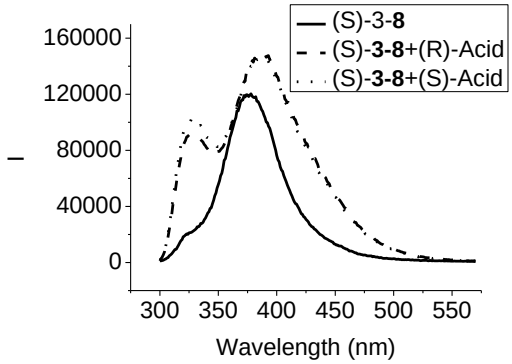

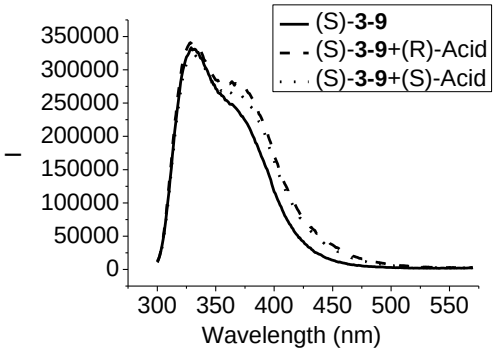

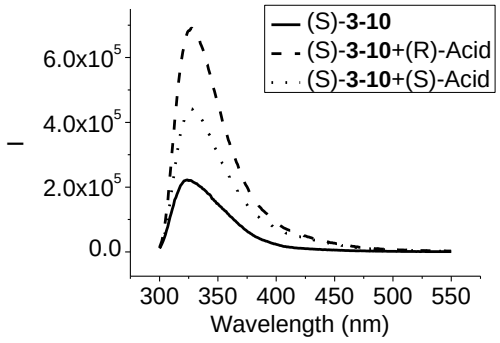

3. Conclusion

We have investigated the fluorescent properties of a series of H_8BINOL-amine

compounds. This study reveals that the intramolecular hydrogen bonds of these compounds can shift the emission of their H_8BINOL unit to a much longer wavelength. In spite of the much shorter conjugation in the H_8BINOL-based fluorophore of (*S*)-**3-5** than that in the BINOL-based compound (*S*)-**3-1**, (*S*)-**3-5** has exhibited very efficient fluorescent response toward MA. Binding of (*S*)-**3-5** with the acid suppresses its intramolecular hydrogen bonding and restores the short wavelength emission of the H_8BINOL unite, giving high sensitivity and good enantioselectivity. Thus, with appropriate design of the structure and functional groups, the H_8BINOL-based molecules are promising as a new class of enantioselective fluorescent sensors. In comparison with their BINOL analogs, the H_8BINOL-based compounds have opened a new window in the shorter emission wavelength to observe the enantioselective fluorescent recognition.[8]

4. Experimental Section

4.1 Synthesis and Characterization of Compounds

Synthesis and Characterization of Sensor (*S*)-3-5. (1) (*S*)-3,3'-Diformyl-H_8BINOL, (*S*)-**3-3** (245 mg, 0.70 mmol), was dissolved in CH_2Cl_2 (22 mL) in the presence of 4 Å molecular sieves and combined with (*S*)-2-amino-1,1,2-triphenylenthanol, (*S*)-**3-4** (607 mg, 2.10 mmol). The reaction mixture was heated at reflux for 30 h, and monitored by using ^{1}H NMR spectroscopy. When the reaction was

complete, the reaction mixture was cooled to room temperature and filtered. The filtrate was concentrated under vacuum and passed through a silica gel column eluted with CH_2Cl_2 to give the corresponding Schiff base. (2) The Schiff base was dissolved in methanol (28 mL) and cooled down to 0 ℃. $NaBH_4$ (106 mg, 2.80 mmol) was added in small portions. The reaction temperature was maintained at 0 ℃ until the solution became colorless and transparent. Then, it was allowed to proceed at room temperature for additional 30 min. Methanol was removed, and the residue was dissolved in ethyl acetate (50 mL) and washed with water (15 mL). The aqueous layer after separation was extracted with ethyl acetate (3 x 30 mL). The combined organic layer was washed with brine (15 mL) and dried over anhydrous Na_2SO_4. After evaporation of the solvent, the residue was purified by flash column chromatography on silica gel eluted with hexanes/ethyl acetate (3/1) to afford (*S*)-**3-5** as a white solid in 71% yield. ^{1}H NMR (300 MHz, $CDCl_3$) δ 1.72 (m, 8H), 2.17 (m, 2H), 2.34 (m, 2H), 2.66 (m, 4H), 3.59 (d, J = 13.5 Hz, 2H), 3.77 (d, J = 13.5 Hz, 2H), 4.63 (s, 2H), 6.58 (s, 2H), 7.02-7.31 (m, 28H), 7.59 (d, J = 7.2 Hz, 2H). ^{13}C NMR (75 MHz, $CDCl_3$) δ 23.5, 23.6, 27.5, 29.5, 49.4, 69.0, 80.5, 121.8, 122.0, 126.4, 126.7, 126.9, 127.6, 127.7, 127.8, 127.9, 128.7, 128.8, 130.1, 130.4, 136.4, 137.4, 144.5, 145.4, 151.4. HRMS Calcd for $C_{62}H_{61}N_2O_4$ (MH^+): 897.4631. Found: 897.4653. m.p. 124-125 ^{0}C. $[\alpha]_D$ = -119.9 (c = 0.865, $CHCl_3$). The enantiomer (*R*)-3-**5** was obtained in the same way by using (*R*)-3,3'-DiformylH_8BINOL and (*R*)-2-amino-1,1,2-triphenylenthanol. $[\alpha]_D$ = 119.3 (c =

0.470, $CHCl_3$).

4.2 Preparation of Samples for Fluorescence Measurement

Sensors were purified by column chromatography and then stored in a refrigerator. The commercially obtained enantiomers of MA were recrystallized from methanol. They were then passed through a short column of silica gel (eluted with diethyl ether) and dried under vacuum. All of the solvents were either HPLC or spectroscopic grade. The stock solutions of the sensors were freshly prepared for each measurement. A 0.01 M stock solution of MA in methylene chloride was freshly prepared. For the fluorescence enhancement study, a sensor solution was mixed with the MA solution at room temperature in a 5 mL volumetric flask and diluted to the desired concentration. The resulting solution was allowed to stand at room temperature for 2 - 3 h before the fluorescence measurement.

References

1. (a) *Fluorescent Chemosensors for Ion and Molecular Recognition*; Czarnik, A. W., Ed.; ACS Symposium Series 538; American Chemical Society: Washington, DC, 1993. (b) de Silva, A. P.; Gunaratne, H. Q. N.; Gunnlaugsson, T.; Huxley, A. J. M.; McCoy, C. P.; Rademacher, J. T.; Rice, T. E. *Chem. Rev.* **1997**, *97*, 1515-1566. (c) Fabbrizzi, L.; Poggi, A. *Chem. Soc. Rev.* **1995**, *24*, 197. (d) *Fluorescent and Luminescent Probes*, 2nd ed.; Mason, W. T., Ed.; Academic: San Diego, 1999.
2. (a) Jelinek, R.; Kolusheva, S. *Chem. Rev.* **2004**, *104*, 5987-6015. (b) Johnson, K. S.; Needoba, J. A.; Riser, S. C.; Showers, W. J. *Chem. Rev.* **2007**, *107*, 623-640. (c) Basabe-Desmonts, L.; Reinhoudt, D. N.; Crego-Calama, M. *Chem. Soc. Rev.*, **2007**, *36*, 993–1017. (d) McDonagh, C.; Burke, C. S.; MacCraith, B. D. *Chem. Rev.* **2008,** *108*, 400-422. (e) Borisov, S. M.; Wolfbeis, O. S. *Chem. Rev.* **2008**, *108*, 423-461. (f) Nolan, E. M.; Lippard, S. J. *Acc. Chem. Res.* **2009**, *42*, 193-203.
3. (a) Thompson, R. B. *Fluorescence Sensors and Biosensors*, CRC: U.S. 2005. (b) James, T. D.; Phillips, M. D.; Shinkai, S. *Boronic Acids in Saccharide Recognition*; RSC: UK, 2006.
4. A review: Pu, L. *Chem. Rev.* **2004**, *104*, 1687-1716.
5. Selected references: (a) James, T. D.; Sandanayake, K. R. A. S.; Shinkai, S. *Nature* **1995**, *374*, 345-347. (b) Klein, G.; Reymond, J.-L. *Helv. Chim. Acta* **1999**, *82*, 400-407. (c) Pugh, V.; Hu, Q. -S.; Pu, L. *Angew. Chem. Int. Ed.* **2000**, *39*, 3638-3641.

(d) Reetz, M. T.; Sostmann, S. *Tetrahedron* **2001**, *57*, 2515-2520. (e) Korbel, G. A.; Lalic, G.; Shair, M. D. *J. Am. Chem. Soc.* **2001**, *123*, 361-362. (f) Jarvo, E. R.; Evans, C. A.; Copeland, G. T.; Miller, S. J. *J. Org. Chem.* **2001**, *66*, 5522-5527. (g) Wong, W.-L.; Huang, K.-H.; Teng, P.-F.; Lee, C.-S.; Kwong, H.-L. *Chem. Commun.* **2004**, 384-385. (h) Zhao, J.-Z.; Fyles, T. M.; James, T. D. *Angew. Chem., Int. Ed.* **2004**, *43*, 3461-3464. (i) Pagliari, S.; Corradini, R.; Galaverna, G.; Sforza, S.; Dossena, A.; Montalti, M.; Prodi, L.; Zaccheroni, N.; Marchelli, R. *Chem. Eur. J.* **2004**, *10*, 2749-2758. (j) Matsushita, H.; Yamamoto, N.; Meijler, M. M.; Wirsching, P.; Lerner, R.A.; Matsushita, M.; Janda, K. D. *Mol. Biosyst.* **2005**, *1*. 303-306. (k). Zhu, L.; Anslyn, E. V. *J. Am. Chem. Soc.* **2004**, *126*, 3676-3677. (l) Mei, X. F.; Wolf, C. *J. Am. Chem. Soc.* **2004**, *126*, 14736-14737.

6. (a) Lin, J.; Hu, Q.-S.; Xu, M. H.; Pu, L. *J. Am. Chem. Soc.* **2002**, *124*, 2088-2089. (b) Xu, M.-H.; Lin, J.; Hu, Q.-S.; Pu, L. *J. Am. Chem. Soc* .**2002**, *124*, 14239-14246. (c) Li, Z.-B.; Lin, J.; Pu, L. *Angew. Chem., Int. Ed.* **2005**, *44*, 1690-1693. (d) Lin, J.; Rajaram, A. R.; Pu, L. *Tetrahedron* **2004**, *60*, 11277-11281. (e) He, X.; Cui, X.; Li, M.; Lin, L.; Liu, X.; Feng, X. *Tetrahedron Lett.* **2009**, *50*, 5853-5856. (f) Liu, H. –L.; Hou, X. –L.; Pu, L. *Angew. Chem. Int. Ed.* **2009**, *48*, 382 –385. (g) Chen, X.; Huang, Z.; Chen, S. –Y.; Li, K.; Yu, X. –Q.; Pu, L. *J. Am. Chem. Soc.* **2010**, *132*, 7297–7299. (h) Liu, H. –L.; Hou, X. –L; Pu, L. *Org. Lett*. **2010,** *12*, 4172-4175.

7. (a) A review: Au-Yeung, T.L.-L.; Chan, S.-S.; Chan. A. S. C. *Adv. Synth. Catal.* **2003**, *345*, 537-555. (b) Matsunaga, S.; Kinoshita, T.; Okada, S.; Harada, S.; Shibasaki, M. *J. Am. Chem. Soc.* **2004**, *126*, 7559-7570. (c) Kumaraswamy, G.; Jena, N.; Sastry, M. N. V.; Padmaja, M.; Markondaiah, B. *Adv. Synth. Catal.* **2005**, *347*, 867 –871. (d) Huang, H.; Liu, X.; Chen, H.; Zheng, Z. *Tetrahedron: Asymmetry* **2005**, *16*, 693–697. (e) Kim, J. G.; Camp, E. H.; Walsh, P. J. *Org. Lett.* **2006**, *8*, 4413-4416. (f) Wu, K.-H.; Gau, H.-M. *J. Am. Chem. Soc.* **2006**, *128*, 14808-14809. (g) Muramatsu, Y.; Harada, T. *Chem. Eur. J.* **2008**, *14*, 10560 – 10563. (h) Jiang, J.; Yu, J.; Sun, X.-X.; Rao, Q.-Q.; Gong, L.-Z. *Angew. Chem. Int. Ed.* **2008**, *47*, 2458 – 2462. (i) Zhou, S.; Wu, K.-H.; Chen, C.-A.; Gau, H.-M. *J. Org. Chem.* **2009**, *74*, 3500–3505.

8. A preliminary study on (*R*)-**3-5**, the enantiomer of (*S*)-**3-5**, was recently communicated: Yu, S.; Pu, L. *J. Am. Chem. Soc.* **2010**, *132*, 17698–17700.

9. Liu, H. -L.; Peng, Q.; Wu, Y. –D.; Chen, D.; Hou, X. –L.; Sabat, M.; Pu, L. *Angew. Chem. Int. Ed.* **2010**, *49*, 602-606.

10. DeBerardinis, A. M.; Turlington, M.; Ko, J; Sole, L; Lin, Pu. *J. Org. Chem.* **2010**, *75*, 2836-2850.

11. Zhang, H. -C.; Huang, W. -S.; Pu, L. *J. Org. Chem.* **2001**, *66*, 481-487.

12. (a) Demas, J. N.; Crosby, J. *J. Phys. Chem.* **1971**, *75*, 991-1024 (see pages 1007-1011). (b) Hu, Q-S; Pugh, V.; Sabat, M.; Pu, L. *J. Org. Chem.* **1999**, *64*, 7528-7536.

13. DeBerardinis, A. M.; Turlington, M.; Ko, J.; Sole, L.; Pu, L. *J. Org. Chem.* **2010**, *75*, 2836–2850.

14. (a) Iwanek, W.; Mattay, J. *J, Photochem. Photobiol. A: Chem.,* **1992**, *67*, 209-226. (b) Ofran, M.; Feitelson, J. *Chem. Phys. Lett.* **1973**, *19*, 427-431. (c) Solntsev, K. M.; Bartolo, E.-A.; Pan, G.; Muller, G.; Bommireddy, S.; Huppert, D.; Tolbert, L. M. *Israel J. Chem*. **2009**, *49*, 227-233. (d) Flegel, M.; Lukeman, M.; Wan, P. *Can. J. Chem*. **2008**, *86*, 161-169. (e) Xu, Y.; McCarroll, M. E. *J. Photochem. Photobiol. A. Chem.* **2006**, *178*, 50-56.

15. Blanda, M. T.; Horner, J. H.; Newcomb, M. *J. Org. Chem.* **1989**, *54*, 4626−4636.

Chapter 4

One Enantiomeric Fluorescent Sensor Pair to Discriminate Four Stereoisomers of Threonines

1. Introduction

The development of enantioselective fluorescent sensors for the recognition of chiral organic molecules has received increasing attention in the past decade because these sensors can potentially provide a real time technique of high sensitivity for high throughput chiral assay.[1,2] Highly enantioselective fluorescent sensors for chiral amines, amino alcohols, α-hydroxycarboxylic acids and amino acids have been obtained. Most of the substrates studied contain only one chiral center except in cases such as the sugar molecules investigated by Shinkai and others.[3-5] No study on the development of a molecular sensor for the fluorescent discrimination of all the four stereoisomers of a compound with two chiral centers, such as threonines and its derivatives (Figure 4-1), was reported before.[4,5] There is significant challenge to carry out the fluorescent recognition of these stereoisomers since it requires a fluorescent sensor to be both enantioselective and diastereoselective.

Figure 4-1. Stereoisomers of Threonines and the N-Cbz-Threonines.

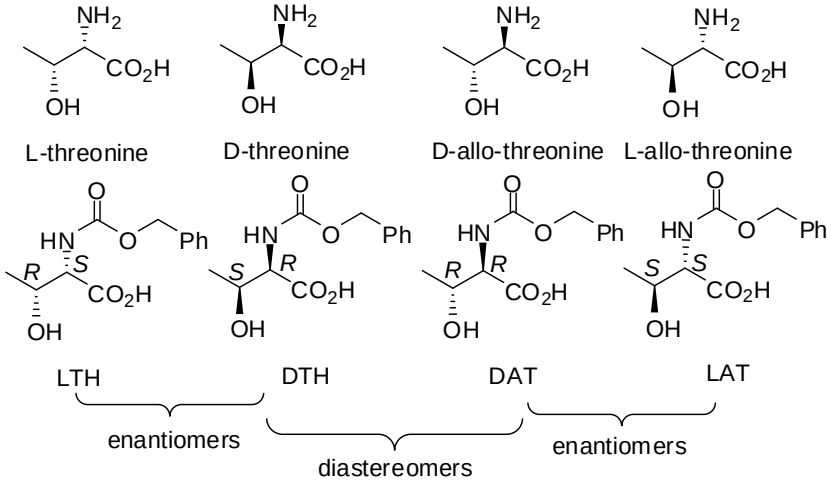

Threonines represent a class of β-hydroxy-α-amino acids that are found to be structural units of many biologically significant natural products such as kaitocephalin, sphingofungins, clithioneine and myriocin. Among the four stereoisomers of threonines, L-threonine is an essential amino acid for humans. Recently, we reported that the 1,1'-bi-2-naphthol (BINOL)-amino alcohol (*S*)-**4-1** is an enantioselective fluorescent sensor for the N-Cbz-serine, a molecule analogous to threonine but without the β-chiral center.[6,7] We have thus studied the interaction of (*S*)-**4-1** and its enantiomer (*R*)-**4-1** with the stereoisomeric N-Cbz-threonines LTH, DTH, LAT and DAT (Figure 4-1). This enantiomeric fluorescent sensor pair is found to exhibit different responses at two emission wavelengths toward the threonine derivatives, leading to both enantioselective and diastereoselective recognition of the threonines. In addition, an enantioselective precipitation is also observed which allows visual discrimination. Herein, these results are reported.

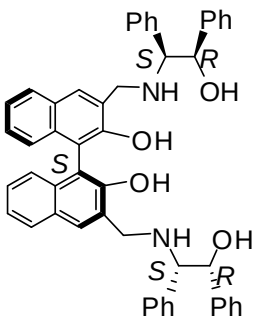

(*S*)-**4-1**

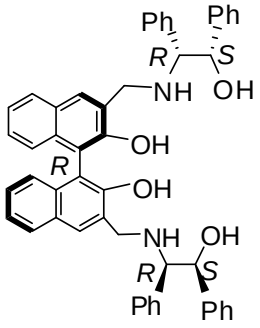

(*R*)-**4-1**

2. Results and Discussion

In toluene solutions [2% 1,2-dimethoxyethane (DME) was added to improve the solubility of the threonines], (*S*)-**4-1** was treated with the threonines. Figure 4-2a gives the fluorescence spectra of (*S*)-**4-1** with or without the four stereoisomeric N-protected amino acids. It shows that (*S*)-**4-1** gives dual emissions with λ_1 = 370 nm and λ_2 = 431 nm. When treated with the four stereoisomers of threonines, the fluorescence responses of (*S*)-**4-1** at the two emission wavelengths are different. LAT causes large fluorescence enhancement at both λ_1 and λ_2. DTH enhances λ_2 greatly but little at λ_1. Both DAT and LTH show smaller enhancement at λ_1 and λ_2, but DAT enhances λ_2 more than LTH.

Figure 4-2. Fluorescence spectra of (a) (*S*)-**4-1** (5.0×10^{-4} M) and (b) (*R*)-**4-1** (5.0×10^{-4} M) with four stereoisomers of α-N-Cbz-amino acid (1.0×10^{-3} M). (Solvent: toluene/2% DME. λ_{exc} = 341 nm, 3.0/3.0 nm)

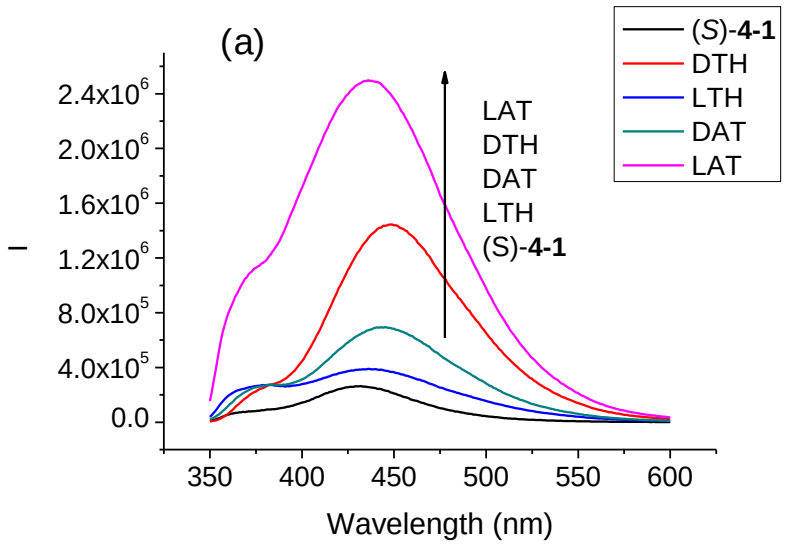

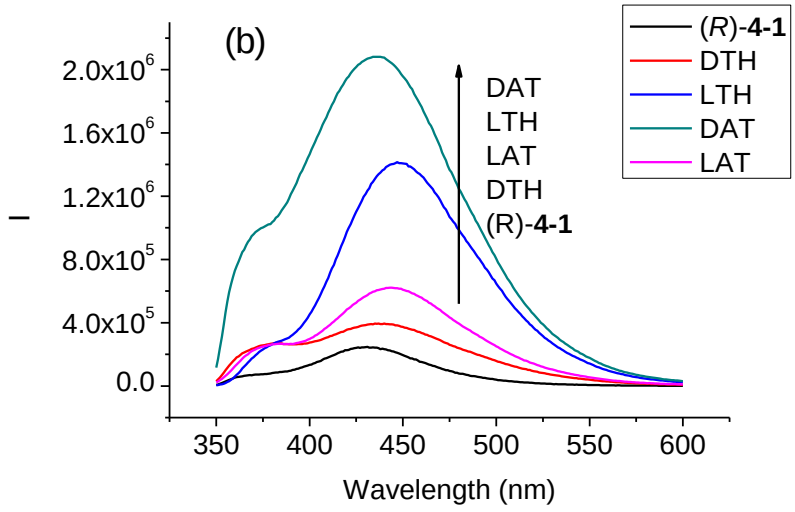

Figure 4-2b gives the fluorescence spectra of (*R*)-**4-1** when treated with the four stereoisomers of the N-protected threonines. The fluorescence responses of Figure 4-2a and Figure 4-2b have a mirror image relationship for the enantiomeric amino acids. As shown in Figure 4-2b, DAT causes large fluorescence enhancement at both λ_1 and λ_2 and LTH enhances λ_2 greatly but not at λ_1. Both LAT and DTH show smaller enhancement at λ_1 and λ_2, but LAT enhances λ_2 more than DTH.

Figure 4-3a plots the fluorescence enhancement of (*S*)-**4-1** at λ_1 (I_1/I_{10}) in the presence of the four stereoisomers of threonines at various concentrations. It shows that in the acid concentration $\leq 2.0 \times 10^{-3}$ M, LAT enhances the fluorescence of (*S*)-**4-1** much greater than the other three stereoisomers with I_1/I_{10} up to 14.3. Thus, the emission of (*S*)-**4-1** at λ_1 can be used to detect LAT. When the concentration of acid was greater than 2.5×10^{-3} M, all the four stereoisomers cause similar fluorescence enhancement of

(*S*)-**4-1**. Figure 4-3b shows that the emission of (*R*)-**4-1** at λ_1 can be used to sense DAT among the four stereoisomers in the acid concentration $\leq 2.0 \times 10^{-3}$ M.

Figure 4-3. Fluorescence enhancements of (a) (*S*)-**4-1** and (b) (*R*)-**4-1** both at 5.0×10^{-4} M with varying acid concentrations. (I_1, fluorescence intensity at 370 nm with the acid, and I_{10} without the acid. λ_{exc} = 341 nm, slit = 3.0/3.0 nm).

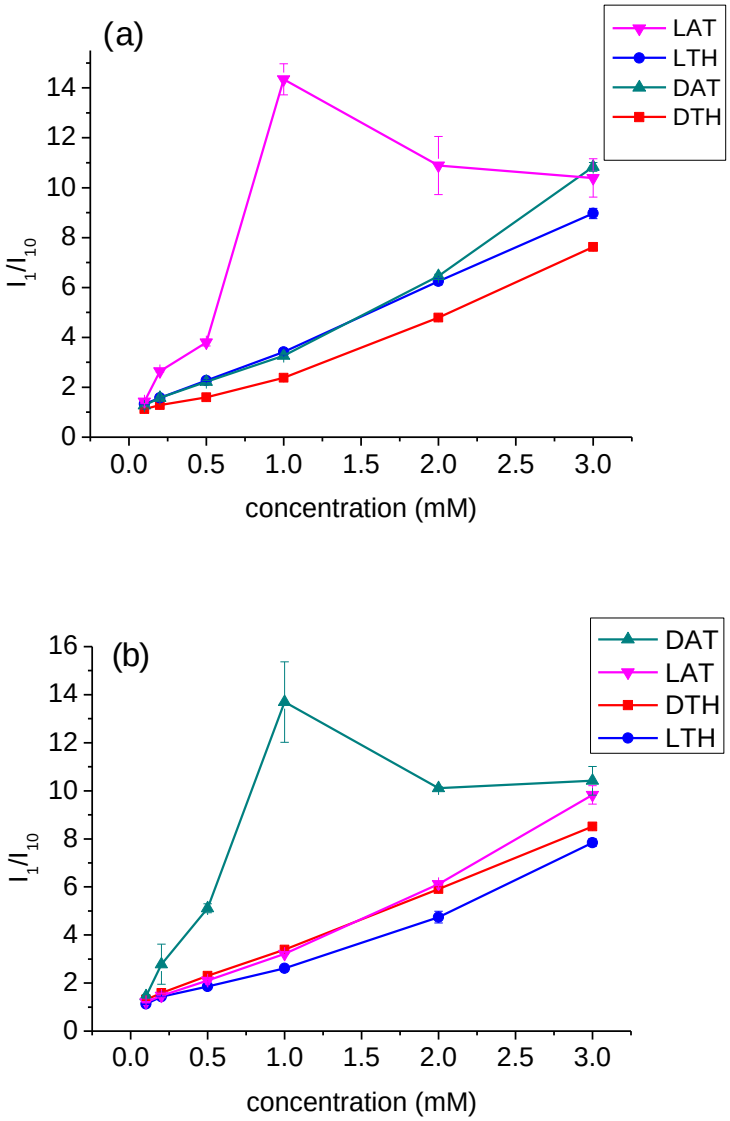

Figure 4-4. Interactions of (*S*)-**4-1** (toluene/2% DME, 5.0 x 10^{-4} M) with LAT at varying concentrations (from left to right: 0, 1E-4, 2E-4, 5E-4, 1E-3, 2E-3, 3E-3, 4E-3, 5E-3 M).

In addition, an enantioselective precipitation was also observed for the interaction of the sensor with LAT and DAT. When LAT ($\geq$ 5.0 x 10^{-4} M) was added to a solution of (*S*)-**4-1** in toluene (2% DME) (5.0 x 10^{-4} M), a white precipitate was produced immediately (Figure 4-4). As the concentration of LAT increased, more precipitates were generated. Under the same conditions, when DAT was added to a solution of (*S*)-**4-1** in the concentration range of 0 - 3 x 10^{-3} M, the solution remained clear. When the enantiomer (*R*)-**4-1** was used, precipitation with DAT was observed but not with LAT. Thus, LAT and DAT can be visually detected by using (*S*)-**4-1** and (*R*)-**4-1**.

Figure 4-5. Plots of I_2/I_1 for (a) (*S*)-**4-1** and (b) (*R*)-**4-1** versus the concentration of the stereoisomeric threonines. (I_1: fluorescence intensity at 370 nm. I_2: fluorescence intensity at 445 nm. Solvent: toluene/2% DME. λ_{exc} = 341 nm, slit = 3.0/3.0 nm)

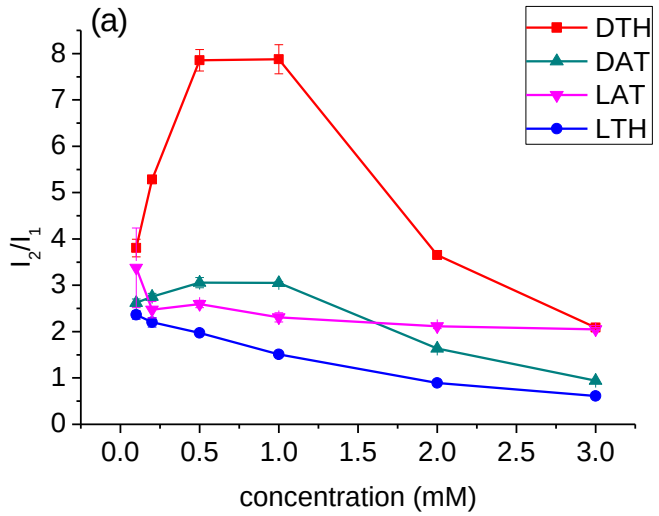

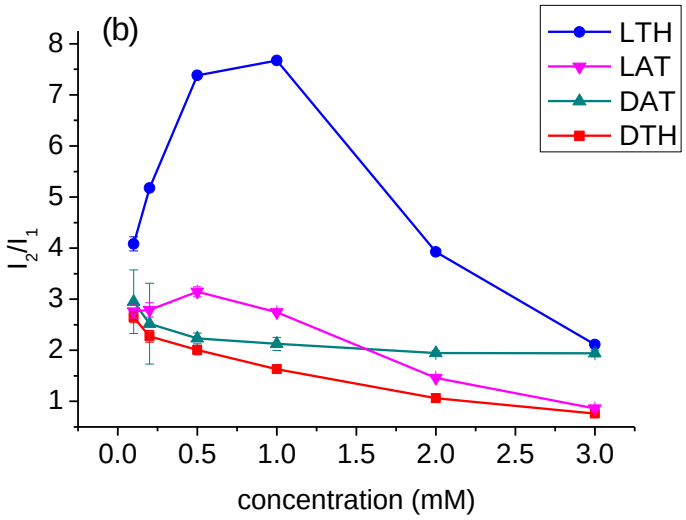

Because the two emission wavelengths of the sensor exhibit different responses toward the stereoisomers of threonines, we have plotted the ratio of the fluorescence intensity of (*S*)-**4-1** at λ_2 and λ_1 (I_2/I_1) against the concentrations of the acids. As shown in Figure 4-5a, when the acid concentration $\leq 2.0 \times 10^{-3}$ M, DTH increases the I_2/I_1 ratio much greater than the other three stereoisomers with I_2/I_1 up to 7.8. Thus, the I_2/I_1 ratio

of (*S*)-**4-1** can be used to sense DTH. When the concentration of acid is greater than 2.5 x 10^{-3} M, the I_2/I_1 ratio of (*S*)-**4-1** in the presence of all the four stereoisomers becomes close. Figure 4-5b shows that the fluorescence intensity ratio I_2/I_1 of (*R*)-**4-1** can be used to detect LTH out of the four stereoisomers when the acid concentration $\leq$ 2.0 x 10^{-3} M.

We have studied the fluorescence responses of (*S*)-**4-1** and (*R*)-**4-1** toward samples containing a mixture of the threonine stereoisomers. The samples were prepared by gradually increasing the percentage of one stereoisomer in the mixture of three other stereoisomers whose proportion was maintained at 1:1:1. The top curve of Figure 4-6a shows the fluorescence enhancement of (*S*)-**4-1** at λ_1 (I_1/I_{10}) versus the increasing percentage of LAT in the mixture. The bottom curve of Figure 4-6a shows the fluorescence enhancement of (*S*)-**4-1** at λ_1 (I_1/I_{10}) when treated with the optically pure LAT at concentrations corresponding to those in the mixture. Thus, at the same amount of LAT, the mixture causes a greater fluorescence enhancement than the optically pure LAT because of the influence of the other three stereoisomers. Figure 4-6a indicates that (*S*)-**4-1** can be used to estimate the relative concentration of LAT in the mixture of the four stereoisomers assuming that changing the ratio of the other three stereoisomers should have small effect on the overall fluorescence enhancement. This is supported by Figure 4-3a which shows much smaller effects of the other three stereoisomers on the fluorescence of (*S*)-**4-1** than LAT. Figure 4-6b plots the fluorescence enhancement of

(*R*)-**4-1** at λ_1 (I_1/I_{10}) against the increasing percentage of DAT in the mixture as well as the optically pure DAT. Similar to the interaction of (*S*)-**4-1** with LAT, (*R*)-**4-1** can be used to estimate the relative concentration of DAT in the mixture of the four stereoisomers. The differences between Figure 4-6a and 4-6b are attributed to the experimental errors in measuring the fluorescence of the mixtures. Therefore, these plots only provide estimates for the relative concentration of LAT and DAT.

Figure 4-6. (a) Plots of I_1/I_0 of (*S*)-**4-1** versus the concentration of the optically pure LAT and the percent of LAT in the mixture of the four stereoisomers. (b) Plots of I_1/I_0 of (*R*)-**4-1** versus the concentration of the optically pure DAT and the percent of DAT in the mixture of the four stereoisomers (total acid concentration in the mixture: 0.5 mM. Solvent: toluene/2% DME. λ_{exc} = 341 nm, slit = 3.0/3.0 nm)

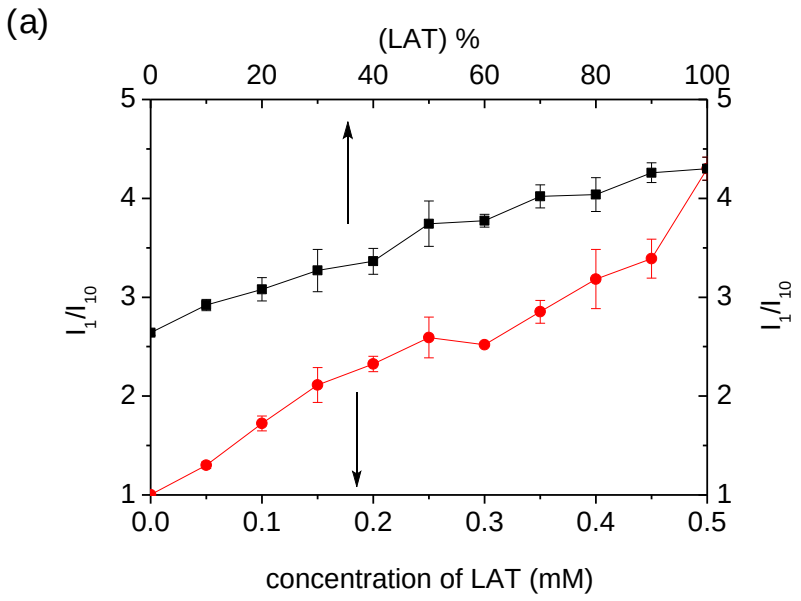

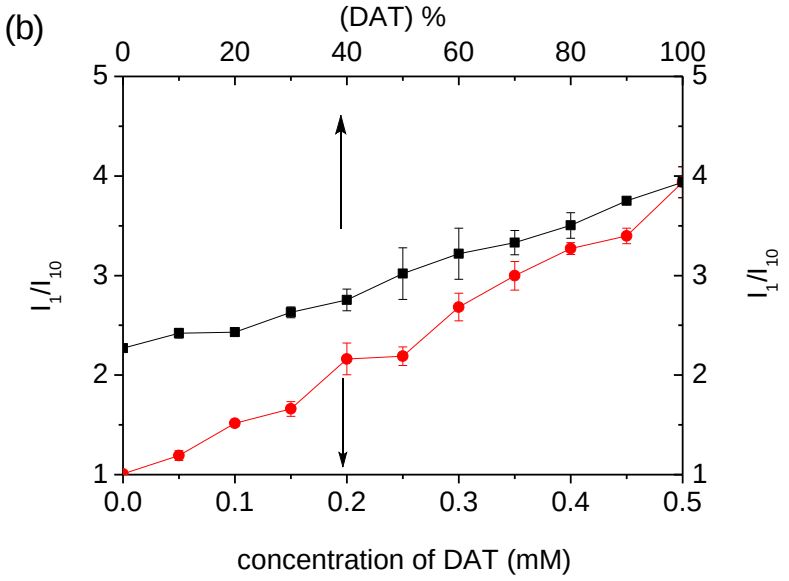

The fluorescence intensity ratio (I_2/I_1) of (*S*)-**4-1** versus the increasing percentage of DTH in the mixture of the stereoisomers is given by the bottom curve of Figure 4-7a. The top curve of Figure 4-7a gives the fluorescence intensity ratio (I_2/I_1) of (*S*)-**4-1** when treated with the optically pure DTH at concentrations corresponding to those in the mixture. At the same amount of DTH, the optically pure DTH generates a greater I_2/I_1 than the mixture due to the effect of the other stereoisomers. Assuming that the effect of the ratio among the other three stereoisomers in the mixture on I_2/I_1 is small as indicated by Figure 4-5a, Figure 4-7a would allow the relative concentration of DTH in the mixture of the four stereoisomers to be estimated. Similarly, from Figure 4-7b, (*R*)-**4-1** can be used to estimate the relative concentration of DTH in the mixture of the four stereoisomers.

Figure 4-7. (a) Plots of I_2/I_1 of (*S*)-**4-1** versus the concentration of the optically pure DTH as well as the percent of DTH in the mixture of four stereoisomers. (a) Plots of I_2/I_1 of (*R*)-**4-1** versus the concentration of the optically pure LTH as well as the percent of LTH in the mixture of four stereoisomers. (Total acid concentration in the mixture: 0.5 mM. Solvent: toluene/2% DME. λ_{exc} = 341 nm, slit = 3.0/3.0 nm)

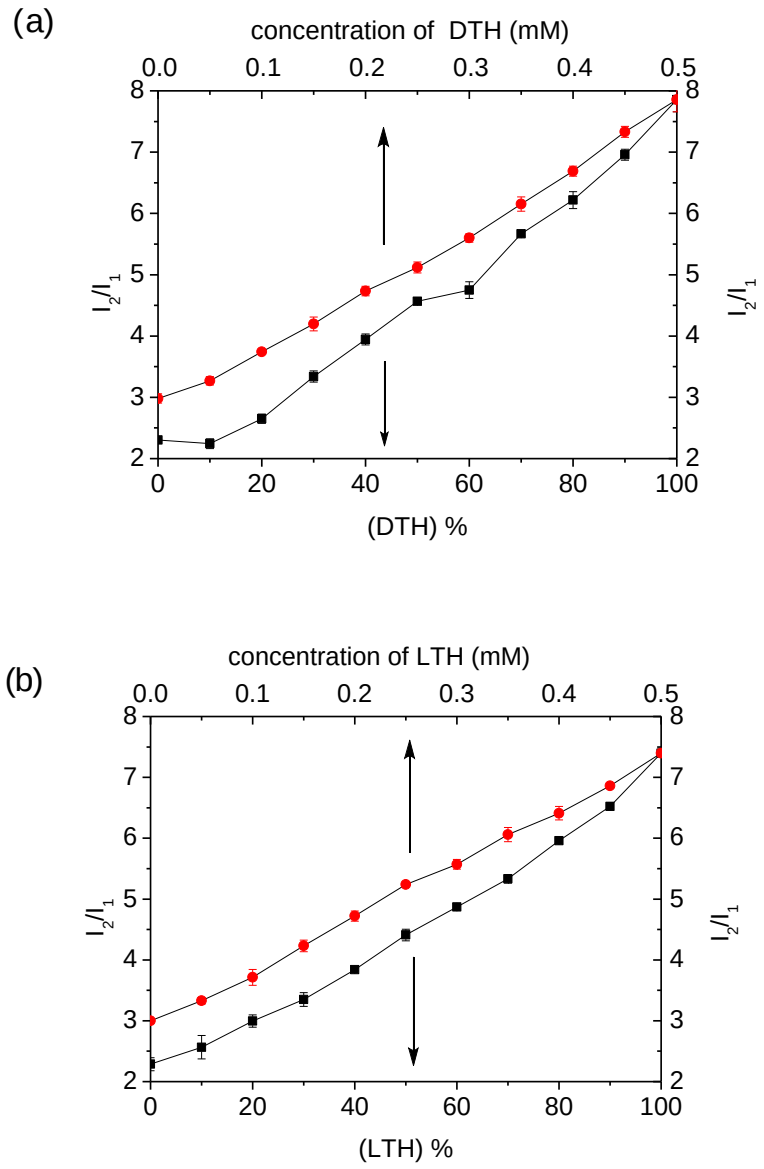

3. Conclusion

In summary, the chiral BINOL-amino alcohol enantiomeric pair (*S*)-**4-1** and (*R*)-**4-1** is found to be an efficient enantioselective and diastereoselective fluorescent sensor pair for the detection of all the four stereoisomers of the threonine derivatives. This work represents the first example that the four stereoisomers of a compound with two chiral centers can be discriminated by using a molecular fluorescent sensor. The enantioselective precipitation of the sensor by the amino acids also makes it possible for visual discrimination. In this study, we have utilized a sensor that exhibits different responses toward the stereoisomeric substrates at two emission wavelengths to expand its capability for both enantioselective and diastereoselective fluorescent sensing. Further development of this strategy has potential to significantly facilitate the discovery of stereoselective fluorescent sensors for chiral organic compounds.

4. Experimental section

4.1 General Data

All reactions were carried out under nitrogen unless otherwise noted. All chemicals were purchased from Sigma Aldrich Chemical Co. or Alfa Aesar. THF was distilled over sodium and benzophenone under nitrogen atmosphere. Methylene chloride and diethyl ether were dried by passing through activated alumina columns under nitrogen. Solvents were stored over 4 Å molecular sieves.

NMR spectra were recorded on a Varian-300 MHz spectrometer. High resolution mass spectra were obtained from the University of Illinois at Urbana-Champaign (UIUC) Mass Spectrometry Facility. Steady-state fluorescence emission spectra were recorded on a Horiba FluoroMax-4 spectrofluorometer.

4.2 Synthesis and Characterization of Compounds.

Synthesis and Characterization of Sensor (S)-4-1 and (*R*)-4-1. Our previously reported procedure was applied: (*S*)-3,3'-DiformylBINOL (224 mg, 0.65 mmol) was dissolved in CH_2Cl_2 (20 mL) in the presence of 4 Å molecular sieves and combined with (1*R*, 2*S*)-2-amino-1,2-diphenylenthanol (279 mg, 1.30 mmol). The reaction mixture was heated at reflux for overnight, and monitored by using ^{1}H NMR spectroscopy. When the reaction was complete, the solution was cooled to room temperature. After filtration and evaporation, the resulting yellow condensation compound was dissolved in methanol (25 mL) and cooled down to 0 ℃. $NaBH_4$ (99 mg, 2.60 mmol) was added in small portions. The reaction temperature was maintained at 0 ℃ until the solution became colorless and transparent. Then, it was allowed to proceed at room temperature for additional 30 min. Methanol was removed by roto-evaporation, and the residue was dissolved in ethyl acetate (50 mL) and washed with water (15 mL). The aqueous layer after separation was extracted with ethyl acetate (3 x 30 mL). The combined organic layer was washed with brine (15 mL) and dried over anhydrous Na_2SO_4. After

evaporation of the solvent, the residue was purified by flash column chromatography on silica gel eluted with hexanes/ethyl acetate (3/1) to afford (*S*)-**4-1** as a white solid in 85% yield. ^{1}H NMR (300 MHz, $CDCl_3$) δ 3.86 (d, J = 13.5 Hz, 2H), 3.92 (d, J = 4.8 Hz, 2H), 4.16 (d, J = 13.8 Hz, 2H), 4.98 (d, J = 5.1 Hz, 2H), 6.96-6.99 (m, 4H), 7.06-7.31 (m, 22H), 7.48 (s, 2H), 7.73 (d, J = 6.3 Hz, 2H). The enantiomer (*R*)-**4-1** was obtained in the same way by using (*R*)-3,3'-DiformylBINOL and (1S, 2R)-2-amino-1,2-diphenylenthanol.

Synthesis and Characterization of DAT and LAT. D-allo-threonine (101.4 mg, 0.85 mmol) was dissolved in a mixture of saturated $NaHCO_3$ (10 mL) and THF (10 mL), and the whole mixture was cooled to 0 ^{0}C. To this solution, benzyl chloroformate (146 μL, 1.02 mmol) was added at 0 ^{0}C and the resulting mixture was stirred for 1 h at 0 ^{0}C. After quenching the reaction with 3M aqueous HCl at 0 ^{0}C, the organic layer was washed with 3M aqueous HCl and brine and dried over anhydrous sodium sulfate. After evaporation of the solvent, the residue was purified by flash column chromatography on silica gel eluted with methylene chloride/methanol (10/1) to afford DAT as a white solid in 75% yield. ^{1}H NMR (300 MHz, $CDCl_3$) δ 1.25 (d, J = 6.3 Hz, 3H), 4.14 (br, 1H), 4.37 (br, 1H), 5.09 (s, 2H), 5.94 (d, J = 7.5 Hz, 1H), 6.06 (br, 2H), 7.32 (br, 5H). ^{13}C NMR (75 MHz, $CDCl_3$) δ 19.2, 59.5, 67.8, 69.3, 128.4, 128.6, 128.8, 136.0, 157.0, 173.5. HRMS Calcd for $C_{12}H_{15}NO_5$ (MH^+): 276.0848. Found: 276.0846. The enantiomer LAT was obtained in the same way by using L-allo-threonine.

4.3 Preparation of Samples for Fluorescence Measurement

Sensors were purified by column chromatography and then stored in a refrigerator. N-benzyloxycabonyl-L-threonine and N-benzyloxycabonyl-D-threonine were purchased from Alfa Aesar. N-benzyloxycabonyl-D-allothreonine and N-benzyloxycabonyl-L-allothreonine were purified by column chromatography and recrystallized with ethyl acetate/hexanes. All of the solvents were either HPLC or spectroscopic grade. The 0.0025 M stock solutions of the sensors in toluene were freshly prepared for each measurement. A 0.025 M stock solution of α-N-Cbz-amino acids was freshly prepared using toluene containing 10% (v) DME. DME was added to improve the solubility of the substrates. For the fluorescence enhancement study, a sensor solution was mixed with α-N-Cbz-amino acid solution at room temperature in a 5 mL volumetric flask and diluted to the desired concentration. The resulting solution was allowed to stand at room temperature for 2 h before the fluorescence measurement.

References

1. A review: Pu, L. *Chem. Rev.* **2004**, *104*, 1687-1716.

2. Selected references: (a) James, T. D.; Sandanayake, K. R. A. S.; Shinkai, S. *Nature* **1995**, *374*, 345-347. (b) Pugh, V.; Hu, Q. -S.; Pu, L. *Angew. Chem. Int. Ed.* **2000**, *39*, 3638-3641. (c) Reetz, M. T.; Sostmann, S. *Tetrahedron* **2001**, *57*, 2515-2520. (d) Korbel, G. A.; Lalic, G.; Shair, M. D. *J. Am. Chem. Soc.* **2001**, *123*, 361-362. (e) Jarvo, E. R.; Evans, C. A.; Copeland, G. T.; Miller, S. J. *J. Org. Chem*. **2001**, *66*, 5522-5527. (f) Beer, G.; Rurack, K.; Daub, J. *J. Chem. Soc., Chem. Commun*. **2001**, 1138-1139. (g) McCarroll, M. E.; Haddadian, F.; Warner, I. M. *J. Am. Chem. Soc.* **2001**, *123*; 3173-3174. (h) Wong, W.-L.; Huang, K.-H.; Teng, P.-F.; Lee, C.-S.; Kwong, H.-L. *Chem. Commun.* **2004**, 384-385. (i) Zhao, J.-Z.; Fyles, T. M.; James, T. D. *Angew. Chem. Int. Ed.* **2004**, *43*, 3461-3464. (h) Pagliari, S.; Corradini, R.; Galaverna, G.; Sforza, S.; Dossena, A.; Montalti, M.; Prodi, L.; Zaccheroni, N.; Marchelli, R. *Chem. Eur. J.* **2004**, *10*, 2749-2758. (i) Zhu, L.; Anslyn, E. V. *J. Am. Chem. Soc*. **2004**, *126*, 3676-3677. (j) Mei, X. F.; Wolf, C. *J. Am. Chem. Soc.* **2004**, *126*, 14736-14737. (k) Matsushita, H.; Yamamoto, N.; Meijler, M. M.; Wirsching, P.; Lerner, R.A.; Matsushita, M.; Janda, K. D. *Mol. Biosyst.* **2005**, *1*, 303-306. (l) Dai, Z. H.; Xu, X. D.; Canary, J. W. *Chirality* **2005**, *17*, S227-S233. (m) Yu, S.; Pu, L. *J. Am. Chem. Soc.* **2010**, *132*, 17698–17700.

3. James,T. D.; Phillips, M. D.; Shinkai, S. *Boronic Acids in Saccharide Recognition*;

RSC: UK, 2006.

4. Fluorescent discrimination of the two enantiomers of amino alcohols, diamines or diacids with two chiral centers was reported: (a) Grady, T.; Harris, S. J.; Smyth, M. R.; Diamond, D.; Hailey, P. *Anal. Chem.* **1996**, *68*, 3775-3782. (b) Zhao, J. Z.; James, T. D. *Chem. Comm*. **2005**, 1889-1891. (c) Wang, Q.; Chen, X.; Tao, L.; Wang, L.; Xiao, D.; Yu, X. –Q.; Pu, L. *J. Org. Chem.* **2007**, *72*, 97-101. (d) Zheng, Y. –S.; Hu, Y. -J. *J. Org. Chem*. **2009**, *74*, 5660–5663.

5. A fluorescent sensor was reported to discriminate L- and D-threonines: Wang, H.; Chan, W. –H.; Lee, A. W. M. *Org. Biomol. Chem*. **2008**, *6*, 929-934.

6. Liu, H. L.; Hou, X. L; Pu, L. *Org. Lett*. **2010,** *12*, 4172-4175.

7. For an account on the enantioselective fluorescent sensors developed in our laboratory, see: Pu, L. *Acc. Chem. Res*. **2012**, *45*, 150-163.

Chapter 5

Simultaneous Determination of Both the Enantiomeric Composition and Concentration of a Chiral Substrate with One Fluorescent Sensor

1. Introduction

The potential application of enantioselective fluorescent sensors in rapid chiral assay has attracted significant research activity in this area. In recent years, a number of highly enantioselective fluorescent sensors have been developed for the recognition of chiral substrates such as carboxylic acids, amino acids, amines and amino alcohols.[1,2] These sensors can be used to determine the enantiomeric composition of a chiral substrate at a given concentration. Thus, an independent method to determine the concentration of the substrate is generally required. That is, two separate measurements are needed in order to determine both the concentration and the enantiomeric composition of a sample.[3]

In 2007, Anslyn reported the use of two UV absorption sensors (one chiral and one achiral with distinctively different absorptions) placed separately in a dual-chamber quartz cuvette to determine both the enantiomeric composition and concentration in one absorption measurement.[4] In 2010, we reported the use of a pseudoenantiomeric sensor pair in a fluorescent chiral assay.[5] A pseudoenantiomeric sensor pair contains a mixture of two sensors that have emissions at two different wavelengths (λ_1 and λ_2) with the opposite fluorescent responses to the two enantiomers of a chiral molecule. When this pseudoenantiomeric sensor pair is applied to a chiral assay, we have demonstrated that using the fluorescent intensity difference (I_1-I_2) (I_1: fluorescence intensity at λ_1. I_2: fluorescence intensity at λ_2) can determine the enantiomeric composition of the substrate

and using the fluorescence intensity sum (I_1+I_2) can determine the concentration. That is, one fluorescent measurement could give both data with the use of the sensor mixture.

The above study leads us to propose another fluorescent method to determine both the concentration and enantiomeric composition of a chiral molecule: If a dual emission fluorescent sensor could exhibit a highly concentration dependent emission at λ_1 and a highly enantioselective emission at λ_2, it might be possible to use the fluorescent responses of this sensor at the two emission wavelengths to determine both the concentration and the enantiomeric composition of a chiral molecule. Herein, we wish to report our discovery of the first example of such a system to simultaneously determine both the enantiomeric composition and the concentration of a chiral diamine with one fluorescent sensor.

2. Results and Discussions

We synthesized the 1,1'-bi-2-naphthol-based trifluoromethyl ketone molecule (*S*)-**5-3** and its enantiomer (*R*)-**5-3** as a potential fluorescent sensor for chiral amines according to Scheme 5-1. When (S)-2,2'-bis(methoxymethoxy)-1,1'-binaphthyl, (S)-**5-1**, is deprotonated by *n*-BuLi followed by addition of ethyl trifluoroacetate, (S)-**5-2** is obtained as a yellow oil in 62%. CF_3COOH is then added to remove MOM groups to generate the desired compound (S)-**5-3** as an orange solid in 84% yield. Its specific optical rotation was $[\alpha]_D$ = -167.5 (c = 0.355, $CHCl_3$). The ^{19}F NMR spectrum of (*S*)-**5-3** in

$CDCl_3$ shows a singlet at δ -70.06. The enantiomer (R)-**5-3** is also prepared by using the enantiomer of the starting material.

Scheme 5-1. Preparation of Compounds (*S*)- and (*R*)-**5-3**.

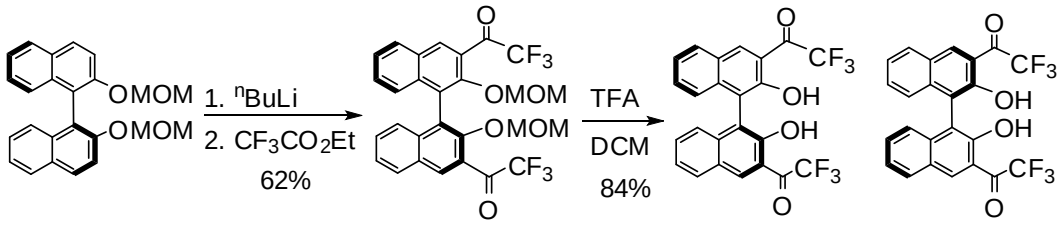

The use of trifluoromethyl ketone-based molecular sensors have been studied previously. In 1974, Herman reported the use of a trifluoromethyl aryl ketone for the selective electrochemical detection of carbonates.[6] It was later established that this selectivity is due to the nucleophilic addition of carbonates to the highly electrophilic trifluoromethyl ketone.[7] In 1991, Simon reported the use of the trifluoromethyl aryl ketone-based membranes as optical sensors for humidity and ethanol.[8] In these studies, the nucleophilic addition of water or ethanol to the trifluoromethyl carbonyl group disrupts the extended conjugation, leading to hypsochromic shifts of the absorption band. Further development of the trifluoromethyl ketone-based absorption and fluorescence sensors have been achieved in recent years for the recognition of many nucleophilic species such as alcohols, amines, and various anions.[9] In 2010, Anh also reported that a binaphthyl-based chiral trifluoromeththyl ketone could be used to distinguish the enantiomers of amino acids by using NMR spectroscopic methods.[10] In spite of these

studies, however, no report has appeared on using the trifluoromethyl ketone-based molecules for enantioselective fluorescent recognition.

We studied the optical properties of (*S*)-**5-3**. The UV spectrum of (*S*)-**5-3** in methylene chloride displays absorptions at $\lambda_{max}(\varepsilon)$ = 228 ($4.5x10^4$), 263 ($5.2x10^4$), 319 ($3.0x10^4$) and 432 ($4.8x10^3$) nm (Figure 5-1a). When (*S*)-**5-3** (1.0×10^{-5} M in CH_2Cl_2) was treated with a chiral diamine *trans*-1,2-diaminocyclohexane (*R,R*)- or (*S,S*)-**5-4** (5.0 x 10^{-3} M), there were large absorption decreases at λ_{max} = 263, 319 and 432 nm, a large increase at λ_{max} = 231 nm and a new absorption at λ_{max} = 345 nm, but no enantioselectivity was observed (Figure 5-1a).

Figure 5-1. UV/Vis absorption spectra (a) and fluorescence spectra (b) of (*S*)-**5-3** (1.0×10^{-5} M) with/without (*R,R*)- and (*S,S*)-**5-4** (5.0×10^{-3} M) (Solvent: CH_2Cl_2. λ_{exc} = 343 nm, slit = 2/2 nm.).

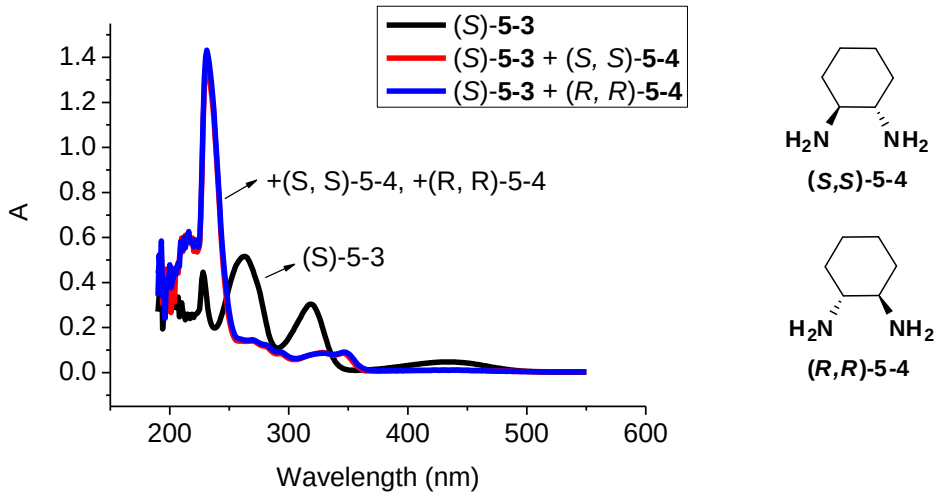

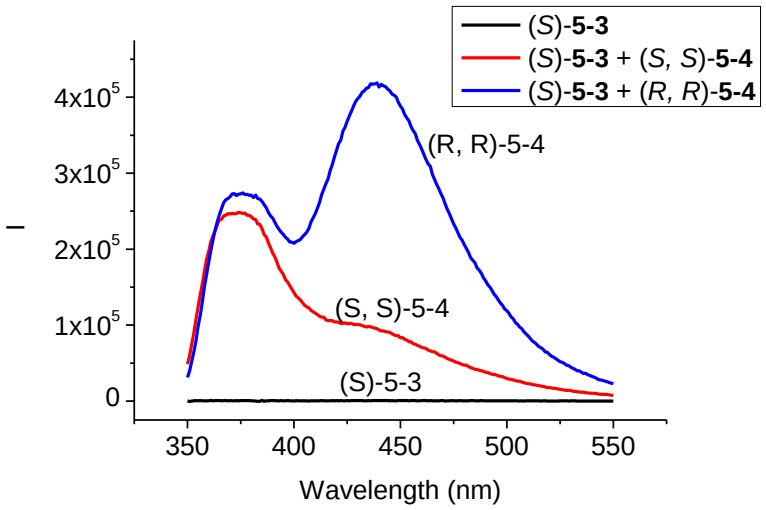

Unlike many 1,1'-binaphthyl molecules, (*S*)-**5-3** was found to be nonemissive at all in solution (Figure 5-1b). When its solution (1.0×10^{-5} M in CH_2Cl_2) was treated with (*R,R*)-**5-4** (5.0×10^{-3} M), a dramatic fluorescent enhancement was observed with dual emissions at 370 (λ_1) and 438 (λ_2) nm (Figure 5-1b). When (*S*)-**5-3** was treated with (*S,S*)-**5-4**, a similar large fluorescence enhancement at λ_1 was also observed, but the fluorescence enhancement at λ_2 was much smaller. Thus, (*S*)-**5-3** exhibits high sensitivity toward the chiral diamine at λ_1 and high enantioselectivity at λ_2. This molecule represents a rare example of an enantioselective fluorescent *enhancement* sensor for a chiral diamine.[11] We also studied the fluorescence response of (*R*)-**5-3**, the enantiomer of (*S*)-**5-3**, toward the chiral diamine. The expected mirror image responses were observed which confirmed the observed chiral discrimination.

Figure 5-2. Plots of I_1 (a), I_2 (b), I_1/I_2 (c) for (*S*)-**5-3** (1.0×10^{-5} M) in the presence of

varying concentrations of (*R,R*)- and (*S,S*)-**5-4**. (Fluorescence intensity I_1 at λ_1 = 370 nm and I_2 at λ_2 = 438 nm. Solvent: CH_2Cl_2. λ_{exc} = 343 nm, slit = 2/2 nm.)

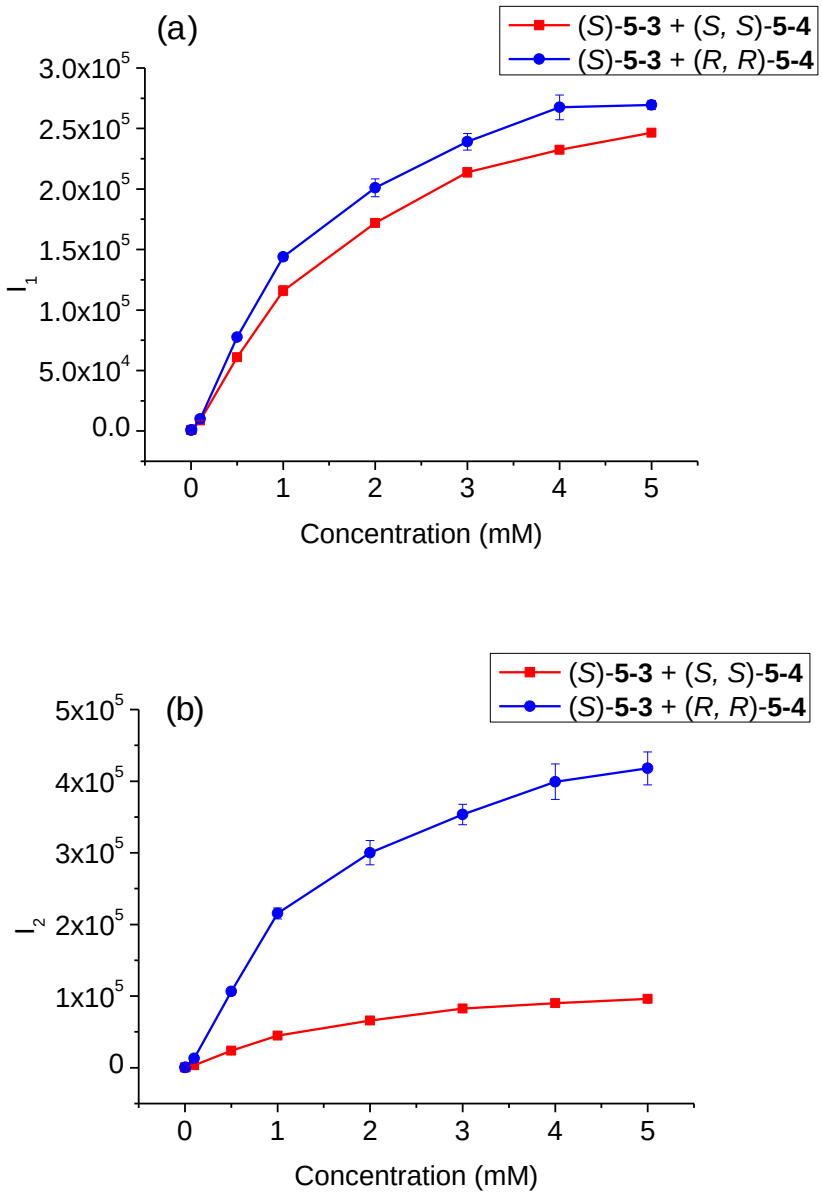

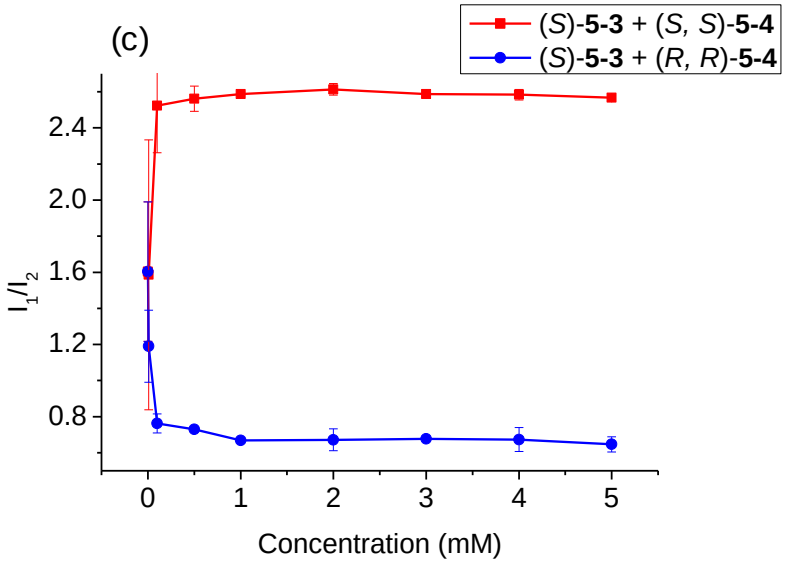

We have studied the effects of the concentration of the chiral diamine on the fluorescence responses of (*S*)-**5-3** at λ_1 and λ_2. Figure 5-2a plots the fluorescence intensity (I_1) of (*S*)-**5-3** at λ_1 versus the increasing concentration of (*R,R*)- and (*S,S*)-**5-4**. It shows that I_1 is strongly dependent on the concentration of the dimine but not significantly on its chiral configuration. Figure 5-2b plots the fluorescence intensity (I_2) of (*S*)-**5-3** at λ_2 versus the increasing concentration of (*R,R*)- and (*S,S*)-**5-4** which shows high enantioselectivity. We further found that the fluorescence intensity ratio I_1/I_2 is independent of the concentration of the chiral diamine in the range of 5.0×10^{-4} M to 5.0×10^{-3} M but is only dependent of the chiral configuration of the substrate. As shown in Figure 5-2c, the I_1/I_2 ratio for (*S,S*)-**5-4** remains to be constant at 2.60 and that for (*R,R*)-**5-4** at 0.67.

We have plotted I_1/I_2 of (*S*)-**5-3** (1.0×10^{-5} M in CH_2Cl_2) versus (*S,S*)-**5-4**% for the

chiral diamine samples with varying enantiomeric composition and concentration (5.0 x 10^{-4} M – 5.0 x 10^{-3} M) in Figure 5-3. This plot demonstrates that the enantiomeric purity of the chiral diamine can be determined by measuring the fluorescence responses of (*S*)-**5-3** at λ_1 and λ_2 without the need to know the concentration of the sample.

Figure 5-3. Plots of I_1/I_2 vs (*S*,*S*)-**5-4**% at various diamine concentrations (mM) (Solvent: CH_2Cl_2. λ_{exc} = 343 nm, slit = 2/2 nm.).

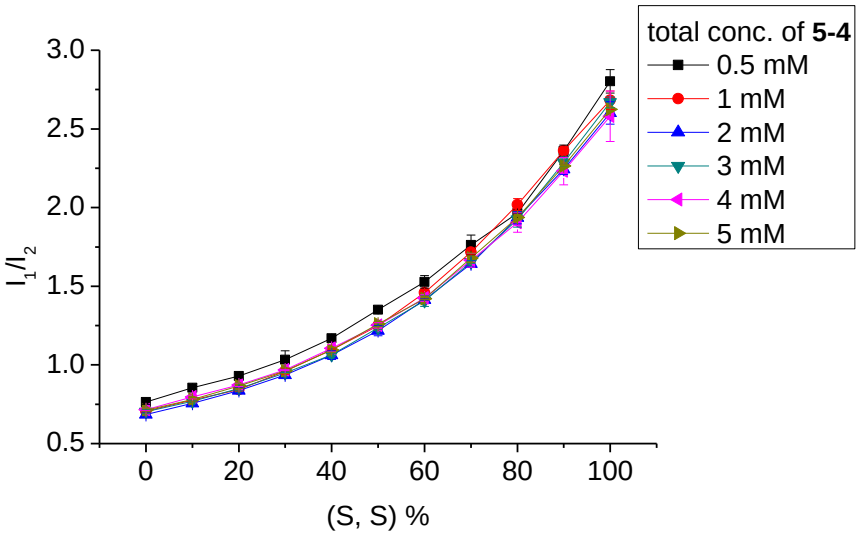

As described above, I_1 is strongly influenced by both (*S*,*S*)- and (*R*,*R*)-**5-4** (Figure 5-2a) and I_1/I_2 is only dependent on the enantiomeric composition (Figure 5-3). Figure 5-2a also shows that the chiral configuration of the diamine has a small effect on I_1. In order to more accurately determine the concentration of the substrate, we have plotted I_1 and I_1/I_2 of (*S*)-**5-3** against the diamine concentration of the samples containing varying

compositions of (*S,S*)- and (*R,R*)-**5-4** in Figure 5-4. This plot takes into consideration the effects of the chiral configuration of the diamine. It demonstrates that the concentration of a chiral diamine sample can be determined by measuring the fluorescence responses I_1 and I_2 of the sensor (*S*)-**5-3**.

Figure 5-4. Plot of I_1, I_1/I_2 vs the total concentration of **5-4** with various enantiomeric composition.

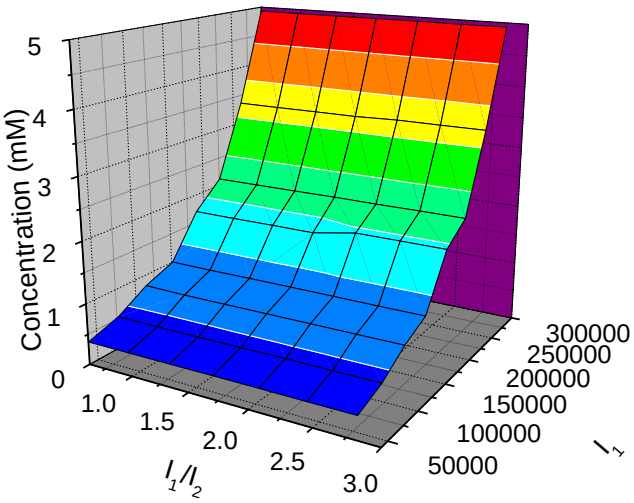

In the above experiments, when a given sample of the chiral diamine is treated with the fluorescent sensor (*S*)-**5-3**, one fluorescence measurement will give the fluorescence intensity I_1 and I_2. By using I_1/I_2, the enantiomeric composition of the sample can be determined from Figure 5-3. By using I_1 and I_1/I_2, the total concentration of the two enantiomers of the diamine can be determined from Figure 5-4. Therefore, both the

concentration and the enantiomeric composition of a chiral molecule can be simultaneously determined by one fluorescence measurement with the use of only one fluorescent sensor.

We have applied Figure 5-3 and 5-4 to ananlyze the ee and concentration of five test samples of the chiral dimaine **5-4**. As the results summarized in Table 5-1, the values of (S, S)-**5-4**% and the sample concentration from the fluorescent measurements had average errors of 10.6% and 8%, respectively.

Table 5-1. Determination of (S,S)-**5-4**% and concentration of test samples.

sample	1	2	3	4	5
measured (S, S) %	99	80	55	26	96
actual (S, S) %	95	75	50	20	95
error	4%	7%	10%	30%	1%
measured concentration (mM)	0.6	0.9	1.6	2.9	3.4
actual concentration (mM)	0.6	1	1.8	2.5	3.5
error	0%	10%	11%	16%	3%

In order to gain further understanding on the interaction of (*S*)-**5-3** with the chiral diamine, we have conducted a ^{19}F NMR titration for the interaction of (*S*)-5-**3** with (*S,S*)-**5-4**. To an NMR tube containing (*S*)-**5-3** (0.4 mL, 5 mM) in $CDCl_3$, (*S,S*)-**5-4** was gradually added. After each addition the solution was mixed well before its ^{19}F NMR spectrum was taken. The ^{19}F NMR spectrum of (*S*)-**5-3** gave a singlet at δ -70.06. With the addition of (*S,S*)-**5-4**, two new peaks at δ -69.94 and -83.83 started to appear with the same integration, while the signal of (*S*)-**5-3** at δ -70.06 was decreasing and then

completely disappeared with the addition of 4.7 equiv of the diamine. This indicates the formation of the 1:1 adduct homosemiaminal **5-5** at this stage (Scheme 5-2).[9c,12a] After that, the signal at δ -69.94 started to decrease while the signal at δ -83.83 was increasing until all the peaks were converted to the peak at δ -83.83 with the addition of 27 equiv of the diamine. This indicates the formation of the 2:1 adduct disemiaminal **5-6**. [9c,12a] Further addition of the diamine didn't change the ^{19}F NMR spectra during the 2 h period. In the subsequent several days, slow appearance of new peaks at δ -72.09 and -80.64 was observed, which were then slowly converted to the peak at δ -80.64. The signal at δ -72.09 is attributed to the formation of **5-7**[12b] and that at δ -80.64 is attributed to the formation of aminal **5-8**.[12c] Compound **5-8** was also prepared from the reaction of (*S*)-**5-3** with (*S,S*)-**5-4** in the presence of molecular sieves at room temperature in 2 d. ^{19}F NMR titration of (*S*)-**5-3** with (*R,R*)-**5-4** exhibited similar responses.

The above NMR study has revealed that the addition of the chiral diamine to (*S*)-**5-3** led to a fast formation of the amine-ketone adducts **5-5** and **5-6**, but the formation of the condensation product **5-7** and the subsequent cycloaddition product **5-8** was slow. Therefore, the observed large fluorescence enhancement of (*S*)-**5-3** in the presence of the chiral diamine can be attributed to the formation of **5-5** and **5-6**. We have examined the fluorescence spectra of the (*S*)-**5-3** solution (1×10^{-5} M) with (*S*, *S*)-**5-4** or (*R*, *R*)-**5-4** (5×10^{-3} M) over five hours after mixing, and we found no significant change in both the shape and intensity (Figure 5-5).

Scheme 5-2. A proposed mechanism for the reaction of (*S*)-**5-3** with the chiral diamine.

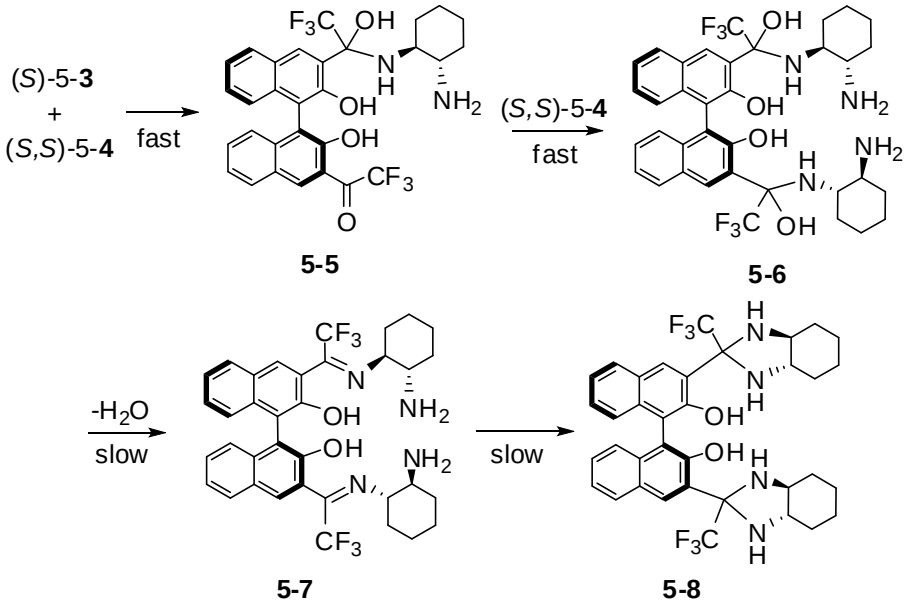

Figure 5-5. Time dependent fluorescence spectra of (*S*)-**3-3** solution (1×10^{-5} M) with (a) (*S*, *S*)-**5-4** (5×10^{-3} M) and (b) (*R*, *R*)-**5-4** (5×10^{-3} M). (Solvent: CH_2Cl_2. λ_{exc} = 343 nm, slit = 2/2 nm.)

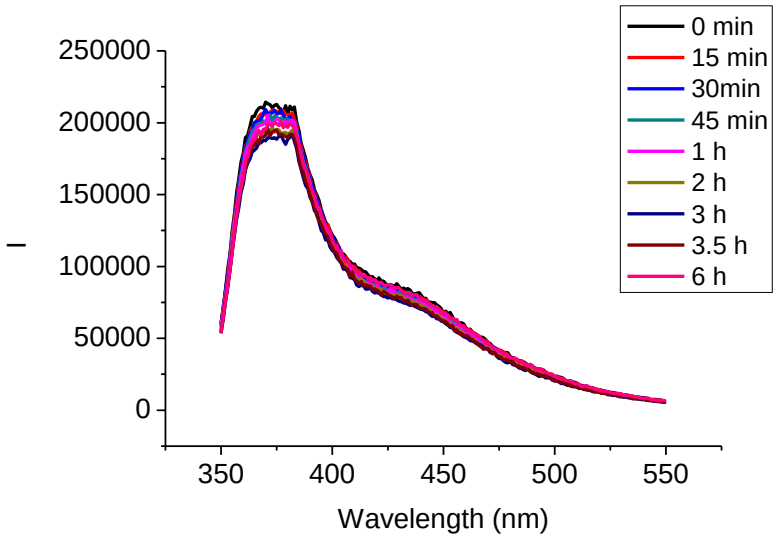

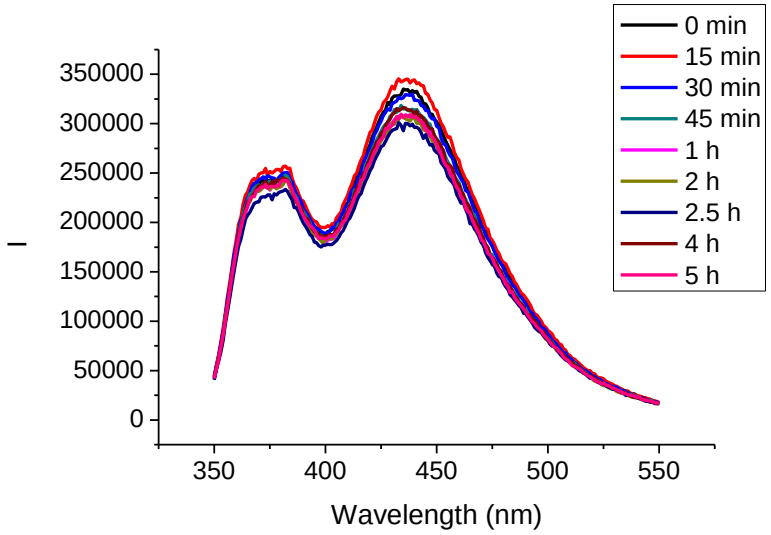

3. Conclusion

In summary, we have discovered a fluorescent sensor that exhibits very different fluorescence responses at two emission wavelengths toward a chiral diamine, one with high sensitivity and one with high enantioselectivity. On the basis of this difference in fluorescence response, it has been demonstrated for the first time that both the concentration and enantiomeric composition of a chiral substrate can be determined simultaneously by one fluorescence measurement with the use of only one fluorescent sensor. This system should significantly simplify the application of the enantioselective fluorescent sensor.

4. Experimental section

4.1 General Data

All reactions were carried out under nitrogen unless otherwise noted. All chemicals were purchased from Sigma Aldrich Chemical Co. or Alfa Aesar. THF was distilled over sodium and benzophenone under nitrogen atmosphere. Methylene chloride and diethyl ether were dried by passing through activated alumina columns under nitrogen. Solvents were stored over 4 Å molecular sieves.

Melting points were uncorrected and obtained on a Mel-Temp II capillary melting point apparatus. Optical rotations were measured on a Jasco P-2000 digital polarimeter. NMR spectra were recorded on a Varian-300 MHz or Bruker-600 MHz spectrometer. Chemical shifts for ^{1}H NMR spectra were reported in parts per million relative to a singlet at 7.26 ppm for deuterated chloroform. Chemical shifts for ^{13}C NMR were reported relative to the centerline of a triplet at 77.16 ppm for deuterated chloroform. The ^{19}F NMR spectra were reported in units of part per million (ppm) relative to trifluoroacetic acid (δ -76.55 ppm) as an external reference. High resolution mass spectra were obtained from the University of Illinois at Urbana-Champaign (UIUC) Mass Spectrometry Facility. UV-Vis spectra were recorded on a Hewlett-Packard 8452A diode-array spectrophotometer. Steady-state fluorescence emission spectra were recorded on a Horiba FluoroMax-4 spectrofluorometer.

4.2 Synthesis and Characterization of Compounds

Synthesis and Characterization of (S)-5-2. Under nitrogen, (*S*)-**5-1** (3.0 mmol, 1.12

g) was dissolved in ether (36 mL). The solution was cooled to 0 ℃, and n-BuLi (12.0 mmol, 2.5 M in hexane, 4.8 mL) was added dropwise. The reaction mixture was stirred for 2 h at room temperature and cooled to 0 ^{0}C, and then ethyl trifluoroacetate (13.5 mmol, 1.6 mL) was added slowly. The reaction mixture was allowed to warm to room temperature and stirred for 1 h to afford a cream-like mixture. A saturated aqueous NH_4Cl solution was added to quench the reaction. The organic layer was separated, and the aqueous layer was extracted with ethyl acetate (three 20 mL aliquots). The combined organic extracts were washed with brine, and dried over Na_2SO_4. After evaporation of the solvent, the residue was purified by column chromatography on silica gel eluted with hexane/methylene chloride (1/3) to afford compound (*S*)-5-**2** as a yellow oil in 62% yield. ^{1}H NMR (300 MHz, $CDCl_3$) δ 2.77 (s, 6H), 4.73 (d, J= 6.3 Hz, 2H), 4.77 (d, J= 6.3 Hz, 2H), 7.25 (d, J = 8.7 Hz, 2H), 7.44-7.50 (m, 2H), 7.53-7.58 (m, 2H), 8.05 (d, J = 8.1 Hz, 2H), 8.43 (s, 2H). ^{19}F NMR (300 MHz, $CDCl_3$) δ -73.62. ^{13}C NMR (75 MHz, $CDCl_3$) δ 56.6, 100.7, 116.5 (q, J = 290 Hz), 126.4, 126.8, 126.9, 127.0, 129.6, 129.8, 130.1, 132.7, 136.2, 151.6, 182.4 (q, J = 35.6 Hz). HRMS Calcd for $C_{28}H_{20}O_6F_6Na$ (MNa^+): 589.1062, Found: 589.1053. $[\alpha]_D$ = -18.056 (c = 0.590, $CHCl_3$).

Synthesis and Characterization of (S)-5-3. After compound (*S*)-**5-2** (134.2 mg, 0.25 mmol) was dissolved in a minimum amount of CH_2Cl_2, trifluroacetic acid (1.0 mL) was added slowly, and the mixture was stirred at room temperature for 10 min. A saturated aqueous $NaHCO_3$ solution was added to quench the reaction. The organic layer was

separated, and the aqueous layer was extracted with CH_2Cl_2 (3 x 20 mL). The combined organic extracts were washed with brine, and dried over Na_2SO_4. After evaporation of the solvent, the residue was purified by column chromatography on silica gel eluted with hexane/methylene chloride (2/1) to afford compound (*S*)-5-**3** as an orange solid in 84% yield. ^{1}H NMR (300 MHz, $CDCl_3$) δ 7.16 (d, J = 7.5 Hz, 2H), 7.41-7.51 (m, 4H), 8.02 (d, J = 7.5 Hz, 2H), 8.70 (s, 2H), 10.51 (s, 2H). ^{19}F NMR (282 MHz, $CDCl_3$) δ -70.06. ^{13}C NMR (150 MHz, $CDCl_3$) δ 115.2, 116.7 (q, J = 289.5 Hz), 117.8, 124.7, 125.3, 127.2, 131.2, 132.2, 136.1 (q, J = 3.75 Hz), 138.5, 155.0, 185.1 (q, J = 36.0 Hz). HRMS Calcd for $C_{24}H_{13}O_4F_6$ (MH^+): 479.0718, Found: 479.0719. m.p. 231 ^{0}C. $[\alpha]_D$ = -167.50 (c = 0.355, $CHCl_3$).

Synthesis and Characterization of (*S, S, S*)-5-8. Under nitrogen, (S)-5-3 (0.1 mmol, 47.8 mg) was dissolved in CH_2Cl_2 (3 mL). (*S,S*)-**5-4** (2.0 mmol, 228.4 mg) and 4 Å molecular sieves were added. The reaction mixture was stirred for 2 days at room temperature. After filtration, the solvent was evaporated and the residue was purified by column chromatography on neutral aluminum oxide eluted with methylene chloride to afford compound (*S,S,S*)-**5-8** as a white solid in 65% yield. ^{1}H NMR (300 MHz, $CDCl_3$) δ 1.20-1.34 (m, 8H), 1.84-1.87 (m, 4H), 2.06-2.09 (m, 2H), 2.25-2.29 (m, 2H), 2.47-2.58 (m, 8H), 7.27-7.29 (m, 6H), 7.78-7.82 (m, 2H), 8.03 (s, 2H), 13.57 (s, 2H). ^{19}F NMR (282 MHz, $CDCl_3$) δ -80.63. ^{13}C NMR (150 MHz, $CDCl_3$) δ 24.8, 24.9, 28.8, 29.5, 64.7, 65.4, 84.3 (q, J = 28.8 Hz), 117.7, 122.0, 123.4, 125.0, 125.7 (q, J = 283.5 Hz), 127.5,

127.6, 128.5, 129.4, 134.5, 152.8. HRMS Calcd for $C_{36}H_{37}N_4O_2F_6$ (MH^+): 671.2821, Found: 671.2831. m.p. 194 ^{0}C. $[\alpha]_D$ = -217.0 (c = 0.52, $CHCl_3$).

Synthesis and Characterization of (*S, R, R*)-5-8. (*S, R, R*)-**5-8** was prepared in a way similar to the preparation of (*S,S,S*)-**5-8** by starting with (*S*)-**5-3** and (*R,R*)-**5-4**. ^{1}H NMR (300 MHz, $CDCl_3$) δ 1.24-1.33 (m, 8H), 1.84 (d, J = 8.1 Hz, 4H), 2.8 (d, J = 13.5 Hz, 2H), 2.25 (d, J = 10.8 Hz, 2H), 2.37 (m, 2H), 2.54-2.66 (m, 6H), 7.07 (d, J = 8.1 Hz, 2H), 7.16-7.28 (m, 4H), 7.81 (d, J = 7.8 Hz, 2H), 8.05 (s, 2H), 13.24 (s, 2H). ^{19}F NMR (282 MHz, $CDCl_3$) δ -80.29. ^{13}C NMR (150 MHz, $CDCl_3$) δ 24.76, 24.82, 29.0, 29.7, 64.8, 65.2, 84.0 (q, J = 29.9 Hz), 117.7, 122.7, 123.2, 124.8, 125.6 (q, J = 279.6 Hz), 127.3, 127.6, 128.6, 129.2, ,134.5, 153.6. HRMS Calcd for $C_{36}H_{37}N_4O_2F_6$ (MH^+): 671.2821, Found: 671.2816. m.p. 236 ^{0}C. $[\alpha]_D$ = -36.3 (c = 1.66, $CHCl_3$).

4.3 Preparation of Samples for Fluorescence Measurement.

Sensors were purified by column chromatography followed by recrystallization and then stored in a refrigerator. The enantiomers of *trans*-1,2-diaminocyclohexane were purchased from Aldrich and redistilled. All of the solvents were either HPLC or spectroscopic grade. The stock solutions of the sensors were freshly prepared for each measurement. A 0.01 M stock solution of *trans*-1,2-diaminocyclohexane in methylene chloride was freshly prepared. For the fluorescence enhancement study, a sensor solution was mixed with the amine solution at room temperature in a 5 mL volumetric

flask and diluted to the desired concentration. The resulting solution was allowed to stand at room temperature for 0.5 h before the fluorescence measurement and all the fluorescence spectra were taken within 2 hours.

4.4 Preparation of Samples for ^{19}F NMR Titration

The $CDCl_3$ solution of (*S*)-**5-3** (0.4 mL, 5.0 mM) was prepared in an NMR tube. The $CDCl_3$ solution of (*S, S*) or (*R, R*)-**5-4** (1 mL, 0.5 M) was prepared in a small vial as the stock solution. The NMR spectrum of the (*S*)-**5-3** solution was first recorded and the stock solution of the diamine was added to the NMR tube in the following fashion: 1 x 2 μL, 1 x 3 μL, 3 x 5 μL, 8 x 10 μL, and then 50 μLs. After each addition the solution was mixed well and the NMR spectra were recorded. (In order to avoid the sensor being diluted with the addition of the diamine during the titration, a small amount of (S)-5-3 (5.0 mM) was pre-added to the diamine stock solution. This way, the total concentration of the sensor was maintained at 5.0 mM throughout the titration.)

References

1. Selected references of enantioselective fluorescent sensors: (a) James, T. D.; Sandanayake, K. R. A. S.; Shinkai, S. *Nature* **1995**, *374*, 345-347. (b) Pugh, V.; Hu, Q. -S.; Pu, L. *Angew. Chem. Int. Ed.* **2000**, *39*, 3638-3641. (c) Reetz, M. T.; Sostmann, S. *Tetrahedron* **2001**, *57*, 2515-2520. (d) Korbel, G. A.; Lalic, G.; Shair, M. D. *J. Am. Chem. Soc.* **2001**, *123*, 361-362. (e) Jarvo, E. R.; Evans, C. A.; Copeland, G. T.; Miller, S. J. *J. Org. Chem*. **2001**, *66*, 5522-5527. (f) Wong, W.-L.; Huang, K.-H.; Teng, P.-F.; Lee, C.-S.; Kwong, H.-L. *Chem. Commun.* **2004**, 384-385. (g) Zhao, J.-Z.; Fyles, T. M.; James, T. D. *Angew. Chem., Int. Ed.* **2004**, *43*, 3461-3464. (h) Pagliari, S.; Corradini, R.; Galaverna, G.; Sforza, S.; Dossena, A.; Montalti, M.; Prodi, L.; Zaccheroni, N.; Marchelli, R. *Chem. Eur. J.* **2004**, *10*, 2749-2758. (i) Matsushita, H.; Yamamoto, N.; Meijler, M. M.; Wirsching, P.; Lerner, R.A.; Matsushita, M.; Janda, K. D. *Mol. Biosyst.* **2005**, *1*. 303-306. (j) Zhu, L.; Anslyn, E. V. *J. Am. Chem. Soc.* **2004**, *126*, 3676-3677. (k) Mei, X. F. ; Wolf, C. *J. Am. Chem. Soc.* **2004**, *126*, 14736-14737. (l) Li, Z.-B.; Lin, J.; Pu, L. *Angew. Chem., Int. Ed.* **2005***, 44,* 1690-1693.

2. For reviews on enantioselective fluorescent recognition: (a) Pu, L. *Chem. Rev.* **2004**, *104*, 1687-1716. (b) Pu, L. *Acc. Chem. Res*. **2012**, *45*, 150–163. (c) A recent review on chiral optical sensors: Leung, D.; Kang, S. O.; Anslyn, E. V. *Chem. Soc. Rev*. **2012**, *41*, 448–479.

3. (a) Mei, X. F.;Wolf, C. *J. Am. Chem. Soc*. **2006**, *128*, 13326-13327. (b) Wolf, C.; Liu, S.; Reinhardt, B. C. *Chem. Commun.* **2006**, 4242-4244.
4. Zhu, L.; Shabbir, S. H.; Anslyn, E. V. *Chem. Eur. J.* **2007**, *13*, 99-104.
5. Yu, S. S.; Pu, L. *J. Am. Chem. Soc*. **2010**, 132, 17698–17700.
6. Herman, H. B.; Rechnitz, G. A. *Science* **1974**, *184*, 1074–1075.
7. Meyerhoff, M. E.; Pretsch, E.; Welti, D. H.; Simon, W. *Anal. Chem*. **1987**, *59*, 144–150.
8. (a) Wang, K.; Seiler, K.; Haug, J. –P.; Lehmann, B.; Hartman, S. W. K.; Simon, W. *Anal. Chem*. **1991**, *63*, 970-974. (b) Seiler, K.; Wang, K.; Kuratli, M.; Simon, W. *Anal. Chim. Act*. **1991**, *244*, 151–160.
9. (a) Mohr, G. J.; Tirelli, N.; Lohse, C.; Spichiger-Keller, U. E. *Adv. Mater*. **1998**, *10*, 1353-1357. (b) Mertz, E.; Zimmerman, S. C. *J. Am. Chem. Soc.* **2003**, *125*, 3424-3425. (c) Sasaki, S. –i.; Kotegawa, Y.; Tamiaki, H. *Tetrahedron Lett*. **2006**, *47*, 4849–4852. (d) Ryu, D.; Park, E.; Kim, D. –S.; Yan, S.; Lee, J. Y.; Chang, B. –Y.; Ahn, K. H. *J. Am. Chem. Soc*. **2008**, *130*, 2394–2395.
10. Sambasivan, S.; Kim, D. –s.; Ahn, K. H. *Chem. Commun*. **2010**, *46*, 541–543.
11. Tumambac, G. E.; Wolf, C. *Org. Lett*. **2005**, *7*, 4045–4048.
12. (a) Mertz, E.; Beil, J. B.; Zimmerman, S. C. *Org. Lett*. **2003**, *5*, 3127–3130. (b) Tamborski, C.; Prabhu, U. D. G.; Eapen, K. C. *J. Fluor. Chem*. **1985**, *28*, 139-150. (c) Prakash, G. K. S.; Mathew, T.; Panja, C.; Vaghoo, H.; Venkataraman, K.; Olah, G. A.

Org. Lett. **2007**, *9*, 179–182.

Chapter 6

Study of BINOL-Dicarbonyl Compounds in Fluorescent Recognition

1. Introduction

Enantioselective fluorescent sensors have been extensively investigated due to their potential application in high-throughput screening of chiral catalyst. In recent years, a number of highly enantioselective fluorescent sensors have been developed for the recognition of chiral substrates such as carboxylic acids, amino acids, amines and amino alcohols.[1,2] Our group has developed a series of BINOL-based fluorescent sensors[3] because BINOL can provide a good fluorophore, axial chirality and binding sites. Most of our sensors are based on hydrogen bonding mechanism, which significantly limits their application in highly polar solvents. The use of trifluoromethyl ketone-based molecular sensors has been studied previously and they could covalently interact with various nucleophiles, such as carbonates, alcohols and amines.[4] Recently we reported the first example of using the trifluoromethyl ketone-based molecule for enantioselective fluorescent recognition.[5] As described in Chapter 5, the BINOL-trifluoromethyl ketone compound (*S*)-**5-3** is nonfluorescent in CH_2Cl_2 and shows dual emissions when treated with both enantiomers of trans-1,2-diaminocyclohexane. It exhibits high sensitivity at one emission wavelength and high enantioselectivity at another. By using this fluorescent sensor, both the concentration and enantiomeric composition of trans-1,2-diaminocyclohexane can be determined simultaneously with one fluorescence measurement which points a new direction for the development of enantioselective fluorescent sensors. In order to gain more understanding on this type of sensors, we have synthesized a series of BINOL-based molecules containing 3,3'- or 6,6'-carbonyl groups and have explored their fluorescent responses towards a variety of amines,

diamines, amino carboxylates and amino alcohols. Herein, these results are reported.

2. Results and Discussion

2.1 Synthesis and Characterization of the BINOL-diketone compounds.

As described in Chapter 5, we synthesized (*S*)-**6-4** according to Scheme 6-1.[5] The ^{1}H NMR spectrum of (*S*)-**6-4** in $CDCl_3$ shows a singlet at δ 10.51 for the hydroxyl group, which indicates strong intramolecular hydrogen bonding.

Scheme 6-1. Synthesis of the BINOL-diketone (*S*)-**6-4**.

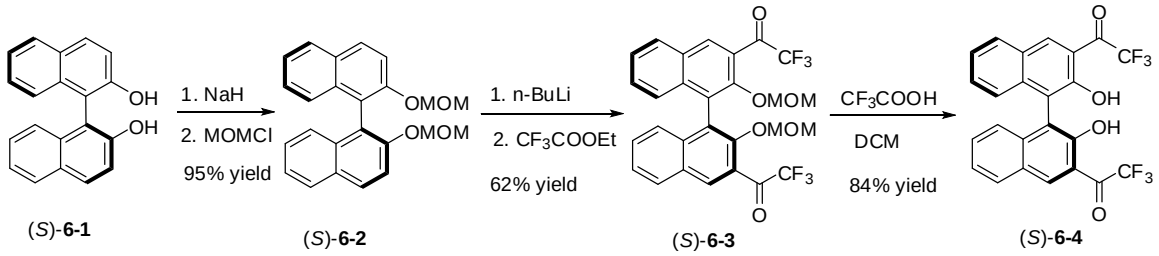

(*S*)-**6-1** (*S*)-**6-2** (*S*)-**6-3** (*S*)-**6-4**

An H_8BINOL analogue (*R*)-**6-8** was prepared by following a similar procedure starting with (*R*)-H_8BINOL (Scheme 6-2). Its specific optical rotation was $[\alpha]_D$ = -38.5 (c = 0.36, $CHCl_3$). The ^{1}H NMR spectrum of (*R*)-**8** in $CDCl_3$ shows a singlet at δ 11.14 for the hydroxyl group.

Scheme 6-2. Synthesis of the H_8BINOL-diketone (*R*)-**6-8**.

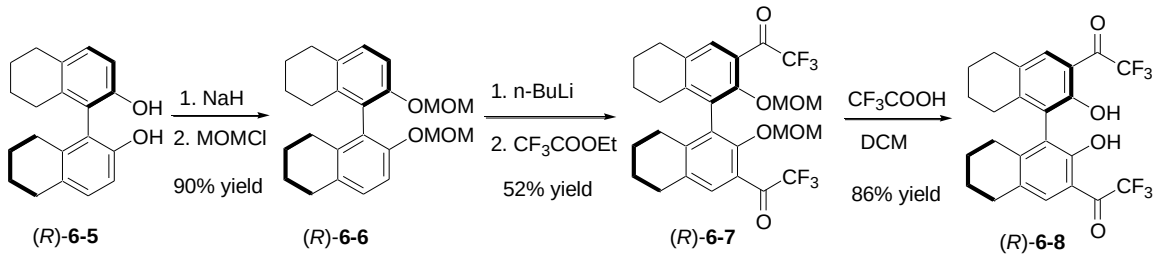

(*R*)-**6-5** (*R*)-**6-6** (*R*)-**6-7** (*R*)-**6-8**

Compounds (*S*)-**6-10** and (*S*)-**6-12** were prepared as the analogues of (*S*)-**6-4** with carbonyl groups of different electronic properties. Following procedures similar to the synthesis of (*S*)-**6-4**, we used DMF to prepare (*S*)-**6-10** (Scheme 6-3)[6] and ethyl difluoroacetate to prepare (*S*)-**6-12** (Scheme 6-4). The specific optical rotation of (*S*)-**6-12** was $[\alpha]_D = 31.9$ (c = 0.19, $CHCl_3$). The ^1H NMR spectrum in $CDCl_3$ shows a singlet at δ 10.59 for the hydroxyl group of (*S*)-**6-10** and at δ 10.75 for (*S*)-**6-12**.

Scheme 6-3. Synthesis of the BINOL-dialdehyde (*S*)-**6-10**.

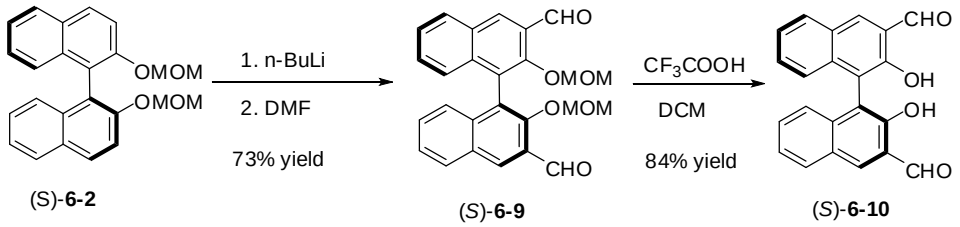

Scheme 6-4. Synthesis of the BINOL-diketone (*S*)-**6-12**.

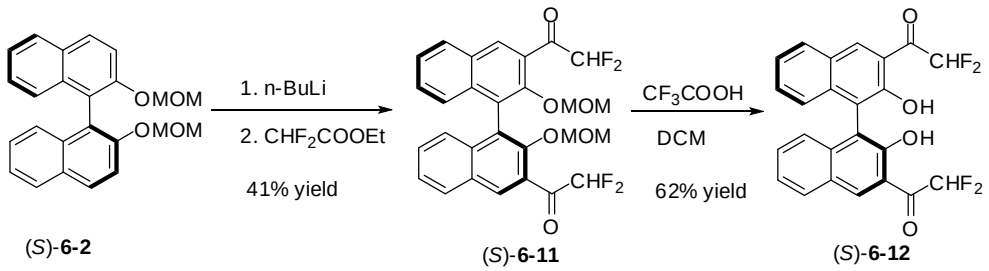

We also introduced trifluoroacetyl group to the 6,6'-postions of BINOL to make compound (*S*)-**6-16**. As shown in Scheme 6-5, (*S*)-**6-1** was treated with bromine to give 6,6'-brominated BINOL in 87% yield.[7] After protected with the MOM group,[7] the resulting compound was reacted with *n*-BuLi and ethyl trifluoroacetate to produce (*S*)-**6-15** in 87% yield.[8] Then TFA was added to remove MOM to generate (*S*)-**6-16** in 89% yield. Its specific optical rotation was $[\alpha]_D = 333.6$ (c = 0.16, $CHCl_3$). The ^1H NMR

spectrum of (*S*)-**16** in $CDCl_3$ shows a singlet at δ 5.33 for the hydroxyl group which is much more upfiled than those of the 3,3'-dicarbonylBINOLs because of the absence of the intramolecular OH···O=C hydrogen bond.

Scheme 6-5. Synthesis of the BINOL-diketone (*S*)-**6-16**.

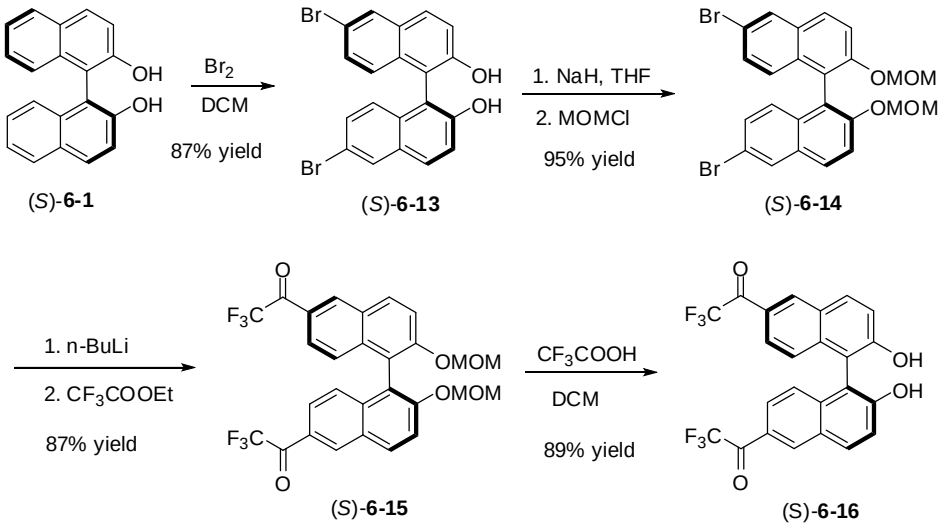

2.2 UV Spectra of Compounds (*S*)-6-3, (*S*)-6-4, (*R*)-6-8, (*S*)-6-10, (*S*)-6-12 and (*S*)-6-16.

Figure 6-1 gives the UV spectra of (*S*)-**6-3**, (*S*)-**6-4**, (*R*)-**6-8**, (*S*)-**6-10**, (*S*)-**6-12** and (*S*)-**6-16** in CH_2Cl_2 at 1.0×10^{-5} M and Table 6-1 summarizes their maximum absorption peaks and their extinction coefficients. As shown in Figure 6-1a, (*S*)-**6-4** displays absorptions at λ_{max} = 228, 263, 319 and 432 nm. Compared to (*S*)-**6-4,** the long wavelength absorption is missing in the MOM protected compound (*S*)-**6-3**, which indicates that the intramolecular hydrogen bonding is responsible for the absorption at 432 nm. H_8BINOL analogue (*R*)-**6-8** exhibits blue shifted absorptions due to its less conjugated structure but with patterns similar to those of (*S*)-**6-4** (Figure 6-1b). The

similar absorption patterns can also be observed in compounds (*S*)-**6-10** and (*S*)-**6-12**. (*S*)-**6-16**, in which two trifluoroacetyl groups are attached to the 6,6'-positions, gives very differently structured absorptions with the long wavelength absorption observed in (*S*)-**6-4** missing. This observation is consistent with our proposed hydrogen bonding origin of the absorption at 432 nm in (*S*)-**6-4**.

Figure 6-1. UV spectra of (a) (*S*)-**6-3**, (b) (*R*)-**6-8**, (c) (*S*)-**6-10**, (*S*)-**6-12** and (d) (*S*)-**6-16** (1.0×10^{-5} M) in comparison with that of (*S*)-**6-4** in CH_2Cl_2.

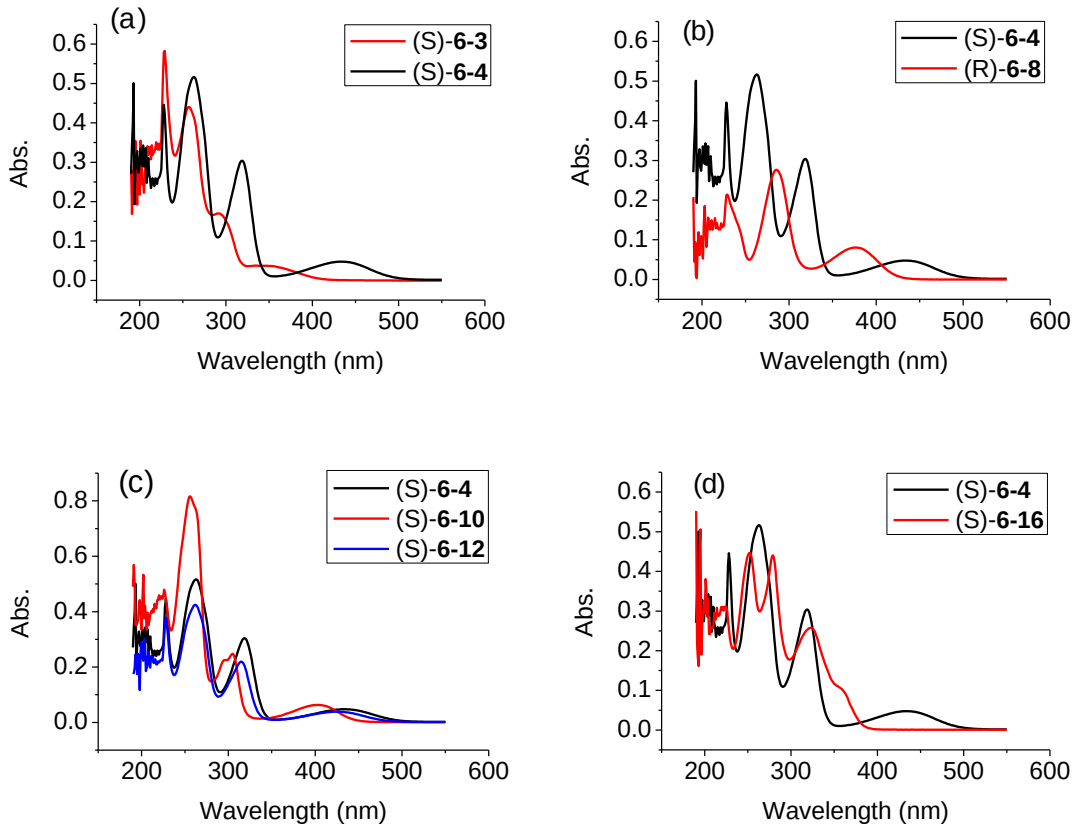

Table 6-1. Maximum absorption peaks and extinction coffecient of (*S*)-**6-3**, (*S*)-**6-4,** (*R*)-**6-8**, (*S*)-**6-10**, (*S*)-**6-12** and (*S*)-**6-16** ($1.0x10^{-5}$ M in CH_2Cl_2).

	$\lambda_{max}(\varepsilon)$
(*S*)-**6-3**	229 ($5.8x10^4$), 257 ($4.4x10^4$), 291 ($1.7x10^4$), 357 ($3.5x10^3$) nm.
(*S*)-**6-4**	228 ($4.5x10^4$), 263 ($5.2x10^4$), 319 ($3.0x10^4$), 432 ($4.8x10^3$) nm
(*R*)-**6-8**	229 ($2.1x10^4$), 285 ($2.8x10^4$), 377 ($8.1x10^3$) nm
(*S*)-**6-10**	255 ($8.1x10^4$), 305 ($2.5x10^4$), 402 ($6.3x10^3$) nm
(*S*)-**6-12**	228 ($3.8x10^4$), 262 ($4.2x10^4$), 315 ($2.2x10^4$), 425 ($3.9x10^3$) nm
(*S*)-**6-16**	252 ($4.5x10^4$), 279 ($4.4x10^4$), 323 ($2.6x10^4$), 359 ($1.0x10^4$) nm

2.3 Fluorescence Spectra of Compounds (*S*)-6-3, (*S*)-6-4, (*R*)-6-8, (*S*)-6-10, (*S*)-6-12 and (*S*)-6-16.

The fluorescence spectrum of (*S*)-**6-4** is compared with those of (*S*)-**6-3**, (*R*)-**6-8**, (*S*)-**6-10**, (*S*)-**6-12** and (*S*)-**6-16** in CH_2Cl_2 at 1.0×10^{-5} M. As shown by Figure 6-2, similar to (*S*)-**6-4**, compounds (*R*)-**6-8**, (*S*)-**6-10** and (*S*)-**6-12** containing the intramolecular hydrogen bonds are found to be nonemissive. The MOM protected compound (*S*)-**6-3**, however, shows a very strong emission at 495 nm. (*S*)-**6-16** gives an even stronger emission at 444 nm. The emissions of (*S*)-**6-3** and (*S*)-**6-16** could be attributed to their internal charge transfer states.

Figure 6-2. Fluorescence spectra of (*S*)-**6-3,** (*S*)-**6-4**, (*R*)-**6-8**, (*S*)-**6-10**, (*S*)-**6-12** and (*S*)-**6-16** (1.0×10^{-5} M) in CH_2Cl_2. (λ_{exc} = 343 nm for (*S*)-**6-3,** (*S*)-**6-4**, (*S*)-**6-10**, (*S*)-**6-12** and (*S*)-**6-16**, λ_{exc} = 290 nm for (*R*)-**6-8**, slit = 2.0/2.0 nm).

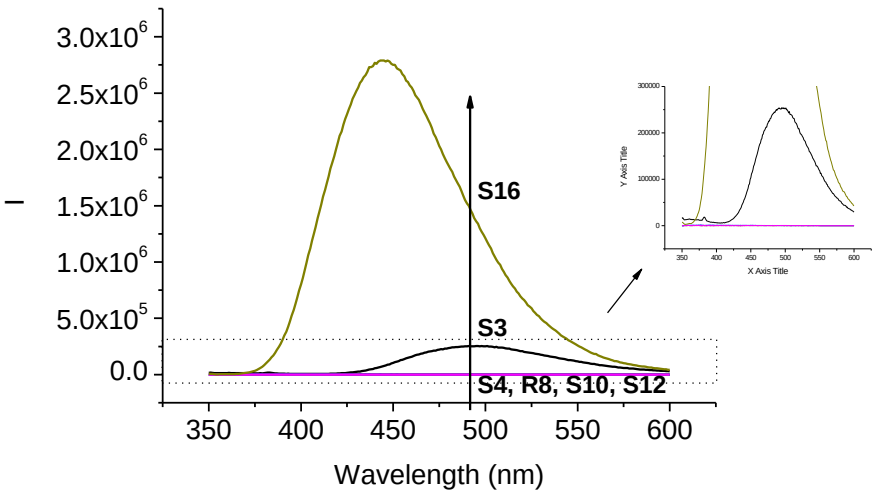

We have studied the solvent effect on the fluorescence properties of these compounds. As shown in Figure 6-3a, (*S*)-**6-4** showed very little emission in CH_2Cl_2, $CHCl_3$ and CH_3CN, moderate emission in THF, DMSO and very strong emission in MeOH. Changing the solvent from CH_3CN to CH_3CN/H_2O (1:1) and from THF to THF/H_2O (1:1) caused significant fluorescence enhancement. However, changing the solvent from CH_2Cl_2 to CH_2Cl_2/H_2O (1:1) and from $CHCl_3$ to $CHCl_3/H_2O$ (1:1) barely affect the fluorescent emission. Moreover, the colors of the solutions change accordingly with the fluorescence. When there is no emission or very weak fluorescence, the solution is light yellow, and when it shows strong emission, the solution becomes colorless.

Compound (*S*)-**6-12** shows similar solvent effect but the fluorescence is much weaker than (*S*)-**6-4** (Figure 6-3c). (*S*)-**6-10** shows no fluorescence or very weak fluorescence in all of the tested solvents (Figure 6-3b).

Figure 6-3. Fluorescence spectra of (a) (*S*)-**6-4**, (b) (*S*)-**6-10** and (c) (*S*)-**6-12** (1.0×10^{-5} M) in various solvents. (λ_{exc} = 343 nm, slit = 2.0/2.0 nm).

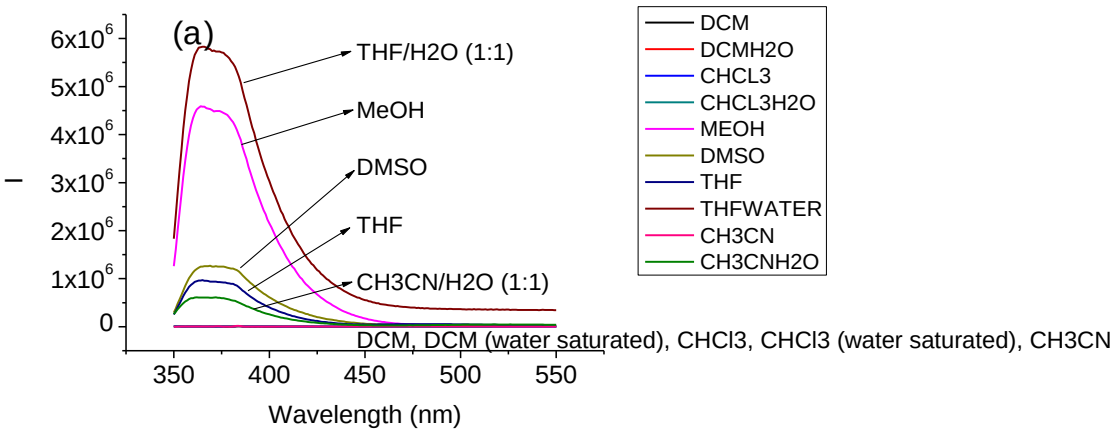
(a)
6x10^6
5x10^6
4x10^6
3x10^6
2x10^6
1x10^6
0
I
350
400
450
500
550
Wavelength (nm)
THF/H2O (1:1)
MeOH
DMSO
THF
CH3CN/H2O (1:1)
DCM, DCM (water saturated), CHCl3, CHCl3 (water saturated), CH3CN
DCM
DCMH2O
CHCL3
CHCL3H2O
MEOH
DMSO
THF
THFWATER
CH3CN
CH3CNH2O

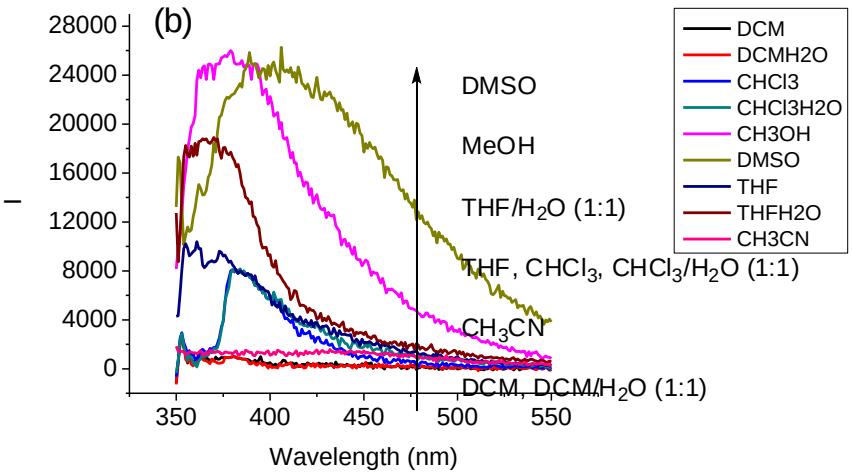
(b)
28000
24000
20000
16000
12000
8000
4000
0
I
350
400
450
500
550
Wavelength (nm)
DMSO
MeOH
THF/H2O (1:1)
THF, CHCl3, CHCl3/H2O (1:1)
CH3CN
DCM, DCM/H2O (1:1)
DCM
DCMH2O
CHCl3
CHCl3H2O
CH3OH
DMSO
THF
THFH2O
CH3CN

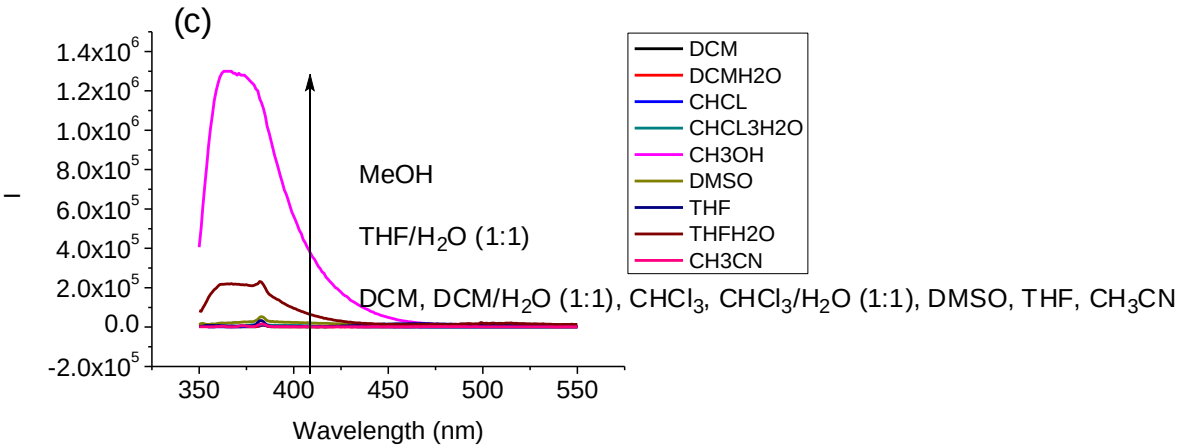
(c)
1.4x10^6
1.2x10^6
1.0x10^6
8.0x10^5
6.0x10^5
4.0x10^5
2.0x10^5
0.0
-2.0x10^5
I
350
400
450
500
550
Wavelength (nm)
MeOH
THF/H2O (1:1)
DCM, DCM/H2O (1:1), CHCl3, CHCl3/H2O (1:1), DMSO, THF, CH3CN
DCM
DCMH2O
CHCL
CHCL3H2O
CH3OH
DMSO
THF
THFH2O
CH3CN

On the basis of the above observations, we propose that the quenched fluorescence of compound (*S*)-**6-4** might be due to the excited state intramolecular proton transfer process.[9] Absorption of photons frequently changes the electron distribution within a fluorophore.[10] Aromatic alcohols or protonated amines become more acidic in the excited state than in the ground state because the electrons on the hydroxyl group or protonated amine are shifted into the aromatic ring in the excited state.[11] Aromatic carboxylic acids and esters usually become more basic in the excited state because electron acceptors have vacant π orbitals into which electrons can be transferred. In the case of 2-naphthol the pK_A decreased from 9.2 in the ground state to 2.0 in the excited state.[12] In acid solution the emission is from naphthol with an emission maximum at 357 nm. In basic solution the emission is from the naphtholate anion with an emission maximum at 409 nm. At intermediate pH values emission from both species is observed in water.[13] It has been proposed that water cluster serves as proton acceptor which explains why naphtholate emission disappears in nonaquous solvents.[14] When a molecule contains both the proton donor and acceptor, excited state proton transfer is facile to happen within the molecule since the transferring proton is very close to the acceptor. For example, Methyl 2-hydroxy-3-naphtholat (MNA), which contains both the proton donor and acceptor, is known to undergo intramolecular excited state proton transfer reaction.[15] The transferring proton, which is already hydrogen bonded with ester group, is very easy to move to its adjacent oxygen atom in the excited state. This theory can also apply to compounds (*S*)-**6-4**, (*R*)-**6-8**, (*S*)-**6-10** and (*S*)-**6-12**, in which the intramolecular hydrogen bond is formed. When methanol or water is added to the (*S*)-**6-4**

solutions, nucleophilic attack happens, which changes the structure of the original intramolecular hydrogen bond and thus changes its fluorescent property.

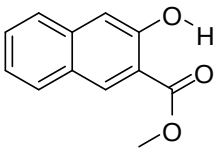

MNA

The following scheme shows a proposed mechanism for the fluorescence of (*S*)-**6-4**. In nonaqueous solution, the excited state proton transfer of (*S*)-**6-4** upon irradiation could generate a nonemissive species (*S*)-**6-17**. In the presence of water or alcohol, (*S*)-**6-18** could be generated. The excited state proton transfer of (*S*)-**6-4** upon irradiation could generate the naphthalate (*S*)-**6-19** that could undergo both radiative and nonradiative decay.

Scheme 6-6. Proposed mechanism for the fluorescent responses of (*S*)-**6-4**.

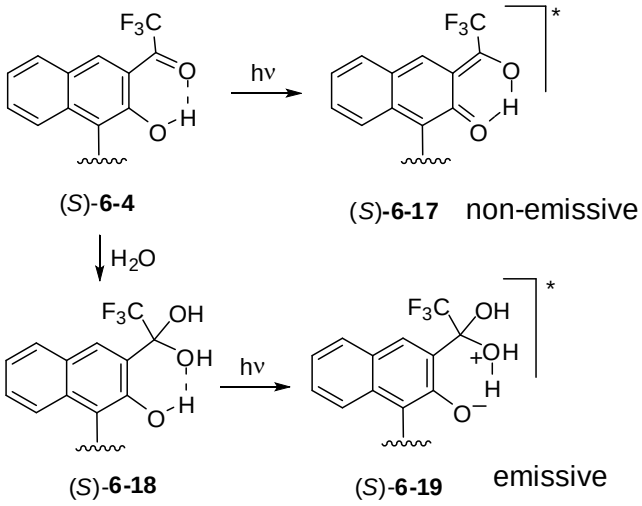

2.4 Interaction of (*S*)-6-4 with Amines.

In Chapter 5, we described the interaction of (*S*)-**6-4** with the two enantiomers of trans-cyclohexanediamine. We have further studied the interaction of (*S*)-**6-4** with many other amines and diamines as listed in Figure 6-4.

Figure 6-4. Structures of various amines.

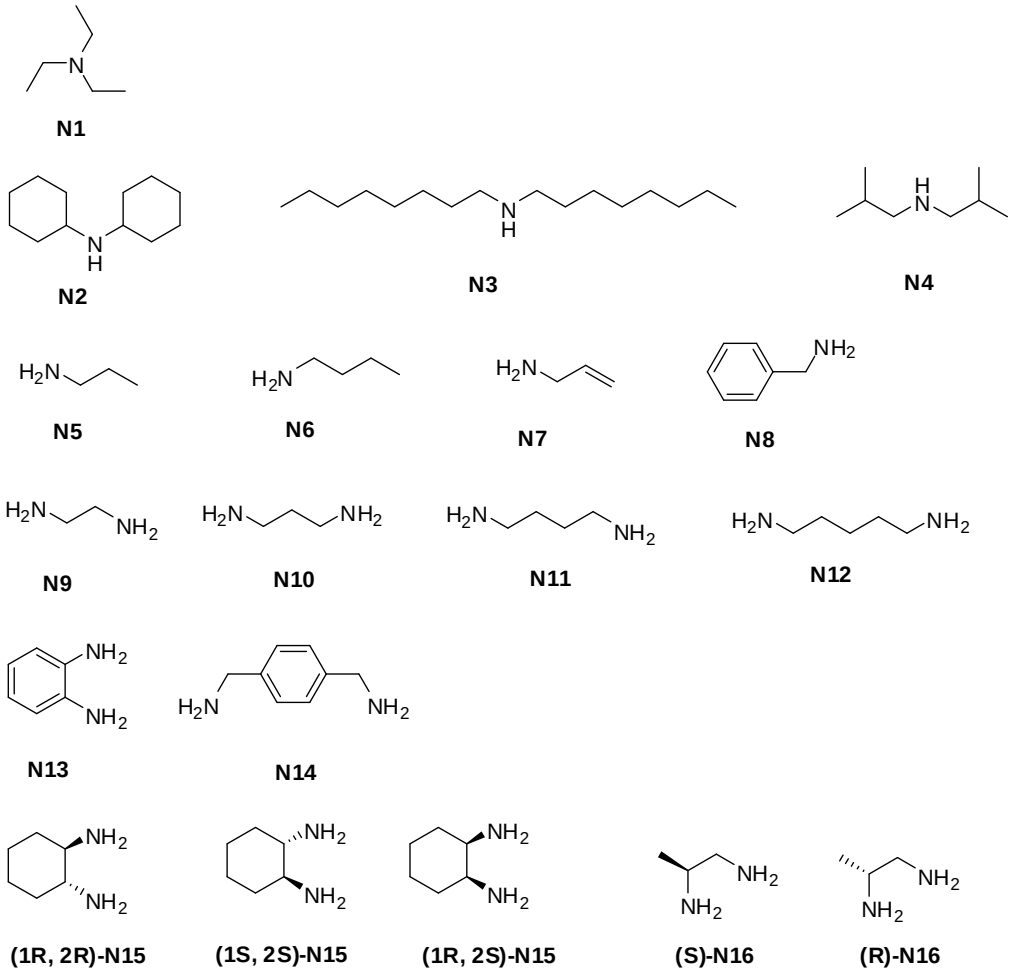

A. Fluorescence Study.

When (*S*)-**6-4** (1.0×10^{-5} M in CH_2Cl_2) was treated with various monoamines **N1-N8** (1.0×10^{-3} M), including tertiary, secondary and primary monoamines, very little change

in the fluorescence was observed (Figure 6-5a). When linear aliphatic diamines (**N9-N12**) were used under the same conditions, the fluorescence changed dramatically. Both 1,2-diaminoethane **N9** and 1,5-diaminopentane **N12** showed significant fluorescence enhancement and gave dual emission peaks with λ_1 = 370 nm and λ_2 = 438 nm for **N9** and λ_1 = 384 nm and λ_2 = 438 nm for **N12**. Both diamines enhanced the short wavelength emission more than long wavelength emission. In contrast, 1,3-diaminopropane **N10** and 1,4-diaminobutane **N11** displayed much smaller fluorescence enhancement which is approximately only 3% of **N9**. The aromatic diamine **N13** and the benzylic diamine **N14** didn't turn on the fluorescence at all.

We have compared the fluorescence responses of (*S*)-**6-4** toward the trans-cyclohexane-1,2-diamine [(*R,R*)-N**15,** (*S,S*)-N**15]** described in Chapter 5 with those toward the *meso-cis*-cyclohexane-1,2-diamine [(*S,R*)-N**15]**. As shown in Figure 6-5b, these three stereoisomers showed very interesting fluorescence enhancement. All three isomers turned on the fluorescence of (*S*)-**6-4** and showed dual emission at λ_1 = 370 and λ_2 = 438 nm but the fluorescence responses at the two emission wavelengths are different. (1*R*, 2*R*)-N**15** causes large fluorescence enhancement at both λ_1 and λ_2, in which one at λ_1 is smaller than λ_2. (1*S*, 2*S*)-N**15** enhances λ_1 greatly but much smaller at λ_2. The meso isomer (1*S*, 2*R*)-N**15** enhances λ_1 greatly and a little smaller at λ_2. Similarly, both enantiomers of chiral 1,2-diaminopropane **N16** cause significant fluorescence enhancement at both λ_1 and λ_2, in which (*R*)-**N16** enhances more at λ_2 than (*S*)-**N16** (Figure 6-5c) does.

Figure 6-5. Fluorescence spectra of (*S*)-**6-4** (1.0×10^{-5} M) in the presence of (a) various

achiral amines **N1-N14**, (b) three isomers of **N15** and (c) two enantiomers of **N16** (1.0×10^{-3} M). (λ_{exc} = 343 nm, slit = 2.0/2.0 nm).

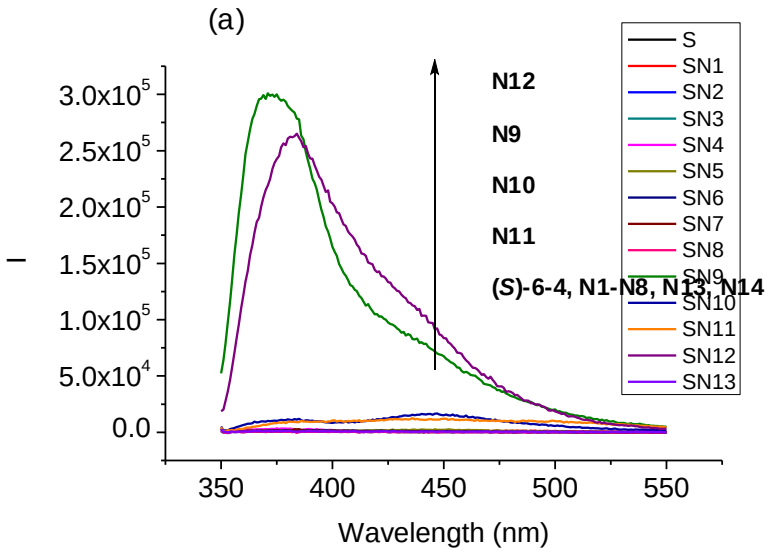

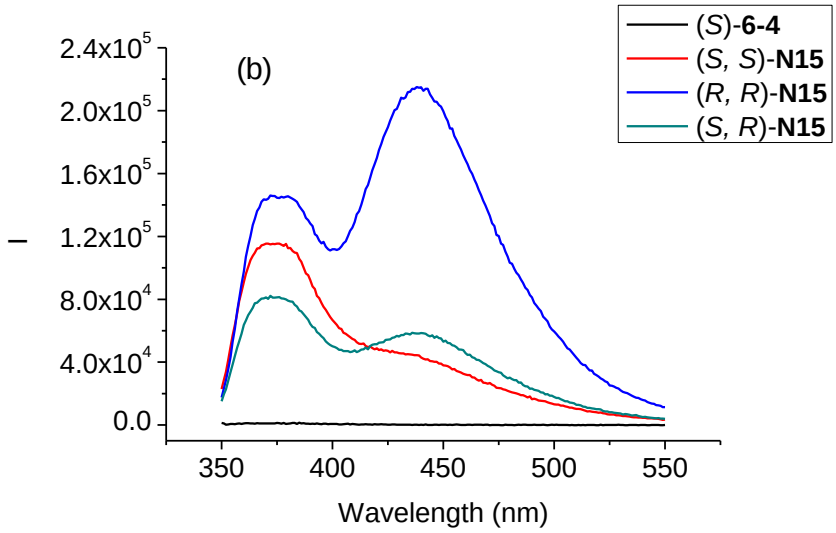

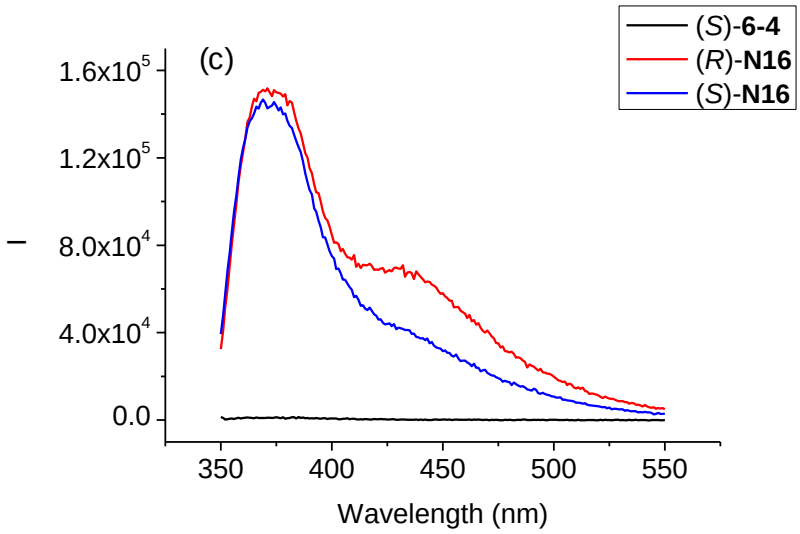

In Chapter 5, we described that the ratio of the fluorescence intensity of (*S*)-**6-4** at I_1 and I_2 (I_1/I_2) in the presence of *trans*-cyclohexanediamine only depends on the configuration of the enantiomer and is independent of the concentration. We also studied the effect of the concentration of *meso-cis*-cyclohexanediamine on I_1/I_2. As shown in Figure 6-6, similar to that observed for the enantiomers of *trans*-cyclohexanedimine, the I_1/I_2 remains constant (1.4) while the concentration of meso-cis-cyclohexanedimine varies. Therefore, using I_1/I_2 we can distinguish all the three stereoisomers of cyclohexanediamine.

Figure 6-6. Plots of I_1/I_2 for (*S*)-**6-4** (1.0×10^{-5} M) in the presence of varying concentrations of (*R,R*)- (*S, R*)- and (*S,S*) -**N15.** (Fluorescence intensity I_1 at λ_1 = 370 nm and I_2 at λ_2 = 438 nm. Solvent: CH_2Cl_2. λ_{exc} = 343 nm, slit = 2/2 nm.)

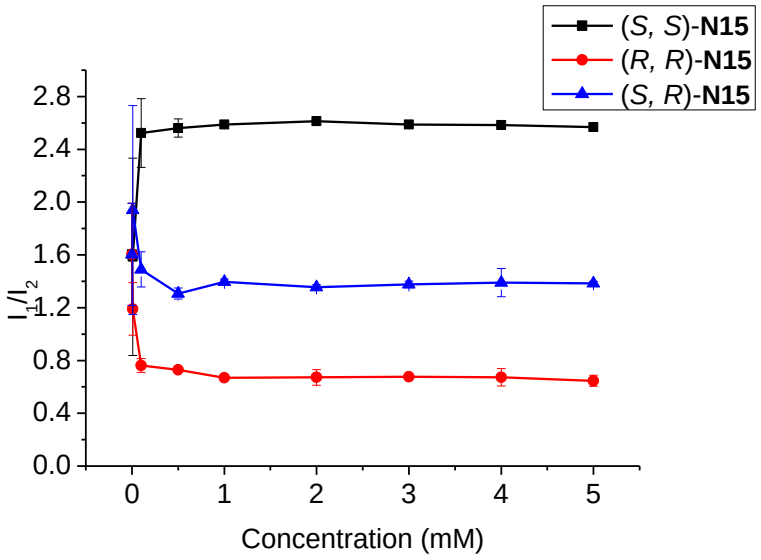

Similar study was also conducted on chiral diamine **N16** in the concentration range of 5.0×10^{-4} M to 5.0×10^{-3} M. As expected, (*S*)-**6-4** showed similar fluorescent responses when treated with **N16**. Figure 6-7a plots the fluorescent intensity of (*S*)-**6-4** at λ_1 versus increasing concentration of (*R*)- and (*S*)-**N16**. It shows that I_1 is strongly dependent on the concentration of the diamine but not significantly on its chiral configuration. Figure 2b plots the fluorescent intensity at λ_2 versus increasing concentration of (*R*)- and (*S*)-**N16** which shows significant enantioselectivity. We also found the I_1/I_2 ratio is nearly independent of the concentration and remains at 3.3-3.7 for (*S*)-**N16** and 2.3-2.1 for (*R*)-**N16** in the concentration range of 5.0×10^{-4} M to 5.0×10^{-3} M.

Figure 6-7. Plots of (a) I_1, (b) I_2 and (c) I_1/I_2 for (*S*)-**6-4** (1.0×10^{-5} M) in the presence of varying concentrations of (R)- and (S)-**N16**. (Fluorescence intensity I_1 at λ_1 = 370 nm and I_2 at λ_2 = 438 nm. Solvent: CH_2Cl_2. λ_{exc} = 343 nm, slit = 2/2 nm.)

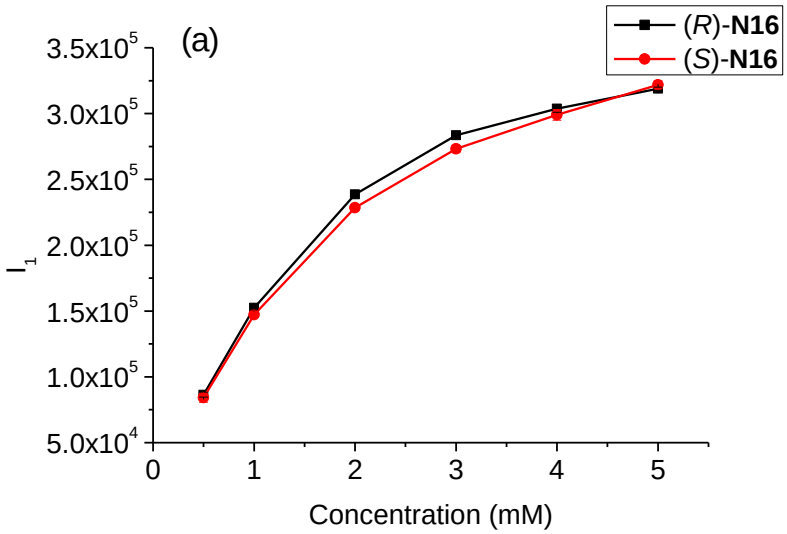
(a)
(*R*)-**N16**
(*S*)-**N16**
3.5x10^5
3.0x10^5
2.5x10^5
2.0x10^5
1.5x10^5
1.0x10^5
5.0x10^4
I1
0
1
2
3
4
5
Concentration (mM)

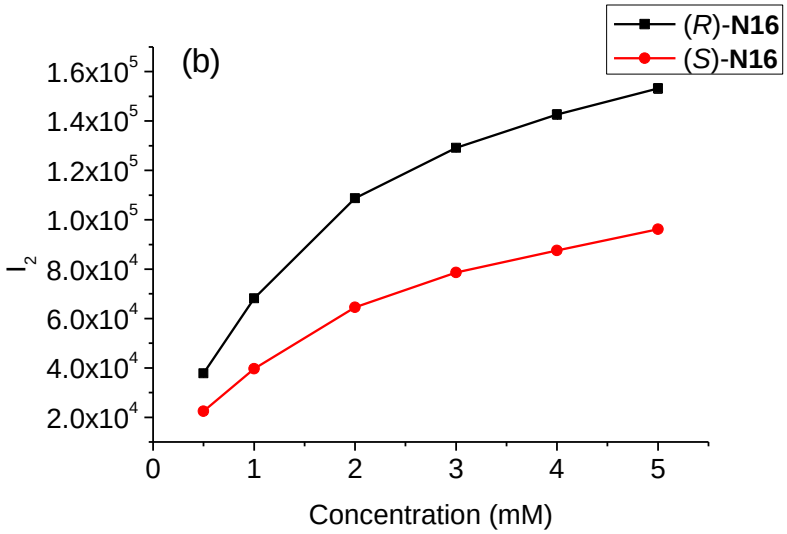
(b)
(*R*)-**N16**
(*S*)-**N16**
1.6x10^5
1.4x10^5
1.2x10^5
1.0x10^5
8.0x10^4
6.0x10^4
4.0x10^4
2.0x10^4
I2
0
1
2
3
4
5
Concentration (mM)

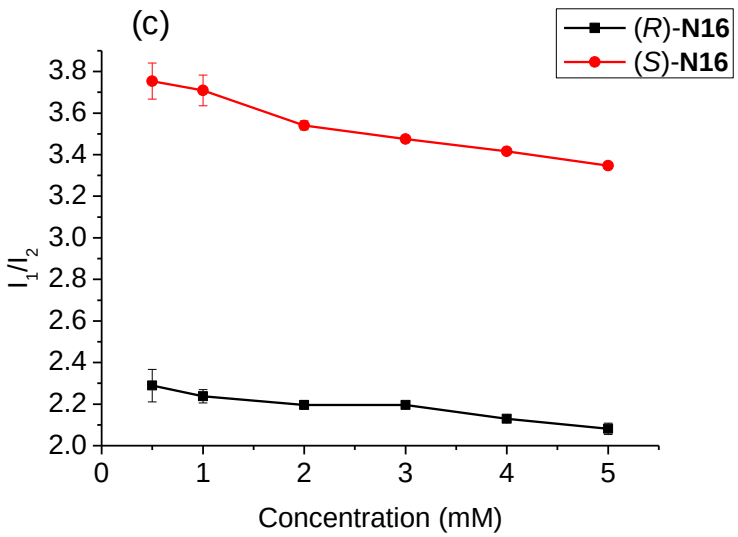

To better understand the dual emissions of (*S*)-**6-4** when treated with chiral diamines **N15** or **N16**, the excitation spectra were recorded for (*S*)-**6-4** (1×10^{-5} M) in the presence of (*R, R*)- and (*S, S*)-**N15** (4×10^{-3} M). As shown in Figure 6-8, both samples give the same excitation spectra with emissions at 370 or 438 nm, which means both emissions at 370 and 438 nm are from the same ground state species. Lifetimes were also measured and it is 1 ns for emission at 370 and 1.7 ns for emission at 438. The difference in lifetime indicates that the two emission peaks are from two different emitting states. Therefore, after (*S*)-**6-4** interacts with diamine, the resulting complex experiences excited state reactions and forms two different emitting species.

Figure 6-8. Excitation spectra of (*S*)-**6-4** (1.0×10^{-5} M, CH_2Cl_2) in the presence of (a) (*R, R*)- or (b) (*S, S*)-**N15** (4.0×10^{-3} M). (slit = 2.0/2.0 nm).

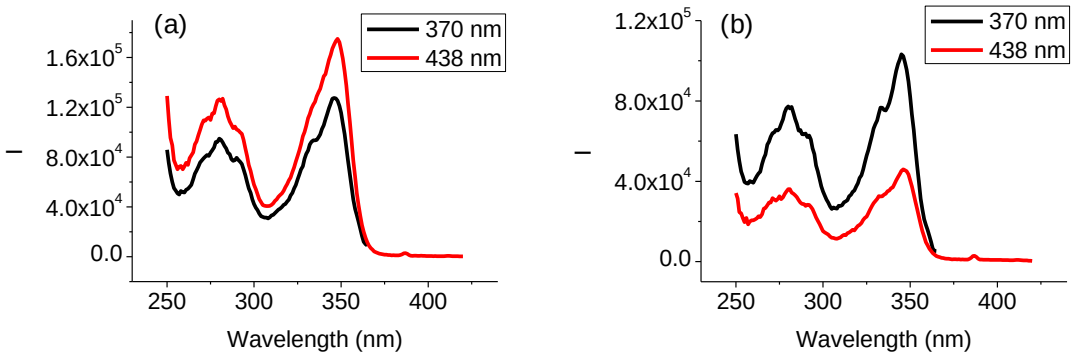

As shown in Figure 6-9, Job plots have been obtained for the interaction of (*S*)-**6-4** with **N9** and **N12** at a total concentration of 0.1 mM. For **N9** the fluorescence emission reached maximum at 30% of (*S*)-**6-4**, which indicates a 1:2 [(*S*)-**6-4**:**N9**] binding. However, for **N12**, the maximum fluorescence was shown at 50% of (*S*)-**6-4** and the fluorescence emission stayed high in the range of 30% -50% of (*S*)-**6-4**, which indicates more complicated binding mechanism. Both 1:1 and 1:2 [(*S*)-**6-4**:**N12**] bindings could exist in this system.

Figure 6-9. Job plot of (*S*)-**6-4** (1.0×10^{-5} M) with (a) **N9** and (b) **N12**. (total concentration = 0.1 mM, λ_{exc} = 343 nm, slit = 2.0/2.0 nm).

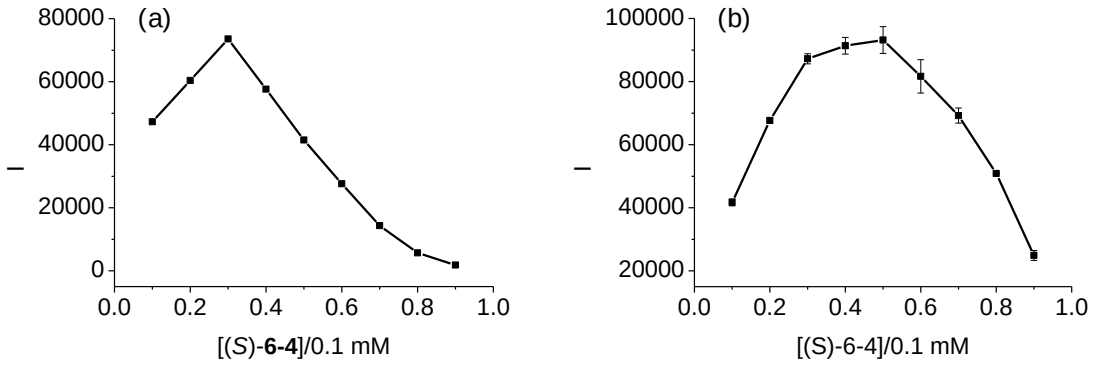

To better understand different fluorescence responses of (*S*)-**6-4** with monoamines and diamines, we recorded the fluorescence spectra of (*S*)-**6-4** (1.0×10^{-5} M in CH_2Cl_2) with propylamine (**N5**) at higher concentrations. As is shown in Figure 6-10, **N5** could not turn on the fluorescence of (*S*)-**6-4** at 0.001 M. However, as the concentration of N5 increased, (S)-6-4 started to show dual emissions at λ = 380 and 436 nm but the fluorescence intensities were still much lower than that with aliphatic diamines.

Figure 6-10. Fluorescence spectra of (*S*)-**6-4** (1.0×10^{-5} M in CH_2Cl_2) in the presence of propylamine **N5** at various concentrations (0 – 0.05 M). (λ_{exc} = 343 nm, slit = 2.0/2.0 nm).

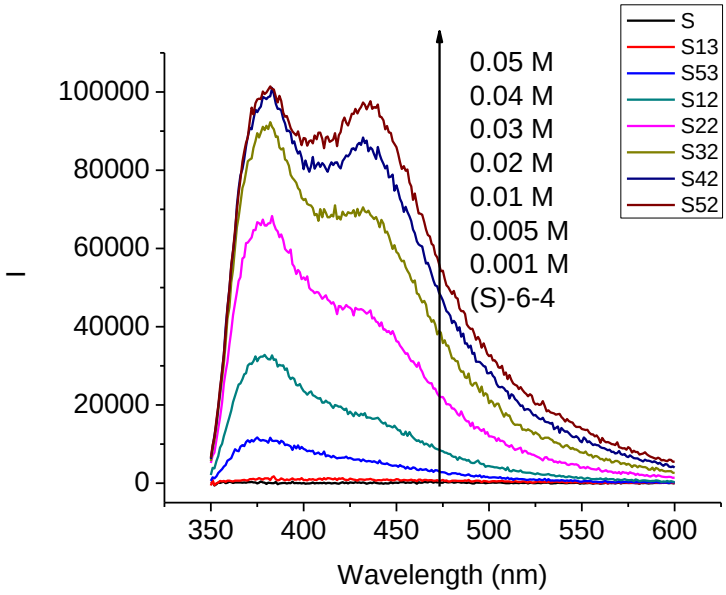

B. UV Study.

We have measured the UV-Vis absorption spectra of (*S*)-**6-4** (1.0×10^{-5} M), amines (1.0×10^{-3} M) and their mixtures. As shown in Figure 6-11, for **N1**-**N8** and **N13**-**N14**, the UV spectra of the mixtures are simple addition of those of (*S*)-**6-4** and amines, and the

amines don't change the absorption of (*S*)-**6-4** at all. The aliphatic diamines **N9**-**N12** and the three stereoisomers of **N15** caused similar changes to the UV absorption of (*S*)-**6-4**, including a significant decrease in the absorbance intensity at λ 263, 319 and 432 nm, an increase at 231 nm and the appearance of a new absorption peak at 345 nm. This indicates significant structural changes of (*S*)-**6-4** when interacted with the diamines.

Figure 6-11. UV spectra of (*S*)-**6-4** (1.0×10^{-5} M), amines (1.0×10^{-3} M) and their mixtures. (The black line represents UV absorption of (*S*)-**6-4**, the blue line represents amine and the red line represents the mixture.)

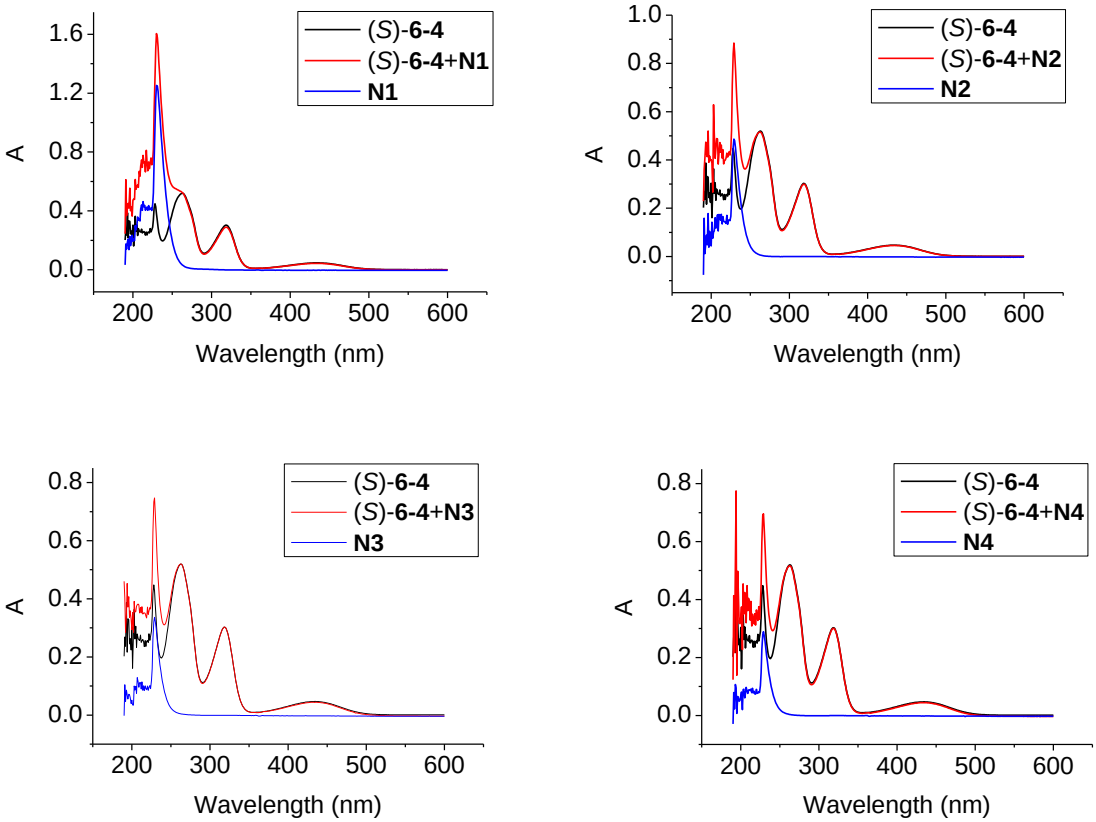

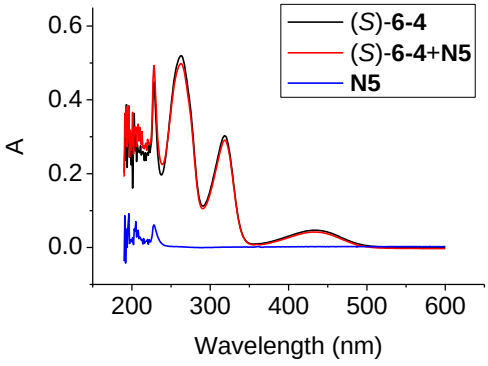
(S)-6-4
(S)-6-4+N5
N5
A
Wavelength (nm)

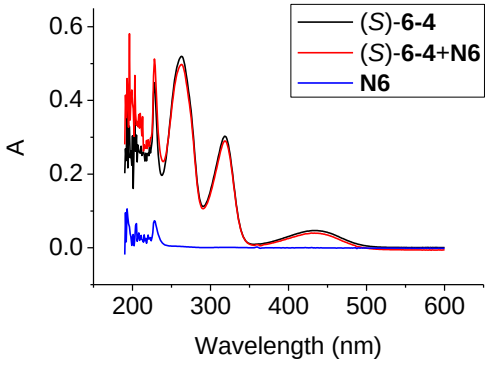
(S)-6-4
(S)-6-4+N6
N6
A
Wavelength (nm)

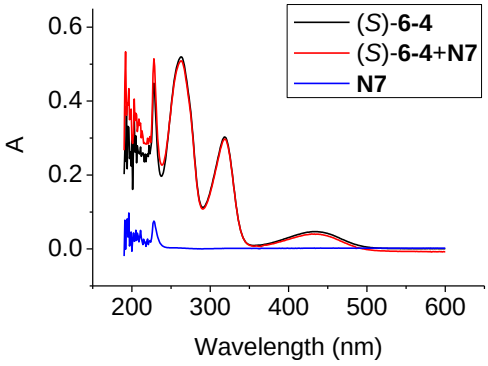
(S)-6-4
(S)-6-4+N7
N7
A
Wavelength (nm)

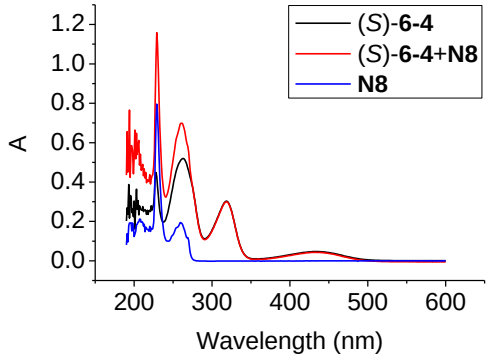
(S)-6-4
(S)-6-4+N8
N8
A
Wavelength (nm)

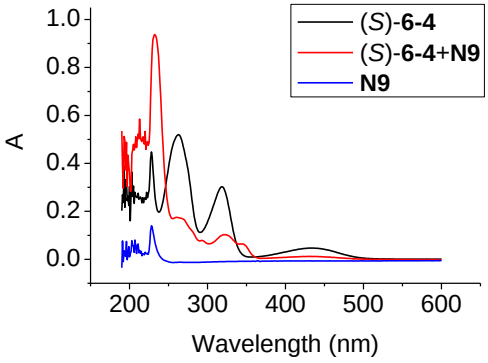
(S)-6-4
(S)-6-4+N9
N9
A
Wavelength (nm)

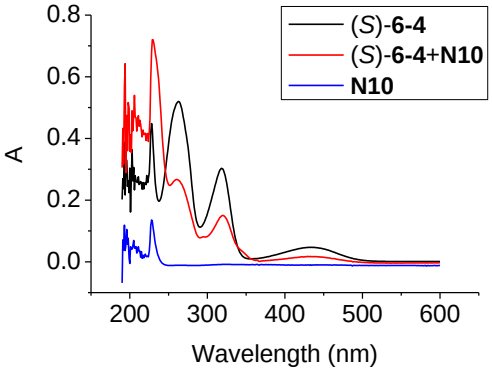
(S)-6-4
(S)-6-4+N10
N10
A
Wavelength (nm)

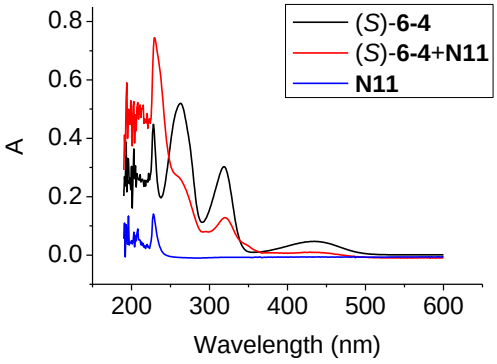
(S)-6-4
(S)-6-4+N11
N11
A
Wavelength (nm)

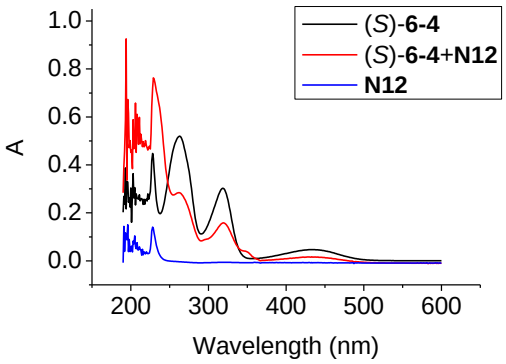
(S)-6-4
(S)-6-4+N12
N12
A
Wavelength (nm)

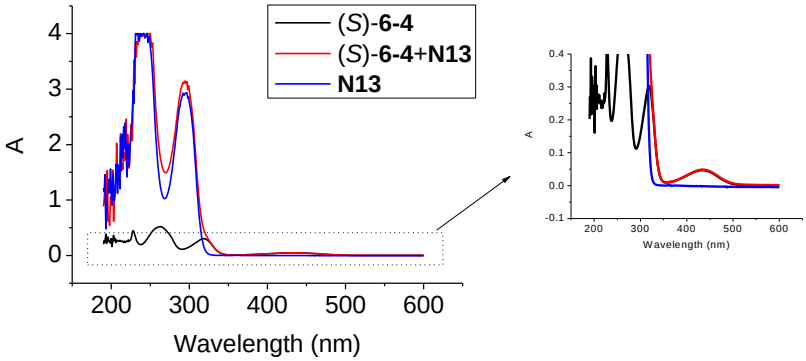
(S)-6-4
(S)-6-4+N13
N13
A
Wavelength (nm)

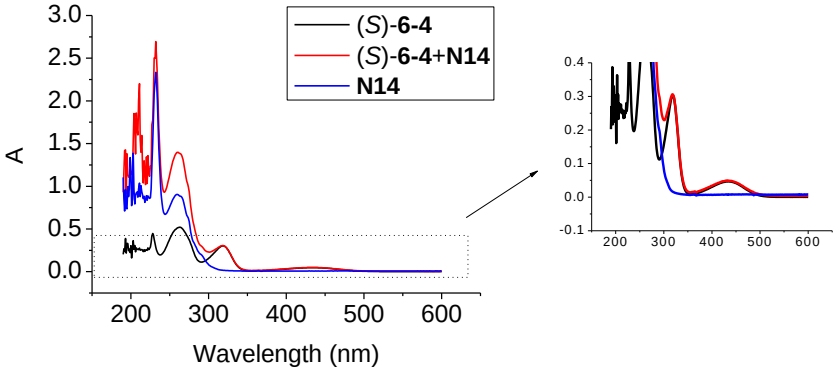
(S)-6-4
(S)-6-4+N14
N14
A
Wavelength (nm)

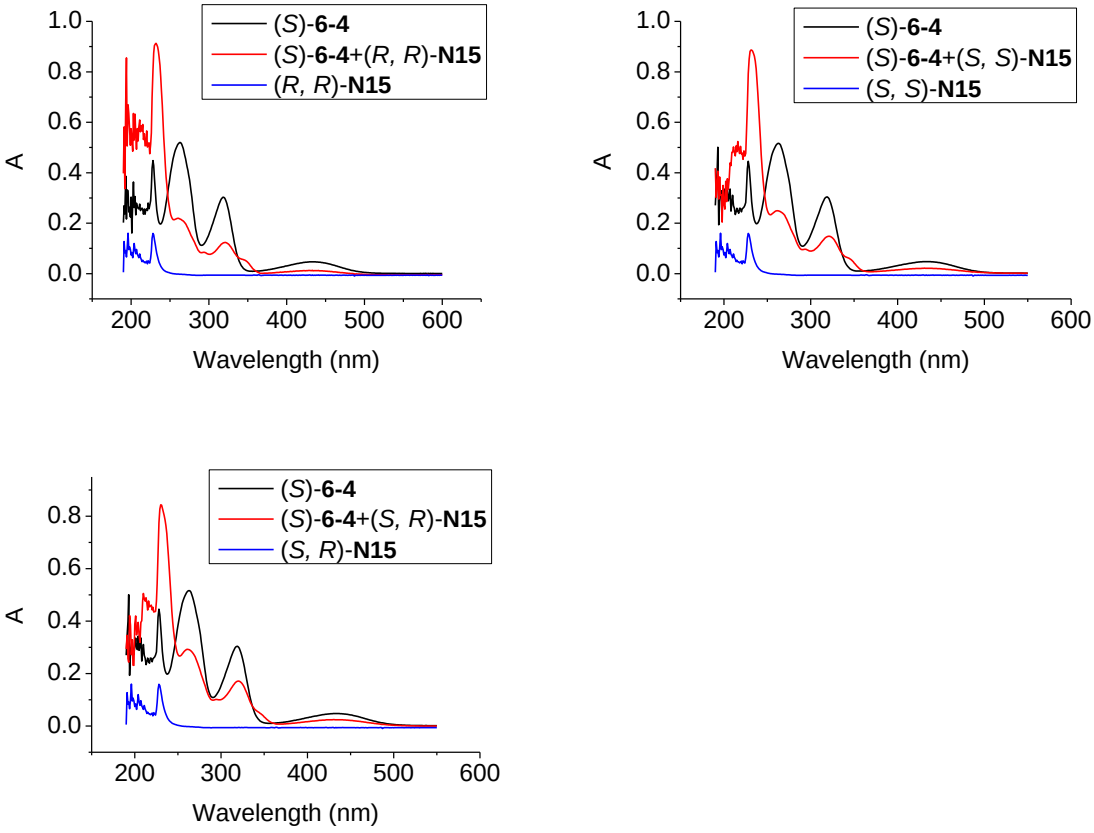

We further examined the UV absorption of (*S*)-**6-4** (1.0×10^{-5} M in CH_2Cl_2) with propylamine **N5** at higher concentrations. As is shown in Figure 6-12, at concentrations higher than 0.005 M, N5 started to cause similar changes to the UV absorption of (S)-6-4 as the aliphatic diamines. This observation, along with fluorescence study, suggests that monoamines and diamines could cause similar structural changes to (*S*)-**6-4** but much higher concentration is needed for the use of the monoamines.

Figure 6-12. UV-Vis absorption spectra of (*S*)-**6-4** (1.0×10^{-5} M in CH_2Cl_2) in the presence of propylamine **N5** at various concentrations (0 – 0.05 M).

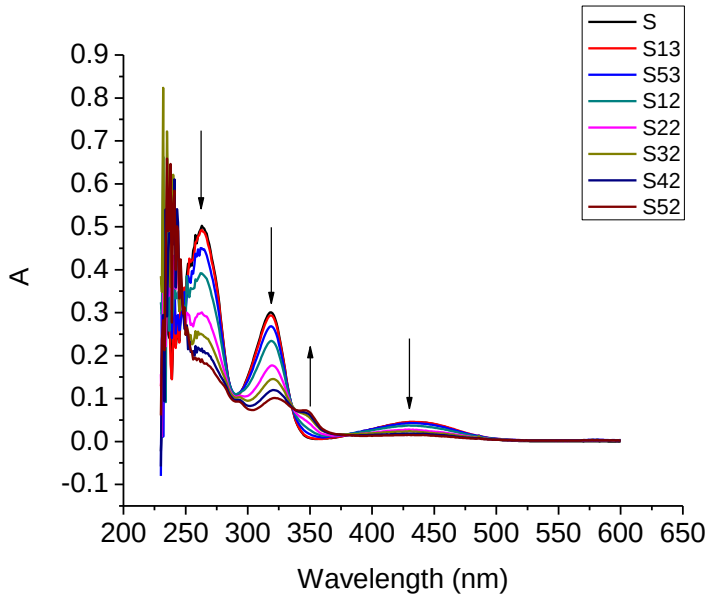

C. NMR Study.

In Chapter 5, we described the study of the ^{19}F NMR spectra of (*S*)-**6-4** in the presence of trans-cyclohexanediamine. We have further conducted a ^{19}F NMR titration of (*S*)-**6-4** with **N9**, **N12** and the meso isomer of **N15** in $CDCl_3$. The $CDCl_3$ solution of (*S*)-**6-4** (0.4 mL, 5.0 mM) was prepared in an NMR tube. The $CDCl_3$ solution of diamine (1 mL, 0.5 M) was prepared in a small vial as the stock solution. The NMR spectrum of the (*S*)-**6-4** was first recorded and the stock solution of the diamine was gradually added to the NMR tube. After each addition the solution was mixed well and the NMR spectra were recorded. In order to avoid the sensor being diluted with the addition of the diamine during the titration, a small amount of (*S*)-**6-4** (5.0 mM) was pre-added to the diamine solution.

(*S*)-**6-4** showed a singlet ^{19}F signal at δ -70.06. With addition of 0.2 eq **N9**, two peaks at δ -69.98 and -83.64 appeared with the same integration. These two new peaks kept

increasing while the signal at δ -70.06 decreased until addition of 0.8 eq **N9**. These two peaks were assigned to the monohemiaminal product (*S*)-**6-20**. After that a new peak at δ -83.53 started to show up and all other signals decreased until addition of 7.1 eq **N9** when all other signals converted to the peak at δ -83.53, which is assigned to the dihemiaminal product (*S*)-**6-21**. Further addition of amine generated new peaks at around δ -72.58 and -80.20, which were assigned to imine (*S*)-**6-22** and aminal (*S*)-**6-23** respectively. The signal at δ -72.58 remained at a low intensity all the time and the signal at around δ -80.20 increased while signal at δ -83.53 decreased. This indicates that once the hemiaminal is converted to imine, the imine is converted to the aminal quickly. After 108 eq of amine was added over 2 h, there was still an intense peak at δ -83.44. After overnight, the hemiaminal signal was significantly reduced while the aminal signal was increased, which indicated that the conversion from the hemiaminal (*S*)-**6-21** to the aminal (*S*)-**6-23** was slowly proceeding.

The NMR titration of (*S*)-**6-4** with **N12** showed more complicated chemical shift changes. With addition of 0.19 eq **N12**, a new peak at δ -83.81 appeared and the signal of (*S*)-**6-4** became a little broader, which became even broader and shifted upfield with more amine addition. With addition of 0.94 eq N12, two new peaks at δ -85.80 and -86.65 appeared. When amine addition increased to 5.3 eq, the broad peak completely disappeared and only three peaks at δ -83.80, -85.81 and -86.41 left. With even more amine added, the NMR spectrum started to become complicated.

The NMR titration of (*S*)-**6-4** with the three stereo isomers of **N15** exhibited responses similar to those by **N9** but with much slower reaction. When (*S*)-**6-4** was

titrated with cyclohexanediamine, only hemiaminal signals could be observed in the first several hours and the signals of imines and aminals started to show up after overnight.

Scheme 6-7. Proposed binding mechanisms.

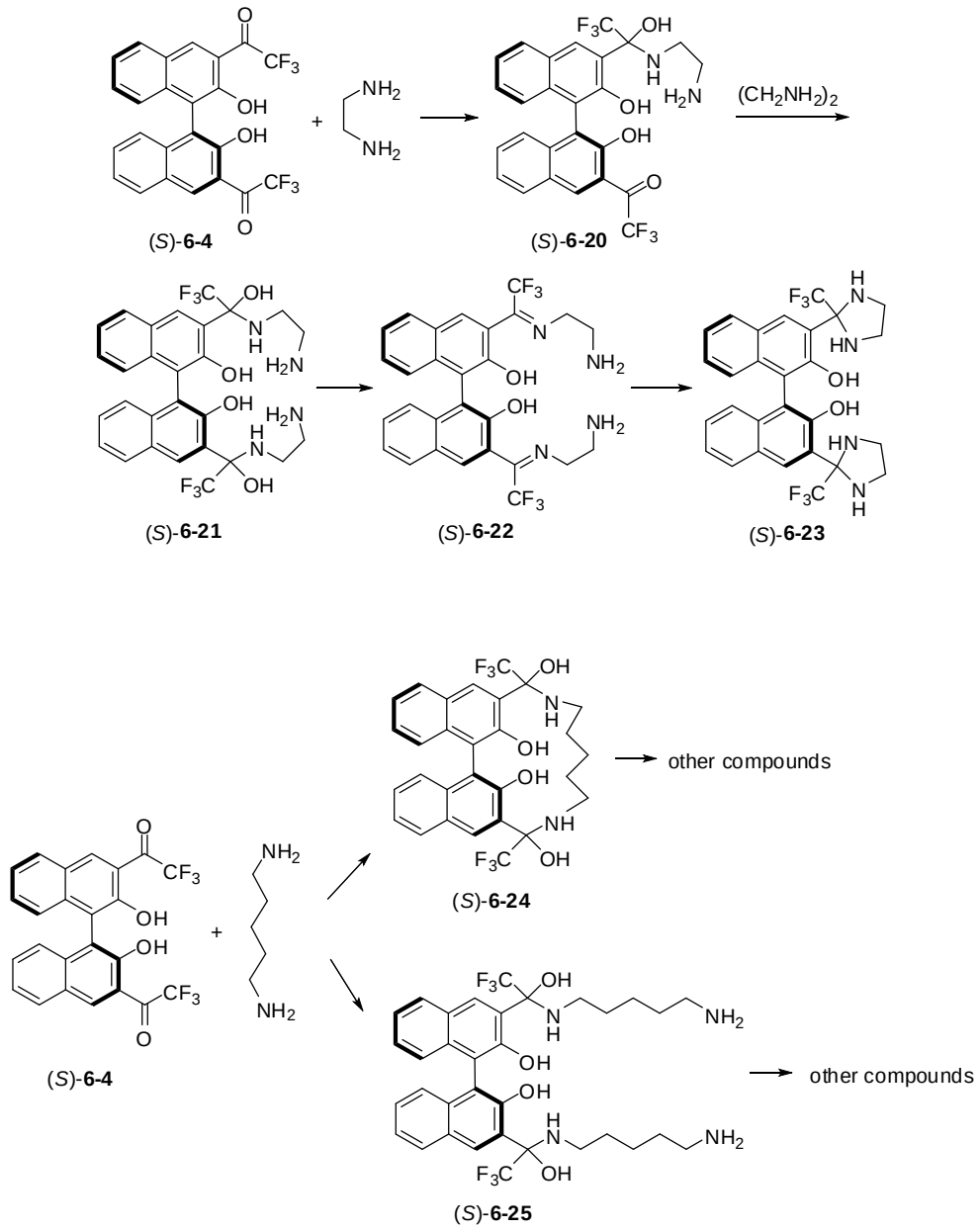

On the basis of the above observations, we propose the following binding mechanisms. The reaction of ethylenediamine (**N9**) with (*S*)-**6-4** is similar to that described for the reaction with trans-cyclohexanediamine in Chapter 5. As shown in Scheme 6-7, the 1,2-diamine favors 1:2 (ligand:diamine) binding and undergoes amine addition, water elimination and addition to imine to form an aminal of five-member ring. In contrast, the 1,5-diamine could form both 1:1 and 1:2 binding as indicated by its Job plot. One possible structure for the 1:1 adduct between 1,5-diaminopentane (**N12**) could be that generated from the addition to both of the $COCF_3$ group. Formation of oligomers is also possible.

The ^{19}F NMR titration of (*S*)-**6-16** with (*S, S*)-**N15** in $CDCl_3$ was also conducted. Similar to (*S*)-**6-4**, the fluorine signals were converting to a peak at -83.84 with addition of (S, S)-N15, which indicated that addition of amino group to carbonyl also happened for (*S*)-**6-16**.

We also conducted a ^{19}F NMR study for the reaction of (*S*)-**6-4** with propylamine. For the NMR study, a much higher concentration of (*S*)-**6-4** (5 mM) in $CDCl_3$ than that used in the fluorescence and UV experiments (10^{-5} M) was needed for the signal detection. However, at this high concentration, when (*S*)-**6-4** was treated with propylamine, the NMR spectrum showed the disappearance of the signal of (*S*)-**6-4** with formation of a very weak and broad signal. Sometimes formation of a yellowish precipitate could be observed. This indicates that the solubility of the addition product of (*S*)-**6-4** with propylamine is probably lower than the detection limit of the NMR experiments for characterization. In order to characterize the product for the reaction of

(*S*)-**4** with propylamine, we switched the solvent to DMSO-d_6 for the ^{19}F NMR titration of (*S*)-**4** with propylamine. In DMSO-d_6, the ^{19}F NMR spectrum of (*S*)-**6-4** showed multiple signals probably due to the reaction of the nucleophilic solvent and water molecules with the trifluoroacetyl groups of (*S*)-**6-4**. Addition of 20 equiv propylamine converted all the signals to a singlet at δ -81.51. The product was isolated and further characterized by ^{1}H/^{13}C NMR and mass spectroscopes as a hemiaminal compound (*S*)-**6-26**.

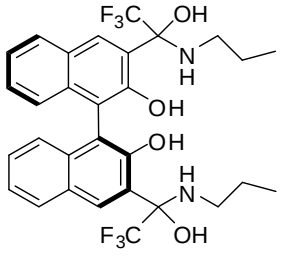

(*S*)-**6-26**

D. X-Ray Structures.

The crystals of the aminal product isolated from the reaction of (*S*)-**4** with (*S,S*)-N**15** were obtained by slow evaporation of its chloroform solution and were used for X-ray analysis. Crystals of the final addition products for the reactions of (*S*)-**4** with ethylenediamine **N9** and propylenediamine **N10** were obtained by mixing the sensor with the diamines in 1:10 ratio in chloroform followed by slow evaporation. The X-ray analyses of these crystals have confirmed their bis(cyclic aminal) structures (Figure 6-13). In these structures, intramolecular hydrogen bonding between the central hydroxyl groups and the nitrogen atoms of the aminal rings are observed.

Figure 6-13. X-ray structures of the complexes of (*S*)-**6-4** with (a) **N9**, (b) **N10** and (c) (*S*, *S*)-**N15**.

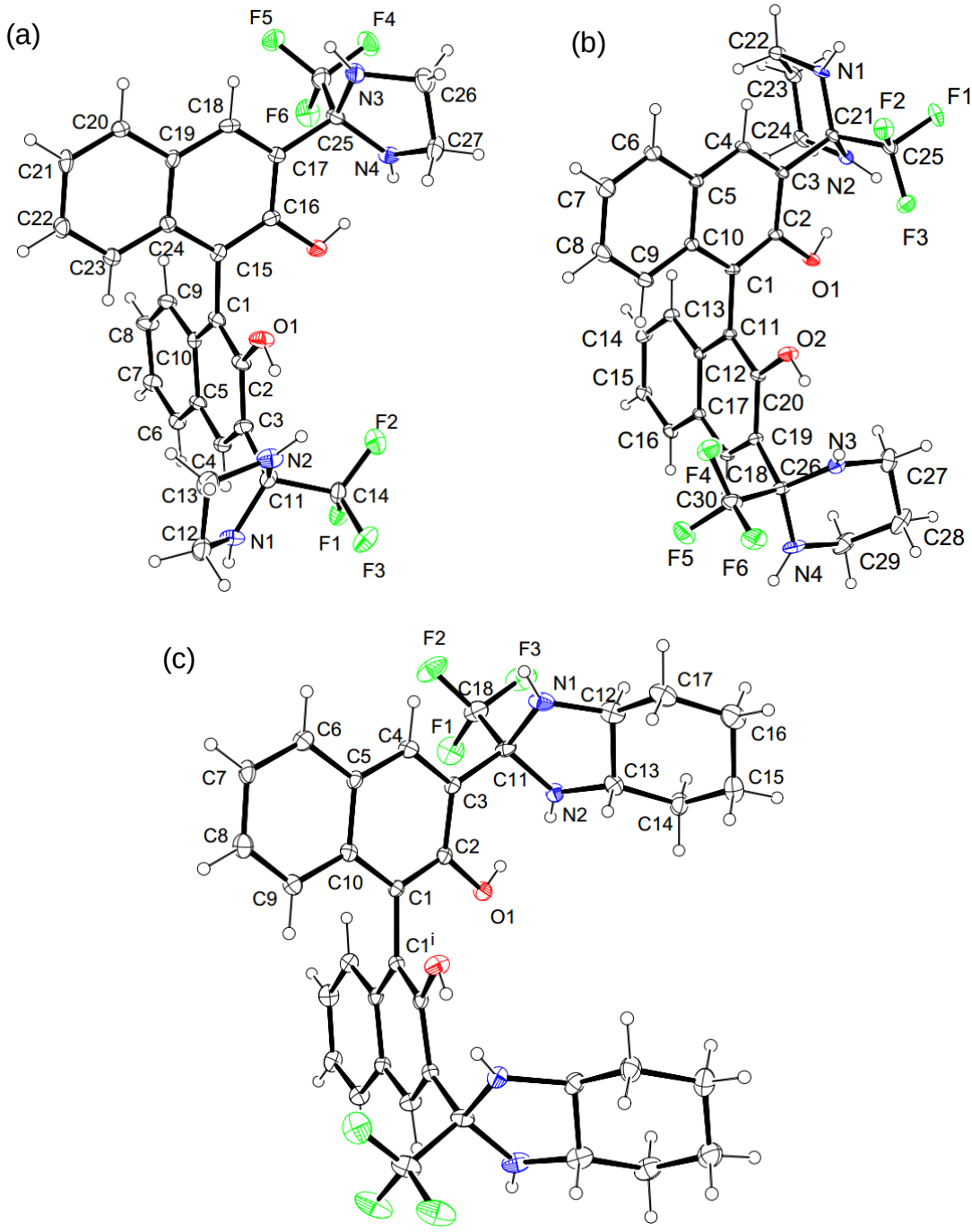

On the basis of the above observations for the interaction of (*S*)-**6-4** with various amines, we found that the reactions of (*S*)-**6-4** with the aliphatic primary diamines are much more facile than those with the primary monoamines, which lead to much greater fluorescence enhancement at lower concentration. The fluorescence responses of the sensor toward the 1,2-diamine and 1,5-diamine are much greater than those of the 1,3- and 1,4-diamines. As shown in Scheme 6-8, it is proposed that the intermolecular hydrogen bond as shown by (*S*)-**6-27** could facilitate the reaction with the 1,2-diamines. In the resulting compound such as (*S*)-**6-28**, the original hydrogen bond of O-H···O=C has been disrupted which could contribute to the fluorescence enhancement. That is, although the O-H···O=C hydrogen bonds of the sensor completely quench its fluorescence, the new O-H···N hydrogen bonds do not. In addition, the much greater fluorescence enhancement of the sensor caused by the 1,2-diamine than by propylamine could be further attributed to the formation of more rigid structures of (*S*)-**6-28** and (*S*)-**6-29** that contain multiple new hydrogen bonds of O-H···N. The interaction of the second amine group of ethylenediamine with the two central hydroxyl groups of the sensor could also explain the observed highly enantioselective fluorescent response in the presence of the chiral 1,2-diamines. When the 1,3- and 1,4-diamines are used, there may be greater ring strains for the hydrogen bonding interactions similar to those shown by (*S*)-**6-27** - (*S*)-**6-28**. Therefore, their fluorescence enhancements are much smaller. When the 1,5-diamine is used, the large fluorescence enhancement could be attributed to the formation of a compound like (*S*)-**6-24** where both carbonyl groups of the sensor could react with the amine to generate a rigid macrocyclic structure.

Scheme 6-8. A proposed mechanism for the reaction of (*S*)-**6-4** with ethylene diamine.

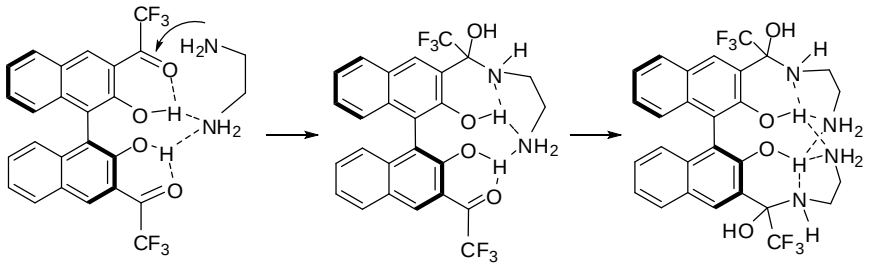

We have also isolated the final reaction product between (*S*)-**6-4** and (*R, R*)-**N15**, compound (*S, R, R*)-**6-30**. Figure 6-14 gives the fluorescent spectrum of this compound. It gives a maximum emission at 383 nm and the fluorescent intensity is much higher than those intermediates.

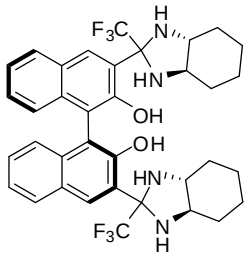

Figure 6-14. Fluorescence spectrum of (*S, R, R*)-**6-30** (1×10^{-5} M in CH_2Cl_2). (λ_{exc} = 343 nm, slit = 2.0/2.0 nm)

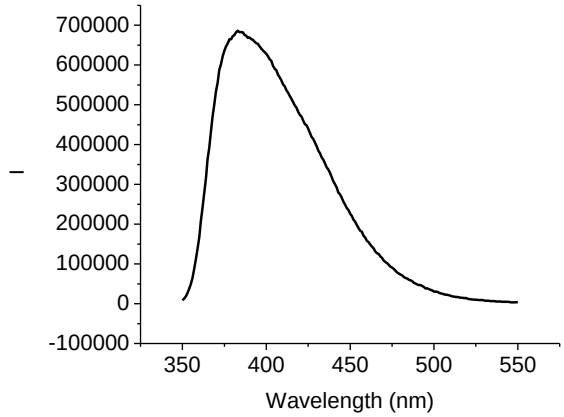

2.5 Interaction of the other analogs of (*S*)-6-4 with amines

The interactions of compounds (*R*)-**6-8**, (*S*)-**6-10**, (*S*)-**6-12** and (*S*)-**6-16** (1×10^{-5} M) with various amines in CH_2Cl_2 were also studied. The amines **N1**, **N2**, **N5**, **N9**, (*R, R*)- or (*S, S*)-**N15** were selected as typical examples of tertiary, secondary and primary amines, achiral and chiral diamines. As shown in Figure 6-15a, b, monoamines **N1**, **N2** and **N5** caused very little change to the fluorescence of the H_8BINOL analogue (*R*)-**6-8**. The diamines turned on the fluorescence of (*R*)-**6-8** with dual emissions. A low enantioselective fluorescence response was observed in the presence of (*R, R*)- and (*S, S*)-**N15** (Figure 6-15b). Thus, this compound could be used to sense the diamines but the sensitivity and enantioselectivity are much lower than those of (*S*)-**6-4**. The UV spectrum of (*R*)-**6-8** in the presence of 500 equiv of the chiral diamine RR- and SS-N15 showed little change (Figure 6-15c).

Figure 6-15. Fluorescence spectra of (*R*)-**6-8** in the presence of **N1**, **N2**, **N5**, **N9** (a), and (*R, R*)- or (*S, S*)-**N15** (b) (amine: 1.0×10^{-3} M). (λ_{exc} = 286 nm, slit = 2.0/2.0 nm). UV spectra of (*R*)-**6-8** in the presence of (*R, R*)- and (*S, S*)-**N15** (5×10^{-3} M) (c). (sensor: 1.0×10^{-5} M in CH_2Cl_2)

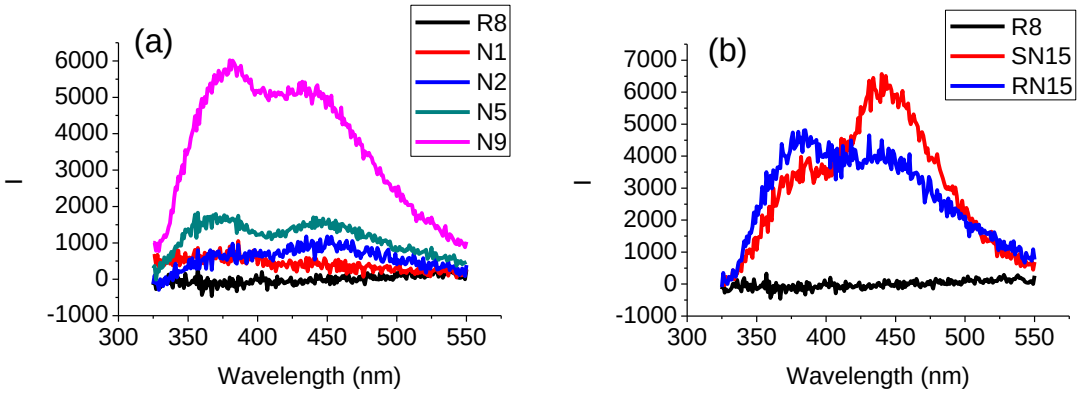

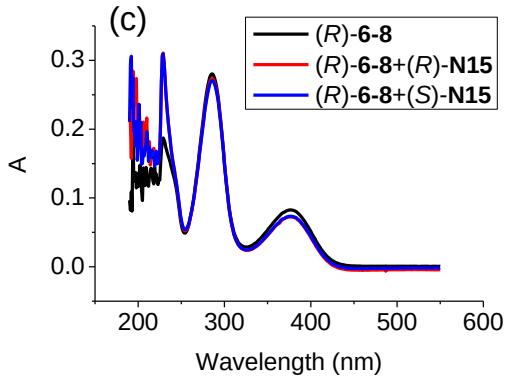

(*S*)-**6-10**, the BINOL-dialdehyde analogue, showed different fluorescence responses when treated with various amines. All of the tested monoamines and achiral diamines didn't turn on its fluorescence (Figure 6-16a). The chiral diamine **N15** caused enantioselective fluorescence enhancement with I_R/I_S = 2.6 at λ = 395 nm (Figure 6-16b). Figure 6-16c gives the UV absorption responses of (*S*)-**6-10** when treated with (*R, R*)- or (*S, S*)-**N15.** It shows that there were absorption increases at λ = 228, 256, 265, 293 and 304 nm, an decrease at λ = 405 nm, an new absorption at λ = 382nm.

Figure 6-16. Fluorescence spectra of (*S*)-**6-10** in the presence of **N1**, **N2**, **N5**, **N9** (a), and (*R, R*)- or (*S, S*)-**N15** (b). (λ_{exc} = 343 nm, slit = 2.0/2.0 nm). UV spectra of (*S*)-**6-10** in the presence of (*R, R*)- and (*S, S*)-**N15** (c). (sensor: 1.0×10^{-5} M in CH_2Cl_2. amine: 5.0×10^{-3} M)

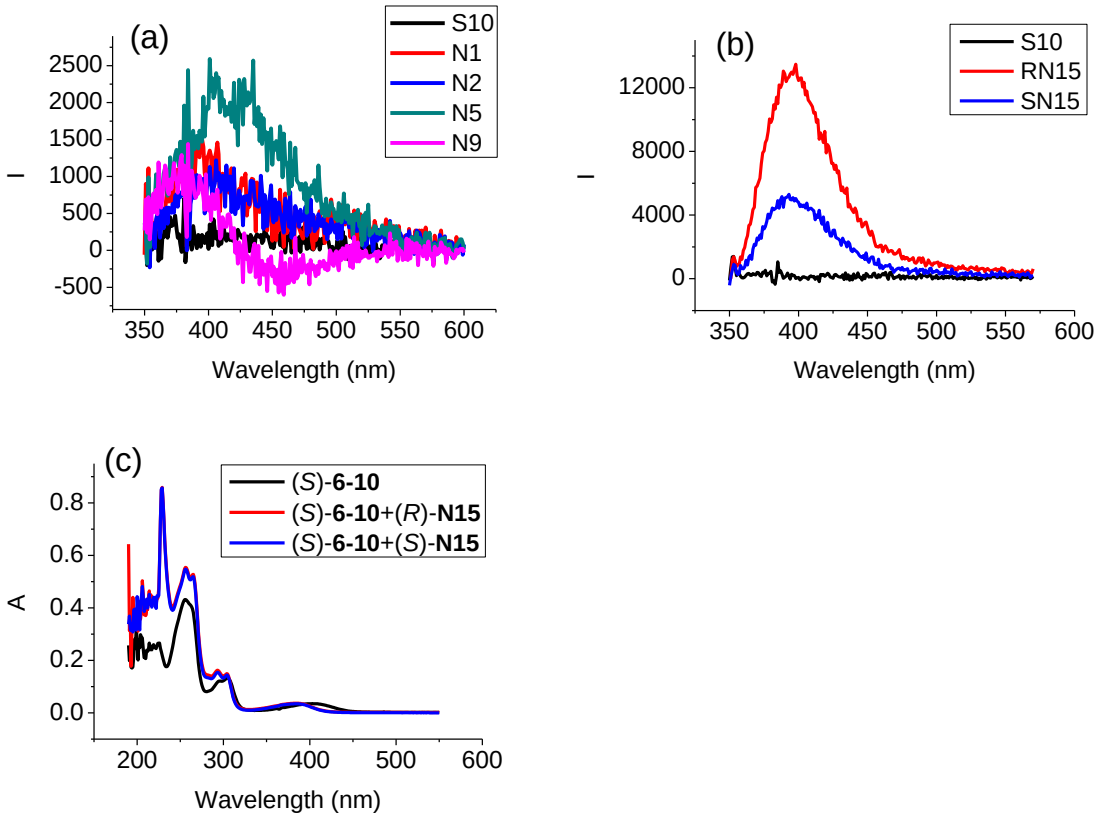

(*S*)-**6-12**, the BINOL-$COCHF_2$ analogue, showed similar fluorescence responses as (*S*)-**6-4** toward various amines (Figure 6-17). When its solution (1.0×10^{-5} M in CH_2Cl_2) was treated with (*R,R*)-**N15** (5.0×10^{-3} M), a dramatic fluorescent enhancement was observed with dual emissions at 385 (λ_1) and 438 (λ_2) nm with $I_1/I_2 = 0.64$. When (*S*)-**6-12** was treated with (*S,S*)-**N15**, a similar large fluorescence enhancement at λ_1 was also observed, but the fluorescence enhancement at λ_2 was much smaller with $I_1/I_2 = 1.47$. Therefore, it can serve as an alternative sensor for the enantioselective fluorescent recognition of the chiral diamines.

Figure 6-17. Fluorescence spectra of (*S*)-**6-12** (1.0×10^{-5} M in CH_2Cl_2) in the presence of **N1**, **N2**, **N5**, **N9**, (*R, R*)- or (*S, S*)-**N15** (5.0×10^{-3} M). (λ_{exc} = 343 nm, slit = 3.0/3.0 nm).

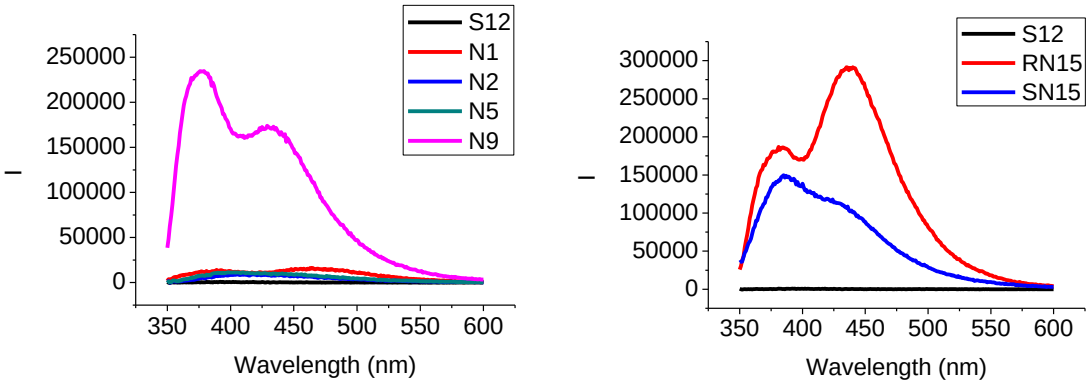

The 6, 6'-analogue (*S*)-**6-16** exhibited significant fluorescence quenching with all of the tested amines, in which chiral diamine **N15** quenched over 90% of its fluorescence with no enantioselectivity (Figure 6-18a,b). Since (*S*)-**6-16** does not have the intramolecular OH...O=C hydrogen bonds of (*S*)-**6-4**, it is strongly emissive. Therefore, the mechanism of fluorescence enhancement for (*S*)-**6-4** in the presence of **N15** to disrupte the intramolecular OH...O=C hydrogen bonds cannot operate with (*S*)-**6-16**. The 6,6'-positions of the two trifluoroacetyl groups of (*S*)-**6-16** also make it unlikely to form a cyclic rigid structure with **N15**. It was reported[16] that the fluorescence of BINOL can be quenched by amines in various solvents. Our observed fluorescence quneching of (*S*)-**6-16** by the amines appears to be much more efficient than that of BINOL by amines. It was proposed that the fluorescence quenching of BINOL by amines could be attributed to the formation of hydrogen bonded complexes between the BINOL hydroxyl groups and the amine nitrogen as well as the corresponding excited state proton transfer complex. The increased fluorescence quenching of (*S*)-**6-16** by the amines could be attributed to the increased acidity of the hydroxyl groups of (*S*)-**6-16** caused by the two electron-withdrawing 6,6'-trifluoroacetyl groups which should increase their interaction with the

amine bases. Figure 6-18c gives the UV responses of (*S*)-**6-16** when treated with R and S-**N15**. It shows an absorption increase at 228 nm, an decrease at 251, 279 and 323 nm, and an new absorption at 370 nm. No enantioselectivity is observed in the UV absorptions.

Figure 6-18. Fluorescence spectra of (*S*)-**6-16** in the presence of **N1**, **N2**, **N5**, **N9**, **N12 (a)**, and (*R*, *R*)- or (*S*, *S*)-**N15** (b) . (λ_{exc} = 343 nm. slit = 1.0/1.0 nm for **N1**, **N2**, **N5**, **N9** and **N12**. slit = 2.0/2.0 nm for (*R*, *R*)- or (*S*, *S*)-**N15**). UV spectra of (*S*)-**6-16** in the presence of (*R*, *R*)- and (*S*, *S*)-**N15** (c). (sensor: 1.0×10^{-5} M in CH_2Cl_2. amine: 5.0×10^{-3} M)

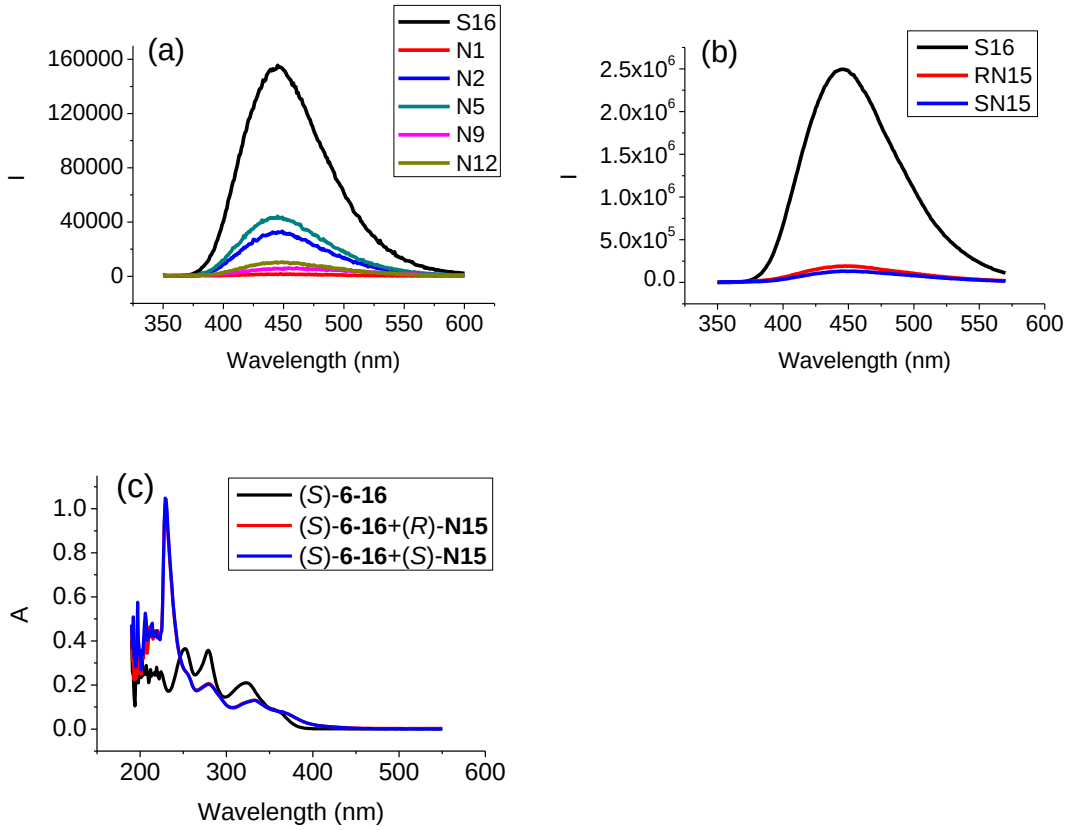

The MOM protected analogue (*S*)-**6-3** was also examined for the interaction with the chiral diamine (*R, R*)- and (*S, S*)-**N15** in CH_2Cl_2 (Figure 6-19). Without the intramolecular OH···O=C hydrogen bonds of (*S*)-**6-4**, (*S*)-**6-3** is also strongly emissive. Both enantiomers of **N15** caused a small (~10%) fluorescence quenching of (*S*)-**6-3** with no enantioselectivity. This demonstrates that the hydroxyl groups of (*S*)-**6-4** are essential for its highly sensitive fluorescence enhancement and excellent enantioselectivity. The UV spetrum of (*S*)-**6-3** showed little change in the presence of R or SN15 except an increase at l = 230 nm (Figure 6-19b).

Figure 6-19. (a) Fluorescence spectra of (*S*)-**6-3** in the presence of (*R, R*)- and (*S, S*)-**N15**. (λ_{exc} = 343 nm, slit = 2.0/2.0 nm). (b) UV spectra of (*S*)-**6-3** in the presence of (*R, R*)- and (*S, S*)-**N15**. (sensor: 1.0×10^{-5} M in CH_2Cl_2. amine: 5.0×10^{-3} M)

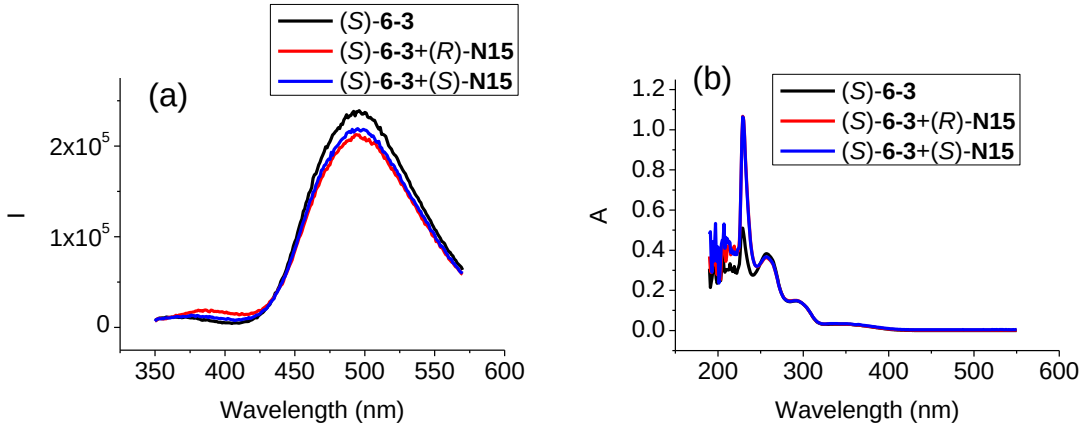

When the excitation wavelength was set to 290 nm, (*S*)-**6-3** showed dual emissions at 359 and 494 nm, in which the emission at 359 nm is much weaker than that at 494 nm (Figure 6-20). (*S*)-**6-16** also showed a shoulder peak at 359 nm after treatment with **N15**. We attribute the short wavelength emission to the locally excited state of binaphthol and

the long wavelength emission to internal charge shift state.

Figure 6-20. Fluorescence spectra of (*S*)-**6-3** (a) and (*S*)-**6-16** (b) in the presence of (*R*, *R*)- and (*S*, S)-**N15** (sensor: 1.0×10^{-5} M in CH_2Cl_2, amine: 5.0×10^{-3} M) (λ_{exc} = 290 nm, slit = 2.0/2.0 nm).

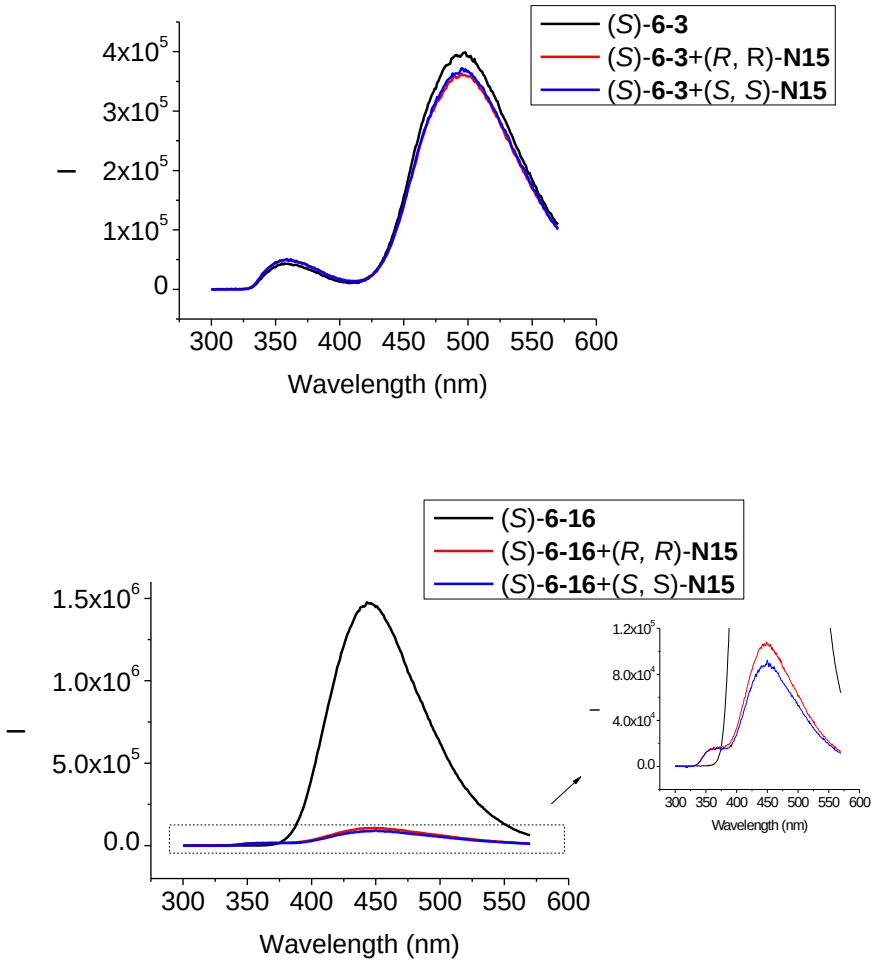

2.6 Interaction of (*S*)-6-4 with Tetrabutylammonium Salts of Amino Acids.

Interactions of (*S*)-**6-4** (1×10^{-5} M) with various amino acids (as tetrabutylammonium salts, 2.0×10^{-4} M) in CH_2Cl_2 were also studied. Figure 6-21 gives the fluorescence

spectra of (*S*)-**6-4** in the presence of the tetrabutylammonium salts of D- and L-amino acids. All of the tested amino acids turned on the fluorescence of (*S*)-**6-4.** The maximum emission of (*S*)-**6-4** located at 450 nm when treated with Ser, Ala, Val, Leu, Tyr and at 460 nm with Asp. Moreover, it showed enantioselectivity toward different enantiomers of amino acids with higher fluorescence intensity for the D-enantiomer. The ratios of I_D/I_L for tested amino acids were summarized in table 6-2.

Table 6-2. The ratio of I_D/I_L of tested amino acid salts. (I_D: the fluorescence intensity maximum of (*S*)-**6-4** when treated with D-amino acid salts. I_L: the fluorescence intensity at maximum of (*S*)-**6-4** when treated with L-amino acid salts.)

	Ser	Ala	Val	Leu	Asp	Tyr
I_D/I_L	2.0	1.9	2.8	1.6	3.2	1.5

Figure 6-21. Fluorescence spectra of (*S*)-**6-4** (1.0×10^{-5} M) in the presence of the tetrabutylammonium salts of D- and L-amino acids (2.0×10^{-4} M). (λ_{exc} = 343 nm, slit = 2.0/2.0 nm).

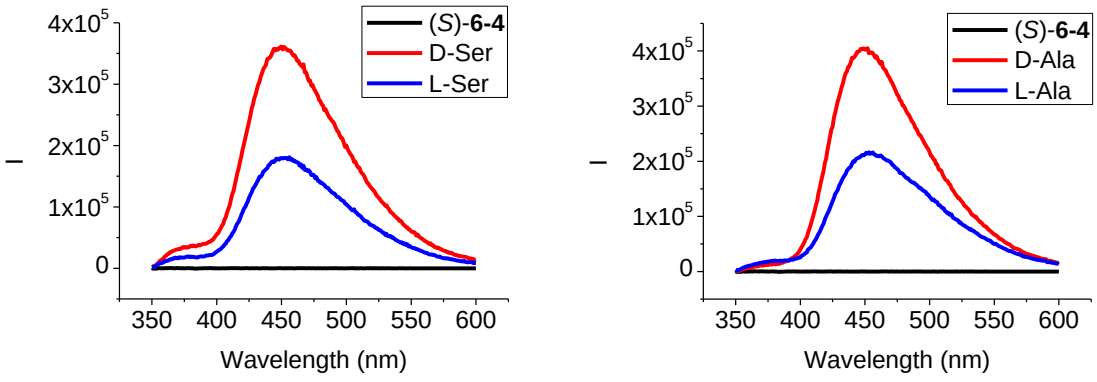

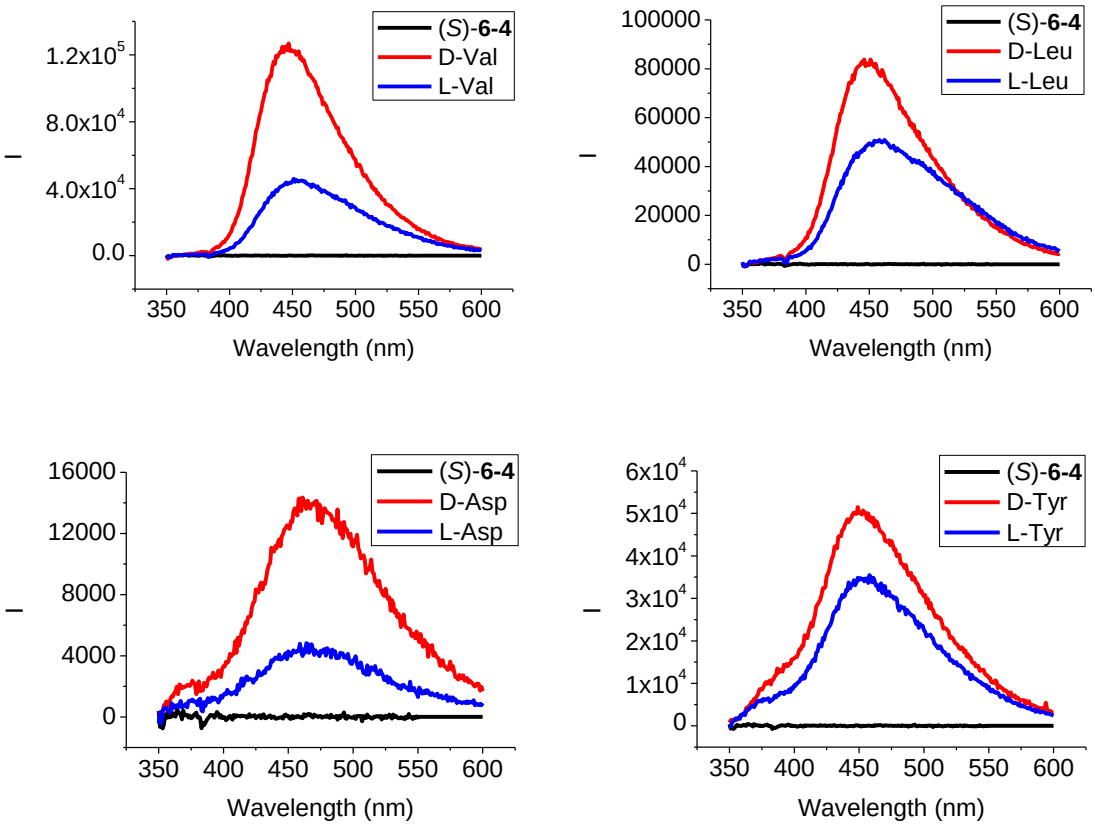

2.7 Interaction of (*S*)-6-4 with Chiral Amino Alcohols.

Interactions of (*S*)-**6-4** (1×10^{-5} M) with chiral amino alcohols **AA1**, **AA2** and **AA3** in CH_2Cl_2 were also studied. As shown in Figure 6-23, treatment with (*S*)-**AA1** turned on the fluorescence of (*S*)-**6-4** with maximum emission at 375 nm while (*R*)-**AA1** only caused very little change to the (*S*)-**6**-4 solution. The fluorescence intensity ratio I_S/I_R (I_S: the fluorescence intensity of (*S*)-**6-4** at 375 nm when treated with (*S*)-**AA**. I_R: the fluorescence intensity of (*S*)-**6-4** at 375 nm when treated with (*R*)-**AA**.) reached 13.4 when the concentration of **AA1** was 2.0 mM. Both enantiomers of **AA2** turned on the fluorescence of (*S*)-**6-4** and showed maximum emission at 375 nm. Similar to **AA1**, (*S*)-**AA2** enhanced the fluorescence of (*S*)-**6-4** more than (*R*)-**AA2** did, with I_S/I_R = 3.3 at

concentration 2.0 mM. When **AA3** was used, the ratio I_S/I_R reached 5.1 at concentration 5.0 mM. It was noted that treatment of (*R*)-**AA2** showed dual emissions at 375 nm and 425 nm. With addition of increasing concentration of (*R*)-**AA2**, the ratio of fluorescence intensities at these two wavelengths, $\lambda_{375}/\lambda_{425}$, was decreasing.

Time-dependent fluorescence was also monitored for the mixture of (*S*)-**6-4** with (*S*)-**AA1** and the fluorescence kept increasing even after overnight. Therefore, the reaction of (*S*)-**6-4** with amino alcohols was much slower than that with diamines. The spectra shown in Figure 6-23 were taken two hours after preparation. When amino alcohols with higher concentration were used, consistent fluorescent results could not be obtained, which make it difficult for this sensor to be used in quantitative measurement.

Figure 6-22. Structures of tested chiral amino alcohols.

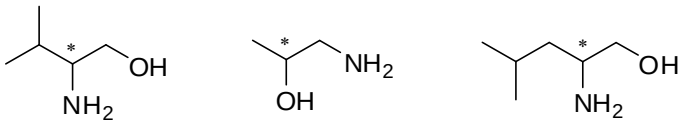

AA1 **AA2** **AA3**

Figure 6-23. Fluorescence spectra of (*S*)-**6-4** (1.0×10^{-5} M, in CH_2Cl_2) in the presence of chiral amino alcohols (2.0×10^{-4} M) and the maximum emission change with increasing concentrations. (λ_{exc} = 343 nm, slit = 2.0/2.0 nm).

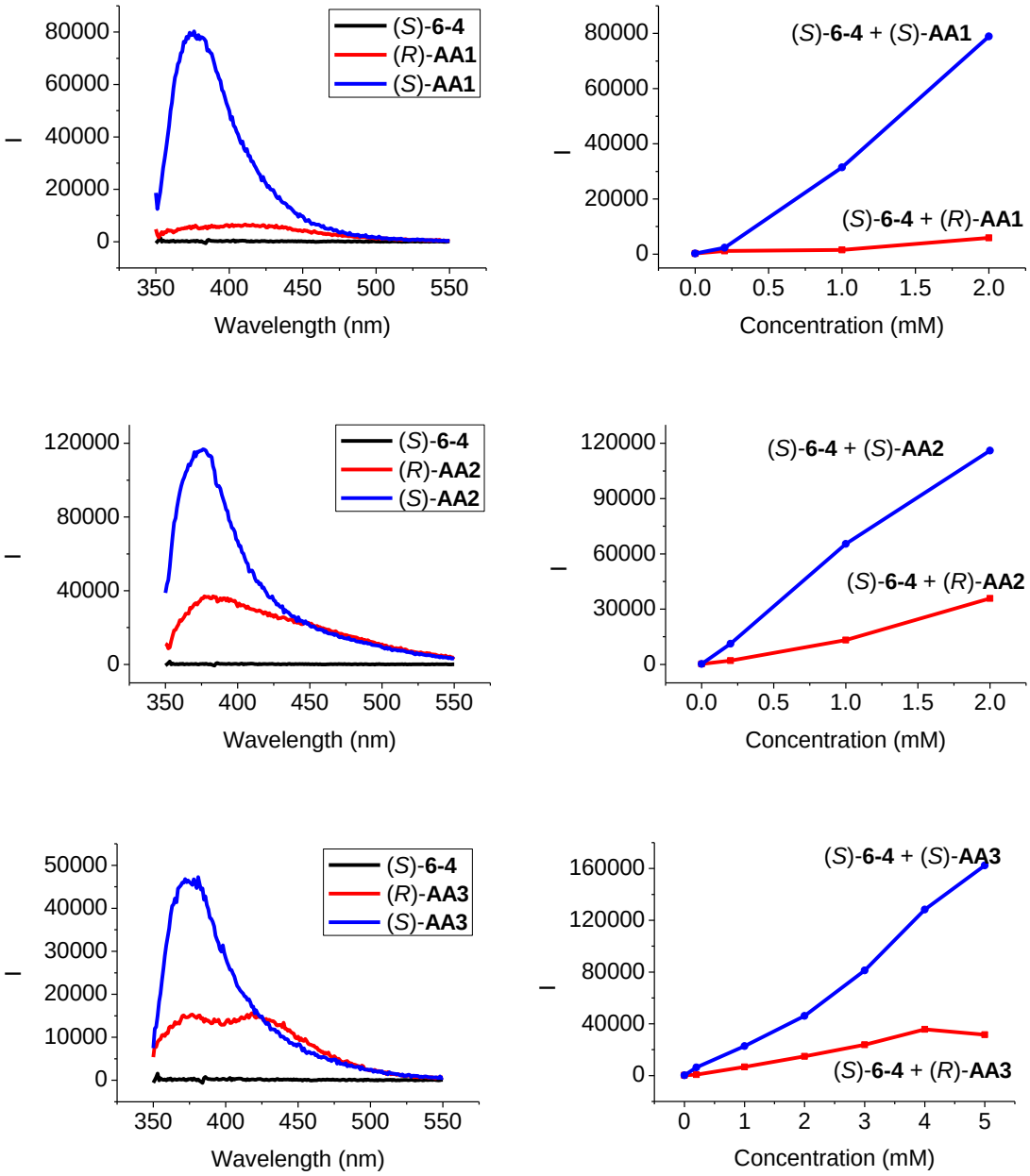

3. Conclusion

We have synthesized and studied a series of BINOL-dicarbonyl compounds for fluorescent recognition. This study reveals that the intramolecular hydrogen bonds between the BINOL hydroxyl groups and the carbonyl units of these compounds can turn

off the fluorescence of the BINOL unit. Binding with nucleophilic substrates transforms the original hydrogen binding and turns on the fluorescence. Formation of more rigid structures with the substrates further enhances the fluorescence. (*S*)-**6-4** was proved to be a general enantioselective fluorescent sensor for a variety of substrates with two nucleophilic groups, such as diamines, amino carboxylates and amino alcohols. Some analogs of (*S*)-**6-4**, such as compounds (*R*)-**6-10** and (*S*)-**6-12**, also exhibit enantioselective fluorescent responses in the interaction with chiral diamines. Therefore, the BINOL-dicarbonyl compounds represent a promising class of enantioselective fluorescent sensors for functional chiral amines.

4. Experimental Section

4.1 General Data:

All reactions were carried out under nitrogen unless otherwise noted. All chemicals were purchased from Sigma Aldrich Chemical Co. or Alfa Aesar. THF was distilled over sodium and benzophenone under nitrogen atmosphere. Methylene chloride and diethyl ether were dried by passing through activated alumina columns under nitrogen. Solvents were stored over 4 Å molecular sieves.

Melting points were uncorrected and obtained on a Mel-Temp II capillary melting point apparatus. Optical rotations were measured on a Jasco P-2000 digital polarimeter. NMR spectra were recorded on a Varian-300 MHz or Bruker-600 MHz spectrometer. Chemical shifts for ^{1}H NMR spectra were reported in parts per million relative to a singlet at 7.26 ppm for deuterated chloroform. Chemical shifts for ^{13}C NMR were

reported relative to the centerline of a triplet at 77.16 ppm for deuterated chloroform. The ^{19}F NMR spectra were reported in units of part per million (ppm) relative to trifluoroacetic acid (δ -76.55 ppm) as an external reference. High resolution mass spectra were obtained from the University of Illinois at Urbana-Champaign (UIUC) Mass Spectrometry Facility. UV-Vis spectra were recorded on a Hewlett-Packard 8452A diode-array spectrophotometer. Steady-state fluorescence emission spectra were recorded on a Horiba FluoroMax-4 spectrofluorometer.

4.2 Preparation of Samples for Fluorescence Measurement.

Materials: Sensors were purified by column chromatography followed by recrystallization and then stored in a refrigerator. All of the tested amines were purchased and redistilled. All of the solvents were either HPLC or spectroscopic grade. The stock solutions of the sensors and amines were freshly prepared for each measurement. For the fluorescence study, a sensor solution was mixed with the amine solution at room temperature in a 5 mL volumetric flask and diluted to the desired concentration. The resulting solution was allowed to stand at room temperature for 0.5 h before the fluorescence measurement and all the fluorescence spectra were taken within 2 hours.

4.3 Synthesis and Characterization of Compounds

Synthesis and Characterization of (S)-6-2.[17] Under nitrogen, (*S*)-1,1'-binaphthyl-2,2'-diol, (*S*)-**6-1** (17.5 mmol, 5.0 g), was dissolved in THF (200 mL). The solution was cooled to 0 ℃, and NaH (43.75 mmol, 60% in mineral oil, 1.75 g) was added in small portions. The reaction mixture was stirred for 15 min and then chloromethyl methyl ether (43.75 mmol, 3.3 mL) was added slowly. The reaction mixture was allowed to warm to

room temperature and stirred for 1 h. Water was added slowly to quench the reaction. The organic layer was separated, and the aqueous layer was extracted with ethyl acetate (three 30 mL aliquots). The combined organic extracts were washed with brine, and dried over Na_2SO_4. After evaporation of the solvent, the residue was purified by column chromatography on silica gel eluted with hexane/ethyl acetate (15/1) to afford compound (*S*)-**6-2** as a white solid in 95% yield (16.6 mmol, 6.22g). ^{1}H NMR (300 MHz, $CDCl_3$) δ 3.15 (s, 6H), 4.98 (d, J = 6.9 Hz, 2H), 5.09 (d, J = 6.6 Hz, 2H), 7.14-7.25 (m, 4H), 7.32-7.37 (m, 2H), 7.58 (d, J = 9.3 Hz, 2H), 7.88 (d, J = 8.1 Hz, 2H), 7.96 (d, J = 9.0 Hz, 2H).

Synthesis and Characterization of (S)-6-3. Under nitrogen, 2,2'-bis-methoxymethyl-1,1'-binaphthyl, (*S*)-**6-2** (3.0 mmol, 1.12 g), was dissolved in diethyl ether (36 mL). The solution was cooled to 0 ℃, and n-BuLi (12.0 mmol, 2.5 M in hexane, 4.8 mL) was added dropwise. The reaction mixture was stirred for 2 h at room temperature and cooled to 0 ^{0}C, and then ethyl trifluoroacetate (13.5 mmol, 1.6 mL) was added slowly. The reaction mixture was allowed to warm to room temperature and stirred for 1 h to afford a cream-like mixture. A saturated aqueous NH_4Cl solution was added to quench the reaction. The organic layer was separated, and the aqueous layer was extracted with ethyl acetate (three 20 mL aliquots). The combined organic extracts were washed with brine, and dried over Na_2SO_4. After evaporation of the solvent, the residue was purified by column chromatography on silica gel eluted with hexane/methylene chloride (1/3) to afford compound (*S*)-**2** as a yellow oil in 62% yield (1.86 mmol, 1.05 g). ^{1}H NMR (300 MHz, $CDCl_3$) δ 2.77 (s, 6H), 4.73 (d, J= 6.3 Hz, 2H), 4.77 (d, J= 6.3 Hz, 2H), 7.25 (d, J = 8.7 Hz, 2H), 7.44-7.50 (m, 2H), 7.53-7.58 (m, 2H), 8.05 (d, J = 8.1 Hz, 2H), 8.43 (s, 2H).

^{19}F NMR (282 MHz, $CDCl_3$) δ -73.62. ^{13}C NMR (75 MHz, $CDCl_3$) δ 56.6, 100.7, 116.5 (q, J = 290 Hz), 126.4, 126.8, 126.9, 127.0, 129.6, 129.8, 130.1, 132.7, 136.2, 151.6, 182.4 (q, J = 35.6 Hz). HRMS Calcd for $C_{28}H_{20}O_6F_6Na$ (MNa^+): 589.1062, Found: 589.1053. $[\alpha]_D$ = -18.056 (c = 0.590, $CHCl_3$).

Synthesis and Characterization of (S)-6-4. After compound (*S*)-**6-3** (0.25 mmol, 134.2 mg) was dissolved in a minimum amount of CH_2Cl_2, trifluroacetic acid (1.0 mL) was added slowly, and the mixture was stirred at room temperature for 10 min. A saturated aqueous $NaHCO_3$ solution was added to quench the reaction. The organic layer was separated, and the aqueous layer was extracted with CH_2Cl_2 (3 x 20 mL). The combined organic extracts were washed with brine, and dried over Na_2SO_4. After evaporation of the solvent, the residue was purified by column chromatography on silica gel eluted with hexane/methylene chloride (2/1) to afford compound (*S*)-**6-4** as an orange solid in 84% yield (0.21 mmol, 100 mg). ^{1}H NMR (300 MHz, $CDCl_3$) δ 7.16 (d, J = 7.5 Hz, 2H), 7.41-7.51 (m, 4H), 8.02 (d, J = 7.5 Hz, 2H), 8.70 (s, 2H), 10.51 (s, 2H). ^{19}F NMR (282 MHz, $CDCl_3$) δ -70.06. ^{13}C NMR (150 MHz, $CDCl_3$) δ 115.2, 116.7 (q, J = 289.5 Hz), 117.8, 124.7, 125.3, 127.2, 131.2, 132.2, 136.1 (q, J = 3.75 Hz), 138.5, 155.0, 185.1 (q, J = 36.0 Hz). HRMS Calcd for $C_{24}H_{13}O_4F_6$ (MH^+): 479.0718, Found: 479.0719. m.p. 231 ^{0}C. $[\alpha]_D$ = -167.50 (c = 0.355, $CHCl_3$).

Synthesis and Characterization of (*R*)-6-6.[18] Under nitrogen, (*R*)-5,5',6,6',7,7',8,8'-octahydro-1,1'-binaphthyl-2,2'-diol (H_8BINOL), (*R*)-**6-5** (25 mmol, 7.4 g), was dissolved in THF (300 mL). The solution was cooled to 0 ℃, and NaH (62.8 mmol, 60% in mineral oil, 2.52 g) was added in small portions. The reaction mixture was stirred for 30

min and then chloromethyl methyl ether (62.8 mmol, 4.8 mL) was added slowly. The reaction mixture was allowed to warm to room temperature and stirred for overnight. Water was added slowly to quench the reaction. The organic layer was separated, and the aqueous layer was extracted with ethyl acetate (three 30 mL aliquots). The combined organic extracts were washed with brine, and dried over Na_2SO_4. After evaporation of the solvent, the residue was purified by column chromatography on silica gel eluted with hexane/ethyl acetate (15/1) to afford compound (*R*)-**6-6** as a white solid in 90% yield (22.5 mmol, 8.6 g). ^{1}H NMR (300 MHz, $CDCl_3$) δ 1.65-1.76 (m, 8H), 2.07-2.17 (m, 2H), 2.27-2.37 (m, 2H), 2.78 (t, J = 6.0 Hz, 4H), 3.30 (s, 6H), 4.97 (d, J = 6.6 Hz, 2H), 5.03 (d, J = 6.6 Hz, 2H), 6.99 (d, J = 8.4 Hz, 2H), 7.05 (d, J = 8.4Hz, 2H).

Synthesis and Characterization of (*R*)-6-7. Under nitrogen, (*R*)-2,2'-bis(methoxymethoxy)-5,5',6,6',7,7',8,8'-octahydro-1,1'-binaphthyl, (*R*)-**6-6** (4.4 mmol, 1.7 g), was dissolved in diethyl ether (50 mL). The solution was cooled to 0 ℃, and n-BuLi (17.8 mmol, 2.5 M in hexane, 7.1 mL) was added dropwise. The reaction mixture was stirred for 4 h at room temperature and cooled to 0 ^{0}C, and then ethyl trifluoroacetate (20.0 mmol, 2.4 mL) was added slowly. The reaction mixture was allowed to warm to room temperature and stirred for 2.5 h to afford a cream-like mixture. A saturated aqueous NH_4Cl solution was added to quench the reaction. The organic layer was separated, and the aqueous layer was extracted with ethyl acetate (three 20 mL aliquots). The combined organic extracts were washed with brine, and dried over Na_2SO_4. After evaporation of the solvent, the residue was purified by column chromatography on silica gel eluted with hexane/methylene chloride (1/3) to afford compound (*R*)-**6-7** as a yellow

oil in 52% yield (2.3 mmol, 1.31 g). ^{1}H NMR (300 MHz, $CDCl_3$) δ 1.65-1.82 (m, 8H), 2.12-2.22 (m, 2H), 2.47-2.57 (m, 2H), 2.83-2.87 (m, 10H), 4.79 (d, J = 6.6 Hz, 2H), 4.83 (d, J = 6.6 Hz, 2H), 7.49 (s, 2H). ^{13}C NMR (75 MHz, $CDCl_3$) δ 22.5, 28.5, 29.6, 56.2, 100.8, 116.4 (q, J = 290 Hz), 123.2, 130.47, 130.51,132.2, 133.9, 145.4, 153.5, 181.4 (q, J = 34.5 Hz). HRMS Calcd for $C_{28}H_{28}O_6F_6Na$ (MNa^+): 597.1688, Found: 197.1678. $[\alpha]_D$ = 43.34 (c = 0.39, $CHCl_3$).

Synthesis and Characterization of (*R*)-6-8. After compound (*R*)-**6-7** (237.8 mg, 0.41 mmol) was dissolved in a minimum amount of CH_2Cl_2, trifluroacetic acid (1.0 mL) was added slowly, and the mixture was stirred at room temperature for 10 min. A saturated aqueous $NaHCO_3$ solution was added to quench the reaction. The organic layer was separated, and the aqueous layer was extracted with CH_2Cl_2 (3 x 20 mL). The combined organic extracts were washed with brine, and dried over Na_2SO_4. After evaporation of the solvent, the residue was purified by column chromatography on silica gel eluted with hexane/methylene chloride (2/1) to afford compound (*R*)-**6-8** as a yellow solid in 86% yield (0.35 mmol, 172 mg). ^{1}H NMR (300 MHz, $CDCl_3$) δ 1.71-1.88 (m, 8H), 2.25-2.35 (m, 2H), 2.50-2.60 (m, 2H), 2.88 (m, 4H), 7.67 (s, 2H), 11.1 (s, 2H). ^{13}C NMR (75 MHz, $CDCl_3$) δ 22.4, 22.6, 28.3, 29.4, 112.2, 116.8 (q, J = 288 Hz), 124.4, 129.9, 130.6 (q, J = 3.0 Hz), 150.0, 159.4, 184.1 (q, J = 34.5 Hz). HRMS Calcd for $C_{24}H_{21}O_4F_6$ (MH^+): 487.1344, Found: 487.1338. m.p. 209 ^{0}C. $[\alpha]_D$ = -38.5 (c = 0.36, $CHCl_3$).

Synthesis and Characterization of (*S*)-6-9.[6] Under nitrogen, 2,2'-bis-methoxymethyl-1,1'-binaphthyl, (*S*)-**6-2** (3.0 mmol, 1.12 g), was dissolved in diethyl ether (33 mL). The solution was cooled to 0 ℃, and n-BuLi (10.5 mmol, 2.5 M in hexane, 4.2 mL) was

added dropwise. The reaction mixture was stirred for 3 h at room temperature and cooled to 0 ^{0}C, and then anhydrous DMF (12.0 mmol, 1.3 mL) was added slowly. The reaction mixture was allowed to warm to room temperature and stirred for 2 h to afford a cream-like mixture. A saturated aqueous NH_4Cl solution was added to quench the reaction. The organic layer was separated, and the aqueous layer was extracted with ethyl acetate (three 20 mL aliquots). The combined organic extracts were washed with brine, and dried over Na_2SO_4. After evaporation of the solvent, the residue was purified by column chromatography on silica gel eluted with hexane/ethyl acetate (4/1) to afford compound (*S*)-**6-9** as a yellow oil in 73% yield (2.2 mmol, 943 mg). ^{1}H NMR (300 MHz, $CDCl_3$) δ 2.88 (s, 6H), 4.76 (d, J= 1.2 Hz, 2H), 4.78 (d, J= 1.5 Hz, 2H), 7.27 (d, J = 8.4 Hz, 2H), 7.42 (t, J = 6.9 Hz, 2H), 7.53 (d, J = 6.9 Hz, 2H), 8.10 (d, J = 8.1 Hz, 2H), 8.67 (s, 2H), 10.59 (s, 2H).

Synthesis and Characterization of (*S*)-6-10.[6] After compound (*S*)-**6-9** (1.1 mmol, 471mg) was dissolved in a minimum amount of CH_2Cl_2, trifluroacetic acid (1.0 mL) was added slowly, and the mixture was stirred at room temperature for 1 h. A saturated aqueous Na_2CO_3 solution was added to quench the reaction. The organic layer was separated, and the aqueous layer was extracted with CH_2Cl_2 (3 x 20 mL). The combined organic extracts were washed with brine, and dried over Na_2SO_4. After evaporation of the solvent, the residue was purified by recrystallization with CH_2Cl_2/ethanol to afford compound (*S*)-**6-10** as a yellow solid in 84% yield (0.92 mmol, 316 mg). ^{1}H NMR (300 MHz, $CDCl_3$) δ 7.19-7.22 (m, 2H), 7.38-7.43 (m, 4H), 7.98-8.02 (m, 2H), 8.35 (s, 2H), 10.19 (s, 2H), 10.59 (s, 2H).

Synthesis and Characterization of (*S*)-6-11. Under nitrogen, 2,2'-bis-methoxymethyl-1,1'-binaphthyl, (*S*)-**6-2** (3.0 mmol, 1.12 g), was dissolved in diethyl ether (36 mL). The solution was cooled to 0 ℃, and n-BuLi (10.5 mmol, 2.5 M in hexane, 4.2 mL) was added dropwise. The reaction mixture was stirred for 3 h at room temperature and cooled to 0 ^{0}C, and then ethyl difluoroacetate (12.0 mmol, 1.3 mL) was added slowly. The reaction mixture was allowed to warm to room temperature and stirred for 2 h to afford a cream-like mixture. A saturated aqueous NH_4Cl solution was added to quench the reaction. The organic layer was separated, and the aqueous layer was extracted with ethyl acetate (three 20 mL aliquots). The combined organic extracts were washed with brine, and dried over Na_2SO_4. After evaporation of the solvent, the residue was purified by column chromatography on silica gel eluted with hexane/methylene chloride (1/2) to afford compound (*S*)-**6-11** as a yellow oil in 41% yield (1.23 mmol, 652 mg). ^{1}H NMR (300 MHz, $CDCl_3$) δ 2.90 (s, 6H), 4.60 (d, J= 5.7 Hz, 2H), 4.66 (d, J= 5.7 Hz, 2H), 6.69 (t, J = 54 Hz, 2H), 7.20 (d, J = 8.4 Hz, 2H), 7.44 (m, 2H), 7.54 (m , 2H), 8.05 (d, J = 8.1 Hz, 2H), 8.44 (s, 2H). ^{19}F NMR (282 MHz, $CDCl_3$) δ -127.93 (dd, J1 = 321 Hz, J2 = 54 Hz, 2F), -126.57 (dd, J1 = 321 Hz, 54 Hz, 2F). ^{13}C NMR (75 MHz, $CDCl_3$) δ 57.0, 100.2, 110.0 (t, J = 249 Hz), 125.4, 125.9, 126.6, 129.4, 129.7, 129.9, 130.0, 133.1, 136.0, 151.0, 190.6 (t, J = 25.5 Hz). HRMS Calcd for $C_{28}H_{22}O_6F_4Na$ (MNa^+): 553.1250, Found: 553.1259. $[\alpha]_D$ = 31.9 (c = 0.19, $CHCl_3$).

Synthesis and Characterization of (S)-6-12. After compound (*S*)-**6-11** (0.94 mmol, 500 mg) was dissolved in a minimum amount of CH_2Cl_2, trifluroacetic acid (1.0 mL) was added slowly, and the mixture was stirred at room temperature for 1 h. A saturated

aqueous $NaHCO_3$ solution was added to quench the reaction. The organic layer was separated, and the aqueous layer was extracted with CH_2Cl_2 (3 x 20 mL). The combined organic extracts were washed with brine, and dried over Na_2SO_4. After evaporation of the solvent, the residue was purified by column chromatography on silica gel eluted with hexane/methylene chloride (1/1) to afford compound (*S*)-**6-12** as a light yellow solid in 62% yield (0.58 mmol, 258 mg). ^{1}H NMR (600 MHz, $CDCl_3$) δ 6.53 (t, J = 53.4 Hz, 2H), 7.17 (d, J = 7.8 Hz, 2H), 7.40-7.46 (m, 4H), 8.00 (d, J = 7.8 Hz, 2H), 8.76 (s, 2H), 10.75 (s, 2H). ^{19}F NMR (282 MHz, $CDCl_3$)) δ -121.31 (dd, J1 = 351 Hz, J2 = 57 Hz, 2F), -119.82 (dd, J1 = 351 Hz, 57 Hz, 2F). ^{13}C NMR (150 MHz, $CDCl_3$) δ 111.3 (t, J = 252 Hz), 116.6, 117.6, 124.7, 124.9, 127.2, 130.8, 131.6, 135.4 (t, J = 4.5 Hz), 138.1, 154.8, 192.2 (t, J = 25.5 Hz). HRMS Calcd for $C_{24}H_{15}O_4F_4$ (MH^+): 443.0906, Found: 443.0907. m.p. 271 ^{0}C. $[\alpha]_D$ = -153.5 (c = 0.21, $CHCl_3$).

Synthesis and Characterization of (S)-6-13.[7] (*S*)-**6-1** (14.7 mmol, 4.2 g) was dissolved in CH_2Cl_2 (150 mL) and the solution was cooled to -78 ^{0}C. Br_2 (37.8 mmol, 2 mL) was added dropwise. After the reaction mixture was stirred for 2.5 h, it was warmed up to room temperature and stirred for additional 30 min. 10% $NaHSO_3$ solution (100 mL) was added to quench the reaction. The organic layer was separated, and the aqueous layer was extracted with CH_2Cl_2 (20 mL x 3). The combined organic extracts were washed with brine, and dried over Na_2SO_4. After evaporation of the solvent, the residue was purified by column chromatography on silica gel eluted with hexane/ethyl acetate (4/1) to afford compound (*S*)-**6-13** as a white solid in 87% yield (12.8 mmol, 5.68 g). ^{1}H NMR (300 MHz, $CDCl_3$) δ 5.01 (s, 2H), 6.96 (d, J = 9.0 Hz, 2H), 7.34-7.41 (m, 4H), 7.89

(d, J = 9.0 Hz, 2H), 8.05 (s, 2H).

Synthesis and Characterization of (S)-6-14.[7] Under nitrogen, (*S*)-**6-13** (8.0 mmol, 3.55 g) was dissolved in THF (150 mL). The solution was cooled to 0 °C, and NaH (20 mmol, 60% in mineral oil, 0.8 g) was added in small portions. The reaction mixture was stirred for 30 min and then chloromethyl methyl ether (20 mmol, 1.5 mL) was added slowly. The reaction mixture was allowed to warm to room temperature and stirred for 1 h. Water was added slowly to quench the reaction. The organic layer was separated, and the aqueous layer was extracted with ethyl acetate (three 30 mL aliquots). The combined organic extracts were washed with brine, and dried over Na_2SO_4. After evaporation of the solvent, the residue was purified by column chromatography on silica gel eluted with hexane/ethyl acetate (10/1) to afford compound (*S*)-**6-14** as a white solid in 95% yield (7.6 mmol, 4.04 g). ^{1}H NMR (300 MHz, $CDCl_3$) δ 3.15 (s, 6H), 4.98 (d, J = 6.9 Hz, 2H), 5.09 (d, J = 6.9 Hz, 2H), 6.98 (d, J = 9.0 Hz, 2H), 7.29 (dd, J1 = 9.0 Hz, J2 = 2.1 Hz, 2H), 7.60 (d, J = 9.0 Hz, 2H), 7.86 (d, J = 9.0 Hz, 2H), 8.03 (d, J = 2.1 Hz, 2H).

Synthesis and Characterization of (S)-6-15. Under nitrogen, (*S*)-**6-14** (1.0 mmol, 532 mg) was dissolved in THF (15 mL). The solution was cooled to -78 ^{0}C, and n-BuLi (4.4 mmol, 2.5 M in hexane, 1.8 mL) was added dropwise. The reaction mixture was stirred for an additional 3 h at the same temperature, and then ethyl trifluoroacetate (6.6 mmol, 0.8 mL) was added slowly. The reaction mixture was stirred for 30 min at –78 ^{0}C and for 30 min at rt. A saturated aqueous NH_4Cl solution was added to quench the reaction. The organic layer was separated, and the aqueous layer was extracted with ethyl acetate (20 mL x 3). The combined organic extracts were washed with brine, and dried over Na_2SO_4.

After evaporation of the solvent, the residue was purified by column chromatography on silica gel eluted with hexane/methylene chloride (1/2) to afford compound (*S*)-**6-15** as a light yellow oil in 87% yield (0.87 mmol, 493 mg). ^{1}H NMR (300 MHz, $CDCl_3$) δ 3.24 (s, 6H), 5.12 (d, J = 7.2 Hz, 2H), 5.21 (d, J = 7.2 Hz, 2H), 7.27 (d, J = 9.0 Hz, 2H), 7.77 (d, J = 9.0 Hz, 2H), 7.88 (d, J = 9.0 Hz, 2H), 8.20 (d, J = 9.0 Hz, 2H), 8.72 (s, 2H). ^{19}F NMR (282 MHz, $CDCl_3$) δ -71.63. ^{13}C NMR (75 MHz, $CDCl_3$) δ 56.2, 94.5, 117.0 (t, J = 290 Hz), 117.6, 119.8, 125.1, 125.6, 126.1, 128.4, 132.7, 133.7, 137.4, 156.2, 180.2 (t, J = 34.5 Hz). HRMS Calcd for $C_{28}H_{20}O_6F_6Na$ (MNa^+): 589.1062, Found: 589.1063. $[\alpha]_D$ = 36.35 (c = 0.305, $CHCl_3$).

Synthesis and Characterization of (S)-6-16. After compound (*S*)-**6-15** (320 mg, 0.56 mmol) was dissolved in a minimum amount of CH_2Cl_2, trifluroacetic acid (1 mL) was added slowly, and the mixture was stirred at room temperature for 2 h. A saturated aqueous Na_2CO_3 solution was added to quench the reaction. The organic layer was separated, and the aqueous layer was extracted with CH_2Cl_2 (20 mL x 3). The combined organic extracts were washed with brine, and dried over Na_2SO_4. After evaporation of the solvent, the residue was purified by column chromatography on silica gel eluted with hexane/methylene chloride (2/1) to afford compound (*S*)-**6-16** as a light yellow solid in 89% yield (0.50 mmol, 238 mg). ^{1}H NMR (300 MHz, $CDCl_3$) δ 5.33 (s, 2H), 7.19 (d, J = 8.7 Hz, 2H), 7.53 (d, J = 9.0 Hz, 2H), 7.92 (d, J = 9.0 Hz, 2H), 8.21 (d, J = 9.0 Hz, 2H), 8.69 (s, 2H). ^{19}F NMR (282 MHz, $CDCl_3$) δ -71.78. ^{13}C NMR (150 MHz, DMSO) δ 115.0, 116.8 (t, J = 291 Hz), 120.2, 123.3, 124.4, 125.3, 126.7, 132.5, 133.6, 137.7, 179.1 (t, J = 33 Hz). $[\alpha]_D$ = 333.6 (c = 0.16, $CHCl_3$). m.p. 244 ^{0}C. HRMS Calcd for

$C_{24}H_{13}O_4F_6$ (MH^+): 479.0718, Found: 479.0714.

References

1. Selected references of enantioselective fluorescent sensors: (a) James, T. D.; Sandanayake, K. R. A. S.; Shinkai, S. *Nature* **1995**, *374*, 345-347. (b) Pugh, V.; Hu, Q. -S.; Pu, L. *Angew. Chem. Int. Ed.* **2000**, *39*, 3638-3641. (c) Reetz, M. T.; Sostmann, S. *Tetrahedron* **2001**, *57*, 2515-2520. (d) Korbel, G. A.; Lalic, G.; Shair, M. D. *J. Am. Chem. Soc.* **2001**, *123*, 361-362. (e) Jarvo, E. R.; Evans, C. A.; Copeland, G. T.; Miller, S. J. *J. Org. Chem*. **2001**, *66*, 5522-5527. (f) Wong, W.-L.; Huang, K.-H.; Teng, P.-F.; Lee, C.-S.; Kwong, H.-L. *Chem. Commun.* **2004**, 384-385. (g) Zhao, J.-Z.; Fyles, T. M.; James, T. D. *Angew. Chem., Int. Ed.* **2004**, *43*, 3461-3464. (h) Pagliari, S.; Corradini, R.; Galaverna, G.; Sforza, S.; Dossena, A.; Montalti, M.; Prodi, L.; Zaccheroni, N.; Marchelli, R. *Chem. Eur. J.* **2004**, *10*, 2749-2758. (i) Matsushita, H.; Yamamoto, N.; Meijler, M. M.; Wirsching, P.; Lerner, R.A.; Matsushita, M.; Janda, K. D. *Mol. Biosyst.* **2005**, *1*. 303-306. (j) Zhu, L.; Anslyn, E. V. *J. Am. Chem. Soc.* **2004**, *126*, 3676-3677. (k) Mei, X. F. ; Wolf, C. *J. Am. Chem. Soc.* **2004**, *126*, 14736-14737.
2. For reviews on enantioselective fluorescent recognition: (a) Pu, L. *Chem. Rev.* **2004**, *104*, 1687-1716. (b) Pu, L. *Acc. Chem. Res*. **2012**, *45*, 150–163. (c) A recent review on chiral optical sensors: Leung, D.; Kang, S. O.; Anslyn, E. V. *Chem. Soc. Rev*. **2012**, *41*, 448–479.
3. (a) Lin, J.; Hu, Q.-S.; Xu, M. H.; Pu, L. *J. Am. Chem. Soc.* **2002**, *124*, 2088-2089. (b) Xu, M.-H.; Lin, J.; Hu, Q.-S.; Pu, L. *J. Am. Chem. Soc.* **2002**, *124*, 14239-

14246. (c) Li, Z.-B.; Lin, J.; Pu, L. *Angew. Chem., Int. Ed.* **2005**, *44*, 1690-1693. (d) Lin, J.; Rajaram, A. R.; Pu, L. *Tetrahedron* **2004**, *60*, 11277-11281. (e) He, X.; Cui, X.; Li, M.; Lin, L.; Liu, X.; Feng, X. *Tetrahedron Lett.* **2009**, *50*, 5853-5856. (f) Liu, H. –L.; Hou, X. –L.; Pu, L. *Angew. Chem. Int. Ed.* **2009**, *48*, 382 –385. (g) Chen, X.; Huang, Z.; Chen, S. –Y.; Li, K.; Yu, X. –Q.; Pu, L. *J. Am. Chem. Soc.* **2010**, *132*, 7297–7299. (h) Liu, H. –L.; Hou, X. –L; Pu, L. *Org. Lett*. **2010,** *12*, 4172-4175. (i) Liu, H. -L.; Peng, Q.; Wu, Y. –D.; Chen, D.; Hou, X. –L.; Sabat, M.; Pu, L. *Angew. Chem. Int. Ed.* **2010**, *49*, 602-606. (j) Yu, S.; Pu, L. *J. Am. Chem. Soc.* **2010**, *132*, 17698–17700. (k) Yu, S.; DeBerardinis, A. M.; Turlington, M.; Pu, L. *J. Org. Chem.* **2011**, *76*, 2814–2819. (l) Yu, S.; Pu, L. *Sci. China. Chem.* **2013**, *56*, 301–306.

4. (a) Herman, H. B.; Rechnitz, G. A. *Science* **1974**, *184*, 1074–1075. (b) Meyerhoff, M. E.; Pretsch, E.; Welti, D. H.; Simon, W. *Anal. Chem*. **1987**, *59*, 144–150. (c) Wang, K.; Seiler, K.; Haug, J. –P.; Lehmann, B.; Hartman, S. W. K.; Simon, W. *Anal. Chem*. **1991**, *63*, 970-974. (d) Seiler, K.; Wang, K.; Kuratli, M.; Simon, W. *Anal. Chim. Act*. **1991**, *244*, 151–160. (e) Mohr, G. J.; Tirelli, N.; Lohse, C.; Spichiger-Keller, U. E. *Adv. Mater*. **1998**, *10*, 1353-1357. (f) Mertz, E.; Zimmerman, S. C. *J. Am. Chem. Soc.* **2003**, *125*, 3424-3425. (g) Sasaki, S. –i.; Kotegawa, Y.; Tamiaki, H. *Tetrahedron Lett*. **2006**, *47*, 4849–4852. (h) Ryu, D.; Park, E.; Kim, D. –S.; Yan, S.; Lee, J. Y.; Chang, B. –Y.; Ahn, K. H. *J. Am. Chem. Soc*. **2008**, *130*, 2394–2395. (i) Sambasivan, S.; Kim, D. –s.; Ahn, K. H. *Chem. Commun*. **2010**, *46*, 541–543.

5. Yu, S.; Plunkett, W.; Kim, M.; Pu, L. *J. Am. Chem. Soc.* **2012**, *134*, 20282–20285.

6. Cox, P. J.; Wang, W.; Snieckus, V. *Tetrahedron Lett.* **1992**, 33, 2253–2256.

7. Hu, Q. S.; Zheng, X. F.; Pu, L. *J. Org. Chem.* **1996**, 61, 5200.

8. Abou-Eikhair, R. A. I.; Dixon, D. W.; Netzel, T. L. *J. Org. Chem.* **2009**, 74, 4712.

9. (a) Hou, S. Y.; Hetherington, W. M.; Korenowski, G. M.; Eisenthal, K. B. *Chem. Phys. Lett.* **1979**, 68, 282. (b) Ford, D.; Thistlethwaite, P. J.; Woolfe, G. J. *Chem. Phys. Lett.* **1980**, 69, 246.

10. Forster, T. *Z. Electrochem.* **1950**, 54, 531.

11. Wan, P.; Shukla, D. *Chem. Rev.* **1993**, 93, 571.

12. Djoufac-Woumfo, E.; Arnaud, N.; Georges, J. *Analyst.* **1988**, 113, 447.

13. Ofran, M.; Feitelson, J. *Chem. Phys. Lett.* **1973**, 19, 427.

14. Lee, J.; Griffin, R. D.; Robinson, G. W. *J. Chem. Phys*. **1985**, 82, 4920.

15. Law, K-Y.; Shoham, J. *J. Phys. Chem.* **1994**, 98, 3114.

16. Iwanek, W.; Mattay, J. *J. Photochem. Photobiol. A.* **1992**, 67, 209.

17. Yue, Y.; Turlington, M.; Yu, X-Q.; Lin, P. *J. Org. Chem*. **2009**, 74, 8681.

18. DeBerardinis, A. M.; Turlington, M.; Ko, J.; Sole, L.; Lin, P. *J. Org. Chem*. **2010**, 75, 2836.

Appendix

Appendix to Chapter 2

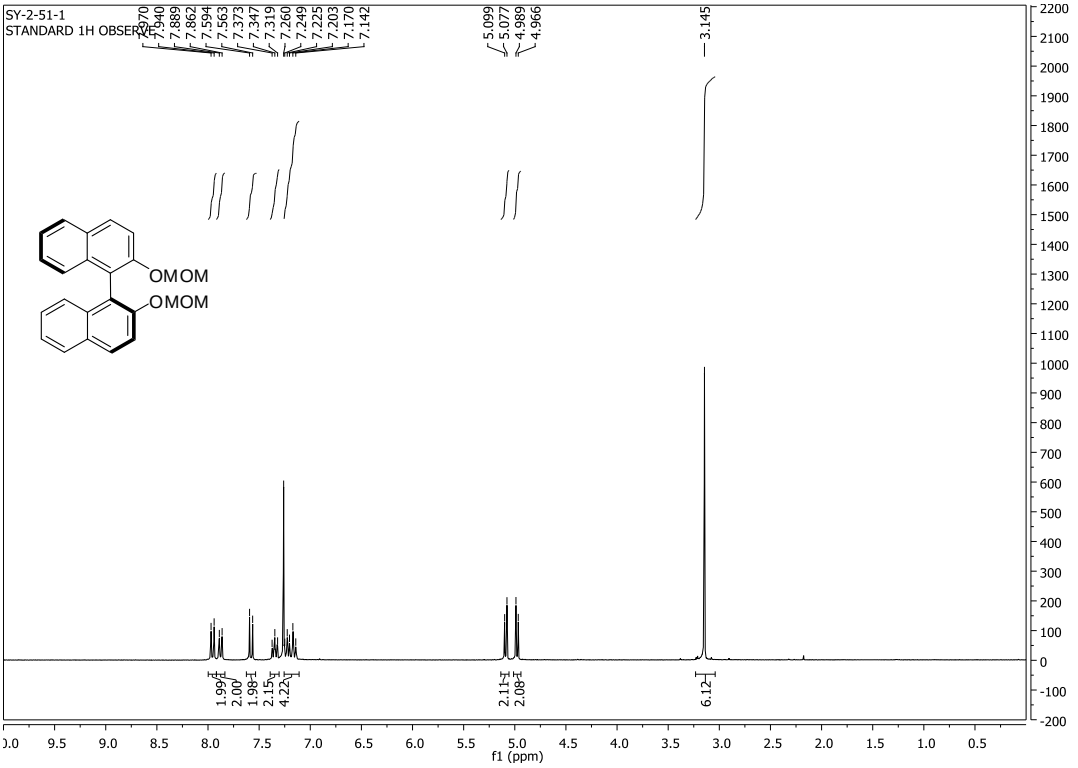

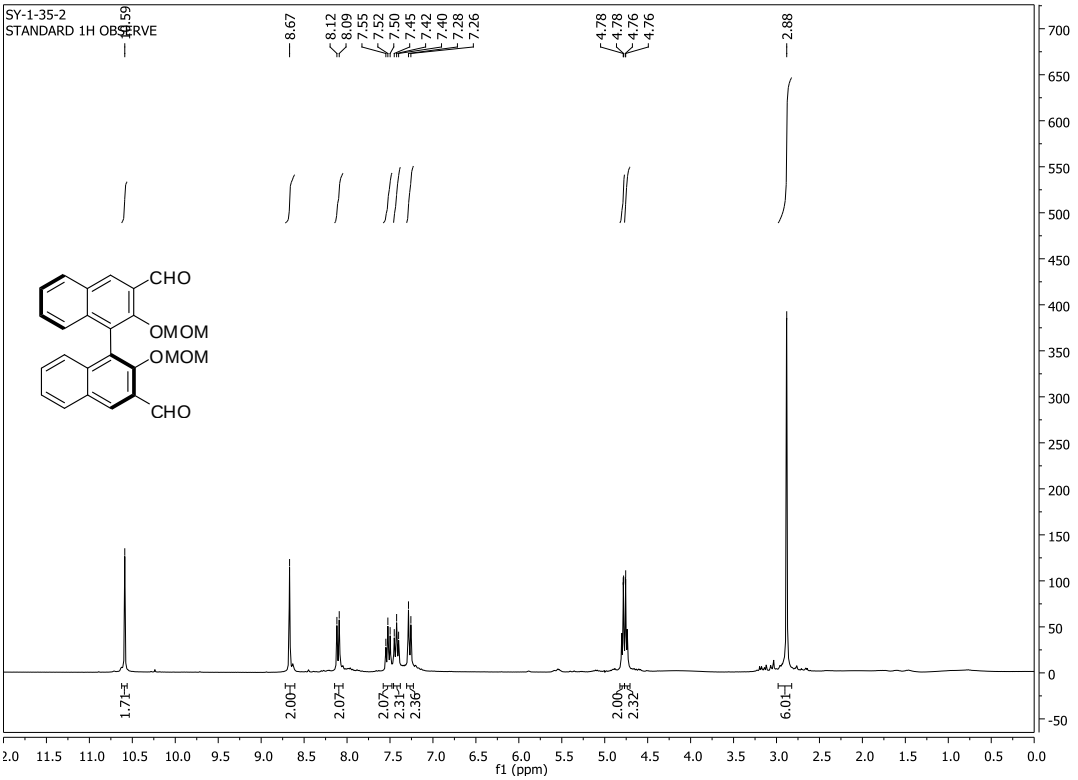

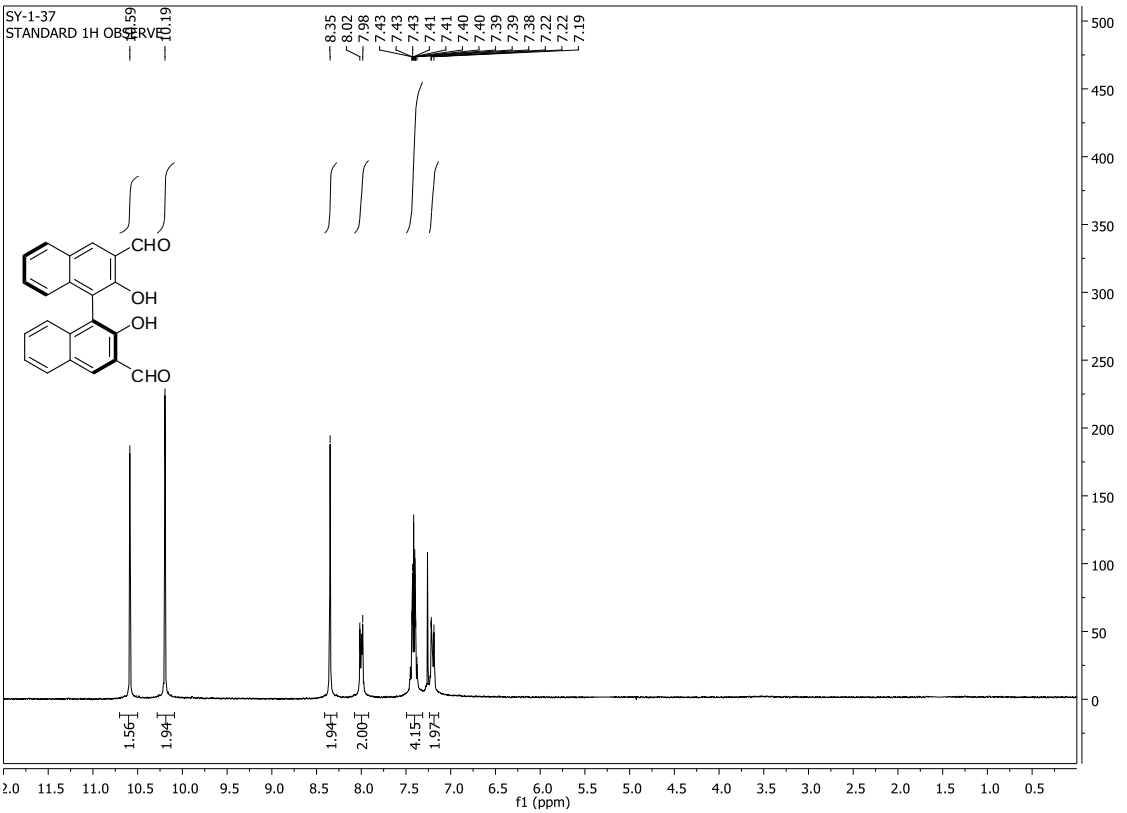
SY-1-37
STANDARD 1H OBSERVE
10.59
10.19
8.35
8.02
7.98
7.43
7.43
7.43
7.41
7.41
7.40
7.40
7.39
7.39
7.38
7.22
7.22
7.19
CHO
OH
OH
CHO
1.56
1.94
1.94
2.00
4.15
1.97
f1 (ppm)

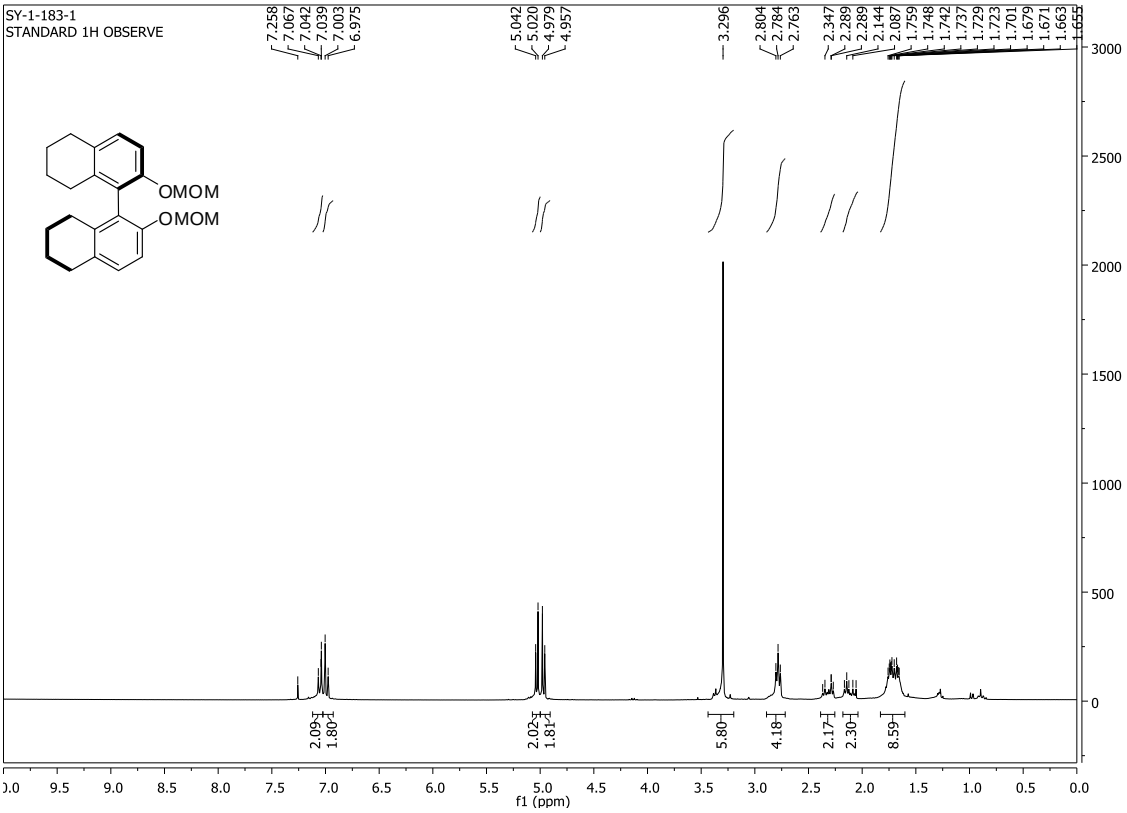
SY-1-183-1
STANDARD 1H OBSERVE
7.258
7.067
7.042
7.039
7.003
6.975
5.042
5.020
4.979
4.957
3.296
2.804
2.784
2.763
2.347
2.289
2.289
2.144
2.087
1.759
1.748
1.742
1.737
1.729
1.723
1.701
1.679
1.671
1.663
1.655
OMOM
OMOM
2.09
1.80
2.02
1.81
5.80
4.18
2.17
2.30
8.59
f1 (ppm)

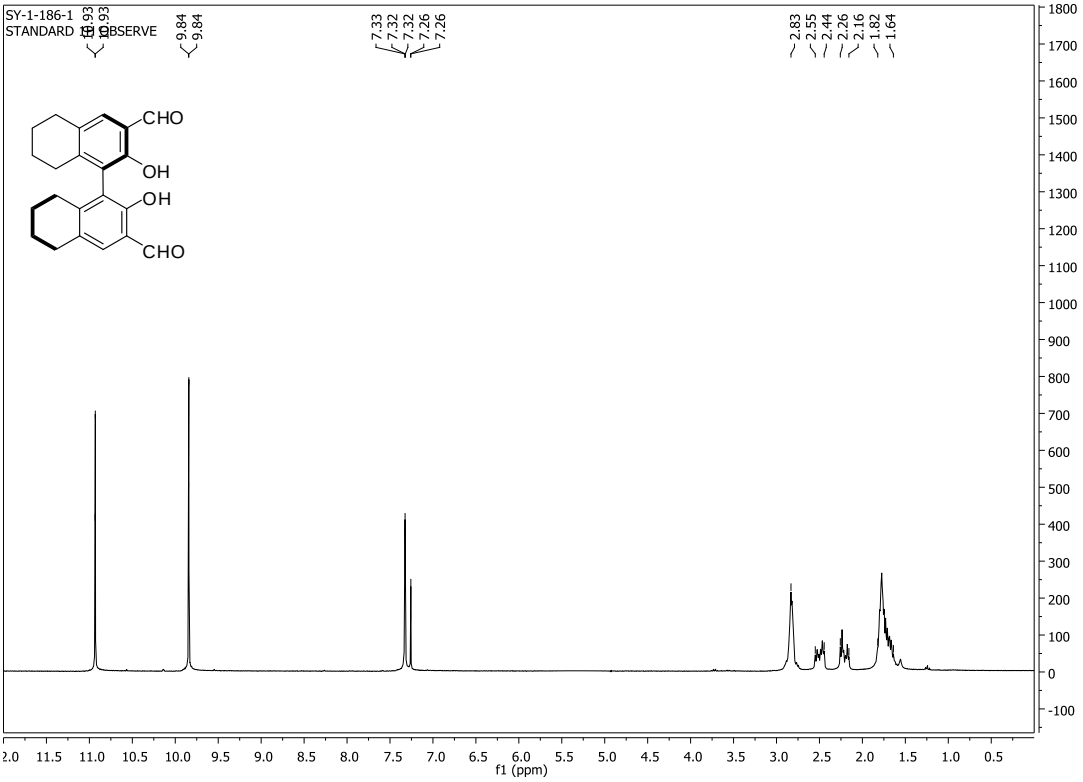
SY-1-186-1
STANDARD 1H OBSERVE
10.93
9.84
7.33
7.32
7.32
7.26
7.26
2.83
2.55
2.44
2.26
2.16
1.82
1.64
CHO
OH
OH
CHO
f1 (ppm)

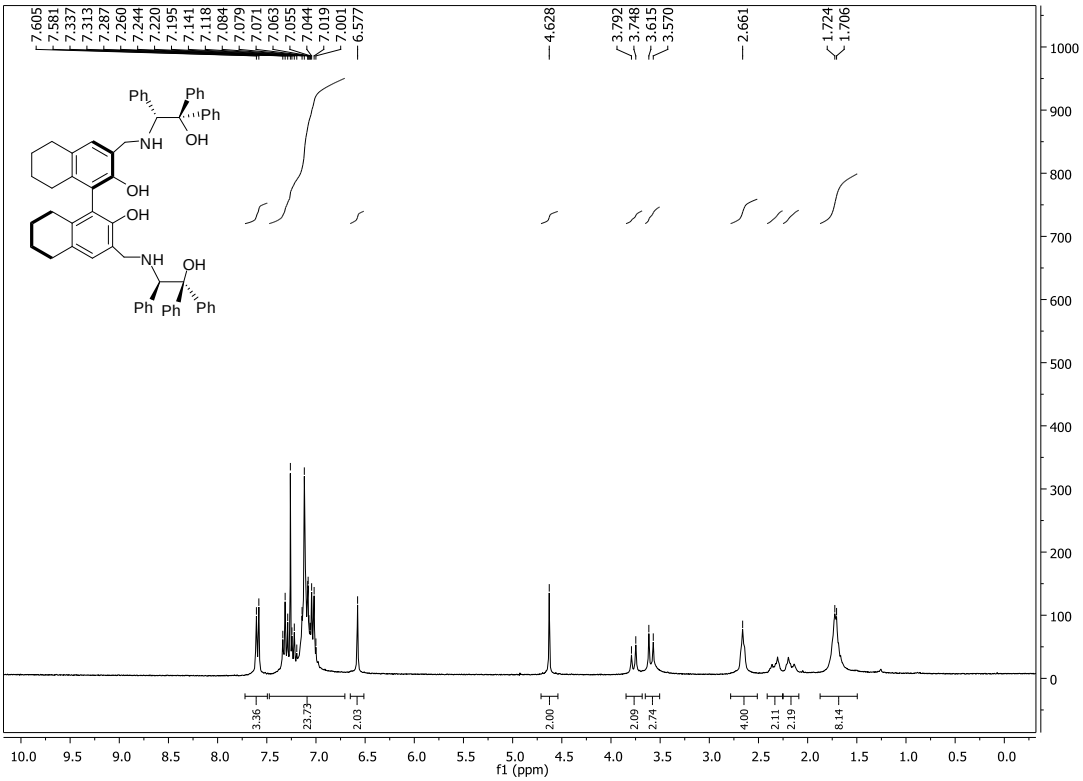
7.605
7.581
7.337
7.313
7.287
7.260
7.244
7.220
7.195
7.141
7.118
7.084
7.079
7.071
7.063
7.055
7.044
7.019
7.001
6.577
4.628
3.792
3.748
3.615
3.570
2.661
1.724
1.706
Ph
Ph
Ph
NH
OH
OH
OH
NH
OH
Ph
Ph
Ph
3.36
23.73
2.03
2.00
2.09
2.74
4.00
2.11
2.19
8.14
f1 (ppm)

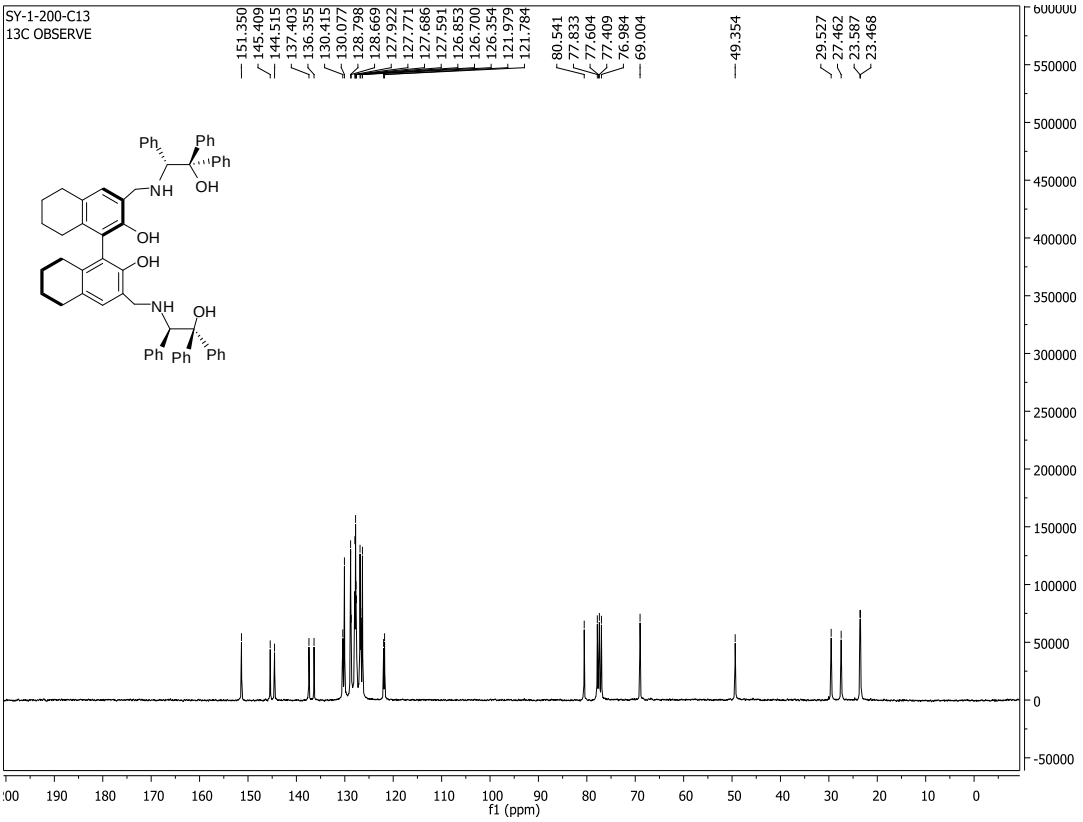
SY-1-200-C13
13C OBSERVE
151.350
145.409
144.515
137.403
136.355
130.415
130.077
128.798
128.669
127.922
127.771
127.686
127.591
126.853
126.700
126.354
121.979
121.784
80.541
77.833
77.604
77.409
76.984
69.004
49.354
29.527
27.462
23.587
23.468
Ph
Ph
Ph
NH
OH
OH
OH
NH
OH
Ph
Ph
Ph
600000
550000
500000
450000
400000
350000
300000
250000
200000
150000
100000
50000
0
-50000
200
190
180
170
160
150
140
130
120
110
100
90
80
70
60
50
40
30
20
10
0
f1 (ppm)

Appendix to Chapter 3

NMR Experiments for the Interaction of (*S*)-3-5 with (*R*)-MA

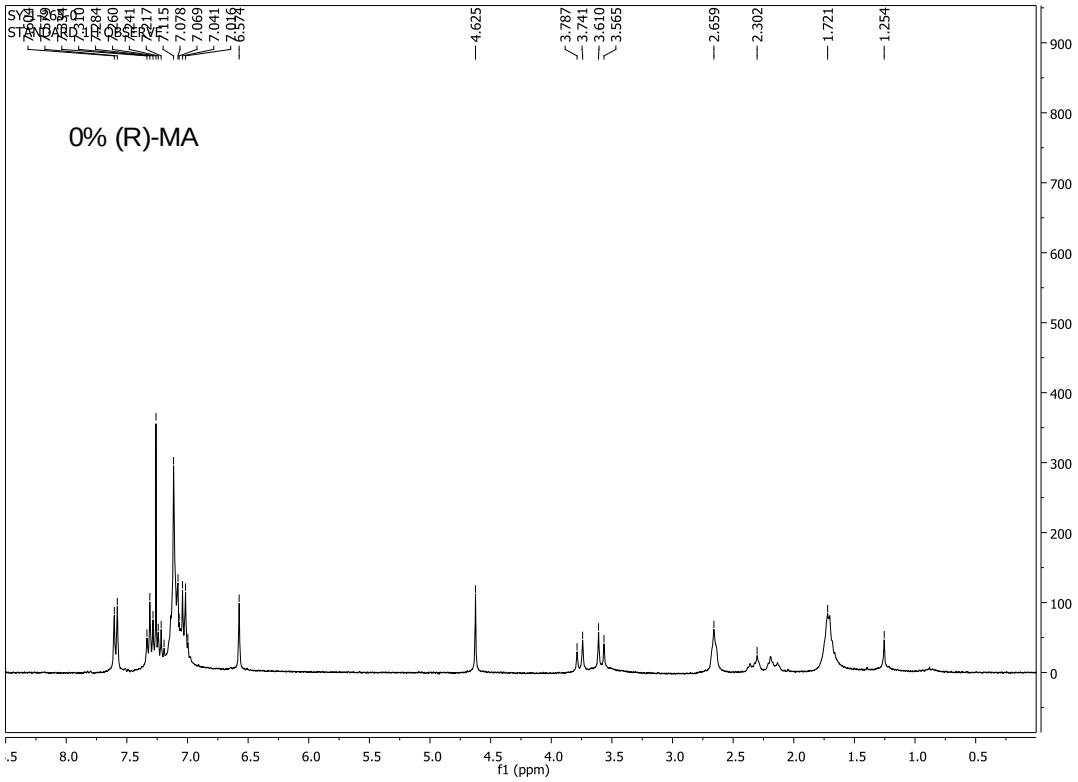

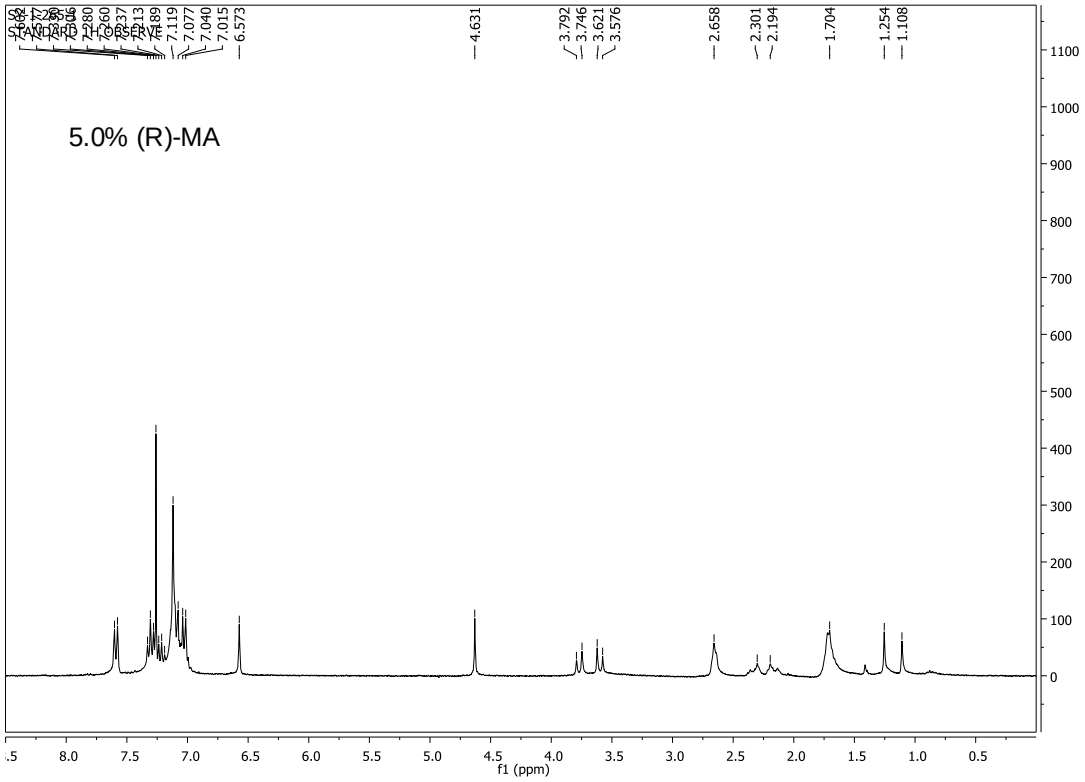
5.0% (R)-MA
f1 (ppm)

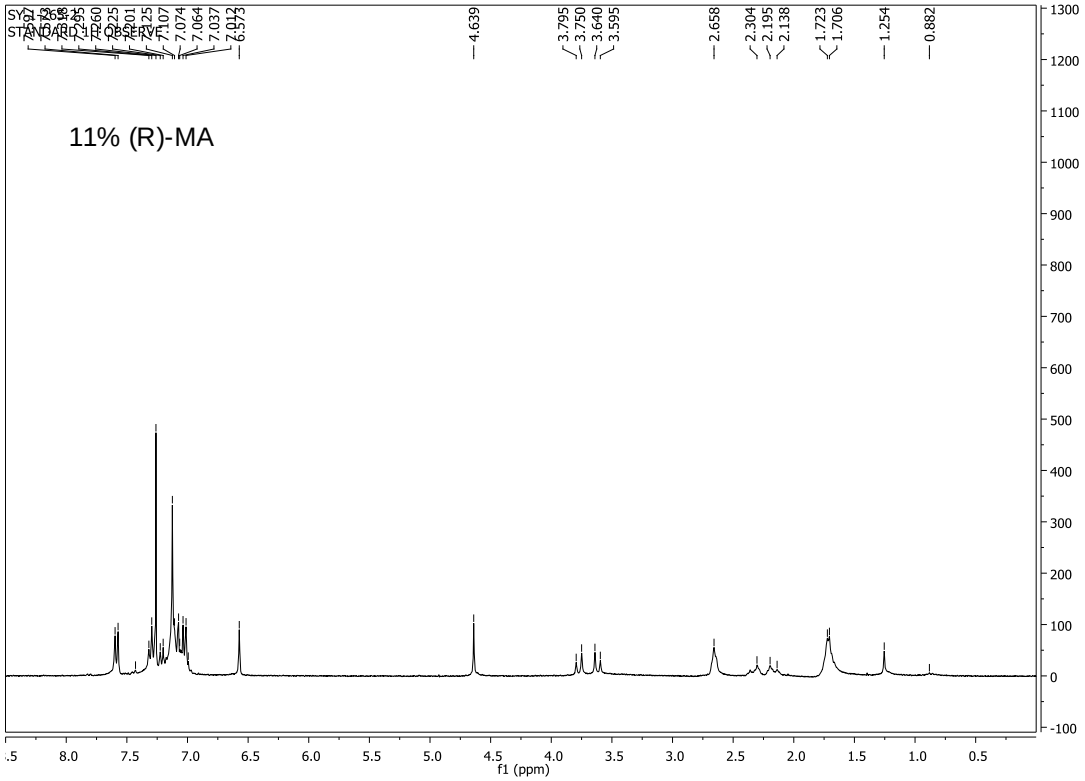
11% (R)-MA
f1 (ppm)

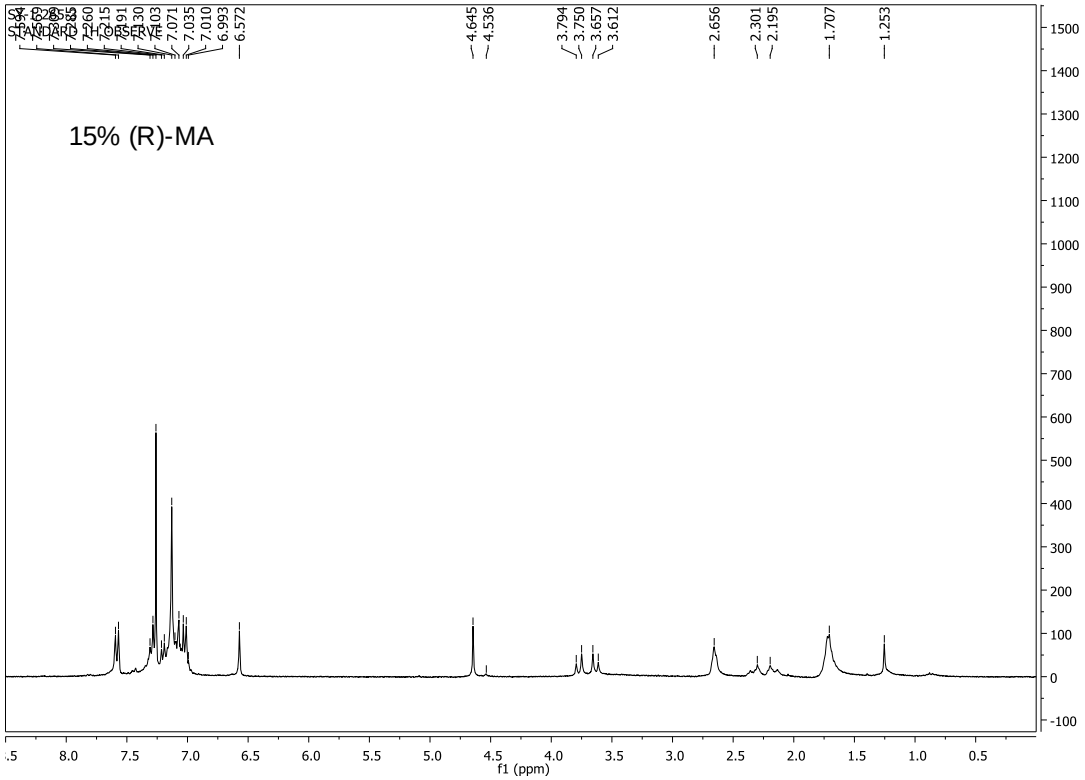
15% (R)-MA
f1 (ppm)

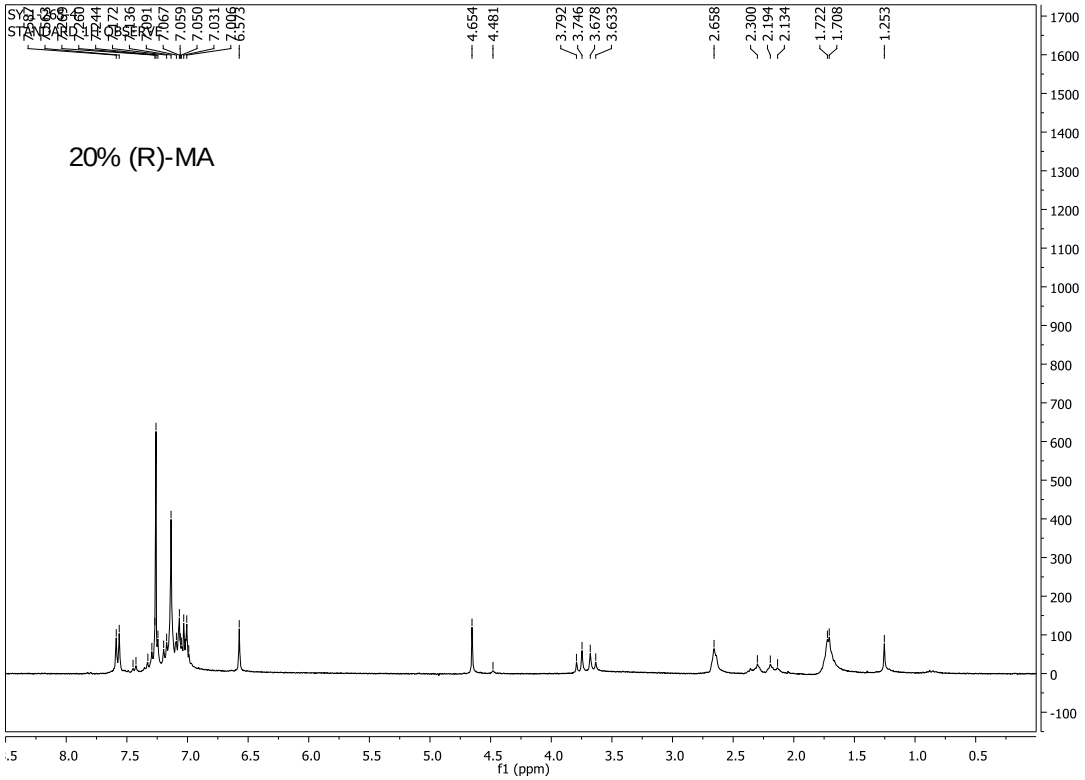
20% (R)-MA
f1 (ppm)

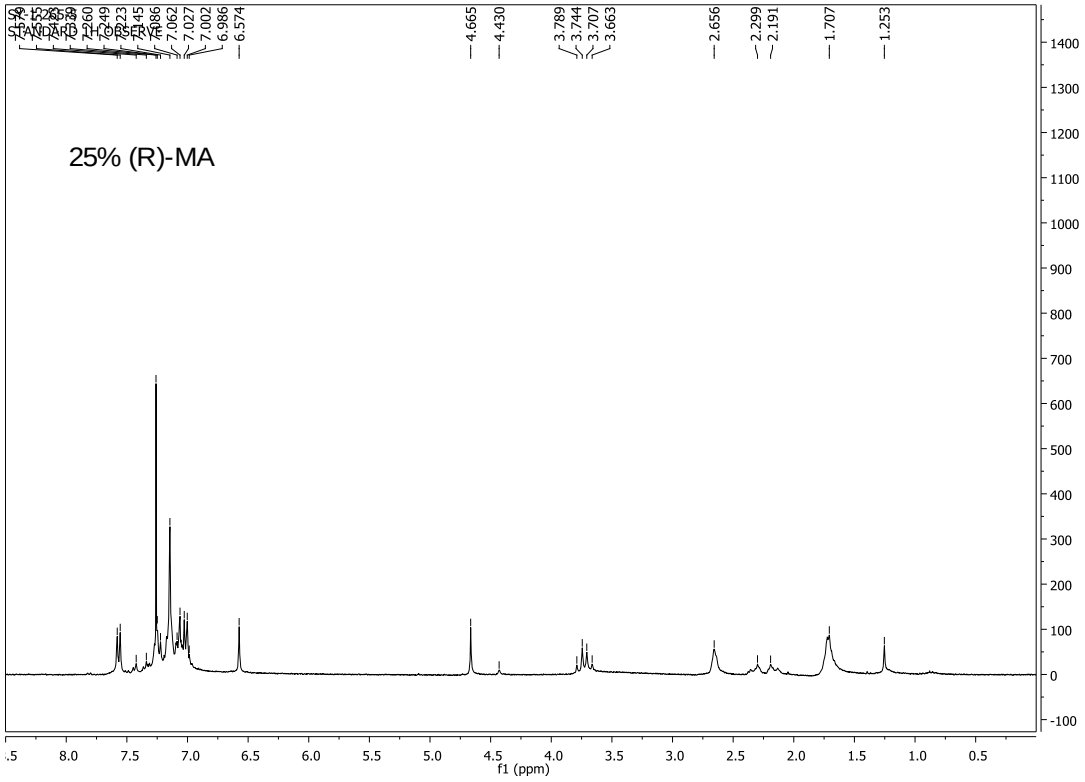
25% (R)-MA
f1 (ppm)

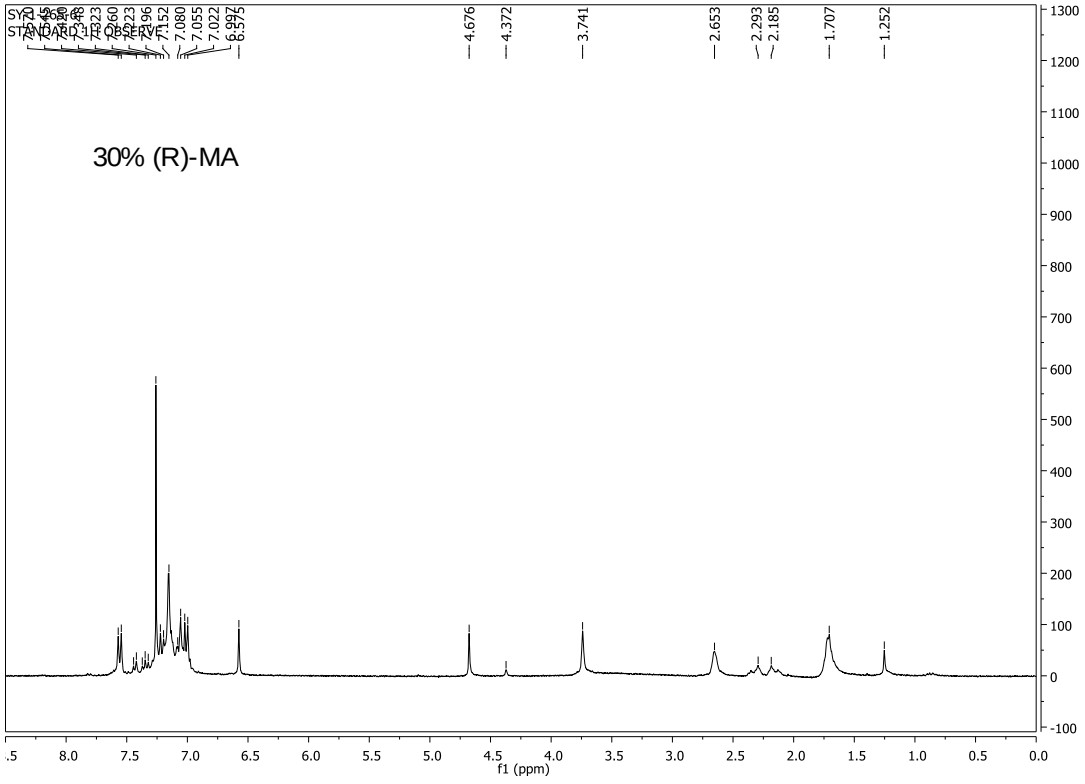
30% (R)-MA
f1 (ppm)

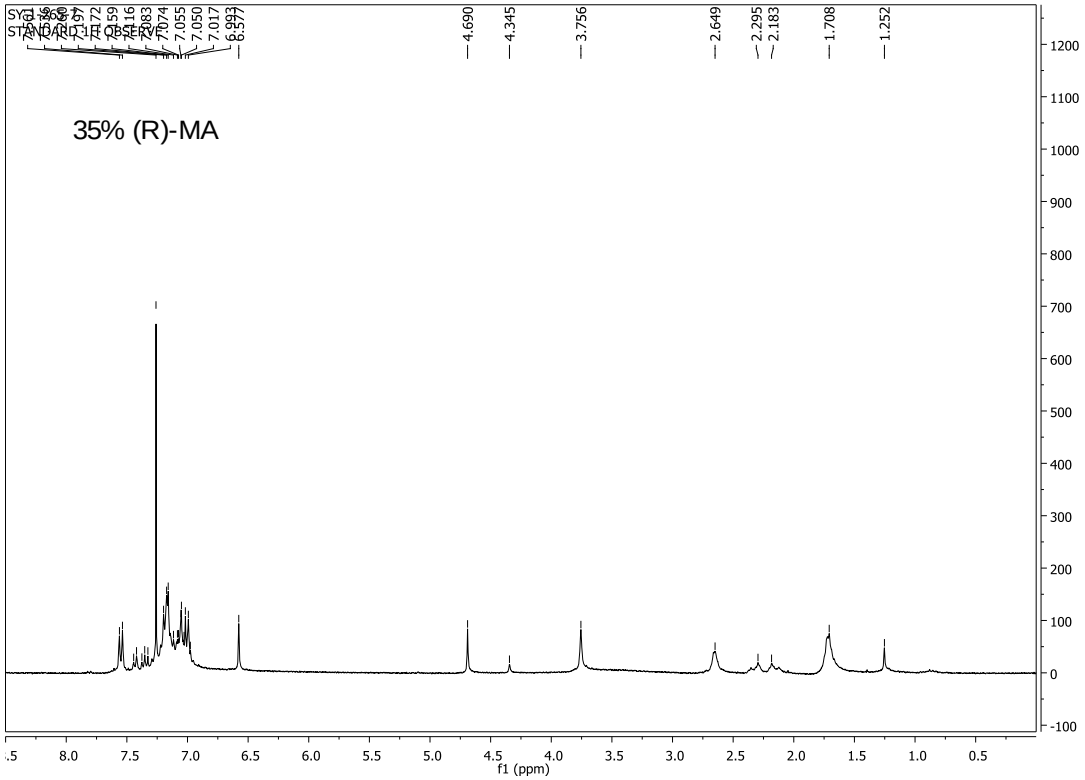
35% (R)-MA
4.690
4.345
3.756
2.649
2.295
2.183
1.708
1.252
6.577
f1 (ppm)

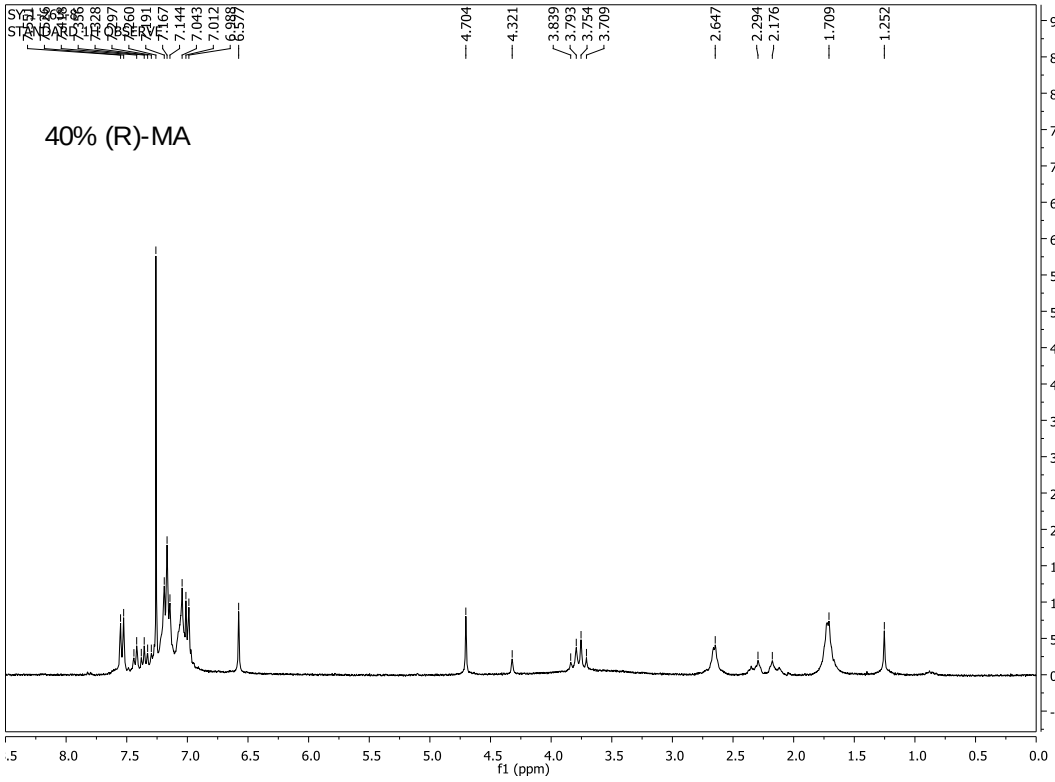
40% (R)-MA
4.704
4.321
3.839
3.793
3.754
3.709
2.647
2.294
2.176
1.709
1.252
6.577
f1 (ppm)

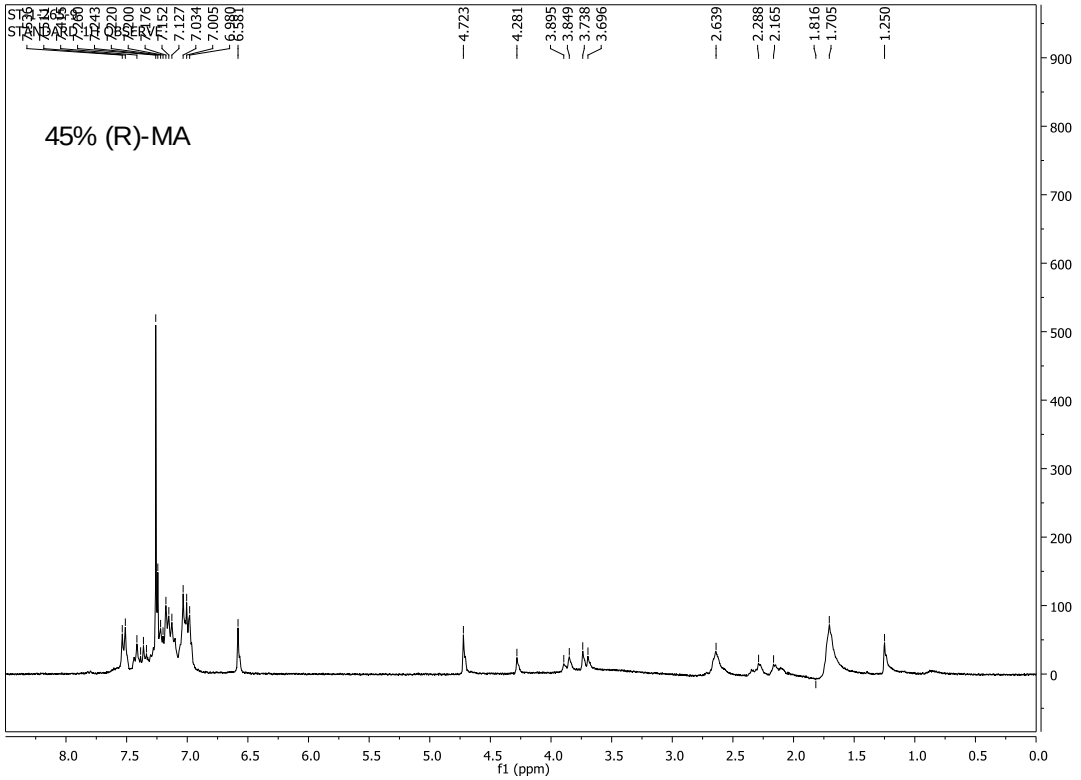
45% (R)-MA
4.723
4.281
3.895
3.849
3.738
3.696
2.639
2.288
2.165
1.816
1.705
1.250
6.581
7.005
7.034
7.127
f1 (ppm)

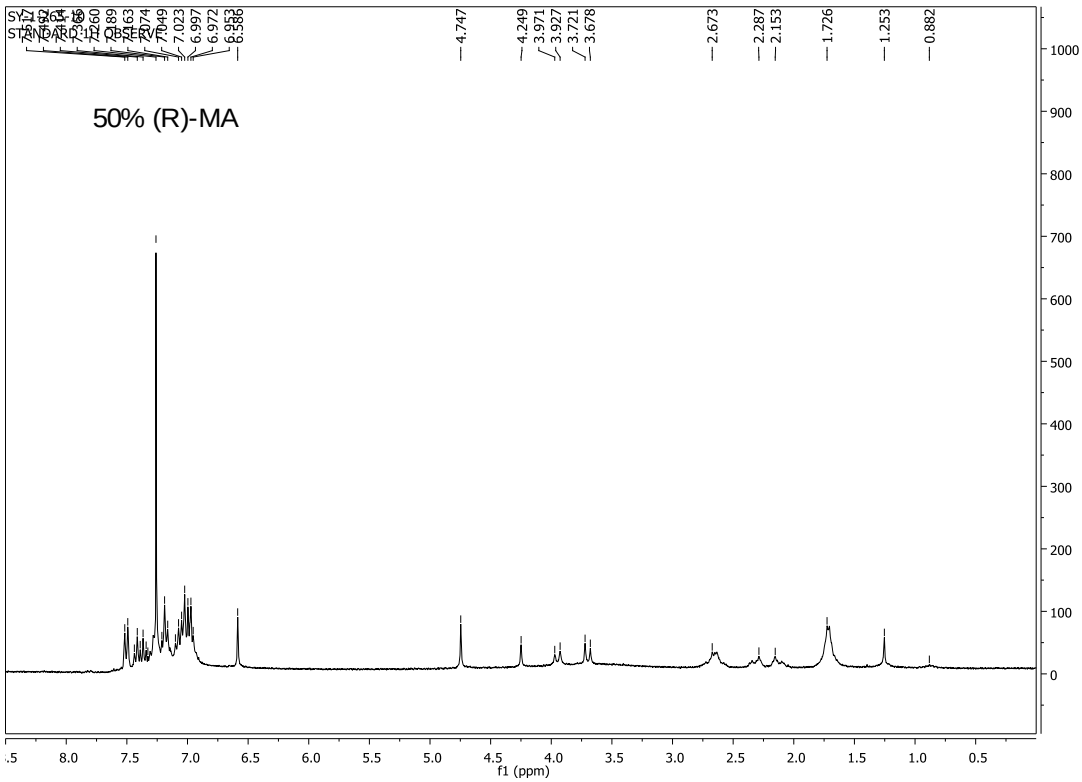
50% (R)-MA
4.747
4.249
3.971
3.927
3.721
3.678
2.673
2.287
2.153
1.726
1.253
0.882
6.586
6.953
6.972
6.997
7.023
f1 (ppm)

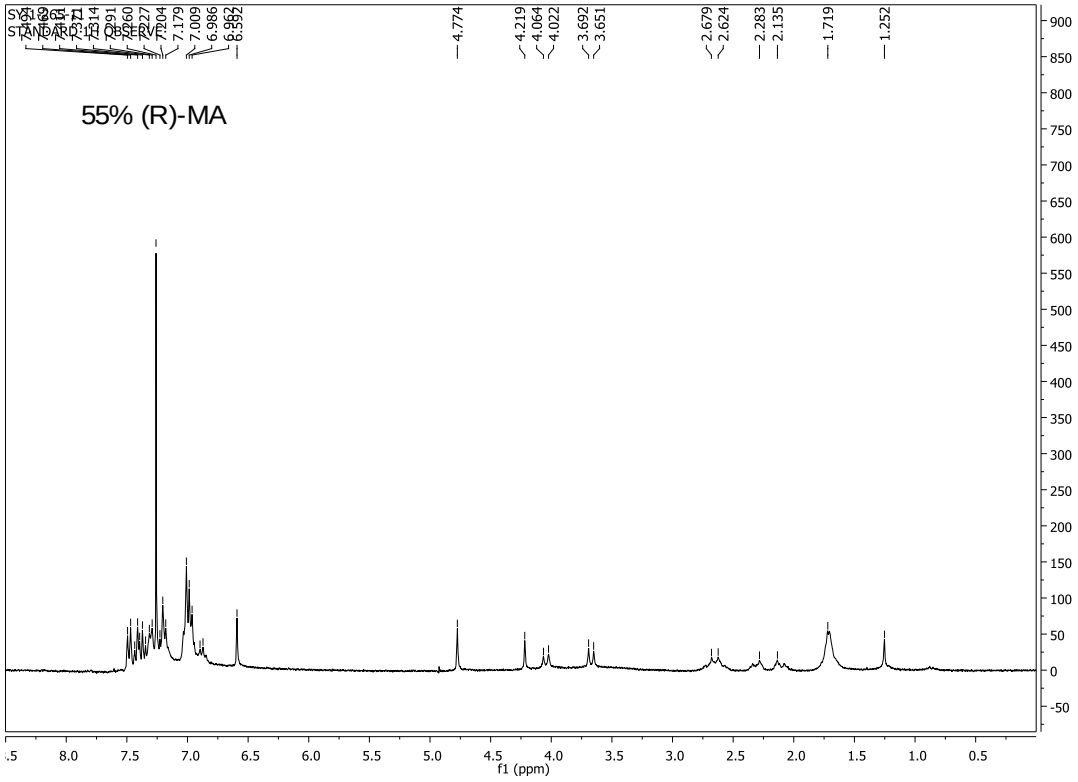
55% (R)-MA
4.774
4.219
4.064
4.022
3.692
3.651
2.679
2.624
2.283
2.135
1.719
1.252
f1 (ppm)

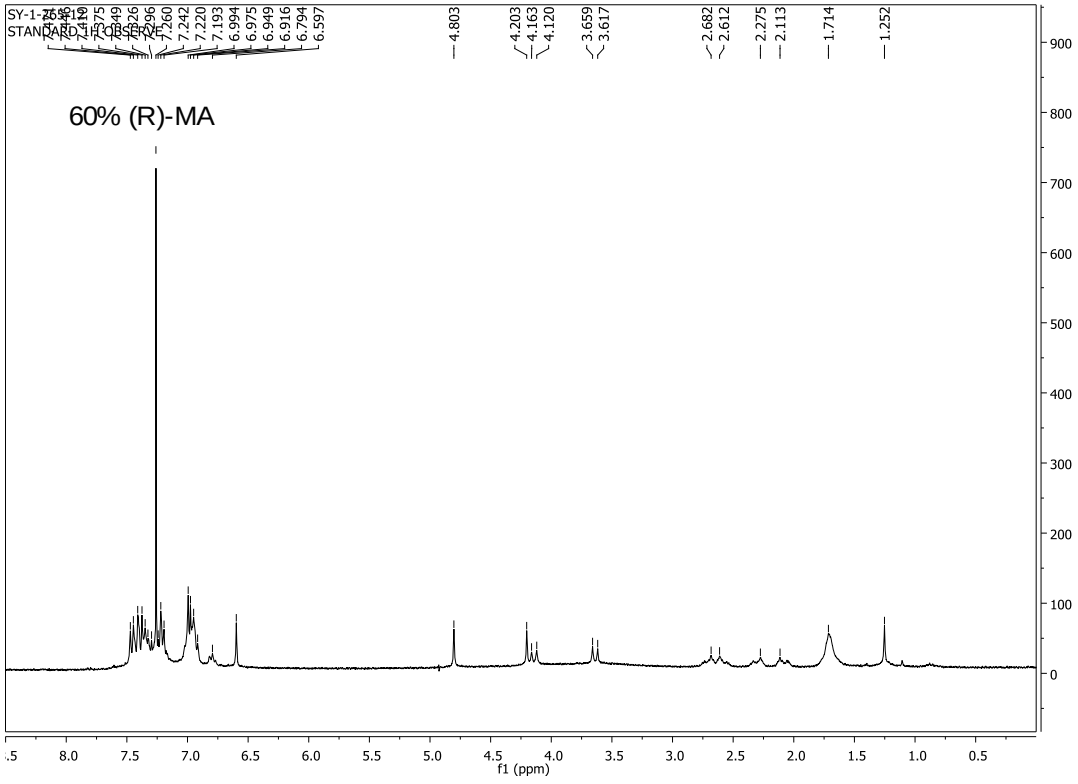
60% (R)-MA
4.803
4.203
4.163
4.120
3.659
3.617
2.682
2.612
2.275
2.113
1.714
1.252
f1 (ppm)

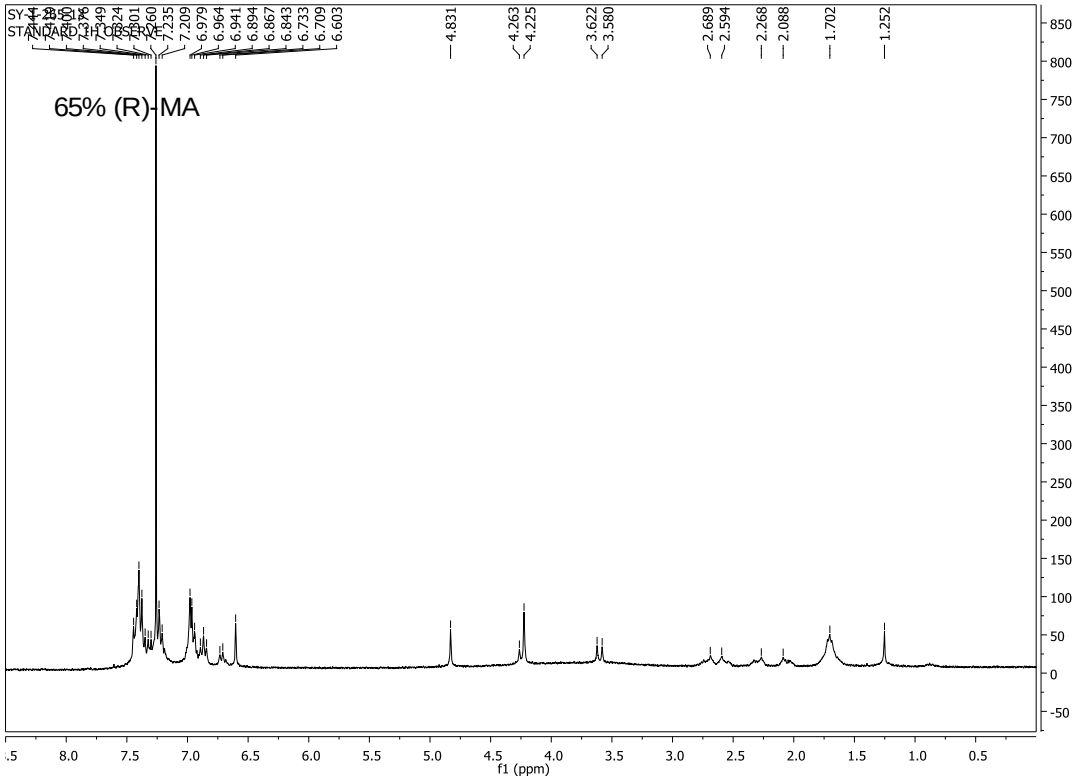
65% (R)-MA
f1 (ppm)

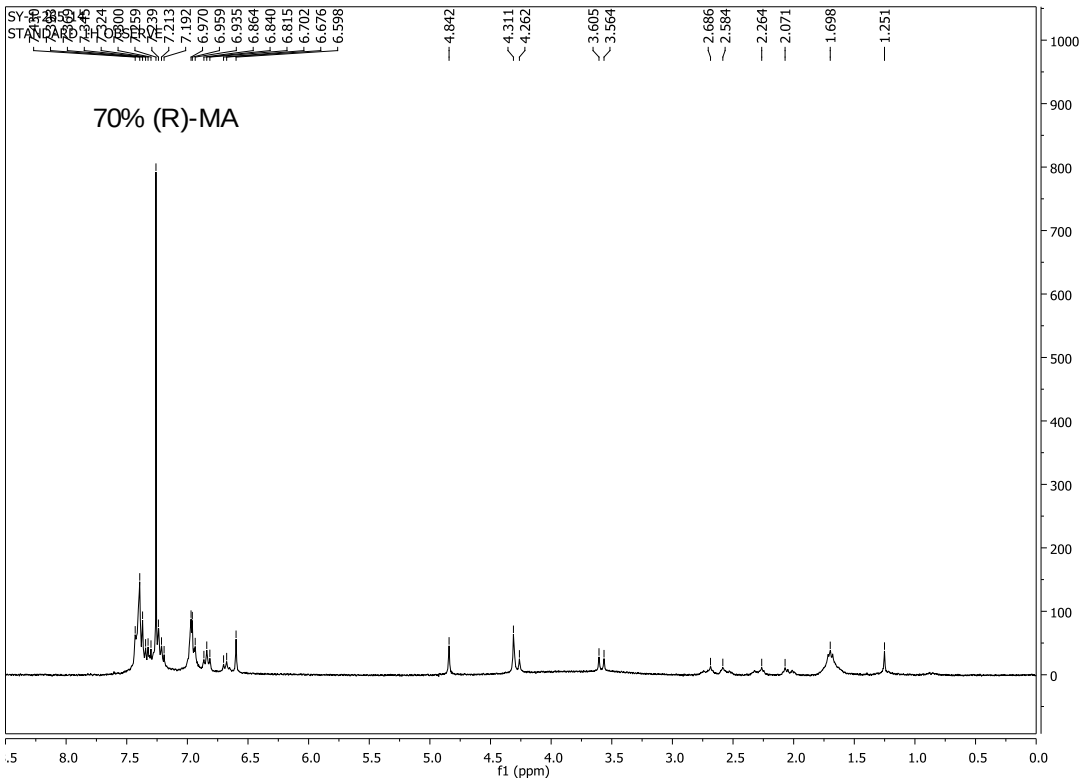
70% (R)-MA
f1 (ppm)

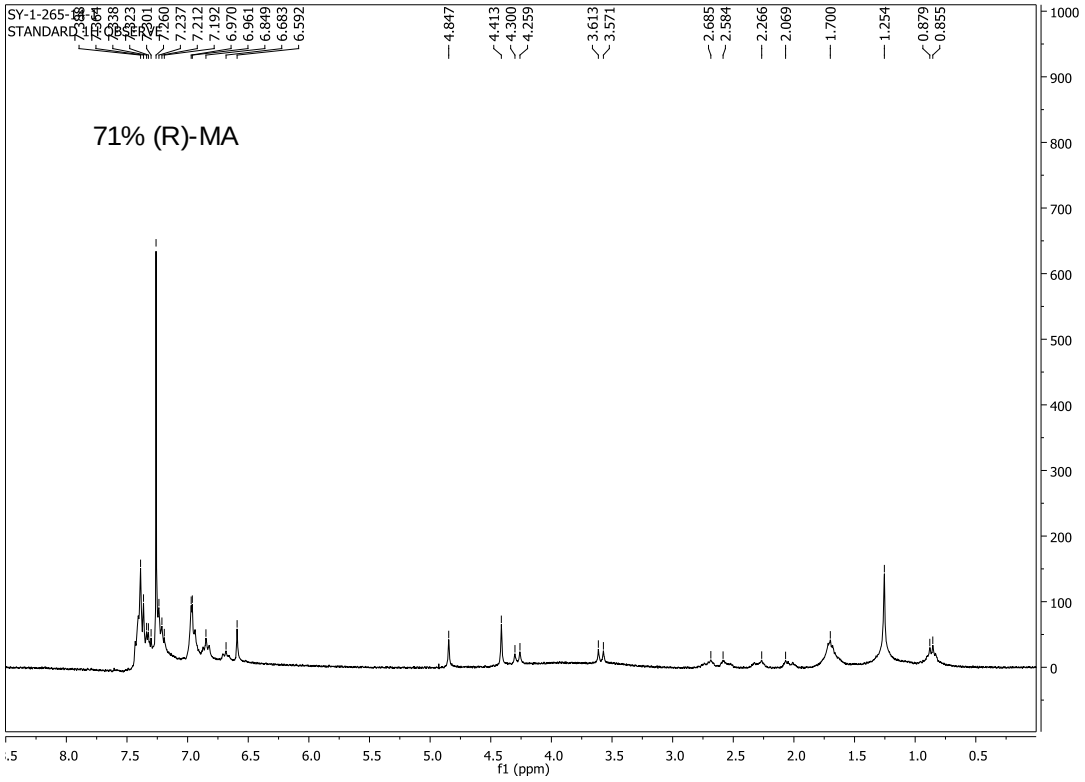
71% (R)-MA
f1 (ppm)

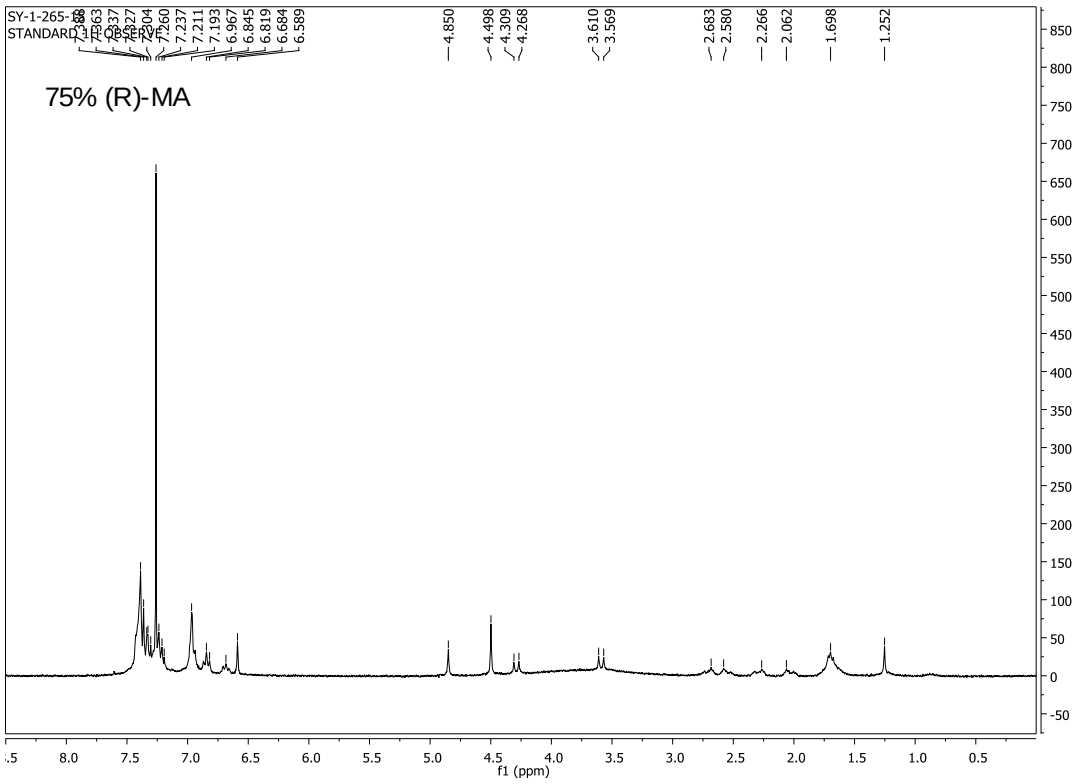
75% (R)-MA
f1 (ppm)

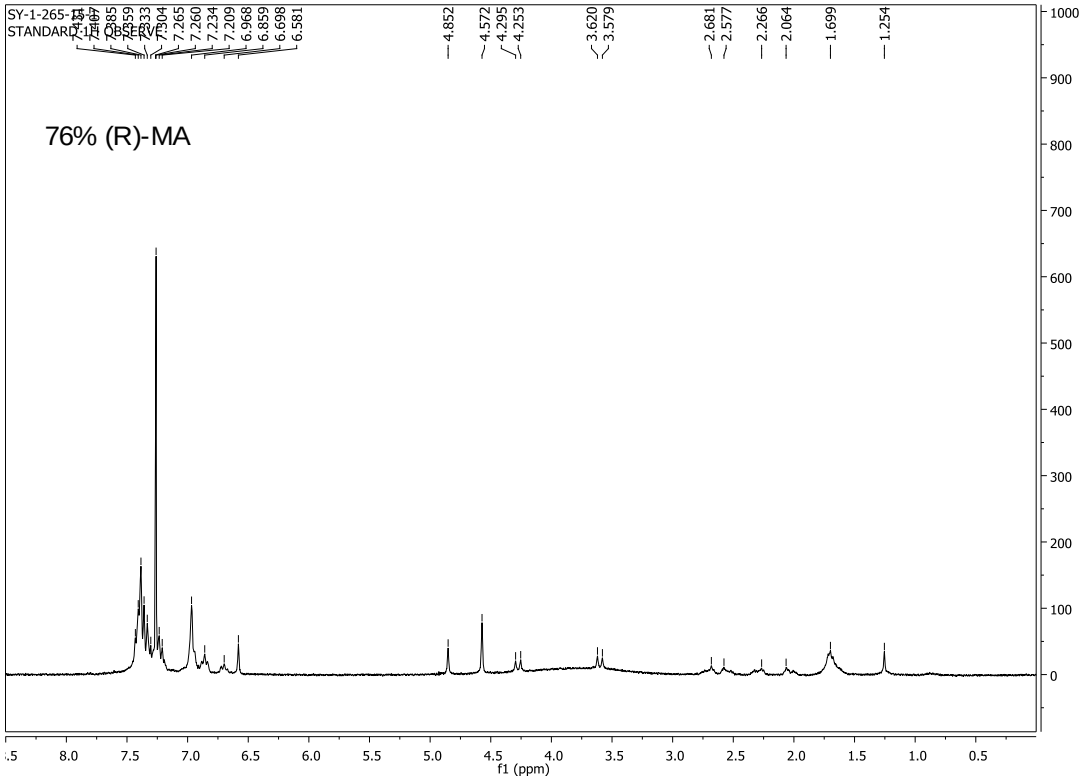
SY-1-265-11
STANDARD 1H OBSERVE
7.367
7.385
7.359
7.333
7.304
7.265
7.260
7.234
7.209
6.968
6.859
6.698
6.581
4.852
4.572
4.295
4.253
3.620
3.579
2.681
2.577
2.266
2.064
1.699
1.254
76% (R)-MA
f1 (ppm)

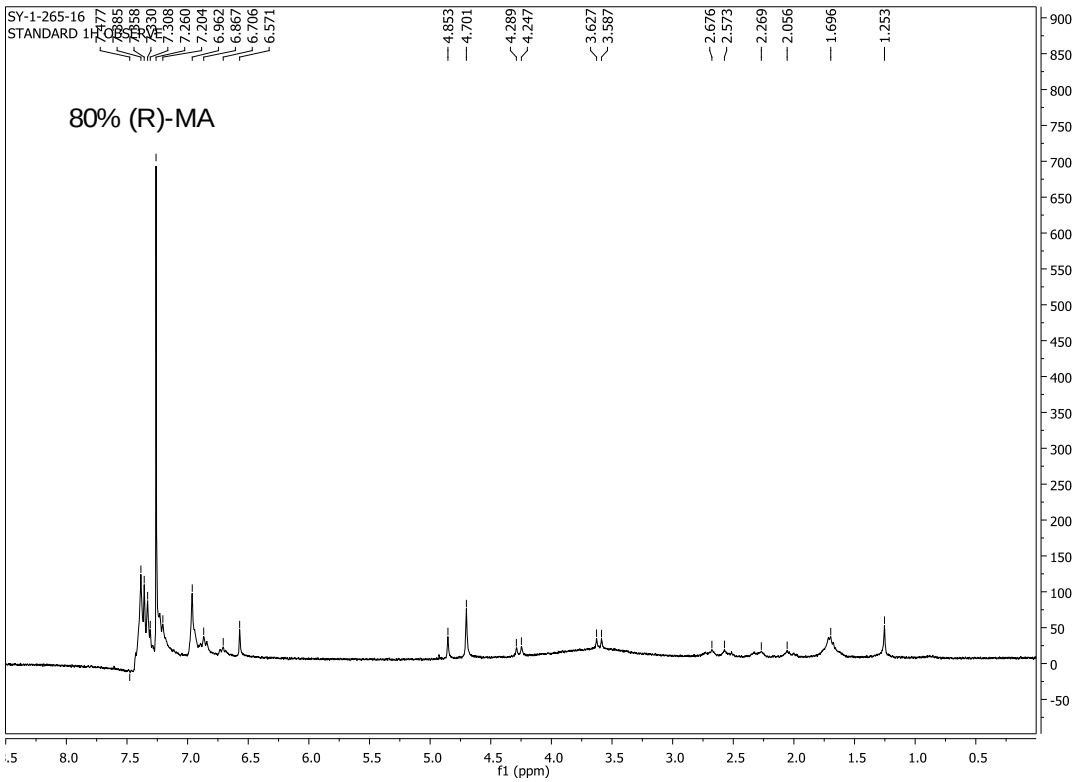
SY-1-265-16
STANDARD 1H OBSERVE
7.377
7.385
7.358
7.330
7.308
7.260
7.204
6.962
6.867
6.706
6.571
4.853
4.701
4.289
4.247
3.627
3.587
2.676
2.573
2.269
2.056
1.696
1.253
80% (R)-MA
f1 (ppm)

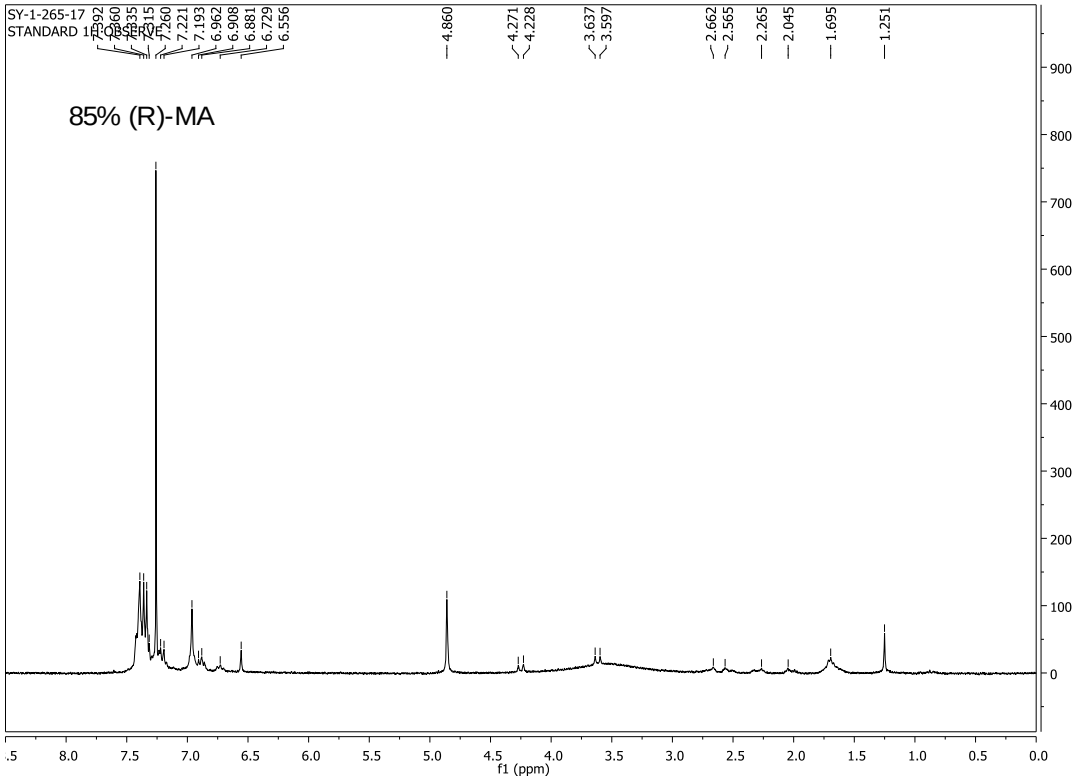
SY-1-265-17
STANDARD 1H OBSERVE
7.392
7.360
7.335
7.315
7.260
7.221
7.193
6.962
6.908
6.881
6.729
6.556
4.860
4.271
4.228
3.637
3.597
2.662
2.565
2.265
2.045
1.695
1.251
85% (R)-MA
f1 (ppm)

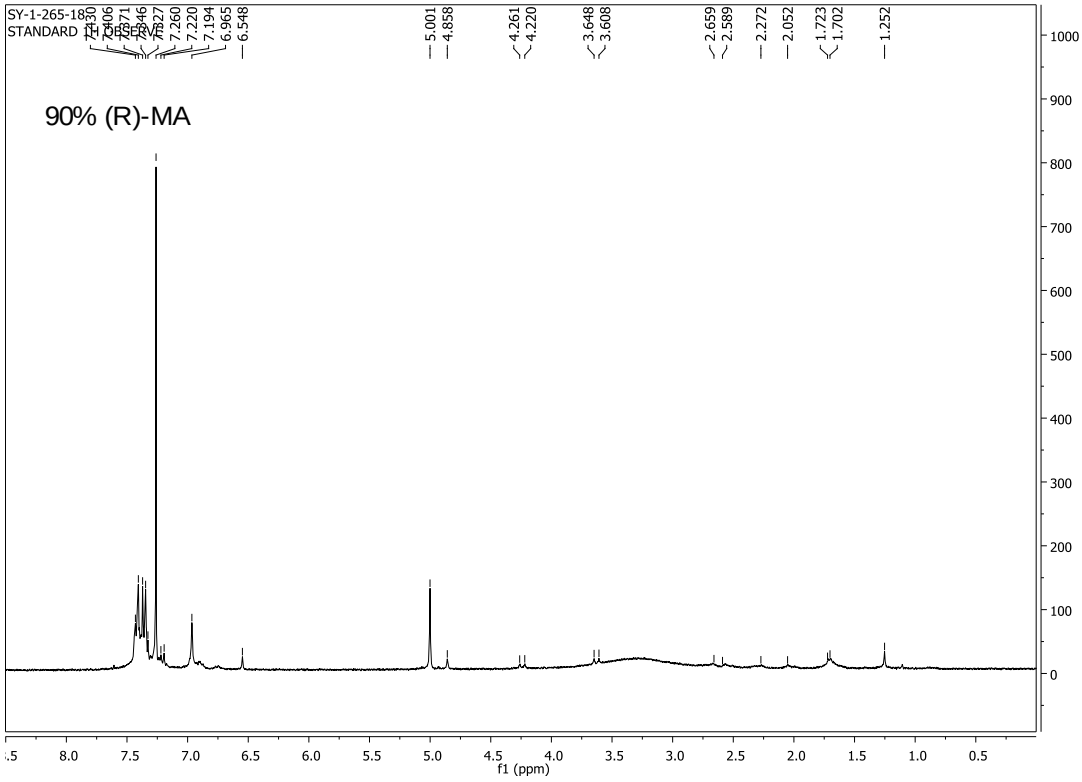
SY-1-265-18
STANDARD 1H OBSERVE
7.330
7.306
7.271
7.246
7.227
7.260
7.220
7.194
6.965
6.548
5.001
4.858
4.261
4.220
3.648
3.608
2.659
2.589
2.272
2.052
1.723
1.702
1.252
90% (R)-MA
f1 (ppm)

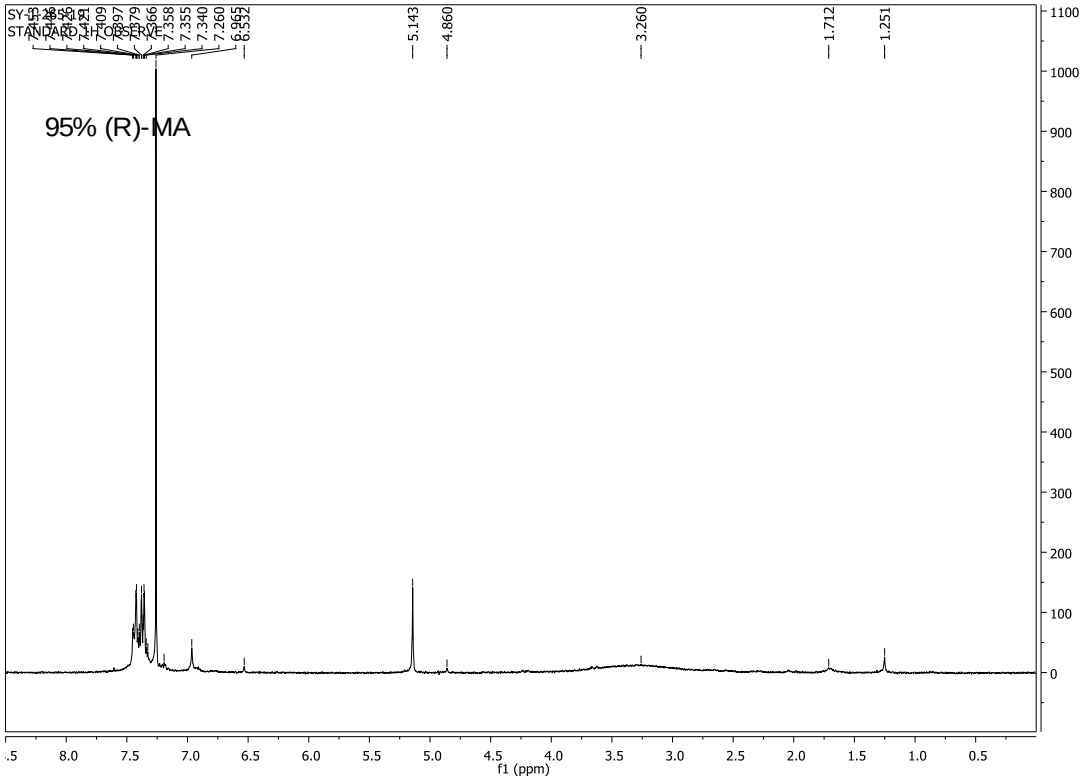
STANDARD 1H OBSERVE
7.358
7.355
7.340
7.260
5.143
4.860
3.260
1.712
1.251
95% (R)-MA
f1 (ppm)

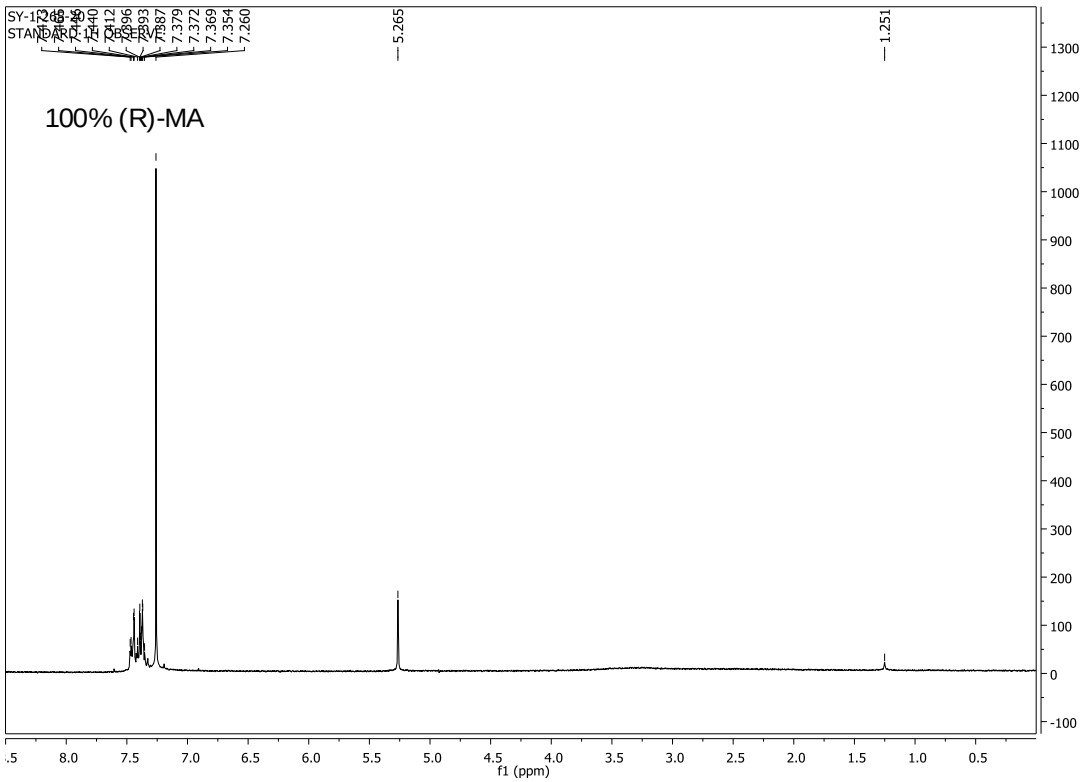
7.379
7.372
7.369
7.354
7.260
5.265
1.251
100% (R)-MA
f1 (ppm)

Appendix to Chapter 4

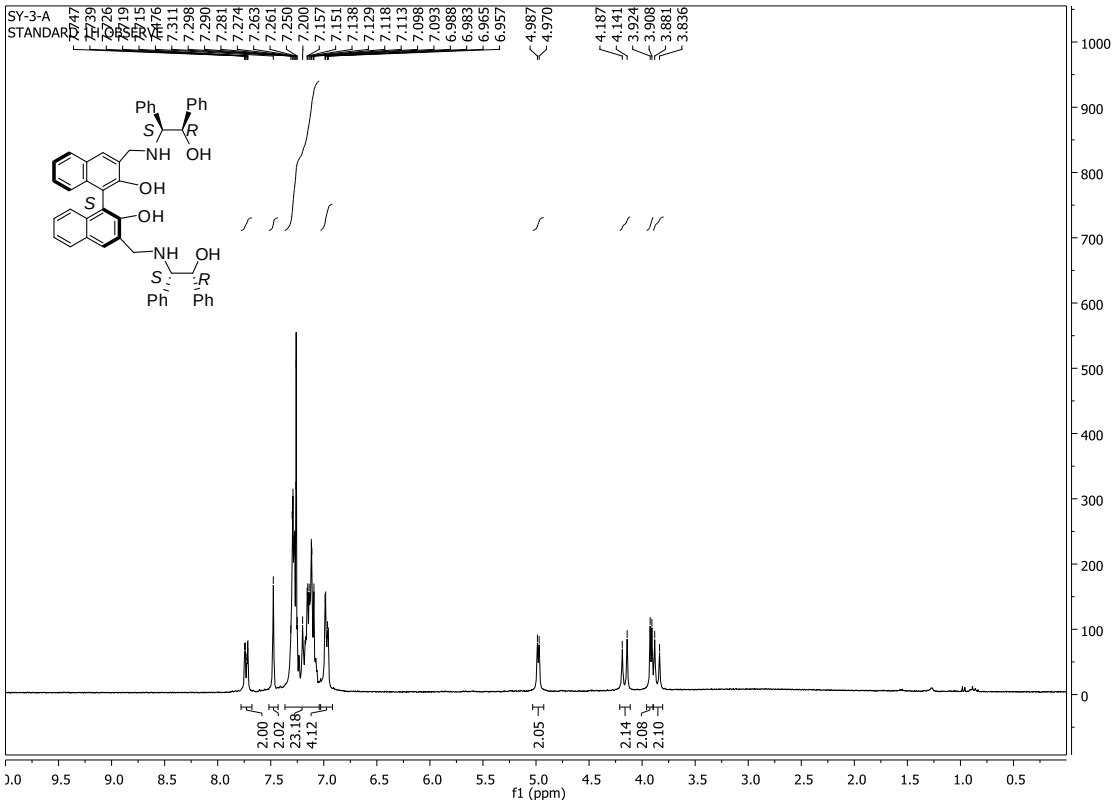

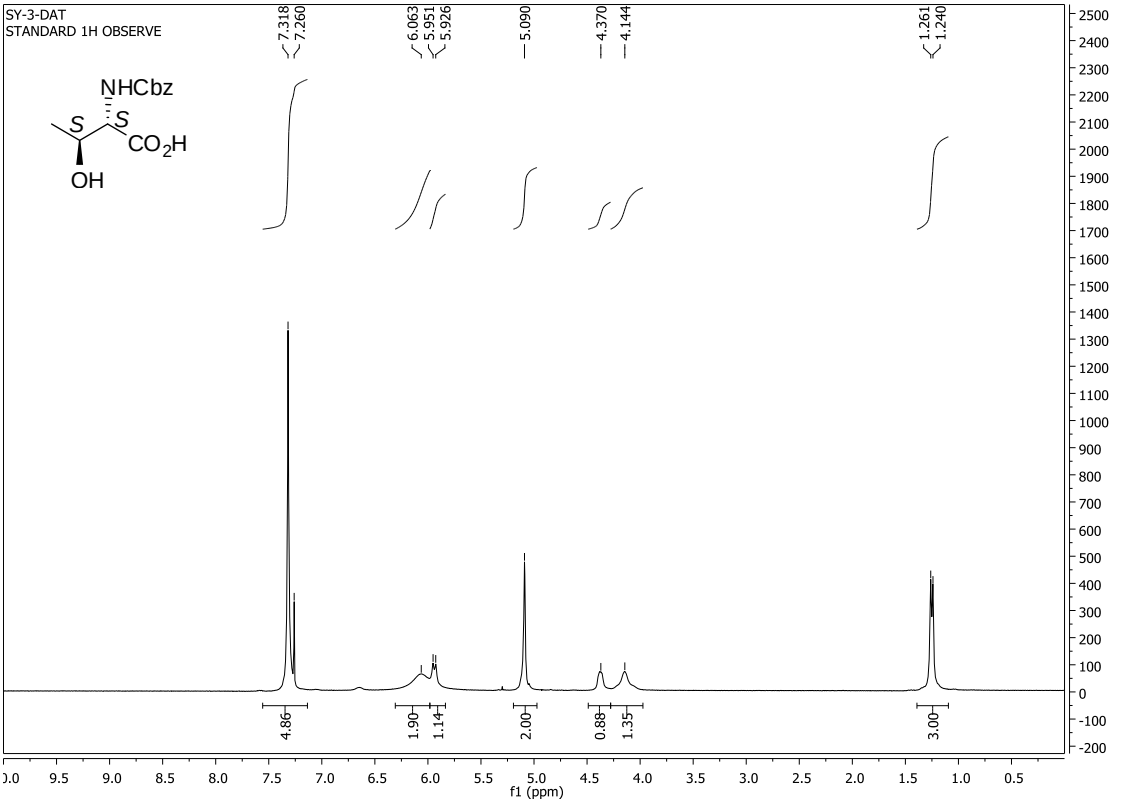
SY-3-DAT
STANDARD 1H OBSERVE
7.318
7.260
6.063
5.951
5.926
5.090
4.370
4.144
1.261
1.240
NHCbz
S
S
CO2H
OH
4.86
1.90
1.14
2.00
0.88
1.35
3.00
f1 (ppm)

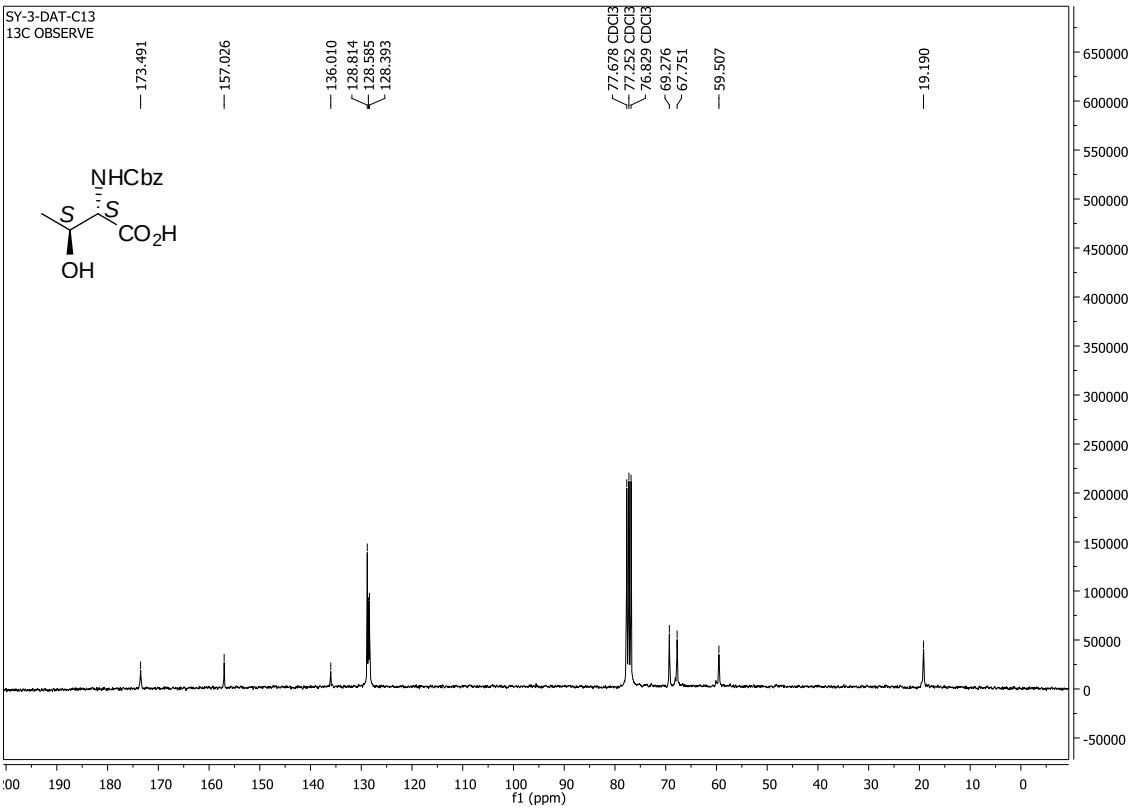
SY-3-DAT-C13
13C OBSERVE
173.491
157.026
136.010
128.814
128.585
128.393
77.678 CDCl3
77.252 CDCl3
76.829 CDCl3
69.276
67.751
59.507
19.190
NHCbz
S
S
CO2H
OH
f1 (ppm)

Appendix to Chapter 5

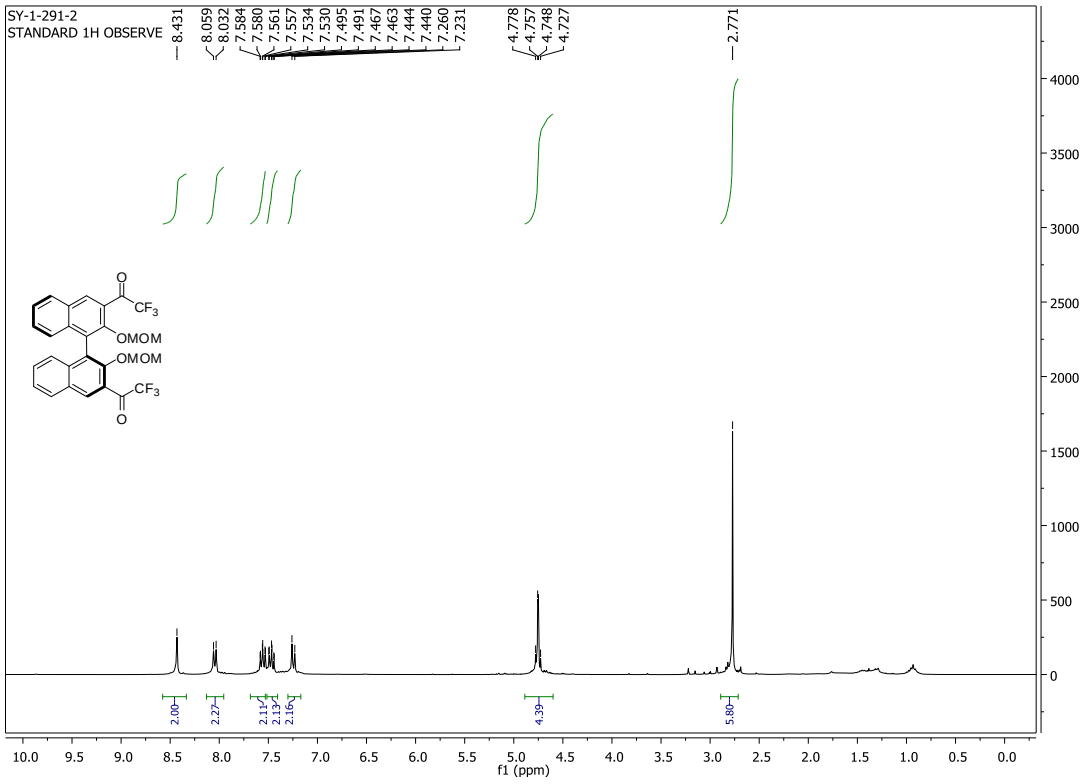

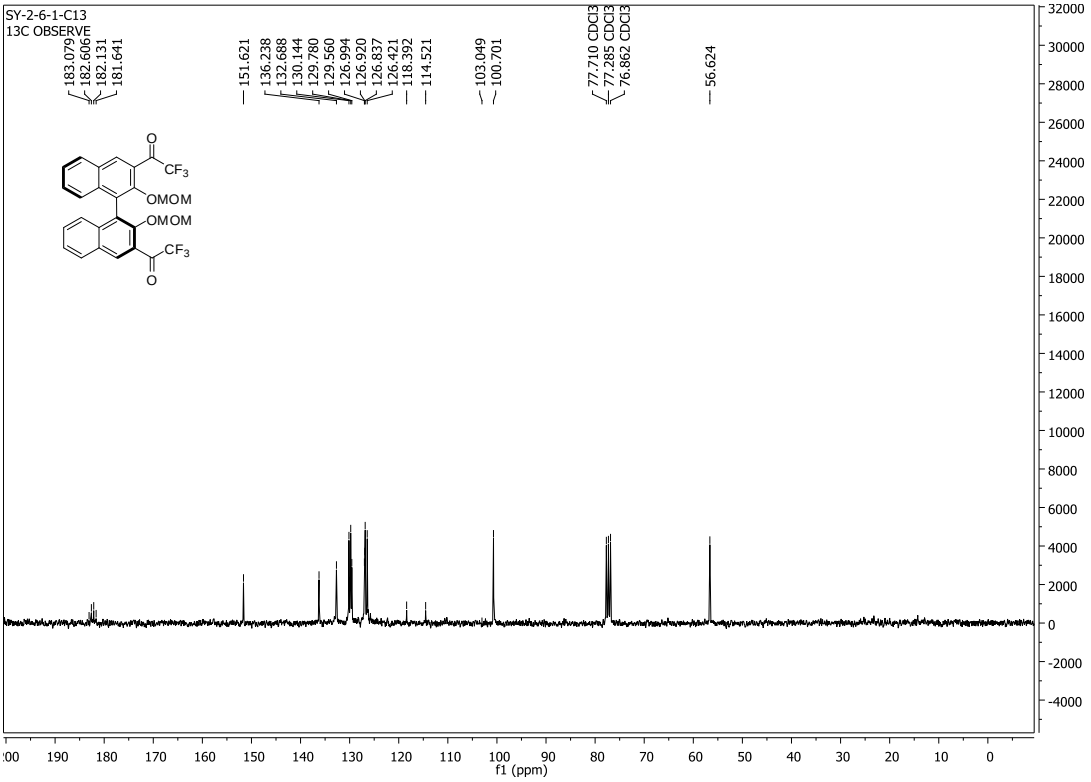
SY-2-6-1-C13
13C OBSERVE
183.079
182.606
182.131
181.641
151.621
136.238
132.688
130.144
129.780
129.560
126.994
126.920
126.837
126.421
118.392
114.521
103.049
100.701
77.710 CDCl3
77.285 CDCl3
76.862 CDCl3
56.624
OMOM
OMOM
CF3
CF3
f1 (ppm)

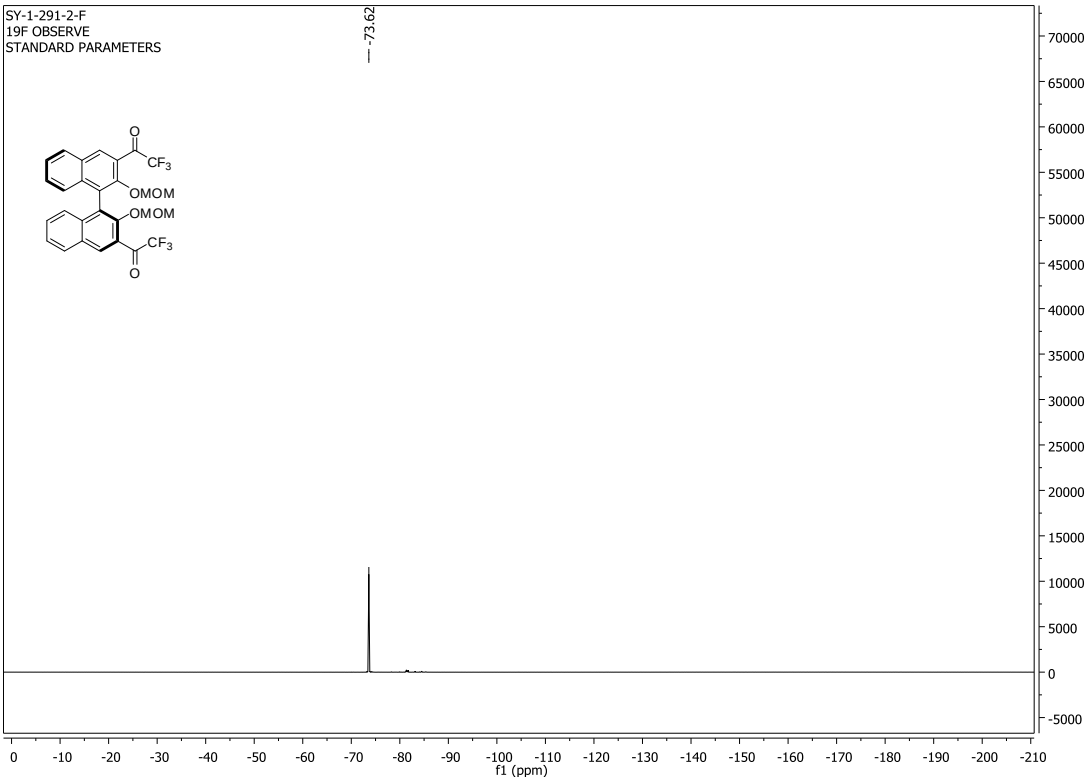
SY-1-291-2-F
19F OBSERVE
STANDARD PARAMETERS
-73.62
OMOM
OMOM
CF3
CF3
f1 (ppm)

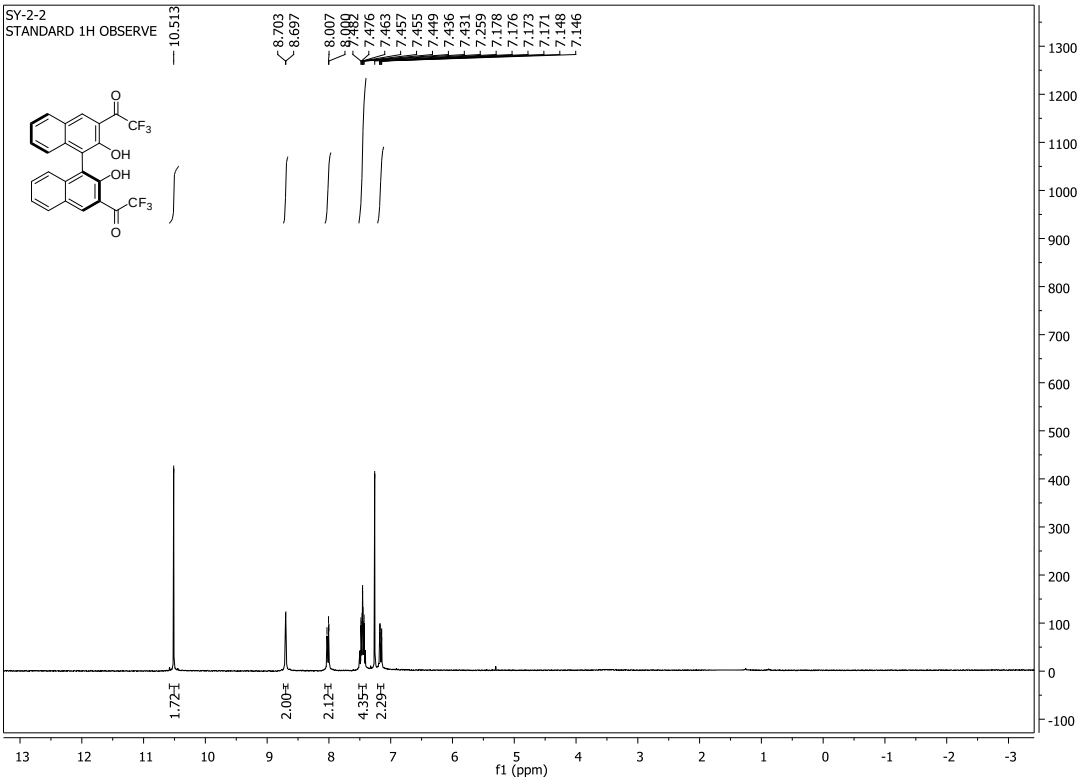
SY-2-2
STANDARD 1H OBSERVE
10.513
8.703
8.697
8.007
7.476
7.463
7.457
7.455
7.449
7.436
7.431
7.259
7.178
7.176
7.173
7.171
7.148
7.146
1.72
2.00
2.12
4.35
2.29
f1 (ppm)

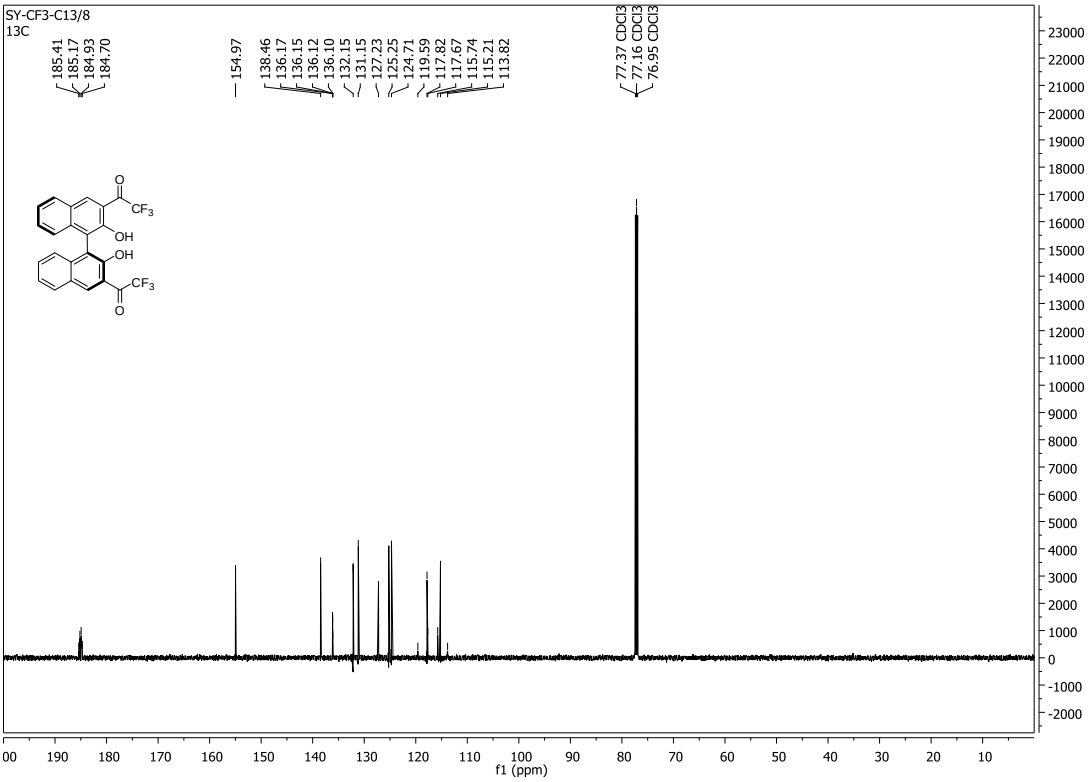
SY-CF3-C13/8
13C
185.41
185.17
184.93
184.70
154.97
138.46
136.17
136.15
136.12
136.10
132.15
131.15
127.23
125.25
124.71
119.59
117.82
117.67
115.74
115.21
113.82
77.37 CDCl3
77.16 CDCl3
76.95 CDCl3
f1 (ppm)

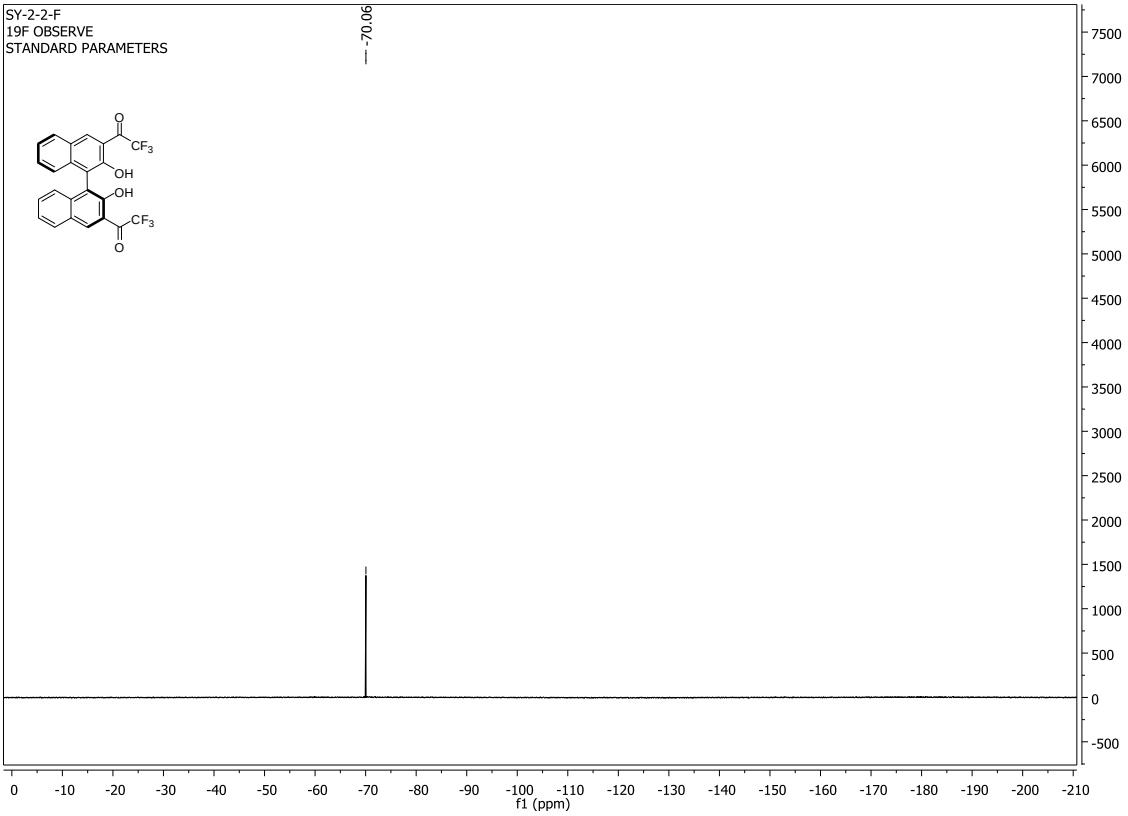
SY-2-2-F
19F OBSERVE
STANDARD PARAMETERS
-70.06
f1 (ppm)

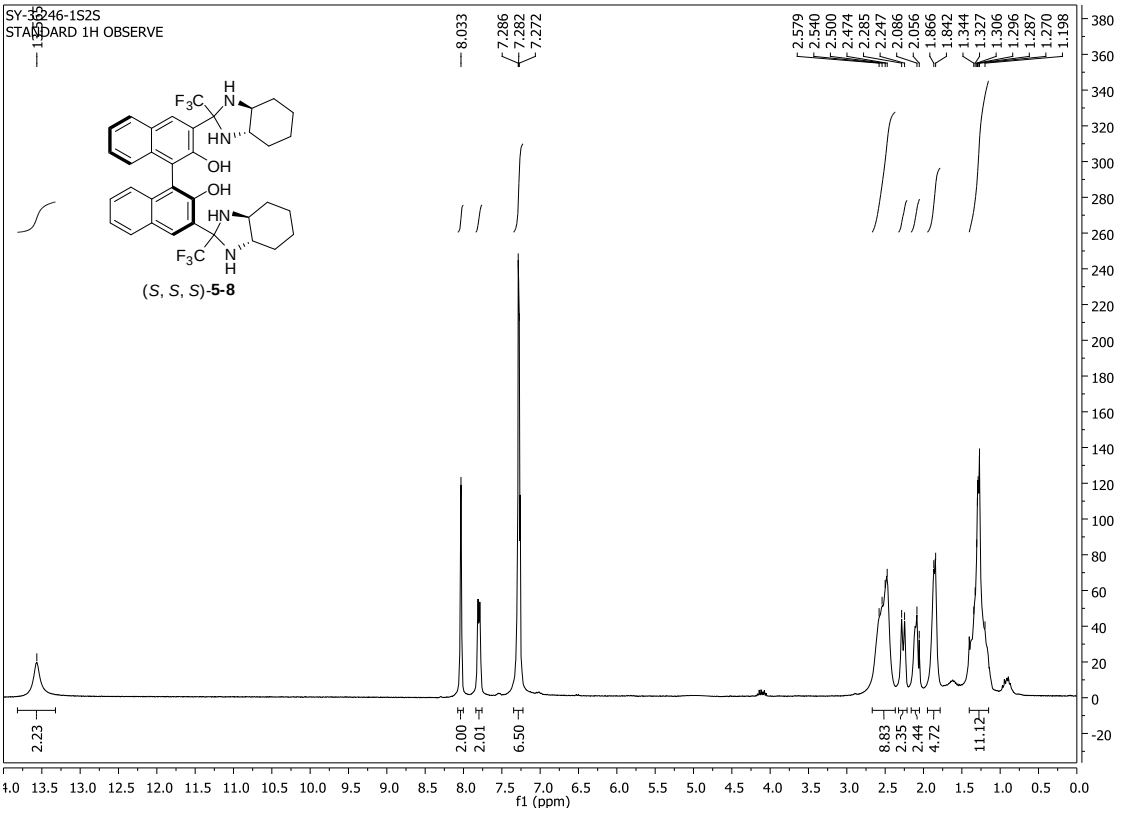
SY-3246-1S2S
STANDARD 1H OBSERVE
8.033
7.286
7.282
7.272
2.579
2.540
2.500
2.474
2.285
2.247
2.086
2.056
1.866
1.842
1.344
1.327
1.306
1.296
1.287
1.270
1.198
2.23
2.00
2.01
6.50
8.83
2.35
2.44
4.72
11.12
f1 (ppm)

(*S*, *S*, *S*)-**5-8**

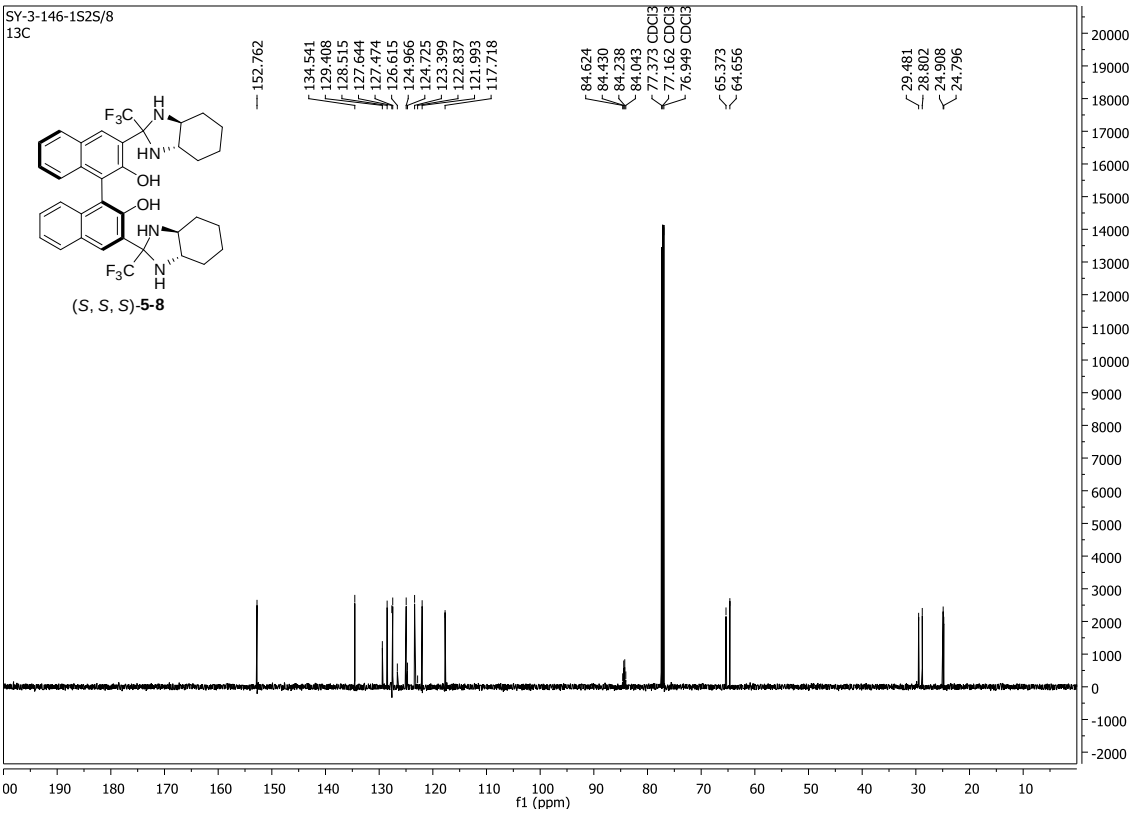
SY-3-146-1S2S/8
13C
152.762
134.541
129.408
128.515
127.644
127.474
126.615
124.966
124.725
123.399
122.837
121.993
117.718
84.624
84.430
84.238
84.043
77.373 CDCl3
77.162 CDCl3
76.949 CDCl3
65.373
64.656
29.481
28.802
24.908
24.796
(S, S, S)-5-8
f1 (ppm)

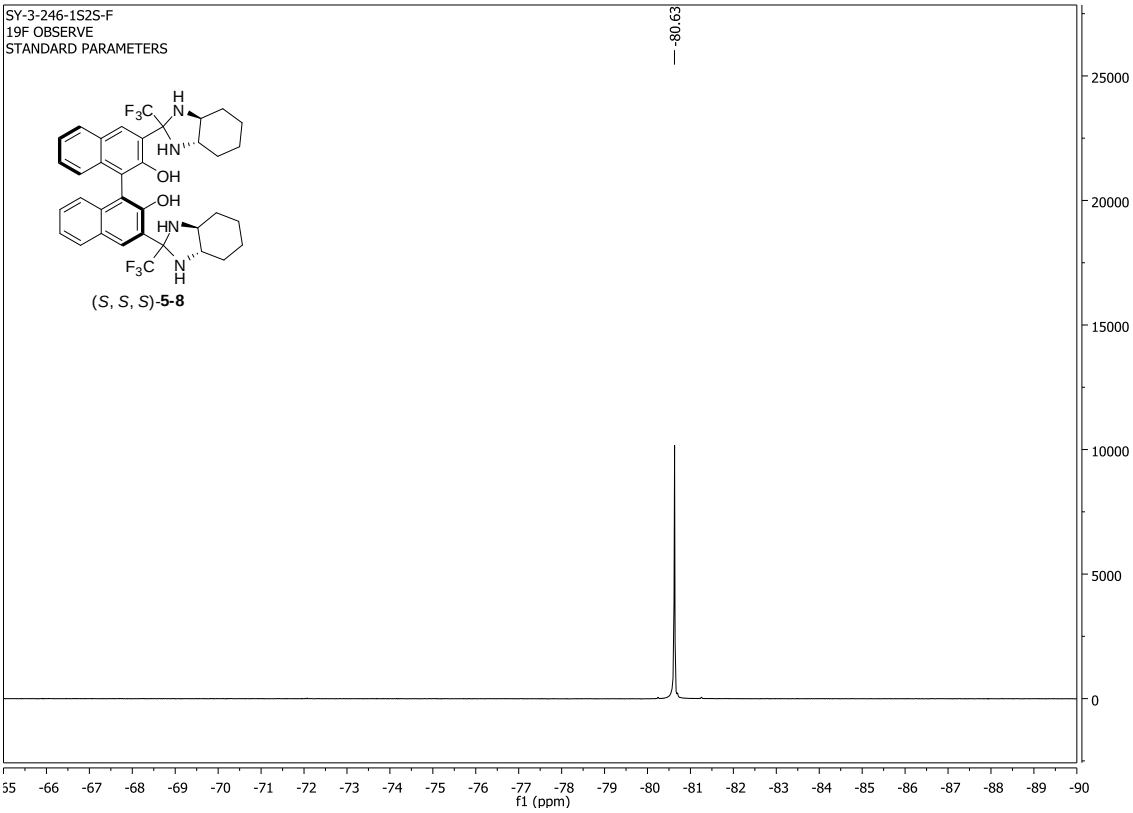
SY-3-246-1S2S-F
19F OBSERVE
STANDARD PARAMETERS
-80.63
(S, S, S)-5-8
f1 (ppm)

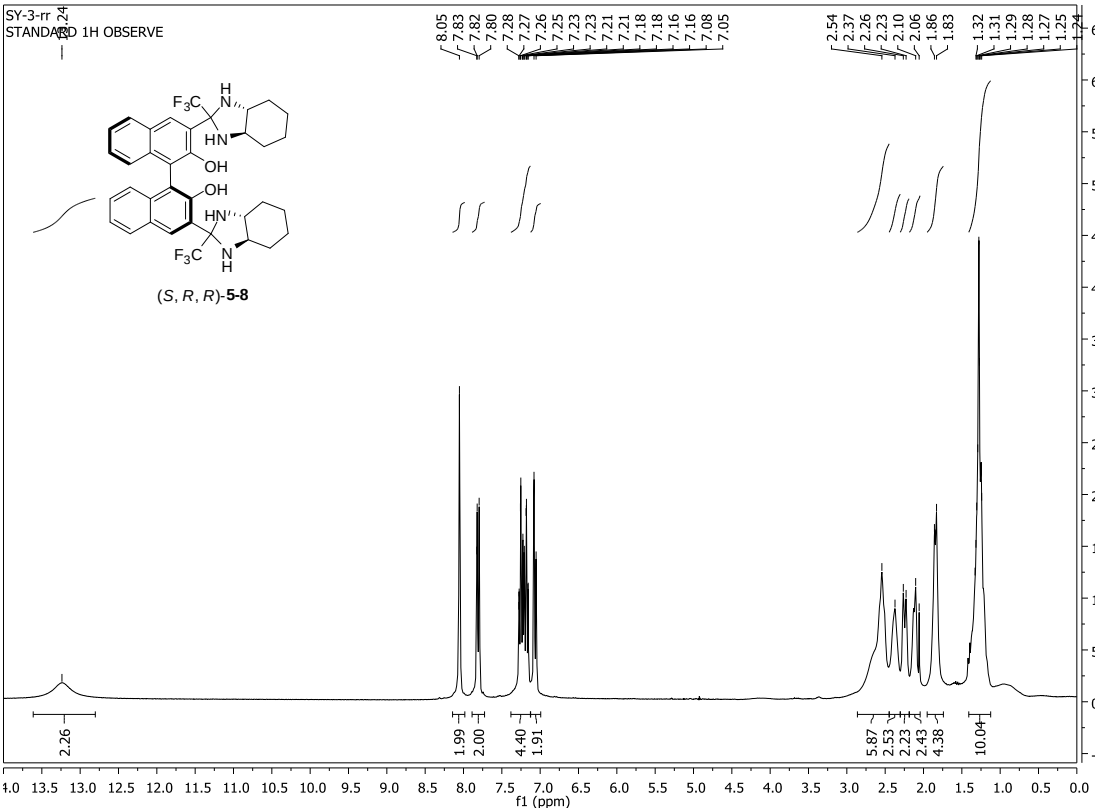
SY-3-rr
STANDARD 1H OBSERVE
(S, R, R)-5-8
f1 (ppm)

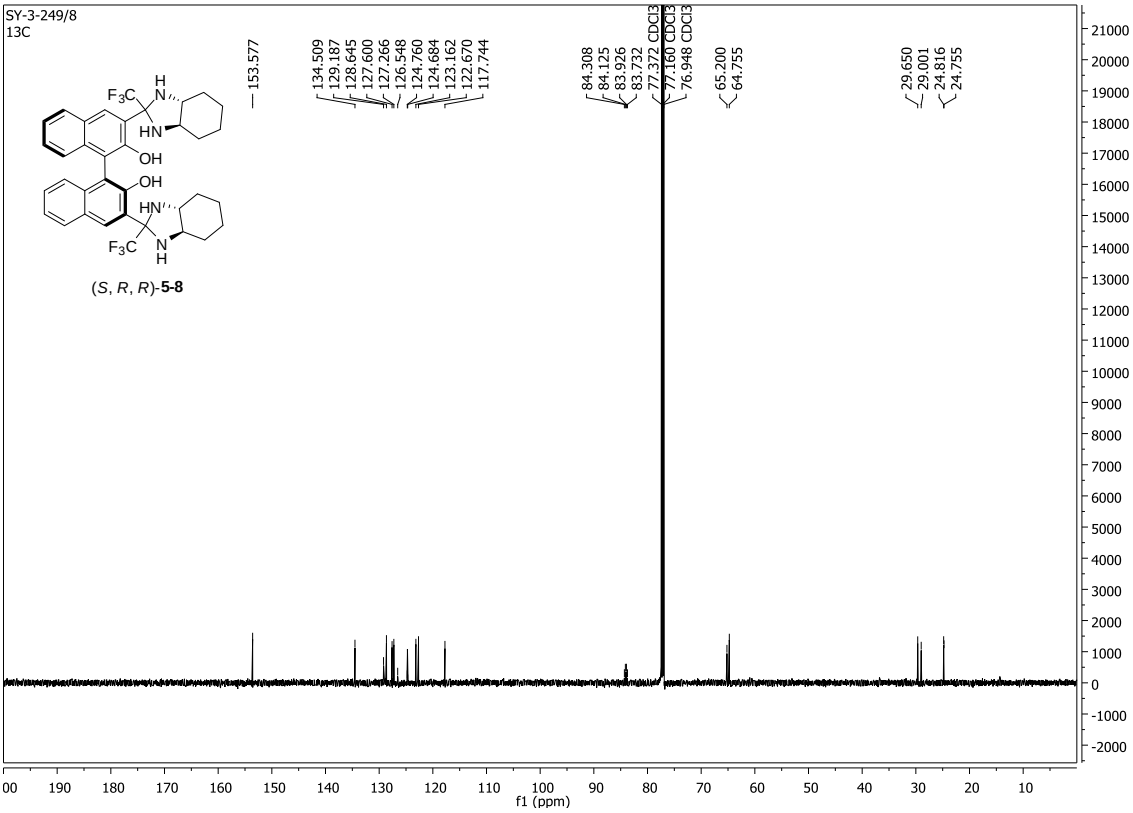
SY-3-249/8
13C
(S, R, R)-5-8
f1 (ppm)

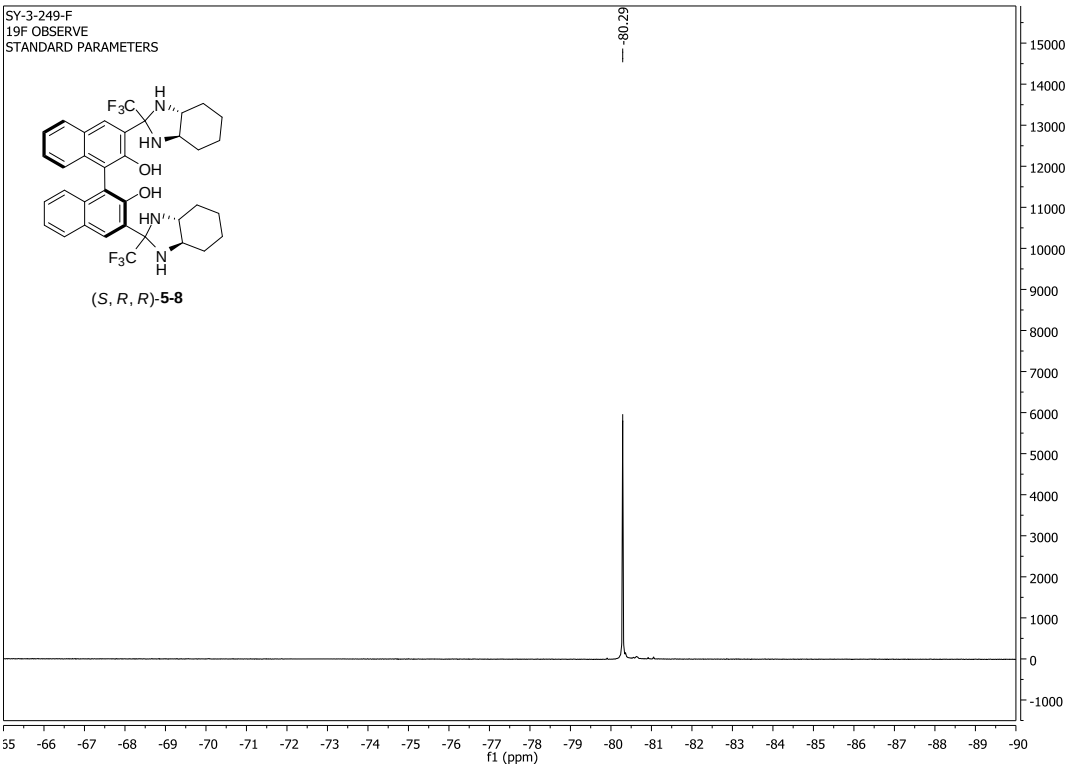

^{19}F NMR Titration of (*S*)-5-3 with (*S*, *S*)-5-4

0 eq of amine

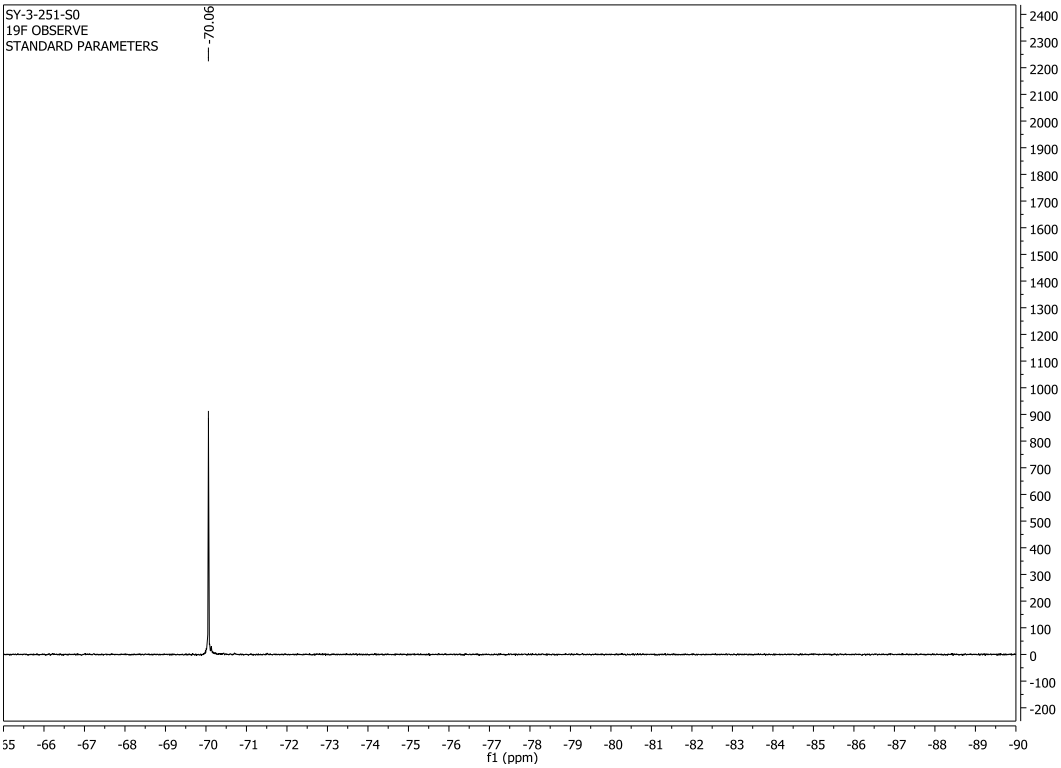

1.2 eq of amine

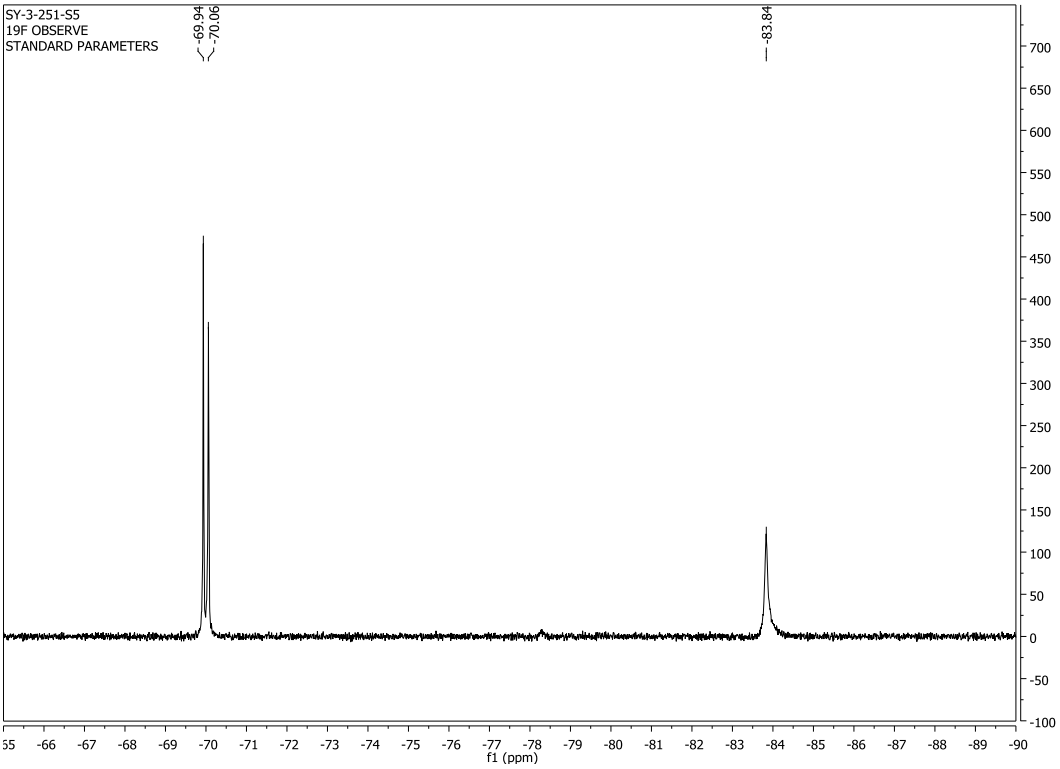

2.4 eq of amine

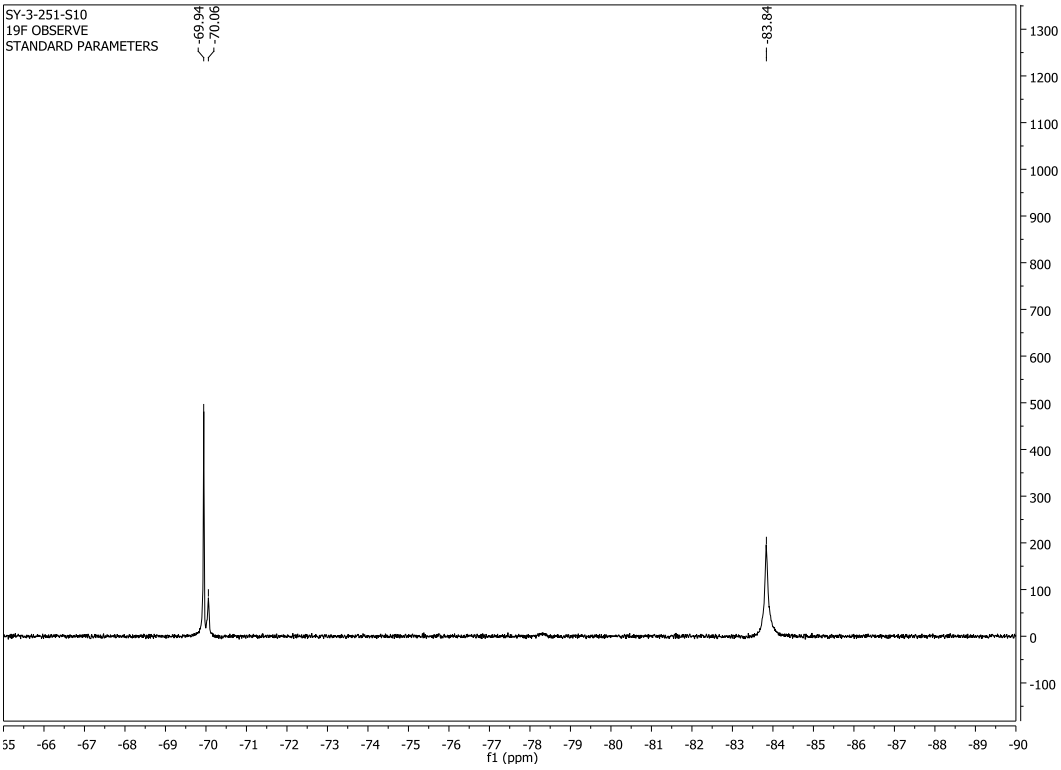

3.6 eq of amine

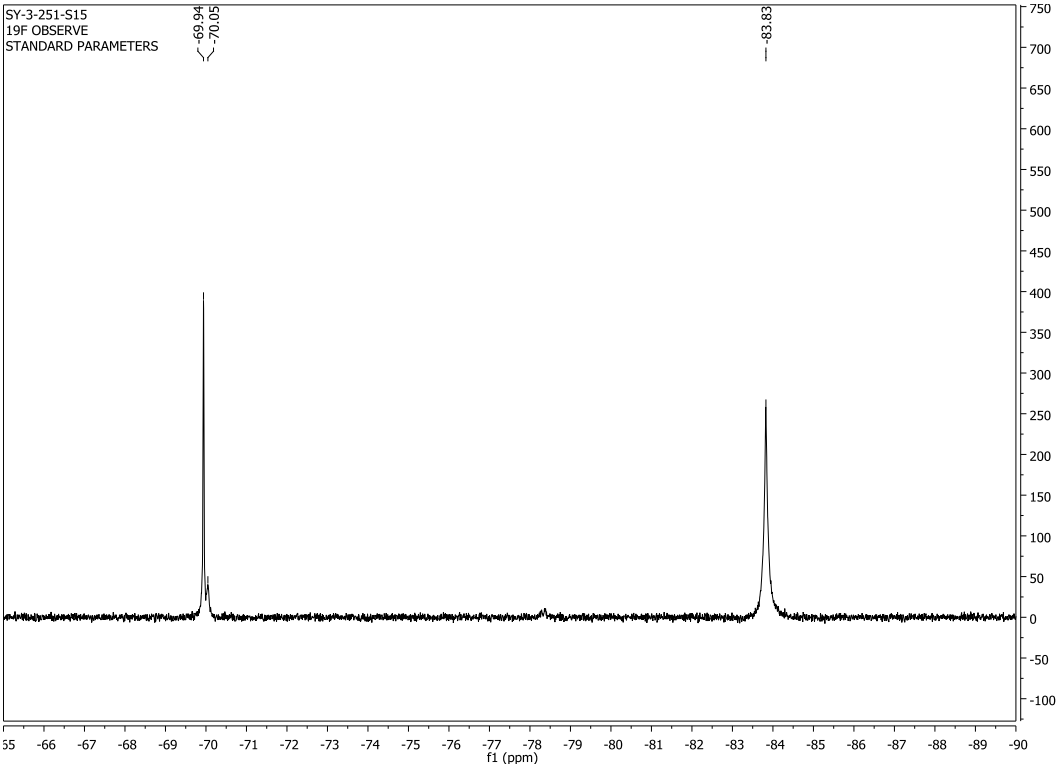

4.8 eq of amine

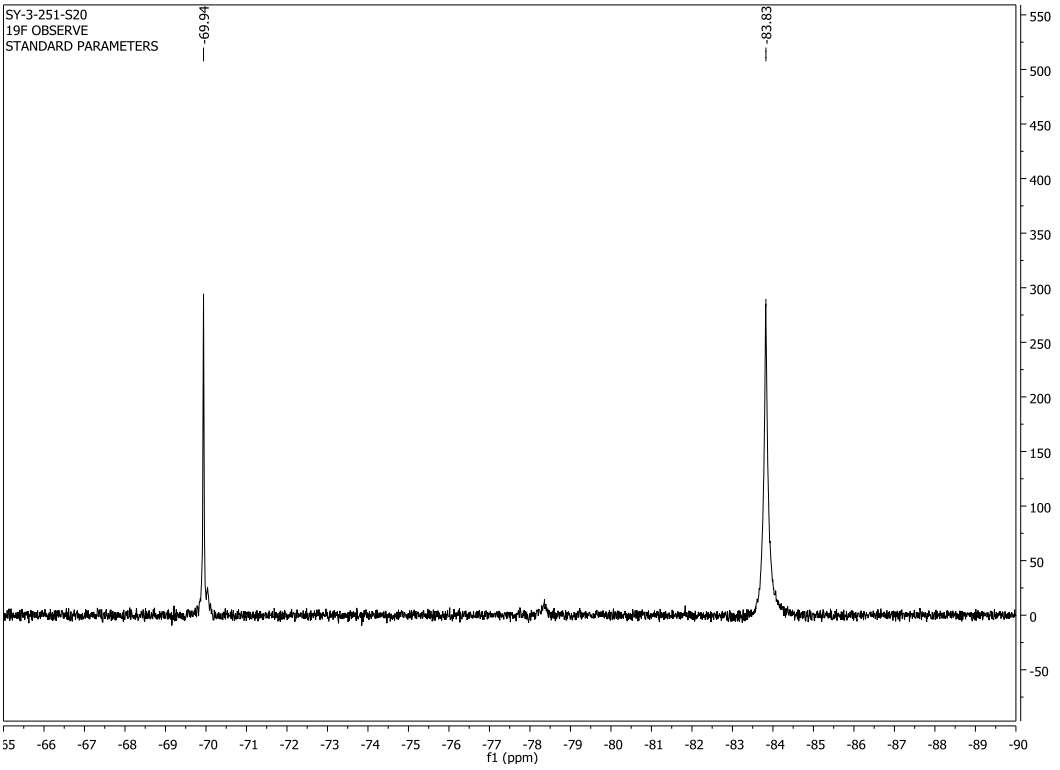

7.0 eq of amine

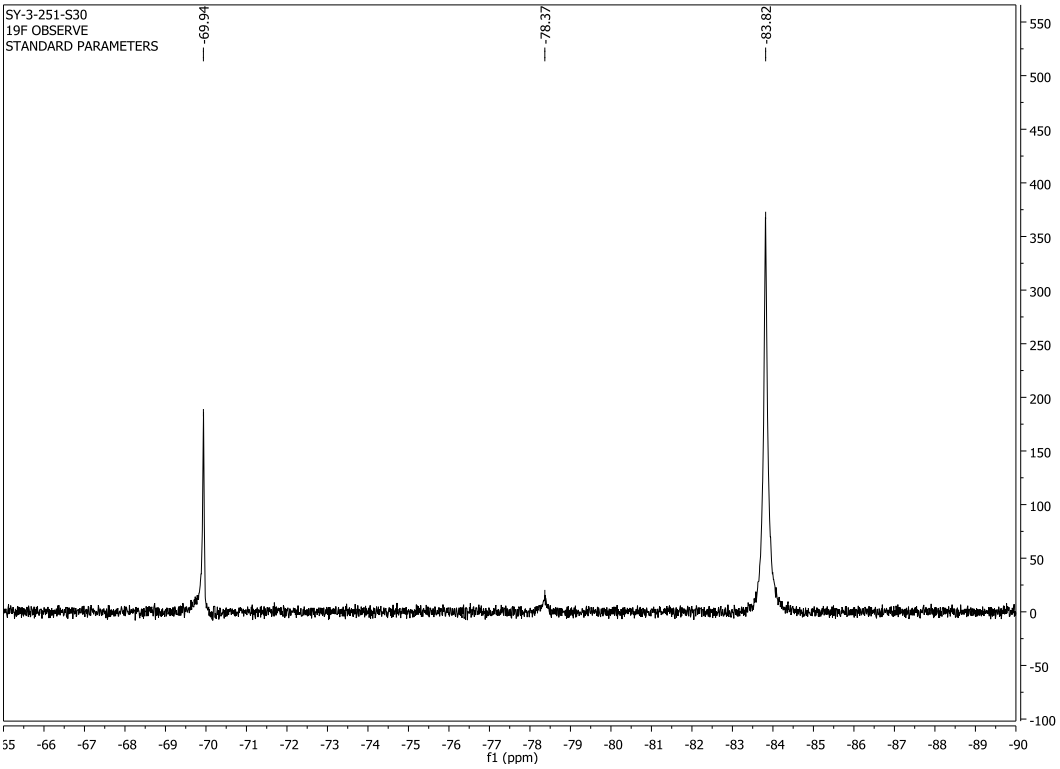

9.1 eq of amine

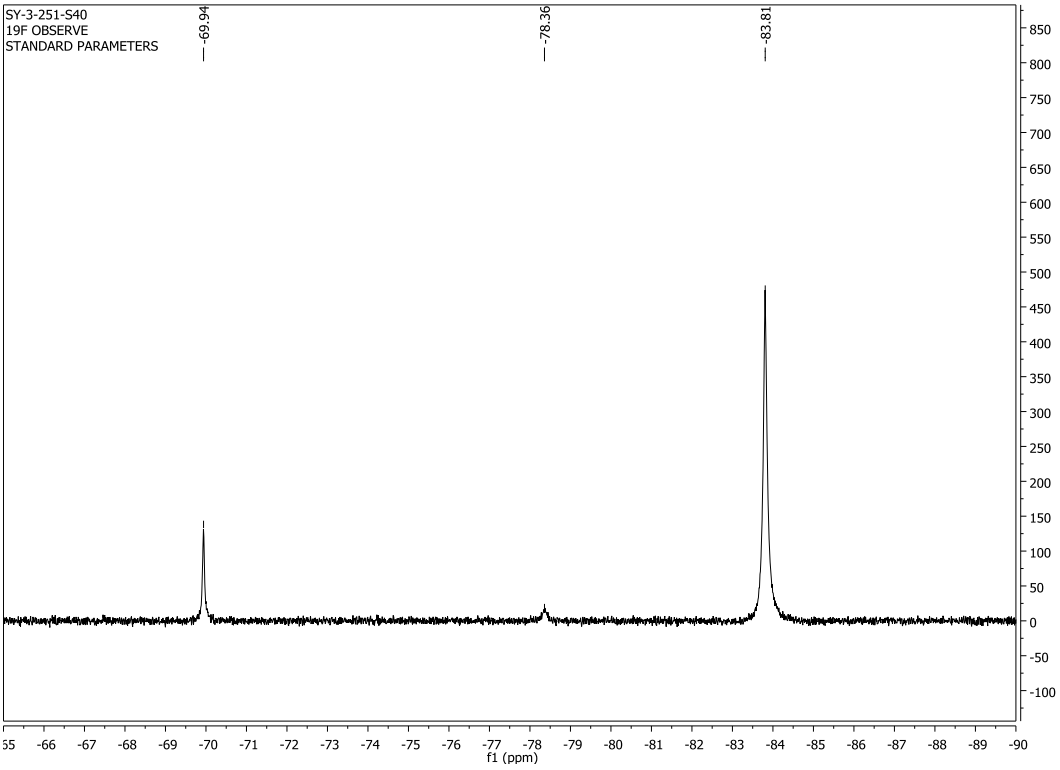

11.1 eq of amine

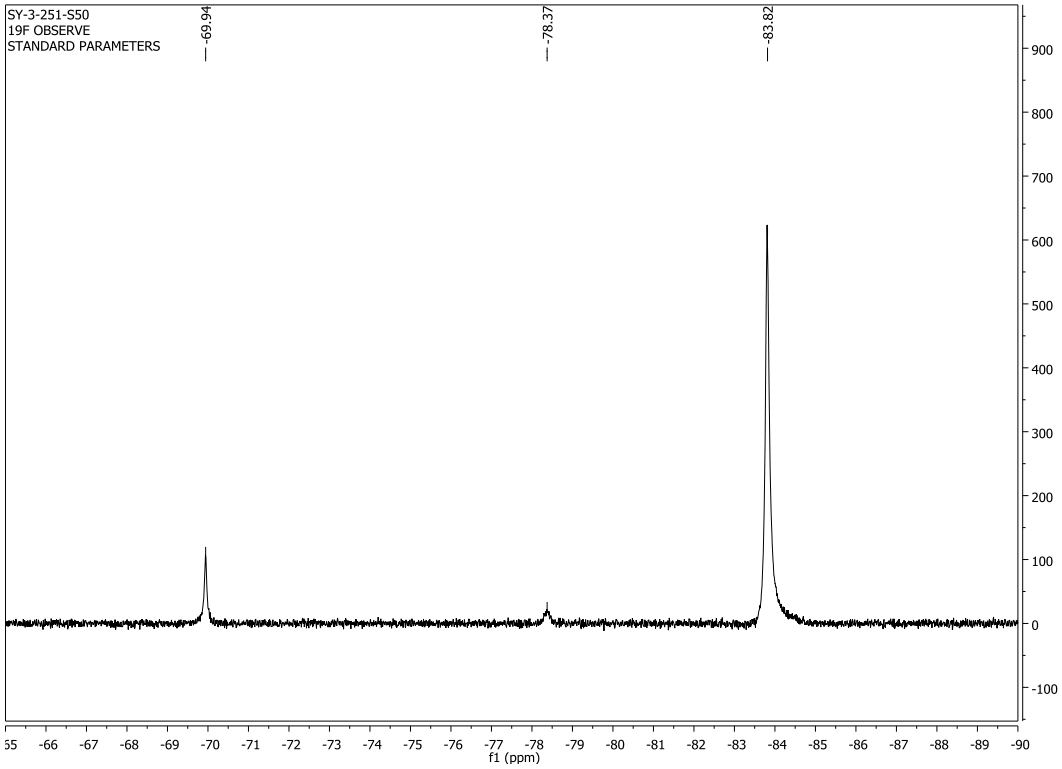

14.9 eq of amine

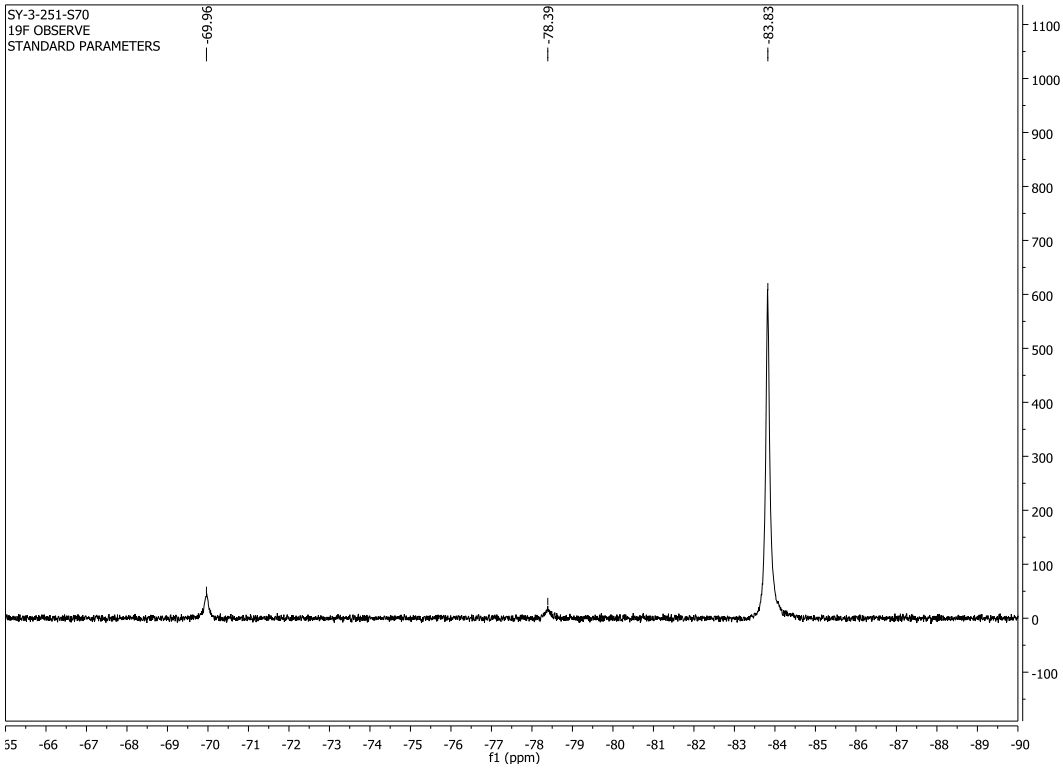

20 eq of amine

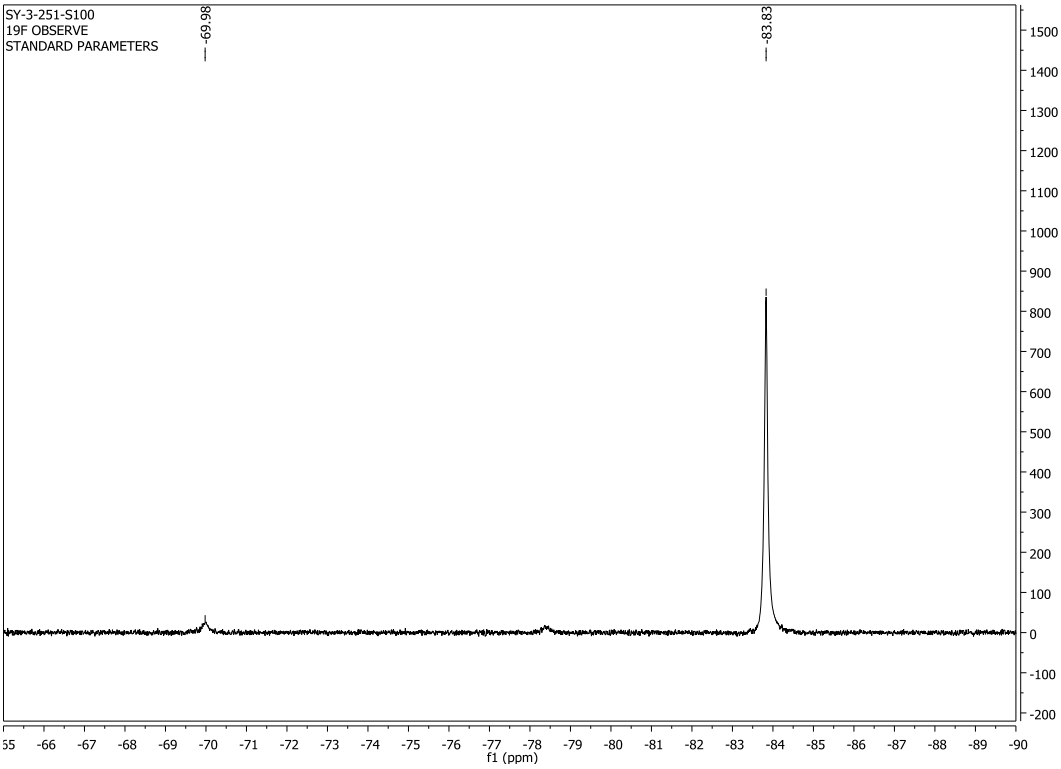

27.3 eq of amine

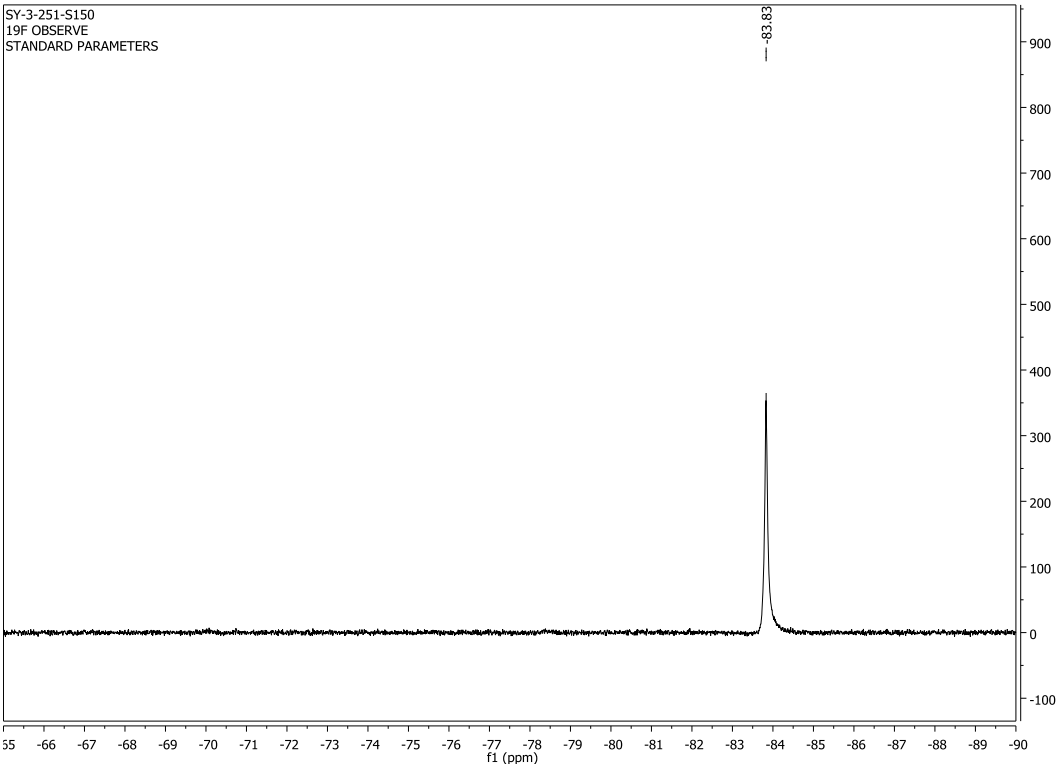

33.3 eq of amine

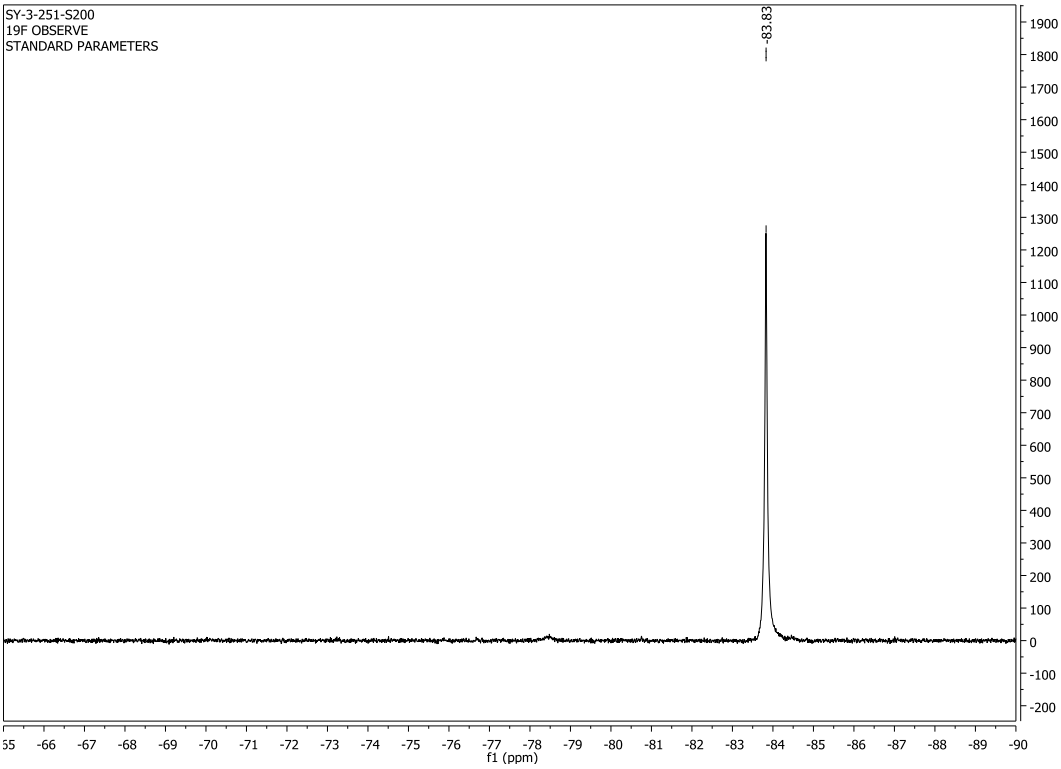

42.9 eq of amine

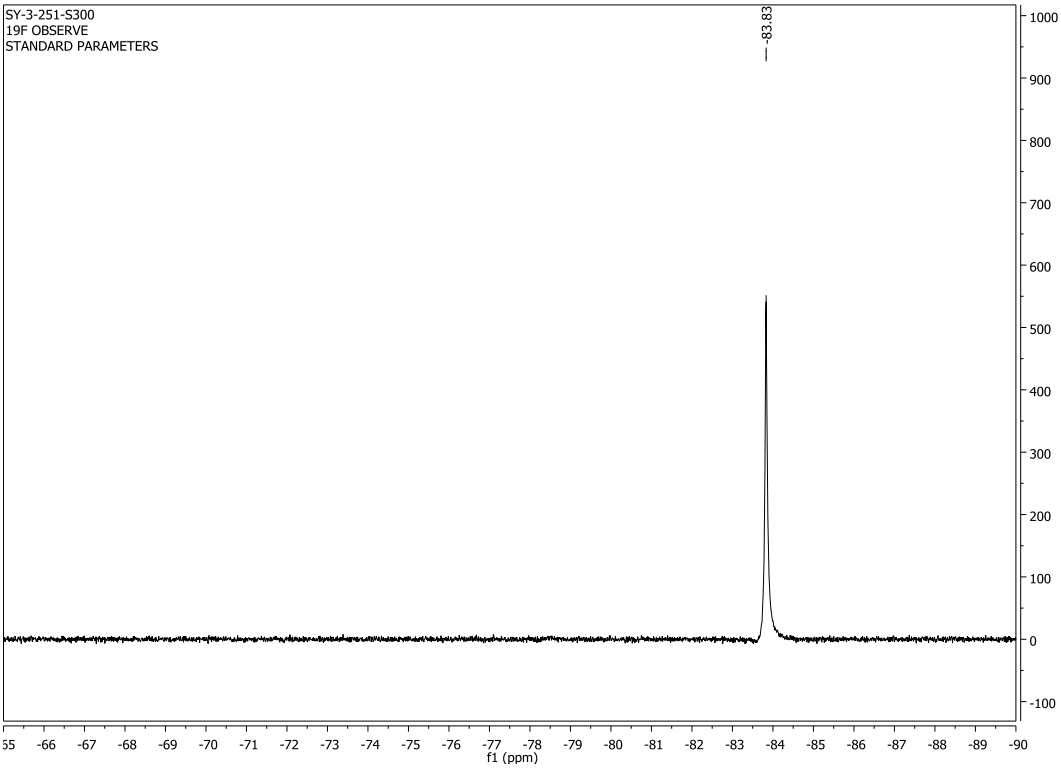

55.6 eq of amine

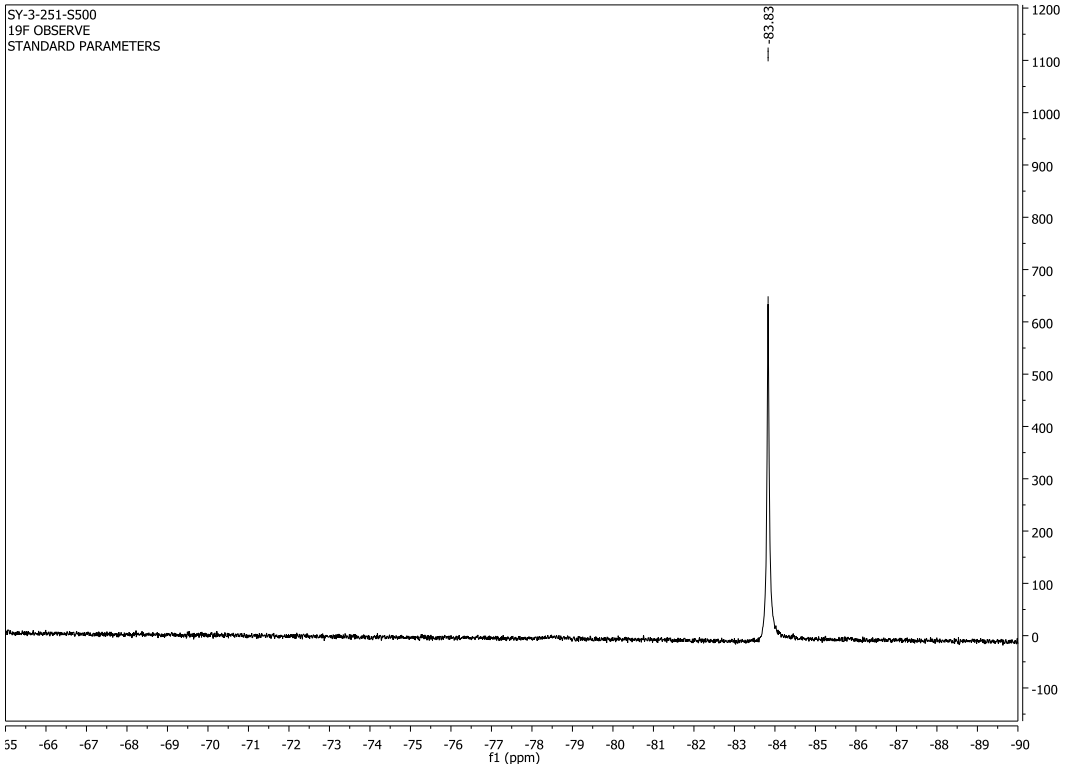

66.7 eq of amine

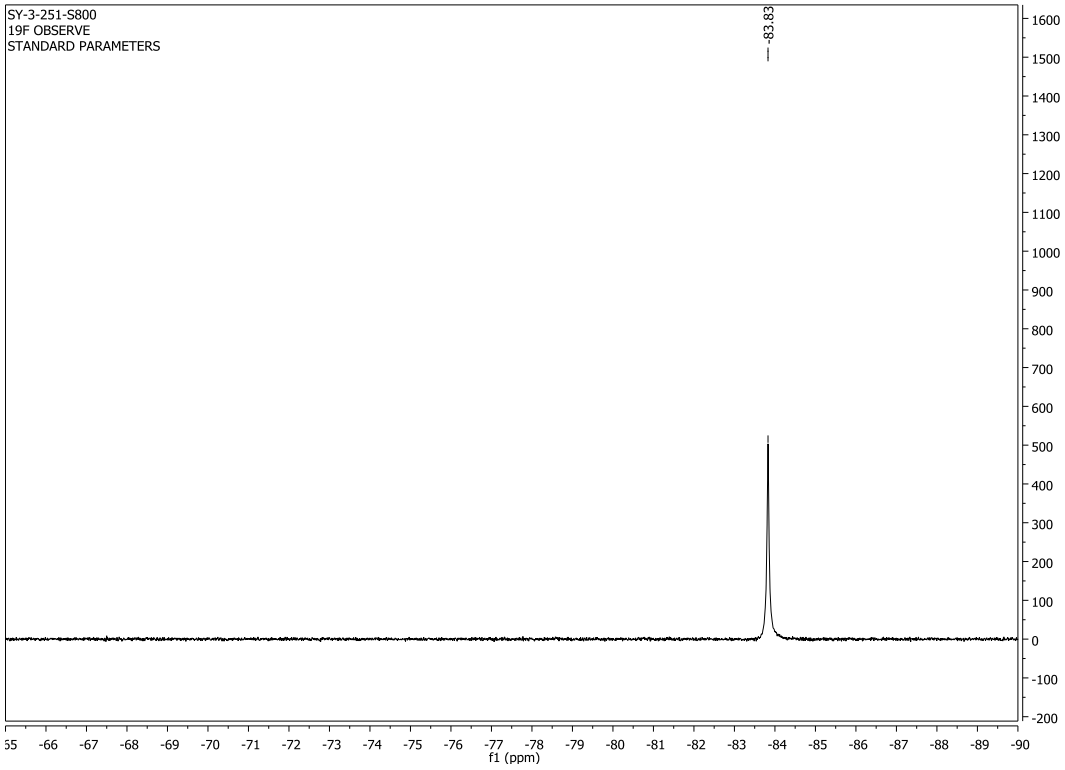

71.0 eq of amine

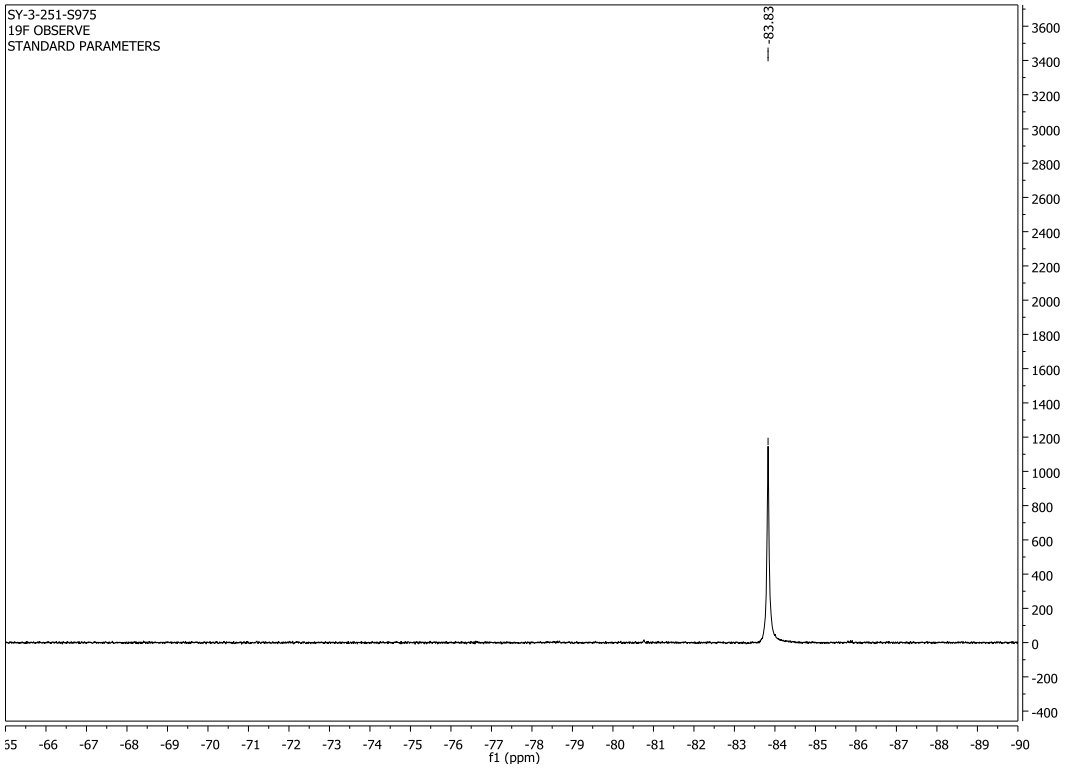

After two days

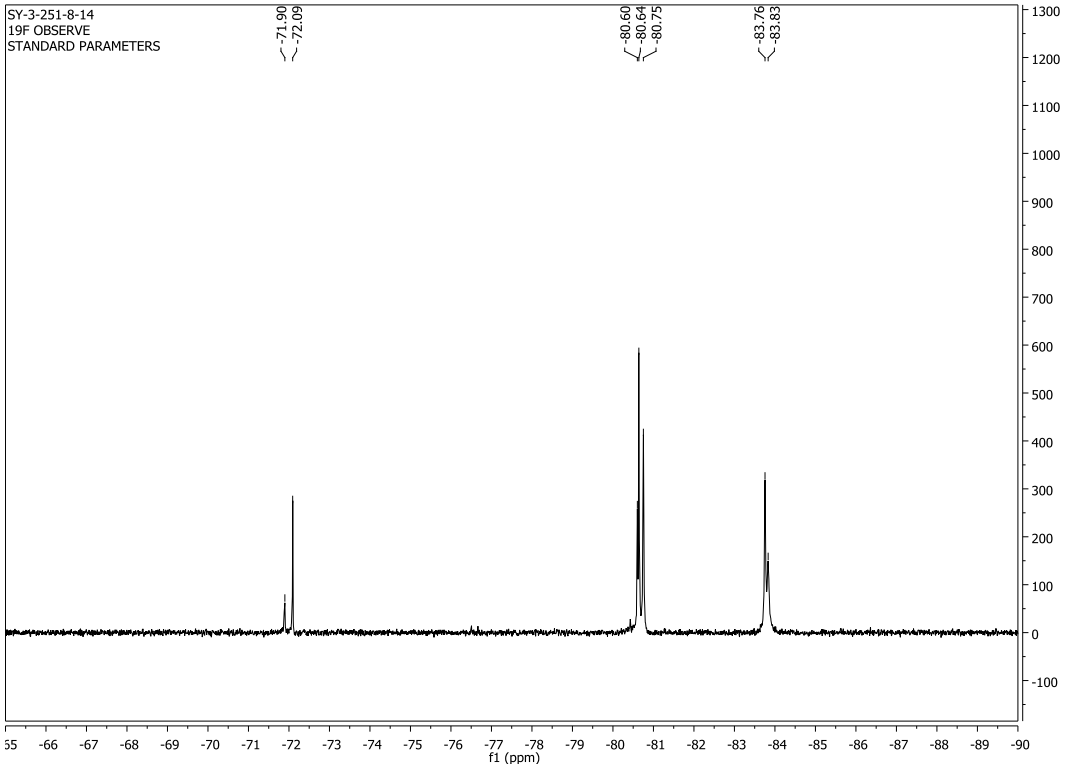

After four days

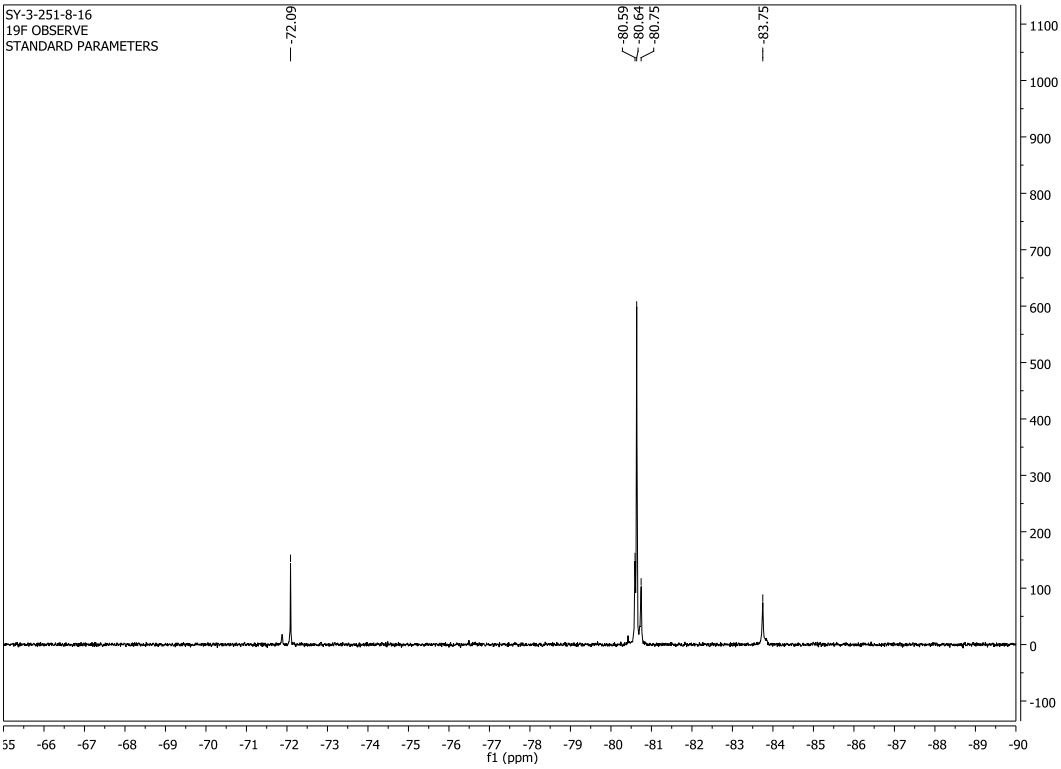

After five days

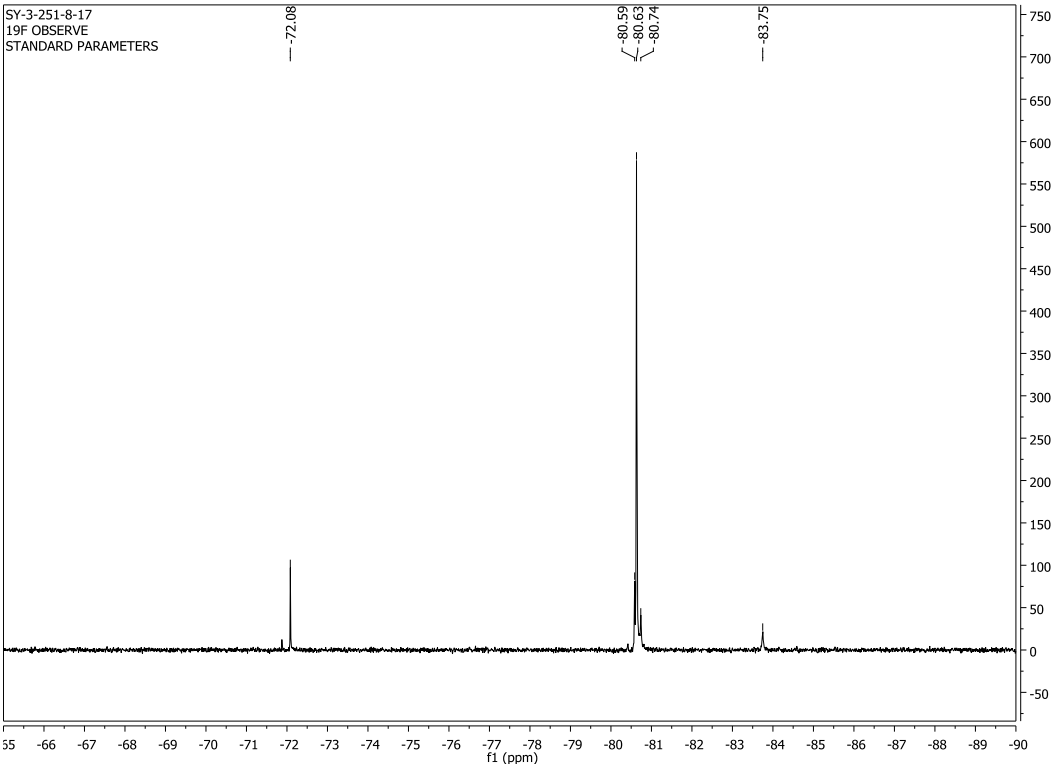

^{19}F NMR Titration of (*S*)-5-3 with (*R*, *R*)-5-4

0 eq of amine

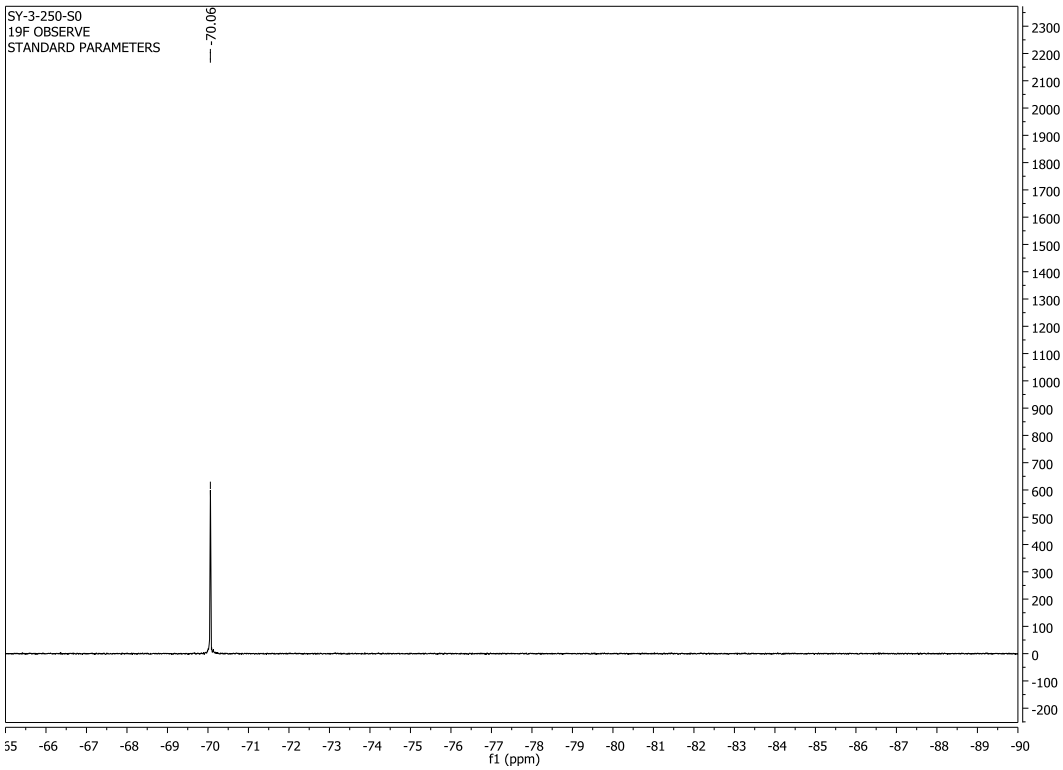

0.5 eq of amine

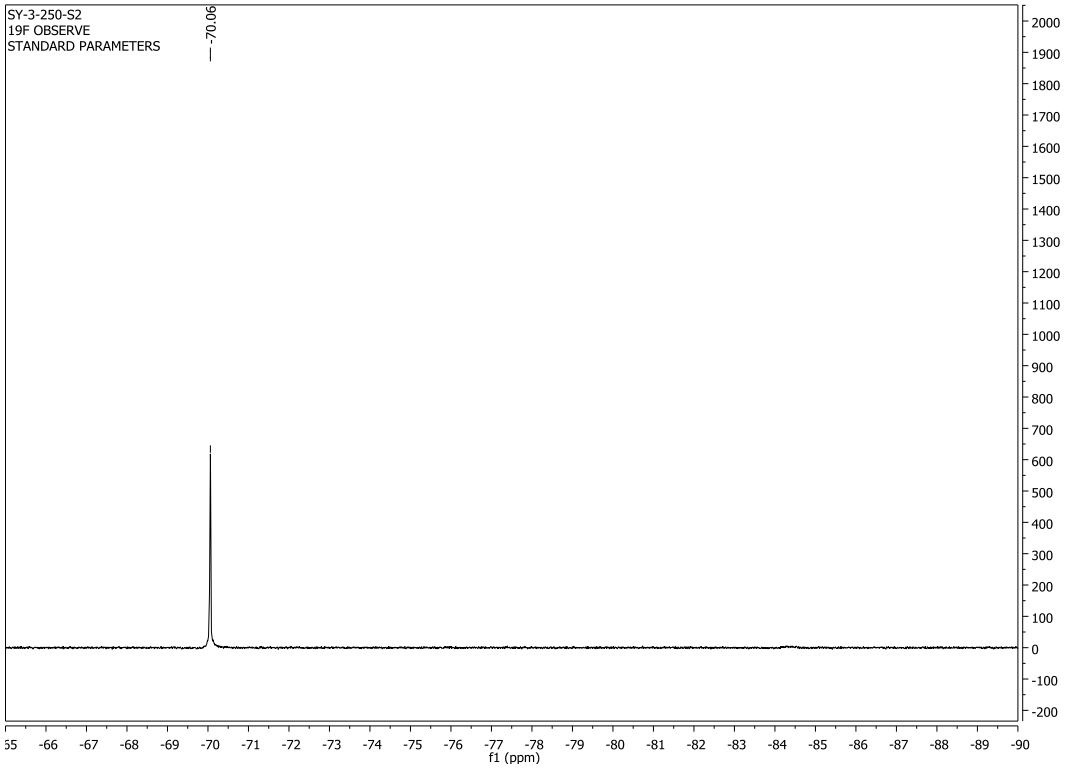

1.2 eq of amine

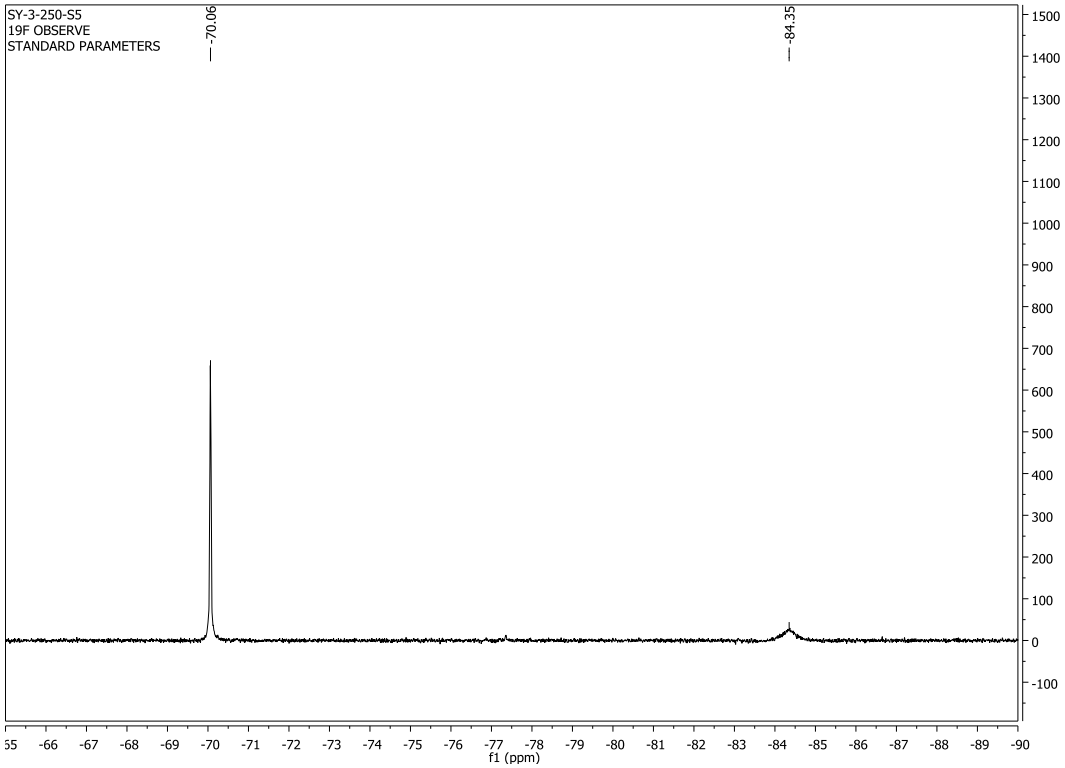

2.4 eq of amine

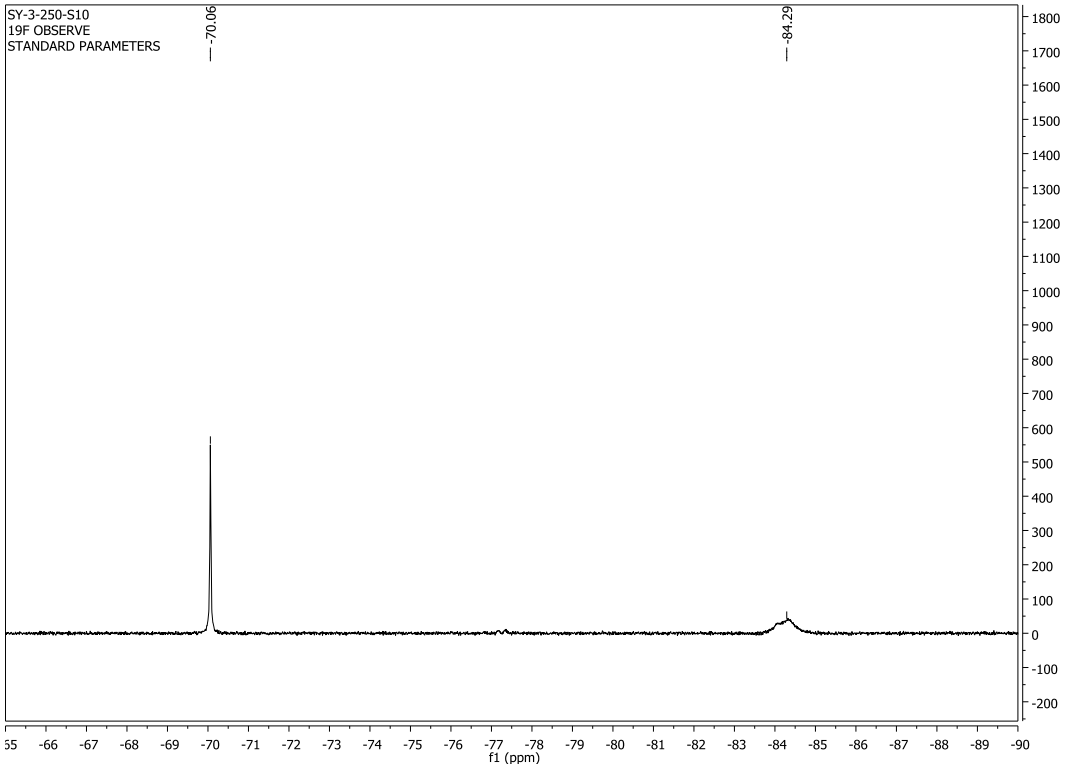

4.8 eq of amine

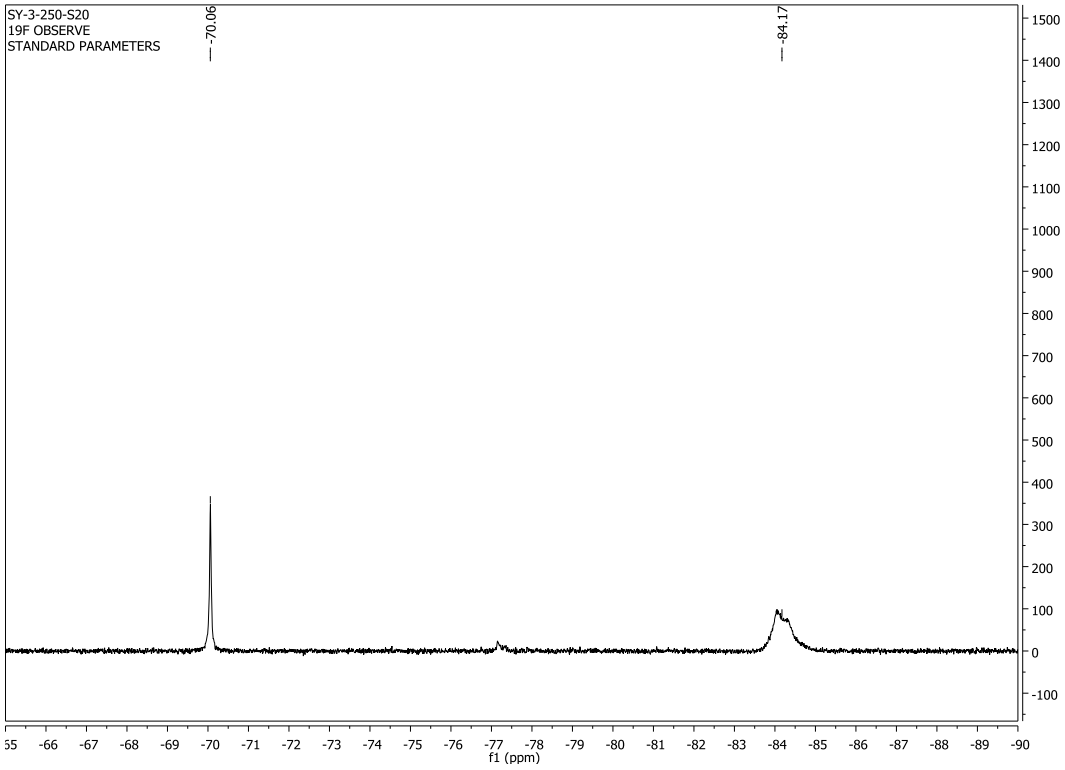

9.1 eq of amine

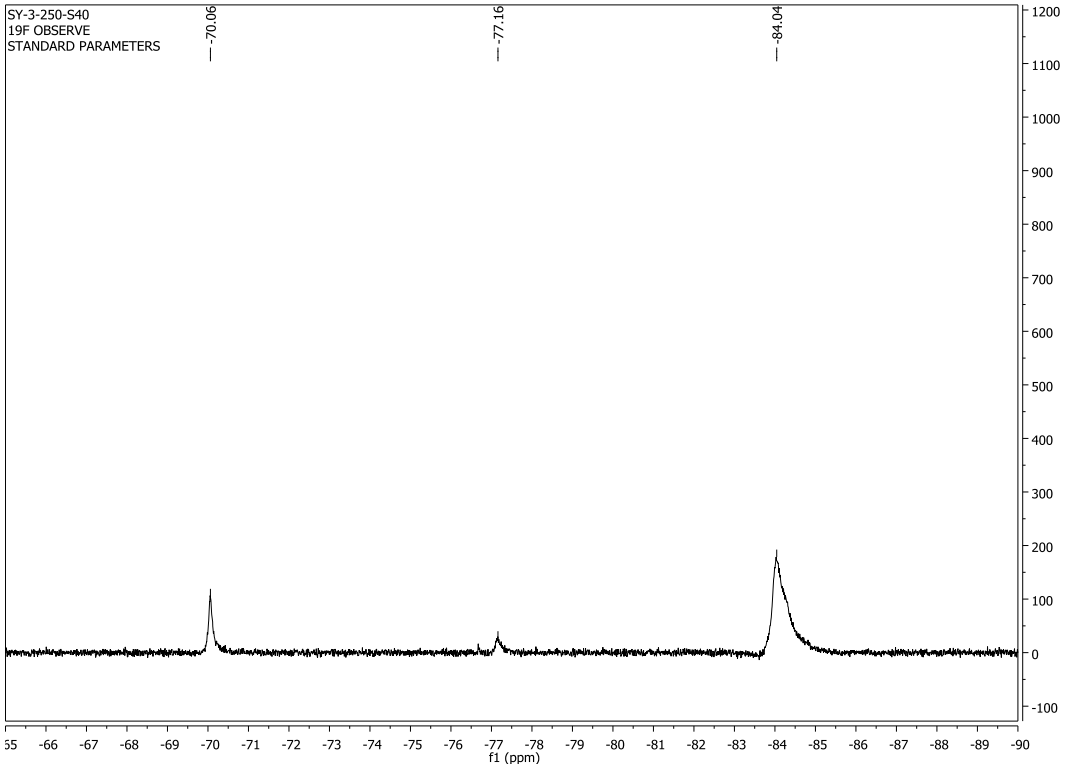

14.9 eq of amine

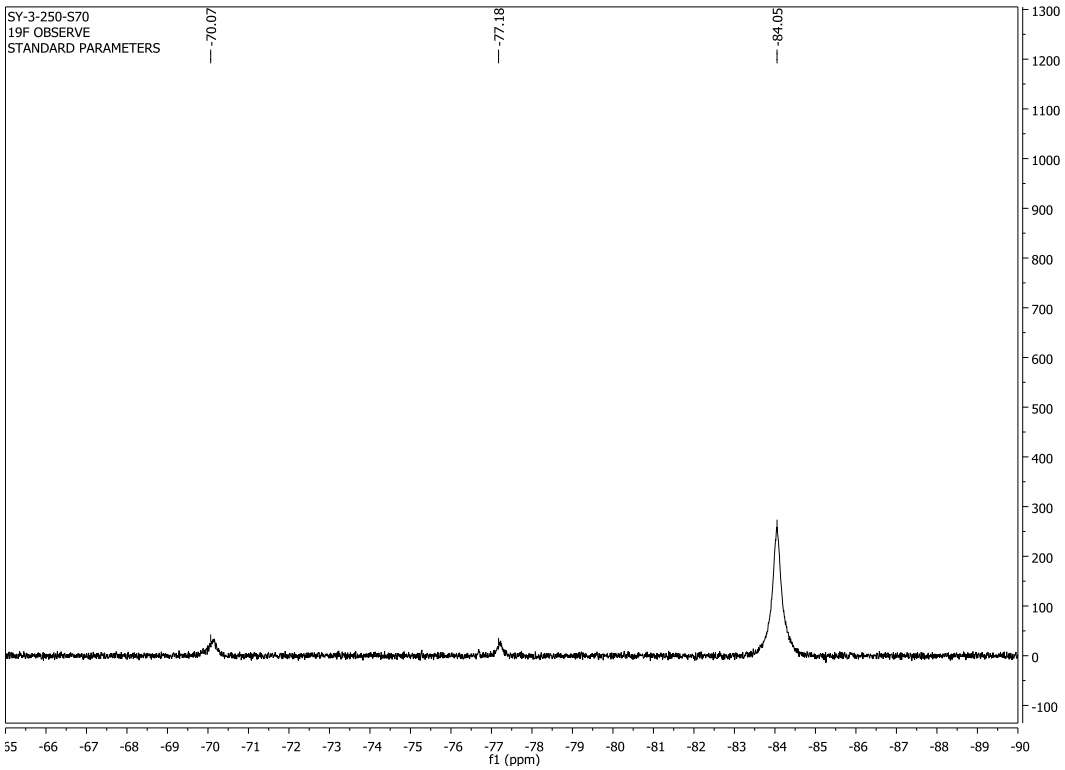

20 eq of amine

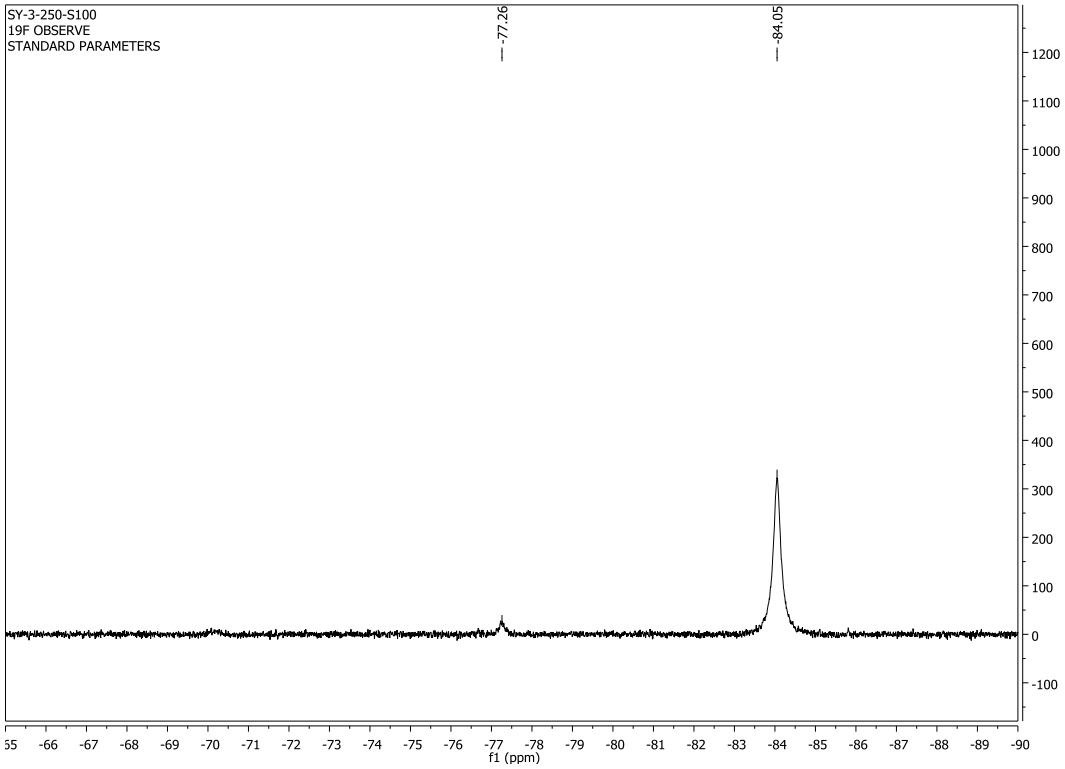

27.3 eq of amine

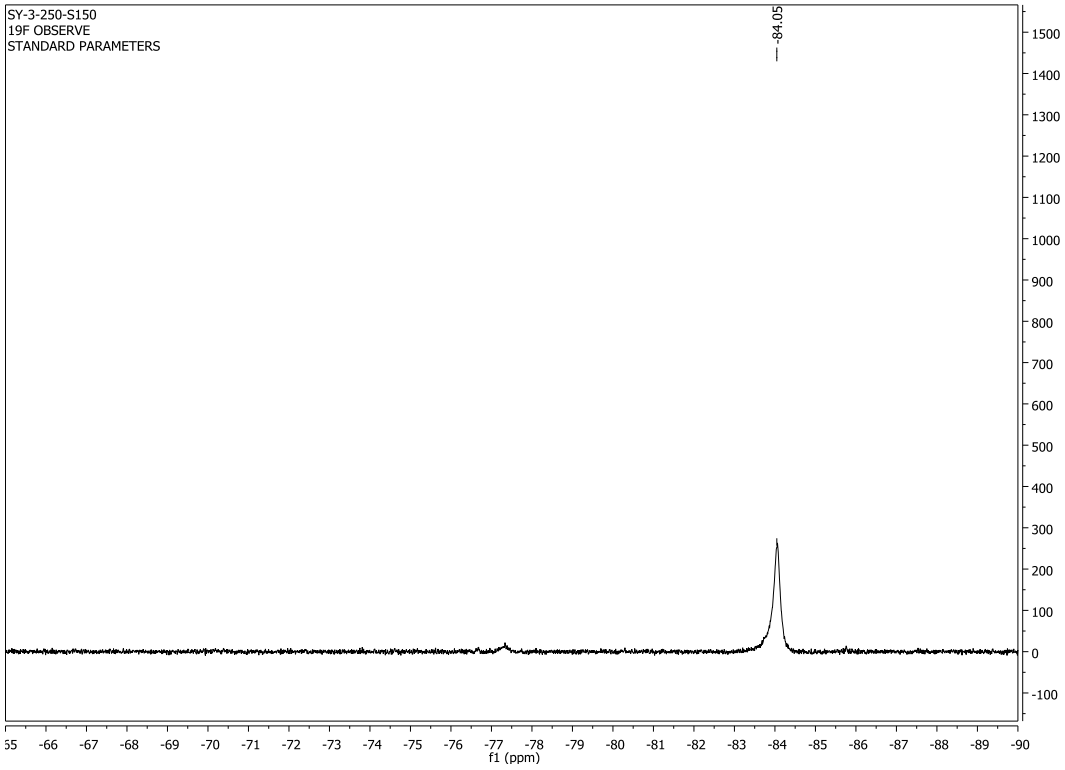

38.5 eq of amine

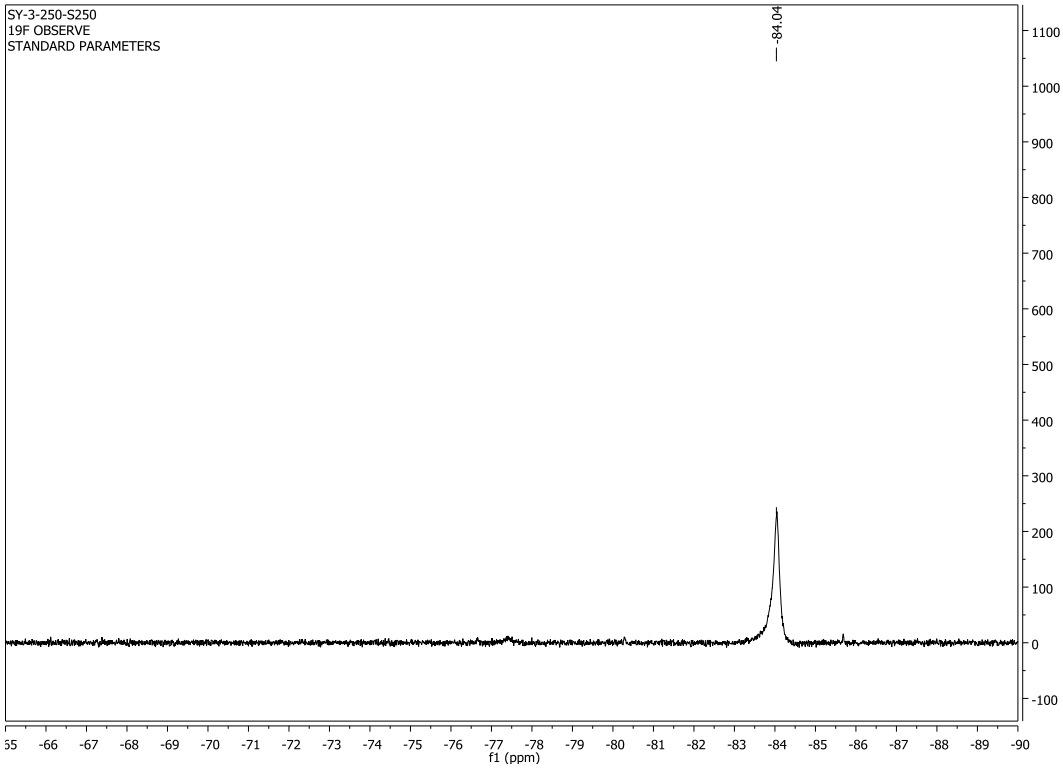

50 eq of amine

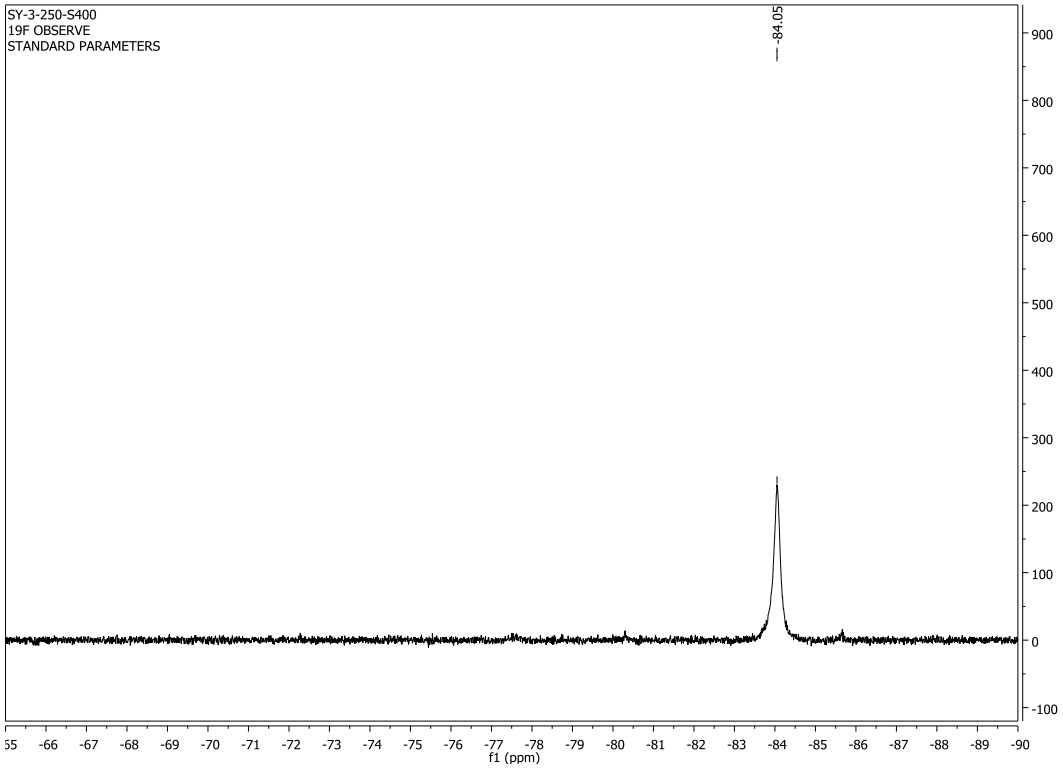

60 eq of amine

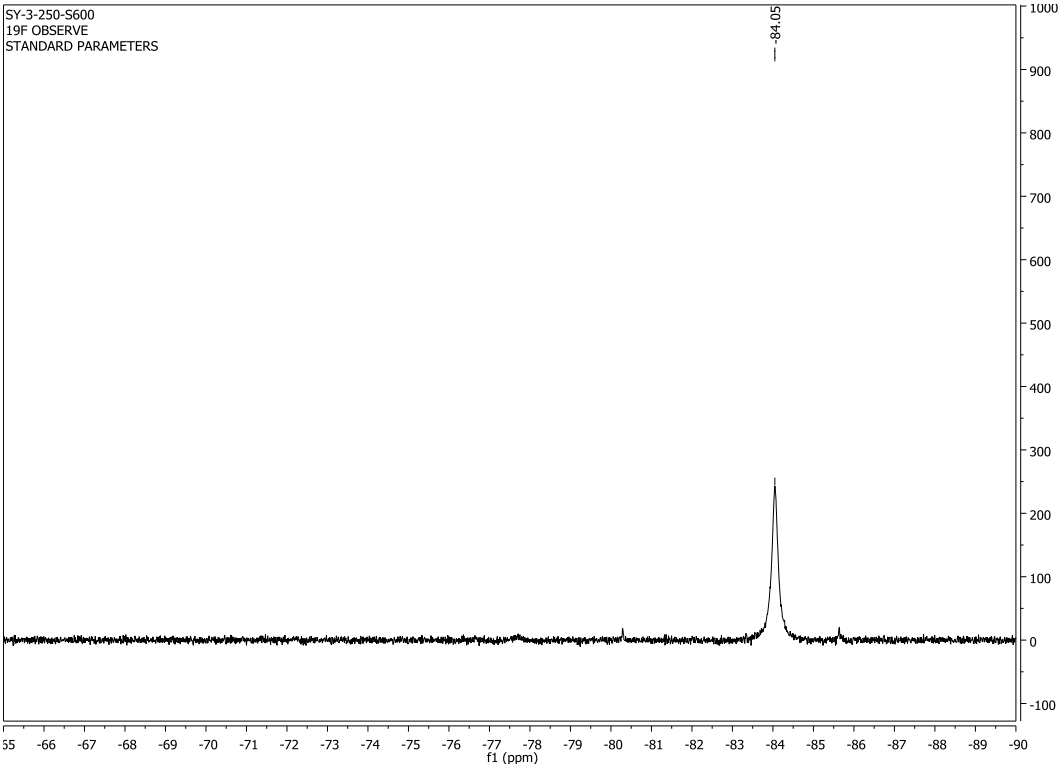

65.5 eq of amine

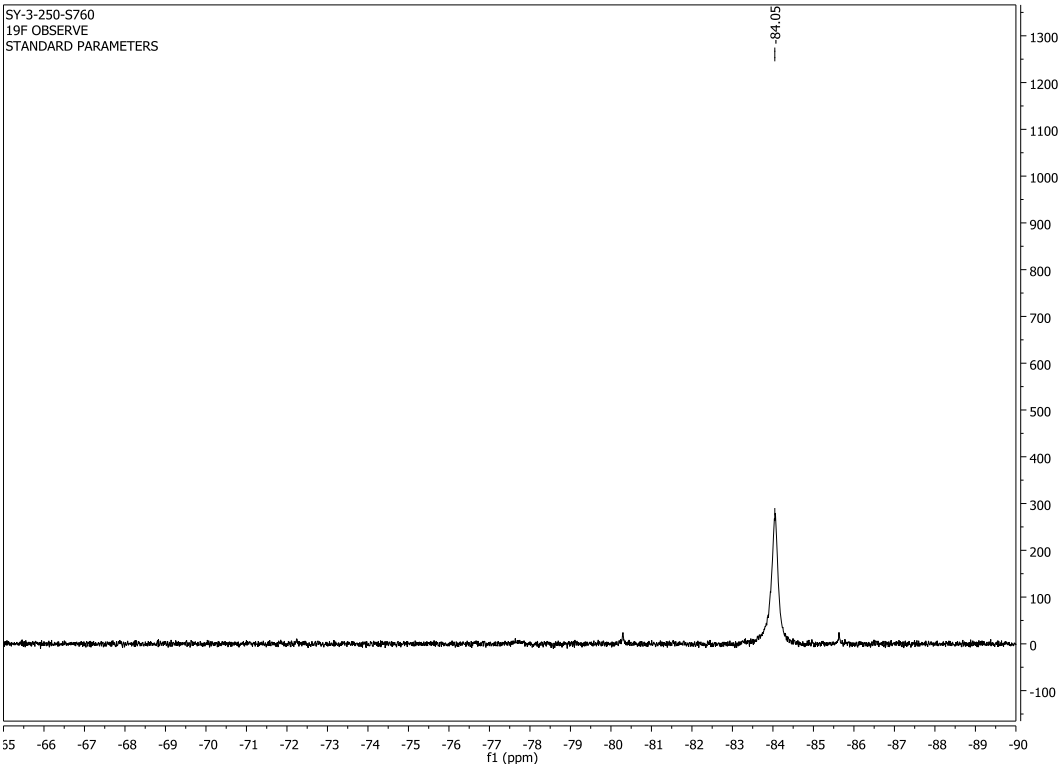

overnight

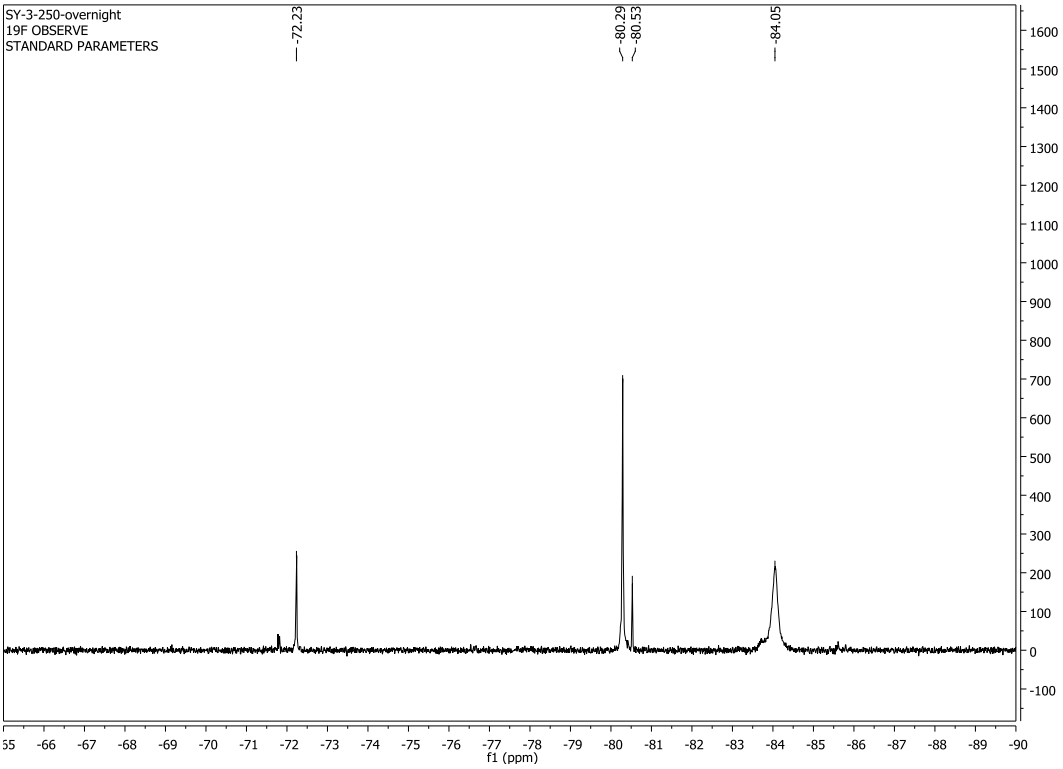

After 3 days

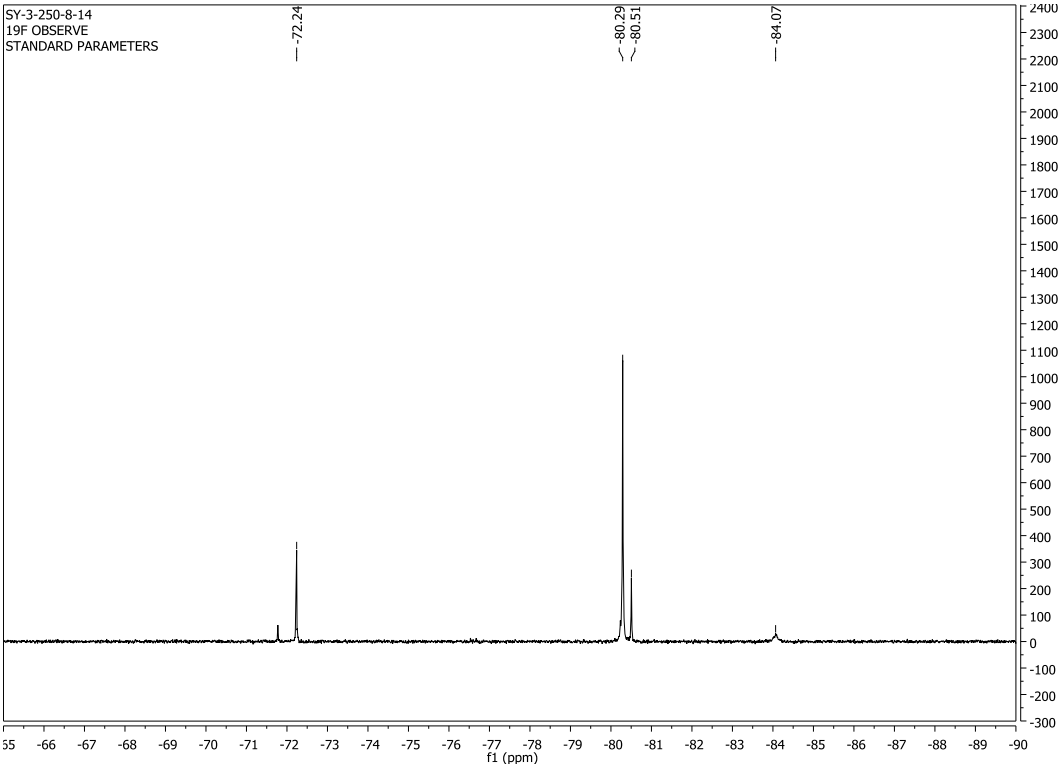

After 5 days

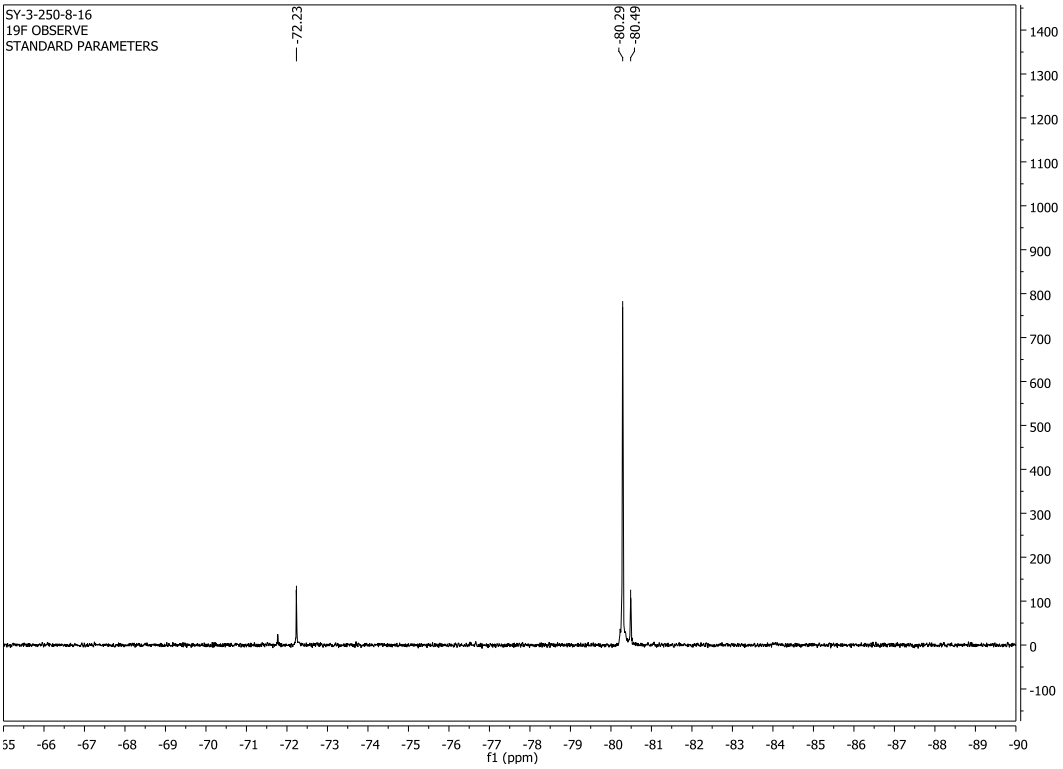

After 6 days

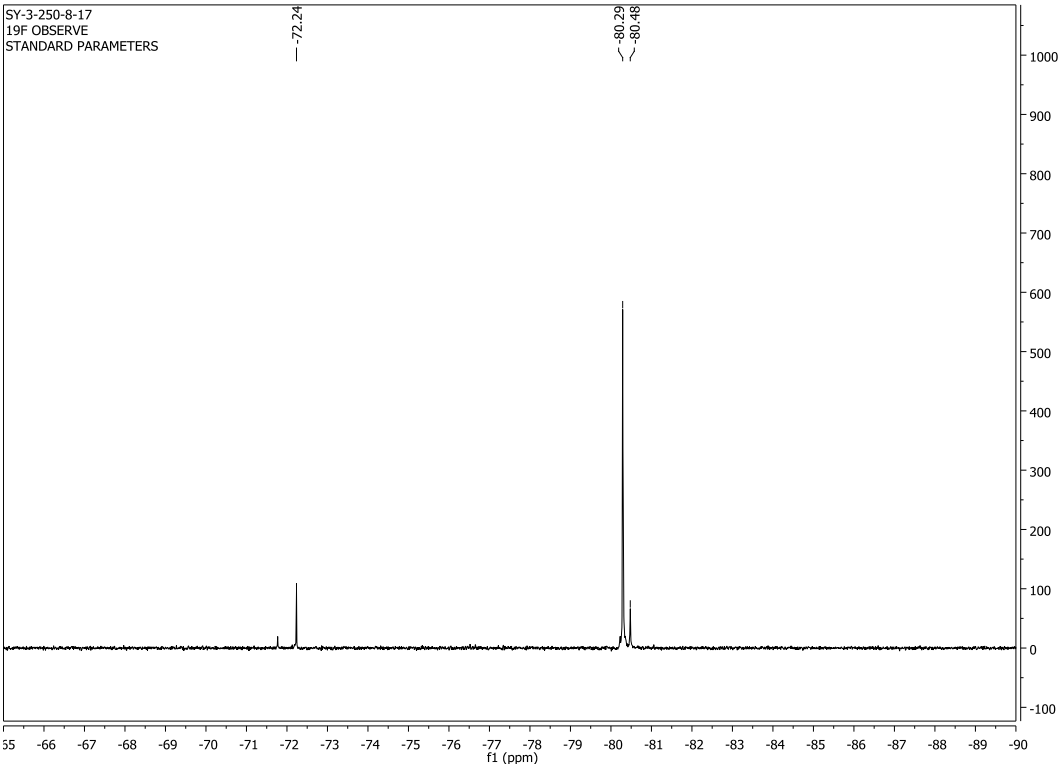

Appendix to Chapter 6

Figure A6-1. Fluorescence spectra of (*S*)-**6-4** (1.0×10^{-5} M, CH_2Cl_2) with increasing concentrations of (a) **N9** (0-1.6 mM), (b) **N12** (0-1.7 mM), (c) (*S, S*)-**N15** (0-5.0 mM), (d) (*R, R*)-**N15** (0-5.0 mM), (e) (*S, R*)-**N15** (0-5.0 mM), (f) (*S*)-**N16** (0-5.0 mM) and (g) (*R*)-**N16** (0-5.0 mM). (λ_{exc} = 343 nm, slit = 2.0/2.0 nm).

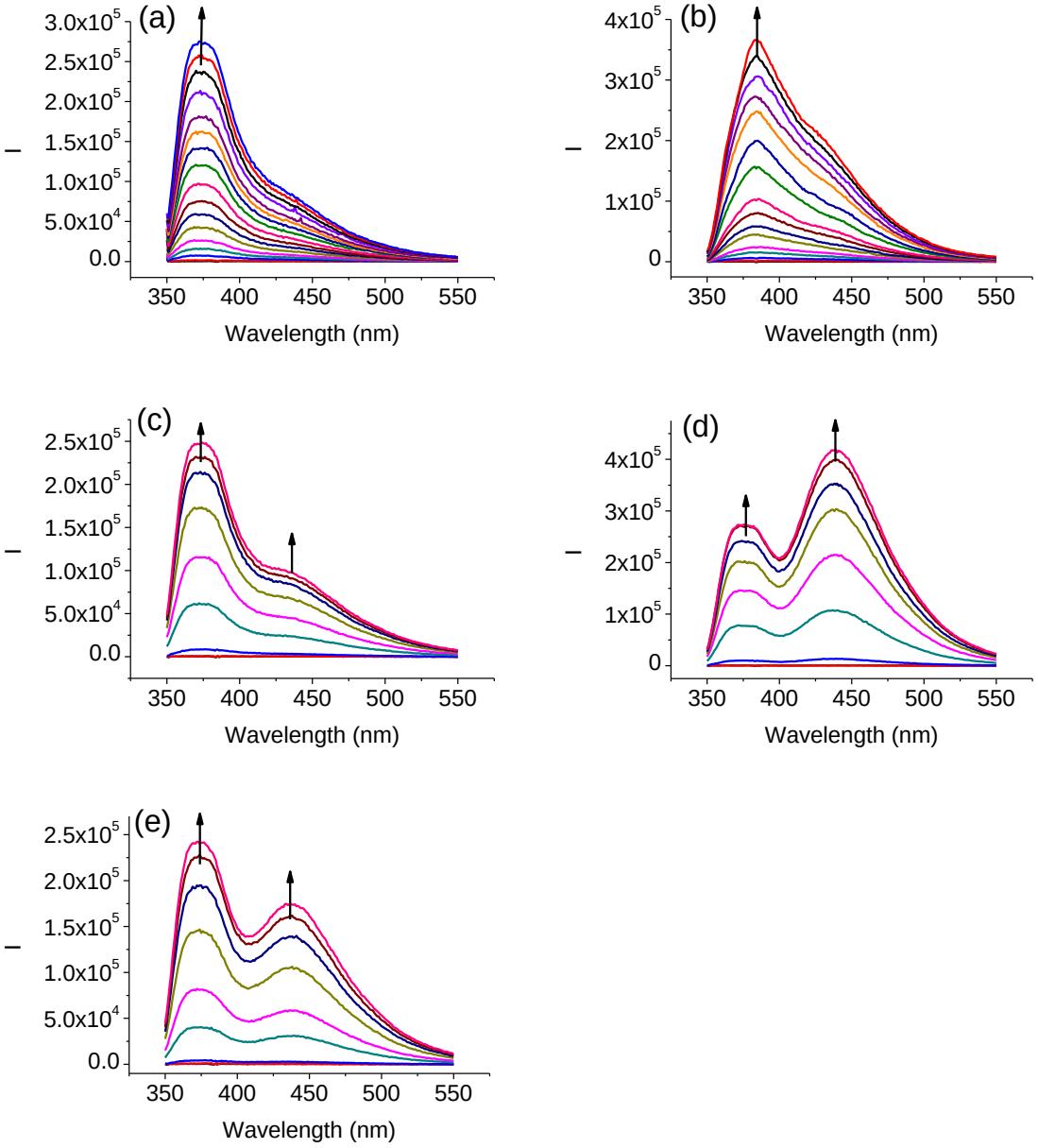

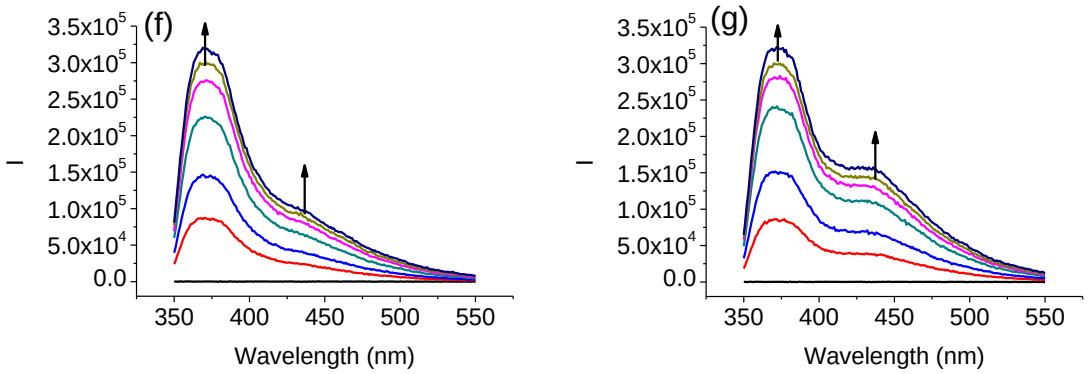

Figure A6-2. UV-Vis absorption spectra of (*S*)-**6-4** (1.0×10^{-5} M, CH_2Cl_2) with increasing concentrations of (a) **N9** (0-8.2 mM), (b) **N10** (0-10.3 mM), (c) **N12** (0-10.9 mM), (d) (*S, S*)-**N15** (0-5.0 mM), (e) (*R, R*)-**N15** (0-5.0 mM), (f) (*S, R*)-**N15** (0-5.0 mM).

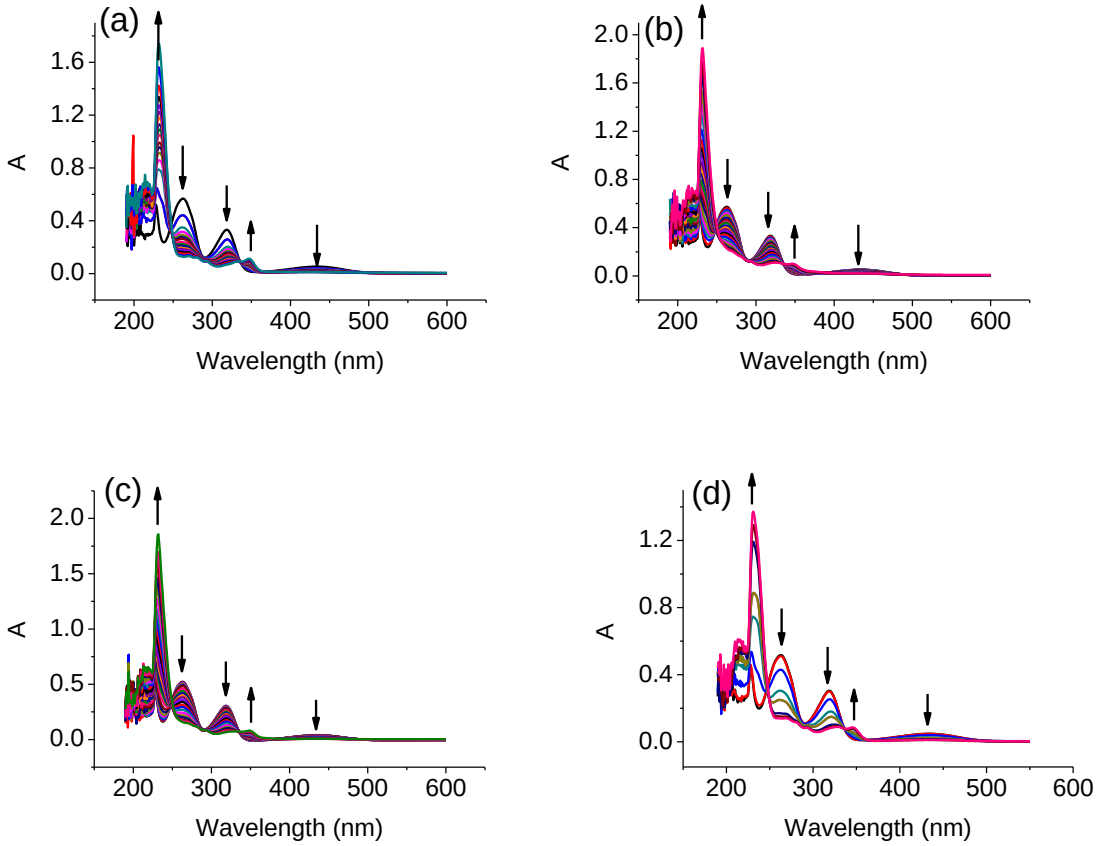

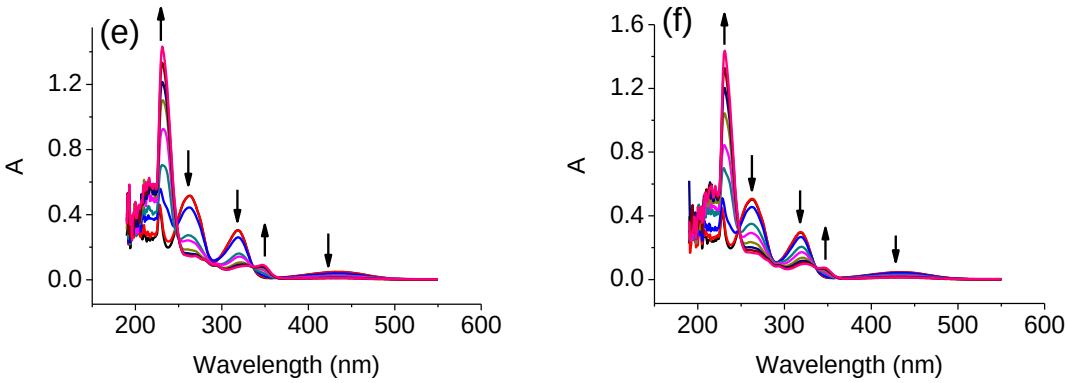

Figure A6-3. Fluorescence spectra of (*S*)-**6-4** (1.0×10^{-5} M, CH_2Cl_2) with increasing concentrations of **AA1**, **AA2** and **AA3**. (λ_{exc} = 343 nm, slit = 2.0/2.0 nm).

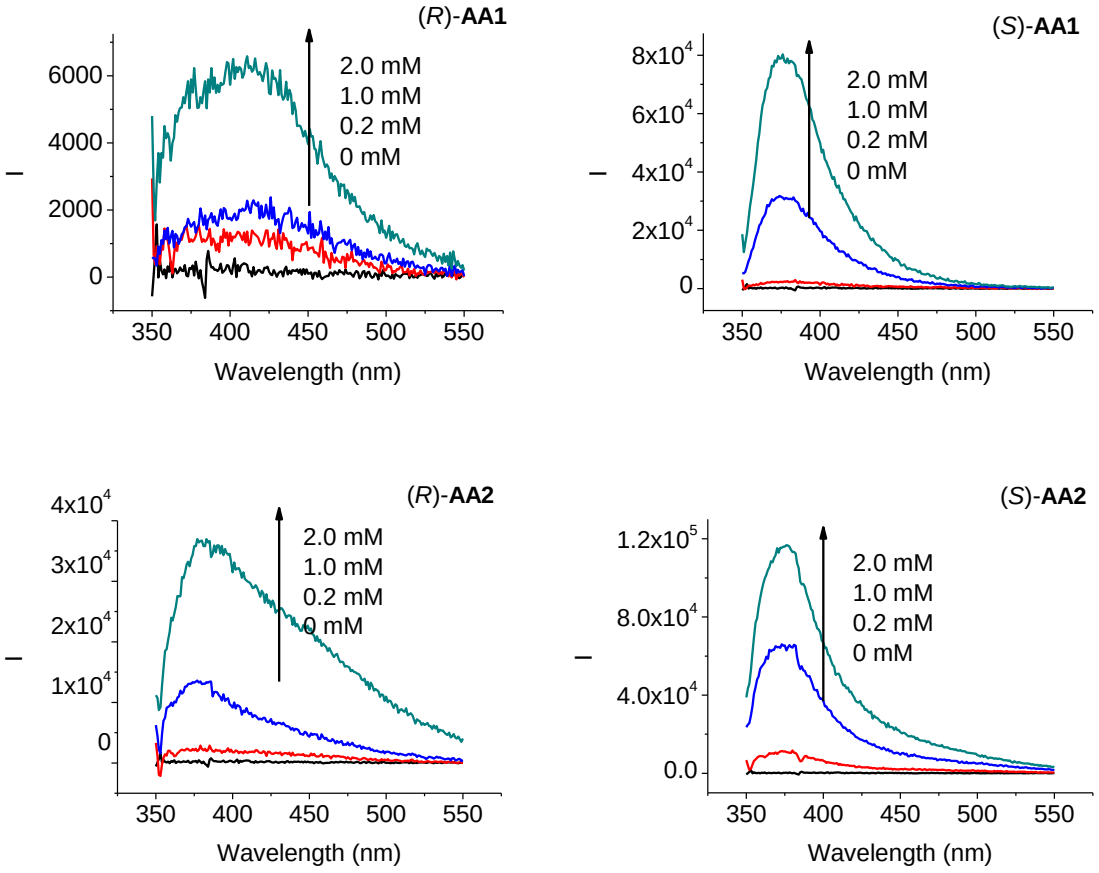

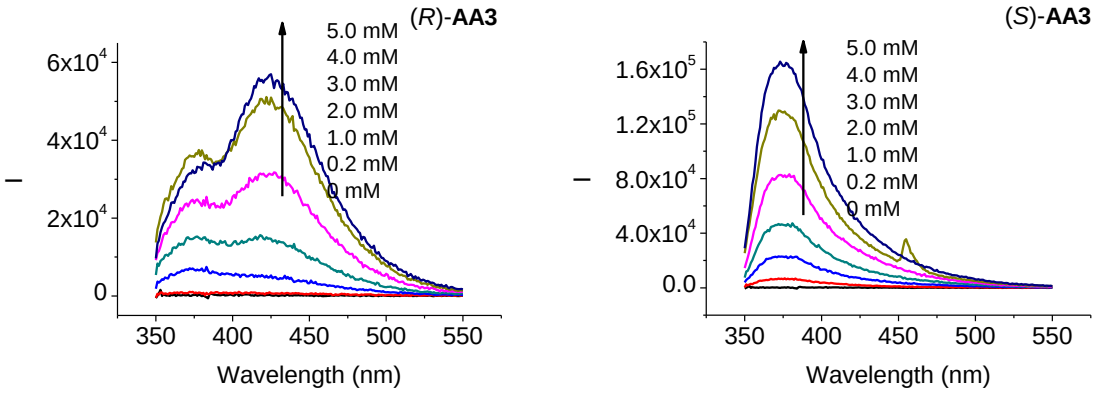

NMR Spectra of Compounds

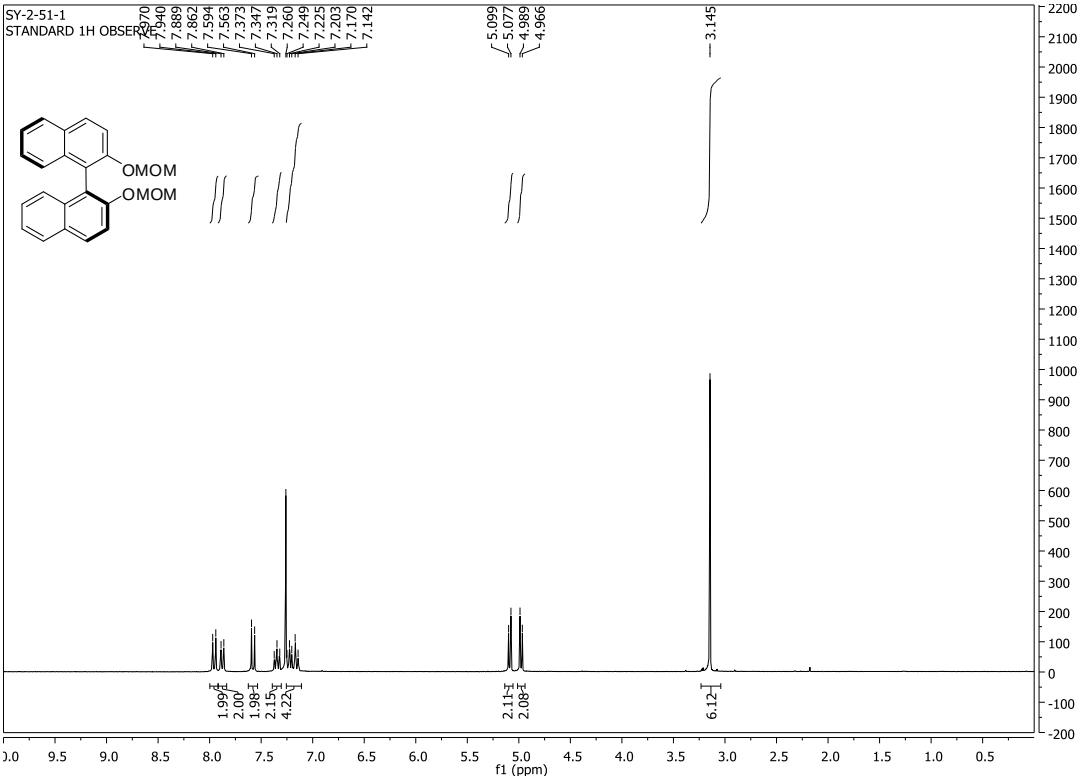

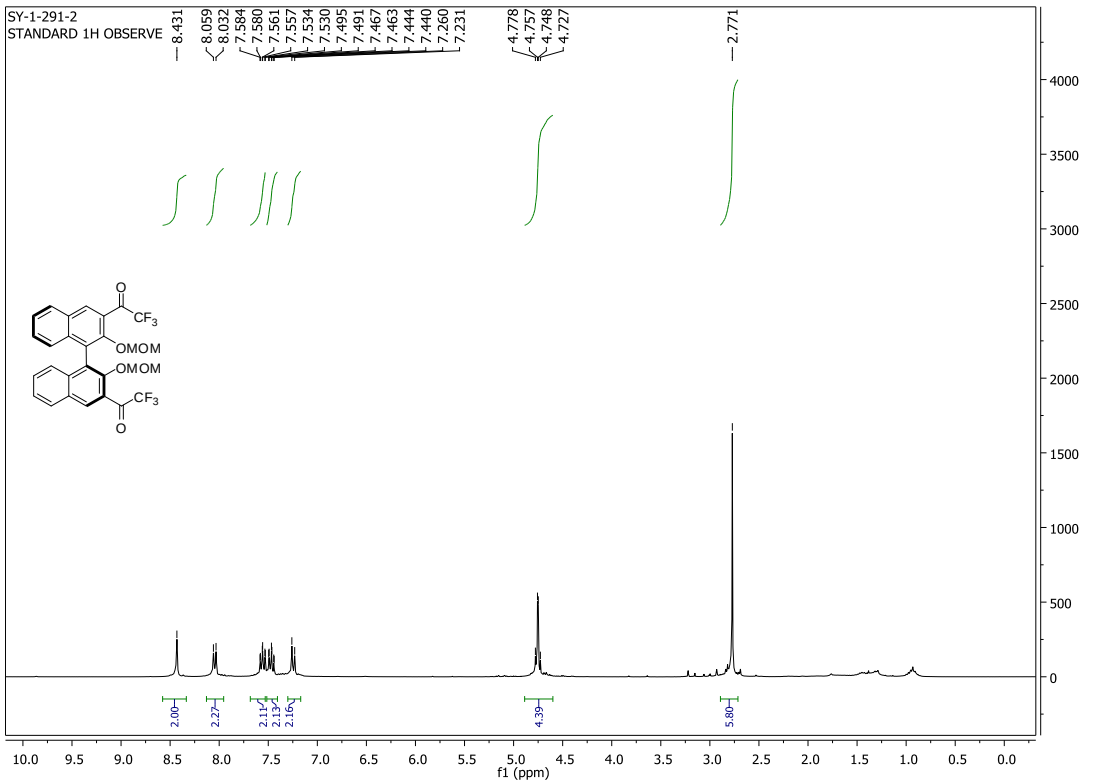
SY-1-291-2
STANDARD 1H OBSERVE
8.431
8.059
8.032
7.584
7.580
7.561
7.557
7.534
7.530
7.495
7.491
7.467
7.463
7.444
7.440
7.260
7.231
4.778
4.757
4.748
4.727
2.771
O
CF3
OMOM
OMOM
CF3
O
2.00
2.27
2.17
2.13
2.16
4.39
5.80
f1 (ppm)

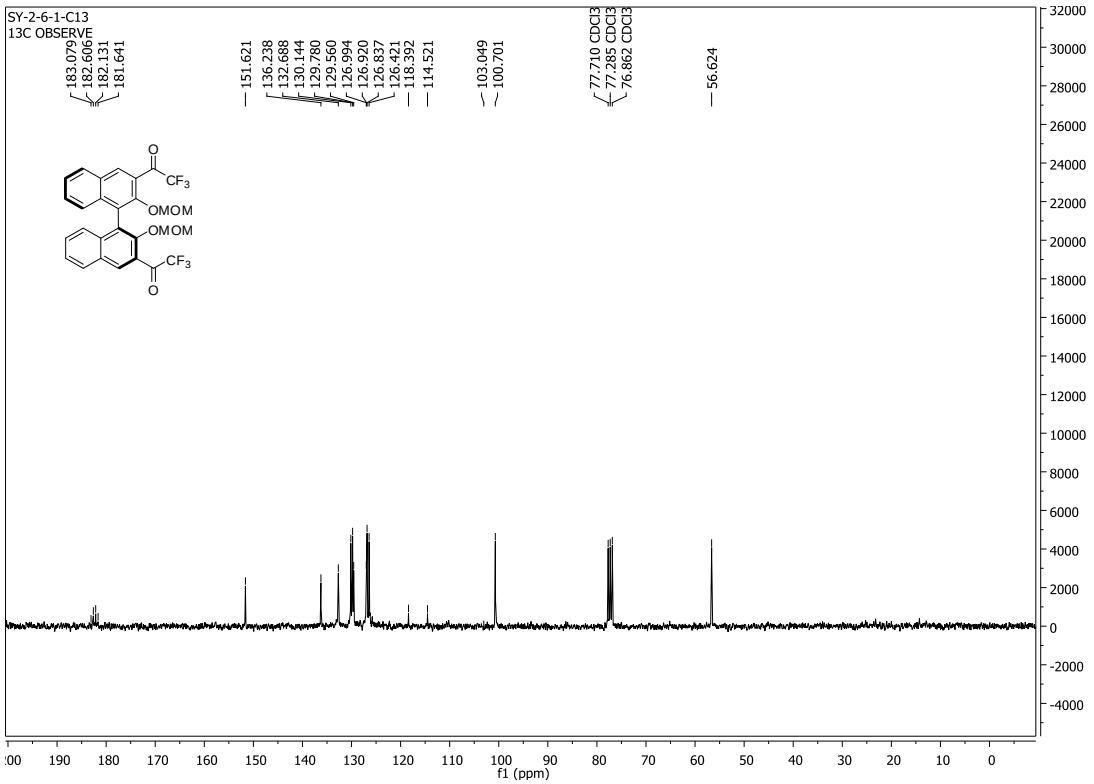
SY-2-6-1-C13
13C OBSERVE
183.079
182.606
182.131
181.641
151.621
136.238
132.688
130.144
129.780
129.560
126.994
126.920
126.837
126.421
118.392
114.521
103.049
100.701
77.710 CDCl3
77.285 CDCl3
76.862 CDCl3
56.624
O
CF3
OMOM
OMOM
CF3
O
f1 (ppm)

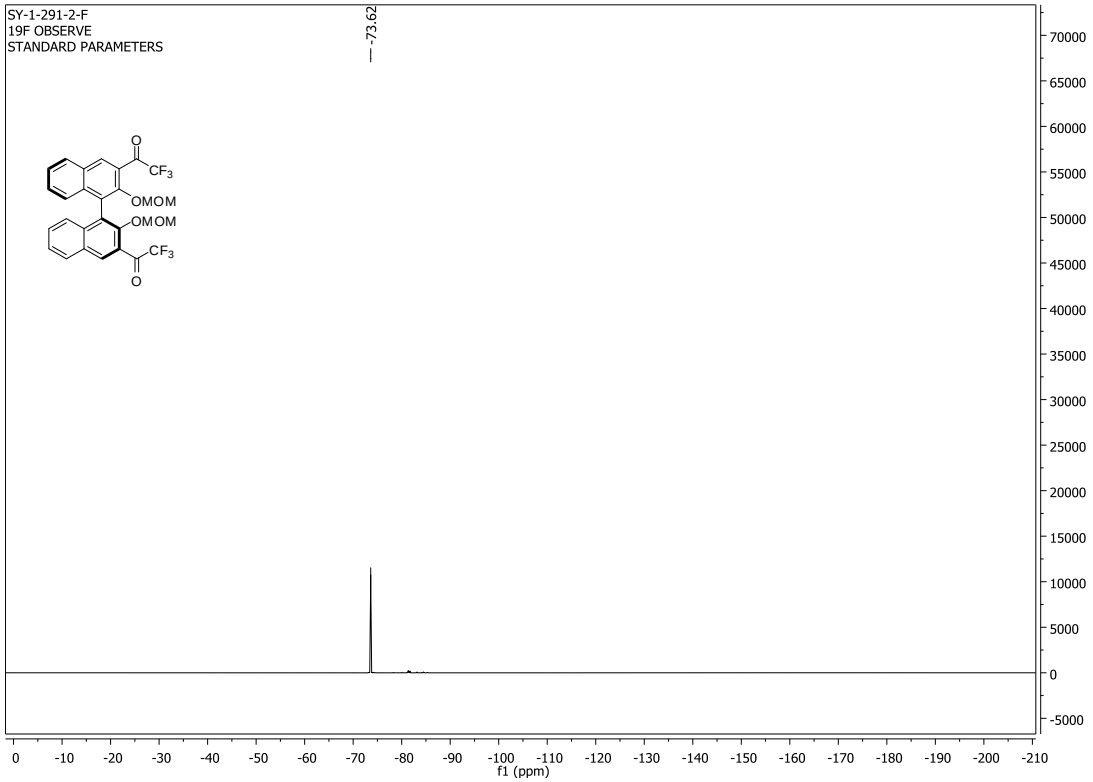
SY-1-291-2-F
19F OBSERVE
STANDARD PARAMETERS
-73.62
f1 (ppm)

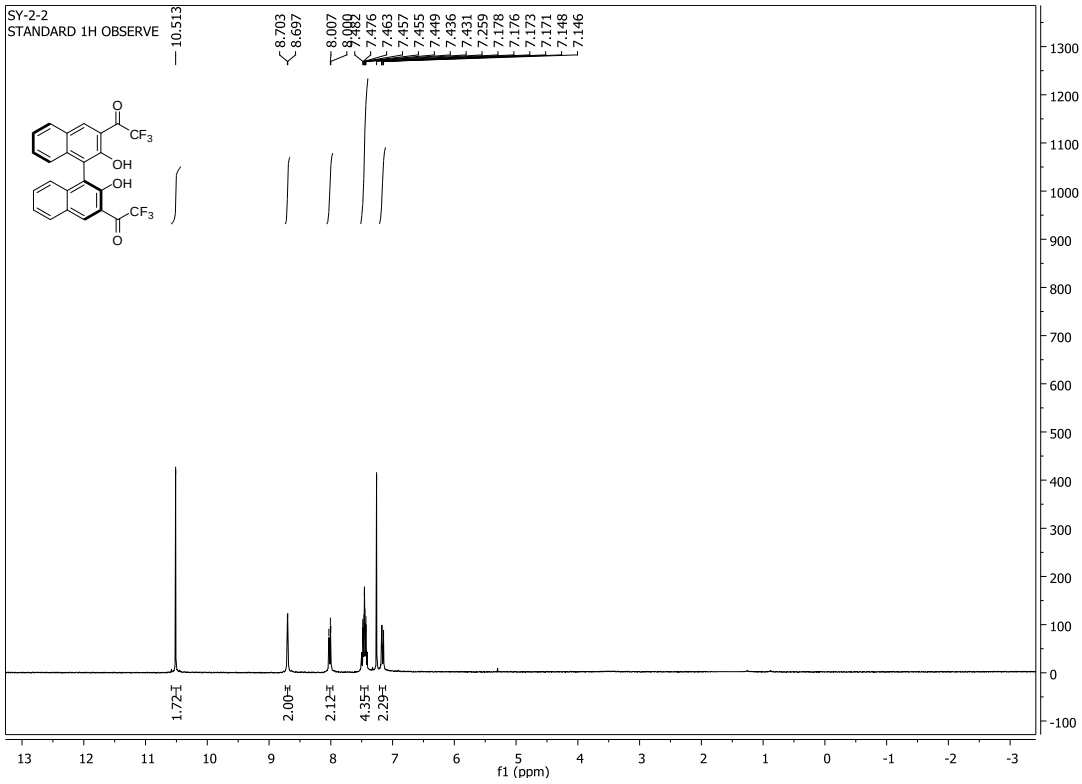
SY-2-2
STANDARD 1H OBSERVE
10.513
8.703
8.697
8.007
7.476
7.463
7.457
7.455
7.449
7.436
7.431
7.259
7.178
7.176
7.173
7.171
7.148
7.146
1.72
2.00
2.12
4.35
2.29
f1 (ppm)

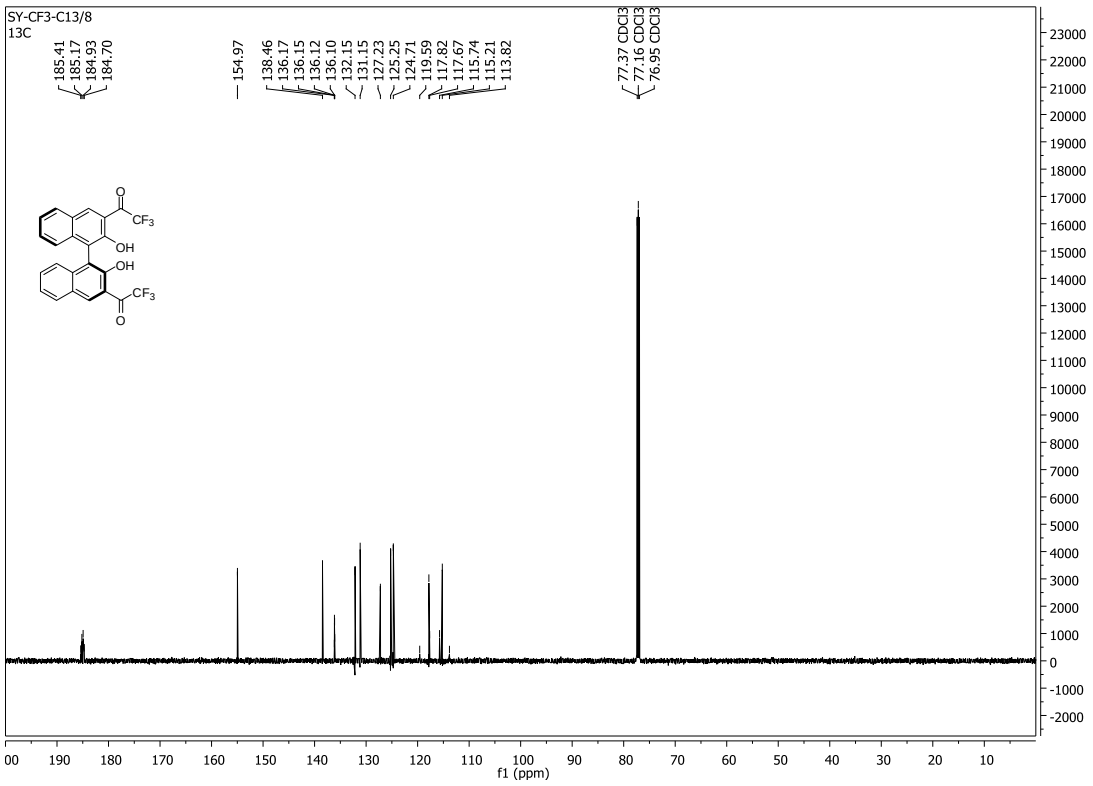
SY-CF3-C13/8
13C
185.41
185.17
184.93
184.70
154.97
138.46
136.17
136.15
136.12
136.10
132.15
131.15
127.23
125.25
124.71
119.59
117.82
117.67
115.74
115.21
113.82
77.37 CDCl3
77.16 CDCl3
76.95 CDCl3
f1 (ppm)

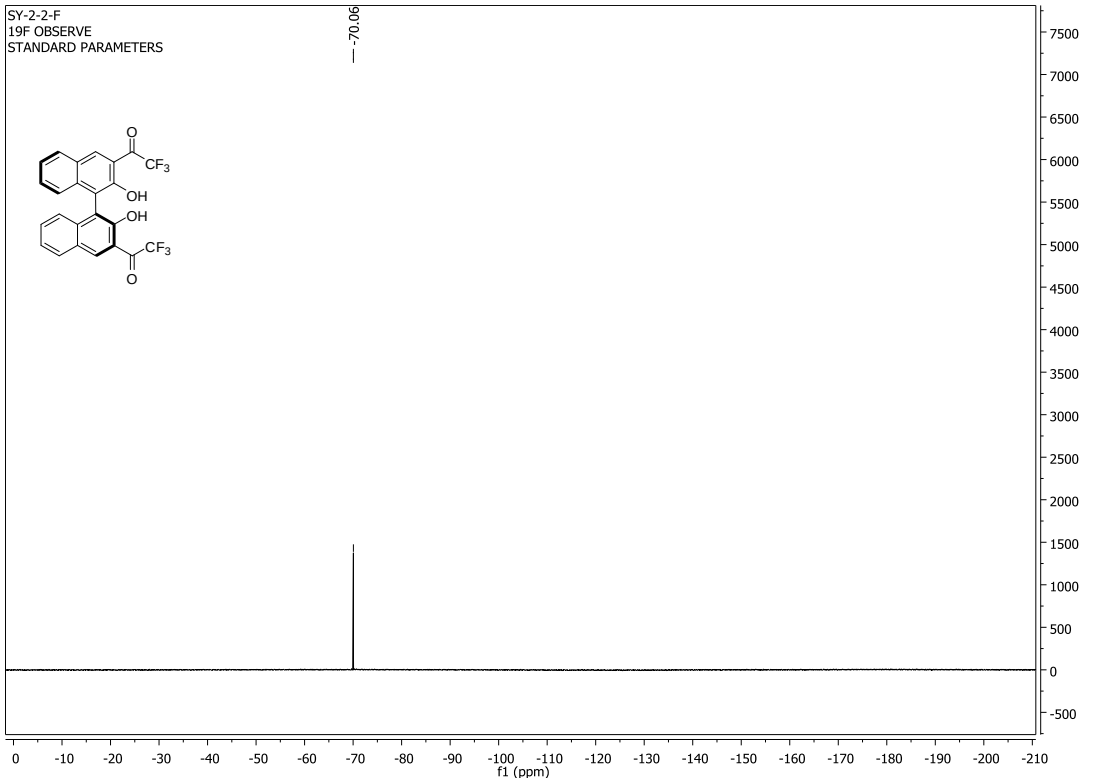
SY-2-2-F
19F OBSERVE
STANDARD PARAMETERS
-70.06
f1 (ppm)

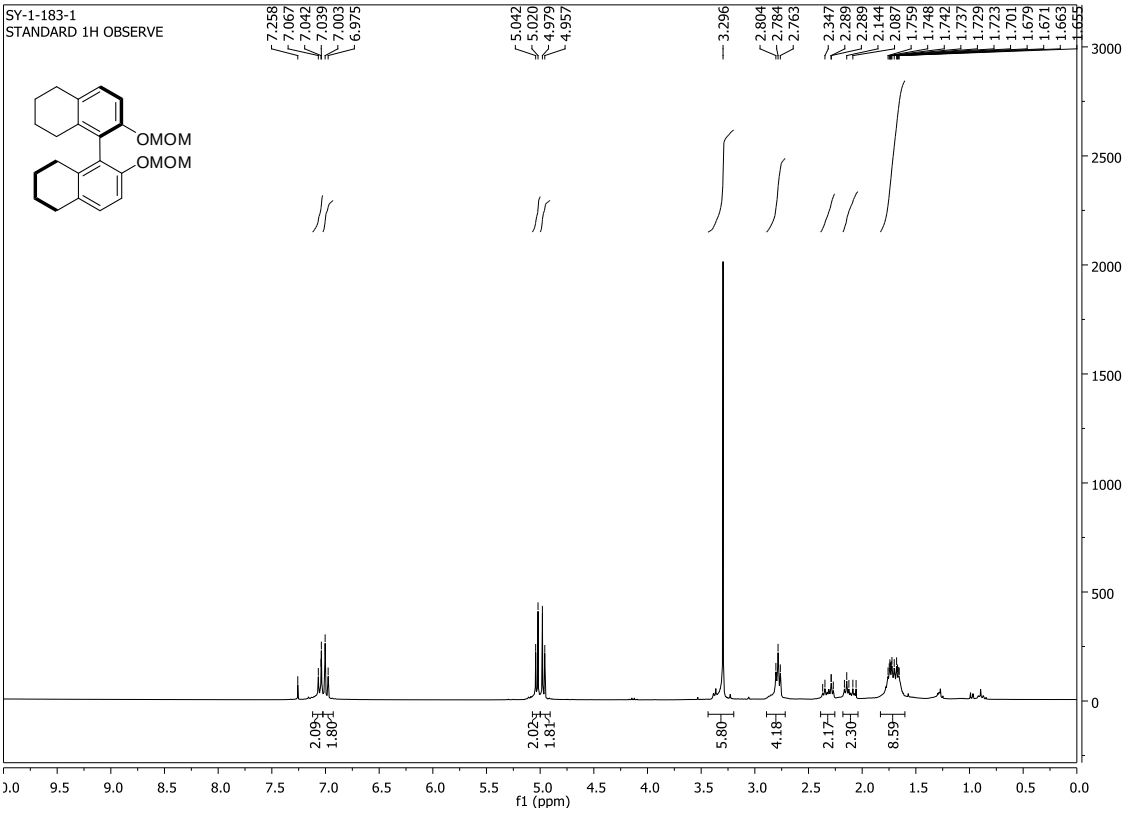
SY-1-183-1
STANDARD 1H OBSERVE
OMOM
OMOM
f1 (ppm)

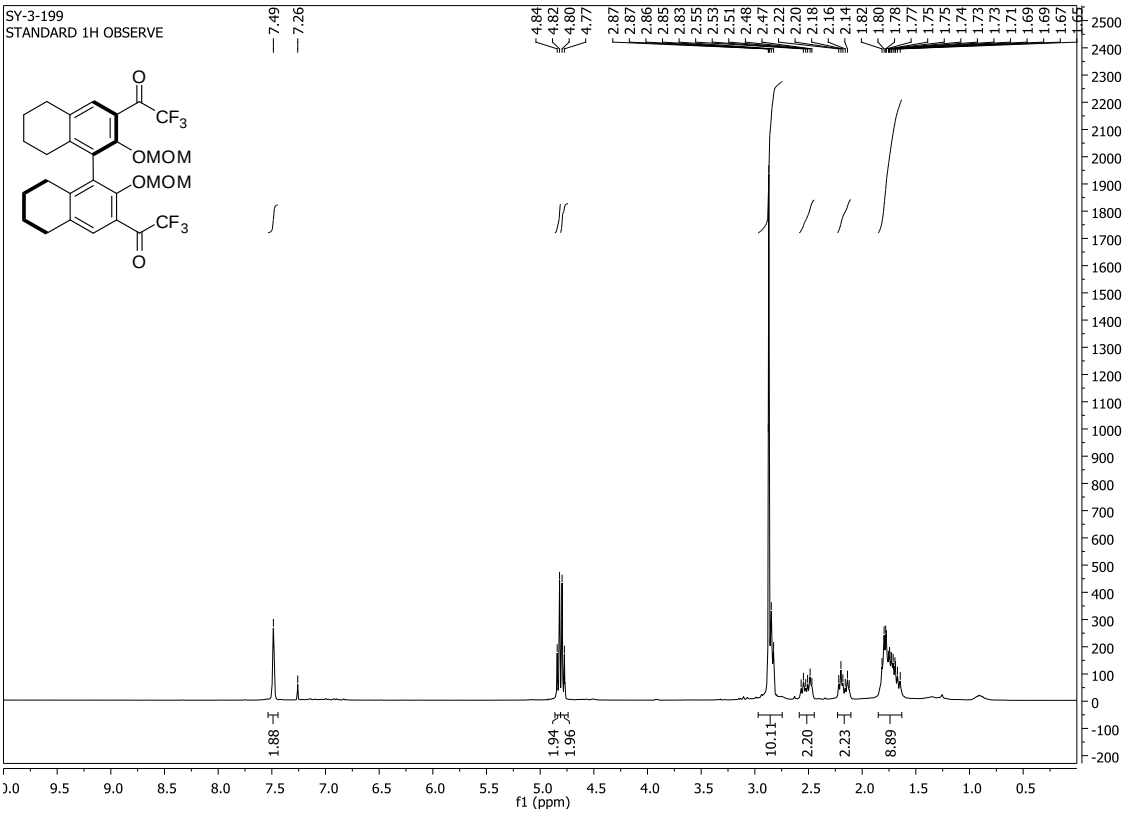
SY-3-199
STANDARD 1H OBSERVE
CF3
OMOM
OMOM
CF3
f1 (ppm)

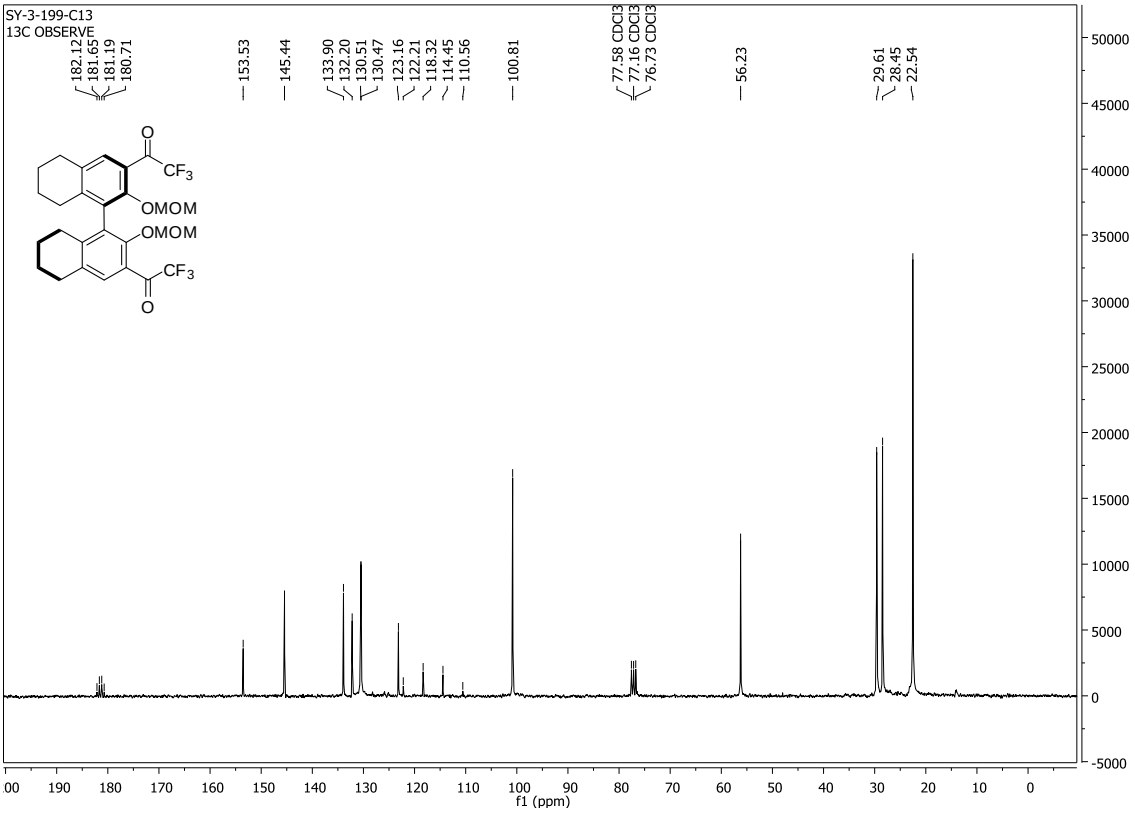
SY-3-199-C13
13C OBSERVE
182.12
181.65
181.19
180.71
153.53
145.44
133.90
132.20
130.51
130.47
123.16
122.21
118.32
114.45
110.56
100.81
77.58 CDCl3
77.16 CDCl3
76.73 CDCl3
56.23
29.61
28.45
22.54
CF3
OMOM
OMOM
CF3
O
O
f1 (ppm)

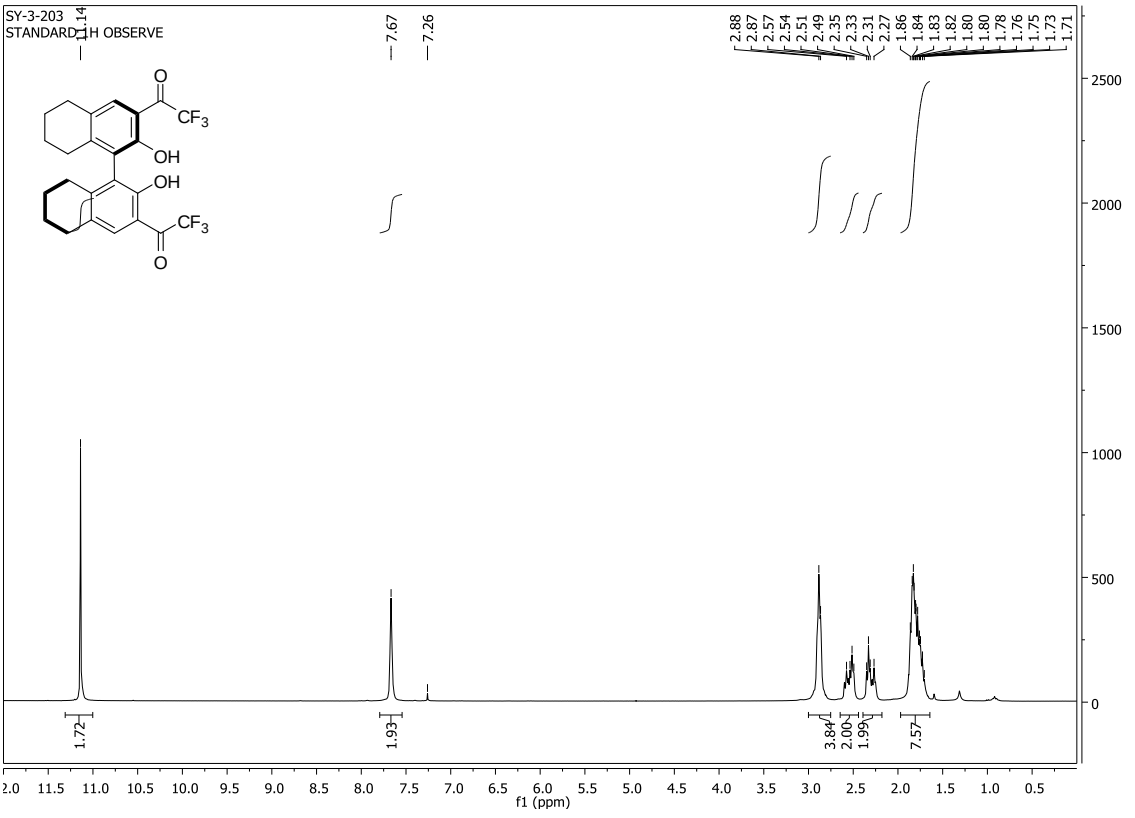
SY-3-203
STANDARD_1H OBSERVE
1.14
7.67
7.26
2.88
2.87
2.57
2.54
2.51
2.49
2.35
2.33
2.31
2.27
1.86
1.84
1.83
1.82
1.80
1.80
1.78
1.76
1.75
1.73
1.71
CF3
OH
OH
CF3
O
1.72
1.93
3.84
2.00
1.99
7.57
f1 (ppm)

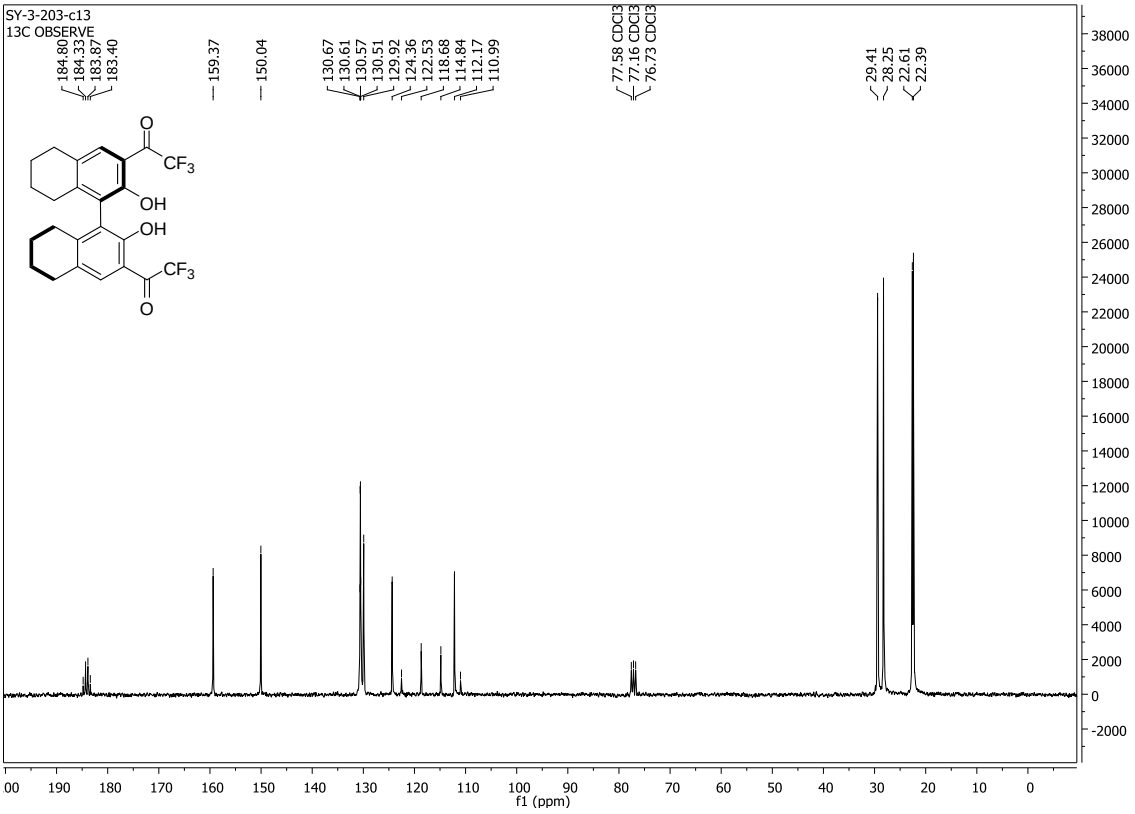
SY-3-203-c13
13C OBSERVE
184.80
184.33
183.87
183.40
159.37
150.04
130.67
130.61
130.57
130.51
129.92
124.36
122.53
118.68
114.84
112.17
110.99
77.58 CDCl3
77.16 CDCl3
76.73 CDCl3
29.41
28.25
22.61
22.39
CF3
OH
OH
CF3
O
O
f1 (ppm)

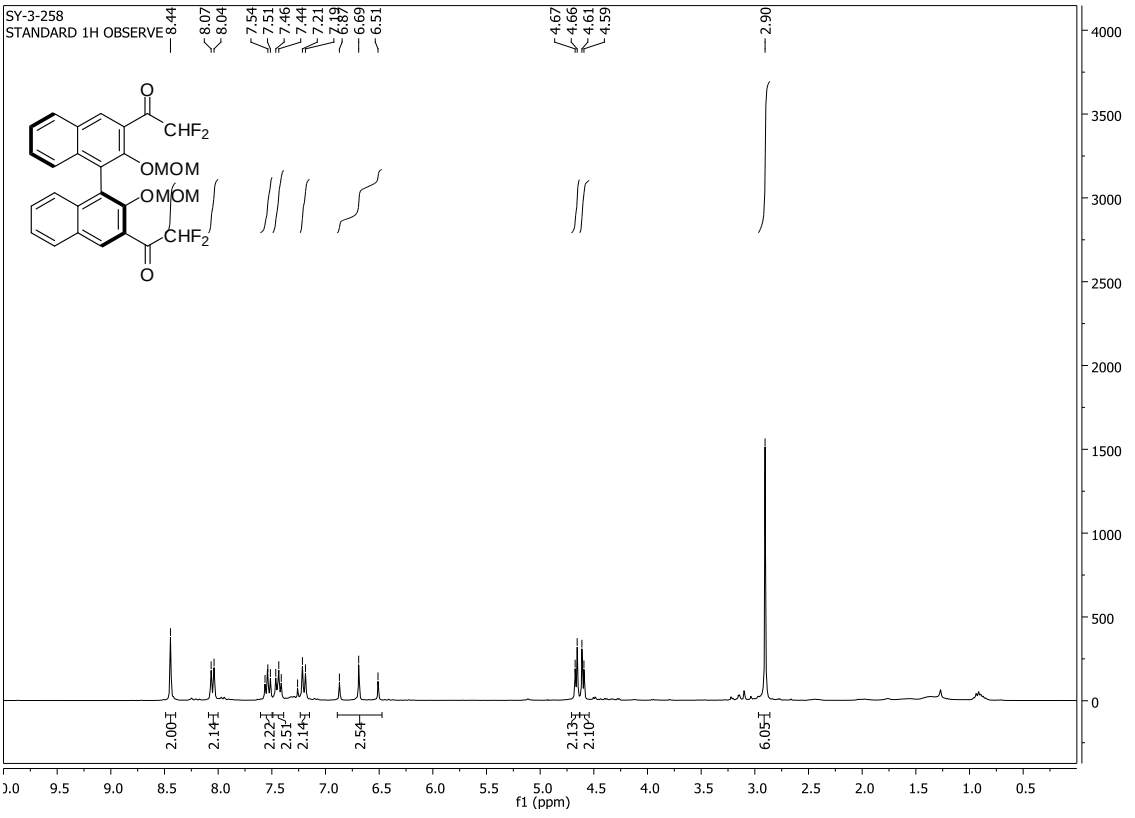
SY-3-258
STANDARD 1H OBSERVE
8.44
8.07
8.04
7.54
7.51
7.46
7.44
7.21
6.69
6.51
4.67
4.66
4.61
4.59
2.90
CHF2
OMOM
OMOM
CHF2
O
O
2.00
2.14
2.22
2.51
2.14
2.54
2.13
2.10
6.05
f1 (ppm)

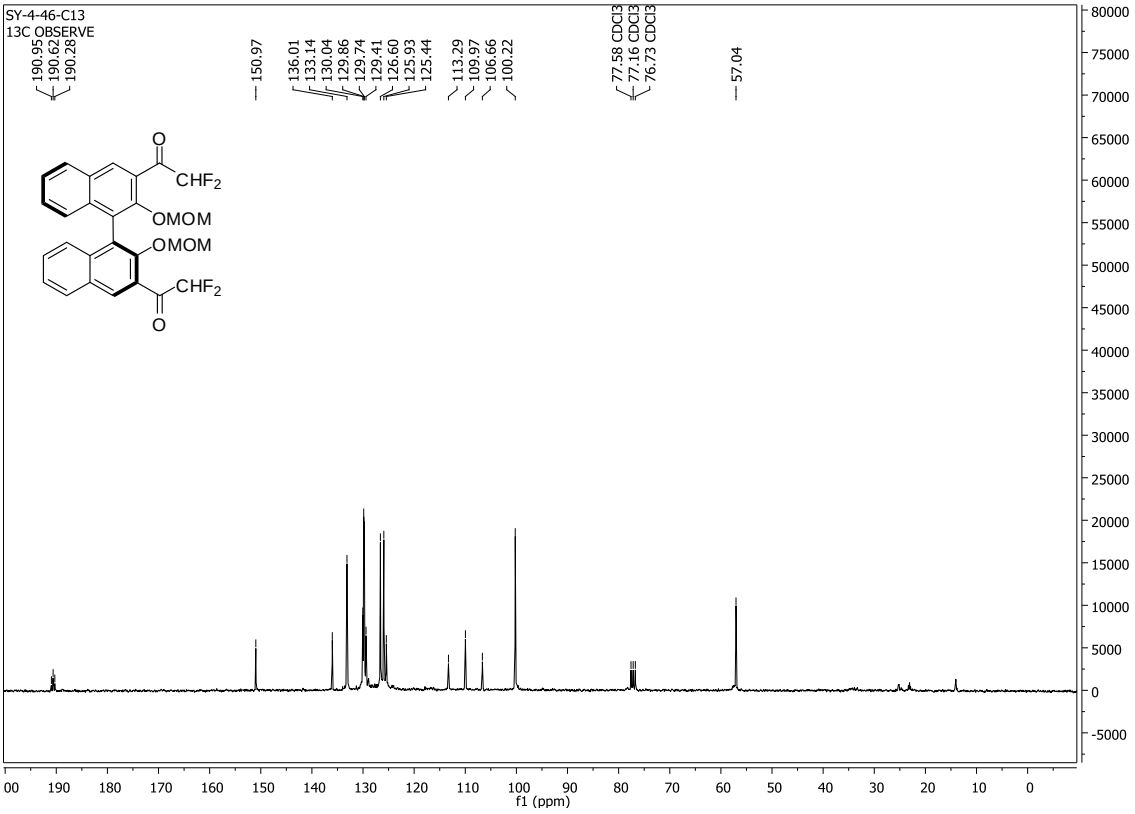
SY-4-46-C13
13C OBSERVE
190.95
190.62
190.28
150.97
136.01
133.14
130.04
129.86
129.74
129.41
126.60
125.93
125.44
113.29
109.97
106.66
100.22
77.58 CDCl3
77.16 CDCl3
76.73 CDCl3
57.04
CHF2
OMOM
OMOM
CHF2
f1 (ppm)

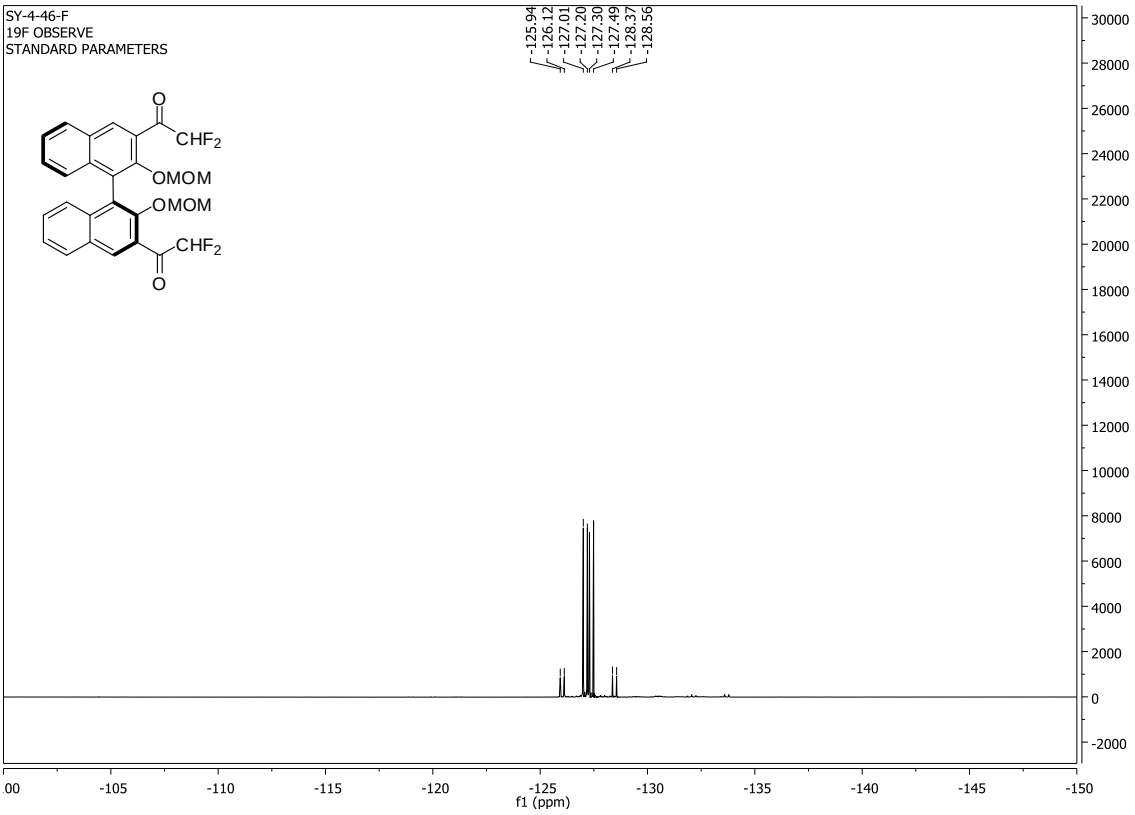
SY-4-46-F
19F OBSERVE
STANDARD PARAMETERS
-125.94
-126.12
-127.01
-127.20
-127.30
-127.49
-128.37
-128.56
CHF2
OMOM
OMOM
CHF2
f1 (ppm)

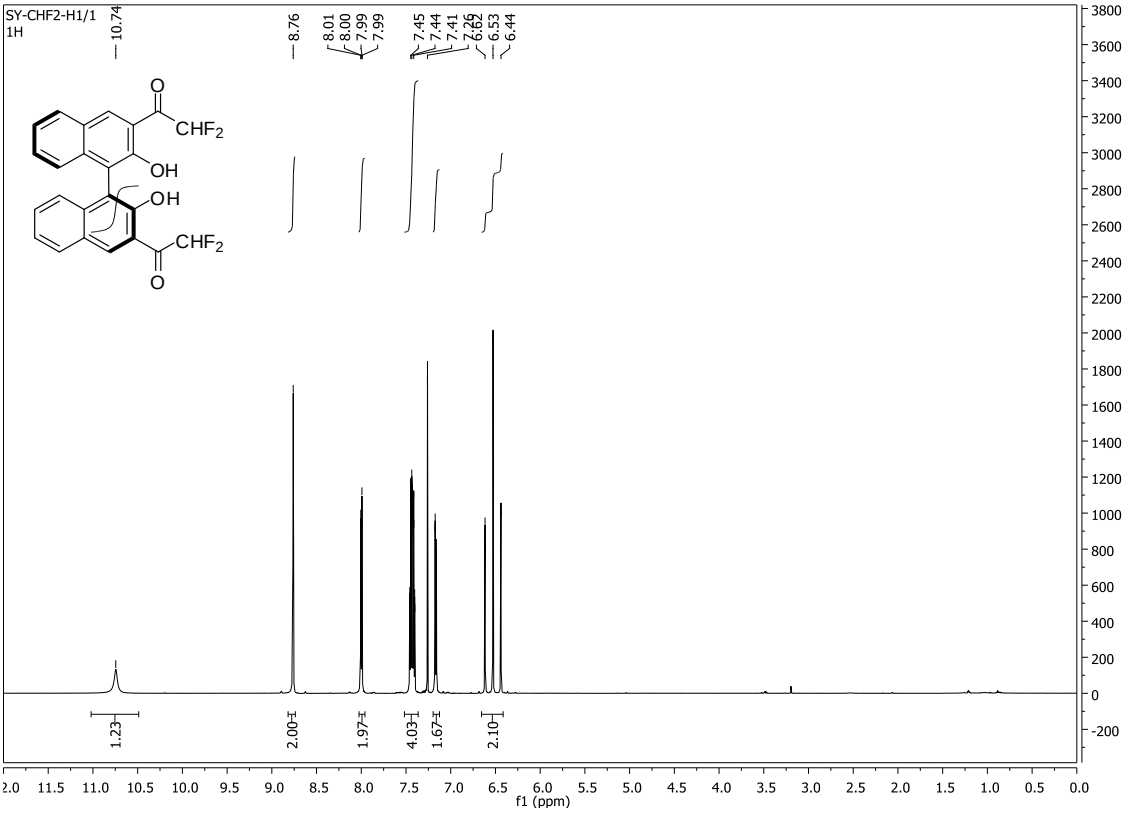
SY-CHF2-H1/1
1H
10.74
8.76
8.01
8.00
7.99
7.99
7.45
7.44
7.41
7.26
6.62
6.53
6.44
CHF2
OH
OH
CHF2
O
O
1.23
2.00
1.97
4.03
1.67
2.10
f1 (ppm)

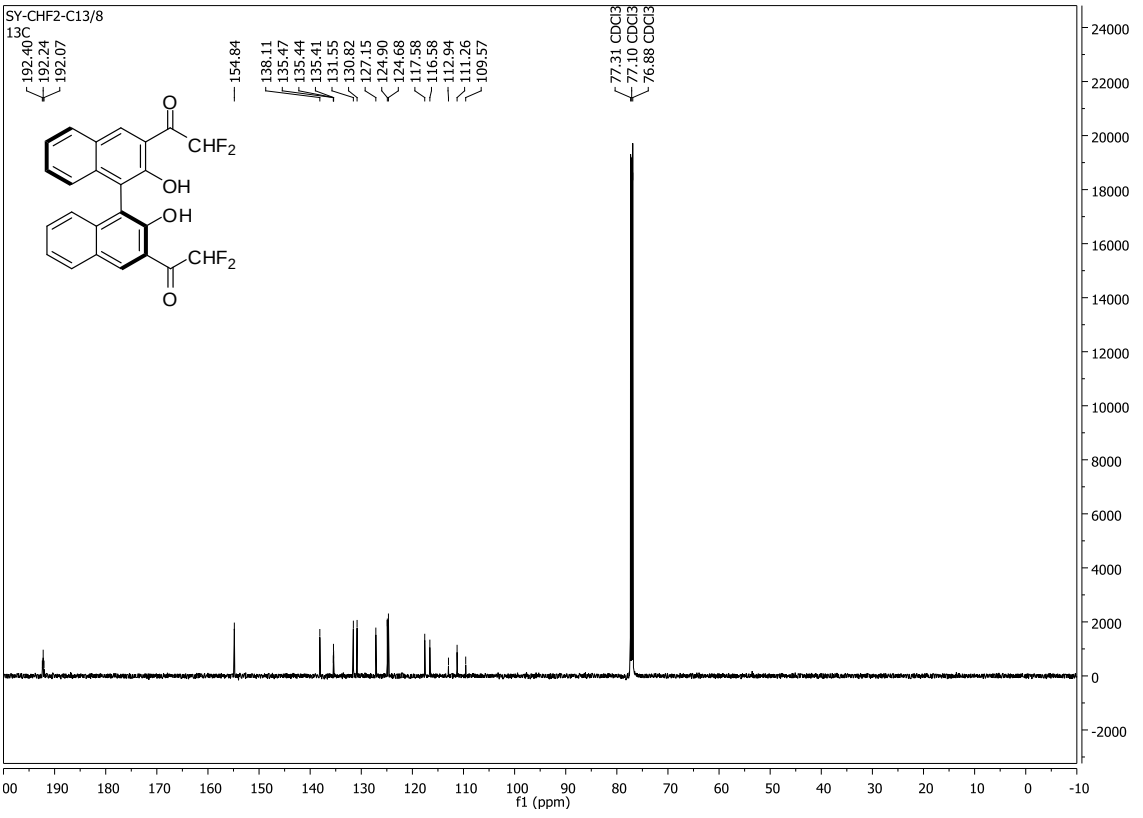
SY-CHF2-C13/8
13C
192.40
192.24
192.07
154.84
138.11
135.47
135.44
135.41
131.55
130.82
127.15
124.90
124.68
117.58
116.58
112.94
111.26
109.57
77.31 CDCl3
77.10 CDCl3
76.88 CDCl3
CHF2
OH
OH
CHF2
O
f1 (ppm)

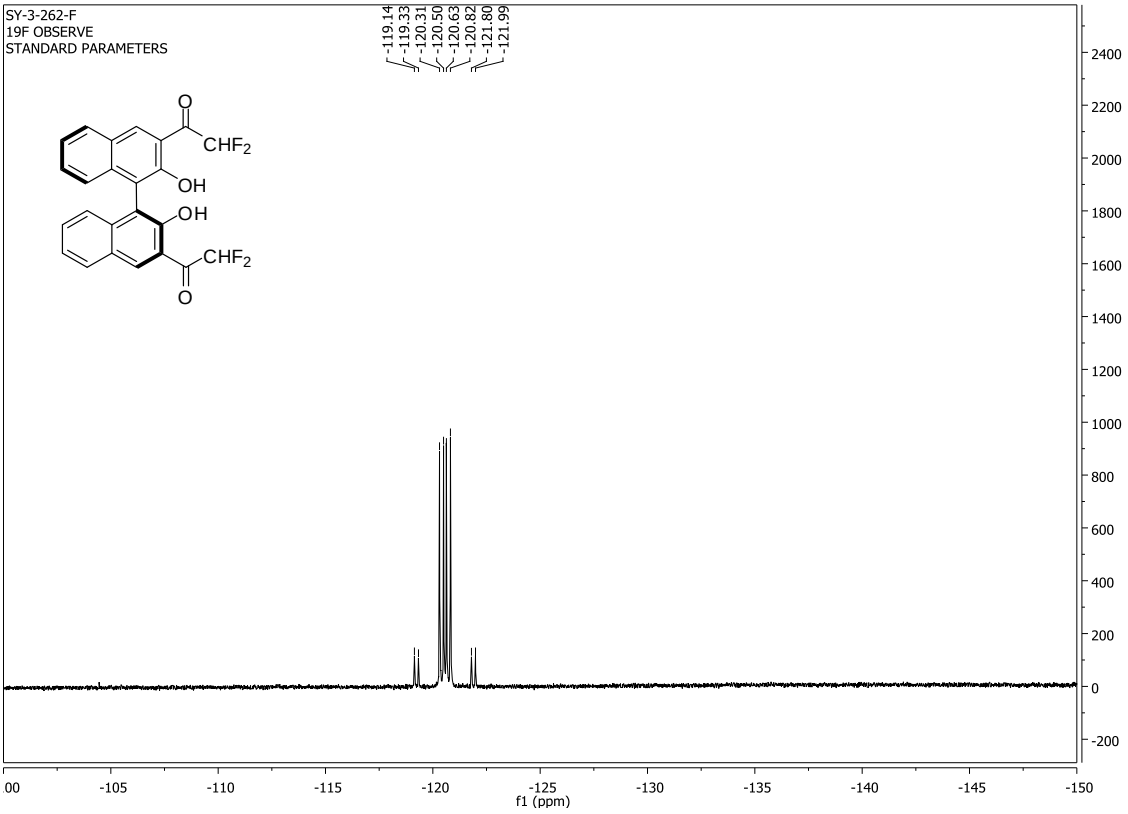
SY-3-262-F
19F OBSERVE
STANDARD PARAMETERS
-119.14
-119.33
-120.31
-120.50
-120.63
-120.82
-121.80
-121.99
O
CHF2
OH
OH
CHF2
O
f1 (ppm)

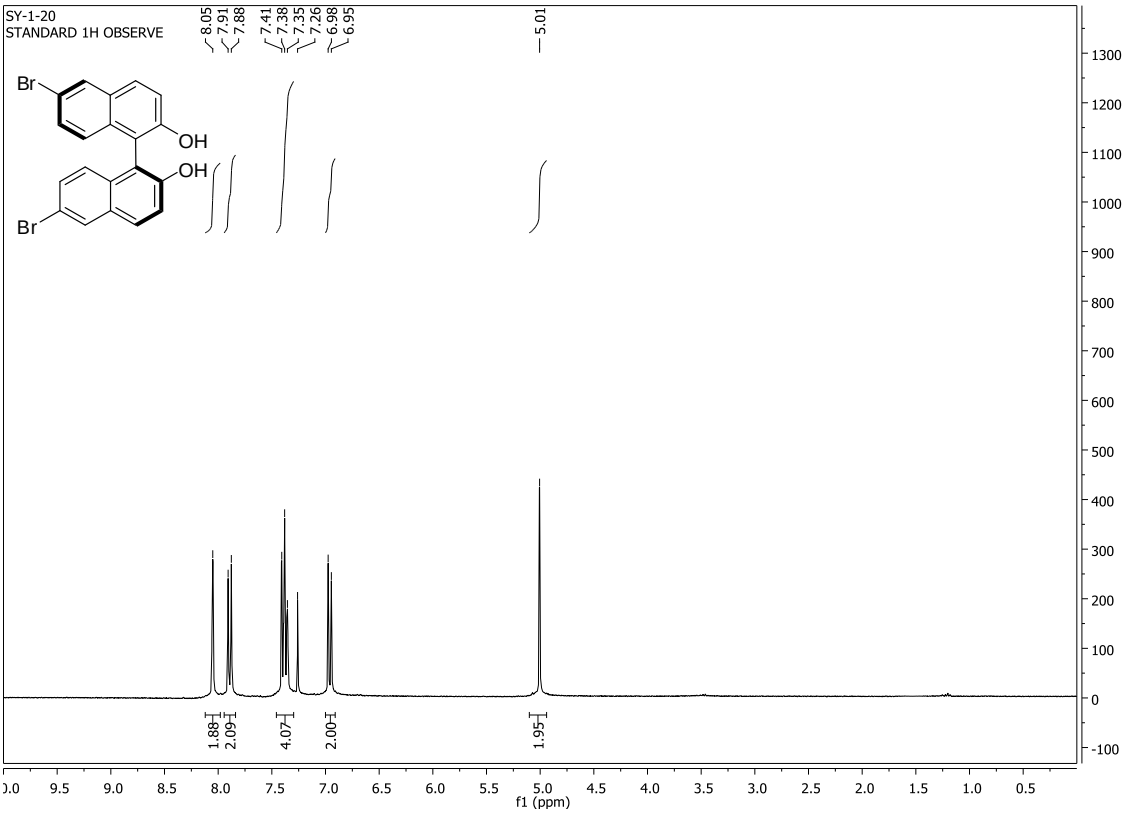
SY-1-20
STANDARD 1H OBSERVE
8.05
7.91
7.88
7.41
7.38
7.35
7.26
6.98
6.95
5.01
Br
OH
OH
Br
1.88
2.09
4.07
2.00
1.95
f1 (ppm)

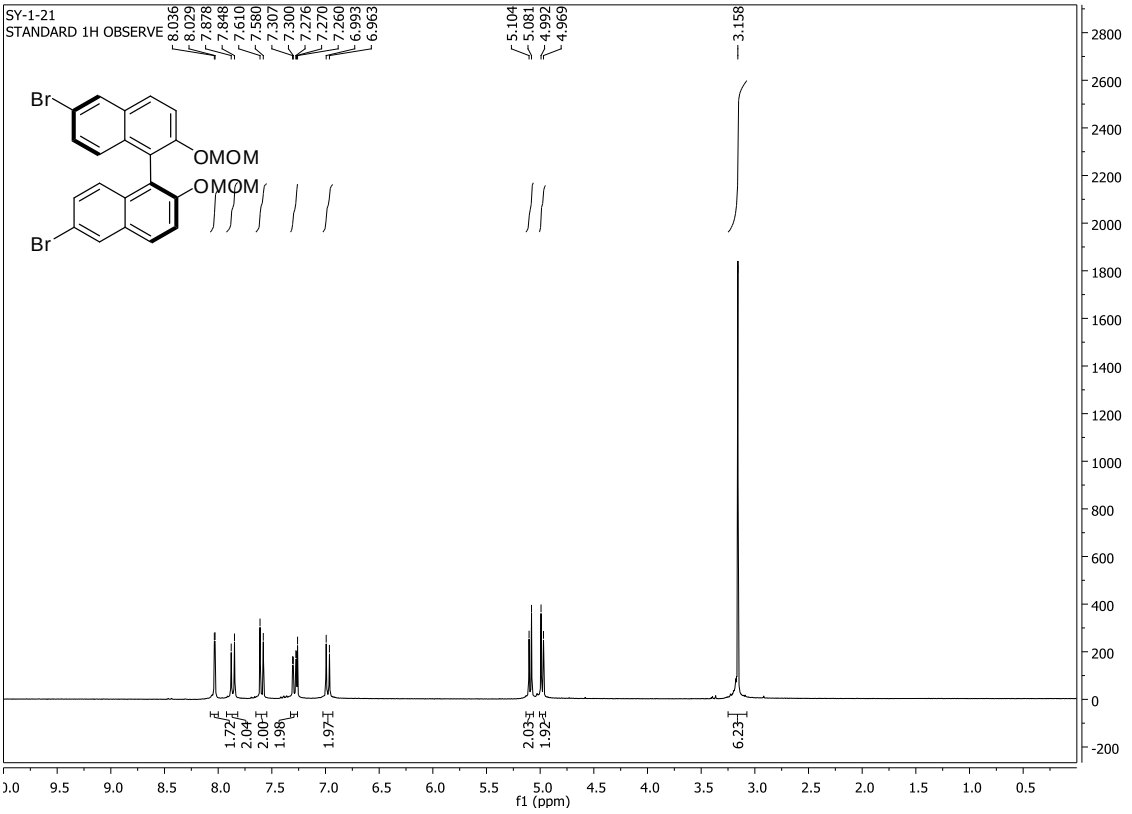
SY-1-21
STANDARD 1H OBSERVE
8.036
8.029
7.878
7.848
7.610
7.580
7.307
7.300
7.276
7.270
7.260
6.993
6.963
5.104
5.081
4.992
4.969
3.158
Br
OMOM
OMOM
Br
1.72
2.04
2.00
1.98
1.97
2.03
1.92
6.23
f1 (ppm)

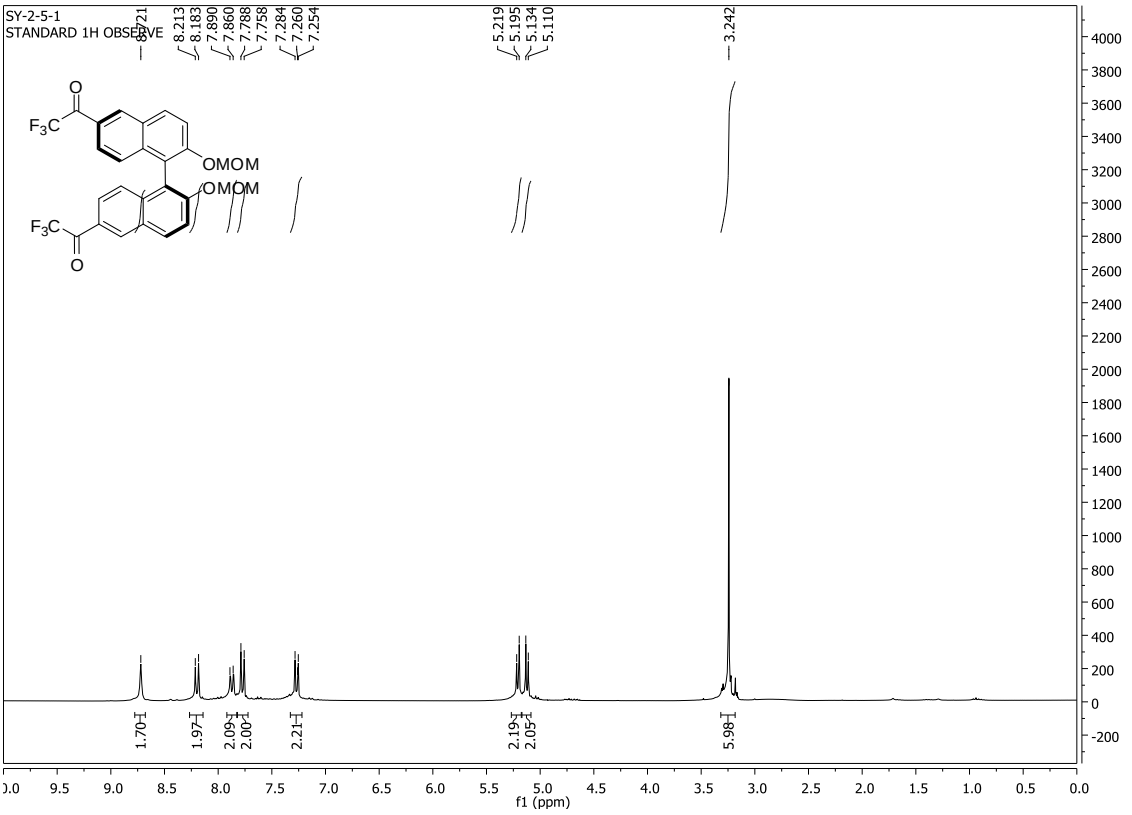
SY-2-5-1
STANDARD 1H OBSERVE
8.721
8.213
8.183
7.890
7.860
7.788
7.758
7.284
7.260
7.254
5.219
5.195
5.134
5.110
3.242
F3C
O
OMOM
OMOM
F3C
O
1.70
1.97
2.09
2.00
2.21
2.19
2.05
5.98
f1 (ppm)

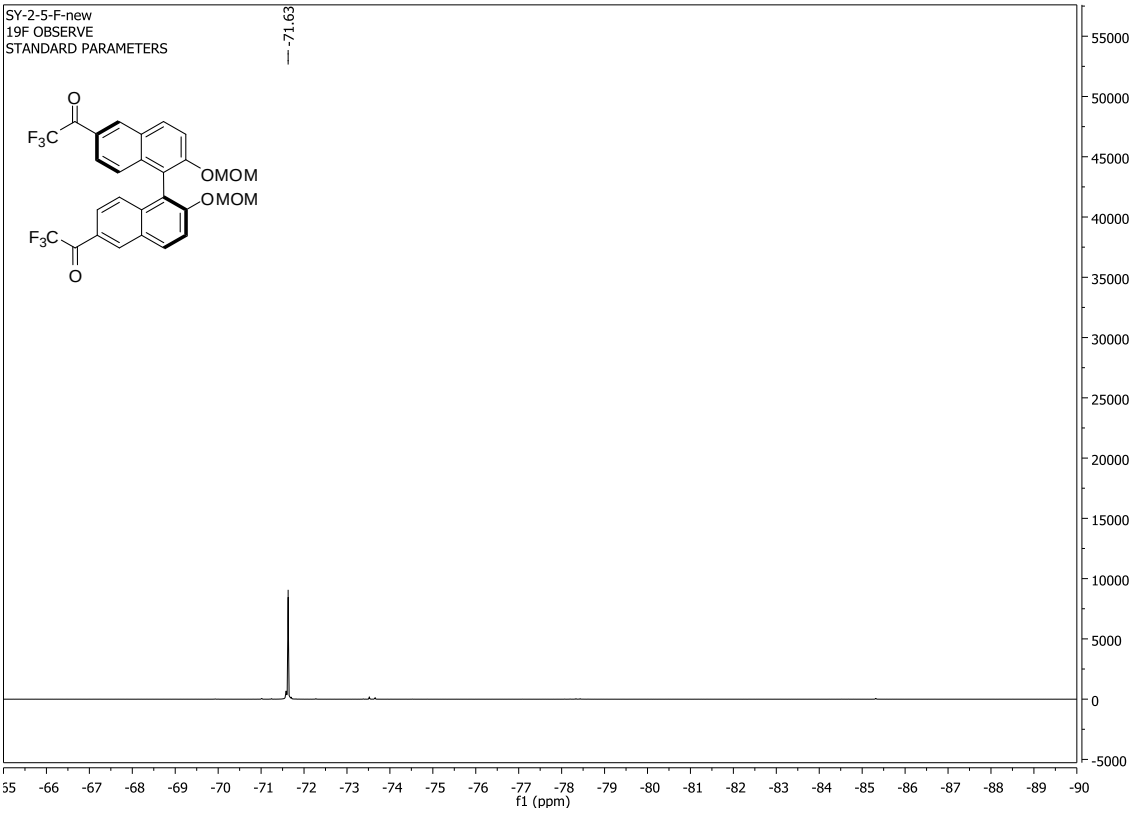
SY-2-5-F-new
19F OBSERVE
STANDARD PARAMETERS
-71.63
OMOM
OMOM
f1 (ppm)

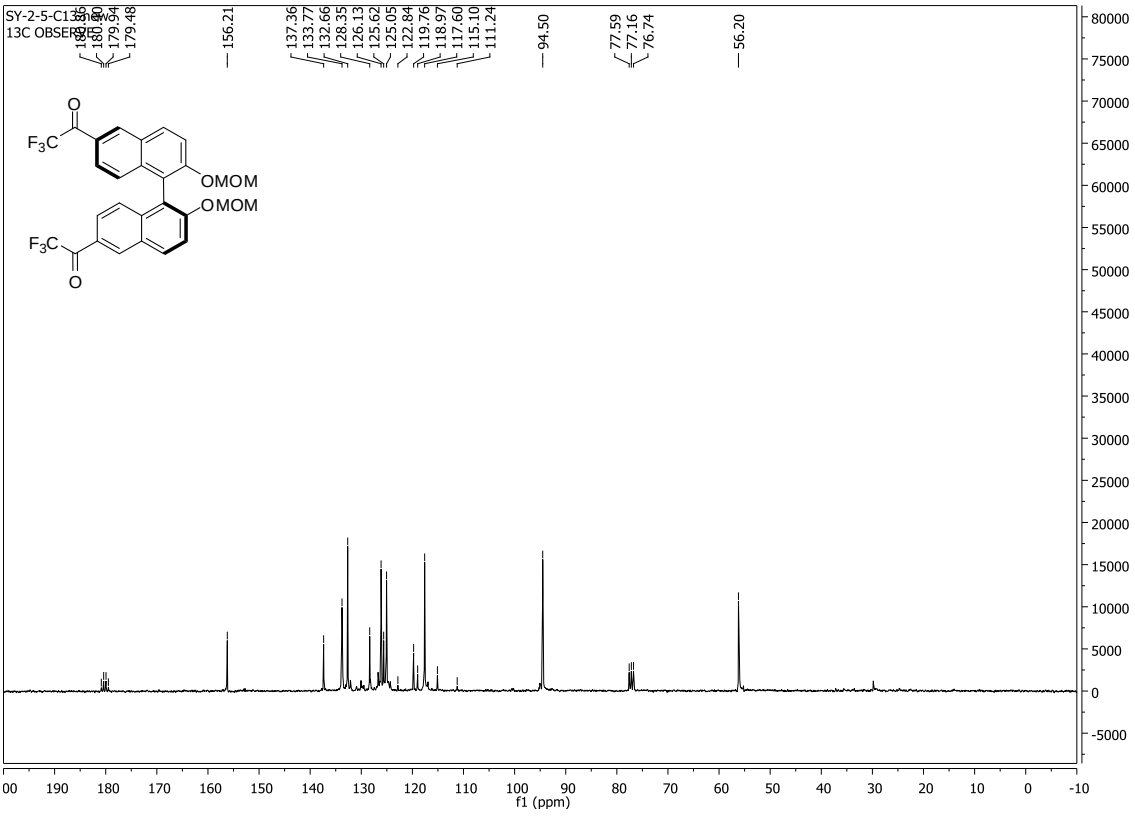
SY-2-5-C13new
13C OBSERVE
179.94
179.48
156.21
137.36
133.77
132.66
128.35
126.13
125.62
125.05
122.84
119.76
118.97
117.60
115.10
111.24
94.50
77.59
77.16
76.74
56.20
OMOM
OMOM
f1 (ppm)

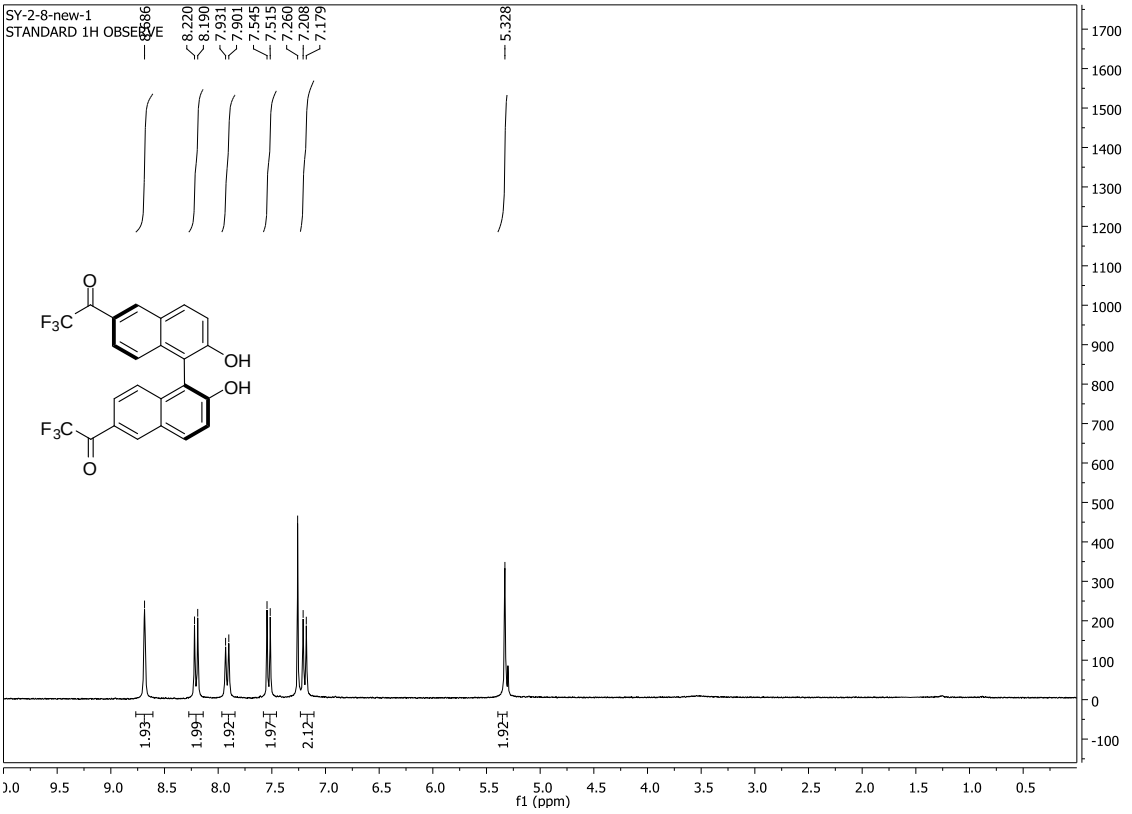
SY-2-8-new-1
STANDARD 1H OBSERVE
8.586
8.220
8.190
7.931
7.901
7.545
7.515
7.260
7.208
7.179
5.328
O
F3C
OH
OH
F3C
O
1.93
1.99
1.92
1.97
2.12
1.92
f1 (ppm)

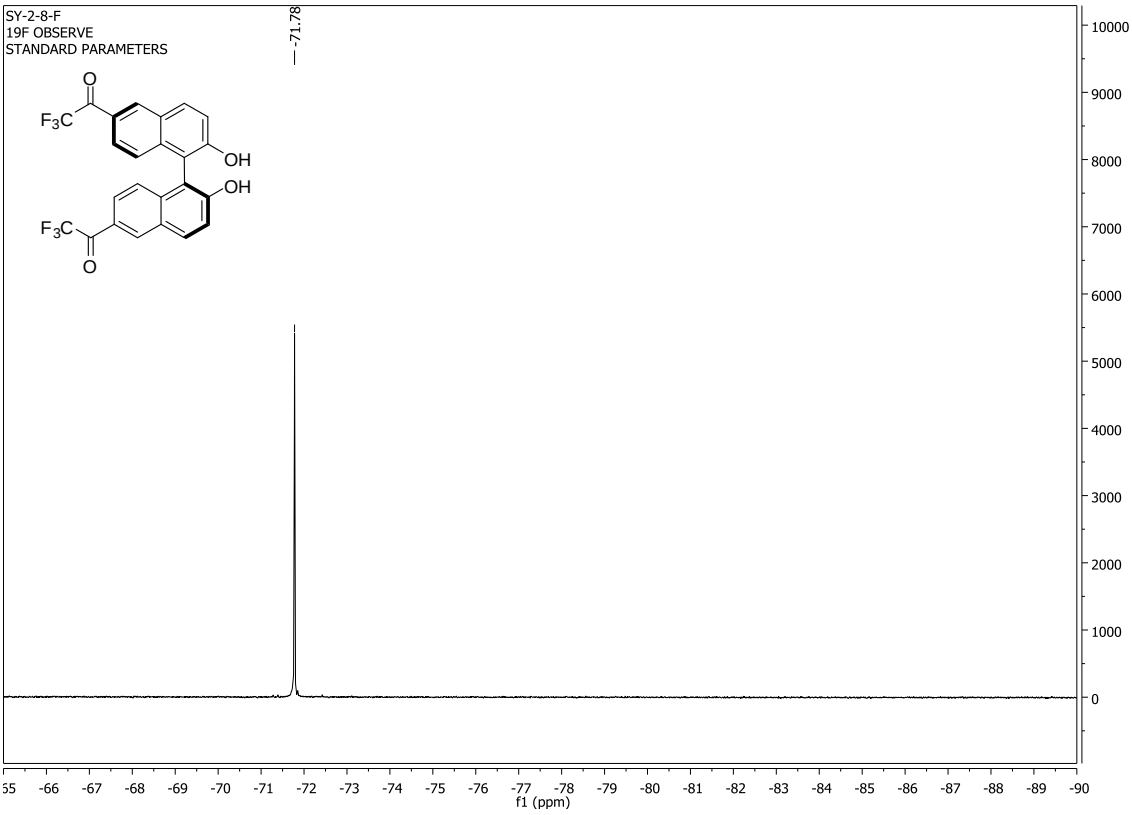
SY-2-8-F
19F OBSERVE
STANDARD PARAMETERS
-71.78
O
F3C
OH
OH
F3C
O
f1 (ppm)

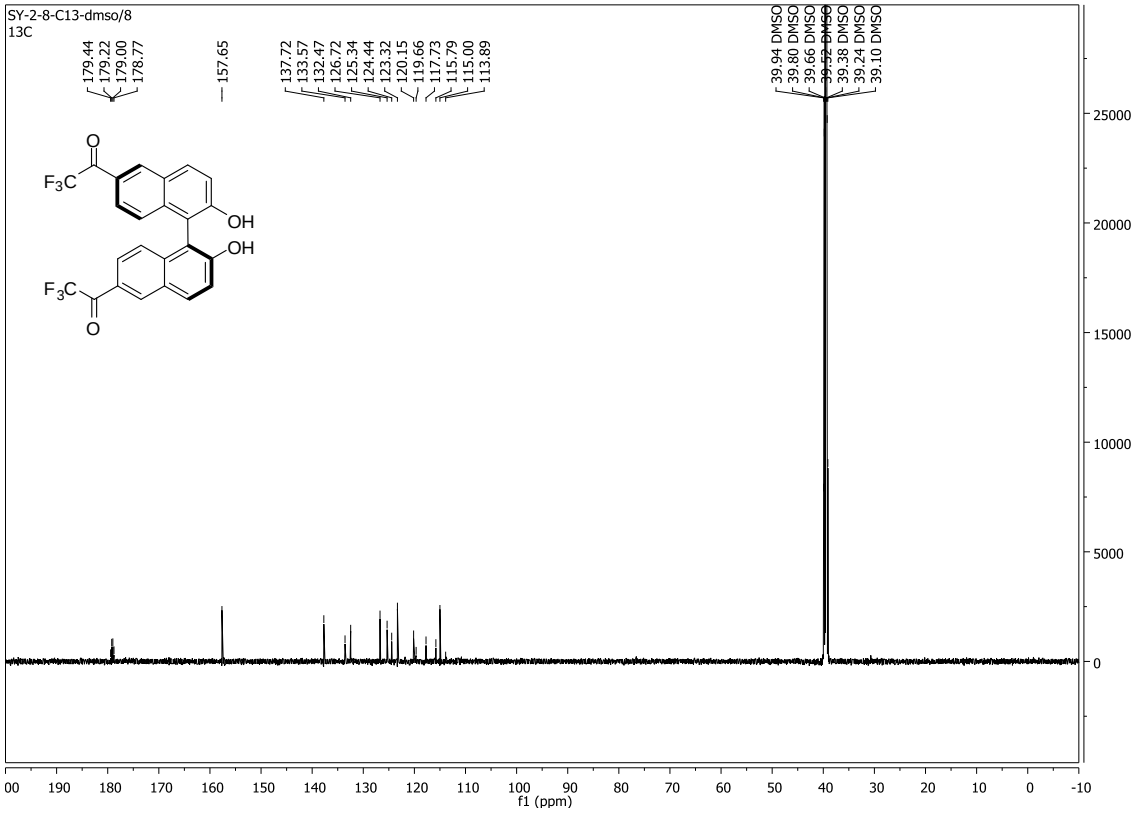
SY-2-8-C13-dmso/8
13C
179.44
179.22
179.00
178.77
157.65
137.72
133.57
132.47
126.72
125.34
124.44
123.32
120.15
119.66
117.73
115.79
115.00
113.89
39.94 DMSO
39.80 DMSO
39.66 DMSO
39.52 DMSO
39.38 DMSO
39.24 DMSO
39.10 DMSO
F3C
O
OH
OH
F3C
O
f1 (ppm)

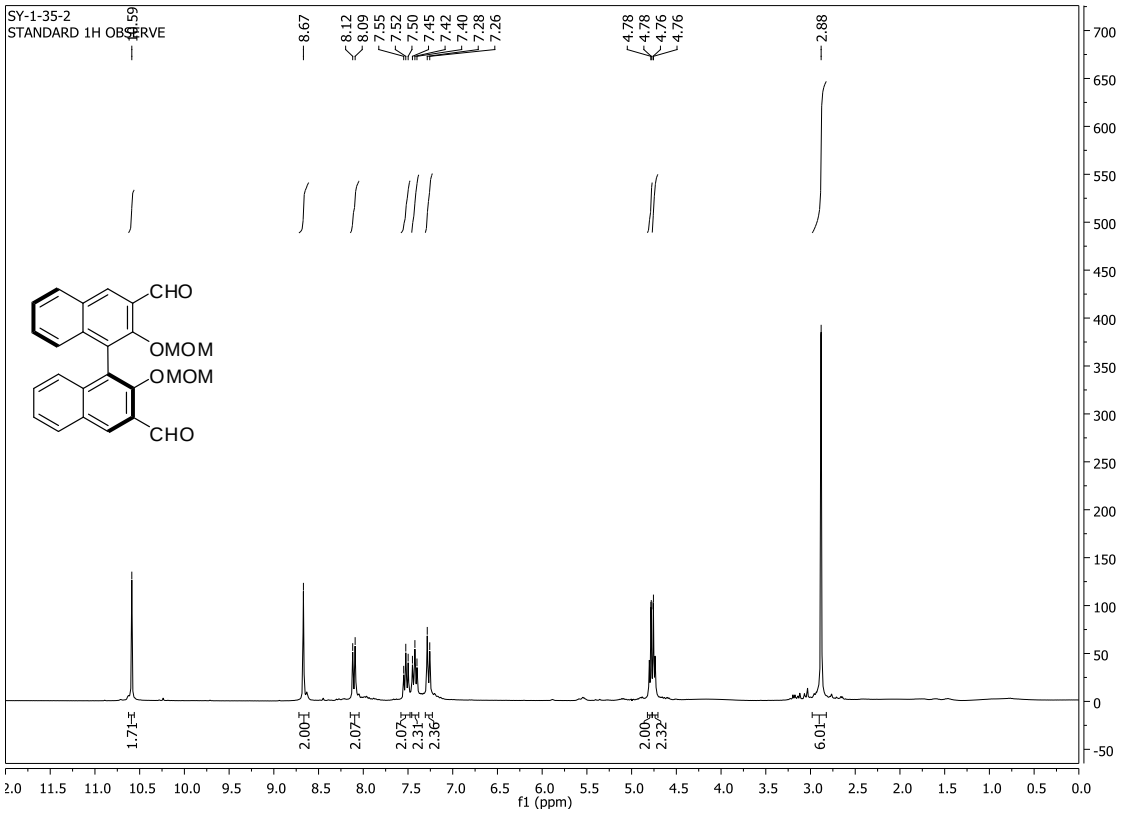
SY-1-35-2
STANDARD 1H OBSERVE
4.59
8.67
8.12
8.09
7.55
7.52
7.50
7.45
7.42
7.40
7.28
7.26
4.78
4.78
4.76
4.76
2.88
CHO
OMOM
OMOM
CHO
1.71
2.00
2.07
2.07
2.31
2.36
2.00
2.32
6.01
f1 (ppm)

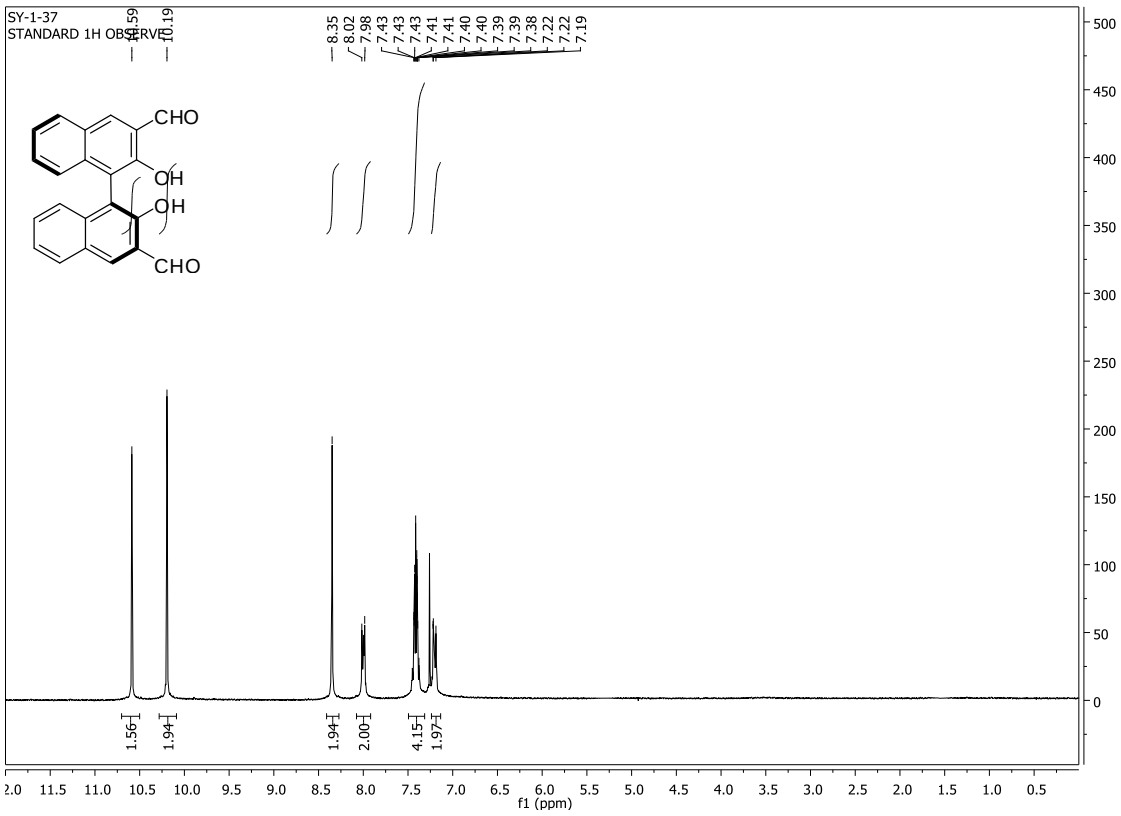
SY-1-37
STANDARD 1H OBSERVE
10.59
10.19
8.35
8.02
7.98
7.43
7.43
7.43
7.41
7.41
7.40
7.40
7.39
7.39
7.38
7.22
7.19
CHO
OH
OH
CHO
1.56
1.94
1.94
2.00
4.15
1.97
f1 (ppm)

^{19}F NMR titration of (*S*)-6-4 with N9

0 eq. of **N9**

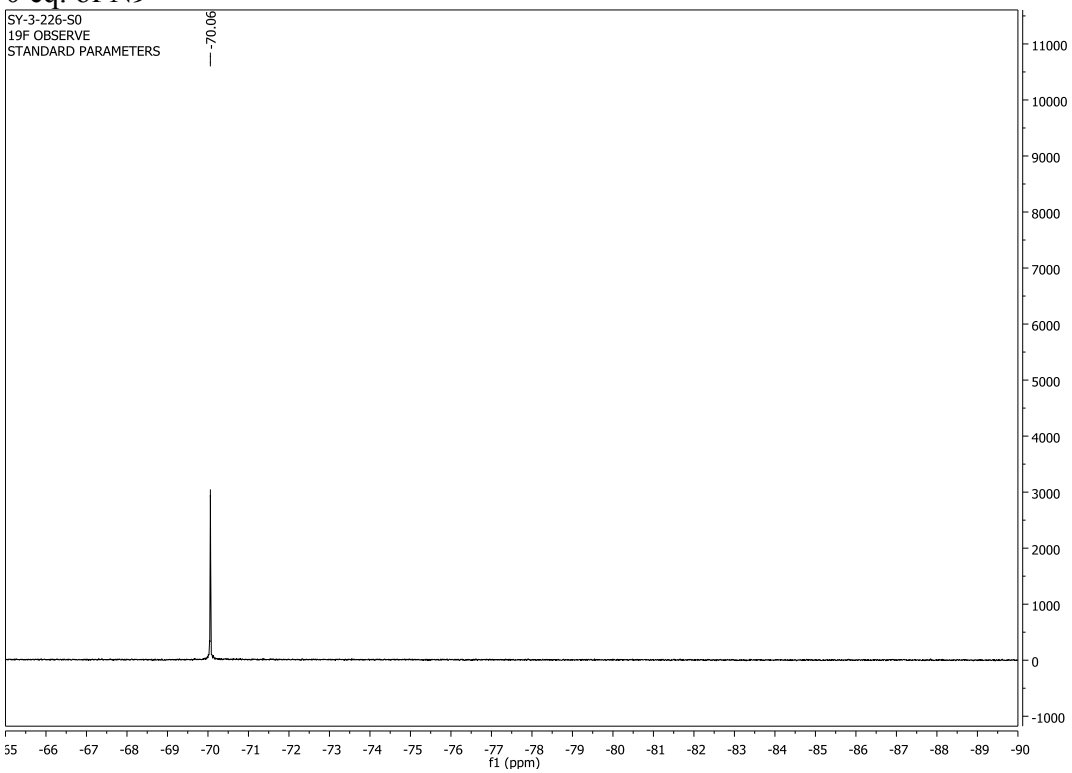

0.2 eq of **N9**

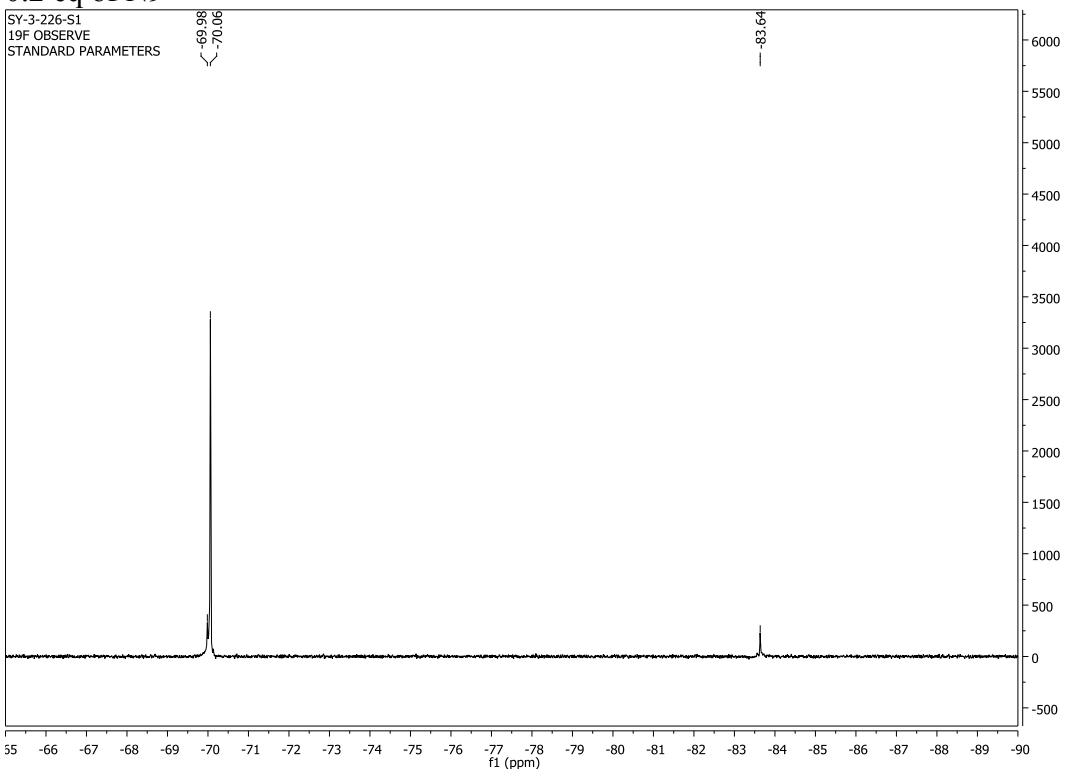

0.4 eq of **N9**

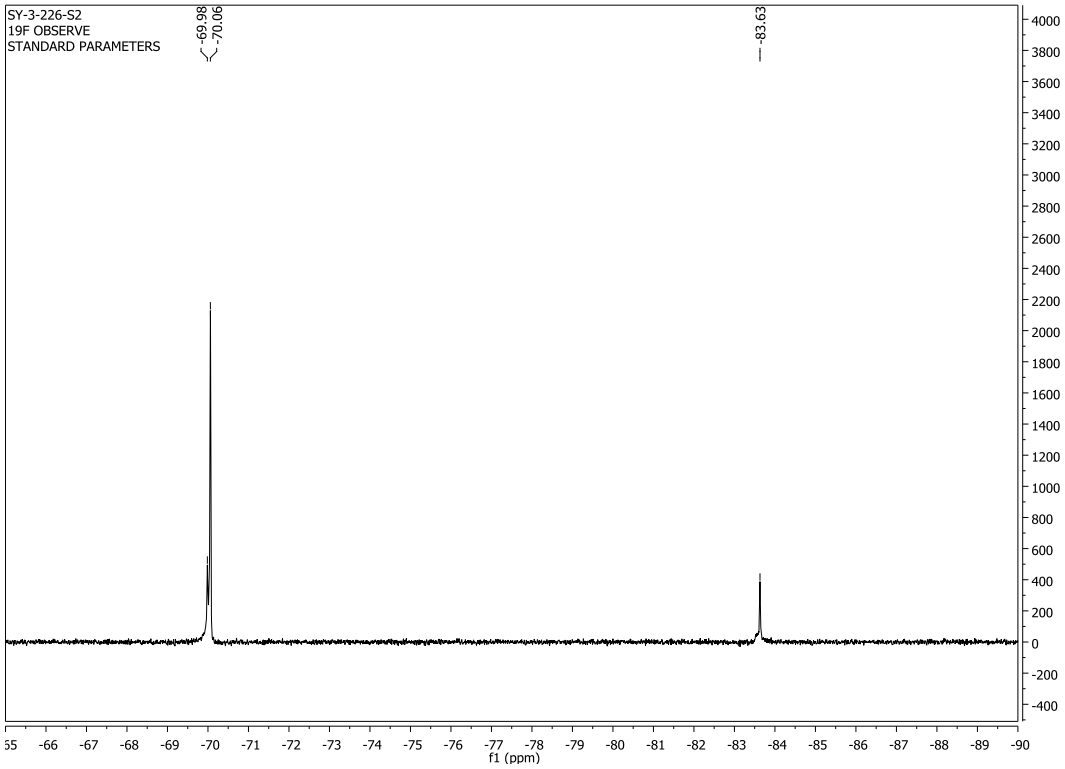

0.6 eq of **N9**

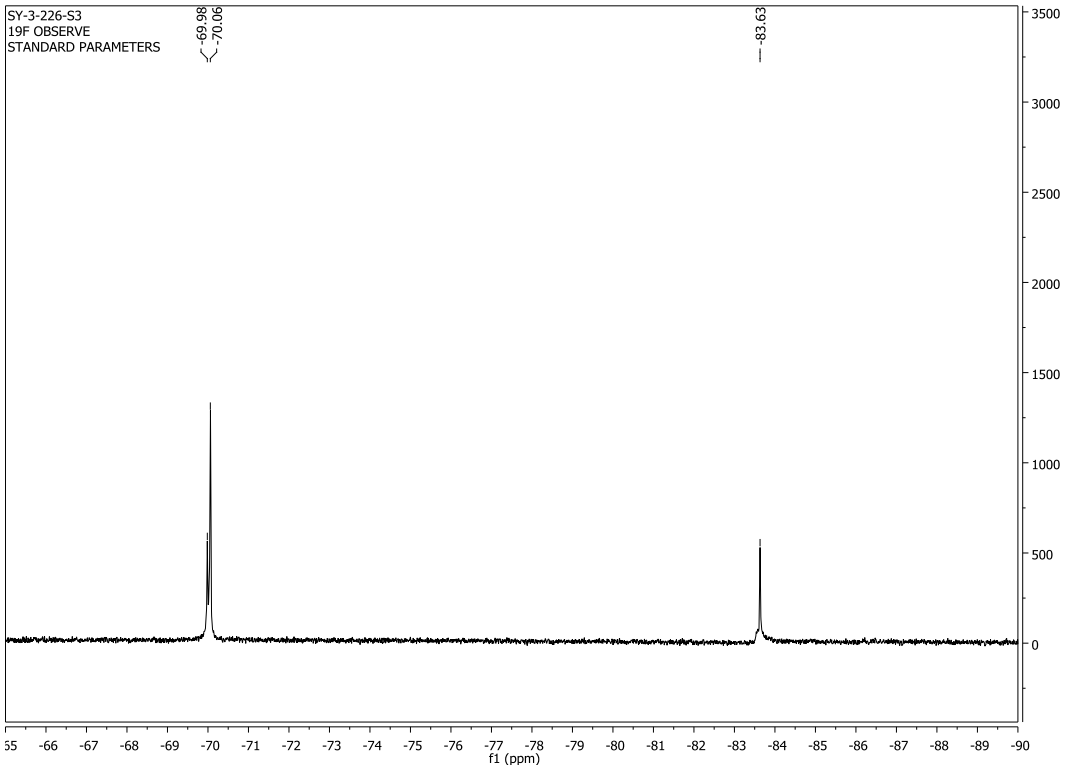

0.8 eq of **N9**

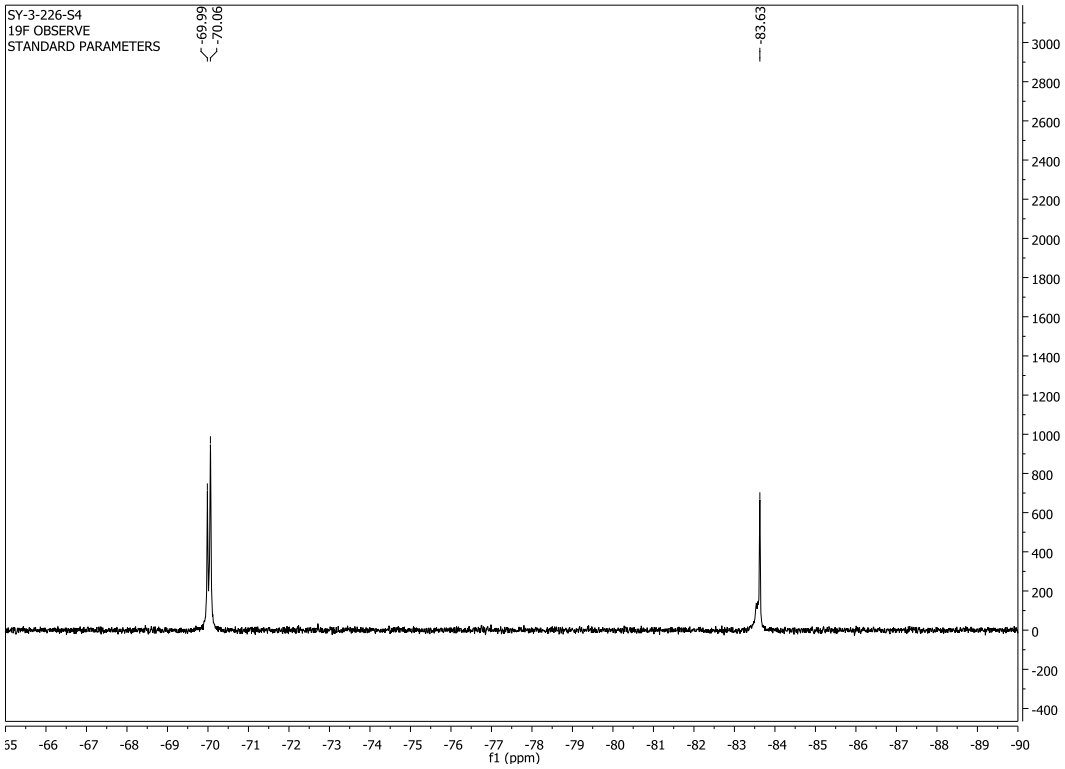

1.15 eq of **N9**

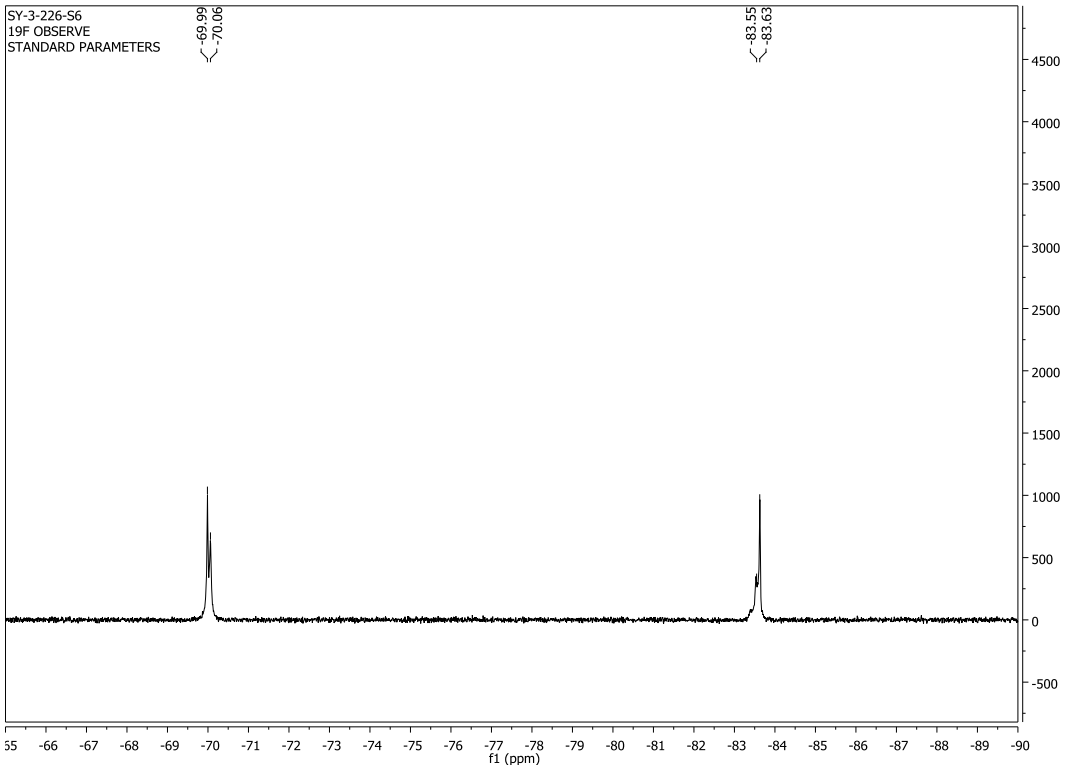

1.9 eq of **N9**

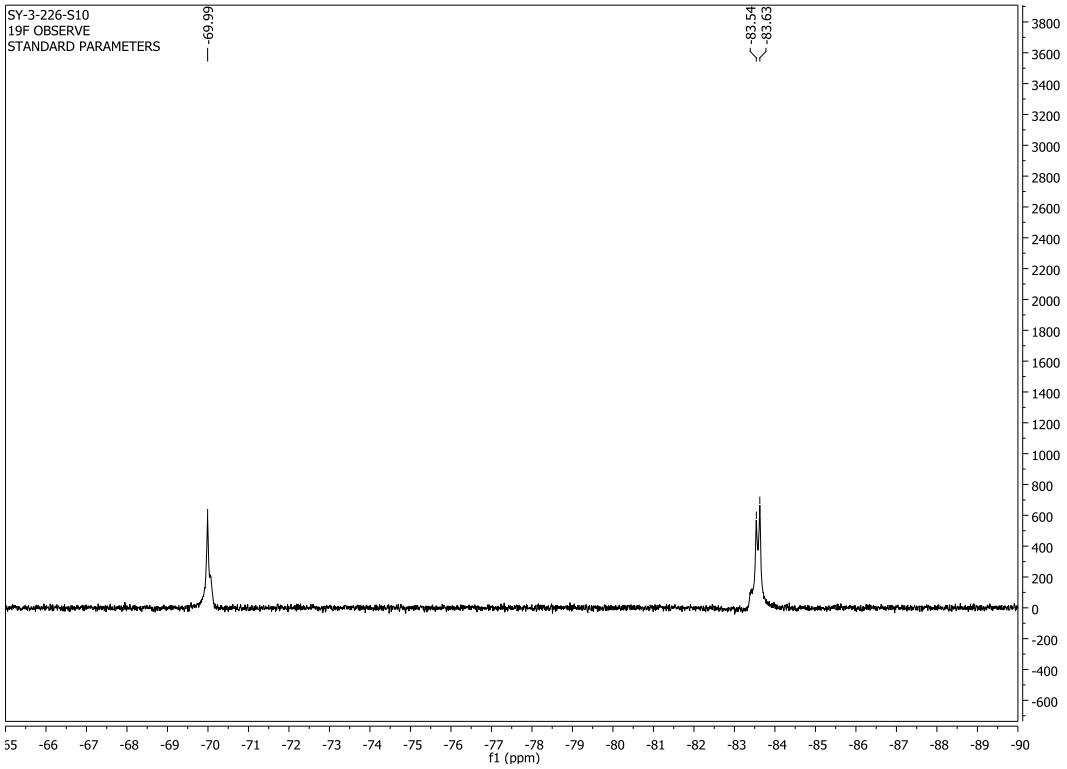

3.7 eq of **N9**

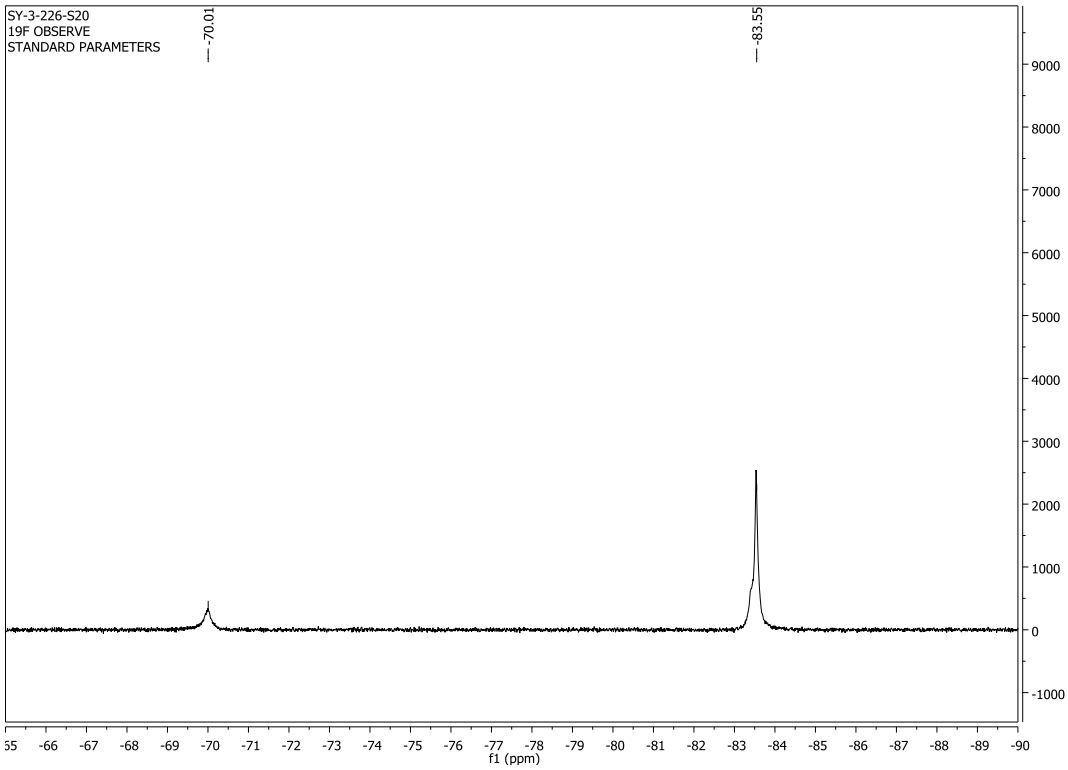

5.4 eq of **N9**

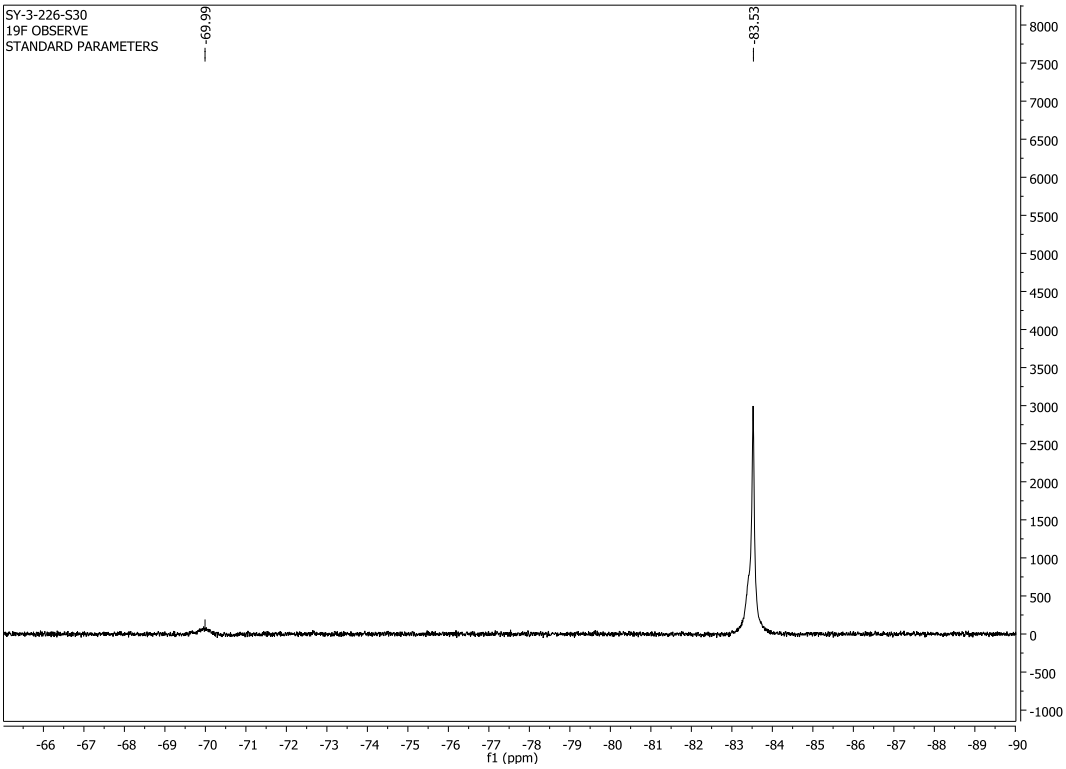

7.1 eq of **N9**

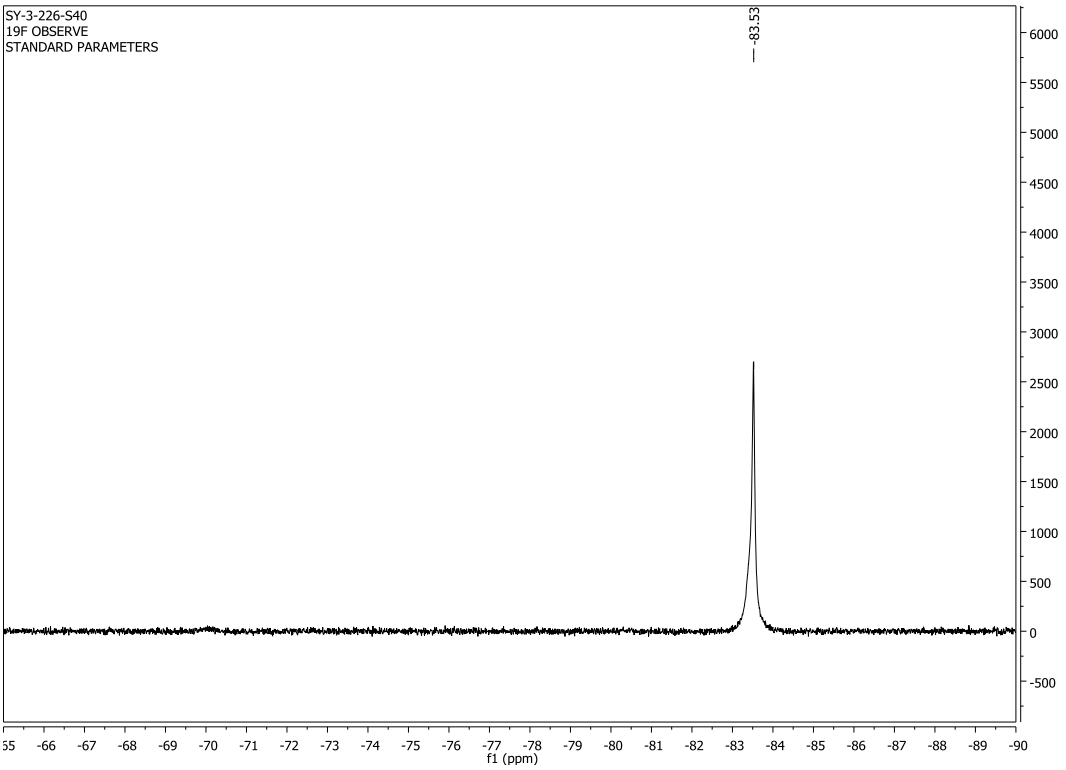

8.7 eq of **N9**

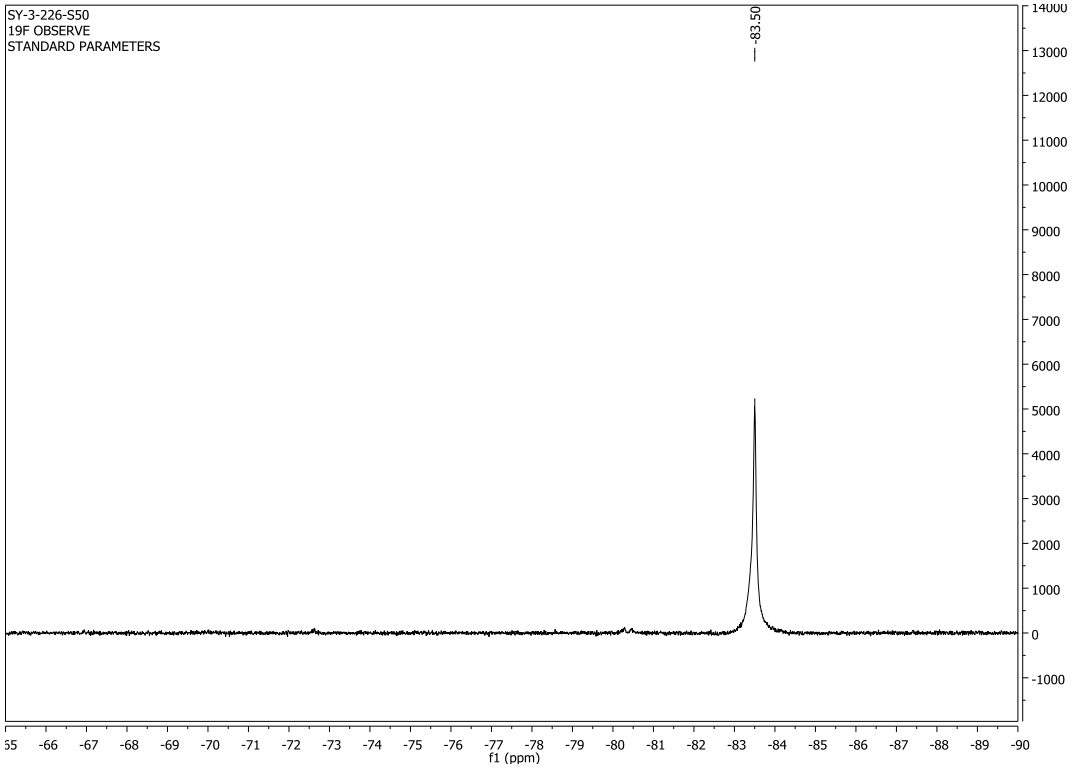

11.6 eq of **N9**

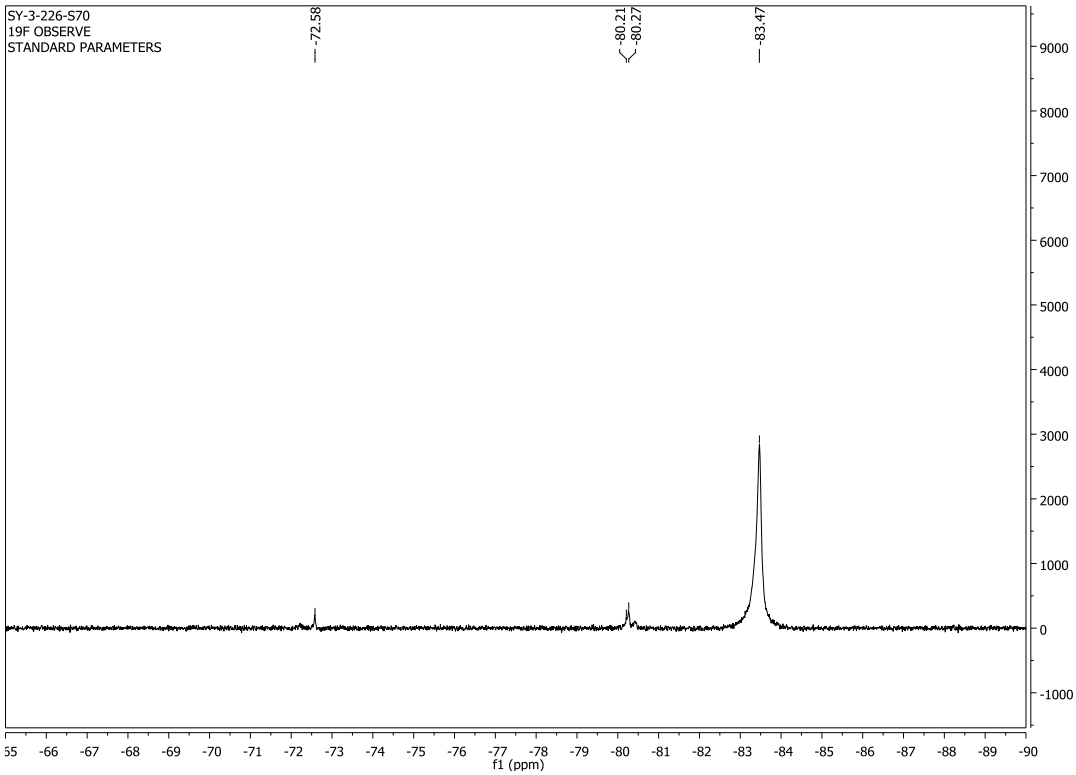

15.6 eq of **N9**

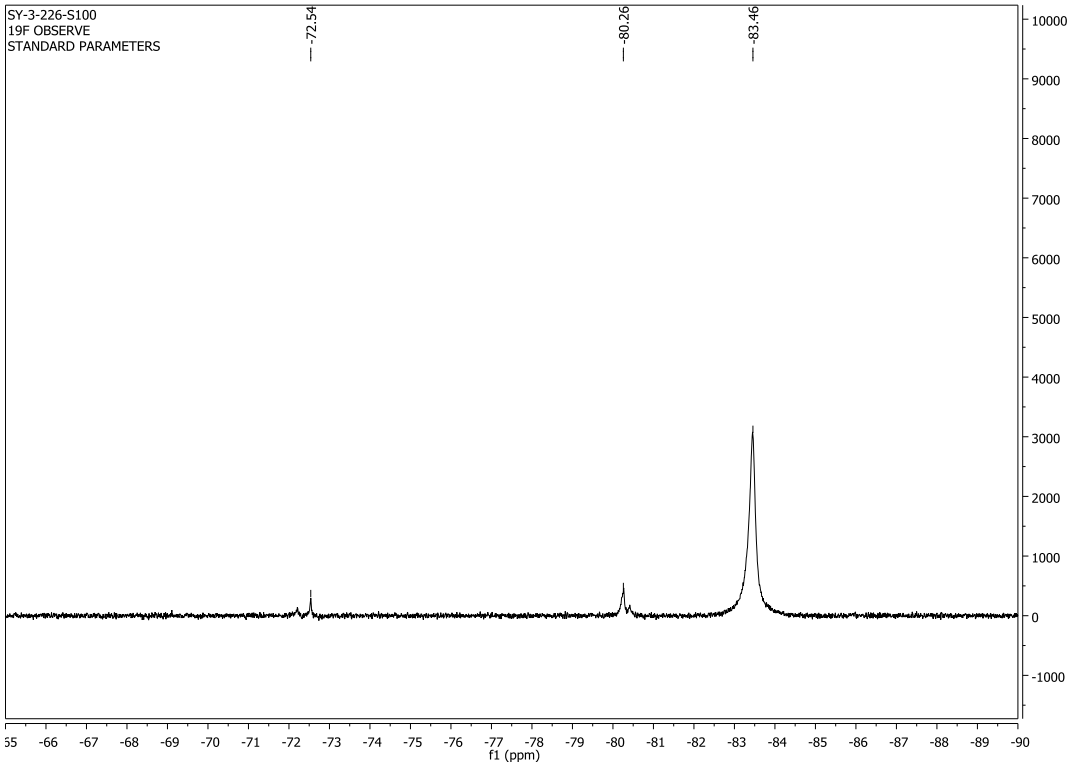

21.3 eq of **N9**

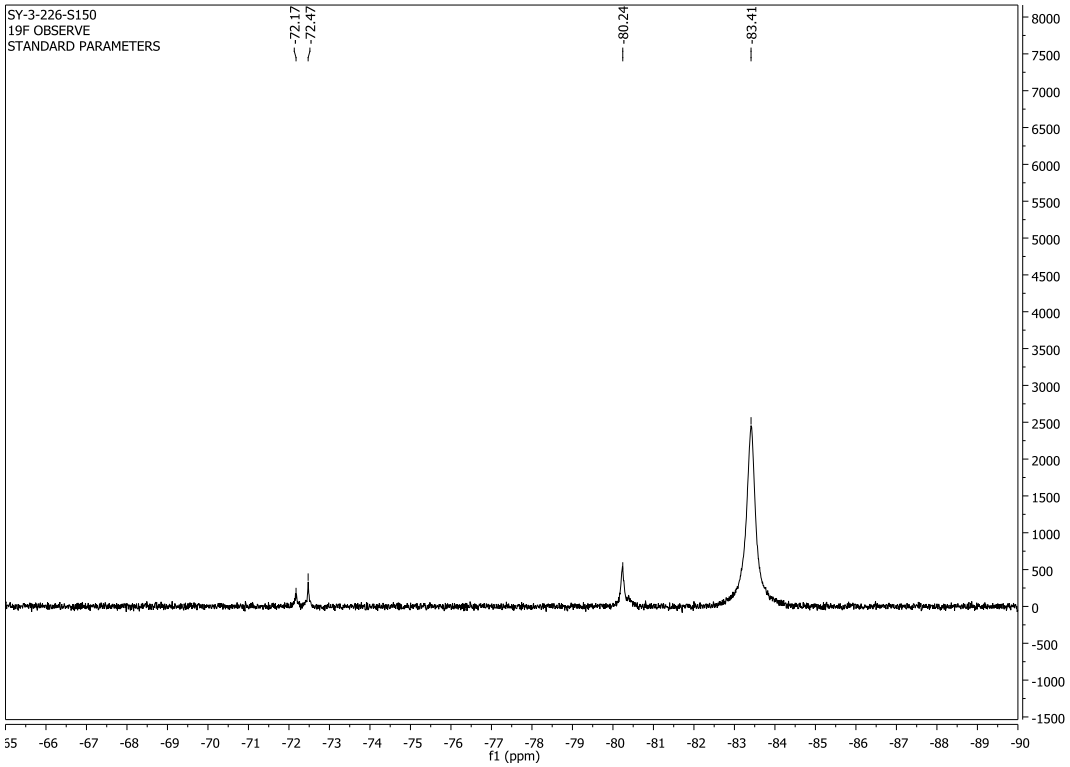

30 eq of **N9**

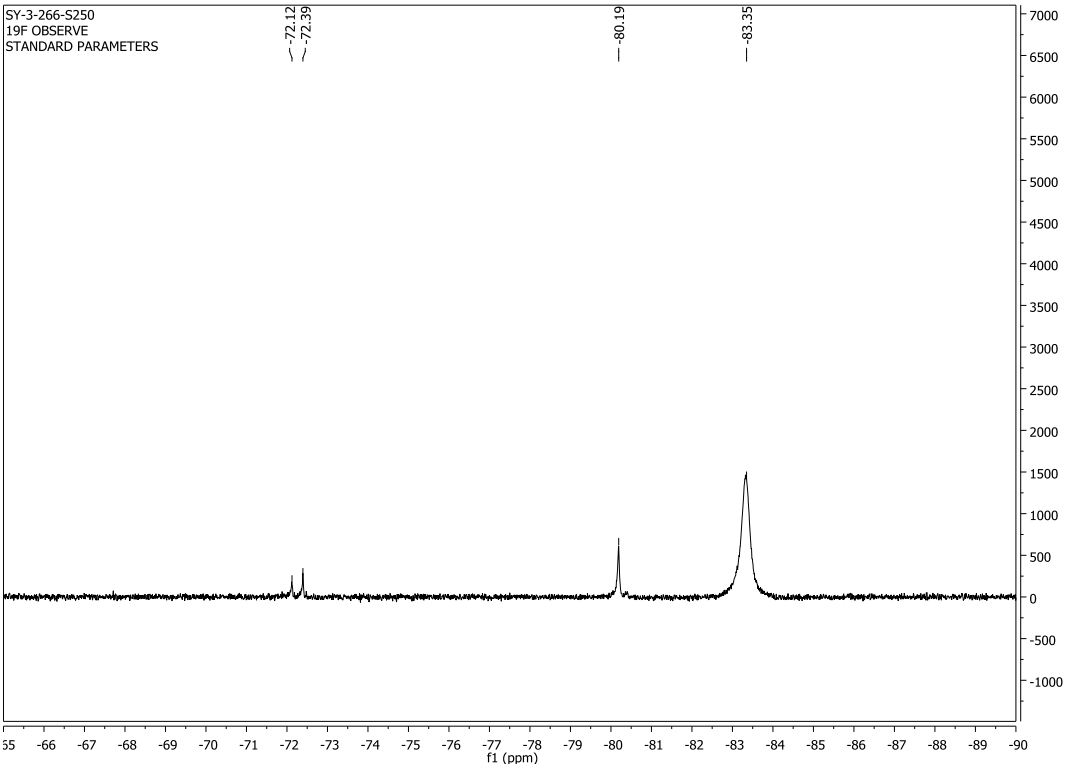

39 eq of **N9**

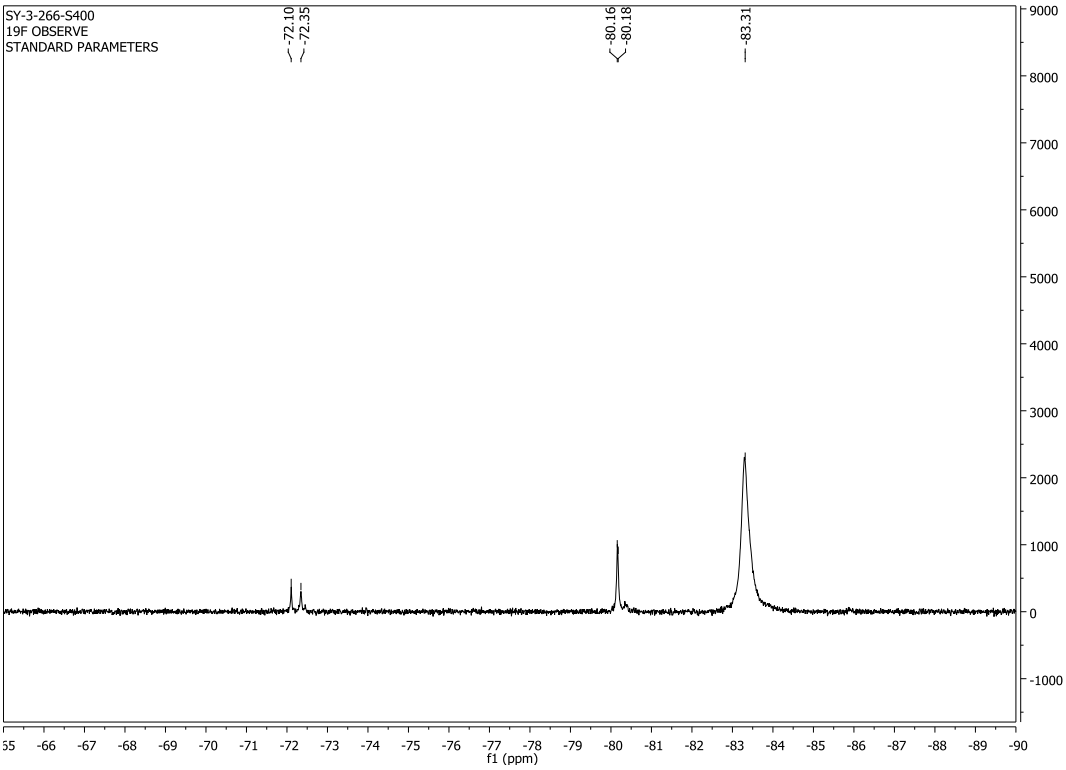

41.9 eq of **N9**

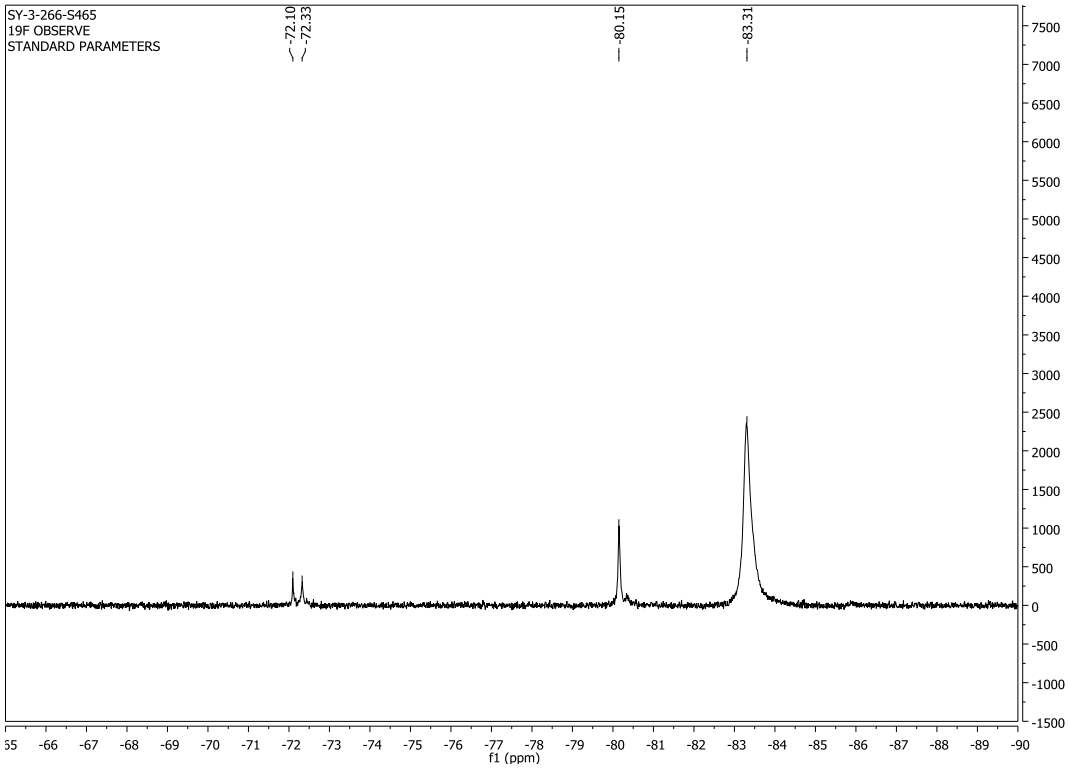

108 eq of **N9**

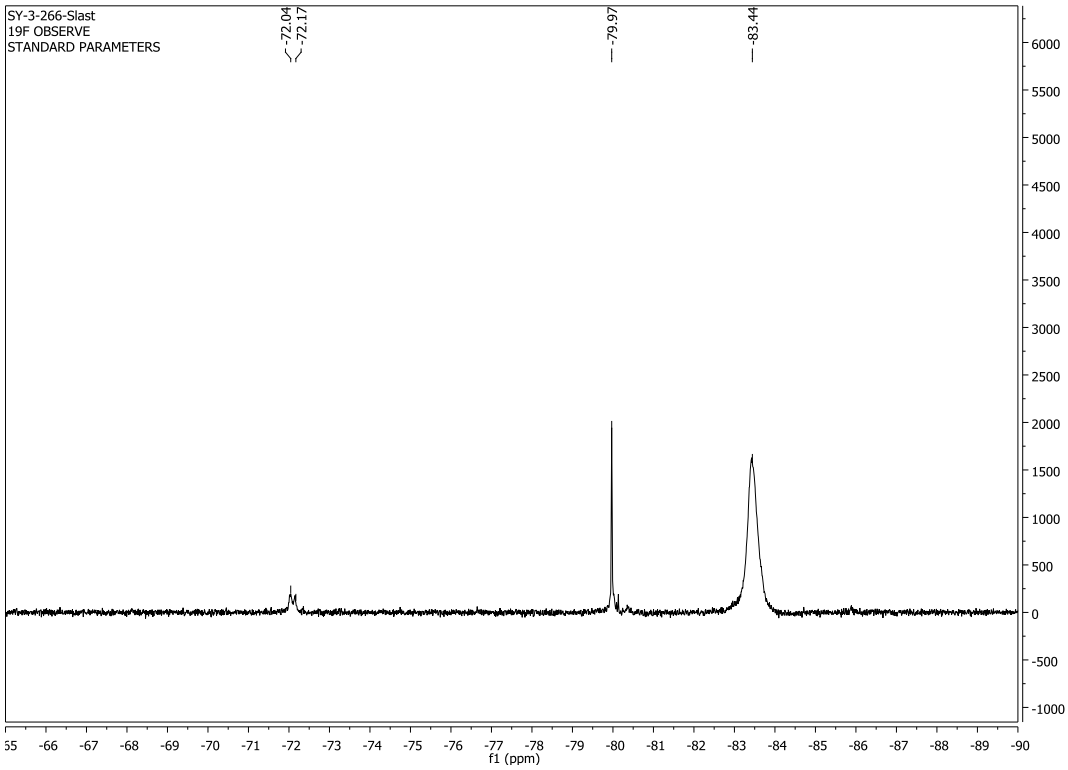

108 eq of **N9** overnight

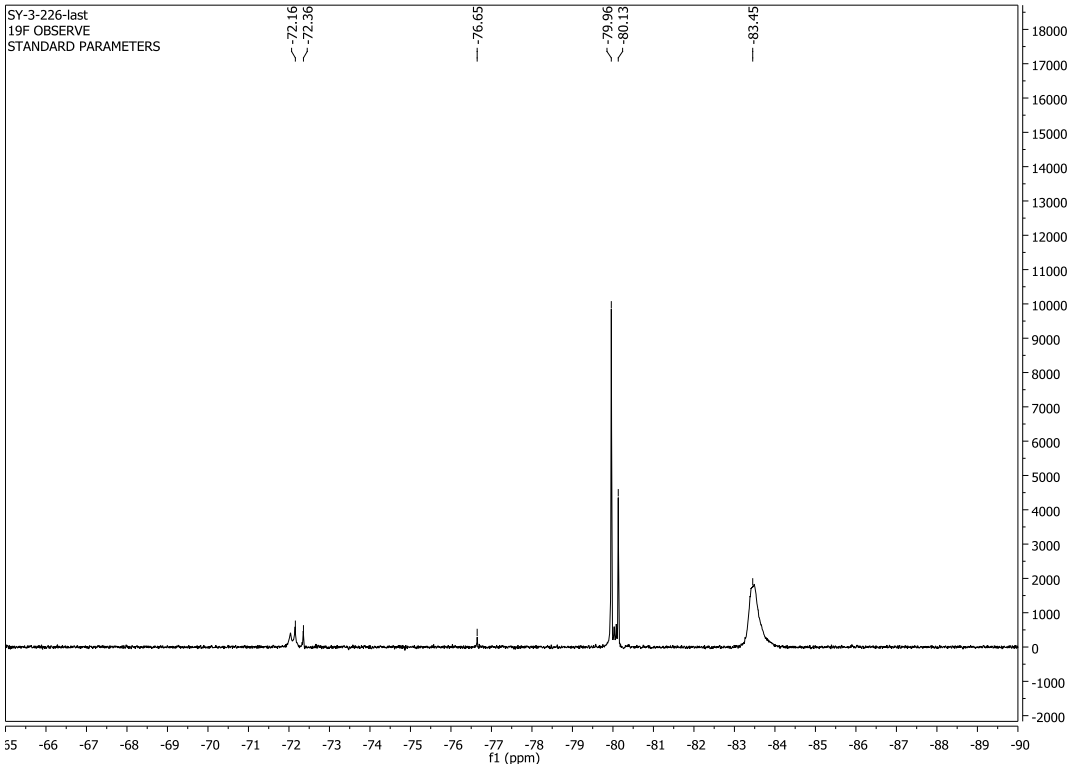

^{19}F NMR titration of (*S*)-6-4 with N12

0 eq of **N12**

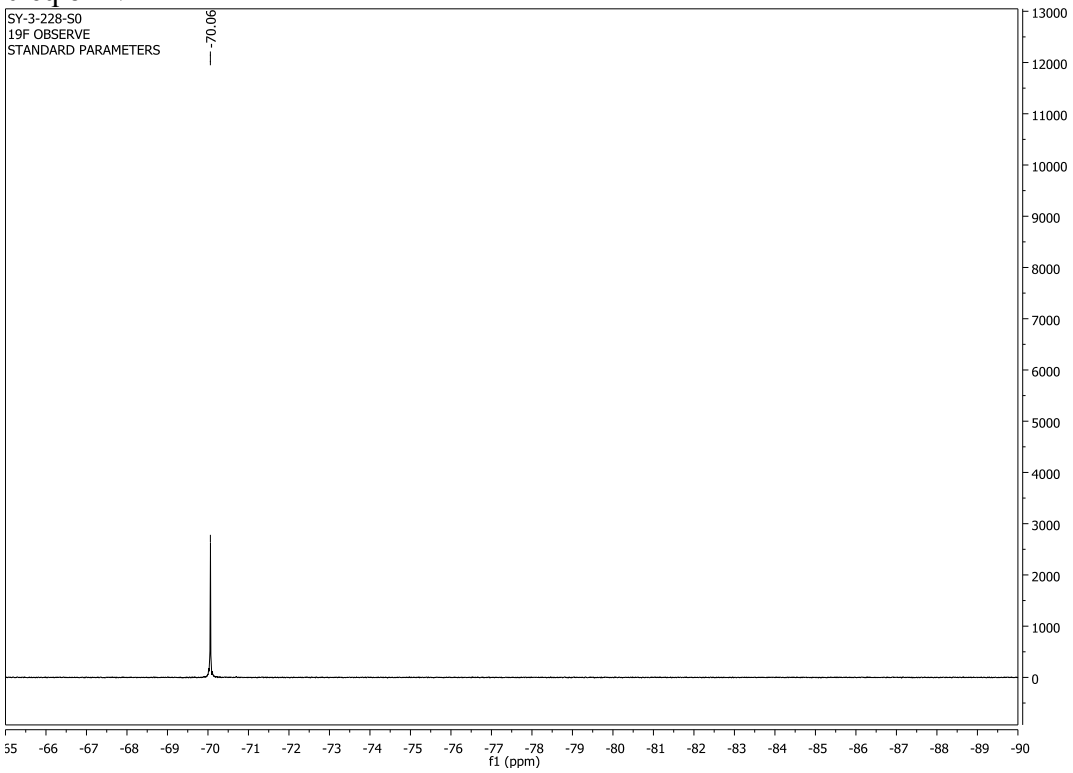

0.19 eq of **N12**

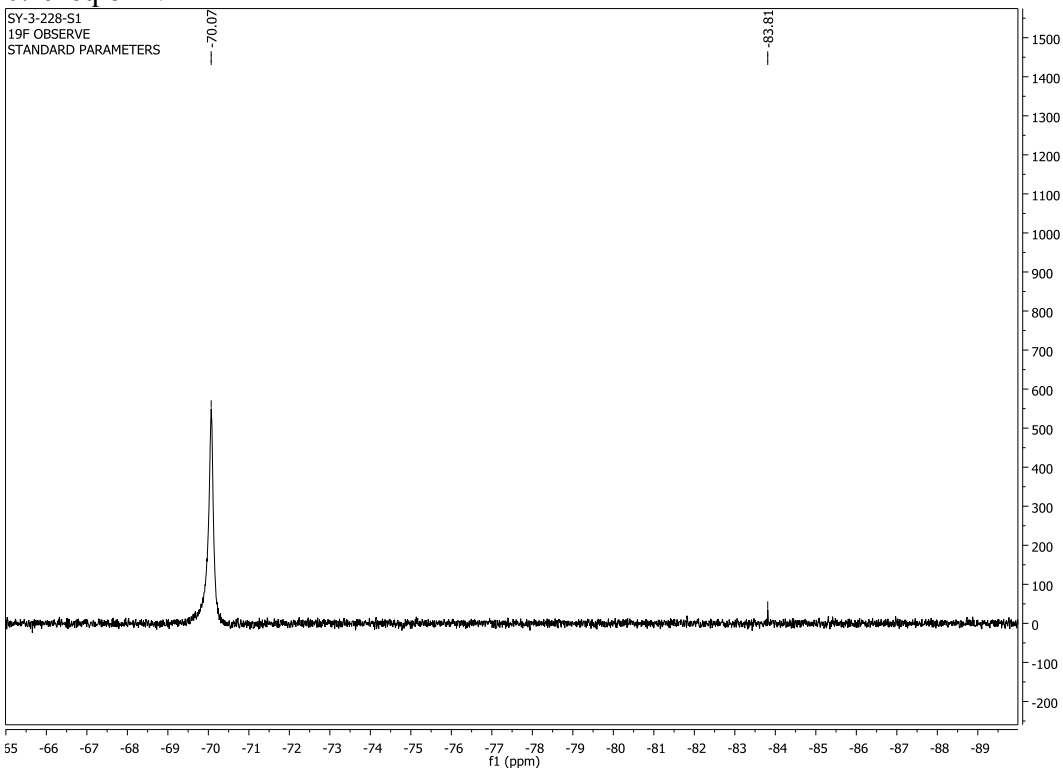

0.57 eq of **N12**

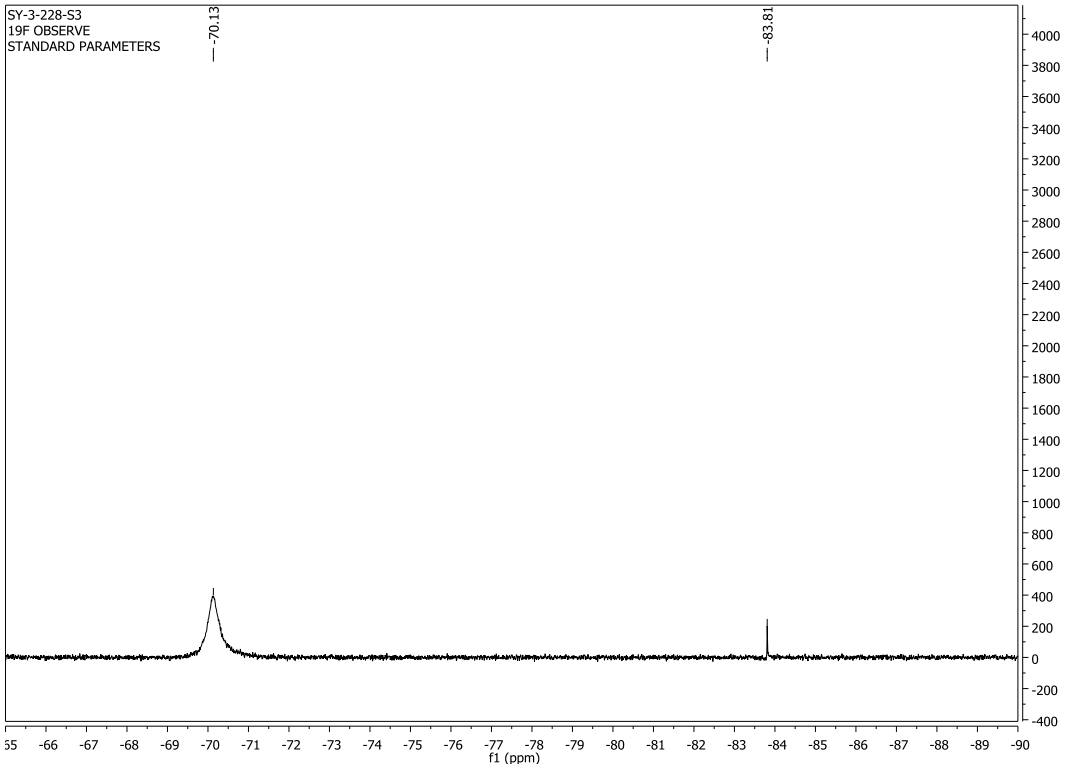

0.94 eq of **N12**

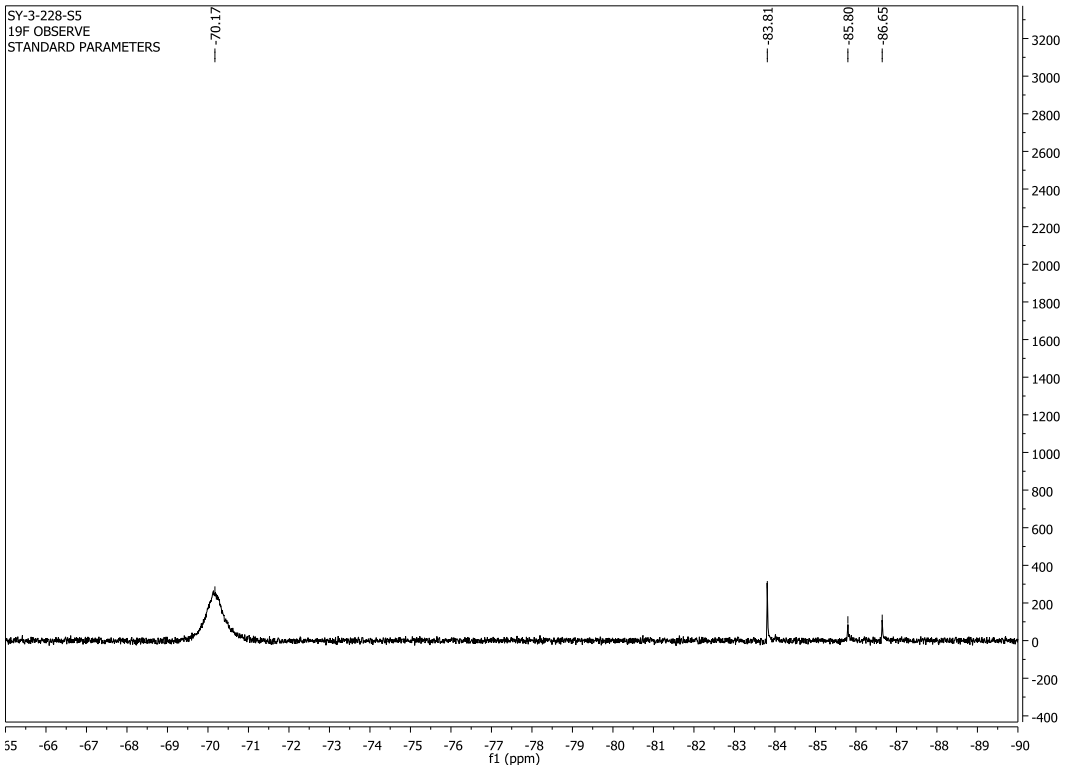

1.5 eq of **N12**

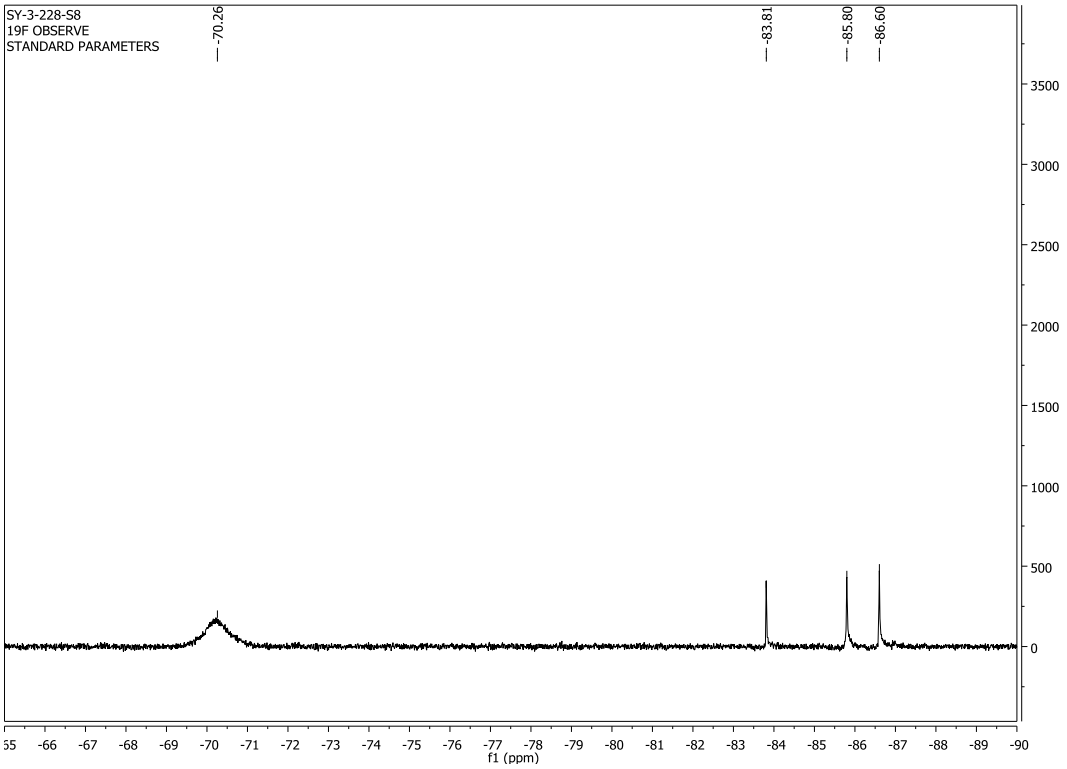

1.86 eq. of **N12**

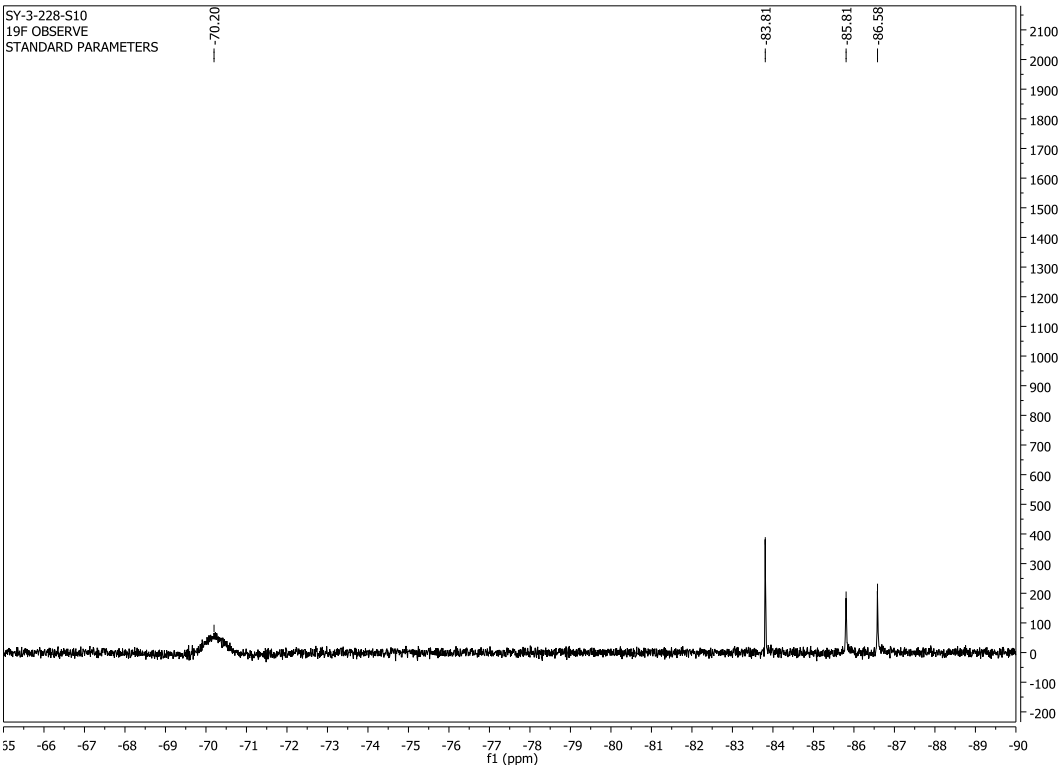

2.05 eq. of **N12**

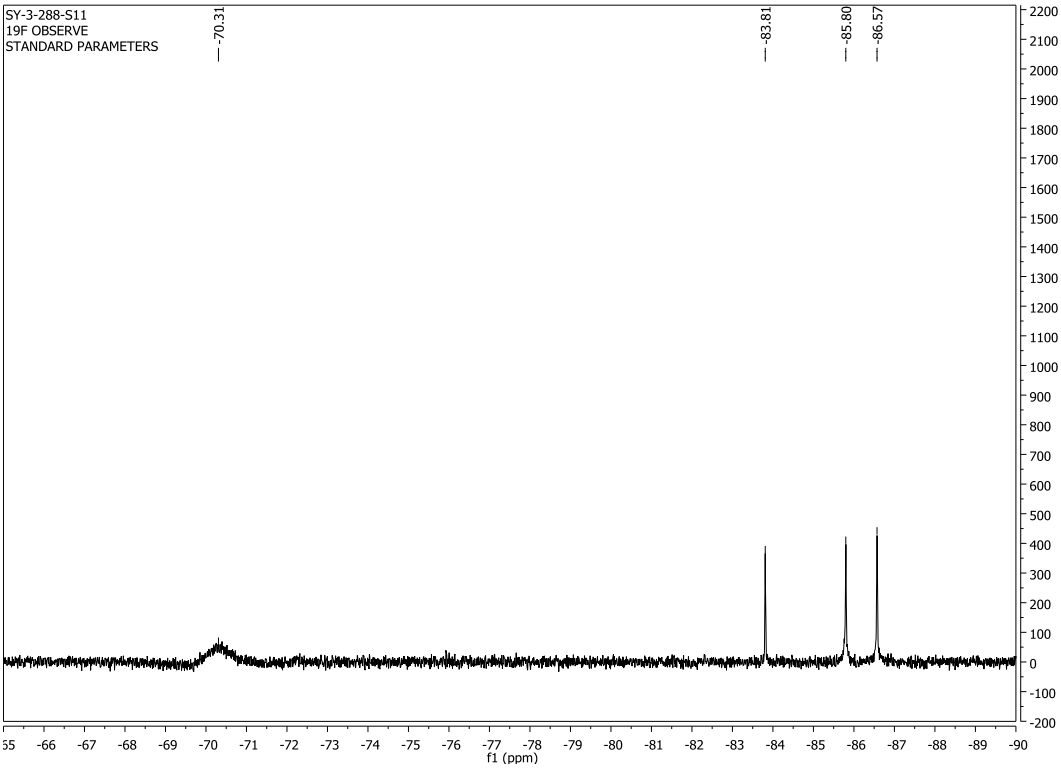

2.76 eq of **N12**

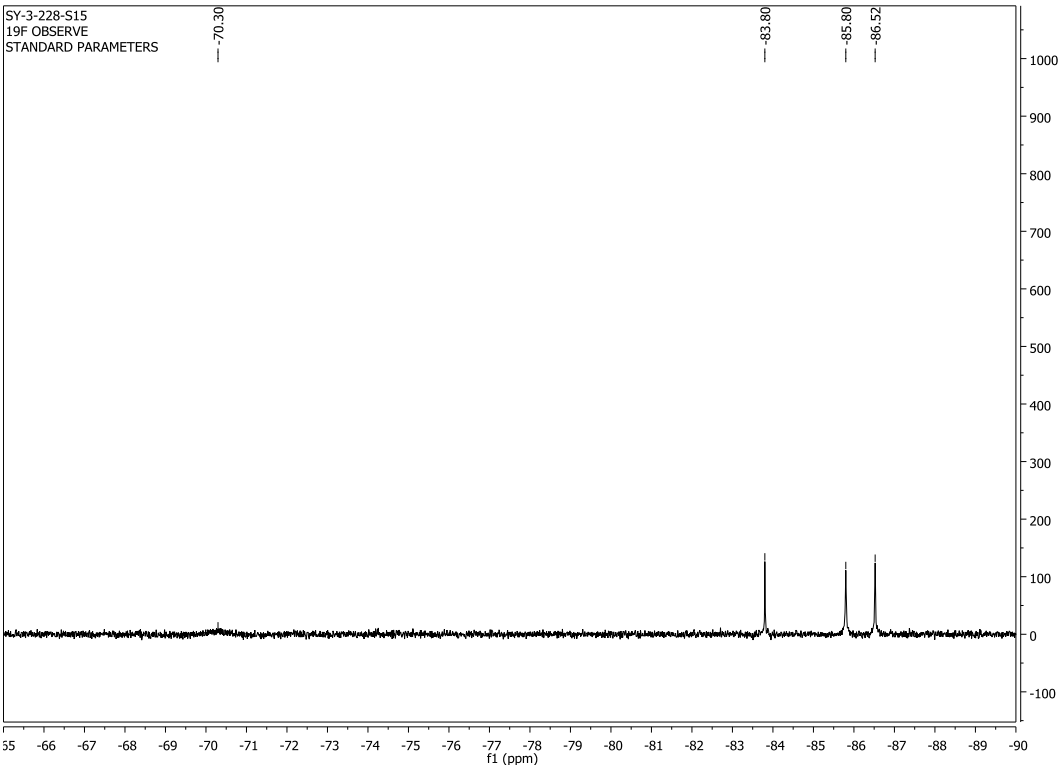

5.33 eq of **N12**

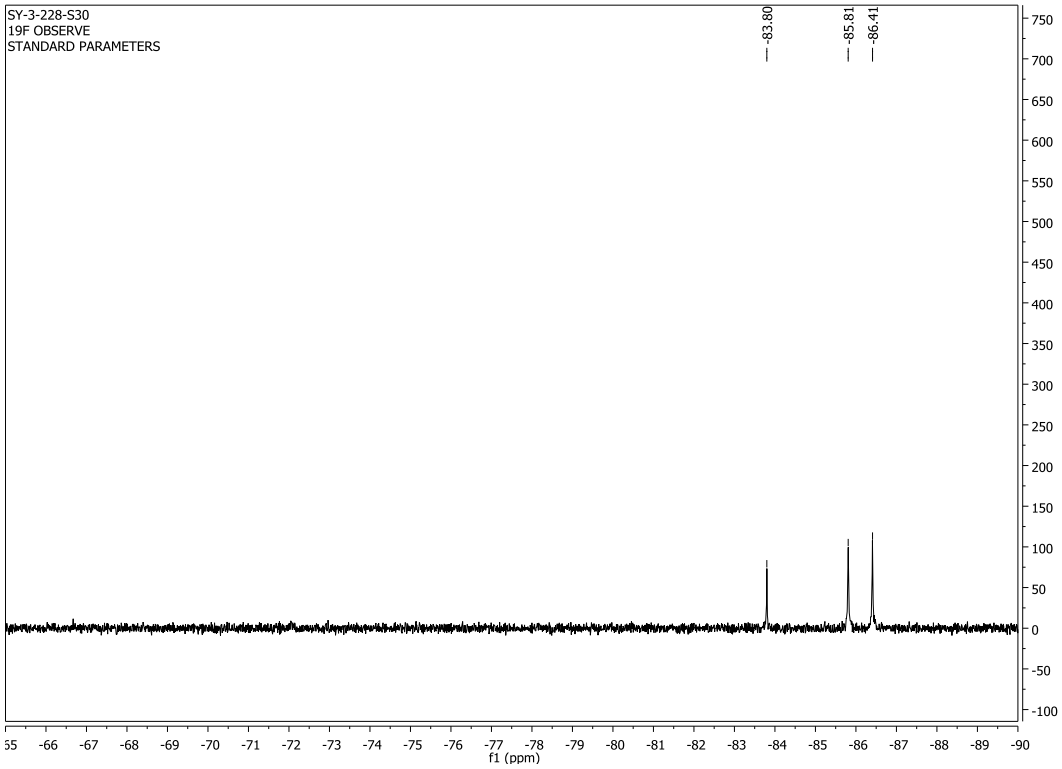

8.49 eq of **N12**

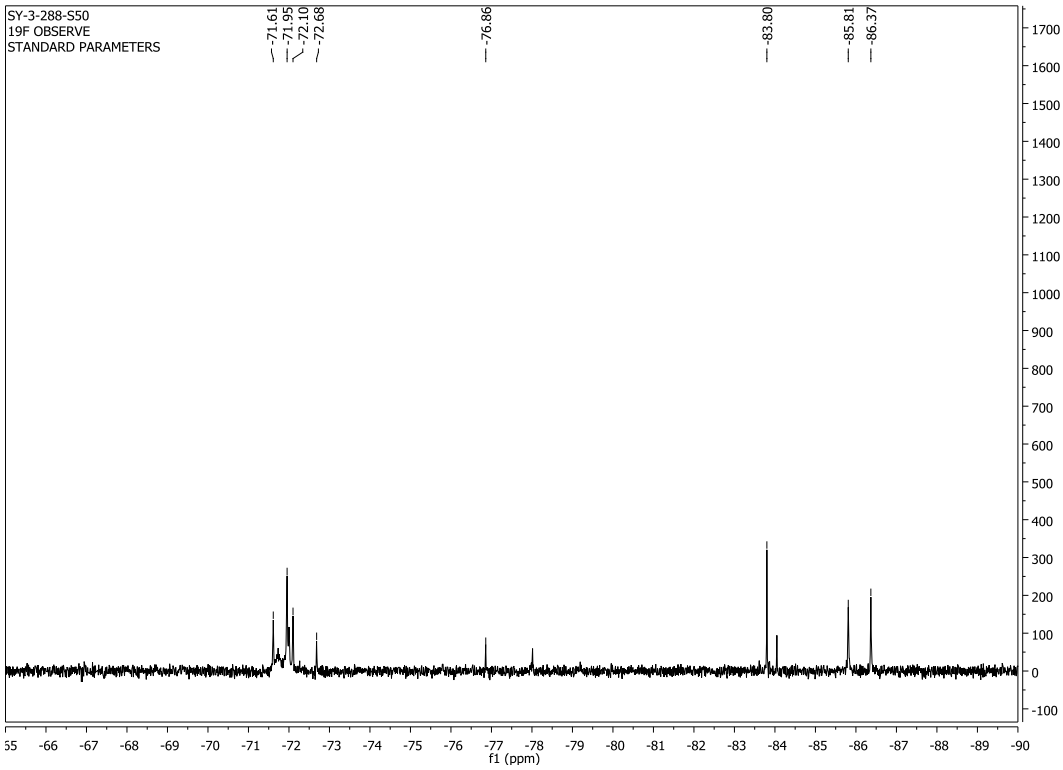

15.3 eq of **N12**

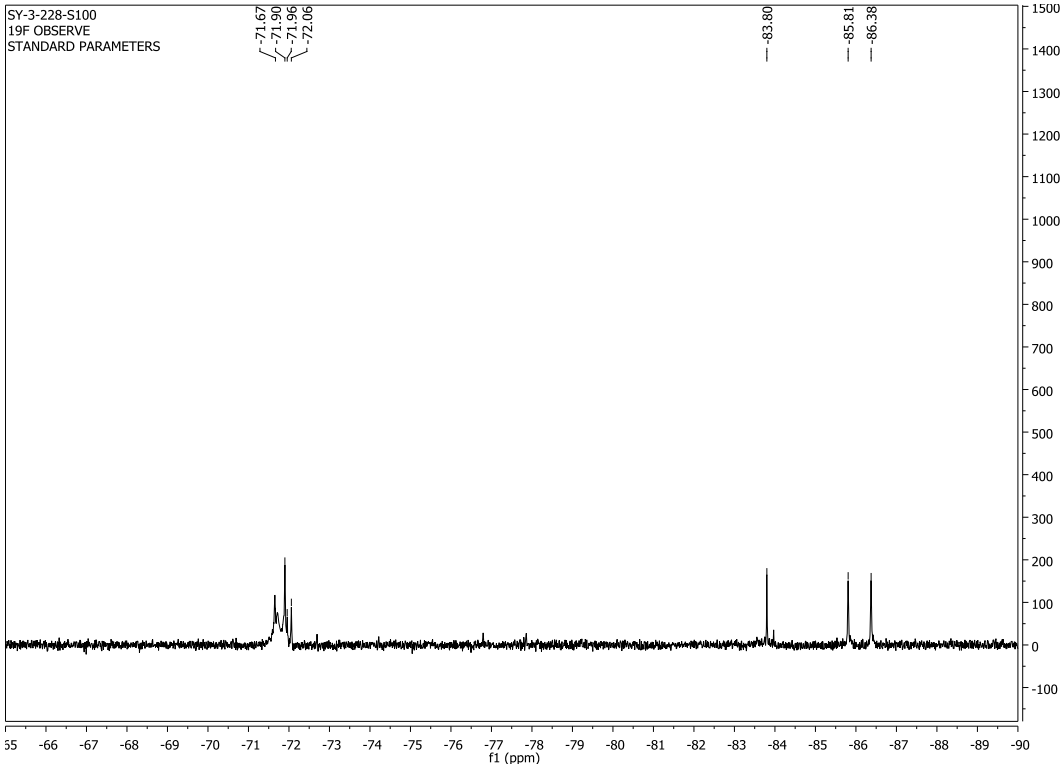

25.5 eq of **N12**

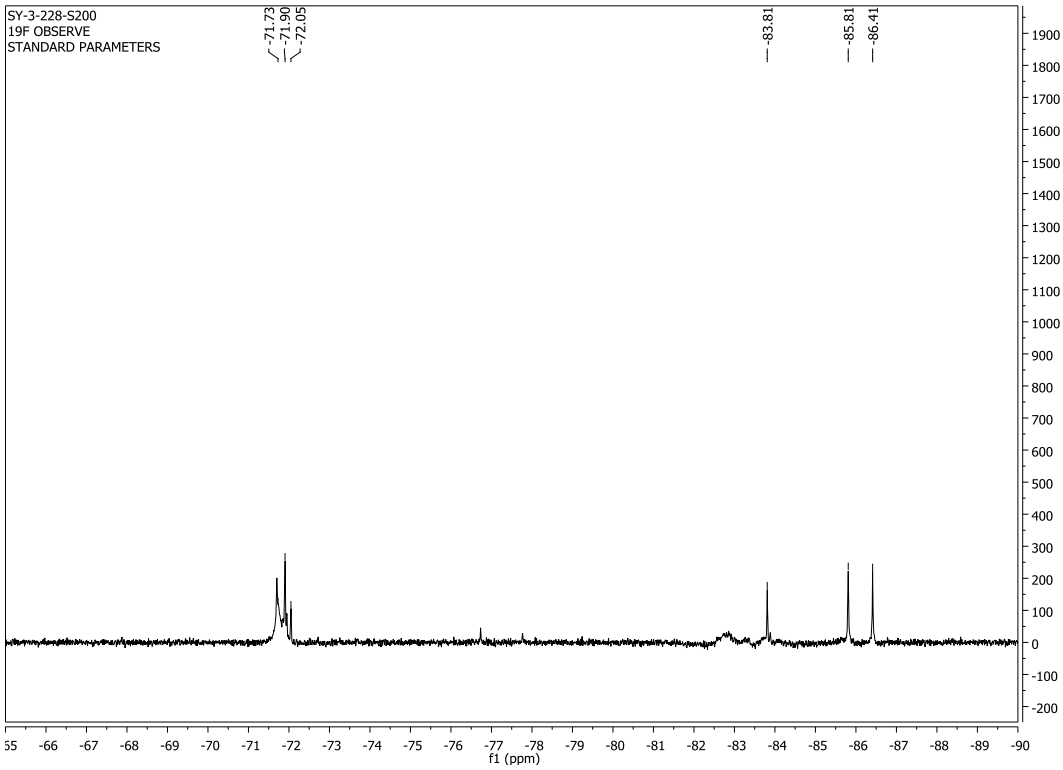

40 eq. of **N12**

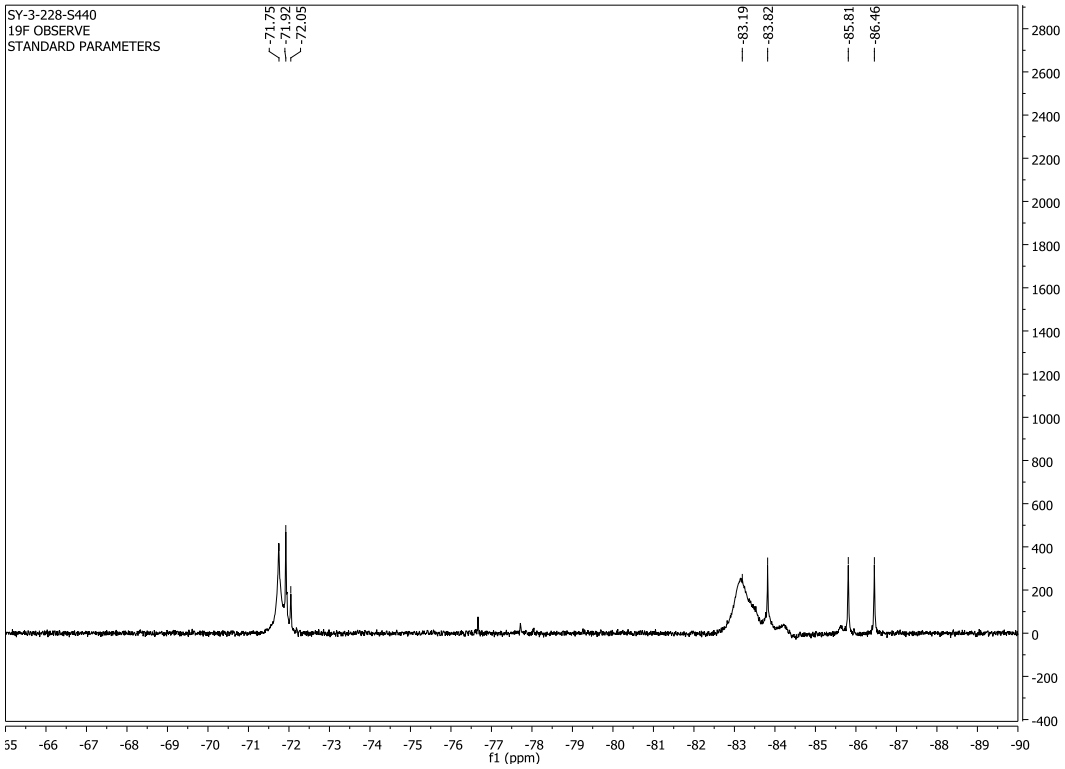
SY-3-228-S440
19F OBSERVE
STANDARD PARAMETERS
-71.75
-71.92
-72.05
-83.19
-83.82
-85.81
-86.46
f1 (ppm)

^{19}F NMR titration of (*S*)-6-4 with N5 in $(CD_3)_2SO$

0 eq of N5

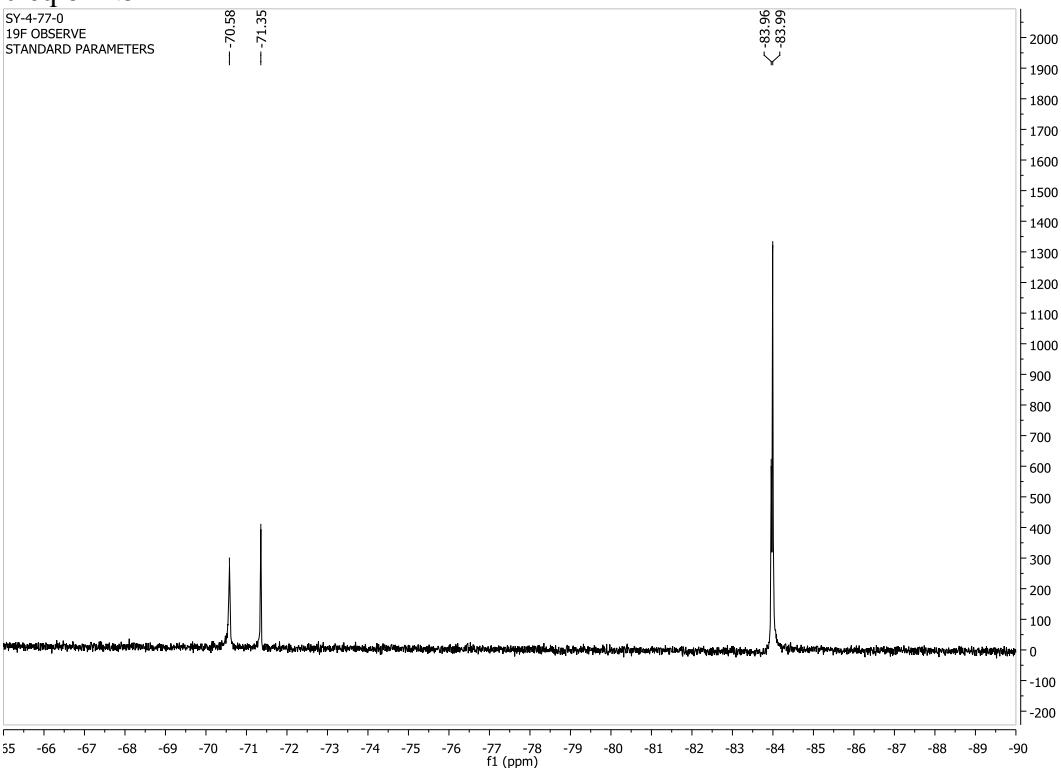

1.2 eq of N5

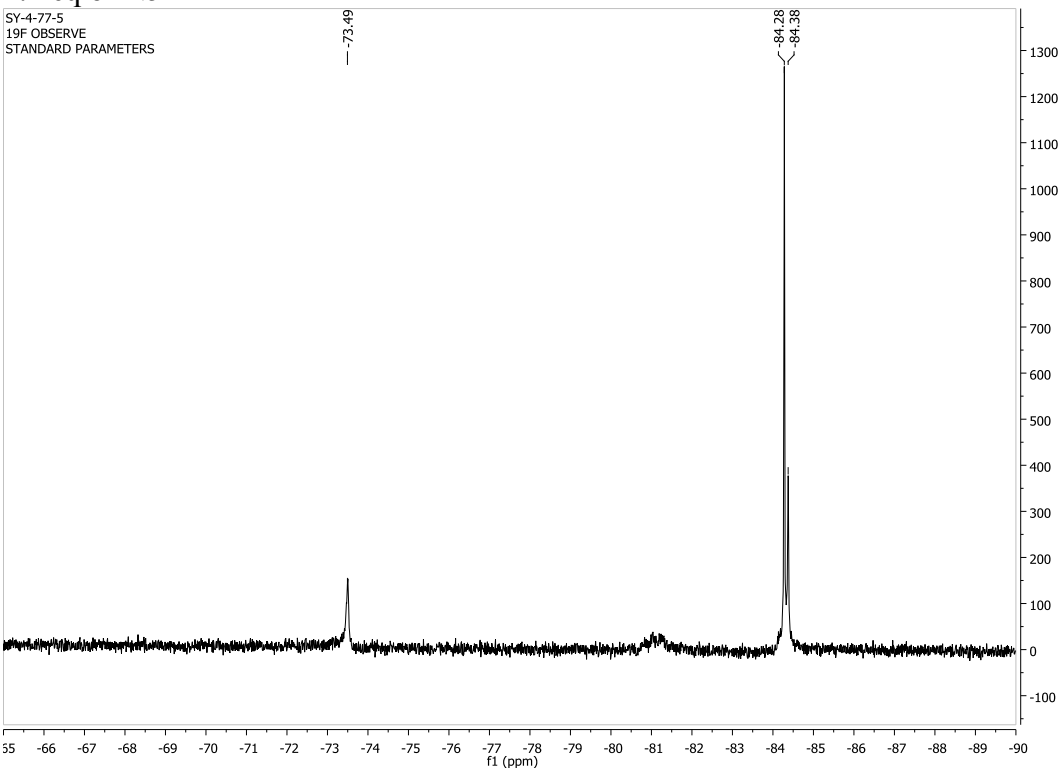

3.6 eq of N5

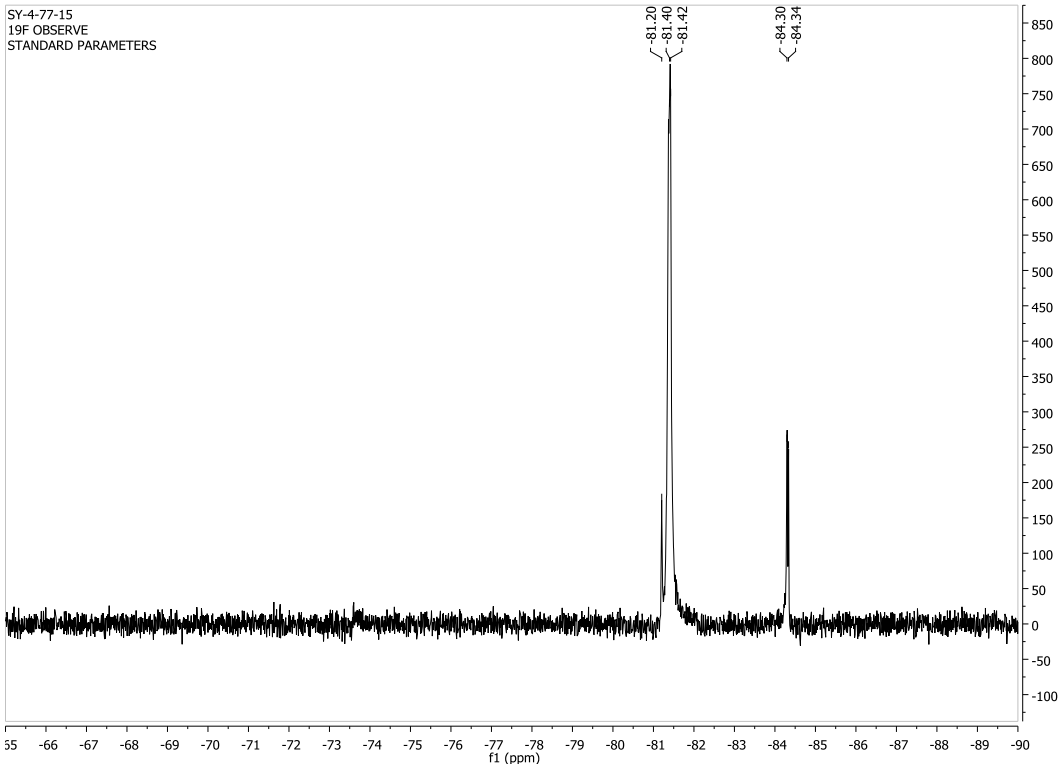

5.9 eq of N5

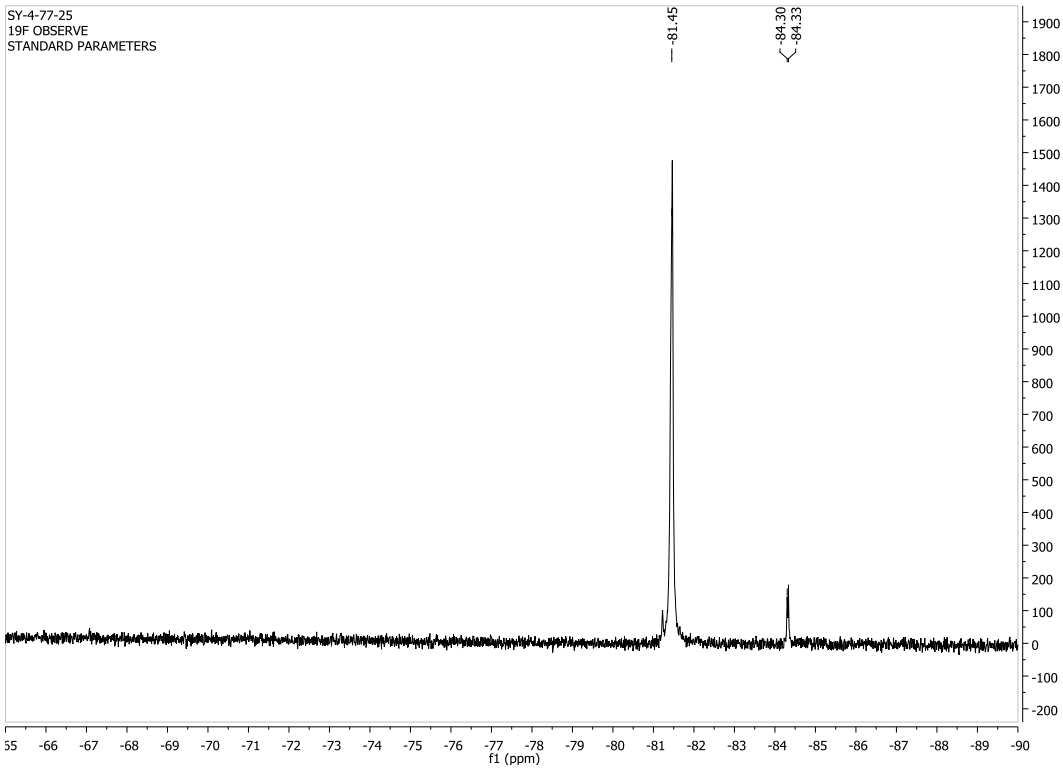

11.1 eq of N5

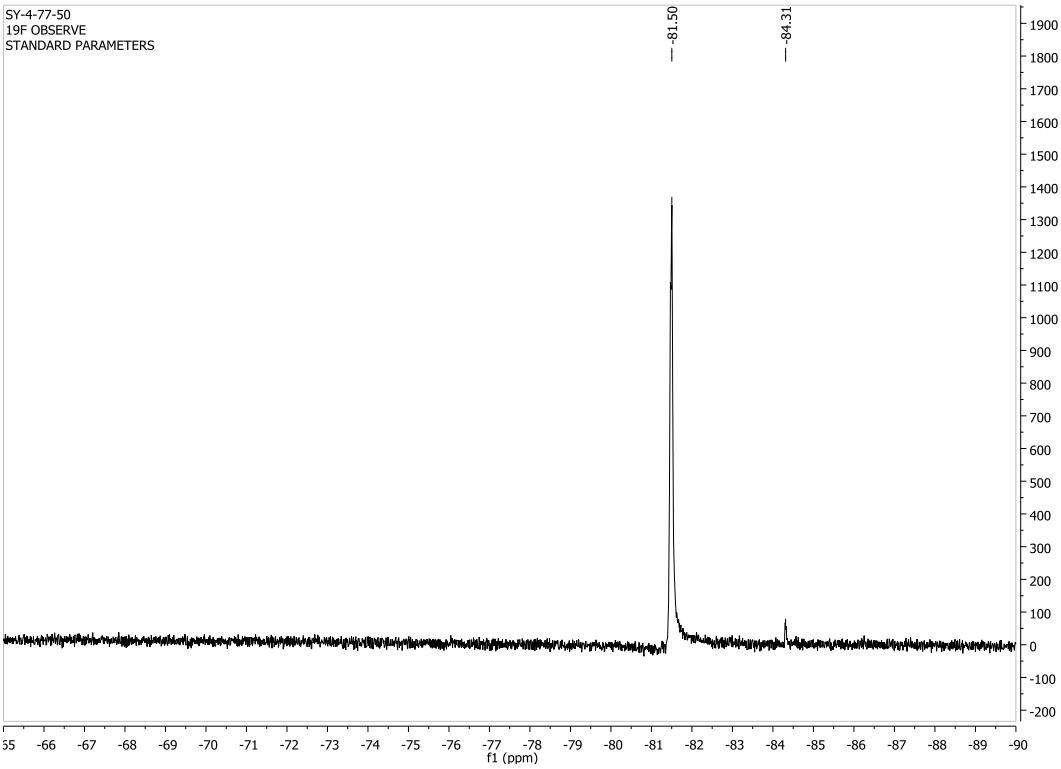

20 eq of N5

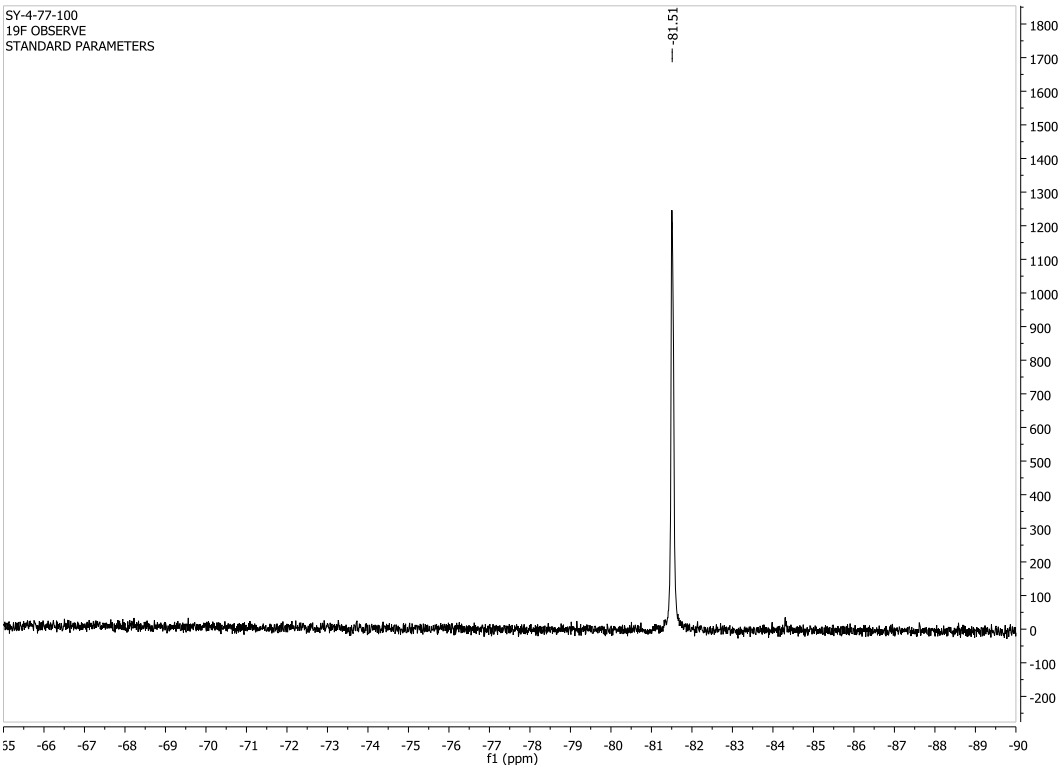

^{1}H NMR spectrum of (S)-**6-4** with 5 eq **N5** in $(CD_3)_2SO$

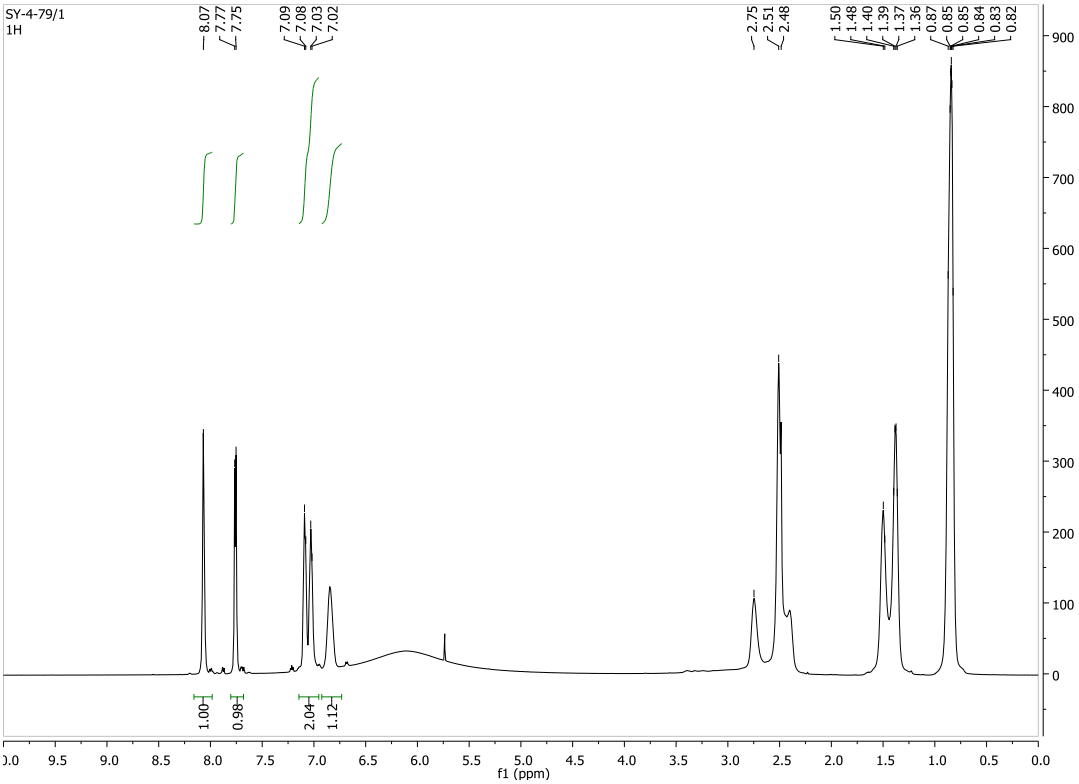

^{13}C NMR spectrum of (S)-**6-4** with 5 eq **N5** in $(CD_3)_2SO$

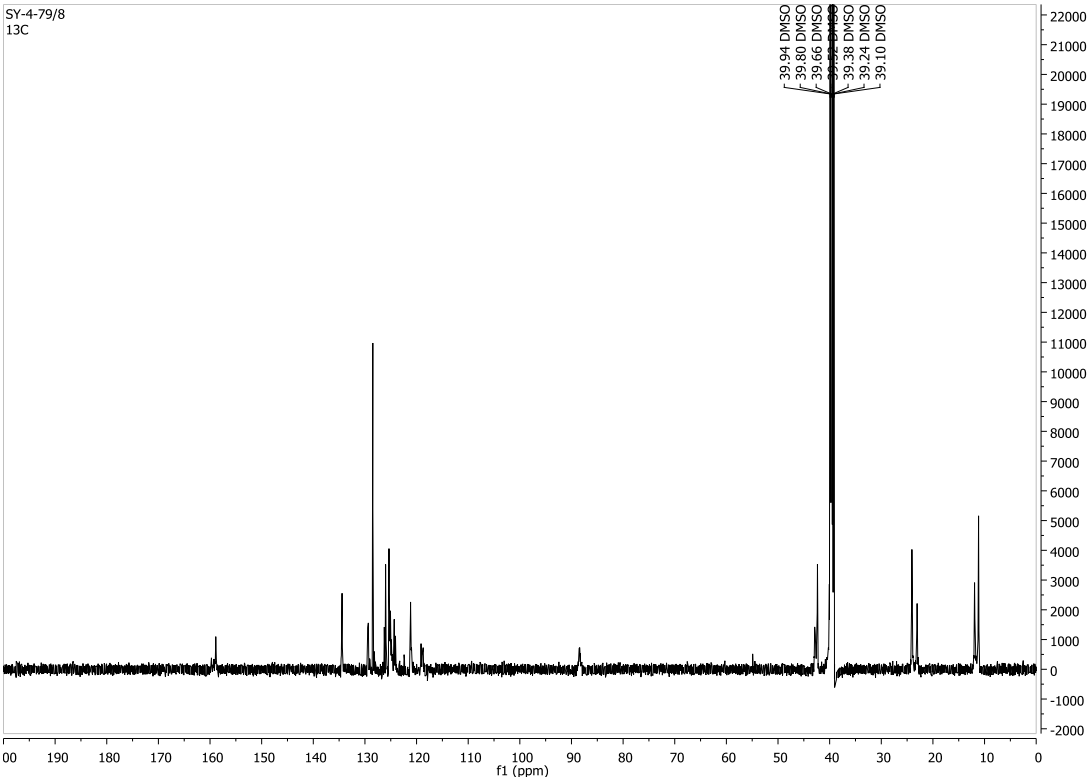

^{19}F NMR titration of (*S*)-6-16 with (*S, S*)-N15 in $CDCl_3$

0 eq of N15

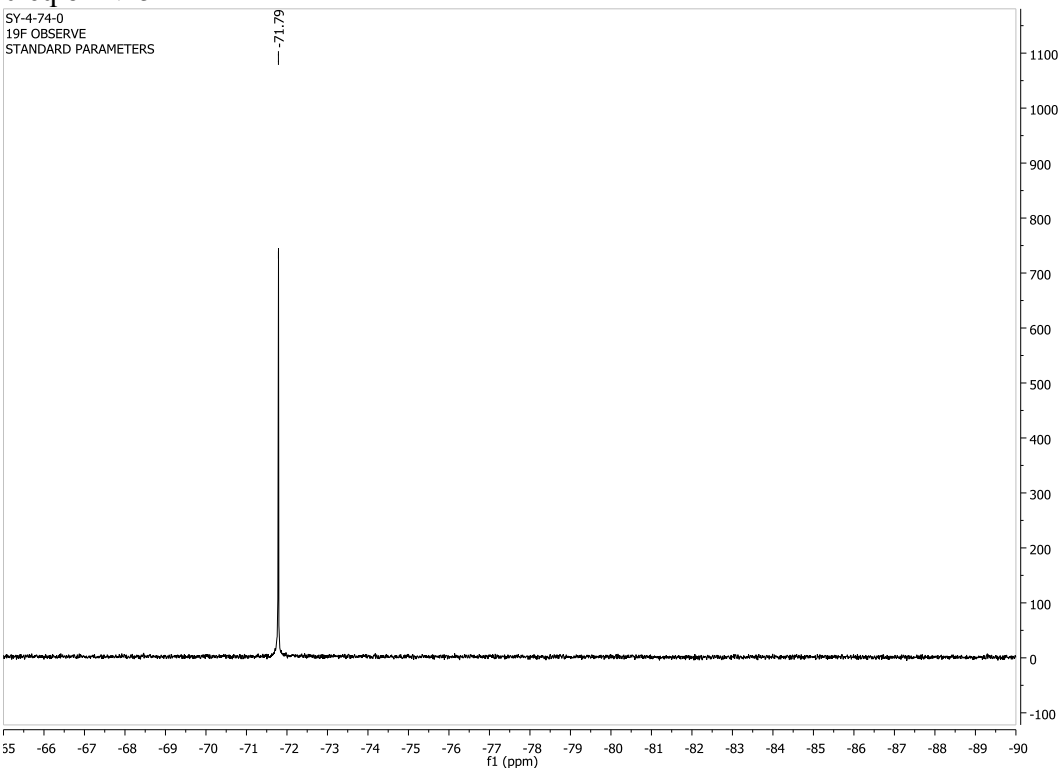

0.2 eq of N15

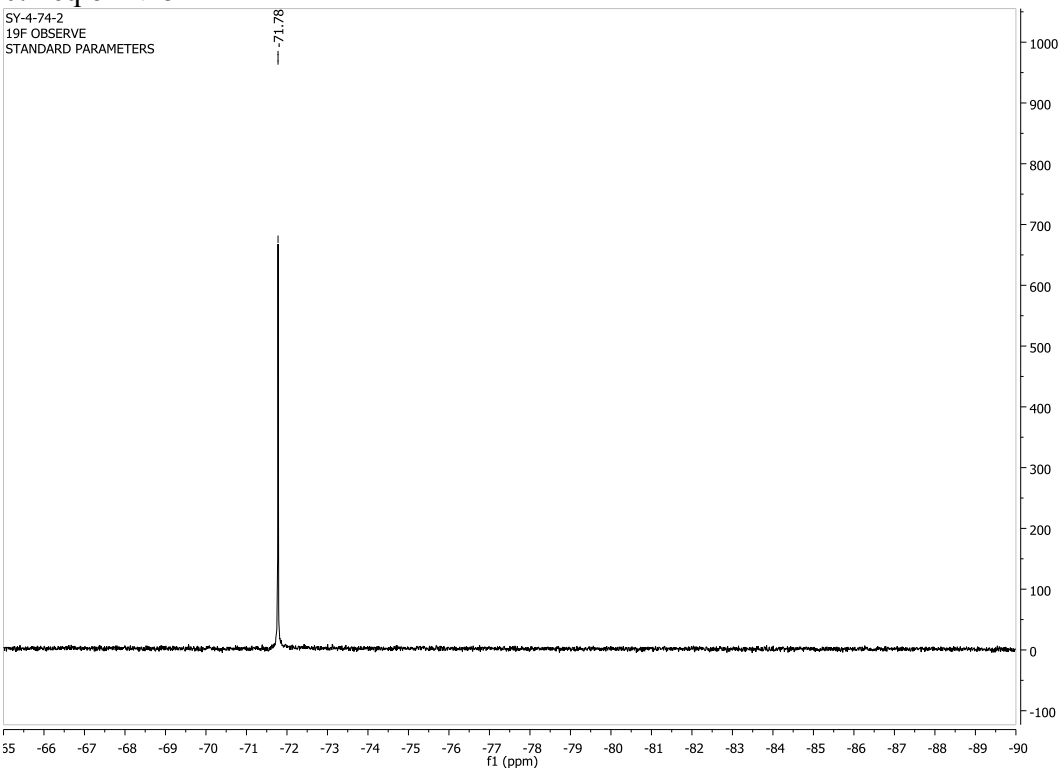

0.7 eq of N15

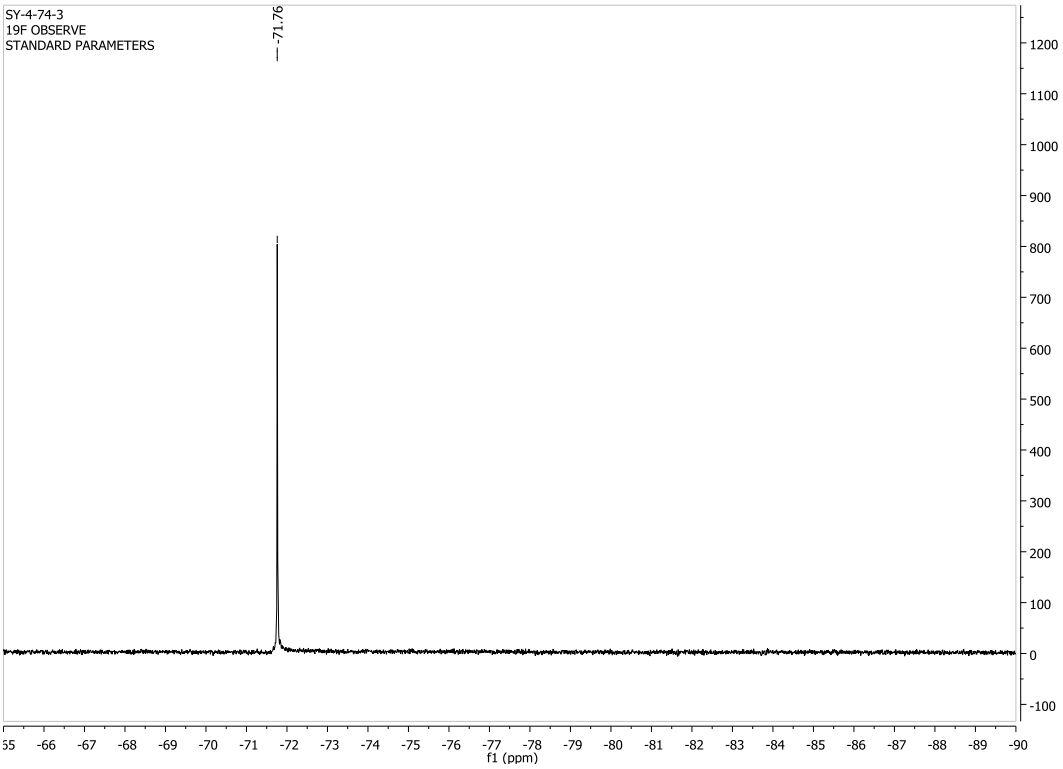

1.2 eq of N15

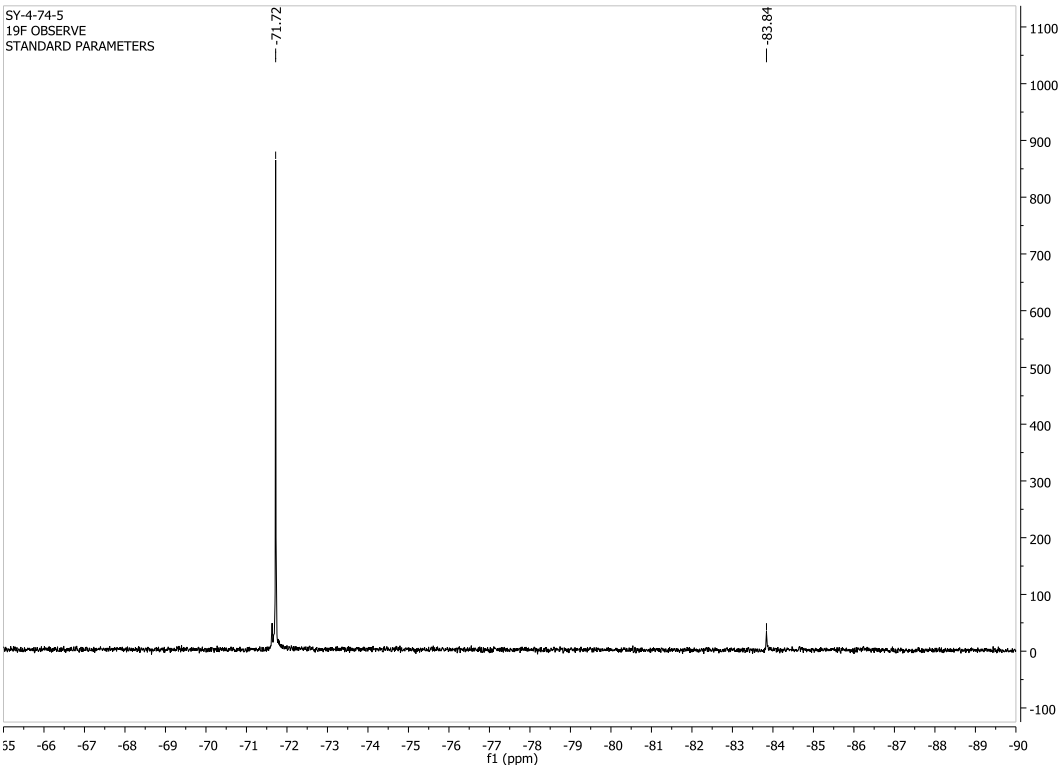

2.4 eq of N15

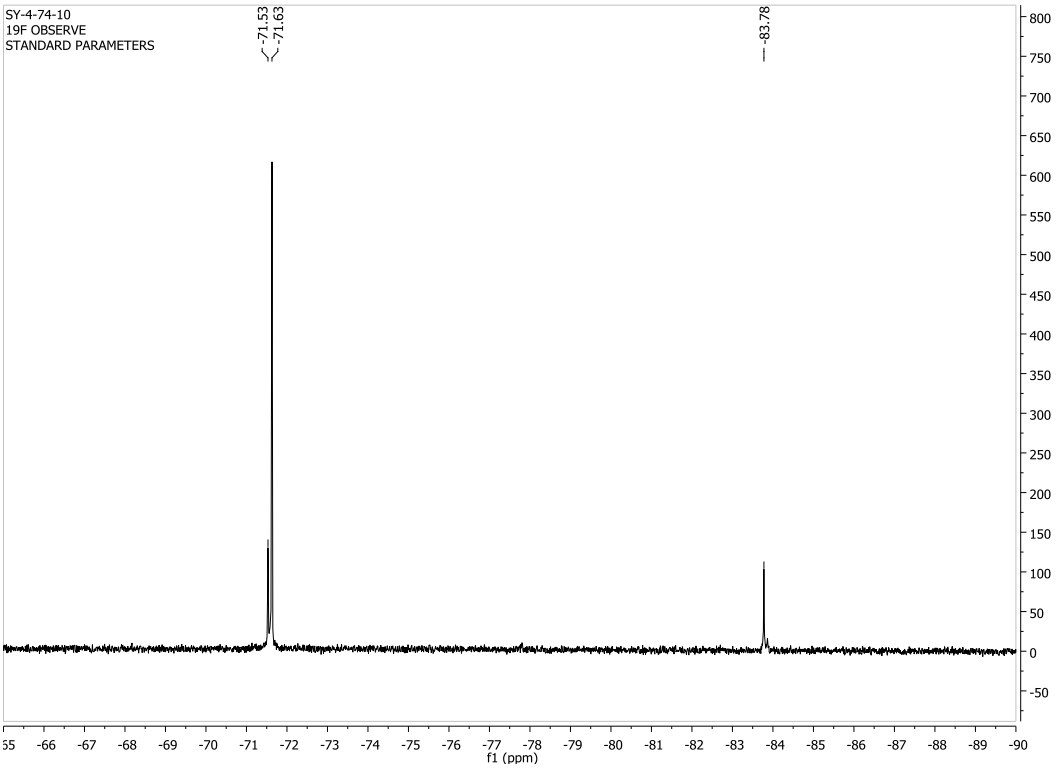

3.6 eq of N15

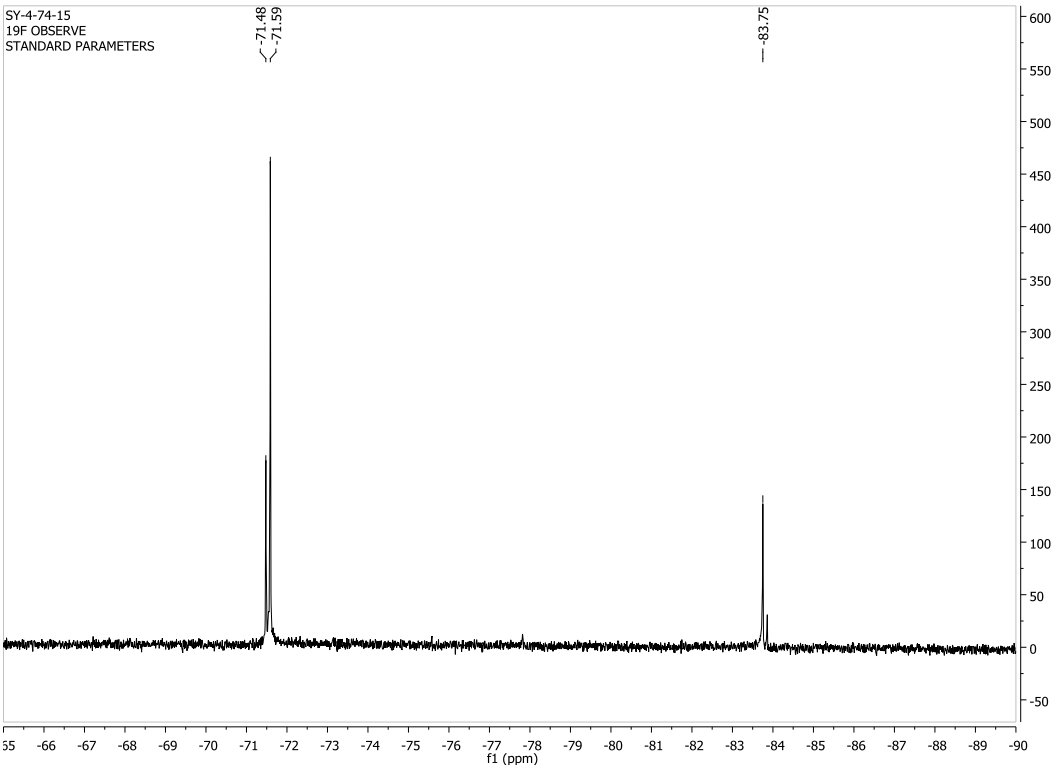

4.8 eq of N15

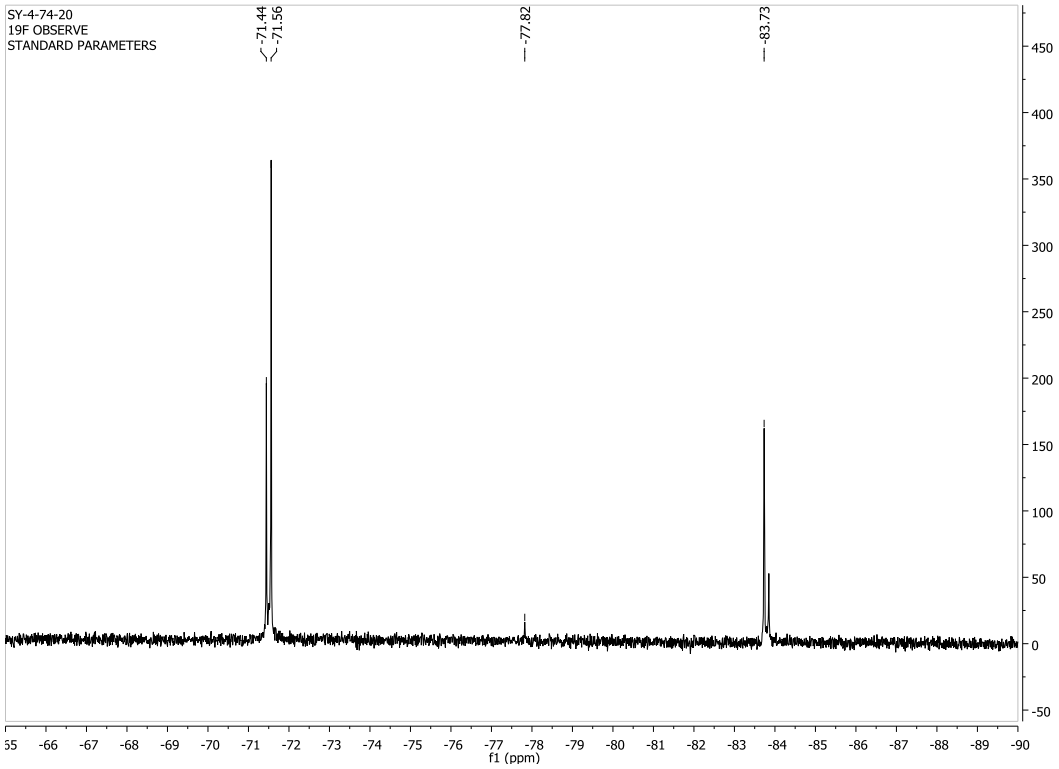

7.0 eq of N15

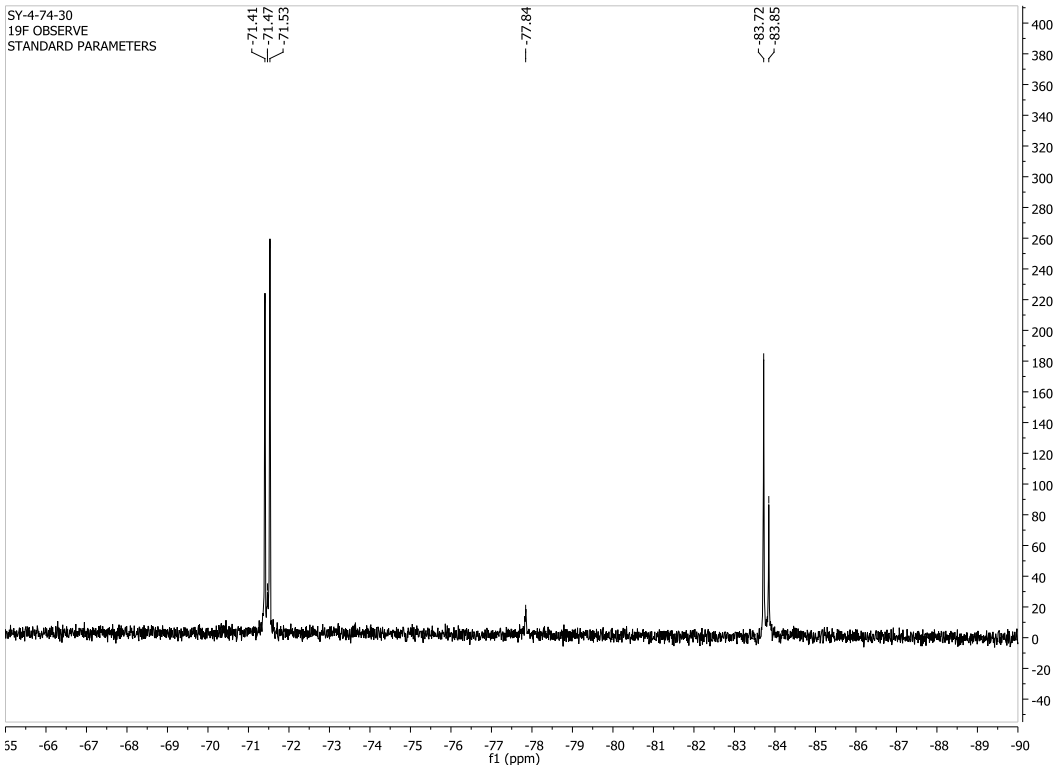

9.1 eq of N15

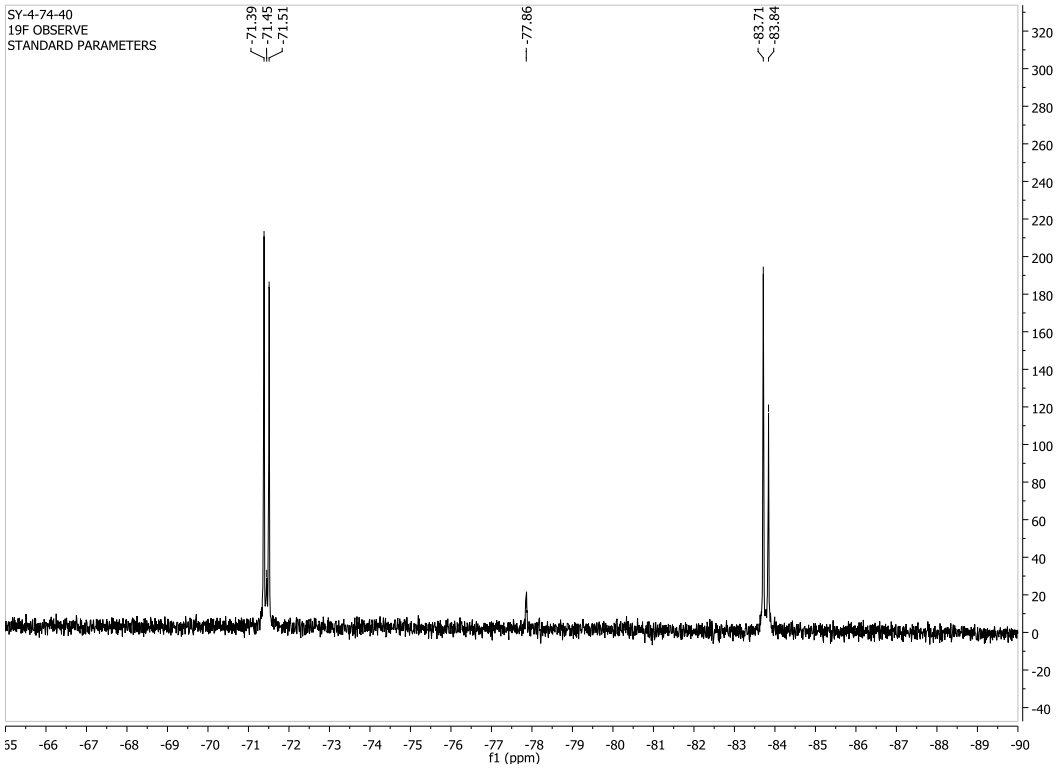

11.1 eq of N15

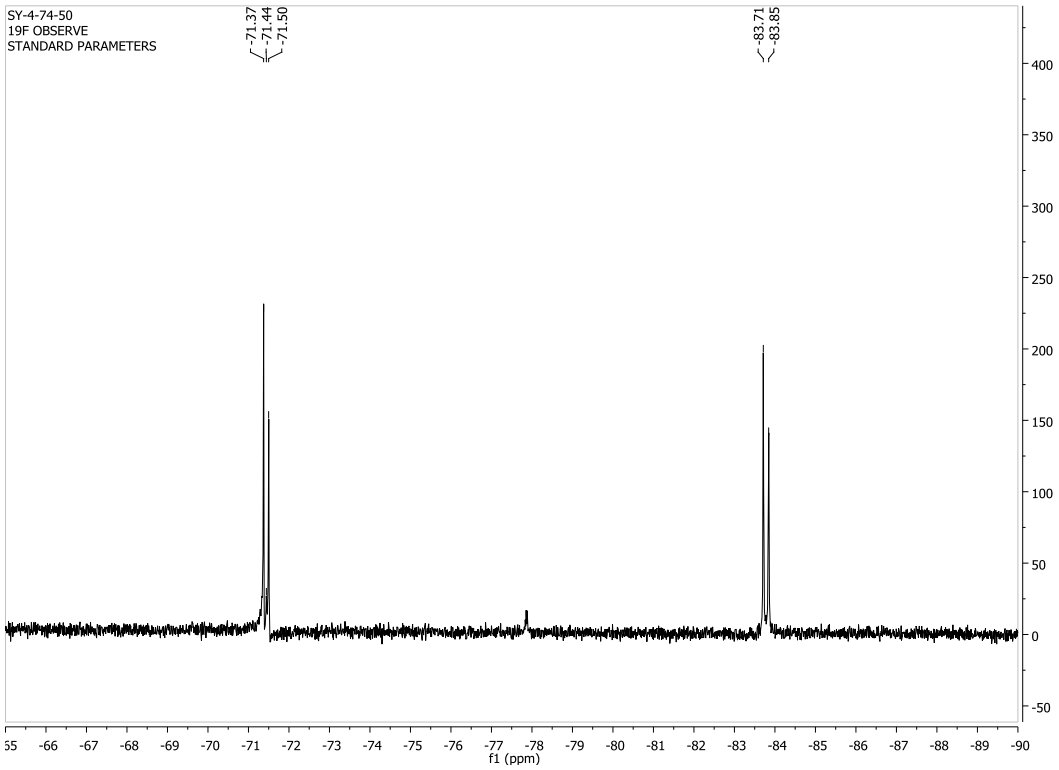

15.8 eq of N15

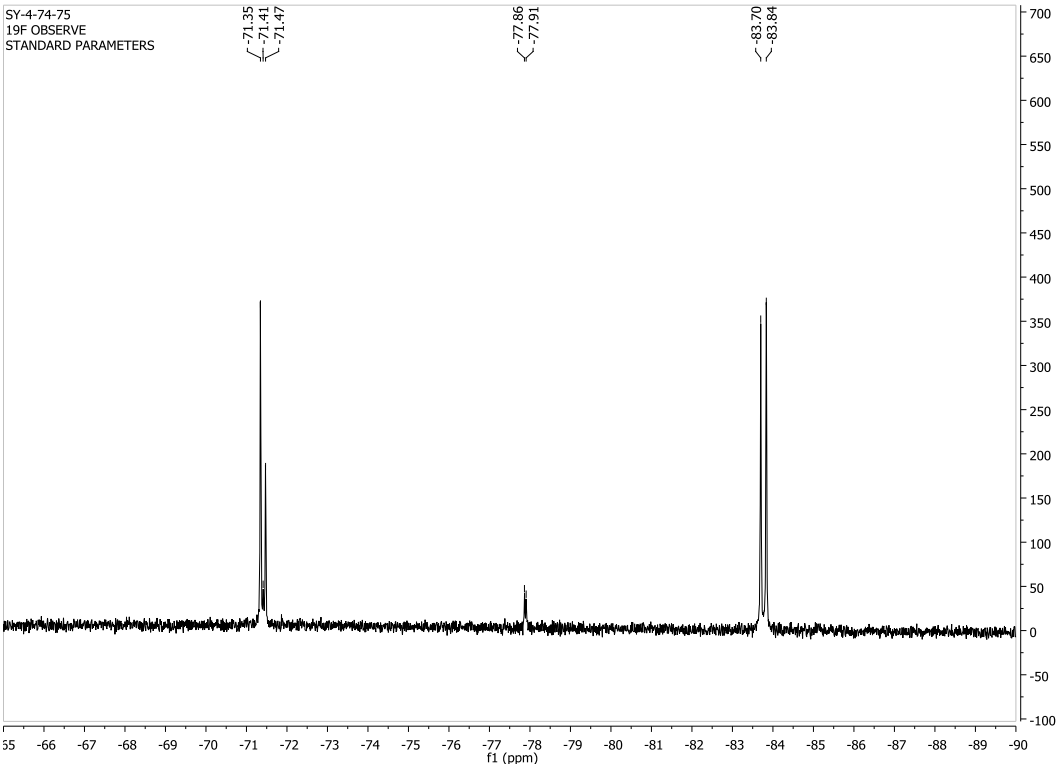

20 eq of N15

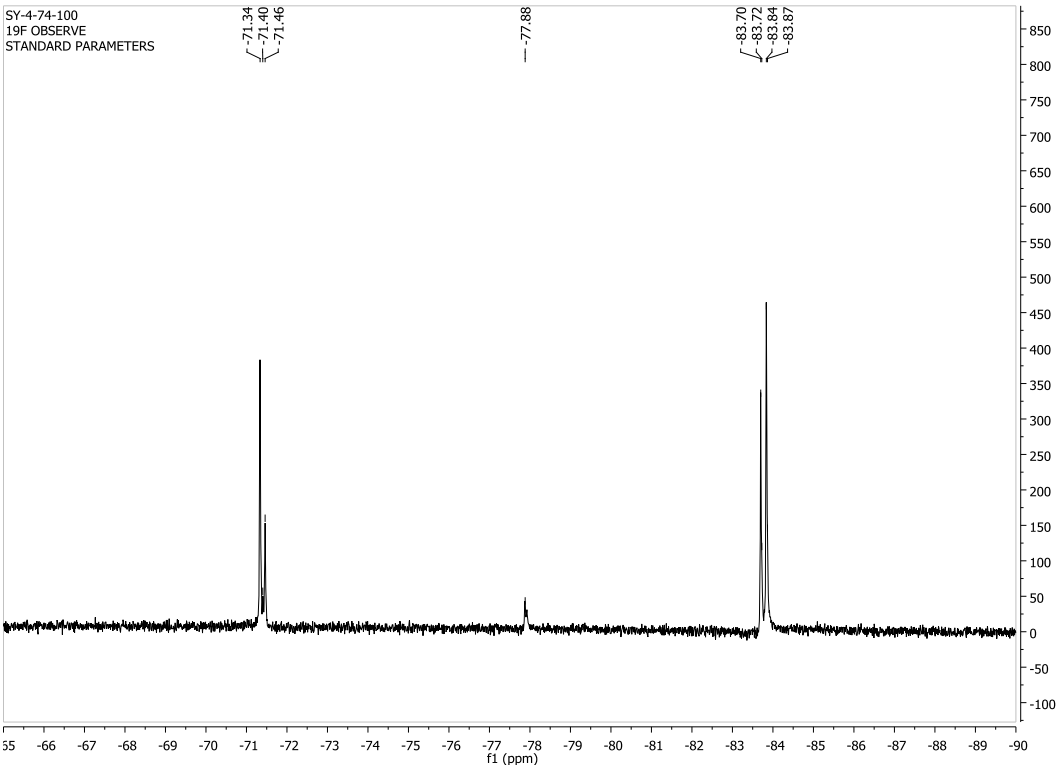

27.3 eq of N15

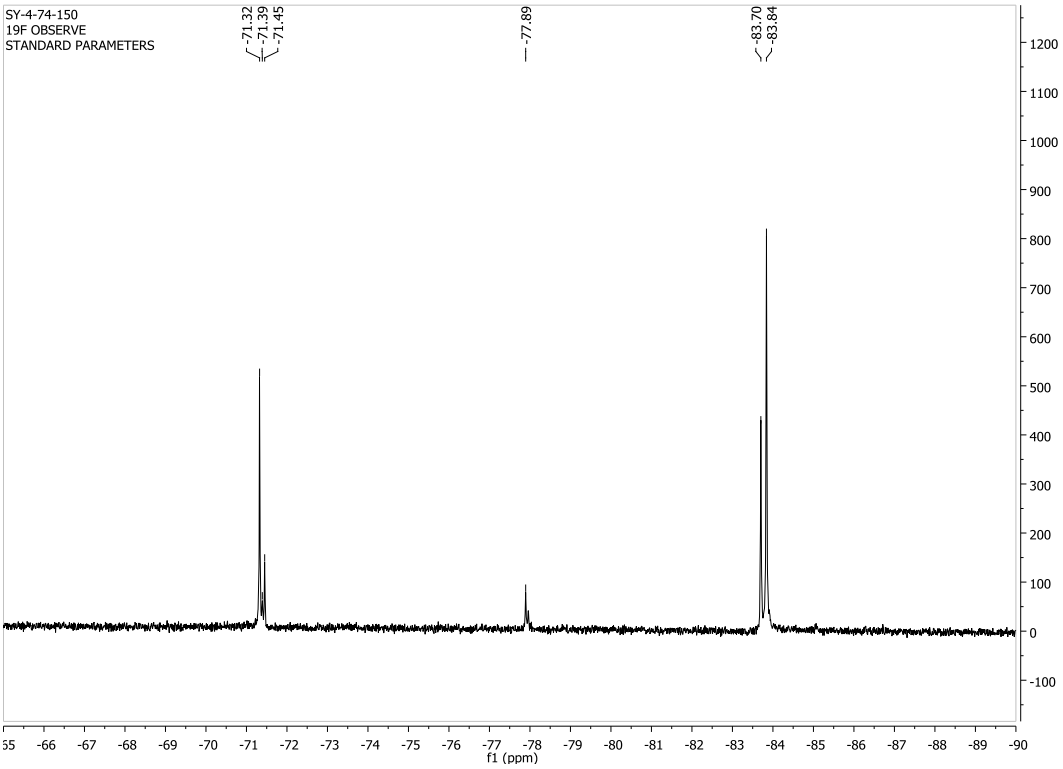

27.3 eq of N15

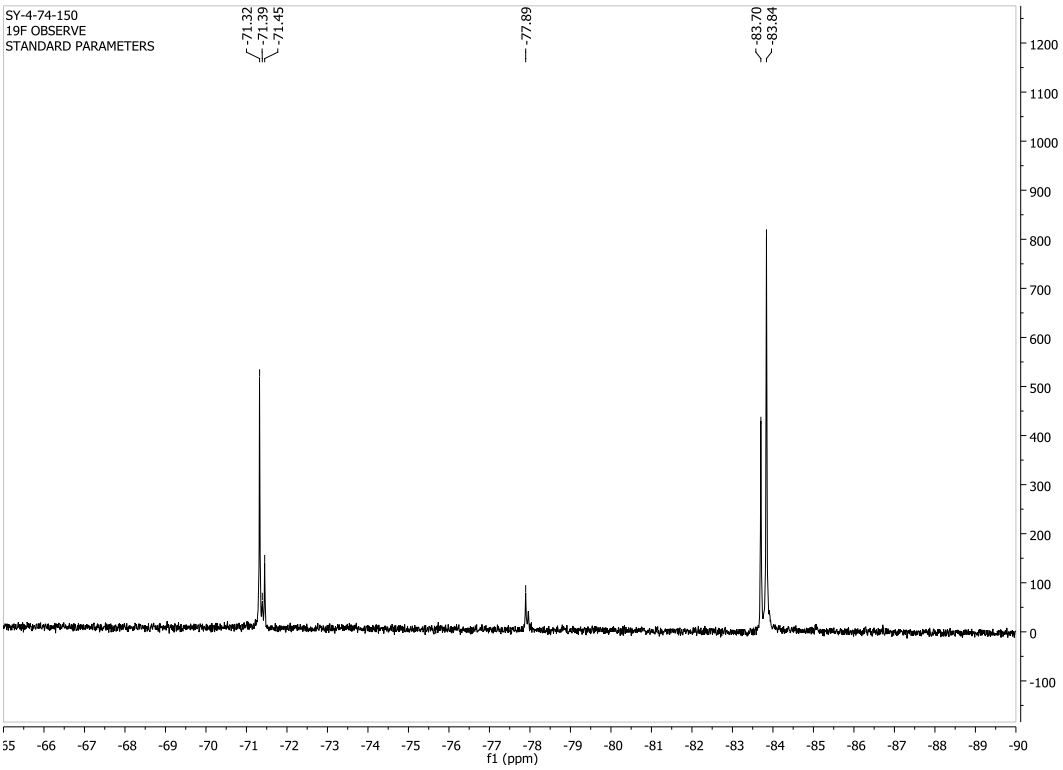

33.3 eq of N15

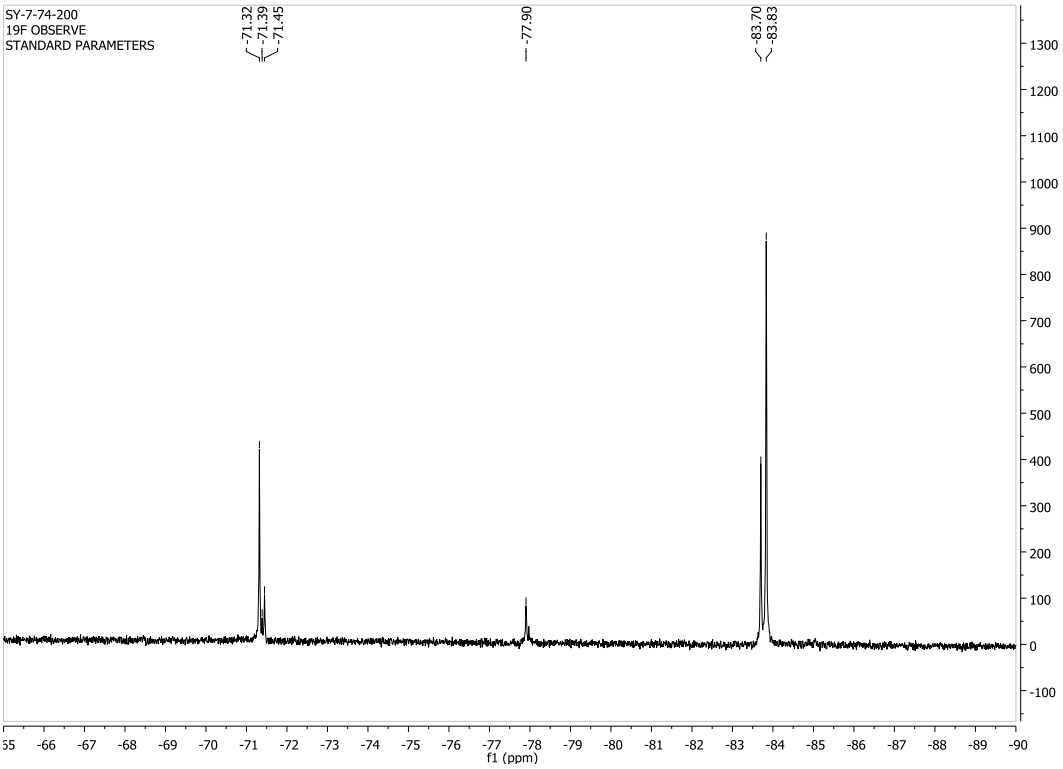

42.9 eq of N15

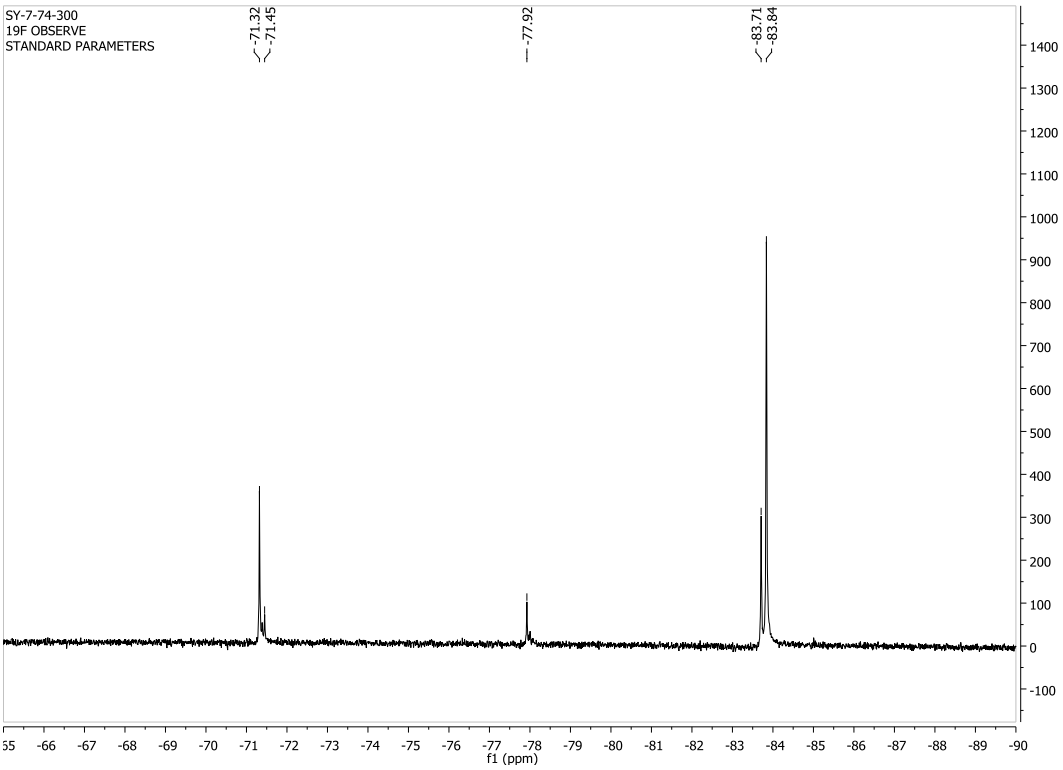

50 eq of N15

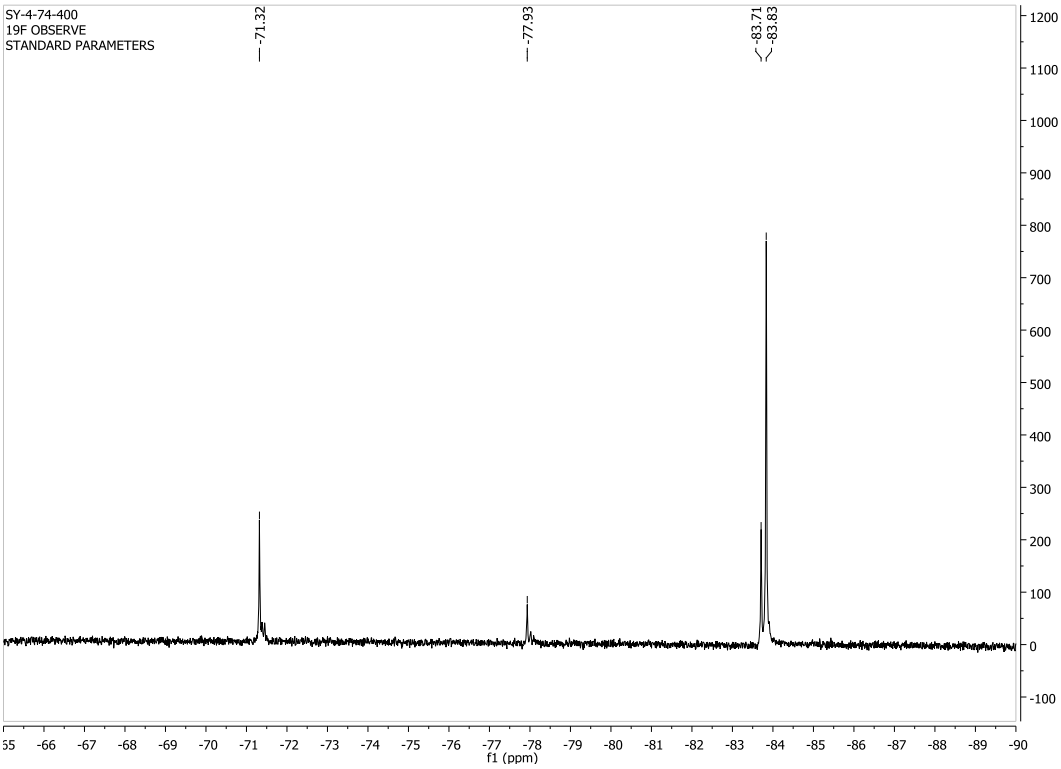

55.6 eq of N15

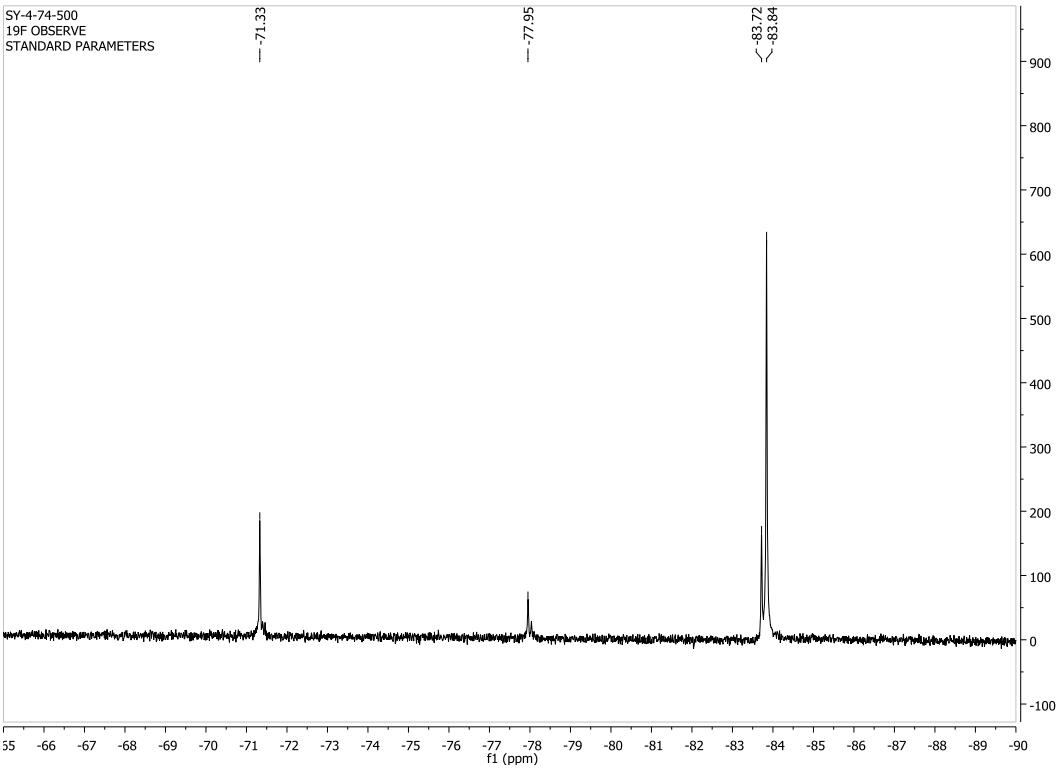

57.2 eq of N15

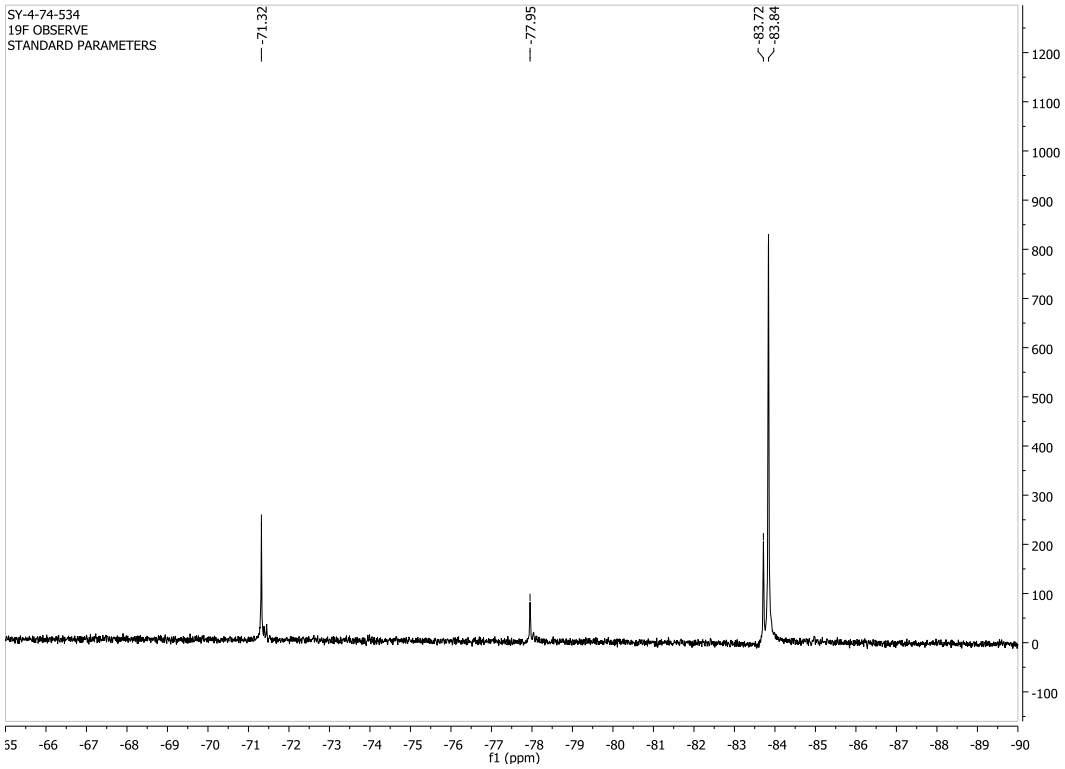
SY-4-74-534
19F OBSERVE
STANDARD PARAMETERS
-71.32
-77.95
-83.72
-83.84
1200
1100
1000
900
800
700
600
500
400
300
200
100
0
-100
55 -66 -67 -68 -69 -70 -71 -72 -73 -74 -75 -76 -77 -78 -79 -80 -81 -82 -83 -84 -85 -86 -87 -88 -89 -90
f1 (ppm)

Table A6-1. Crystal data and structure refinement for C28H24F6N4O2.

Empirical formula	C28 H24 F6 N4 O2
Formula weight	562.51
Temperature	153(2) K
Wavelength	0.71073 Å
Crystal system	Tetragonal
Space group	P4(3)
Unit cell dimensions	a = 10.532(3) Å
	b = 10.532(3) Å
	c = 44.888(12) Å
Volume	4979(2) $Å^3$
Z	8
Density (calculated)	1.501 Mg/m^3
Absorption coefficient	0.127 mm^{-1}
F(000)	2320
Crystal size	0.39 x 0.34 x 0.32 mm^3
Theta range for data collection	3.28 to 25.82 °.
Index ranges	-12<=h<=12, -12<=k<=12, -54<=l<=54
Reflections collected	47263
Independent reflections	9416 [R(int) = 0.0647]
Completeness to theta = 25.82 °	99.1 %
Absorption correction	Empirical
Max. and min. transmission	0.9605 and 0.9522
Refinement method	Full-matrix least-squares on F^2
Data / restraints / parameters	9416 / 1 / 726
Goodness-of-fit on F^2	1.184
Final R indices [I>2sigma(I)]	R1 = 0.0889, wR2 = 0.2121
R indices (all data)	R1 = 0.0910, wR2 = 0.2130
Extinction coefficient	0.0010(3)
Largest diff. peak and hole	0.433 and -0.471 $e.Å^{-3}$

Table A6-2. Atomic coordinates (x 10^4) and equivalent isotropic displacement parameters ($Å^2$x 10^3) for C28H24F6N4O2. U(eq) is defined as one third of the trace of the orthogonalized U^{ij} tensor.

	x	y	z	U(eq)
F(1)	411(4)	9671(4)	1111(1)	42(1)
F(2)	-532(4)	10144(5)	1519(1)	48(1)
F(3)	-147(5)	11596(5)	1195(1)	48(1)
F(4)	-1231(4)	4652(5)	3054(1)	47(1)
F(5)	700(5)	5158(5)	3170(1)	47(1)
F(6)	239(5)	4540(4)	2726(1)	47(1)
F(7)	10358(4)	6220(4)	1354(1)	48(1)
F(8)	10475(4)	4731(5)	1678(1)	49(1)
F(9)	9831(4)	4303(4)	1237(1)	45(1)
F(10)	4840(5)	5527(4)	2886(1)	48(1)
F(11)	3397(5)	5165(5)	3210(1)	50(1)
F(12)	5326(4)	4577(4)	3296(1)	43(1)
O(1)	1405(5)	10113(5)	2104(1)	34(1)
O(2)	294(5)	7004(5)	2230(1)	34(1)
O(3)	7992(5)	4694(5)	2178(1)	36(1)
O(4)	4877(5)	3592(6)	2305(1)	38(1)
N(1)	2486(6)	11333(6)	1247(1)	33(1)
N(2)	1438(6)	11829(6)	1691(1)	33(1)
N(3)	-991(6)	7274(7)	3109(1)	36(2)
N(4)	-1424(6)	6545(5)	2623(1)	28(1)
N(5)	3170(6)	3576(7)	2716(1)	39(2)
N(6)	3660(6)	2504(6)	3159(1)	35(1)
N(7)	8452(5)	6421(6)	1785(1)	28(1)
N(8)	7726(6)	5989(5)	1297(1)	32(1)
C(1)	2460(6)	8180(6)	2035(1)	23(1)
C(2)	1965(6)	9299(6)	1915(1)	25(1)

C(3)	2106(6)	9585(6)	1608(1)	25(1)
C(4)	2692(6)	8688(6)	1427(1)	22(1)
C(5)	3206(6)	7552(6)	1539(1)	23(1)
C(6)	3820(6)	6686(6)	1355(2)	25(1)
C(7)	4367(7)	5602(6)	1465(2)	28(1)
C(8)	4294(7)	5370(7)	1775(2)	31(2)
C(9)	3674(7)	6179(6)	1959(2)	28(1)
C(10)	3095(6)	7301(7)	1851(1)	23(1)
C(11)	1637(6)	10807(6)	1468(1)	26(1)
C(12)	2958(8)	12566(7)	1358(2)	38(2)
C(13)	2621(7)	12548(7)	1689(2)	38(2)
C(14)	329(6)	10552(7)	1324(2)	32(2)
C(15)	2222(6)	7965(6)	2358(1)	21(1)
C(16)	1105(6)	7369(6)	2446(1)	25(1)
C(17)	813(6)	7233(6)	2754(1)	20(1)
C(18)	1641(7)	7648(6)	2961(1)	24(1)
C(19)	2795(6)	8255(6)	2882(1)	22(1)
C(20)	3652(6)	8714(7)	3094(2)	27(1)
C(21)	4745(6)	9333(7)	3018(2)	30(2)
C(22)	5030(6)	9480(6)	2716(2)	26(1)
C(23)	4222(6)	9019(7)	2499(2)	28(1)
C(24)	3093(6)	8403(6)	2573(1)	21(1)
C(25)	-447(6)	6589(7)	2854(2)	26(1)
C(26)	-2360(7)	7443(8)	3043(2)	38(2)
C(27)	-2388(7)	7475(8)	2708(2)	37(2)
C(28)	-184(7)	5236(8)	2951(2)	38(2)
C(29)	7051(6)	2768(6)	2049(1)	21(1)
C(30)	7629(6)	3894(6)	1961(2)	23(1)
C(31)	7763(6)	4177(6)	1656(1)	20(1)
C(32)	7342(6)	3349(7)	1446(2)	28(1)
C(33)	6739(6)	2185(6)	1527(1)	19(1)
C(34)	6292(6)	1338(6)	1307(2)	25(1)
C(35)	5693(6)	258(7)	1390(2)	30(2)
C(36)	5549(7)	-36(6)	1692(2)	30(2)

C(37)	5974(7)	752(7)	1906(2)	29(2)
C(38)	6584(6)	1899(6)	1833(1)	21(1)
C(39)	8420(7)	5444(6)	1551(2)	26(1)
C(40)	7528(9)	7386(8)	1700(2)	42(2)
C(41)	7544(9)	7338(7)	1359(2)	39(2)
C(42)	9750(7)	5177(7)	1453(2)	32(2)
C(43)	6807(6)	2548(6)	2375(1)	24(1)
C(44)	5710(6)	3016(6)	2491(1)	23(1)
C(45)	5419(7)	2893(6)	2800(1)	25(1)
C(46)	6310(6)	2301(6)	2982(1)	23(1)
C(47)	7436(6)	1802(6)	2868(1)	22(1)
C(48)	8317(6)	1165(6)	3053(2)	26(1)
C(49)	9390(7)	613(6)	2936(2)	29(2)
C(50)	9622(7)	688(7)	2632(2)	32(2)
C(51)	8816(7)	1342(6)	2449(2)	26(1)
C(52)	7698(6)	1905(6)	2555(1)	22(1)
C(53)	4176(6)	3382(6)	2939(2)	23(1)
C(54)	2437(7)	2048(7)	3047(2)	39(2)
C(55)	2459(8)	2371(7)	2721(2)	38(2)
C(56)	4448(7)	4677(7)	3081(2)	32(2)

Table A6-3. Bond lengths [Å] and angles [°] for C28H24F6N4O2.

F(1)-C(14)	1.334(9)
F(2)-C(14)	1.333(9)
F(3)-C(14)	1.340(9)
F(4)-C(28)	1.344(9)
F(5)-C(28)	1.357(9)
F(6)-C(28)	1.324(10)
F(7)-C(42)	1.347(9)
F(8)-C(42)	1.350(9)
F(9)-C(42)	1.339(9)
F(10)-C(56)	1.319(9)
F(11)-C(56)	1.352(9)
F(12)-C(56)	1.341(9)
O(1)-C(2)	1.342(8)
O(2)-C(16)	1.351(8)
O(3)-C(30)	1.342(8)
O(4)-C(44)	1.356(8)
N(1)-C(11)	1.446(9)
N(1)-C(12)	1.477(10)
N(2)-C(13)	1.458(10)
N(2)-C(11)	1.483(9)
N(3)-C(25)	1.470(9)
N(3)-C(26)	1.483(9)
N(4)-C(27)	1.462(9)
N(4)-C(25)	1.463(9)
N(5)-C(55)	1.474(10)
N(5)-C(53)	1.472(9)
N(6)-C(53)	1.457(8)
N(6)-C(54)	1.465(10)
N(7)-C(40)	1.459(10)
N(7)-C(39)	1.472(9)
N(8)-C(39)	1.472(8)
N(8)-C(41)	1.461(9)

C(1)-C(2)	1.396(10)
C(1)-C(10)	1.409(9)
C(1)-C(15)	1.490(8)
C(2)-C(3)	1.416(9)
C(3)-C(4)	1.390(9)
C(3)-C(11)	1.516(9)
C(4)-C(5)	1.406(9)
C(5)-C(6)	1.392(9)
C(5)-C(10)	1.426(9)
C(6)-C(7)	1.371(9)
C(7)-C(8)	1.415(10)
C(8)-C(9)	1.354(10)
C(9)-C(10)	1.417(10)
C(11)-C(14)	1.545(9)
C(12)-C(13)	1.527(11)
C(15)-C(16)	1.392(9)
C(15)-C(24)	1.409(9)
C(16)-C(17)	1.419(9)
C(17)-C(18)	1.347(9)
C(17)-C(25)	1.556(9)
C(18)-C(19)	1.419(9)
C(19)-C(20)	1.400(9)
C(19)-C(24)	1.429(9)
C(20)-C(21)	1.366(9)
C(21)-C(22)	1.395(10)
C(22)-C(23)	1.384(9)
C(23)-C(24)	1.395(9)
C(25)-C(28)	1.515(11)
C(26)-C(27)	1.505(12)
C(29)-C(30)	1.391(9)
C(29)-C(38)	1.422(8)
C(29)-C(43)	1.503(8)
C(30)-C(31)	1.409(9)
C(31)-C(32)	1.358(10)

C(31)-C(39)	1.575(9)
C(32)-C(33)	1.428(9)
C(33)-C(34)	1.409(9)
C(33)-C(38)	1.418(9)
C(34)-C(35)	1.352(9)
C(35)-C(36)	1.399(10)
C(36)-C(37)	1.347(10)
C(37)-C(38)	1.407(9)
C(39)-C(42)	1.495(10)
C(40)-C(41)	1.531(11)
C(43)-C(44)	1.359(10)
C(43)-C(52)	1.410(9)
C(44)-C(45)	1.425(9)
C(45)-C(46)	1.390(9)
C(45)-C(53)	1.540(9)
C(46)-C(47)	1.394(9)
C(47)-C(48)	1.415(9)
C(47)-C(52)	1.436(8)
C(48)-C(49)	1.374(10)
C(49)-C(50)	1.390(10)
C(50)-C(51)	1.368(10)
C(51)-C(52)	1.403(10)
C(53)-C(56)	1.532(9)
C(54)-C(55)	1.502(12)

C(11)-N(1)-C(12)	108.3(6)
C(13)-N(2)-C(11)	104.6(6)
C(25)-N(3)-C(26)	106.4(6)
C(27)-N(4)-C(25)	106.3(6)
C(55)-N(5)-C(53)	103.7(6)
C(53)-N(6)-C(54)	107.7(6)
C(40)-N(7)-C(39)	106.5(6)
C(39)-N(8)-C(41)	107.3(6)
C(2)-C(1)-C(10)	120.4(6)

C(2)-C(1)-C(15)	116.1(6)
C(10)-C(1)-C(15)	123.4(6)
O(1)-C(2)-C(1)	117.4(6)
O(1)-C(2)-C(3)	121.7(6)
C(1)-C(2)-C(3)	120.9(6)
C(4)-C(3)-C(2)	118.1(6)
C(4)-C(3)-C(11)	118.6(6)
C(2)-C(3)-C(11)	123.3(6)
C(5)-C(4)-C(3)	122.7(6)
C(4)-C(5)-C(6)	121.6(6)
C(4)-C(5)-C(10)	118.4(6)
C(6)-C(5)-C(10)	120.0(6)
C(7)-C(6)-C(5)	121.6(6)
C(6)-C(7)-C(8)	118.5(6)
C(9)-C(8)-C(7)	121.1(6)
C(8)-C(9)-C(10)	121.5(6)
C(1)-C(10)-C(9)	123.4(6)
C(1)-C(10)-C(5)	119.4(6)
C(9)-C(10)-C(5)	117.2(6)
N(1)-C(11)-N(2)	105.8(6)
N(1)-C(11)-C(3)	114.1(5)
N(2)-C(11)-C(3)	112.5(5)
N(1)-C(11)-C(14)	109.3(6)
N(2)-C(11)-C(14)	106.4(5)
C(3)-C(11)-C(14)	108.5(6)
N(1)-C(12)-C(13)	103.8(6)
N(2)-C(13)-C(12)	102.2(6)
F(2)-C(14)-F(3)	107.1(6)
F(2)-C(14)-F(1)	106.9(6)
F(3)-C(14)-F(1)	106.6(6)
F(2)-C(14)-C(11)	112.7(6)
F(3)-C(14)-C(11)	111.8(6)
F(1)-C(14)-C(11)	111.3(6)
C(16)-C(15)-C(24)	120.2(6)

C(16)-C(15)-C(1)	119.3(6)
C(24)-C(15)-C(1)	120.5(6)
O(2)-C(16)-C(15)	117.2(6)
O(2)-C(16)-C(17)	122.3(6)
C(15)-C(16)-C(17)	120.4(6)
C(18)-C(17)-C(16)	119.8(6)
C(18)-C(17)-C(25)	119.5(6)
C(16)-C(17)-C(25)	120.7(6)
C(17)-C(18)-C(19)	121.9(6)
C(20)-C(19)-C(24)	118.8(6)
C(20)-C(19)-C(18)	122.5(6)
C(24)-C(19)-C(18)	118.7(6)
C(21)-C(20)-C(19)	122.5(6)
C(20)-C(21)-C(22)	118.5(6)
C(23)-C(22)-C(21)	120.9(6)
C(22)-C(23)-C(24)	121.3(6)
C(23)-C(24)-C(15)	122.9(6)
C(23)-C(24)-C(19)	118.0(6)
C(15)-C(24)-C(19)	119.0(6)
N(4)-C(25)-N(3)	107.1(6)
N(4)-C(25)-C(28)	107.5(5)
N(3)-C(25)-C(28)	108.0(6)
N(4)-C(25)-C(17)	114.1(5)
N(3)-C(25)-C(17)	110.2(5)
C(28)-C(25)-C(17)	109.7(6)
N(3)-C(26)-C(27)	102.8(6)
N(4)-C(27)-C(26)	103.5(6)
F(6)-C(28)-F(4)	106.6(6)
F(6)-C(28)-F(5)	106.7(6)
F(4)-C(28)-F(5)	106.7(7)
F(6)-C(28)-C(25)	111.4(7)
F(4)-C(28)-C(25)	112.2(6)
F(5)-C(28)-C(25)	112.9(6)
C(30)-C(29)-C(38)	120.4(6)

C(30)-C(29)-C(43)	118.9(5)
C(38)-C(29)-C(43)	120.4(6)
O(3)-C(30)-C(29)	117.0(6)
O(3)-C(30)-C(31)	122.9(6)
C(29)-C(30)-C(31)	120.1(6)
C(32)-C(31)-C(30)	120.4(6)
C(32)-C(31)-C(39)	118.7(6)
C(30)-C(31)-C(39)	120.9(5)
C(31)-C(32)-C(33)	121.4(6)
C(34)-C(33)-C(32)	121.0(6)
C(34)-C(33)-C(38)	120.4(6)
C(32)-C(33)-C(38)	118.7(5)
C(35)-C(34)-C(33)	119.7(6)
C(34)-C(35)-C(36)	120.2(6)
C(37)-C(36)-C(35)	121.3(7)
C(36)-C(37)-C(38)	120.9(6)
C(37)-C(38)-C(29)	123.4(6)
C(37)-C(38)-C(33)	117.5(6)
C(29)-C(38)-C(33)	119.1(5)
N(8)-C(39)-N(7)	107.0(5)
N(8)-C(39)-C(42)	108.0(6)
N(7)-C(39)-C(42)	108.7(6)
N(8)-C(39)-C(31)	110.1(5)
N(7)-C(39)-C(31)	112.9(5)
C(42)-C(39)-C(31)	109.9(6)
N(7)-C(40)-C(41)	103.5(6)
N(8)-C(41)-C(40)	103.0(6)
F(9)-C(42)-F(8)	105.4(6)
F(9)-C(42)-F(7)	107.0(6)
F(8)-C(42)-F(7)	105.2(6)
F(9)-C(42)-C(39)	113.7(6)
F(8)-C(42)-C(39)	112.0(6)
F(7)-C(42)-C(39)	112.9(6)
C(44)-C(43)-C(52)	121.4(6)

C(44)-C(43)-C(29)	117.5(6)
C(52)-C(43)-C(29)	121.1(6)
O(4)-C(44)-C(43)	118.4(6)
O(4)-C(44)-C(45)	120.1(6)
C(43)-C(44)-C(45)	121.5(6)
C(46)-C(45)-C(44)	117.7(6)
C(46)-C(45)-C(53)	119.0(6)
C(44)-C(45)-C(53)	123.2(6)
C(45)-C(46)-C(47)	122.0(6)
C(46)-C(47)-C(48)	121.5(6)
C(46)-C(47)-C(52)	119.5(6)
C(48)-C(47)-C(52)	119.0(6)
C(49)-C(48)-C(47)	121.0(6)
C(48)-C(49)-C(50)	119.7(7)
C(51)-C(50)-C(49)	120.7(7)
C(50)-C(51)-C(52)	121.9(6)
C(51)-C(52)-C(43)	124.5(6)
C(51)-C(52)-C(47)	117.5(6)
C(43)-C(52)-C(47)	117.9(6)
N(6)-C(53)-N(5)	106.2(5)
N(6)-C(53)-C(56)	110.7(6)
N(5)-C(53)-C(56)	107.1(6)
N(6)-C(53)-C(45)	112.3(5)
N(5)-C(53)-C(45)	112.5(5)
C(56)-C(53)-C(45)	107.9(5)
N(6)-C(54)-C(55)	104.3(6)
N(5)-C(55)-C(54)	102.5(6)
F(10)-C(56)-F(12)	108.4(6)
F(10)-C(56)-F(11)	106.4(6)
F(12)-C(56)-F(11)	106.6(6)
F(10)-C(56)-C(53)	112.8(6)
F(12)-C(56)-C(53)	111.0(6)
F(11)-C(56)-C(53)	111.3(6)

Table A6-4. Anisotropic displacement parameters ($Å^2 x\ 10^3$) for C28H24F6N4O2. The anisotropic displacement factor exponent takes the form: $-2\pi^2[\ h^2\ a^{*2}U^{11} + ...\ + 2\ h\ k\ a^*\ b^*\ U^{12}\ ]$

	U^{11}	U^{22}	U^{33}	U^{23}	U^{13}	U^{12}
F(1)	40(3)	46(3)	42(3)	-10(2)	-14(2)	5(2)
F(2)	32(2)	57(3)	55(3)	3(2)	1(2)	-7(2)
F(3)	45(3)	49(3)	48(3)	6(2)	-15(2)	12(2)
F(4)	33(2)	45(3)	64(3)	17(2)	3(2)	-12(2)
F(5)	42(3)	49(3)	49(3)	23(2)	-10(2)	0(2)
F(6)	48(3)	33(2)	61(3)	-6(2)	2(2)	1(2)
F(7)	42(3)	36(2)	68(3)	6(2)	16(2)	-14(2)
F(8)	32(2)	45(3)	69(4)	5(2)	-7(2)	7(2)
F(9)	42(3)	43(3)	48(3)	-12(2)	19(2)	-6(2)
F(10)	54(3)	35(2)	53(3)	-1(2)	6(2)	1(2)
F(11)	46(3)	47(3)	56(3)	-17(2)	8(2)	19(2)
F(12)	45(3)	45(3)	40(3)	-13(2)	-8(2)	6(2)
O(1)	42(3)	38(3)	22(2)	3(2)	8(2)	3(2)
O(2)	35(3)	50(3)	16(2)	-2(2)	-4(2)	-18(2)
O(3)	58(3)	32(3)	17(2)	-1(2)	-2(2)	-19(2)
O(4)	40(3)	52(3)	24(3)	10(2)	-2(2)	8(3)
N(1)	47(4)	33(3)	18(3)	6(2)	4(2)	1(3)
N(2)	48(4)	27(3)	25(3)	-3(2)	5(3)	5(3)
N(3)	27(3)	61(4)	21(3)	-11(3)	5(2)	5(3)
N(4)	34(3)	30(3)	21(3)	-4(2)	-2(2)	-8(3)
N(5)	36(4)	57(4)	23(3)	7(3)	-2(3)	8(3)
N(6)	43(4)	40(4)	21(3)	6(3)	6(3)	-3(3)
N(7)	34(3)	35(3)	15(3)	-1(2)	-2(2)	-4(3)
N(8)	52(4)	24(3)	20(3)	6(2)	-8(3)	-2(3)
C(1)	25(3)	26(3)	19(3)	-3(2)	1(2)	-11(3)
C(2)	31(3)	28(3)	15(3)	-4(2)	5(2)	-9(3)

C(3)	32(4)	18(3)	24(3)	4(2)	-1(3)	1(3)
C(4)	26(3)	20(3)	19(3)	2(2)	0(2)	-3(2)
C(5)	26(3)	27(3)	16(3)	-2(2)	5(2)	-7(3)
C(6)	27(3)	25(3)	24(3)	-1(3)	3(3)	-1(3)
C(7)	36(4)	18(3)	30(4)	1(3)	0(3)	-1(3)
C(8)	36(4)	25(4)	32(4)	12(3)	8(3)	11(3)
C(9)	35(4)	28(3)	22(3)	6(3)	3(3)	-9(3)
C(10)	15(3)	32(4)	23(3)	2(3)	0(2)	-4(2)
C(11)	25(3)	31(4)	21(3)	-3(3)	-4(2)	7(3)
C(12)	33(4)	37(4)	44(5)	10(3)	-7(3)	-7(3)
C(13)	37(4)	33(4)	44(5)	0(3)	-6(3)	0(3)
C(14)	22(3)	40(4)	34(4)	-1(3)	-4(3)	4(3)
C(15)	26(3)	12(3)	25(3)	-1(2)	-2(2)	3(2)
C(16)	28(3)	28(3)	18(3)	1(3)	-1(3)	2(3)
C(17)	23(3)	18(3)	20(3)	-1(2)	2(2)	0(2)
C(18)	35(4)	26(3)	13(3)	2(2)	2(3)	0(3)
C(19)	19(3)	24(3)	22(3)	0(3)	-2(2)	1(2)
C(20)	25(3)	35(4)	20(3)	3(3)	0(3)	-3(3)
C(21)	19(3)	36(4)	34(4)	-13(3)	-6(3)	-6(3)
C(22)	20(3)	23(3)	36(4)	4(3)	-6(3)	-11(3)
C(23)	25(3)	39(4)	20(3)	0(3)	1(3)	-5(3)
C(24)	23(3)	17(3)	24(3)	5(2)	2(2)	3(2)
C(25)	28(3)	35(4)	17(3)	0(3)	3(3)	-10(3)
C(26)	30(4)	37(4)	48(5)	-7(4)	7(3)	8(3)
C(27)	23(4)	38(4)	49(5)	-11(4)	-9(3)	11(3)
C(28)	26(4)	49(5)	37(4)	3(4)	-6(3)	-3(3)
C(29)	27(3)	26(3)	11(3)	-2(2)	-2(2)	-1(3)
C(30)	20(3)	26(3)	22(3)	0(3)	1(2)	1(2)
C(31)	17(3)	25(3)	19(3)	4(2)	-1(2)	0(2)
C(32)	30(4)	32(4)	21(3)	7(3)	4(3)	3(3)
C(33)	20(3)	16(3)	20(3)	-1(2)	-1(2)	-1(2)
C(34)	32(3)	23(3)	21(3)	2(3)	1(3)	-3(3)
C(35)	24(3)	32(4)	33(4)	-2(3)	-6(3)	-6(3)
C(36)	34(4)	22(3)	33(4)	-2(3)	-9(3)	-6(3)

C(37)	32(4)	35(4)	20(3)	4(3)	-1(3)	-11(3)
C(38)	27(3)	15(3)	22(3)	2(2)	2(3)	-8(2)
C(39)	33(4)	26(3)	18(3)	4(3)	-2(3)	-7(3)
C(40)	55(5)	39(4)	33(4)	-3(3)	-1(4)	12(4)
C(41)	64(5)	24(4)	29(4)	6(3)	-3(4)	-3(3)
C(42)	21(3)	33(4)	41(4)	-2(3)	2(3)	1(3)
C(43)	30(3)	27(3)	17(3)	-2(2)	0(3)	-14(3)
C(44)	27(3)	18(3)	24(3)	2(2)	0(3)	-2(3)
C(45)	36(4)	27(3)	13(3)	-4(2)	2(3)	0(3)
C(46)	29(3)	27(3)	14(3)	3(2)	0(2)	0(3)
C(47)	22(3)	25(3)	18(3)	3(2)	3(2)	0(2)
C(48)	24(3)	28(3)	24(3)	7(3)	-4(3)	0(3)
C(49)	32(4)	27(4)	29(4)	6(3)	-3(3)	-8(3)
C(50)	28(4)	39(4)	30(4)	0(3)	9(3)	3(3)
C(51)	35(4)	23(3)	22(3)	-2(3)	1(3)	-14(3)
C(52)	25(3)	23(3)	18(3)	-2(2)	-1(2)	-6(3)
C(53)	19(3)	22(3)	29(3)	0(3)	0(3)	-1(2)
C(54)	34(4)	23(4)	60(5)	-8(3)	17(4)	-4(3)
C(55)	36(4)	33(4)	46(5)	-10(3)	-7(3)	-7(3)
C(56)	39(4)	28(4)	29(4)	-4(3)	3(3)	-1(3)

Table A6-5. Hydrogen coordinates (x 10^4) and isotropic displacement parameters ($Å^2$x 10^3)
for C28H24F6N4O2.

	x	y	z	U(eq)
H(1O)	1136	10745	2009	51
H(2O)	-362	6691	2307	50
H(3O)	8435	5278	2104	54
H(4O)	4134	3375	2349	58
H(1N)	2688	10978	1076	39
H(2N)	757	11969	1800	40
H(3N)	-584	7532	3270	43
H(4N)	-1431	6055	2464	34
H(5N)	3026	4253	2607	47
H(6N)	4019	2288	3329	42
H(7N)	8934	6423	1945	34
H(8N)	7469	5578	1137	38
H(4)	2748	8850	1220	26
H(6)	3861	6849	1147	30
H(7)	4785	5021	1337	34
H(8)	4686	4634	1856	37
H(9)	3626	5989	2166	34
H(12A)	2532	13280	1255	45
H(12B)	3887	12641	1329	45
H(13A)	3286	12117	1807	45
H(13B)	2494	13418	1767	45
H(18)	1446	7531	3165	29
H(20)	3467	8590	3299	32
H(21)	5298	9656	3167	35
H(22)	5790	9902	2660	32

H(23)	4441	9124	2295	33
H(26A)	-2685	8246	3129	46
H(26B)	-2867	6726	3122	46
H(27A)	-3235	7230	2632	44
H(27B)	-2171	8331	2633	44
H(32)	7452	3548	1241	33
H(34)	6411	1525	1102	30
H(35)	5369	-302	1243	36
H(36)	5143	-806	1747	36
H(37)	5861	530	2110	35
H(40A)	7785	8235	1773	51
H(40B)	6675	7181	1778	51
H(41A)	6733	7648	1274	47
H(41B)	8251	7851	1277	47
H(46)	6146	2236	3189	28
H(48)	8165	1118	3262	31
H(49)	9971	183	3063	35
H(50)	10347	280	2550	39
H(51)	9021	1417	2243	32
H(54A)	1724	2481	3149	47
H(54B)	2352	1120	3077	47
H(55A)	2901	1707	2604	46
H(55B)	1589	2483	2642	46

–

Table A6-6. Crystal data and structure refinement for C31H29F6N4O2Cl3.

Empirical formula	C31 H29 Cl3 F6 N4 O2
Formula weight	709.93
Temperature	153(2) K
Wavelength	0.71073 Å
Crystal system	Orthorhombic
Space group	P2(1)2(1)2(1)
Unit cell dimensions	a = 11.5447(4) Å
	b = 14.4270(5) Å
	c = 19.4717(7) Å
Volume	3243.1(2) $Å^3$
Z	4
Density (calculated)	1.454 Mg/m^3
Absorption coefficient	0.353 mm^{-1}
F(000)	1456
Crystal size	0.44 x 0.28 x 0.26 mm^3
Theta range for data collection	3.49 to 28.81 °.
Index ranges	-15<=h<=15, -19<=k<=19, -26<=l<=26
Reflections collected	54959
Independent reflections	8462 [R(int) = 0.0449]
Completeness to theta = 25.00 °	99.6 %
Absorption correction	Empirical
Max. and min. transmission	0.9138 and 0.8602
Refinement method	Full-matrix least-squares on F^2
Data / restraints / parameters	8462 / 0 / 423
Goodness-of-fit on F^2	0.928
Final R indices [I>2sigma(I)]	R1 = 0.0536, wR2 = 0.1278
R indices (all data)	R1 = 0.0648, wR2 = 0.1349
Absolute structure parameter	0.03(10)
Largest diff. peak and hole	0.549 and -0.649 $e.Å^{-3}$

Table A6-7. Atomic coordinates (x 10^4) and equivalent isotropic displacement parameters ($Å^2$x 10^3)
for C31H29F6N4O2Cl3. U(eq) is defined as one third of the trace of the orthogonalized U^{ij} tensor.

	x	y	z	U(eq)
Cl(1)	457(1)	7043(2)	7424(1)	113(1)
Cl(2)	2327(1)	6659(2)	6476(1)	134(1)
Cl(3)	1428(2)	5270(2)	7358(1)	138(1)
F(1)	-2255(2)	7333(1)	9094(1)	33(1)
F(2)	-2379(1)	8809(1)	8975(1)	31(1)
F(3)	-814(1)	8105(1)	8696(1)	35(1)
F(4)	2845(2)	12196(1)	8066(1)	35(1)
F(5)	4703(2)	12241(1)	8003(1)	40(1)
F(6)	3671(2)	12276(1)	7084(1)	39(1)
O(1)	1231(2)	8476(1)	9505(1)	22(1)
O(2)	1544(2)	10521(1)	8338(1)	24(1)
N(1)	-2230(2)	8259(2)	10335(1)	21(1)
N(2)	-406(2)	7473(1)	10024(1)	20(1)
N(3)	2853(2)	10516(2)	7242(1)	22(1)
N(4)	4921(2)	10623(2)	7350(1)	30(1)
C(1)	1179(2)	10087(2)	9673(1)	15(1)
C(2)	631(2)	9237(2)	9704(1)	15(1)
C(3)	-552(2)	9170(2)	9931(1)	15(1)
C(4)	-1114(2)	9959(2)	10131(1)	17(1)
C(5)	-576(2)	10834(2)	10120(1)	17(1)
C(6)	-1161(2)	11644(2)	10338(1)	24(1)
C(7)	-639(2)	12490(2)	10311(2)	32(1)
C(8)	513(3)	12558(2)	10071(2)	34(1)
C(9)	1107(2)	11792(2)	9856(2)	26(1)
C(10)	584(2)	10900(2)	9875(1)	16(1)

C(11)	2380(2)	10142(2)	9392(1)	14(1)
C(12)	3368(2)	9977(2)	9808(1)	14(1)
C(13)	3286(2)	9753(2)	10512(1)	19(1)
C(14)	4254(2)	9612(2)	10905(1)	24(1)
C(15)	5372(2)	9674(2)	10610(1)	22(1)
C(16)	5485(2)	9878(2)	9929(1)	20(1)
C(17)	4495(2)	10040(2)	9512(1)	14(1)
C(18)	4595(2)	10282(2)	8814(1)	17(1)
C(19)	3653(2)	10463(2)	8411(1)	17(1)
C(20)	2516(2)	10373(2)	8711(1)	16(1)
C(21)	-1208(2)	8250(2)	9896(1)	18(1)
C(22)	-1946(2)	8174(2)	11072(1)	24(1)
C(23)	-1162(2)	7349(2)	11216(1)	26(1)
C(24)	-100(2)	7414(2)	10755(1)	24(1)
C(25)	-1662(2)	8132(2)	9156(1)	23(1)
C(26)	3814(2)	10832(2)	7676(1)	21(1)
C(27)	2954(3)	9512(2)	7087(2)	32(1)
C(28)	4103(3)	9299(3)	6742(2)	42(1)
C(29)	5082(3)	9633(3)	7197(2)	39(1)
C(30)	3746(2)	11891(2)	7706(1)	28(1)
C(31)	1071(4)	6248(4)	6866(2)	81(2)

Table A6-8. Bond lengths [Å] and angles [°] for C31H29F6N4O2Cl3.

Cl(1)-C(31)	1.732(5)
Cl(2)-C(31)	1.741(5)
Cl(3)-C(31)	1.754(7)
F(1)-C(25)	1.346(3)
F(2)-C(25)	1.328(3)
F(3)-C(25)	1.327(3)
F(4)-C(30)	1.329(3)
F(5)-C(30)	1.345(3)
F(6)-C(30)	1.336(3)
O(1)-C(2)	1.355(3)
O(2)-C(20)	1.355(3)
N(1)-C(21)	1.458(3)
N(1)-C(22)	1.477(3)
N(2)-C(24)	1.470(3)
N(2)-C(21)	1.474(3)
N(3)-C(26)	1.468(3)
N(3)-C(27)	1.483(4)
N(4)-C(26)	1.459(3)
N(4)-C(29)	1.470(4)
C(1)-C(2)	1.380(3)
C(1)-C(10)	1.416(3)
C(1)-C(11)	1.493(3)
C(2)-C(3)	1.439(3)
C(3)-C(4)	1.367(3)
C(3)-C(21)	1.531(3)
C(4)-C(5)	1.408(3)
C(5)-C(6)	1.414(3)
C(5)-C(10)	1.425(3)
C(6)-C(7)	1.363(4)
C(7)-C(8)	1.413(4)
C(8)-C(9)	1.366(4)
C(9)-C(10)	1.422(3)

C(11)-C(20)	1.376(3)
C(11)-C(12)	1.419(3)
C(12)-C(13)	1.411(3)
C(12)-C(17)	1.426(3)
C(13)-C(14)	1.370(3)
C(14)-C(15)	1.416(4)
C(15)-C(16)	1.365(4)
C(16)-C(17)	1.421(3)
C(17)-C(18)	1.409(3)
C(18)-C(19)	1.366(3)
C(19)-C(20)	1.442(3)
C(19)-C(26)	1.538(3)
C(21)-C(25)	1.542(3)
C(22)-C(23)	1.521(4)
C(23)-C(24)	1.522(4)
C(26)-C(30)	1.531(4)
C(27)-C(28)	1.519(4)
C(28)-C(29)	1.515(5)

C(21)-N(1)-C(22)	112.91(18)
C(24)-N(2)-C(21)	111.04(19)
C(26)-N(3)-C(27)	111.2(2)
C(26)-N(4)-C(29)	113.6(2)
C(2)-C(1)-C(10)	120.14(19)
C(2)-C(1)-C(11)	119.2(2)
C(10)-C(1)-C(11)	120.5(2)
O(1)-C(2)-C(1)	118.27(19)
O(1)-C(2)-C(3)	121.2(2)
C(1)-C(2)-C(3)	120.5(2)
C(4)-C(3)-C(2)	118.9(2)
C(4)-C(3)-C(21)	119.98(19)
C(2)-C(3)-C(21)	120.96(19)
C(3)-C(4)-C(5)	122.2(2)
C(4)-C(5)-C(6)	121.7(2)

C(4)-C(5)-C(10)	118.7(2)
C(6)-C(5)-C(10)	119.7(2)
C(7)-C(6)-C(5)	121.1(2)
C(6)-C(7)-C(8)	119.4(2)
C(9)-C(8)-C(7)	121.2(2)
C(8)-C(9)-C(10)	120.7(2)
C(1)-C(10)-C(5)	119.6(2)
C(1)-C(10)-C(9)	122.5(2)
C(5)-C(10)-C(9)	117.9(2)
C(20)-C(11)-C(12)	119.89(19)
C(20)-C(11)-C(1)	118.21(19)
C(12)-C(11)-C(1)	121.89(19)
C(13)-C(12)-C(11)	122.6(2)
C(13)-C(12)-C(17)	117.87(19)
C(11)-C(12)-C(17)	119.52(19)
C(14)-C(13)-C(12)	121.5(2)
C(13)-C(14)-C(15)	120.5(2)
C(16)-C(15)-C(14)	119.6(2)
C(15)-C(16)-C(17)	120.9(2)
C(18)-C(17)-C(16)	121.7(2)
C(18)-C(17)-C(12)	118.7(2)
C(16)-C(17)-C(12)	119.6(2)
C(19)-C(18)-C(17)	122.4(2)
C(18)-C(19)-C(20)	118.37(19)
C(18)-C(19)-C(26)	120.2(2)
C(20)-C(19)-C(26)	121.2(2)
O(2)-C(20)-C(11)	117.38(19)
O(2)-C(20)-C(19)	121.53(19)
C(11)-C(20)-C(19)	121.1(2)
N(2)-C(21)-N(1)	114.6(2)
N(2)-C(21)-C(25)	106.71(19)
N(1)-C(21)-C(25)	105.88(18)
N(2)-C(21)-C(3)	109.95(18)
N(1)-C(21)-C(3)	111.51(19)

C(25)-C(21)-C(3)	107.78(19)
N(1)-C(22)-C(23)	112.1(2)
C(22)-C(23)-C(24)	108.9(2)
N(2)-C(24)-C(23)	112.4(2)
F(3)-C(25)-F(2)	107.5(2)
F(3)-C(25)-F(1)	106.9(2)
F(2)-C(25)-F(1)	106.78(19)
F(3)-C(25)-C(21)	112.50(19)
F(2)-C(25)-C(21)	112.3(2)
F(1)-C(25)-C(21)	110.6(2)
N(4)-C(26)-N(3)	110.2(2)
N(4)-C(26)-C(30)	105.5(2)
N(3)-C(26)-C(30)	107.1(2)
N(4)-C(26)-C(19)	116.1(2)
N(3)-C(26)-C(19)	109.71(19)
C(30)-C(26)-C(19)	107.7(2)
N(3)-C(27)-C(28)	110.8(3)
C(29)-C(28)-C(27)	109.2(2)
N(4)-C(29)-C(28)	109.4(2)
F(4)-C(30)-F(6)	106.9(2)
F(4)-C(30)-F(5)	107.0(2)
F(6)-C(30)-F(5)	106.7(2)
F(4)-C(30)-C(26)	113.0(2)
F(6)-C(30)-C(26)	112.6(2)
F(5)-C(30)-C(26)	110.4(2)
Cl(1)-C(31)-Cl(2)	112.9(3)
Cl(1)-C(31)-Cl(3)	106.7(3)
Cl(2)-C(31)-Cl(3)	108.5(3)

Table A6-9. Anisotropic displacement parameters ($Å^2 x\ 10^3$) for C31H29F6N4O2Cl3. The anisotropic displacement factor exponent takes the form: $-2\pi^2[\ h^2\ a^{*2}U^{11} + ...\ + 2\ h\ k\ a^*\ b^*\ U^{12}\ ]$

	U^{11}	U^{22}	U^{33}	U^{23}	U^{13}	U^{12}
Cl(1)	71(1)	147(2)	120(1)	-67(1)	-5(1)	18(1)
Cl(2)	65(1)	243(3)	95(1)	-28(1)	15(1)	-33(1)
Cl(3)	161(2)	139(2)	115(2)	-30(1)	-24(1)	22(2)
F(1)	31(1)	29(1)	39(1)	-5(1)	-14(1)	-8(1)
F(2)	29(1)	32(1)	32(1)	3(1)	-8(1)	5(1)
F(3)	28(1)	50(1)	26(1)	-8(1)	3(1)	0(1)
F(4)	44(1)	27(1)	35(1)	2(1)	9(1)	5(1)
F(5)	44(1)	36(1)	41(1)	8(1)	-8(1)	-16(1)
F(6)	48(1)	40(1)	28(1)	17(1)	2(1)	-3(1)
O(1)	13(1)	15(1)	37(1)	-2(1)	6(1)	2(1)
O(2)	14(1)	40(1)	18(1)	5(1)	-2(1)	2(1)
N(1)	8(1)	26(1)	27(1)	1(1)	0(1)	-3(1)
N(2)	16(1)	15(1)	30(1)	-2(1)	0(1)	1(1)
N(3)	21(1)	29(1)	18(1)	2(1)	-2(1)	4(1)
N(4)	22(1)	46(2)	24(1)	8(1)	10(1)	4(1)
C(1)	10(1)	19(1)	16(1)	2(1)	2(1)	0(1)
C(2)	10(1)	18(1)	19(1)	0(1)	1(1)	2(1)
C(3)	10(1)	16(1)	20(1)	1(1)	-1(1)	0(1)
C(4)	8(1)	20(1)	22(1)	0(1)	1(1)	0(1)
C(5)	12(1)	17(1)	21(1)	-1(1)	0(1)	1(1)
C(6)	16(1)	22(1)	35(1)	-6(1)	2(1)	4(1)
C(7)	26(1)	20(1)	51(2)	-8(1)	3(1)	5(1)
C(8)	27(1)	14(1)	59(2)	-4(1)	7(1)	-3(1)
C(9)	18(1)	19(1)	40(1)	0(1)	7(1)	-1(1)
C(10)	14(1)	16(1)	19(1)	0(1)	0(1)	1(1)
C(11)	11(1)	14(1)	17(1)	0(1)	3(1)	0(1)

C(12)	11(1)	13(1)	17(1)	-1(1)	0(1)	0(1)
C(13)	15(1)	24(1)	19(1)	2(1)	2(1)	1(1)
C(14)	25(1)	28(1)	18(1)	2(1)	0(1)	4(1)
C(15)	15(1)	28(1)	24(1)	0(1)	-7(1)	3(1)
C(16)	12(1)	22(1)	25(1)	-2(1)	-3(1)	1(1)
C(17)	11(1)	14(1)	18(1)	-1(1)	1(1)	0(1)
C(18)	12(1)	19(1)	21(1)	0(1)	4(1)	-1(1)
C(19)	15(1)	19(1)	15(1)	1(1)	3(1)	0(1)
C(20)	10(1)	18(1)	18(1)	1(1)	1(1)	-1(1)
C(21)	11(1)	16(1)	26(1)	-1(1)	-1(1)	0(1)
C(22)	18(1)	27(1)	27(1)	0(1)	3(1)	-2(1)
C(23)	26(1)	25(1)	28(1)	5(1)	-3(1)	-6(1)
C(24)	18(1)	20(1)	34(1)	3(1)	-7(1)	-2(1)
C(25)	16(1)	25(1)	28(1)	-2(1)	-4(1)	-1(1)
C(26)	17(1)	30(1)	16(1)	4(1)	3(1)	1(1)
C(27)	39(2)	31(1)	26(1)	-3(1)	-10(1)	6(1)
C(28)	47(2)	52(2)	25(1)	-10(1)	-2(1)	22(2)
C(29)	33(2)	56(2)	27(1)	-5(1)	2(1)	21(1)
C(30)	29(1)	33(1)	24(1)	9(1)	2(1)	-4(1)
C(31)	43(2)	144(5)	55(2)	-39(3)	-1(2)	-10(3)

Table A6-10. Hydrogen coordinates (x 10^4) and isotropic displacement parameters ($Å^2$x 10^3) for C31H29F6N4O2Cl3.

	x	y	z	U(eq)
H(1)	-2942	8310	10178	25
H(2)	-145	7095	9705	24
H(3)	2290	10874	7092	27
H(4A)	5442	11048	7253	37
H(4)	-1895	9915	10283	21
H(6)	-1932	11596	10506	29
H(7)	-1046	13030	10452	38
H(8)	881	13147	10060	40
H(9)	1878	11857	9691	31
H(13)	2543	9700	10718	23
H(14)	4175	9471	11379	28
H(15)	6041	9574	10885	27
H(16)	6235	9912	9730	24
H(18)	5345	10322	8616	21
H(22A)	-2672	8105	11338	29
H(22B)	-1557	8748	11228	29
H(23A)	-1583	6764	11123	32
H(23B)	-923	7351	11704	32
H(24A)	356	7968	10885	29
H(24B)	394	6861	10830	29
H(27A)	2310	9322	6782	39
H(27B)	2891	9153	7519	39
H(28A)	4175	8624	6664	50
H(28B)	4142	9615	6291	50
H(29A)	5090	9273	7630	46
H(29B)	5833	9538	6961	46
H(31)	494	6072	6506	97
H(1O1)	850(30)	8050(30)	9642(18)	36(10)
H(1O2)	1700(30)	10620(20)	7962(19)	31(9)

Table A6-11. Crystal data and structure refinement for C38H38Cl6F6N4O2.

Empirical formula	C38 H38 Cl6 F6 N4 O2
Formula weight	909.42
Temperature	153(2) K
Wavelength	0.71073 Å
Crystal system	Monoclinic
Space group	C2
Unit cell dimensions	a = 18.621(6) Å
	b = 9.489(3) Å β= 96.732(8) °.
	c = 11.431(3) Å
Volume	2005.8(10) $Å^3$
Z	2
Density (calculated)	1.506 Mg/m^3
Absorption coefficient	0.497 mm^{-1}
F(000)	932
Crystal size	0.44 x 0.34 x 0.16 mm^3
Theta range for data collection	3.94 to 31.46 °.
Index ranges	-26<=h<=26, -13<=k<=13, -16<=l<=16
Reflections collected	16129
Independent reflections	6176 [R(int) = 0.0638]
Completeness to theta = 31.46 °	97.5 %
Absorption correction	Empirical
Max. and min. transmission	0.9248 and 0.8111
Refinement method	Full-matrix least-squares on F^2
Data / restraints / parameters	6176 / 1 / 257
Goodness-of-fit on F^2	1.059
Final R indices [I>2sigma(I)]	R1 = 0.0884, wR2 = 0.1977
R indices (all data)	R1 = 0.1001, wR2 = 0.2050
Absolute structure parameter	0.06(12)
Largest diff. peak and hole	0.539 and -0.631 e.$Å^{-3}$

Table A6-12. Atomic coordinates (x 10^4) and equivalent isotropic displacement parameters ($Å^2$x 10^3) for C38H38Cl6F6N4O2. U(eq) is defined as one third of the trace of the orthogonalized U^{ij} tensor.

	x	y	z	U(eq)
Cl(1)	8769(1)	1822(2)	3162(1)	56(1)
Cl(2)	9360(1)	577(2)	1179(2)	57(1)
Cl(3)	7860(1)	1347(2)	946(1)	48(1)
F(1)	7808(2)	4545(5)	6823(4)	49(1)
F(2)	8437(2)	4612(5)	5361(3)	55(1)
F(3)	7683(2)	2931(5)	5479(3)	54(1)
O(1)	8917(2)	3379(4)	9422(3)	30(1)
N(1)	9079(2)	1908(6)	6020(3)	33(1)
N(2)	8373(2)	1941(4)	7626(3)	24(1)
C(1)	9955(2)	4777(4)	9334(3)	18(1)
C(2)	9392(2)	3985(4)	8764(4)	19(1)
C(3)	9323(2)	3793(5)	7508(3)	18(1)
C(4)	9812(2)	4490(5)	6879(4)	23(1)
C(5)	10356(2)	5378(5)	7430(4)	20(1)
C(6)	10811(2)	6184(6)	6772(4)	26(1)
C(7)	11331(2)	7074(5)	7317(4)	27(1)
C(8)	11419(2)	7168(6)	8558(5)	30(1)
C(9)	10998(2)	6418(5)	9229(4)	25(1)
C(10)	10434(2)	5520(5)	8684(4)	20(1)
C(11)	8755(2)	2860(6)	6836(4)	24(1)
C(12)	8801(2)	483(7)	6207(4)	33(1)
C(13)	8684(2)	518(6)	7496(4)	26(1)
C(14)	8263(3)	-769(6)	7835(5)	33(1)
C(15)	8705(3)	-2080(7)	7571(5)	40(1)
C(16)	8888(3)	-2123(7)	6306(5)	40(1)
C(17)	9258(3)	-757(7)	5946(5)	38(1)
C(18)	8171(3)	3762(7)	6114(5)	36(1)
C(19)	8734(3)	1792(7)	1629(4)	33(1)

Table A6-13. Bond lengths [Å] and angles [°] for C38H38Cl6F6N4O2.

Cl(1)-C(19)	1.746(5)
Cl(2)-C(19)	1.760(6)
Cl(3)-C(19)	1.772(5)
F(1)-C(18)	1.338(7)
F(2)-C(18)	1.318(6)
F(3)-C(18)	1.349(6)
O(1)-C(2)	1.355(5)
N(1)-C(12)	1.472(8)
N(1)-C(11)	1.477(6)
N(2)-C(13)	1.484(6)
N(2)-C(11)	1.495(5)
C(1)-C(2)	1.388(6)
C(1)-C(10)	1.415(5)
C(1)-C(1)#1	1.512(8)
C(2)-C(3)	1.438(5)
C(3)-C(4)	1.391(5)
C(3)-C(11)	1.517(6)
C(4)-C(5)	1.408(6)
C(5)-C(6)	1.421(6)
C(5)-C(10)	1.430(5)
C(6)-C(7)	1.377(6)
C(7)-C(8)	1.412(7)
C(8)-C(9)	1.361(6)
C(9)-C(10)	1.436(6)
C(11)-C(18)	1.545(7)
C(12)-C(17)	1.503(8)
C(12)-C(13)	1.515(7)
C(13)-C(14)	1.526(7)
C(14)-C(15)	1.541(8)
C(15)-C(16)	1.524(8)
C(16)-C(17)	1.546(9)

C(12)-N(1)-C(11)	107.0(3)
C(13)-N(2)-C(11)	104.5(3)
C(2)-C(1)-C(10)	120.7(4)
C(2)-C(1)-C(1)#1	117.5(4)
C(10)-C(1)-C(1)#1	121.8(4)
O(1)-C(2)-C(1)	118.3(4)
O(1)-C(2)-C(3)	120.9(4)
C(1)-C(2)-C(3)	120.8(4)
C(4)-C(3)-C(2)	117.9(4)
C(4)-C(3)-C(11)	118.4(4)
C(2)-C(3)-C(11)	123.7(3)
C(3)-C(4)-C(5)	122.2(4)
C(4)-C(5)-C(6)	121.9(4)
C(4)-C(5)-C(10)	119.2(4)
C(6)-C(5)-C(10)	118.8(4)
C(7)-C(6)-C(5)	121.5(4)
C(6)-C(7)-C(8)	119.1(4)
C(9)-C(8)-C(7)	121.8(4)
C(8)-C(9)-C(10)	120.4(4)
C(1)-C(10)-C(9)	122.8(4)
C(1)-C(10)-C(5)	118.9(4)
C(9)-C(10)-C(5)	118.3(4)
N(1)-C(11)-N(2)	106.5(4)
N(1)-C(11)-C(3)	111.4(3)
N(2)-C(11)-C(3)	112.8(3)
N(1)-C(11)-C(18)	108.4(4)
N(2)-C(11)-C(18)	106.9(3)
C(3)-C(11)-C(18)	110.7(4)
N(1)-C(12)-C(17)	118.2(4)
N(1)-C(12)-C(13)	102.4(4)
C(17)-C(12)-C(13)	111.0(5)
N(2)-C(13)-C(14)	118.9(4)
N(2)-C(13)-C(12)	102.7(4)
C(14)-C(13)-C(12)	111.5(4)

C(13)-C(14)-C(15)	107.0(4)
C(16)-C(15)-C(14)	113.0(5)
C(17)-C(16)-C(15)	112.7(5)
C(12)-C(17)-C(16)	108.8(4)
F(2)-C(18)-F(1)	108.1(6)
F(2)-C(18)-F(3)	106.7(4)
F(1)-C(18)-F(3)	107.2(4)
F(2)-C(18)-C(11)	113.1(4)
F(1)-C(18)-C(11)	111.0(4)
F(3)-C(18)-C(11)	110.6(5)
Cl(1)-C(19)-Cl(2)	110.8(3)
Cl(1)-C(19)-Cl(3)	111.7(3)
Cl(2)-C(19)-Cl(3)	108.7(3)

Symmetry transformations used to generate equivalent atoms:
#1 -x+2,y,-z+2

Table A6-14. Anisotropic displacement parameters ($Å^2 x\ 10^3$) for C38H38Cl6F6N4O2. The anisotropic displacement factor exponent takes the form: $-2\pi^2[\ h^2\ a^{*2}U^{11} + ... + 2\ h\ k\ a^*\ b^*\ U^{12}\ ]$

	U^{11}	U^{22}	U^{33}	U^{23}	U^{13}	U^{12}
Cl(1)	65(1)	70(1)	33(1)	8(1)	9(1)	-25(1)
Cl(2)	29(1)	62(1)	81(1)	3(1)	9(1)	11(1)
Cl(3)	23(1)	74(1)	48(1)	5(1)	6(1)	4(1)
F(1)	30(2)	57(3)	61(2)	3(2)	8(2)	5(2)
F(2)	34(2)	82(3)	46(2)	29(2)	-5(1)	-19(2)
F(3)	28(2)	87(3)	44(2)	13(2)	-8(1)	-18(2)
O(1)	32(2)	33(2)	26(2)	-3(1)	12(1)	-15(2)
N(1)	25(2)	52(3)	24(2)	-5(2)	11(1)	-8(2)
N(2)	21(2)	25(2)	27(2)	-2(2)	10(1)	-3(1)
C(1)	17(2)	17(2)	19(2)	2(1)	4(1)	0(1)
C(2)	21(2)	16(2)	22(2)	0(1)	8(1)	2(1)
C(3)	16(2)	19(2)	21(2)	2(1)	6(1)	1(1)
C(4)	17(2)	32(2)	22(2)	-2(2)	8(1)	-4(2)
C(5)	21(2)	18(2)	22(2)	2(1)	8(1)	-2(1)
C(6)	22(2)	31(2)	27(2)	1(2)	10(2)	-2(2)
C(7)	24(2)	22(2)	36(2)	-2(2)	10(2)	-8(2)
C(8)	21(2)	30(3)	39(2)	0(2)	3(2)	-5(2)
C(9)	22(2)	25(2)	27(2)	-2(2)	3(1)	-1(2)
C(10)	18(2)	18(2)	23(2)	-2(2)	6(1)	4(1)
C(11)	19(2)	35(2)	19(2)	4(2)	7(1)	-4(2)
C(12)	20(2)	48(3)	33(2)	-6(2)	4(2)	0(2)
C(13)	22(2)	27(2)	30(2)	-5(2)	5(2)	3(2)
C(14)	37(2)	25(3)	39(3)	0(2)	12(2)	-5(2)
C(15)	44(3)	27(3)	50(3)	-3(2)	4(2)	0(2)
C(16)	37(3)	41(3)	41(3)	-7(3)	0(2)	10(2)
C(17)	27(2)	52(4)	35(2)	-12(2)	6(2)	2(2)
C(18)	23(2)	51(4)	31(2)	7(2)	-2(2)	-10(2)
C(19)	29(2)	39(3)	32(2)	3(2)	6(2)	-9(2)

Table A6-15. Hydrogen coordinates (x 10^4) and isotropic displacement parameters ($Å^2$x 10^3)
for C38H38Cl6F6N4O2.

	x	y	z	U(eq)
H(1)	9381	2147	5517	40
H(2)	8038	2188	8070	29
H(4)	9777	4364	6050	28
H(6)	10756	6108	5938	31
H(7)	11627	7616	6864	32
H(8)	11782	7772	8935	36
H(9)	11077	6488	10063	30
H(12)	8318	387	5728	40
H(13)	9170	495	7972	32
H(14A)	7779	-796	7370	40
H(14B)	8198	-734	8682	40
H(15A)	9160	-2093	8114	48
H(15B)	8427	-2936	7724	48
H(16A)	9212	-2932	6216	48
H(16B)	8438	-2273	5768	48
H(17A)	9745	-672	6392	45
H(17B)	9313	-783	5095	45
H(19)	8860	2752	1355	39
H(1O)	8670(40)	3080(90)	8970(70)	50(20)

Appendix I. Derivatives of Binol-Pyridine Compounds

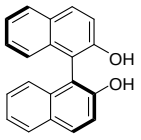

(S)-**7-1**

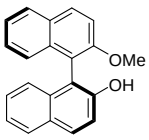

(S)-**7-2**

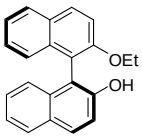

(S)-**7-3**

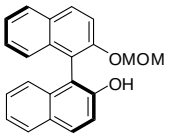

(S)-**7-4**

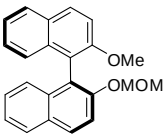

(S)-**7-5**

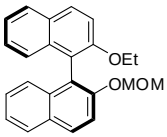

(S)-**7-6**

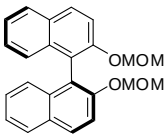

(S)-**7-7**

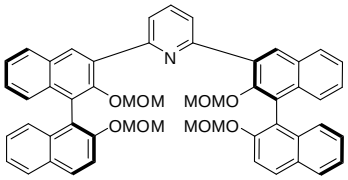

(S)-**7-8**

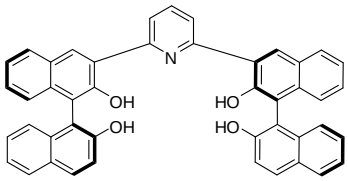

(S)-**7-9**

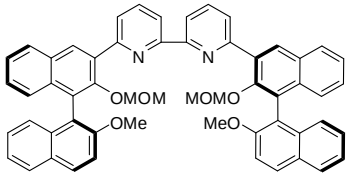

(S)-**7-10**

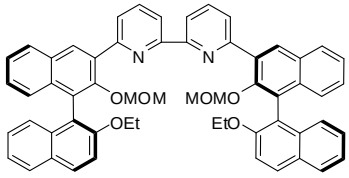

(S)-**7-11**

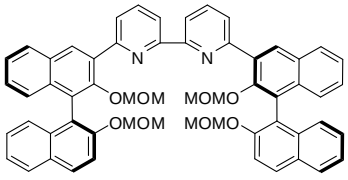

(S)-**7-12**

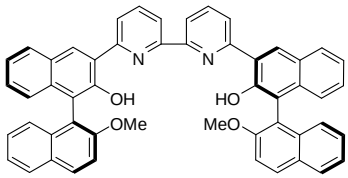

(S)-**7-13**

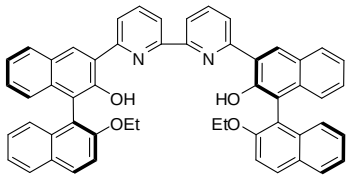

(S)-**7-14**

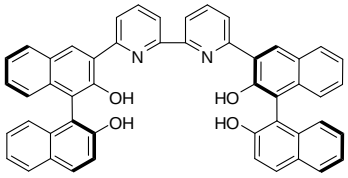

(S)-**7-15**

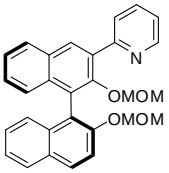

(S)-**7-16**

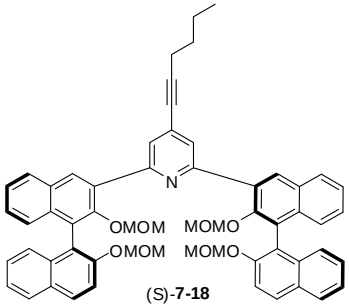

(S)-**7-18**

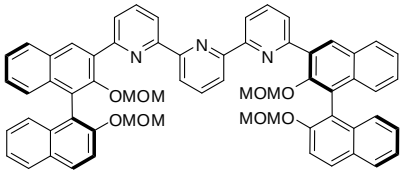

(S)-**7-20**

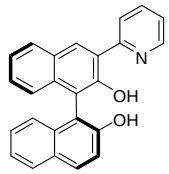

(S)-**7-17**

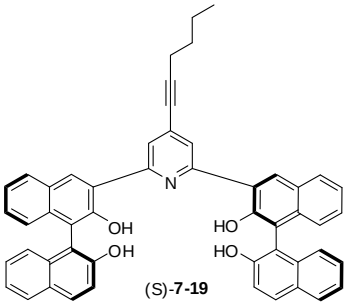

(S)-**7-19**

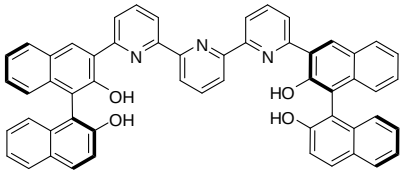

(S)-**7-21**

1. Preparation and Characterization of Compounds

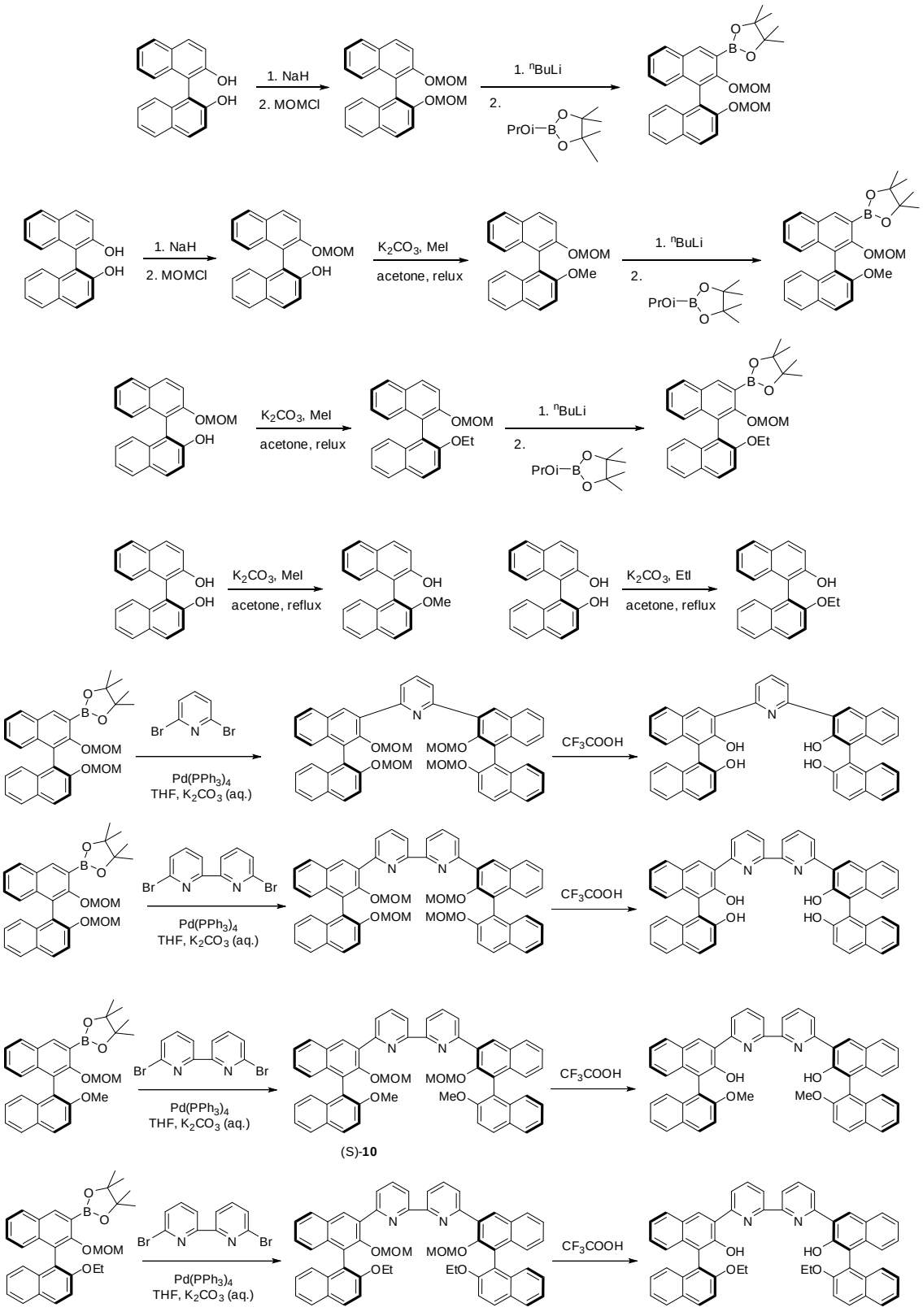

(S)-**10**

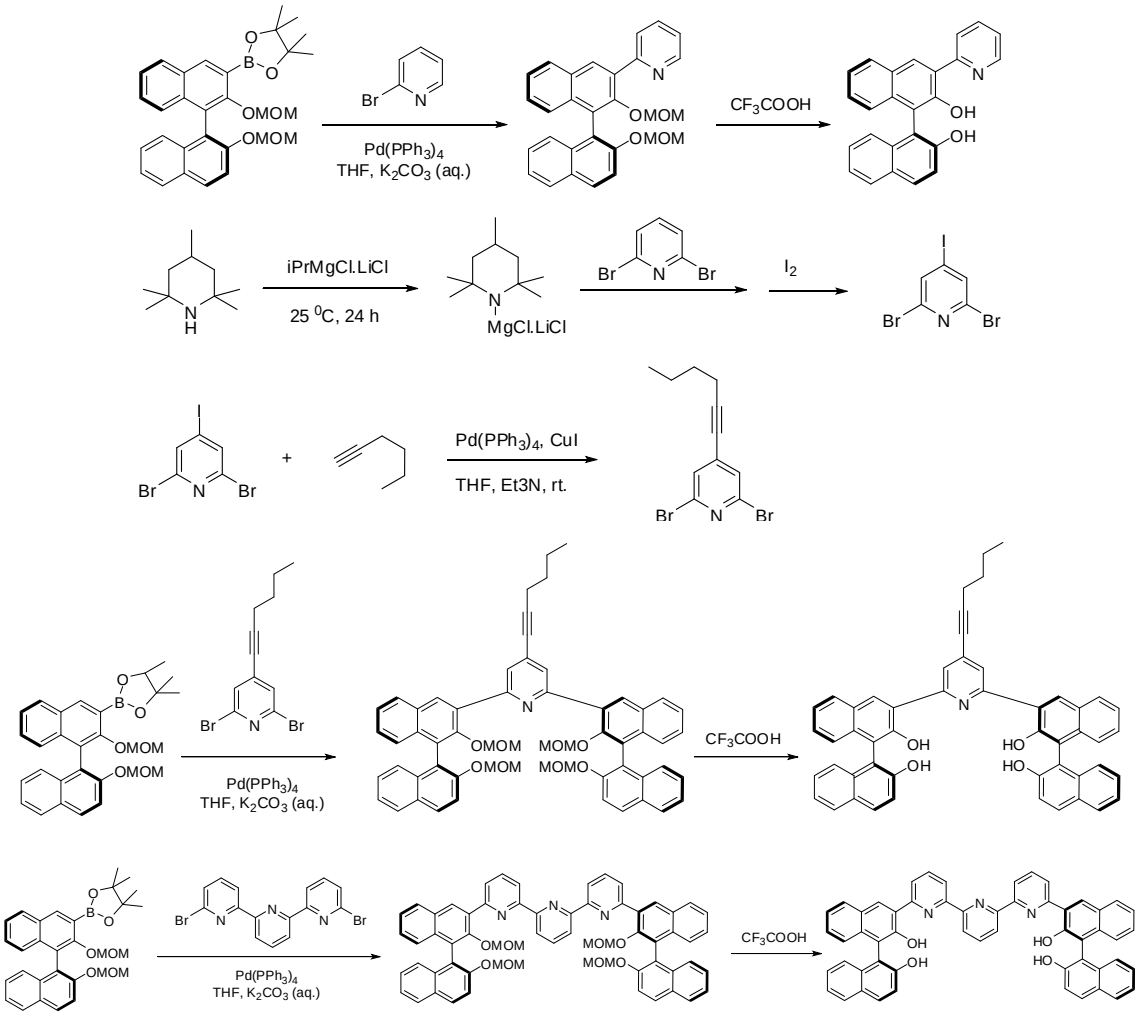
OMOM
OMOM
Br
N
Pd(PPh3)4
THF, K2CO3 (aq.)
CF3COOH
OH
OH
iPrMgCl.LiCl
25 0C, 24 h
MgCl.LiCl
I2
I
Pd(PPh3)4, CuI
THF, Et3N, rt.
MOMO
HO

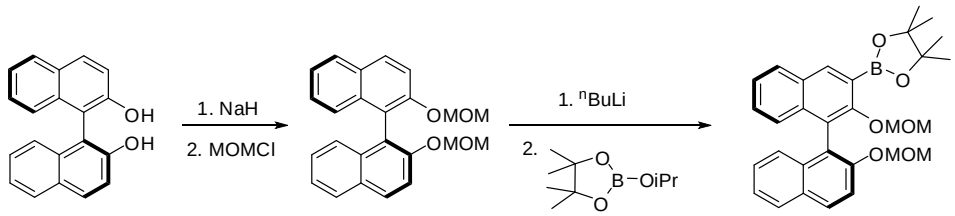

Preparation of (S)-2,2'-bis(methoxymethoxy)-1,1'-binaphthy. Under nitrogen, in a 500 mL flame-dried flask, (S)-BINOL (5.0 g, 17.5 mmol) was dissolved in 200 mL THF and cooled to 0℃. NaH (60% in mineral oil, 1.75 g, 43.75 mmol) was added to the solution in 3 portions. After the mixture was stirred for 15 min, MOMCl (3.3 mL, 43.75 mmol) was added and the reaction mixture was allowed to warm to room temperature. After the mixture was stirred for 1 h, the reaction was quenched with water (20 mL). The organic layer was separated and the aqueous layer was extracted with ethyl acetated (2 x 30 mL). The combined organic layer was washed with brine (30 mL) and dried over anhydrous Na_2SO_4. After evaporation of the solvent, the residue was purified by column chromatography on silica gel eluted with hexanes/ethyl acetate (10/1) to afford desired product as a white solid in 92% yield. ^{1}H NMR (300 MHz, $CDCl_3$) δ 3.15 (s, 6H), 4.98 (d, 2H, J = 6.9 Hz), 5.09 (d, 2H, J = 6.9 Hz), 7.14-7.25 (m, 4H), 7.32-7.37 (m, 2H), 7.58 (d, 2H, J = 9.3 Hz), 7.88 (d, 2H, J = 8.1 Hz), 7.96 (d, 2H, J = 9.0 Hz).

Preparation of (S)-2-(2,2'-bis(methoxymethoxy)-1,1'-binaphthyl-3-yl)-4,4,5,5-tetramethyl-1,3,2-dioxaborolane. Under nitrogen (S)-2,2'-bis(methoxymethoxy)-1,1'-binaphthy (3.74 g, 10 mmol) was dissolved in 110 mL ether and cooled to 0℃. nBuLi (2.5 M, 5.2 mL, 13 mmol) was added dropwise and the reaction mixture was allow to

warm to room temperature over 3 h. Then the reaction mixture was cooled to The reaction mixture was cooled to -78℃ and 2-isopropoxy-4,4,5,5-tetramethyl-1,3,2-dioxaborolane (3 mL, 15.0 mmol) was added. The mixture was allowed to warm to room temperature and stirred for overnight. The generated salts were removed by filtration through a Buchner funnel and rinsed with CH_2Cl_2. The combined organic layer was concentrated and purified by flash chromatography on silica gel eluted with hexanes/ethyl acetate (10/1) to afford desired product as a white solid in 42% yield. ^{1}H NMR (300 MHz, $CDCl_3$) δ 1.39 (s, 2H), 2.39 (s, 2H), 3.11 (s, 2H), 4.84 (d, J = 6.0 Hz, 1H), 4.89 (d, J = 6.0 Hz, 1H), 5.08 (d, J = 6.6 Hz, 1H), 5.16 (d, J = 6.9 Hz, 1H), 6.94 (d, J = 8.4 Hz, 1H), 7.01 (s, J = 8.4 Hz, 1H), 7.25 (t, J = 7.2 Hz, 1H), 7.31-7.41 (m, 2H), 7.43 (t, J = 7.2 Hz, 1H), 7.63 (d, J = 9.0 Hz, 1H), 7.94 (d, J = 8.1 Hz, 1H), 8.04-8.07 (m, 2H), 8.49 (s, 1H).

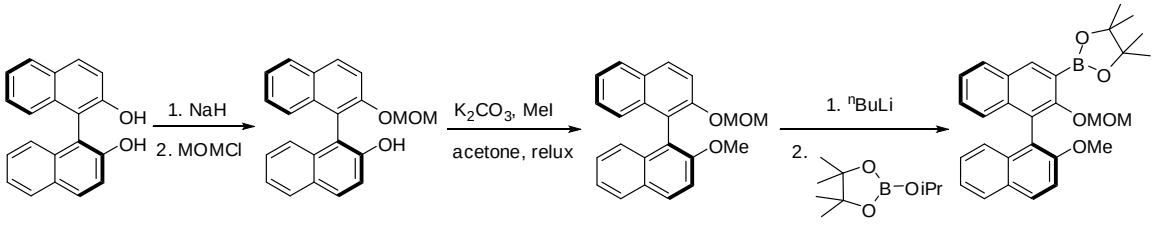

Preparation of (S)-2'-(methoxymethoxy)-1,1'-binaphthyl-2-ol. Under nitrogen, in a 500 mL flame-dried flask, (S)-BINOL (5.0 g, 17.5 mmol) was dissolved in 200 mL THF and cooled to 0℃. NaH (60% in mineral oil, 0.77 g, 19.2 mmol) was added to the solution in 3 portions. After the mixture was stirred for 15 min, MOMCl (1.5 mL, 19.2 mmol) was added and the reaction mixture was allowed to warm to room temperature.

After the mixture was stirred for 1 h, the reaction was quenched with water (20 mL). The organic layer was separated and the aqueous layer was extracted with ethyl acetated (2 x 30 mL). The combined organic layer was washed with brine (30 mL) and dried over anhydrous Na_2SO_4. After evaporation of the solvent, the residue was purified by column chromatography on silica gel eluted with hexanes/ethyl acetate (15/1) to afford desired product as a white solid in 71% yield. ^{1}H NMR (300 MHz, $CDCl_3$) δ 3.19 (s, 3H), 4.95 (s, 1H), 5.06 (d, J = 6.9 Hz, 1H), 5.11 (d, J = 6.9 Hz, 1H), 7.08 (d, J = 7.8 Hz, 1H), 7.18-7.43 (m, 6H), 7.60 (d, J = 9.0 Hz, 1H), 7.86 (d, J = 8.1Hz, 1H), 7.91 (d, J = 8.7 Hz, 2H), 8.03 (d, J = 9.0 Hz, 1H).

Preparation of (S)-2-methoxy-2'-(methoxymethoxy)-1,1'-binaphthyl. To a 100 mL flask, (S)-2'-(methoxymethoxy)-1,1'-binaphthyl-2-ol (1.65g, 5 mmol), K_2CO_3 (0.864 g, 6.26 mmol) and 50 mL acetone were added. After the reaction mixture was stirred under reflux for 1 h, MeI (0.47 mL, 7.5 mmol) was added and the resulting mixture was stirred under relux overnight. When it cooled down, the reaction mixture was poured in to 100 mL water and extracted with CH_2Cl_2 (3 x 30 mL). The combined organic layer was washed with brine (30 mL) and dried over anhydrous Na_2SO_4. After evaporation of the solvent, the residue was purified by column chromatography on silica gel eluted with hexanes/ethyl acetate (15/1) to afford desired product as a white solid in 81% yield. ^{1}H NMR (300 MHz, $CDCl_3$) δ 3.17 (s, 3H), 3.77 (s, 3H), 4.99 (d, J = 6.6 Hz, 1H), 5.07 (d, J = 6.6 Hz, 1H), 7.13 (d, J = 8.4 Hz, 2H), 7.20-7.38 (m, 4H), 7.46 (d, J = 9.0 Hz, 1H), 7.58

(d, J = 9.0 Hz, 1H), 7.87 (d, J = 8.1 Hz, 1H), 7.88 (d, J = 8.1 Hz, 1H), 7.97 (t, J = 9.6 Hz, 2H).

Preparation of (S)-2-(2'-methoxy-2-(methoxymethoxy)-1,1'-binaphthyl-3-yl)-4,4,5,5-tetra-methyl-1,3,2-dioxaborolane. Under nitrogen (S)-2-methoxy-2'-(methoxymethoxy)-1,1'-binaphthyl (1.20 g, 3.5 mmol) was dissolved in 40 mL ether and cooled to 0℃. nBuLi (2.5 M, 1.67 mL, 4.2 mmol) was added dropwise and the reaction mixture was allow to warm to room temperature over 3 h. Then the reaction mixture was cooled to The reaction mixture was cooled to -78 ℃ and 2-isopropoxy-4,4,5,5-tetramethyl-1,3,2-dioxaborolane (1.1 mL, 5.2 mmol) was added. The mixture was allowed to warm to room temperature and stirred for overnight. The generated salts were removed by filtration through a Buchner funnel and rinsed with CH_2Cl_2. The combined organic layer was concentrated and purified by flash chromatography on silica gel eluted with hexanes/ethyl acetate (10/1) to afford desired product as a white solid in 78% yield. ^{1}H NMR (300 MHz, $CDCl_3$) δ 1.39 (s, 12H), 2.42 (s, 3H), 3.77 (s, 3H), 4.82 (d, J = 6.0 Hz, 1H), 4.88 (d, J = 5.7 Hz, 1H), 7.13-7.44 (m, 7H), 7.83 (d, J = 8.1 Hz, 1H), 7.94 (t, J = 9.0 Hz, 2H), 8.49 (s, 1H). ^{13}C NMR (75 MHz, $CDCl_3$) δ 25.1, 55.9, 56.1, 56.8, 84.0, 100.2, 113.7, 120.0, 123.7, 124.9, 126.0, 126.1, 126.4, 126.6, 127.6, 127.8, 128.8, 129.1, 129.6, 130.6, 134.6, 136.0, 139.5, 155.4, 156.9. HRMS Calcd for $C_{29}H_{31}BO_5Na$ (MNa^+): 493.2162. Found: 493.2162. m.p. 73-74 ^{0}C. $[\alpha]_D$ = -55.441 (c = 0.43, $CHCl_3$).

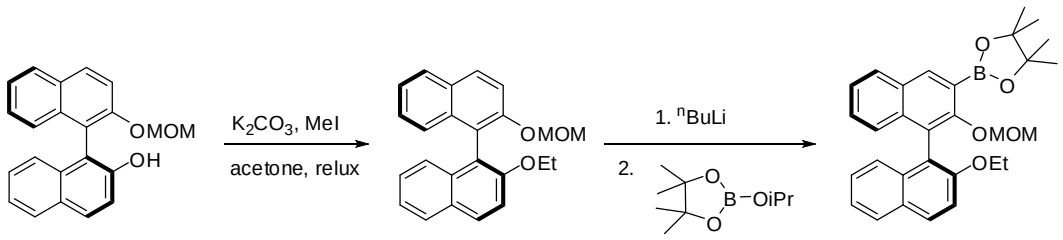

Preparation of (S)-2-ethoxy-2'-(methoxymethoxy)-1,1'-binaphthyl. To a 100 mL flask, (S)-2'-(methoxymethoxy)-1,1'-binaphthyl-2-ol (1.65g, 5 mmol), K_2CO_3 (1.04 g, 7.5 mmol) and 50 mL acetone were added. After the reaction mixture was stirred under reflux for 1 h, EtI (0.8 mL, 10 mmol) was added and the resulting mixture was stirred under relux overnight. When it cooled down, the reaction mixture was poured in to 100 mL water and extracted with CH_2Cl_2 (3 x 30 mL). The combined organic layer was washed with brine (30 mL) and dried over anhydrous Na_2SO_4. After evaporation of the solvent, the residue was purified by column chromatography on silica gel eluted with hexanes/ethyl acetate (15/1) to afford desired product as a white solid in 85% yield. ^{1}H NMR (300 MHz, $CDCl_3$) δ 1.17 (t, J = 6.9 Hz, 3H), 3.29 (s, 3H), 4.15 (m, 2H), 5.10 (d, J = 6.6 Hz, 1H), 5.20 (d, J = 6.6 Hz, 1H), 7.31-7.48 (m, 6H), 7.53 (d, J = 9.0 Hz, 1H), 7.73 (d, J = 9.0 Hz, 1H), 7.98 (d, J = 8.1 Hz, 2H), 8.05 (d, J = 9.0 Hz, 2H). ^{13}C NMR (75 MHz, $CDCl_3$) δ 15.4, 56.1, 65.4, 95.6, 116.0, 117.7, 120.7, 121.2, 124.0, 124.2, 124.3, 125.8, 126.0, 126.5, 126.7, 128.3, 129.6, 129.7, 130.3, 134.5, 134.6, 153.1, 154.7. HRMS Calcd for $C_{24}H_{22}O_3Na$ (MNa^+): 381.1467. Found: 381.1473. m.p. 62 ^{0}C. $[\alpha]_D$ = -76.367 (c = 0.29, $CHCl_3$).

Preparation of (S)-2-(2'-ethoxy-2-(methoxymethoxy)-1,1'-binaphthyl-3-yl)-

4,4,5,5-tetra-methyl-1,3,2-dioxaborolane. Under nitrogen (S)-2-ethoxy-2'-(methoxymethoxy)-1,1'-binaphthyl (1.20 g, 3.5 mmol) was dissolved in 30 mL ether and cooled to 0℃. nBuLi (2.5 M, 1.27 mL, 3.2 mmol) was added dropwise and the reaction mixture was allow to warm to room temperature over 3 h. Then the reaction mixture was cooled to The reaction mixture was cooled to -78 ℃ and 2-isopropoxy-4,4,5,5-tetramethyl-1,3,2-dioxaborolane (0.81 mL, 4.0 mmol) was added. The mixture was allowed to warm to room temperature and stirred for overnight. The generated salts were removed by filtration through a Buchner funnel and rinsed with CH_2Cl_2. The combined organic layer was concentrated and purified by flash chromatography on silica gel eluted with hexanes/ethyl acetate (10/1) to afford desired product as a white solid in 82% yield. ^{1}H NMR (300 MHz, $CDCl_3$) δ 1.03 (td, J1 = 6.9 Hz, J2 = 3.6 Hz, 3H), 1.41 (d, J = 3.6, 12H), 2.45 (d, J = 4.2 Hz, 3H), 4.15 (m, 2H), 4.86 (dd, J1 = 5.4 Hz, J2 = 3.9 Hz, 1H), 5.20 (dd, J1 = 6.0 Hz, J2 = 3.9 Hz, 1H), 7.16-7.42 (m, 7H), 7.82 (dd, J1 = 8.1 Hz, J2 = 3.3 Hz, 1H), 7.93 (dd, J1 = 8.7 Hz, J2 = 3.6 Hz, 2H), 8.48 (d, J = 3.9 Hz, 2H). ^{13}C NMR (75 MHz, $CDCl_3$) δ 15.2, 25.1, 25.2, 56.1, 65.2, 84.0, 100.2, 115.3, 120.8, 123.7, 124.8, 125.8, 126.1, 126.2, 126.5, 127.4, 127.7, 128.7, 129.2, 129.5, 130.6, 134.6, 136.0, 139.2, 154.8, 156.9. HRMS Calcd for $C_{30}H_{33}BO_5Na$ (MNa^+): 507.2319. Found: 507.2318. m.p. 64 ^{0}C. $[\alpha]_D$ = -77.764 (c = 0.34, $CHCl_3$).

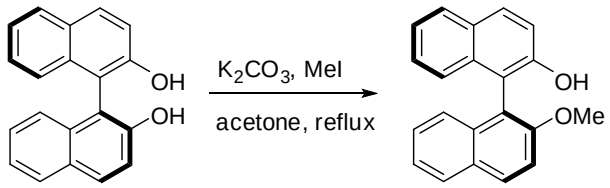

Preparation of (S)-2'-methoxy-1,1'-binaphthyl-2-ol. To a 100 mL flask, (S)-BINOL (1.44 g, 5.0 mmol), K_2CO_3 (0.76 g, 5.5 mmol) and 50 mL acetone were added. After the reaction mixture was stirred under reflux for 2 h, MeI (0.374 mL, 6.0 mmol) was added and the resulting mixture was stirred under reflux overnight. When it cooled down, the reaction mixture was poured in to 100 mL water and extracted with CH_2Cl_2 (3 x 30 mL). The combined organic layer was washed with brine (30 mL) and dried over anhydrous Na_2SO_4. After evaporation of the solvent, the residue was purified by column chromatography on silica gel eluted with hexanes/CH_2Cl_2 (2/1) to afford desired product as a white solid in 79% yield. ^{1}H NMR (300 MHz, $CDCl_3$) δ 3.81 (s, 3H), 4.91 (s, 1H), 7.05 (d, J = 9.0 Hz, 1H), 7.16-7.41 (m, 6H), 7.49 (d, 1H, 9.3 Hz), 7.85-7.92, (m, 3H), 7.86 (d, J = 9.0Hz, 1H).

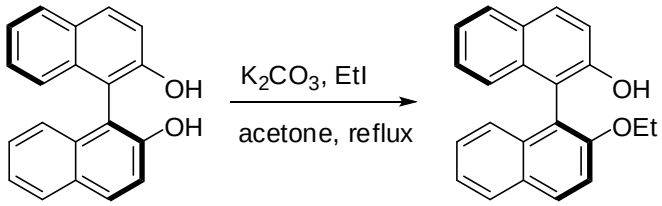

Preparation of (S)-2'-ethoxy-1,1'-binaphthyl-2-ol. To a 100 mL flask, (S)-BINOL (1.44 g, 5.0 mmol), K_2CO_3 (1.04 g, 7.5 mmol) and 50 mL acetone were added. After the reaction mixture was stirred under reflux for 2 h, EtI (0.60 mL, 7.5 mmol) was added and the resulting mixture was stirred under reflux overnight. When it cooled down, the

reaction mixture was poured in to 100 mL water and extracted with CH_2Cl_2 (3 x 30 mL). The combined organic layer was washed with brine (30 mL) and dried over anhydrous Na_2SO_4. After evaporation of the solvent, the residue was purified by column chromatography on silica gel eluted with hexanes/ethyl acetate (15/1) to afford desired product as a white solid in 83% yield. ^{1}H NMR (300 MHz, $CDCl_3$) δ 1.11 (t, J = 6.9 Hz, 3H), 4.01-4.16 (m, 2H), 4.97 (s, 1H), 7.07 (d, J = 8.4 Hz, 1H), 7.17-7.40 (m, 6H), 7.46 (d, J = 9.0 Hz, 1H), 7.85-7.92 (m, 3H), 8.02 (d, J = 9.0 Hz, 1H).

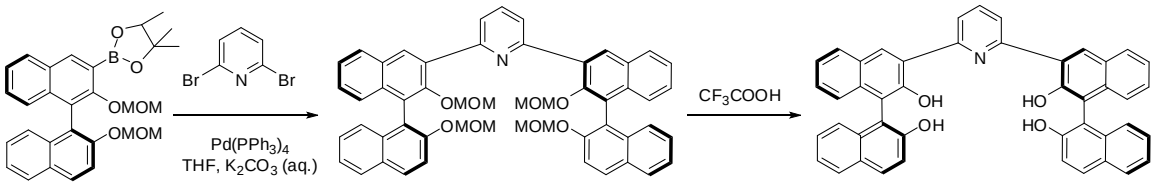

Preparation of 2,6-bis((S)-2,2'-bis(methoxymethoxy)-1,1'-binaphthyl-3-yl)pyridine. Under nitrogen, to a 100 mL flame-dried Schlenk flask was loaded (S)-2-(2,2'-bis(methoxymethoxy)-1,1'-binaphthyl-3-yl)-4,4,5,5-tetramethyl-1,3,2-dioxabo rolane (1.0 g, 2.0 mmol), 2,6-dibromopyridine (189.5 mg, 0.8 mmol), $Pd(PPh_3)_4$ (92 mg, 0.08 mmol). Degassed THF (10 mL) and 2M K_2CO_3 (10 mL) were transferred into the flask via cannula. The reaction mixture was stirred under reflux for overnight. After it cooled to room temperature, the organic layer was separated and the aqueous layer was extracted with CH_2Cl_2 (3 x 30 mL). The combined organic layer was washed with brine (30 mL) and dried over anhydrous Na_2SO_4. After evaporation of the solvent, the residue was purified by column chromatography on silica gel eluted with hexanes/ethyl acetate

(6/1) to afford desired product as a white solid in 88% yield. ^{1}H NMR (300 MHz, $CDCl_3$) δ 2.51 (s, 6H), 3.29 (s, 6H), 4.59 (d, J = 6.0 Hz, 2H), 4.61 (d, J = 6.0 Hz, 2H), 5.14 (d, J = 6.9 Hz, 2H), 5.23 (d, J = 6.9 Hz, 2H), 7.32-7.50 (m, 12H), 7.69 (d, J = 9.0 Hz, 2H), 7.85-7.94 (m, 3H), 8.01-8.05 (m, 4H), 8.11 (d, J = 8.1 Hz, 2H), 8.66 (s, 2H). ^{13}C NMR (75 MHz, $CDCl_3$) δ56.3, 56.5, 95.3, 99.5, 116.9, 121.3, 124.1, 124.5, 125.6, 126.1, 126.85, 126.95, 127.0, 128.2, 129.0, 130.0, 130.1, 131.5, 131.8, 134.4, 134.5, 134.8, 136.2, 151.1, 153.3, 157.0. HRMS Calcd for $C_{53}H_{46}NO_8$ (MH^+): 824.3223. Found: 824.3228. m.p. 110 ^{0}C. $[\alpha]_D$ = -98.860 (c = 0.275, $CHCl_3$).

Preparation of (1S,1''S)-3,3'-(pyridine-2,6-diyl)di-1,1'-bibenzobenzene-2,2'-diol. Under nitrogen, 2,6-bis((S)-2,2'-bis(methoxymethoxy)-1,1'-binaphthyl-3-yl)pyridine (576.8 mg, 0.7 mmol) was dissolved in 10 ml CH_2Cl_2 and trifluoroacetic acid (1.0 mL) was added. After the reaction mixture was stirred at room temperature of 2 h, saturated $NaHCO_3$ (aq.) was added to adjust the pH to 8. Then the mixture was extracted with CH_2Cl_2 (3 x 30 mL) washed with brine (30 mL) and dried over anhydrous Na_2SO_4. After evaporation of the solvent, the residue was purified by column chromatography on silica gel eluted with hexanes/ethyl acetate (2/1) to afford desired product as a light yellow solid in 97% yield. ^{1}H NMR (300 MHz, $CDCl_3$) δ 7.11-7.37 (m, 14H), 7.86 (d, J = 8.1 Hz, 2H), 7.92 (d, J = 9.0 Hz, 4H), 8.00-8.08 (m, 3H), 8.46 (s, 2H). ^{13}C NMR (300 MHz, $CDCl_3$) δ 113.2, 113.6, 118.0, 121.8, 123.9, 124.4, 124.6, 124.8, 127.3, 128.5, 128.7, 129.3, 129.6, 130.7, 131.0, 133.7, 134.7, 138.5, 152.4, 152.9, 155.4. HRMS Calcd for

$C_{45}H_{30}NO_4$ (MH^+): 648.2175. Found: 648.2175. m.p. 225 ^{0}C. $[\alpha]_D$ = -194.4 (c = 0.355, $CHCl_3$).

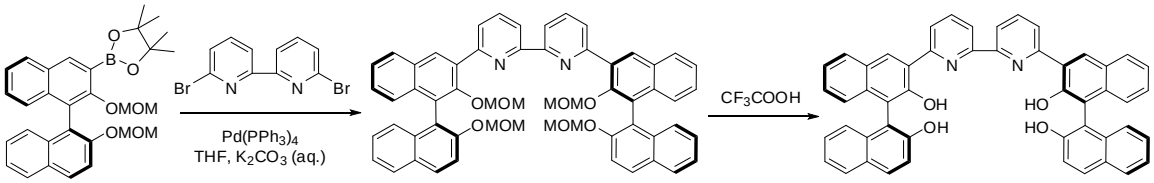

Preparation of 6,6'-bis((S)-2,2'-bis(methoxymethoxy)-1,1'-binaphthyl-3-yl)-2,2'-bipyridine. Under nitrogen, to a 100 mL flame-dried Schlenk flask was loaded (S)-2-(2,2'-bis(methoxymethoxy)-1,1'-binaphthyl-3-yl)-4,4,5,5-tetramethyl-1,3,2-dioxaborolane (1.0 g, 2.0 mmol), 6,6'-dibromo-2,2'-bipyridine (250 mg, 0.8 mmol), $Pd(PPh_3)_4$ (92 mg, 0.08 mmol). Degassed THF (10 mL) and 2M K_2CO_3 (10 mL) were transferred into the flask via cannula. The reaction mixture was stirred under reflux for overnight. After it cooled to room temperature, the organic layer was separated and the aqueous layer was extracted with CH_2Cl_2 (3 x 30 mL). The combined organic layer was washed with brine (30 mL) and dried over anhydrous Na_2SO_4. After evaporation of the solvent, the residue was purified by column chromatography on silica gel eluted with hexanes/ethyl acetate (6/1) to afford desired product as a white solid in 90% yield. ^{1}H NMR (300 MHz, $CDCl_3$) δ 2.41 (s, 3H), 3.26 (s, 3H), 4.49 (dd, J1 = 5.4 Hz, J2 = 1.2 Hz, 2H), 4.52 (dd, J1 = 5.4 Hz, J2 = 1.2 Hz, 2H), 5.10 (dd, J1 = 6.9 Hz, J2 = 0.9 Hz, 2H), 5.19 (dd, J1 = 6.9 Hz, J2 = 0.9 Hz, 2H), 7.24-7.48 (m, 12H), 7.63 (dd, J1 = 9.0 Hz, J2 = 0.9 Hz, 2H), 7.87-8.06 (m, 10H), 8.54 (s, 2H), 8.68 (d, J = 7.8 Hz, 2H). ^{13}C NMR (300 MHz, $CDCl_3$) δ 56.2, 56.4, 95.2,

99.5, 116.8, 119.9, 121.2, 124.4, 125.5, 125.6, 126.0, 126.1, 126.8, 126.9, 128.1, 128.9, 129.9, 130.0, 131.3, 131.7, 134.3, 134.4, 134.6, 137.2, 151.2, 153.2, 156.2, 156.5. HRMS Calcd for $C_{58}H_{49}N_2O_8$ (MH^+): 901.3489. Found: 901.3484. m.p. 113-115 ^{0}C. $[\alpha]_D$ = -108.80 (c = 0.365, $CHCl_3$).

Preparation of (1S,1''S)-3,3'-(2,2'-bipyridine-6,6'-diyl)di-1,1'-bibenzobenzene-2,2'-diol. Under nitrogen, 6,6'-bis((S)-2,2'-bis(methoxymethoxy)-1,1'-binaphthyl-3-yl)-2,2'-bipyridine (630.7 mg, 0.7 mmol) was dissolved in 10 ml CH_2Cl_2 and trifluoroacetic acid (0.5 mL) was added. After the reaction mixture was stirred at room temperature for overnight, the solvent was evaporated and saturated $NaHCO_3$ (aq.) was added. Then the mixture was filtered and the residue was washed with water, methanol and CH_2Cl_2 to afford desired product as a yellow solid in 95% yield. ^{1}H NMR (300 MHz, $(CD)_2SO$) δ 6.95 (d, J = 7.8 Hz, 2H), 7.02 (d, J = 8.4 Hz, 2H), 7.15-7.39 (m, 10H), 7.90 (t, J = 7.8 Hz, 4H), 8.02 (t, J = 8.4 Hz, 4H), 8.29 (t, J = 8.1 Hz, 2H), 8.67 (d, J = 8.4 Hz, 2H), 8.93 (s, 2H), 9.31 (s, 2H). ^{13}C NMR (75 MHz, $(CD)_2SO$) δ 115.9, 118.4, 119.3, 120.3, 121.6, 122.8, 123.1, 123.8, 124.8, 125.0, 126.8,, 128.1, 128.2, 128.6, 128.8, 128.9, 129.5, 129.7, 134.7, 135.6, 141.2, 151.9, 153.7, 154.6, 158.0. HRMS Calcd for $C_{50}H_{33}N_2O_4$ (MH^+): 725.2440. Found: 725.2437. m.p. higher than 400 ^{0}C. $[\alpha]_D$ = -301.13 (c = 0.355, DMSO).

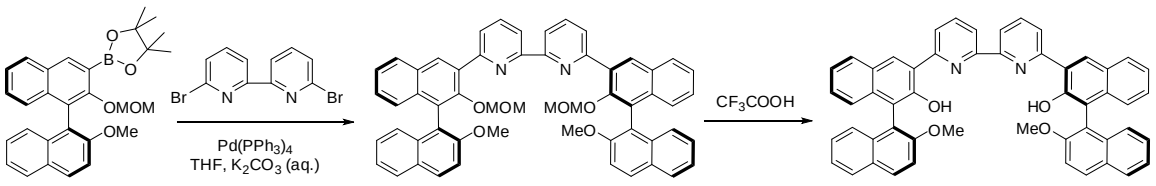

Preparation of 6,6'-bis((S)-2'-methoxy-2-(methoxymethoxy)-1,1'-binaphthyl-3-yl)-2,2'-bipyridine. Under nitrogen, to a 50 mL flame-dried Schlenk flask was loaded (S)-2-(2'-methoxy-2-(methoxymethoxy)-1,1'-binaphthyl-3-yl)-4,4,5,5-tetramethyl-1,3,2-dioxaborolane (706 mg, 1.5 mmol), 6,6'-dibromo-2,2'-bipyridine (188 mg, 0.6 mmol), $Pd(PPh_3)_4$ (69 mg, 0.06 mmol). Degassed THF (8 mL) and 2M K_2CO_3 (8 mL) were transferred into the flask via cannula. The reaction mixture was stirred under reflux for overnight. After it cooled to room temperature, the organic layer was separated and the aqueous layer was extracted with CH_2Cl_2 (3 x 30 mL). The combined organic layer was washed with brine (30 mL) and dried over anhydrous Na_2SO_4. After evaporation of the solvent, the residue was recrystallized with hexanes/ethyl acetate (1/1) to afford desired product as a white solid in 71% yield. ^{1}H NMR (300 MHz, $CDCl_3$) δ 2.44 (s, 6H), 3.85 (s, 6H), 4.47 (d, J = 5.4 Hz, 2H), 4.54 (d, J = 5.4 Hz, 2H), 7.21-7.38 (m, 10H), 7.43-7.50 (m, 4H), 7.87-8.01 (m, 10H), 8.52 (s, 2H), 8.68 (d, J = 7.8 Hz, 2H). ^{13}C NMR (75 MHz, $CDCl_3$) δ 56.5, 56.9, 99.5, 113.9, 119.9, 123.9, 125.4, 125.7, 126.0, 126.8, 126.9, 128.1, 128.9, 129.3, 130.1, 131.3, 131.6, 134.3, 134.4, 134.7, 137.1, 151.2, 155.4, 156.3, 156.4. HRMS Calcd for $C_{56}H_{45}N_2O_6$ (MH^+): 841.4278. Found: 841.3282. m.p. 242 ^{0}C. $[\alpha]_D$ = -106.99(c = 0.175, $CHCl_3$).

Preparation of (1S,1''S)-3,3'-(2,2'-bipyridine-6,6'-diyl)bis(2'-methoxy-1,1'-bibenzobenzen-2-ol). Under nitrogen, 6,6'-bis((S)-2'-methoxy-2-(methoxymethoxy)-1,1'-binaphthyl-3-yl)-2,2'-bipyridine (251.7 mg, 0.3 mmol) was dissolved in 10 ml CH_2Cl_2

and trifluoroacetic acid (0.1 mL) was added. After the reaction mixture was stirred at room temperature for overnight, saturated NaHCO3 (aq.) was added to adjust the pH to 8. Then the mixture was extracted with CH_2Cl_2 (3 x 30 mL) washed with brine (30 mL) and dried over anhydrous Na_2SO_4. After evaporation of the solvent, the residue was recrystallized with CH_2Cl_2/ hexanes to afford desired product as a light yellow solid in 99% yield. ^{1}H NMR (300 MHz, $(CD_3)_2SO$) δ 3.71 (s, 6H), 6.85 (d, J = 8.1 Hz, 2H), 7.05 (d, J = 8.4 Hz, 2H), 7.04-7.33 (m, 8H), 7.63 (d, J = 9.3 Hz, 2H), 7.95-8.02 (m, 4H), 8.10 (d, J = 9.0 Hz, 2H), 8.26 (t, J = 8.1 Hz, 2H), 8.64 (d, J = 8.1 Hz, 2H), 8.92 (s, 2H). HRMS Calcd for $C_{52}H_{37}N_2O_4$ (MH^+): 753.2753. Found: 753.2758. m.p. 354 ^{0}C. $[\alpha]_D$ = -286.63(c = 0.10, $CHCl_3$).

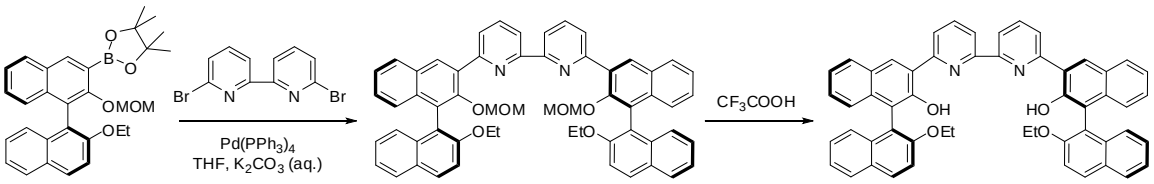

Preparation of 6,6'-bis((S)-2'-ethoxy-2-(methoxymethoxy)-1,1'-binaphthyl-3-yl)-2,2'-bipyridine. Under nitrogen, to a 50 mL flame-dried Schlenk flask was loaded (S)-2-(2'-ethoxy-2-(methoxymethoxy)-1,1'-binaphthyl-3-yl)-4,4,5,5-tetramethyl-1,3,2-dio xaborolane (727mg, 1.5 mmol), 6,6'-dibromo-2,2'-bipyridine (188 mg, 0.6 mmol), $Pd(PPh_3)_4$ (69 mg, 0.06 mmol). Degassed THF (8 mL) and 2M K_2CO_3 (8 mL) were transferred into the flask via cannula. The reaction mixture was stirred under reflux for overnight. After it cooled to room temperature, the organic layer was separated and the

aqueous layer was extracted with CH_2Cl_2 (3 x 30 mL). The combined organic layer was washed with brine (30 mL) and dried over anhydrous Na_2SO_4. After evaporation of the solvent, the residue was purified by column chromatography on silica gel eluted with hexanes/ethyl acetate (6/1) to afford desired product as a white solid in 89% yield. ^{1}H NMR (300 MHz, $CDCl_3$) δ 1.15 (t, J = 6.9 Hz, 6H), 2.44 (s, 6H), 4.06-4.23 (m, 4H), 4.46 (d, J = 5.4 Hz, 2H), 4.54 (d, J = 5.4 Hz, 2H), 7.26-7.48 (m, 14H), 7.86-8.06 (m, 10H), 8.55 (s, 2H), 8.69 (d, J = 7.8 Hz, 2H). ^{13}C NMR (75 MHz, $CDCl_3$) δ 15.4, 56.5, 65.3, 99.5, 115.4, 120.0, 120.4, 123.9, 125.3, 125.78, 125.83, 126.1, 126.8, 126.9, 128.1, 128.9, 129.3, 129.9, 131.3, 131.4, 134.3, 134.4, 134.6, 137.1, 151.2, 154.8, 156.3, 156.5. HRMS Calcd for $C_{58}H_{49}N_2O_6$ (MH^+): 869.3591. Found: 869.3591. m.p. 130 ^{0}C. $[\alpha]_D$ = -112.22(c = 1.05, $CHCl_3$).

Preparation of (1S,1''S)-3,3'-(2,2'-bipyridine-6,6'-diyl)bis(2'-ethoxy-1,1'-bibenzobenzen-2-ol). Under nitrogen, 6,6'-bis((S)-2'-ethoxy-2-(methoxymethoxy)-1,1'-binaphthyl-3-yl)-2,2'-bipyridine (286 mg, 0.33 mmol) was dissolved in 10 ml CH_2Cl_2 and trifluoroacetic acid (0.1 mL) was added. After the reaction mixture was stirred at room temperature for overnight, saturated $NaHCO_3$ (aq.) was added to adjust the pH to 8. Then the mixture was extracted with CH_2Cl_2 (3 x 30 mL) washed with brine (30 mL) and dried over anhydrous Na_2SO_4. After evaporation of the solvent, the residue the residue was purified by column chromatography on silica gel eluted with CH_2Cl_2 to afford desired product as a light yellow solid in 99% yield. ^{1}H NMR (300 MHz, $(CD)_2SO$) δ 0.95 (t, J =

6.9 Hz, 6H), 4.07 (q, J = 6.9 Hz, 4H), 6.90 (d, J = 8.4 Hz, 2H), 7.08 (d, J = 8.4 Hz, 2H), 7.20-7.35 (m, 8H), 7.62 (d, J = 8.7 Hz, 2H), 7.95-8.09 (m, 8H), 8.28 (t, J = 8.4 Hz, 2H), 8.66 (d, J = 7.8 Hz, 2H), 8.92 (s, 2H). ^{13}C NMR (75 MHz, $(CD)_2SO$) δ 15.5, 65.0, 116.6, 118.3, 120.1, 120.5, 121.5, 122.8, 123.8, 124.1, 124.6, 125.4, 127.0, 128.0, 128.2, 128.7, 129.0, 129.6, 129.7, 129.9, 134.2, 135.4, 141.2, 152.1, 154.3, 154.8, 158.0. HRMS Calcd for $C_{54}H_{41}N_2O_4$ (MH^+): 781.3066. Found: 781.3059. m.p. 210 ^{0}C. $[\alpha]_D$ = -298.15(c = 0.285, $CHCl_3$).

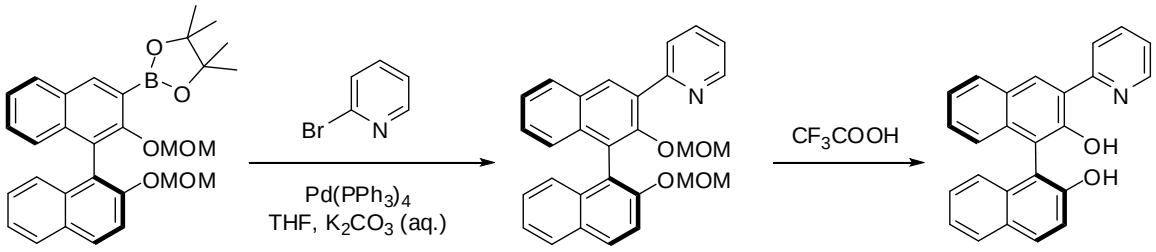

Preparation of (S)-2-(2,2'-bis(methoxymethoxy)-1,1'-binaphthyl-3-yl)pyridine. Under nitrogen, to a 50 mL flame-dried Schlenk flask was loaded (S)-2-(2,2'-bis(methoxymethoxy)-1,1'-binaphthyl-3-yl)-4,4,5,5-tetramethyl-1,3,2-dioxaborolane (438 mg, 0.875 mmol), 2-bromopyridine (67 μL, 0.7 mmol), $Pd(PPh_3)_4$ (40 mg, 0.035 mmol). Degassed THF (5 mL) and 2M K_2CO_3 (5 mL) were transferred into the flask via cannula. The reaction mixture was stirred under reflux for overnight. After it cooled to room temperature, the organic layer was separated and the aqueous layer was extracted with CH_2Cl_2 (3 x 30 mL). The combined organic layer was washed with brine (30 mL) and dried over anhydrous Na_2SO_4. After evaporation of the solvent, the residue

was purified by column chromatography on silica gel eluted with hexanes/ethyl acetate (6/1) to afford desired product as a white solid in 95% yield. ^{1}H NMR (300 MHz, $CDCl_3$) δ 2.45 (s, 3H), 3.24 (s, 3H), 4.47 (d, J = 5.4 Hz, 1H), 4.49 (d, J = 5.7 Hz, 1H), 5.11 (d, J = 6.9 Hz, 1H), 5.20 (d, J = 6.9 Hz, 1H), 7.26-7.47 (m, 7H), 7.65 (d, J = 9.3 Hz, 1H), 7.76 (td, J1 = 7.8 Hz, J2 = 1.5 Hz, 1H), 7.90 (d, J = 7.8 Hz, 2H), 7.98 -8.03 (m, 3H), 8.41 (s, 1H), 8.83 (d, J = 4.8 Hz, 1H). ^{13}C NMR (75 MHz, $CDCl_3$) δ 56.2, 56.4, 95.3, 99.4, 116.9, 121.3, 122.4, 124.5, 125.6, 125.7, 126.0, 126.1, 126.8, 126.9, 127.0, 128.1, 128.9, 130.0, 130.1, 131.3, 131.5, 134.3, 134.4, 134.5, 136.3, 150.0, 150.9, 153.2, 157.0. HRMS Calcd for $C_{29}H_{26}NO_4$ (MH^+): 452.1862. Found: 452.1873. m.p. 136 ^{0}C. $[\alpha]_D$ = -102.11(c = 0.36, $CHCl_3$).

Preparation of (S)-3-(pyridin-2-yl)-1,1'-binaphthyl-2,2'-diol. Under nitrogen, (S)-2-(2,2'-bis(methoxymethoxy)-1,1'-binaphthyl-3-yl)pyridine (149 mg, 0.33 mmol) was dissolved in 10 ml CH_2Cl_2 and trifluoroacetic acid (0.15 mL) was added. After the reaction mixture was stirred at room temperature for overnight, saturated NaHCO3 (aq.) was added to adjust the pH to 8. Then the mixture was extracted with CH_2Cl_2 (3 x 30 mL) washed with brine (30 mL) and dried over anhydrous Na_2SO_4. After evaporation of the solvent, the residue the residue was purified by column chromatography on silica gel eluted with hexanes/ethyl acetate (4/1) to afford desired product as a yellow solid in 90% yield. ^{1}H NMR (300 MHz, $CDCl_3$) δ 7.19-7.37 (m, 7H), 7.45 (d, J = 8.7 Hz, 1H), 7.82 (td, J1 = 8.4 Hz, J2 = 1.8 Hz, 1H), 7.90-7.97 (m, 3H), 8.15 (d, J = 8.1 Hz, 1H), 8.39 (d, J =

5.1 Hz, 1H), 8.52 (s, 1H). ^{13}C NMR (75 MHz, $CDCl_3$) δ 114.8, 115.7, 118.1, 120.5, 121.6, 122.8, 123.6, 124.1, 124.8, 125.3, 126.8, 128.0, 128.3, 128.5, 128.6, 129.3, 129.7, 130.1, 134.1, 135.5, 138.6, 146.1, 151.8, 156.1, 157.5. HRMS Calcd for $C_{25}H_{18}NO_2$ (MH^+): 364.1338. Found: 364.1342. m.p. 177 ^{0}C. $[\alpha]_D$ = -75.720 (c = 0.215, $CHCl_3$).

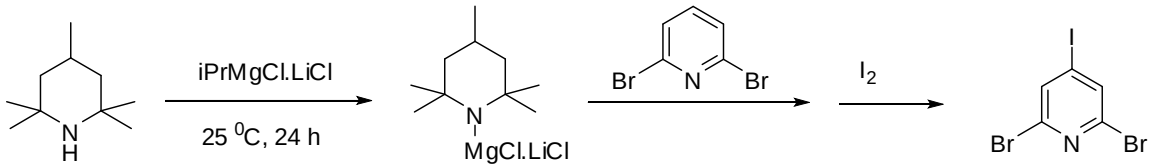

Preparation of 2,6-dibromo-4-iodopyridine. Under nitrogen to a flame-dried flask, *i*PrMgCl·LiCl (1.25 M, 21.4 mL, 26.7 mmol) was added. THF (26 mL) solution of 2,2,4,6,6-pentamethypiperdine (3.67 g, 26.0 mmol) was added dropwise. The mixture was stirred at room temperature for 24 h. Then the mixture was added to the 10 mL THF solution of 2,6-dibromopyridine (3.8 g, 16.0 mmol) via annula at -30^{0}C. After 1 h stirring, I_2 (5.1 g, 20.1 mmol) in THF (10 mL) was added to quench the reaction. The reaction mixture was washed with saturated $NaHSO_3$ (aq. 10 mL) and extracted with ethyl acetate (3 x 30 mL). The combined organic layer was washed with brine (30 mL) and dried over anhydrous Na_2SO_4. After evaporation of the solvent, the residue the residue was purified by column chromatography on silica gel eluted with hexanes/ethyl acetate (8/1) to afford desired product as a white solid in 82% yield. ^{1}H NMR (300 MHz, $CDCl_3$) δ 7.84 (s, 2H).

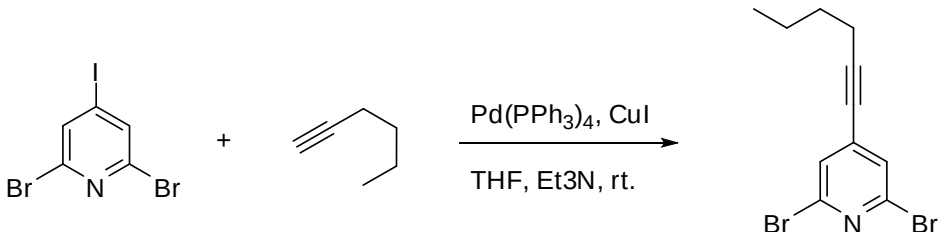

Preparation of 2,6-dibromo-4-(hex-1-ynyl)pyridine. Under nitrogen, to a 50 mL flame-dried Schlenk flask was loaded 2,6-dibromo-4-iodopyridine (363 mg, 2 mmol), $Pd(PPh_3)_4$ (231 mg, 0.02 mmol), CuI (38.2 mg, 0.2 mmol). Degassed THF (64 mL) and Et_3N (16 mL) were transferred into the flask via cannula. 1-Hexyne (290 μL, 2.4 mmol) was added with syringe. The reaction mixture was stirred at room temperature for 24 h. The organic layer was separated and the aqueous layer was extracted with ethyl acetate (3 x 30 mL). The combined organic layer was washed with brine (30 mL) and dried over anhydrous Na_2SO_4. After evaporation of the solvent, the residue was purified by column chromatography on silica gel eluted with hexanes/ethyl acetate (50/1) to afford desired product as colorless liquid in 72% yield. ^{1}H NMR (300 MHz, $CDCl_3$) δ 0.95 (t, J = 7.2 Hz, 3H), 1.39-1.51 (m, 2H), 1.52-1.63 (m, 2H), 2.42 (t, J = 7.2 Hz, 2H), 7.39 (s, 2H). ^{13}C NMR (75 MHz, $CDCl_3$) δ 13.8, 19.5, 22.3, 76.4, 99.9, 129.1, 137.0, 140.8. HRMS Calcd for $C_{11}H_{12}NBr_2$ (MH^+): 315.9336. Found: 315.9344.

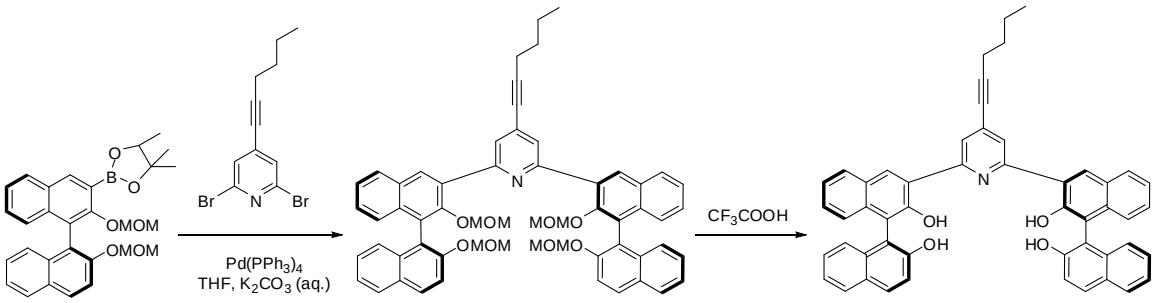

Preparation of 2,6-bis((S)-2,2'-bis(methoxymethoxy)-1,1'-binaphthyl-3-yl)-4-(hex-1-ynyl)pyridine. Under nitrogen, to a 50 mL flame-dried Schlenk flask was loaded (S)-2-(2,2'-bis(methoxymethoxy)-1,1'-binaphthyl-3-yl)-4,4,5,5-tetramethyl-1,3,2-dioxabo

rolane (438 mg, 0.875 mmol), 2,6-dibromo-4-(hex-1-ynyl)pyridine (110.7 mg, 0.35 mmol), $Pd(PPh_3)_4$ (40 mg, 0.035 mmol). Degassed THF (7 mL) and 2M K_2CO_3 (7 mL) were transferred into the flask via cannula. The reaction mixture was stirred under reflux for overnight. After it cooled to room temperature, the organic layer was separated and the aqueous layer was extracted with CH_2Cl_2 (3 x 30 mL). The combined organic layer was washed with brine (30 mL) and dried over anhydrous Na_2SO_4. After evaporation of the solvent, the residue was purified by column chromatography on silica gel eluted with hexanes/ethyl acetate (6/1) to afford desired product as a white solid in 86% yield. ^{1}H NMR (300 MHz, $CDCl_3$) δ 1.02 (t, J = 7.2 Hz, 3H), 1,49-1.59 (m, 2H), 1.64-1.73 (m, 2H), 2.51 (t, J = 6.9 Hz, 2H), 2.60 (s, 6H), 3.27 (s, 6H), 4.65 (d, J = 5.1 Hz, 2H), 4.70 (d, J = 5.1 Hz, 2H), 5.13 (d, J = 6.6 Hz, 2H), 5.25 (d, J = 6.6 Hz, 2H), 7.34-7.49 (m, 12H), 7.69 (d, J = 8.7 Hz, 2H), 7.93 (d, J = 8.4 Hz, 2H), 8.01-8.12 (m, 6H), 8.66 (s, 2H). ^{13}C NMR (75 MHz, $CDCl_3$) δ 14.0, 19.6, 22.4, 30.8, 56.3, 56.6, 77.7, 79.4, 95.3, 95.8, 99.8, 117.0, 121.4, 124.5, 125.6, 126.1, 126.9, 127.0, 127.1, 128.2, 129.0, 130.0, 130.1, 131.4, 131.8, 132.6, 134.4, 151.4, 153.3, 157.0. HRMS Calcd for $C_{59}H_{54}NO_8$ (MH^+): 904.3849. Found: 904.3839. m.p. 120 ^{0}C. $[\alpha]_D$ = -135.14 (c = 0.325, $CHCl_3$).

Preparation of (1S,1''S)-3,3'-(4-(hex-1-ynyl)pyridine-2,6-diyl)di-1,1'-bibenzobenzene-2,2'-diol. Under nitrogen, 2,6-bis((S)-2,2'-bis(methoxymethoxy)-1,1'-binaphthyl-3-yl)-4-(hex-1-ynyl)pyridine (136 mg, 0.15 mmol) was dissolved in 10 ml CH_2Cl_2 and trifluoroacetic acid (0.15 mL) was added. After the reaction mixture was

stirred at room temperature for overnight, saturated NaHCO3 (aq.) was added to adjust the pH to 8. Then the mixture was extracted with CH_2Cl_2 (3 x 30 mL) washed with brine (30 mL) and dried over anhydrous Na_2SO_4. After evaporation of the solvent, the residue the residue was purified by column chromatography on silica gel eluted with hexanes/ethyl acetate (4/1) to afford desired product as an orange yellow solid in 91% yield. ^{1}H NMR (300 MHz, $CDCl_3$) δ 0.99 (t, J = 7.2 Hz, 3H), 1.46-1.58 (m, 2H), 1.61-1.70 (m, 2H), 2.49 (t, J = 7.2 Hz, 2H), 7.12 (t, J = 8.4 Hz, 4H), 7.20-7.39 (m, 10H), 7.84 (d, J = 7.8Hz, 2H), 7.90 (d, J = 8.7 Hz, 4H), 8.01 (s, 2H), 8.41 (s, 2H). ^{13}C NMR (150 MHz, $CDCl_3$) δ 13.8, 19.5, 22.3, 30.6, 78.8, 113.0, 114.0, 118.1, 123.8, 123.9, 124.4, 124.6, 124.7, 127.1, 128.4, 128.5, 128.6, 129.2, 129.5, 130.6, 130.8, 133.6, 134.8, 152.4. HRMS Calcd for $C_{51}H_{38}NO_4$ (MH^+): 728.2801. Found: 728.2791. m.p. 176 ^{0}C. $[\alpha]_D$ = -176.89 (c = 0.205, $CHCl_3$).

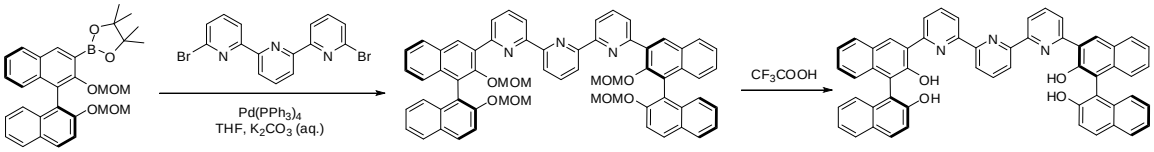

Preparation of 6,6'-bis((S)-2,2'-bis(methoxymethoxy)-1,1'-binaphthyl-3-yl)-2,2':6',2''-terpyridine. Under nitrogen, to a 50 mL flame-dried Schlenk flask was loaded (S)-2-(2,2'-bis(methoxymethoxy)-1,1'-binaphthyl-3-yl)-4,4,5,5-tetramethyl-1,3,2-dioxaborolane (750.6 mg, 1.5 mmol), 6,6''-dibromo-2,2':6',2''-terpyridine (234.6 mg, 0.6 mmol), $Pd(PPh_3)_4$ (57.8 mg, 0.05 mmol). Degassed THF (10 mL) and 2M K_2CO_3 (10 mL) were transferred into the flask via cannula. The reaction mixture was stirred under reflux for

overnight. After it cooled to room temperature, the organic layer was separated and the aqueous layer was extracted with CH_2Cl_2 (3 x 30 mL). The combined organic layer was washed with brine (30 mL) and dried over anhydrous Na_2SO_4. After evaporation of the solvent, the residue was purified by column chromatography on silica gel eluted with hexanes/ethyl acetate (3/1) to afford desired product as a white solid in 92% yield. ^{1}H NMR (600 MHz, $CDCl_3$) δ 2.42 (s, 6H), 3.27 (s, 6H), 4.50 (d, J = 5.4 Hz, 2H), 4.52 (d, J = 5.4 Hz, 2H), 5.19 (d, J = 7.2 Hz, 2H), 5.20 (d, J = 6.6 Hz, 2H), 7.27-7.35 (m, 8H), 7.37-7.40 (m, 2H), 7.45-7.47 (m, 2H), 7.64 (d, J = 9.0 Hz, 2H), 7.89 (d, J = 8.4 Hz, 2H), 7.94-8.00 (m, 4H), 8.03-8.06 (m, 5H), 8.55 (s, 2H), 8.93 (dd, J1 = 7.8Hz, J2 = 1.2 Hz, 2H), 8.77 (d, J = 7.8 Hz, 2H). ^{13}C NMR (150 MHz, $CDCl_3$) δ 56.2, 56.3, 95.1, 99.4, 116.7, 119.6, 121.1, 121.5, 124.3, 125.4, 125.6, 125.9, 126.0, 126.69, 126.73, 126.8, 128.0, 128.8, 129.8, 129.9, 131.6, 134.2, 134.3, 134.5, 137.0, 138.0, 151.0, 153.1, 155.6, 156.1, 156.3. HRMS Calcd for $C_{63}H_{52}N_3O_8$ (MH^+): 978.3754. Found: 978.3763. m.p. 146 ^{0}C. $[\alpha]_D$ = -92.583(c = 0.28, $CHCl_3$).

Preparation of (1S,1''S)-3,3'-(2,2':6',2"-terpyridine-6,6"-diyl)di-1,1'-bibenzobenzene-2,2'-diol. Under nitrogen, **6**,6'-bis((S)-2,2'-bis(methoxymethoxy)-1,1'-binaphthyl-3-yl)-2,2':6',2''-terpyridine (244 mg, 0.25 mmol) was dissolved in 10 ml CH_2Cl_2 and trifluoroacetic acid (0.3 mL) was added. After the reaction mixture was stirred at room temperature for overnight, saturated NaHCO3 (aq.) was added to adjust the pH to 8. Then the mixture was extracted with CH_2Cl_2 (3 x 30 mL) washed with brine

(30 mL) and dried over anhydrous Na_2SO_4. After evaporation of the solvent, the residue the residue was purified by column chromatography on silica gel eluted with CH_2Cl_2/methanol (50/1) to afford desired product as a yellow solid in 95% yield. ^1H NMR (600 MHz, $(CD_3)_2SO$) δ 9.99 (d, J = 8.4 Hz, 2H), 7.09 (d, J = 8.4 Hz, 2H), 7.18 (td, J1 = 7.8 Hz, J2 = 1.8 Hz, 2H), 7.23-7.31 (m, 6H), 7.38 (d, J = 9.0 Hz, 2H), 7.89-7.93 (m, 6H), 8.00 (d, J = 9.6 Hz, 2H), 8.02-8.05 (m, 3H), 8.46 (d, J = 7.8 Hz, 2H), 8.56 (d, J = 8.4 Hz, 2H), 8.89 (s, 2H), 9.29 (s, 2H), 14.62 (s, 2H). ^{13}C NMR (150 MHz, $(CD_3)_2SO$) δ 115.5, 117.7, 118.6, 120.3, 120.8, 120.9, 121.4, 122.4, 124.1, 124.5, 126.0, 127.4, 127.8, 127.9, 128.2, 128.7, 129.0, 134.1, 134.9, 139.7, 151.6, 153.0, 153.1, 154.4, 156.8. HRMS Calcd for $C_{55}H_{36}N_3O_4$ (MH^+): 802.2706. Found: 802.2714. m.p. 248 ^0C. $[\alpha]_D$ = -217.83 (c = 0.165, $CHCl_3$).

2. **Measurement of the Fluorescence Quautum Yield**

The fluorescence quantum yield of compounds was estimated by using a 2-aminopyridine solution in 0.1N H_2SO_4 (ϕ_F= 0.60) as the standard. The fluorescence spectra were recorded on a Horiba FluoroMax-4 spectrofluorometer. Excited wavelength was 290 nm. The excitation slit was set at 1.5 nm and the emission slit at 1.5 nm. The scan speed was set at 1.0 nm/s. After subtracting the solvent background signal and noise signals, the integration of the area under the fluorescence signal of the sensor was calculated from 300 nm to 550 nm. The UV spectra were recorded on a Hewlett-Packard 8452A diode-array spectrophotometer.

Following equation is applied to calculate the quantum yield:

$$\phi_F = \phi_{F,ref}\left(\frac{A_{ref}}{A}\right)\left(\frac{n_D}{n_{D,ref}}\right)^2\left(\frac{a}{a_{ref}}\right)$$

Wherein $\phi_{F,ref}$, A_{ref}, $n_{D,ref}$ and a_{ref} are the reference quantum yield, the reference absorbance, the refraction index of the solvent of the reference, and the integration of the area under the fluorescence signal of the reference, respectively. n_D of THF: 1.4242. $n_{D,ref}$ of 0.1 N sulfuric acid: 1.3330.

Table AI-1. Measurement of fluorescence quantum yield of (*S*)-**7-1** – (*S*)-**7-21**.

Sensor	*A*	*a*	ϕ_F
2-aminopyridine	0.086993	29644375.0000000	0.60
(*S*)-**7-1**	0.066947	2814137.0000000	0.082107
(*S*)-**7-2**	0.063777	1893047.0000000	0.057978
(*S*)-**7-4**	0.078642	3467837.0000000	0.086133
(*S*)-**7-5**	0.085512	17226787.0000000	0.3935
(*S*)-**7-6**	0.079736	16590987.0000000	0.406429
(*S*)-**7-7**	0.101477	17318687.0000000	0.333361
2-aminopyridine	0.097859	1.25497E8	0.60
(*S*)-**7-8**	0.107704	33507480.0000000	0.161739
(*S*)-**7-9**	0.092876	65505.6039700	0.000367
(*S*)-**7-10**	0.099376	31025980.0000000	0.162311
(*S*)-**7-11**	0.093656	29981180.0000000	0.166424
(*S*)-**7-12**	0.103518	34428480.0000000	0.172904
(*S*)-**7-13**	0.104049	17410.0044100	8.7E-05
(*S*)-**7-14**	0.087769	6552.0634100	3.88E-05
(*S*)-**7-15**	0.103434	13024.2522100	6.55E-05
(S)-**7-3**	0.07668	9058540.0000000	0.061416

2-aminopyridine	0.094995	127810657.0000000	0.60
(S)-**7-16**	0.097006	25793500.0000000	0.131543
(S)-**7-17**	0.086143	243608.0000000	0.001399
(S)-**7-18**	0.10428	72424800.0000000	0.343594
(S)-**7-19**	0.092089	572068.0000000	0.003073
(S)-**7-20**	0.085861	29730900.0000000	0.171306
(S)-**7-21**	0.10577	60393.0000000	0.000282

3. Measurement of Lifetime

Table AI-2. Fluorescence lifetime of (*S*)-**7-1** – (*S*)-**7-21**.

(*S*)-**7-1**	0.279 ns	
(*S*)-**7-2**	0.255 ns	
(*S*)-**7-3**	0.292 ns	
(*S*)-**7-4**	0.256 ns	
(*S*)-**7-5**	0.247 ns (97.42%)	5.6 ns (2.58%)
(*S*)-**7-6**	0.244 ns (97.26 %)	5.5 ns (2.74 %)
(*S*)-**7-7**	0.248 ns	
(*S*)-**7-8**	0.266 ns (92.24%)	4.09 ns (7.76%)
(*S*)-**7-9**	0.256 ns	
(*S*)-**7-10**	0.264 ns (91.14 %)	4.01 ns (8.86%)
(*S*)-**7-11**	0.272 ns (90.17%)	3.86 ns (9.83%)
(*S*)-**7-12**	0.271 ns (92.10%)	4.24 ns (7.90 %)
(*S*)-**7-13**	0.251 ns	
(*S*)-**7-14**	0.250 ns	
(*S*)-**7-15**	0.252 ns	
(S)-**7-16**	0.258 ns	
(S)-**7-17**	0.232 ns	
(S)-**7-18**	0.23 ns (94.43%)	3.63 ns (5.57%)
(S)-**7-19**	0.219 ns	
(S)-**7-20**	0.223 ns (94.86%)	4.15 s (5.14%)

4. UV-Vis Absorption of Compounds

Figure AI-1. UV-Vis absorption spectra of compounds ($1.0x10^{-5}$ M in THF).

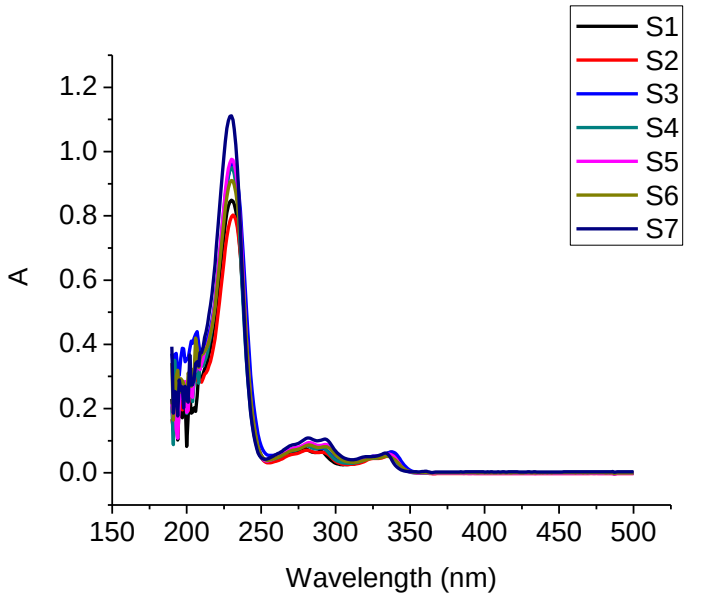

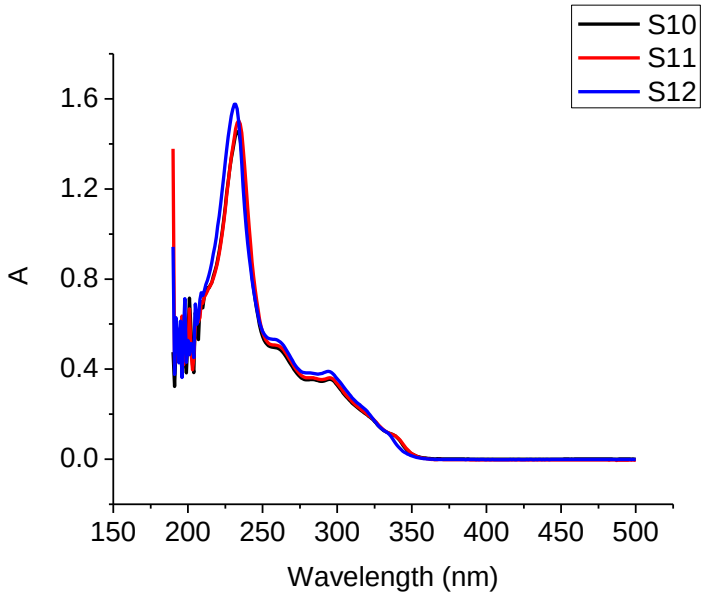

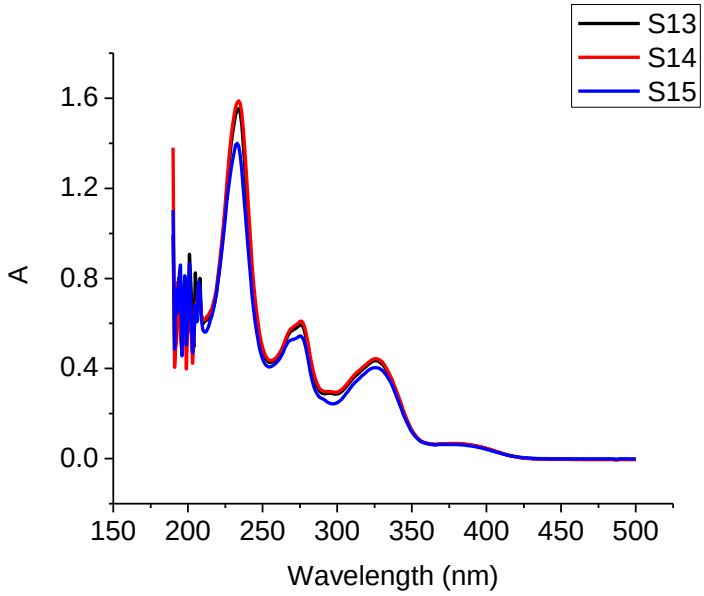
S13
S14
S15
A
1.6
1.2
0.8
0.4
0.0
150
200
250
300
350
400
450
500
Wavelength (nm)

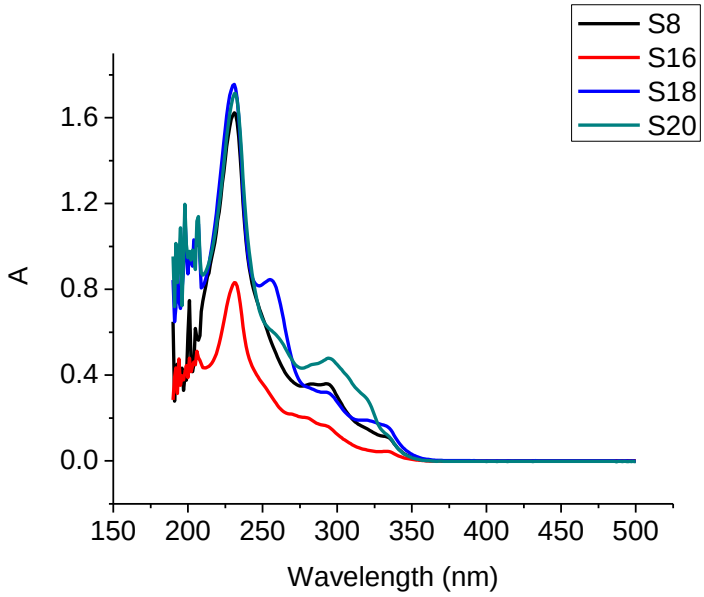
S8
S16
S18
S20
A
1.6
1.2
0.8
0.4
0.0
150
200
250
300
350
400
450
500
Wavelength (nm)

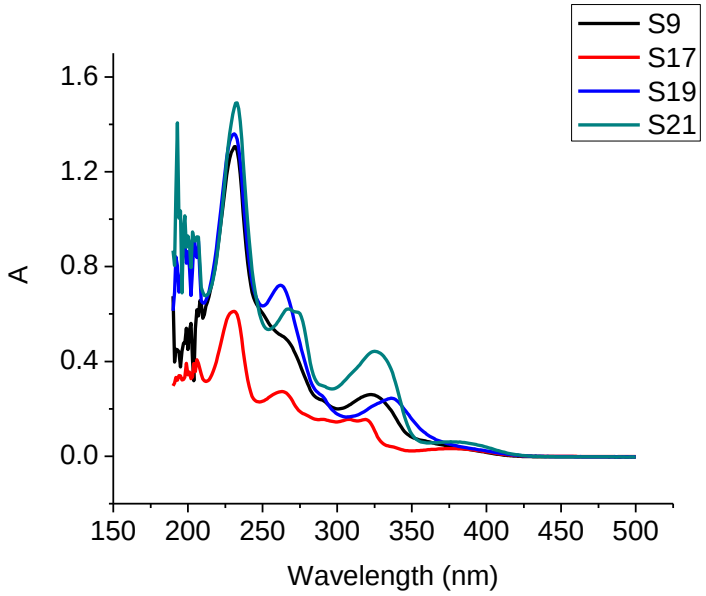

Table AI-3. Maximum absorption peaks and extinction coffecient of (S)-7-1 – (S)-7-21 ($1.0x10^{-5}$ M in THF).

	$\lambda_{max}(\varepsilon)$
(*S*)-**7-1**	230 ($8.5x10^4$), 279 ($7.6x10^3$), 290 ($6.7x10^3$), 325 ($4.7x10^3$), 337 ($6.5x10^3$) nm
(*S*)-**7-2**	231 ($8.0x10^4$), 281 ($7.1x10^3$), 291 ($6.4x10^3$), 326 ($4.5x10^3$), 338 ($5.9x10^3$) nm
(*S*)-**7-3**	231 ($9.6x10^4$), 280 ($8.6x10^3$), 291 ($7.7x10^3$), 326 ($5.2x10^3$), 338 ($6.5x10^3$) nm
(*S*)-**7-4**	230 ($9.5x10^4$), 280 ($8.5x10^3$), 291 ($7.9x10^3$), 326 ($4.6x10^3$), 336 ($5.7x10^3$) nm
(*S*)-**7-5**	230 ($9.8x10^4$), 282 ($9.4x10^3$), 293 ($8.8x10^3$), 325 ($5.1x10^3$), 335 ($5.9x10^3$) nm
(*S*)-**7-6**	230 ($9.1x10^4$), 282 ($8.7x10^3$), 293 ($8.2x10^3$), 325 ($4.6x10^3$), 334 ($5.2x10^3$) nm
(*S*)-**7-7**	230 ($1.1x10^5$), 282 ($1.1x10^4$), 293 ($1.1x10^4$), 323 ($5.1x10^3$), 333 ($6.1x10^3$) nm
(*S*)-**7-8**	231 ($1.6x10^5$), 293 ($3.6x10^4$), 334 ($1.1x10^4$) nm
(*S*)-**7-9**	231 ($1.3x10^5$), 268 ($4.8x10^4$), 323 ($2.6x10^4$) nm
(*S*)-**7-10**	233 ($1.5x10^5$), 261 ($4.9x10^4$), 297 ($3.5x10^4$) nm
(*S*)-**7-11**	234 ($1.5x10^5$), 262 ($5.0x10^4$), 297 ($3.6x10^4$) nm
(*S*)-**7-12**	231 ($1.6x10^5$), 261 ($5.2x10^4$), 295 ($3.9x10^4$) nm
(*S*)-**7-13**	234 ($1.6x10^5$), 276 ($5.9x10^4$), 326 ($4.3x10^4$), 386 ($6.3x10^3$) nm
(*S*)-**7-14**	234 ($1.6x10^5$), 276 ($6.1x10^4$), 326 ($4.4x10^4$), 386 ($6.4x10^3$) nm
(*S*)-**7-15**	233 ($1.4x10^5$), 275 ($5.4x10^4$), 326 ($4.0x10^4$), 386 ($6.0x10^3$) nm

(S)-**7-16**	231 ($8.3x10^4$), 278 ($2.0x10^4$), 294 ($1.6x10^4$), 333 ($4.5x10^3$) nm
(S)-**7-17**	230 ($6.1x10^4$), 263 ($2.7x10^4$), 308 ($1.6x10^4$), 319 ($1.5x10^4$), 376 ($3.2x10^3$) nm
(S)-**7-18**	231 ($1.8x10^5$), 255 ($8.5x10^4$), 293 ($3.2x10^4$), 332 ($1.7x10^4$) nm
(S)-**7-19**	231 ($1.4x10^5$), 262 ($7.2x10^4$), 336 ($2.4x10^4$) nm
(S)-**7-20**	231 ($1.7x10^5$), 295 ($4.8x10^4$) nm
(*S*)-**7-21**	233 ($1.5x10^5$), 267 ($6.2x10^4$), 325 ($4.4x10^4$), 386 ($5.7x10^3$) nm

5. Fluorescent Properties of Compounds

Figure AI-2. Fluorescence spectra of (S)-**7-1** – (S)-**7-21** ($1.0x10^{-5}$ M in THF). (λ_{exc} = 290 nm. slit = 1.5/1.5 nm).

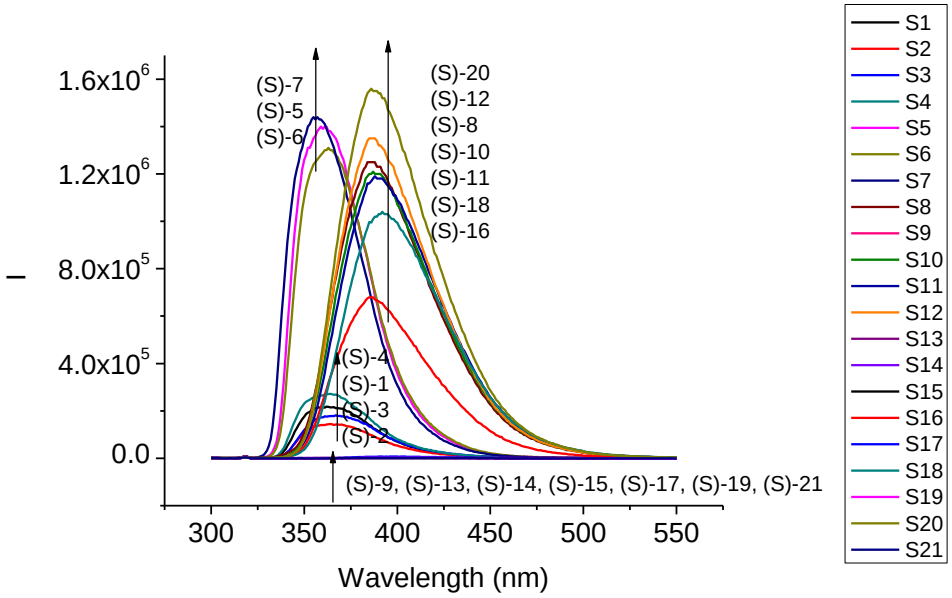

Figure AI-3. Fluorescence spectra of (S)-**7-1** – (S)-**7-21** ($1.0x10^{-5}$ M in THF). (λ_{exc} = 335 nm. slit = 1.5/1.5 nm).

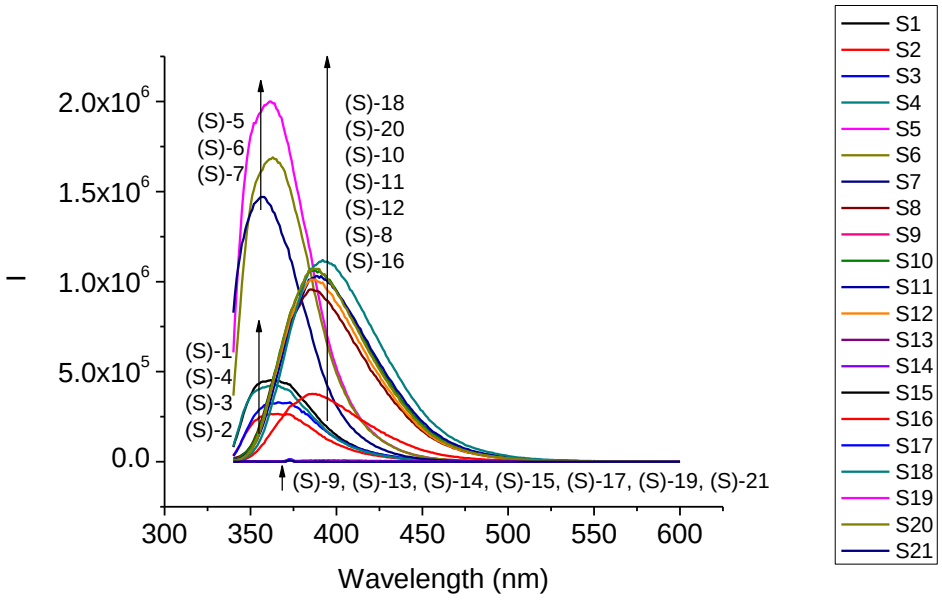

6. Interaction of (S)-7-1 with Pyridine and Bipyridine.

335 nm was used as the excitation wavelength because both pyridine and bipyridine have absorption at 290 nm. Pyridine has no absorption at all at 335 nm even when the concentration is as high as 7 M. Bipyridine started to show absorption at 335 nm when the concentration is higher than 0.01 M. When treated with pyridine, (S)-7-1 showed fluorescence quenching when the pyridine concentration was higher than 0.01 M. Bipyridine caused no change to the fluorescence of (S)-7-1 when its concentration was lower than 0.01 M.

Figure AI-4. UV absorption of pyridine (3.5 M, 7M in THF) and bipyridine (0.01, 0.05, 0.1, 0.2, 0.4, 0.8 M).

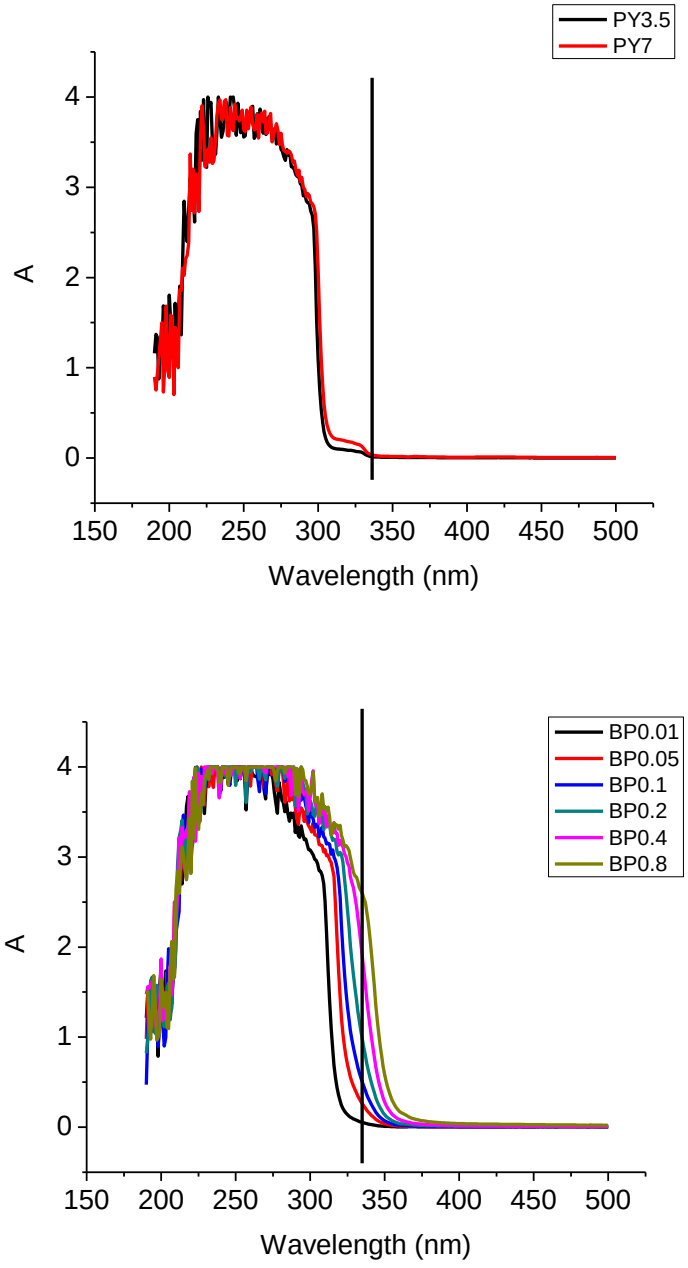

Figure AI-5. Fluorescence spectra of (S)-**7-1**($2.0x10^{-5}$ M in THF) in the presence of pyridine at various concentrations (2E-5, 2E-4, 0.001, 0.002, 0.005, 0.01, 0.02, 0.05, 0.1, 0.2, 0.3, 0.4, 0.5, 0.6, 0.7, 0.8, 0.9, 1, 2, 3, 4, 5, 6, 7M). (λ_{exc} = 335 nm. slit = 1.5/1.5 nm)

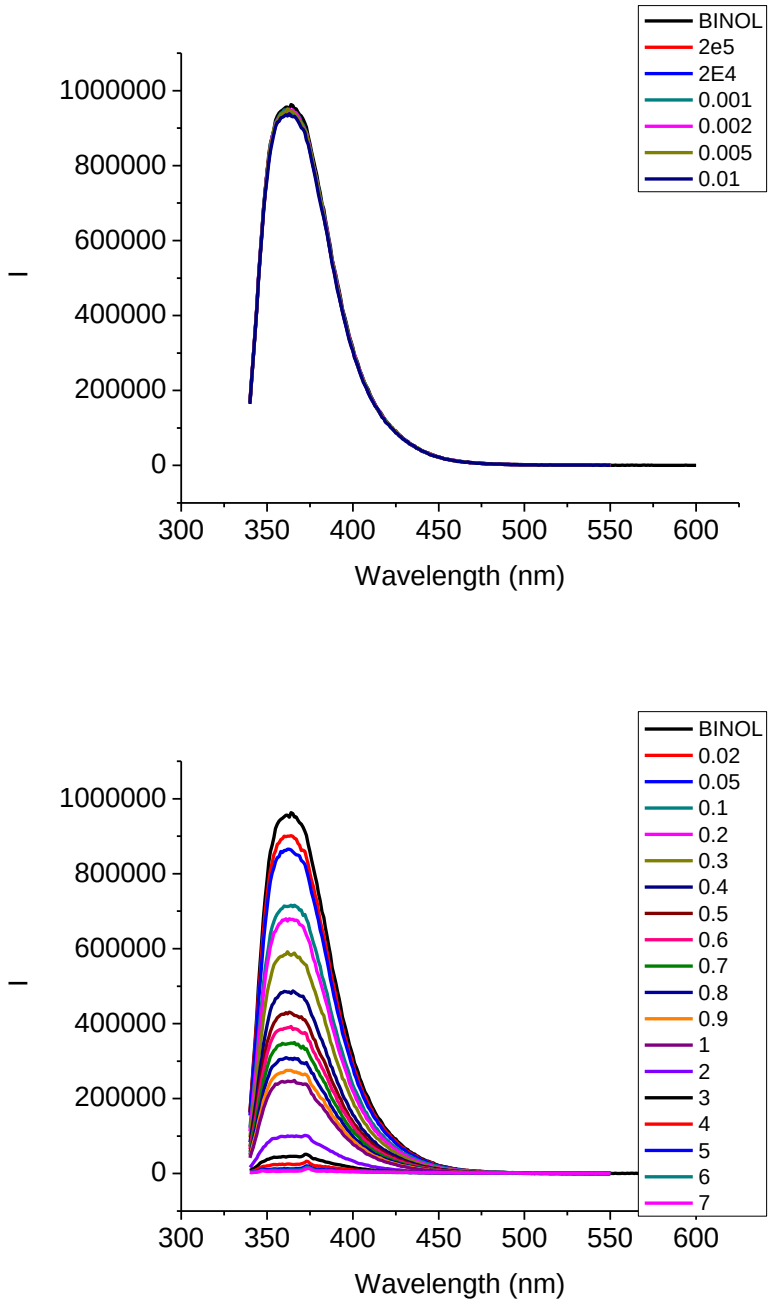

Figure AI-6. Fluorescence spectra of (S)-**7-1**($2.0x10^{-5}$ M in THF) in the presence of bipyridine at various concentrations (2E-5, 2E-4, 0.001, 0.002, 0.005, 0.01, 0.02, 0.05, 0.1, 0.2, 0.3, 0.4, 0.5, 0.6, 0.7, 0.8 M). (λ_{exc} = 335 nm. slit = 1.5/1.5 nm)

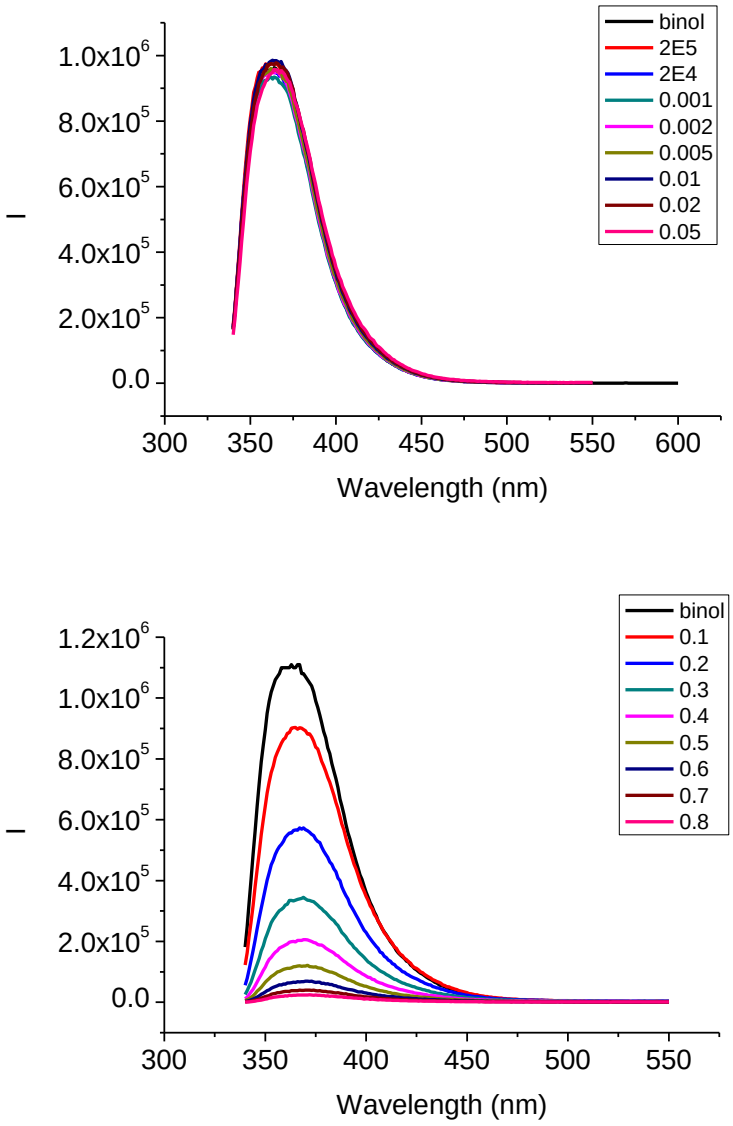

7. Preparation of Cu complex

Copper complex of BINOL-pyridine and BINOL-bipyridine compounds (S)-**7-10** – (S)-**7-15** were prepared by mixing (S)-**7-10** – (S)-**7-15** (0.5 mmol) and $CuCl_2 \cdot 2H_2O$ (0.6 mmol) in methanol (10 mL) at room temperature for about 0.5 h. The reaction was monitored by TLC. After the reaction was complete, the solution was concentrated and

water (2 mL) was added to generate precipitate. The solid was collected through filtration, washed with water (3x1 mL) and methanol (several drops) and then dried under vacuum.

Copper complex of BINOl-terpyridine compounds (S)-**7-20** and (S)-**7-21** were prepared at 70 ^{o}C.

8. pH effect

Figure AI-7. Fluorescence spectra of (S)-**7-9** (1×10^{-5} M in 5 mL THF) with addition of (a) 3M HCl or (b) 3M NaOH (1, 5, 10, 20, 50 μL). (λ_{exc} = 325 nm. slit = 5.0/5.0 nm)

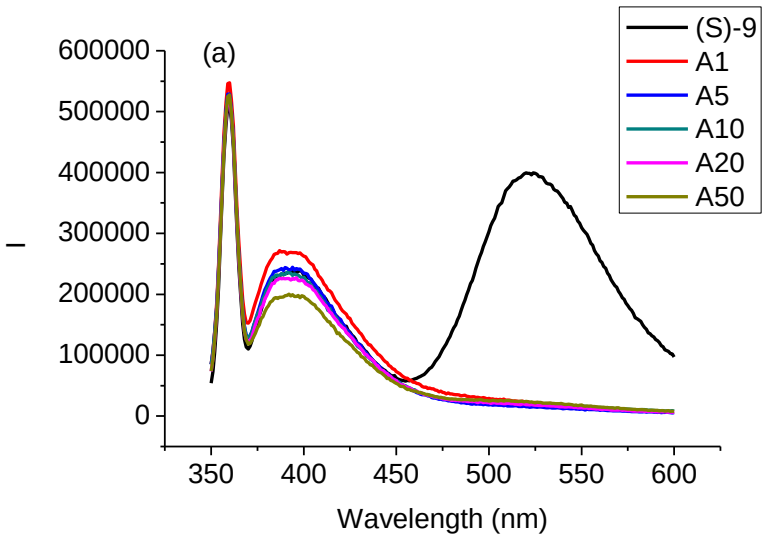

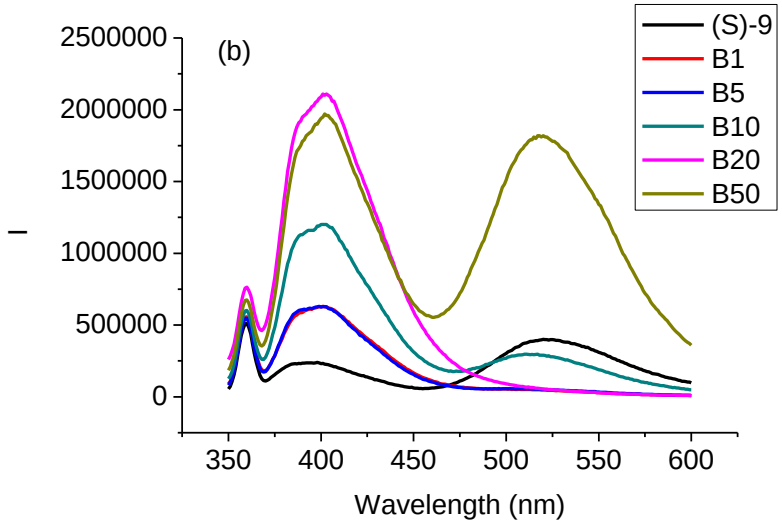

Figure AI-8. Fluorescence spectra of (S)-**7-9** (1×10^{-5} M in 5 mL THF/H_2O 5:1) with addition of 3M NaOH (1, 5, 10, 20μL). (λ_{exc} = 325 nm. slit = 3.0/3.0 nm)

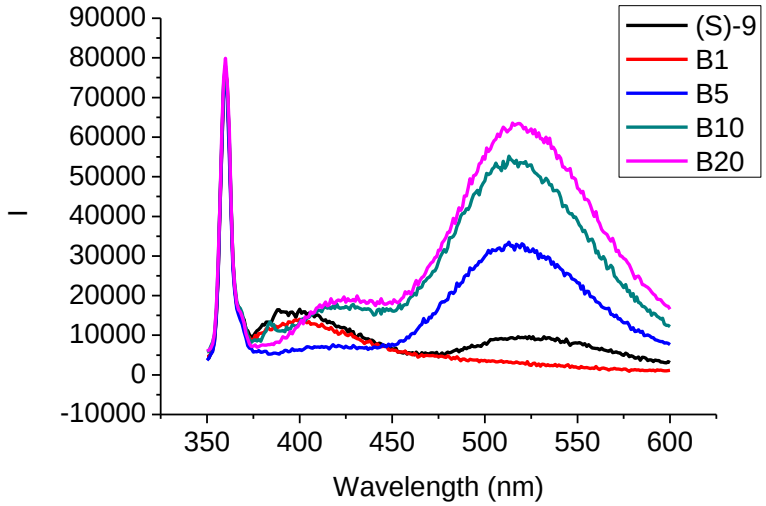

Figure AI-9. Fluorescence spectra of (S)-**7-15** (1×10^{-5} M in 5 mL DMF) with addition of (a) 3M HCl or (b) 3M NaOH (1, 5, 10, 20, 50 μL). (λ_{exc} = 325 nm. slit = 5.0/5.0 nm)

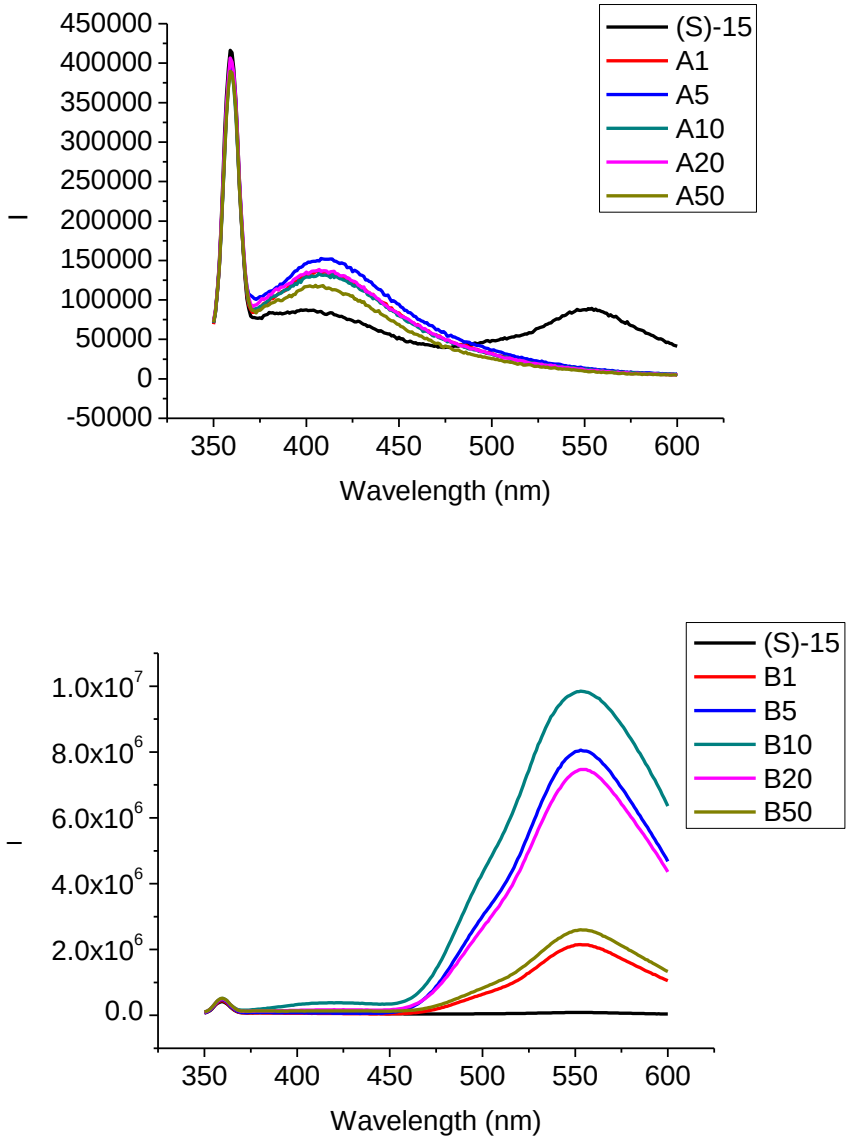

Figure AI-10. Fluorescence spectra of (S)-**7-15** (1×10^{-5} M in 5 mL THF/H_2O 5:1) with addition of 3M NaOH (1, 5, 10, 20μL). (λ_{exc} = 325 nm. slit = 3.0/3.0 nm)

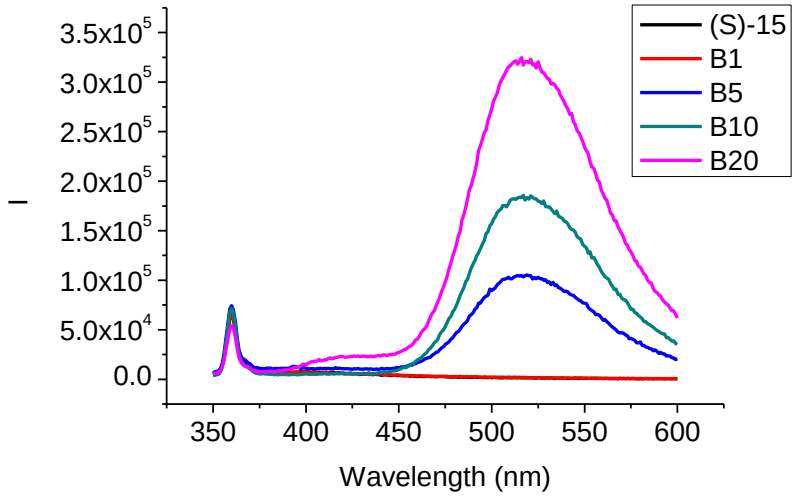

Figure AI-11. Fluorescence spectra of (S)-**7-13** (1×10^{-5} M in 5 mL THF) with addition of (a) 3M HCl or (b) 3M NaOH (1, 5, 10, 20, 50 μL). (λ_{exc} = 325 nm. slit = 5.0/5.0 nm)

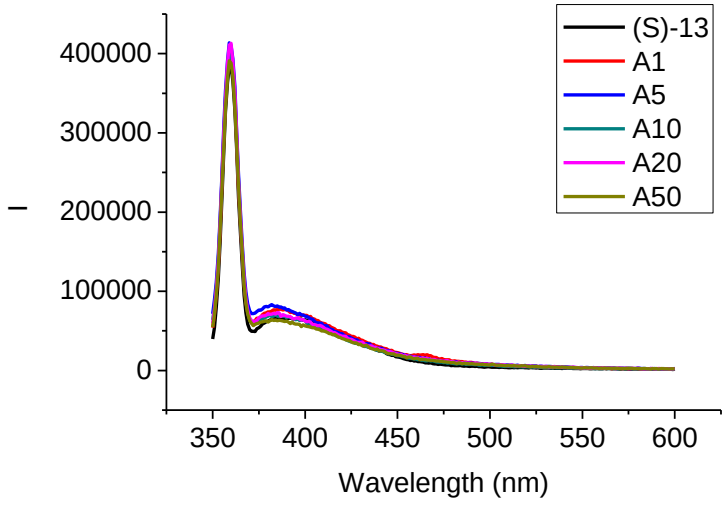

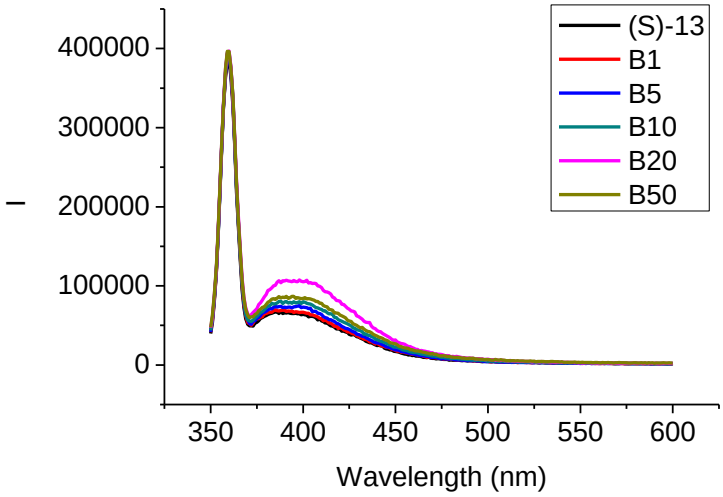

Figure AI-12. Fluorescence spectra of (S)-**7-14** (1×10^{-5} M in 5 mL THF) with addition of (a) 3M HCl or (b) 3M NaOH (1, 5, 10, 20, 50 μL). (λ_{exc} = 325 nm. slit = 5.0/5.0 nm)

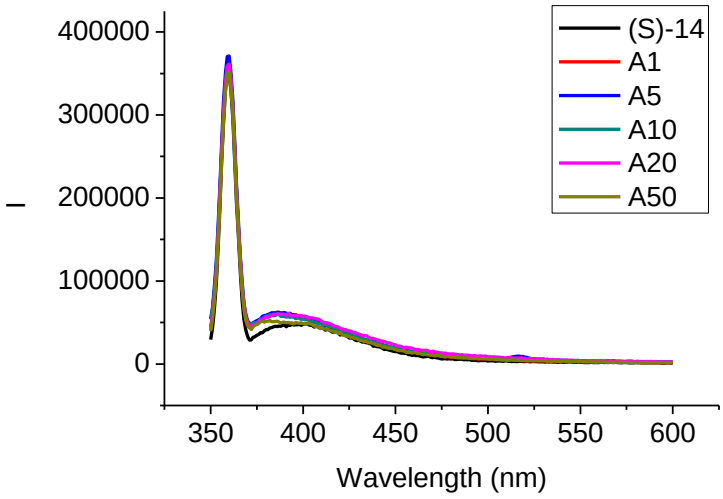

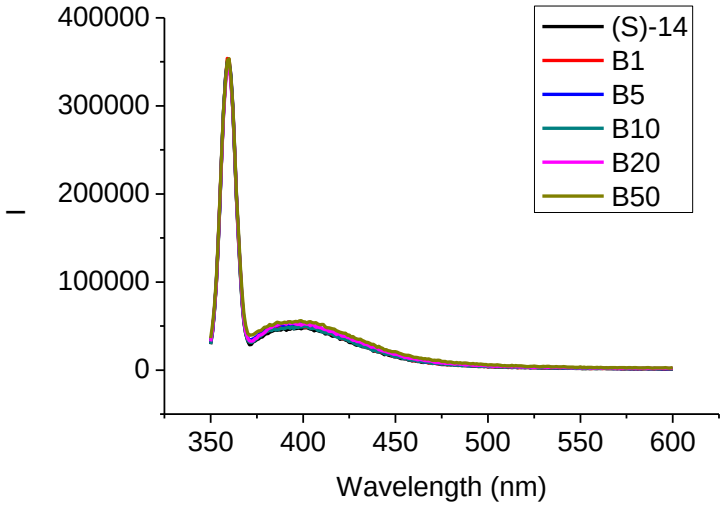

Figure AI-13. Fluorescence spectra of (S)-**7-15** $CuCl_2$ (1×10^{-5} M in 5 mL DMF) at different pH. (λ_{exc} = 320 nm. slit = 5.0/5.0 nm) SY-2-207

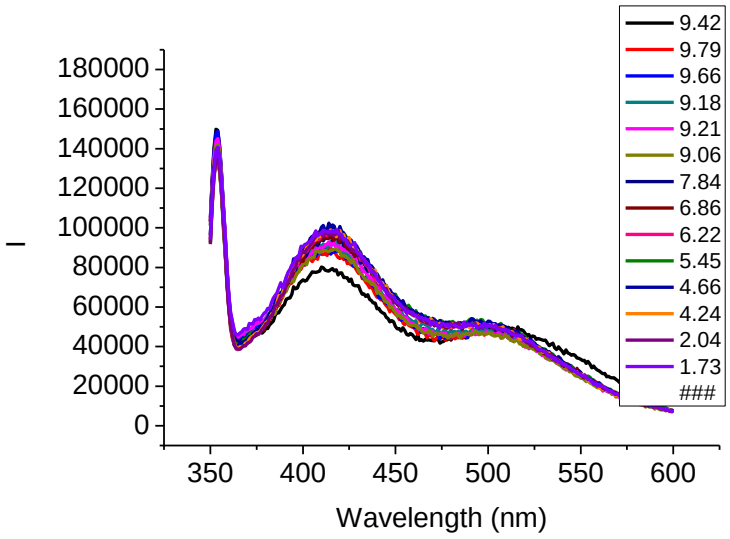

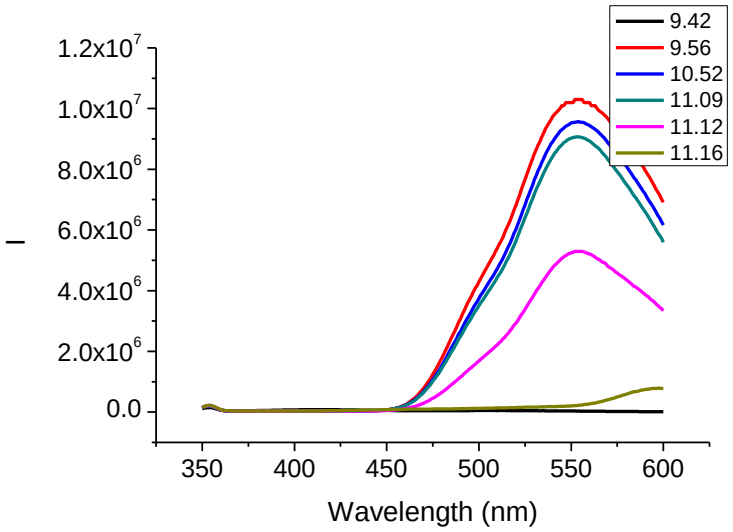

9. Interaction of Cu complexes of (S)-7-9, (S)-7-13, (S)-7-14, (S)-7-15 with substrates

Figure AI-14. UV-Vis absorption spectra of (S)-**7-9** and its copper complex (2×10^{-5} M in THF).

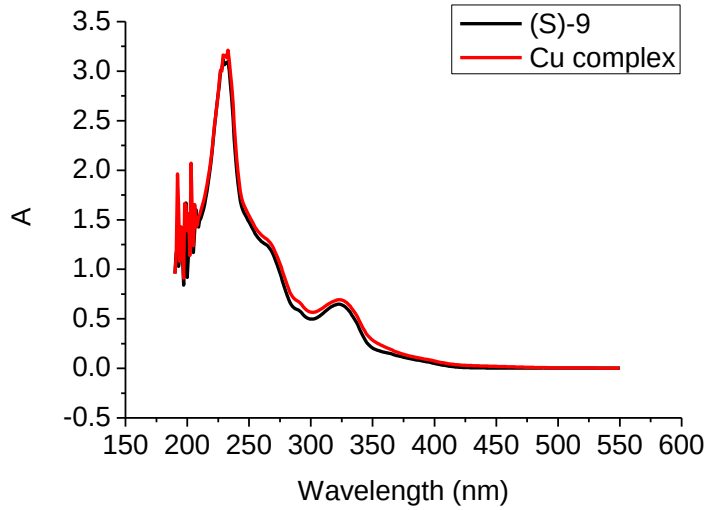

Figure AI-15. Fluorescence spectra of (S)-**7-9**, its copper complex (2×10^{-5} M in

THF/water 4.2/0.8) and its copper complex in the presence of mandelic acid, Leu, Ser and Arg (1×10^{-4} M). (λ_{exc} = 323 nm. slit = 7.0/7.0 nm)

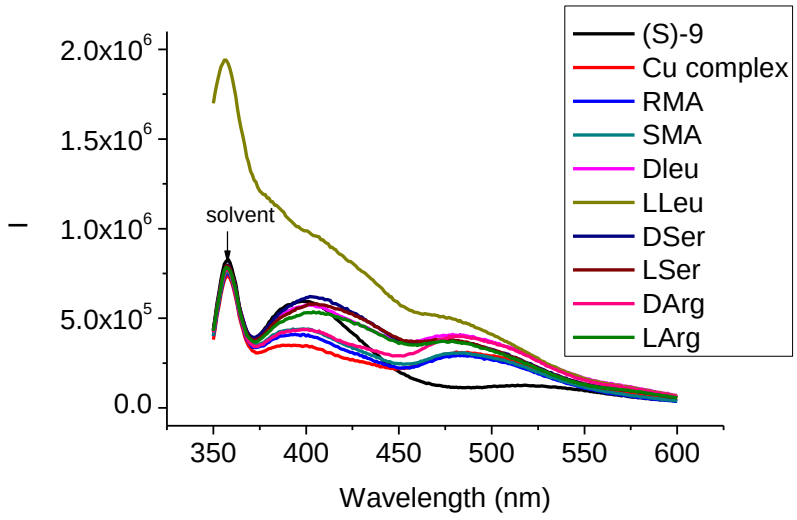

Figure AI-16. UV-Vis absorption spectra of (S)-**7-13** and its copper complex (1×10^{-5} M in THF/H_2O 5:1).

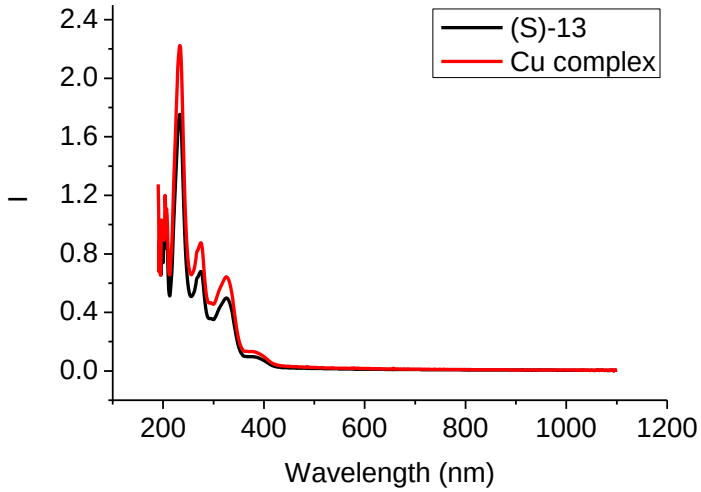

Figure AI-17. Fluorescence spectra of (S)-**7-13**, (S)-**7-13** $CuCl_2$ and (S)-**7-13** $CuCl_2$

(1×10^{-5} M in THF/H_2O 5:1) in the presence of D-Ser, L-Ser and L-His (1×10^{-5} M, 5×10^{-5} M, 1×10^{-4} M). (λ_{exc} = 325 nm. slit =3.0/3.0 nm)

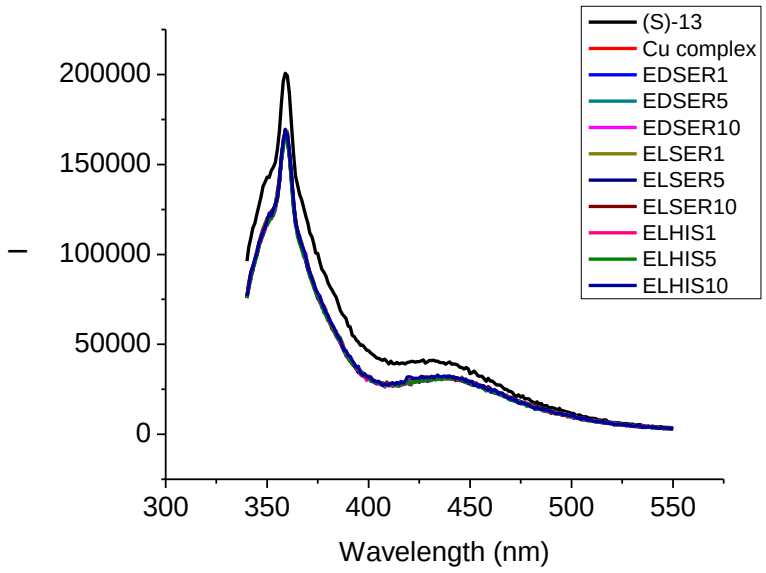

Figure AI-18. UV-Vis absorption spectra of (S)-**7-14** and its copper complex (1×10^{-5} M in THF/H_2O 5:1).

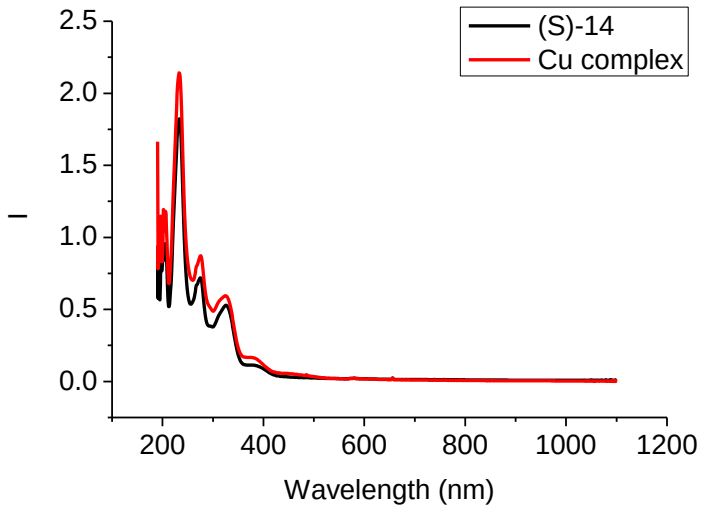

Figure AI-19. Fluorescence spectra of (S)-**7-14**, (S)-**7-14** $CuCl_2$ and (S)-**7-14** $CuCl_2$ (1×10^{-5} M in THF/H_2O 5:1) in the presence of D-Ser, L-Ser and L-His (1×10^{-5} M, 5×10^{-5} M, 1×10^{-4} M). (λ_{exc} = 325 nm. slit =3.0/3.0 nm)

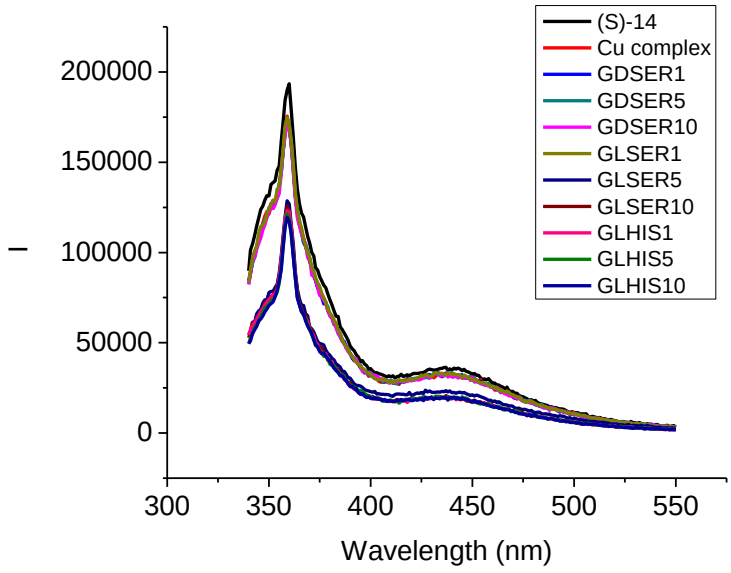

Figure AI-20. UV-Vis absorption spectra of (S)-**7-15** and its copper complex (2×10^{-5} M in DMF).

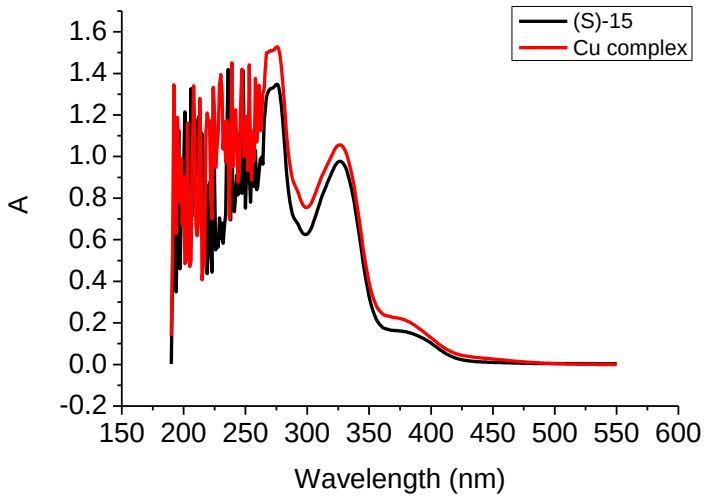

Figure AI-21. Fluorescence spectra of (S)-**7-15**, its copper complex (2×10^{-5} M in DMF/water 4.2/0.8) and its copper complex in the presence of mandelic acid, Leu, Ser and Arg (1×10^{-4} M). (λ_{exc} = 326 nm. slit = 7.0/7.0 nm)

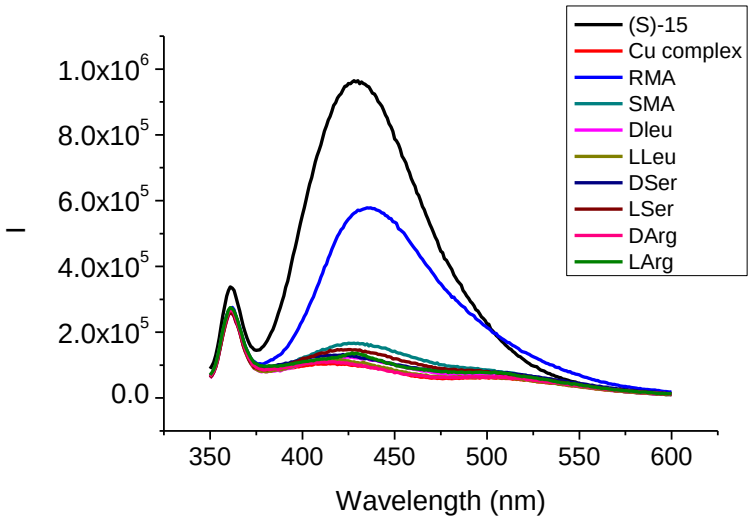

Figure AI-22. Fluorescence spectra of (S)-**7-15** $CuCl_2$ (2×10^{-5} M in DMF) in the presence of phenylalaninol (2×10^{-4} M, 4×10^{-4} M, 6×10^{-4} M). (λ_{exc} = 326 nm. slit = 6/6nm)

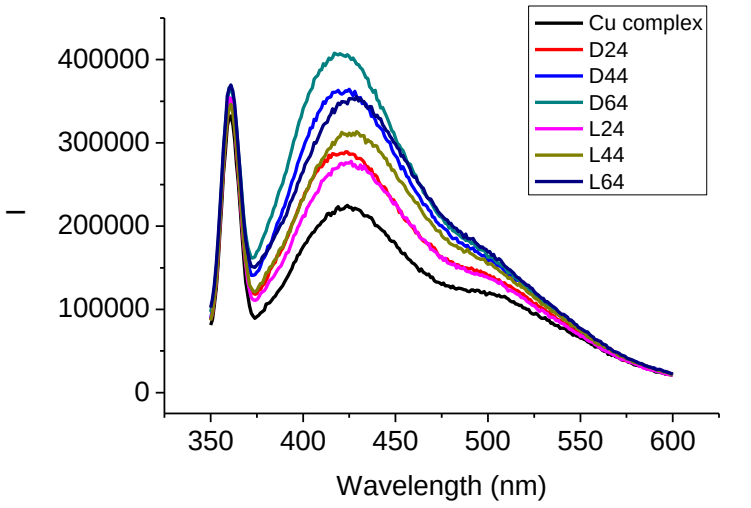

Figure AI-23. Fluorescence spectra of (S)-**7-15** $CuCl_2$ (2×10^{-5} M in DMSO) in the presence of phenylalaninol (2×10^{-4} M, 1×10^{-3} M, 2×10^{-3} M). (λ_{exc} = 326 nm. slit =5.0/5.0 nm)

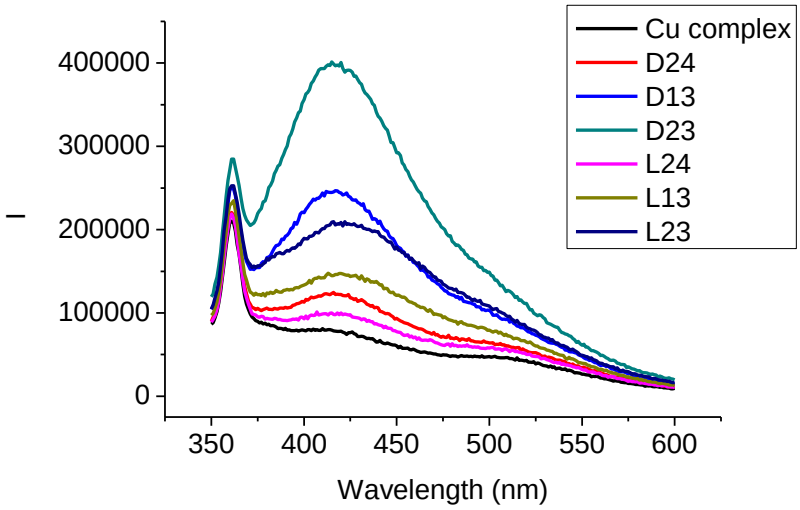

Figure AI-24. Fluorescence spectra of (S)-**7-15** $CuCl_2$ (2×10^{-5} M in DMSO/H_2O 4.1/0.9) in the presence of Leu (2×10^{-4} M, 1×10^{-3} M, 2×10^{-3} M). (λ_{exc} = 326 nm. slit =5.0/5.0 nm)

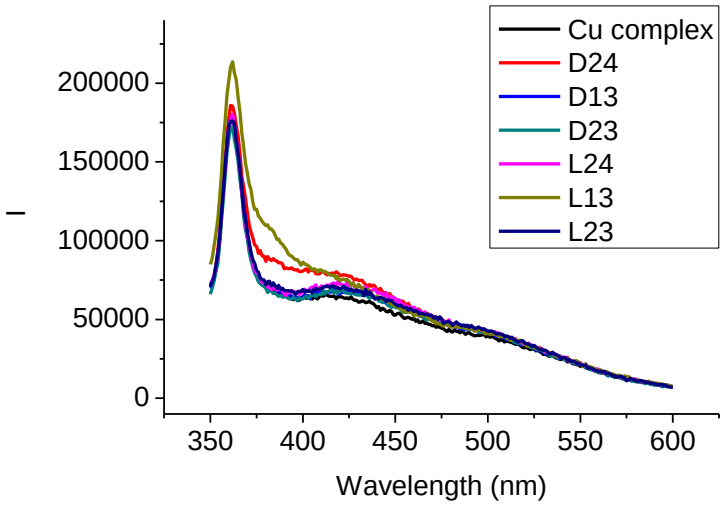

Figure AI-25. Fluorescence spectra of (S)-**7-15** $CuCl_2$ (2×10^{-5} M in DMSO/H_2O 4.1/0.9) in the presence of Ser (2×10^{-4} M, 1×10^{-3} M, 2×10^{-3} M). (λ_{exc} = 326 nm. slit =5.0/5.0 nm)

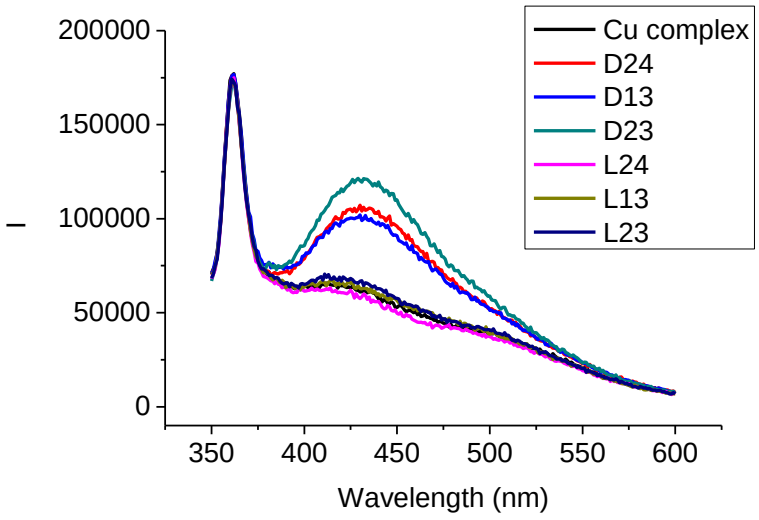

10. Interaction of Cu complexes of (S)-7-10, (S)-7-11, (S)-7-12, (S)-7-20 with substrates

Figure AI-26. UV-Vis absorption spectra of (S)-**7-10** and its copper complex (1×10^{-5} M in THF/H_2O 5:1).

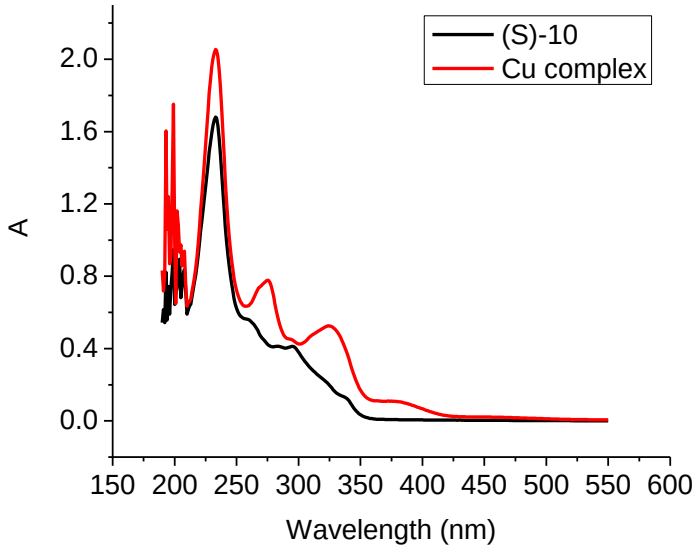

Figure AI-27. Fluorescence spectra of (S)-**7-10** and its copper complex (1×10^{-5} M in THF/H_2O 5:1). (λ_{exc} = 325 nm. slit =1.5/1.5 nm)

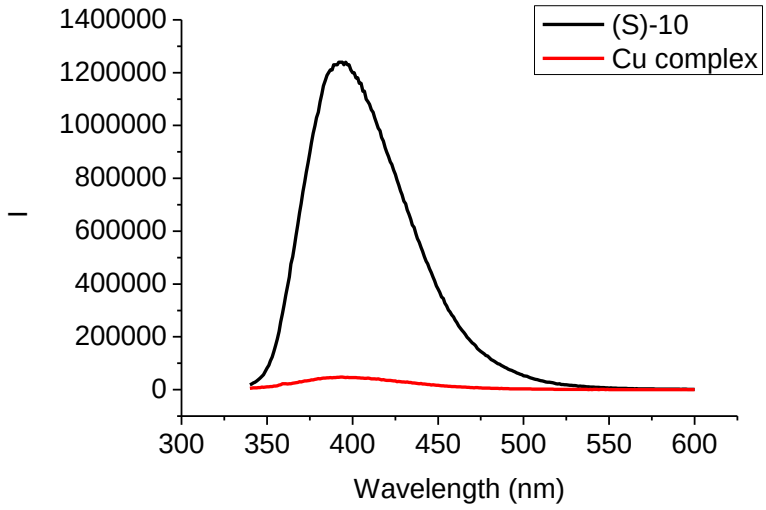

Figure AI-28. Fluorescence spectra of (S)-**7-10** $CuCl_2$ (1×10^{-5} M in THF/H_2O 5:1) in the presence of Ser (1×10^{-5} M, 5×10^{-5} M, 1×10^{-4} M). (λ_{exc} = 325 nm. slit =1.5/1.5 nm)

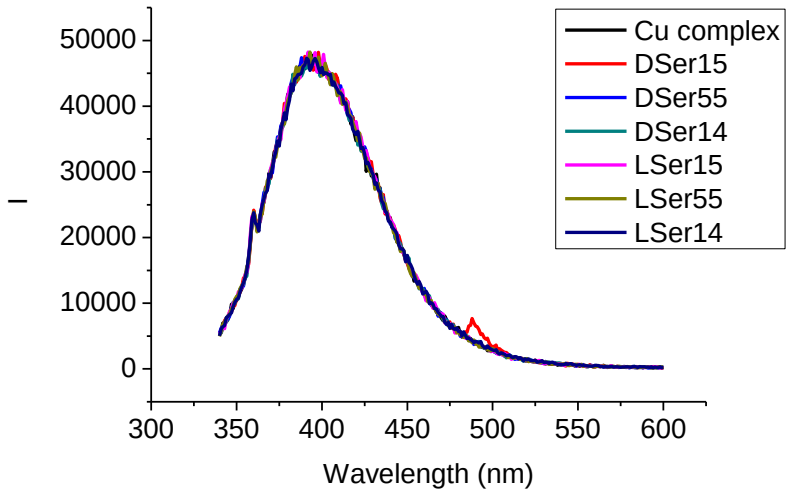

Figure AI-29. Fluorescence spectra of (S)-**7-10** $CuCl_2$ (1×10^{-5} M in THF/H_2O 5:1) in the presence of mandelic acid (1×10^{-4} M, 1×10^{-3} M, 1×10^{-2} M). (λ_{exc} = 325 nm. slit =1.5/1.5 nm)

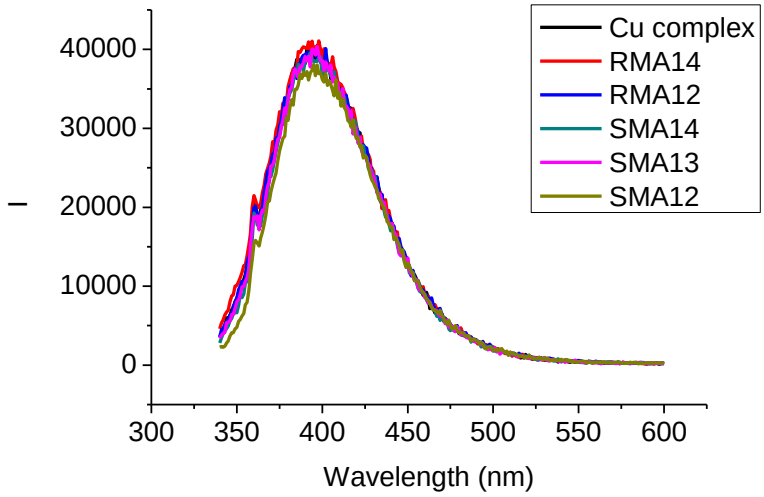

Figure AI-30. Fluorescence spectra of (S)-**7-10** $CuCl_2$ (1×10^{-5} M in THF/H_2O 5:1) in the presence of phenylalaninol (1×10^{-4} M, 1×10^{-3} M, 1×10^{-2} M). (λ_{exc} = 325 nm. slit =1.5/1.5 nm)

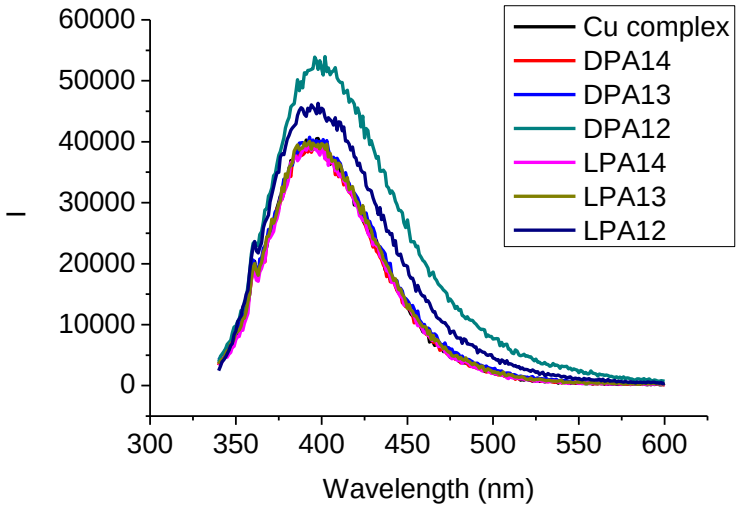

Figure AI-31. Fluorescence spectra of (S)-**7-10** $CuCl_2$ (1×10^{-5} M in THF/H_2O 5:1) in the presence of Alanine (1×10^{-4} M, 1×10^{-3} M, 1×10^{-2} M). (λ_{exc} = 325 nm. slit =1.5/1.5 nm)

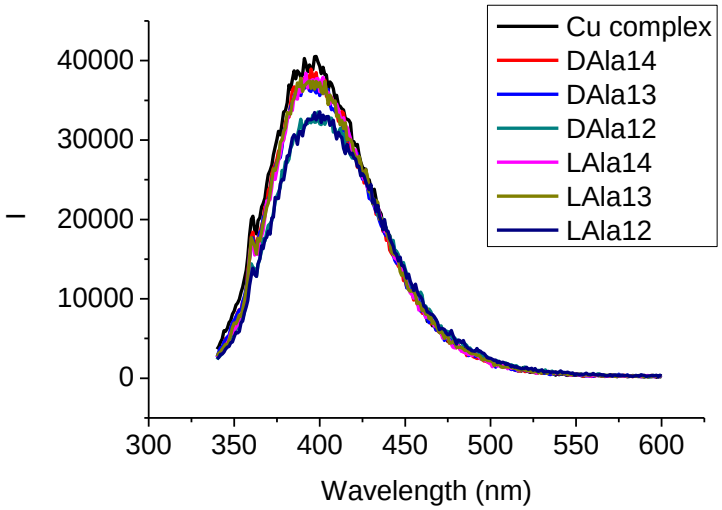

Figure AI-32. Fluorescence spectra of (S)-**7-10** $CuCl_2$ (1×10^{-5} M in THF : CH3OH : water = 1 : 10.8 : 8.5) in the presence of mandelic acid (1×10^{-4} M, 1×10^{-3} M, 1×10^{-2} M). (λ_{exc} = 325 nm. slit =1.5/1.5 nm)

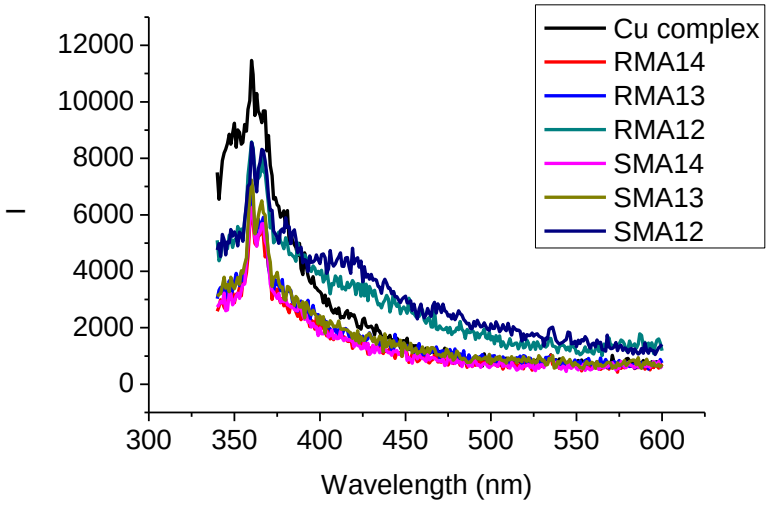

Figure AI-33. Fluorescence spectra of (S)-**7-10** $CuCl_2$ (1×10^{-5} M in THF : CH3OH : water = 1 : 10.8 : 8.5) in the presence of phenylalaninol (1×10^{-4} M, 1×10^{-3} M, 1×10^{-2} M). (λ_{exc} = 325 nm. slit =1.5/1.5 nm)

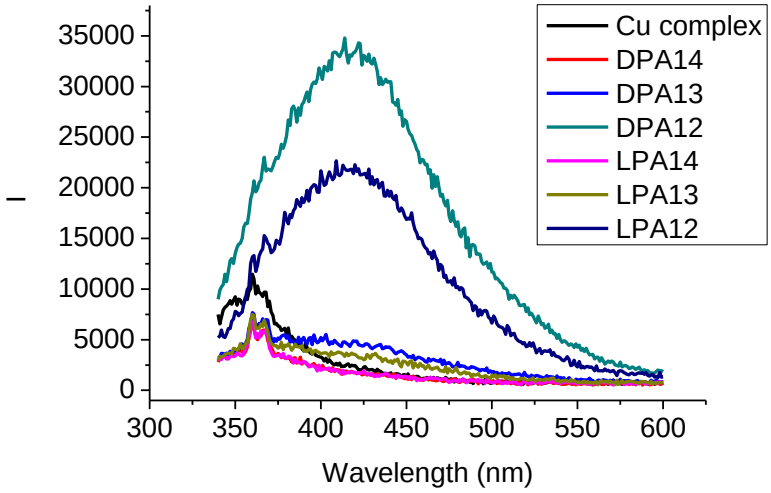

Figure AI-34. Fluorescence spectra of (S)-**7-10** $CuCl_2$ (1×10^{-5} M in THF : CH3OH : water = 1 : 10.8 : 8.5) in the presence of Alanine (1×10^{-4} M, 1×10^{-3} M, 1×10^{-2} M). (λ_{exc} = 325 nm. slit =1.5/1.5 nm)

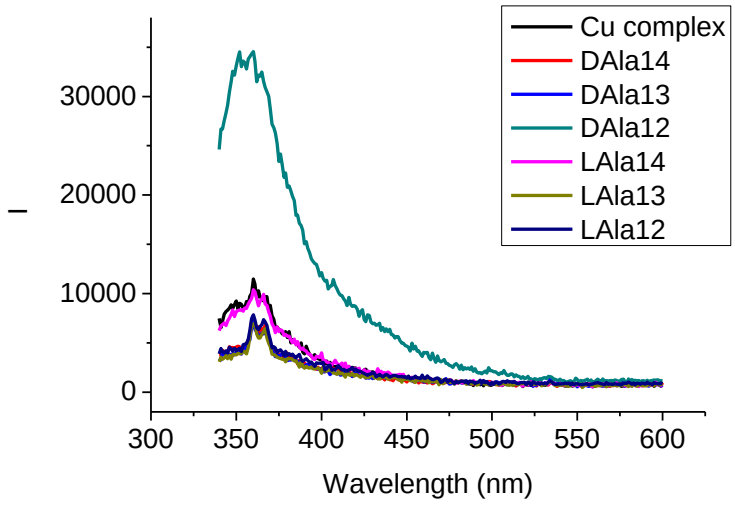

Figure AI-35. UV-Vis absorption spectra of (S)-**7-11** and its copper complex (1×10^{-5} M in THF/H_2O 5:1).

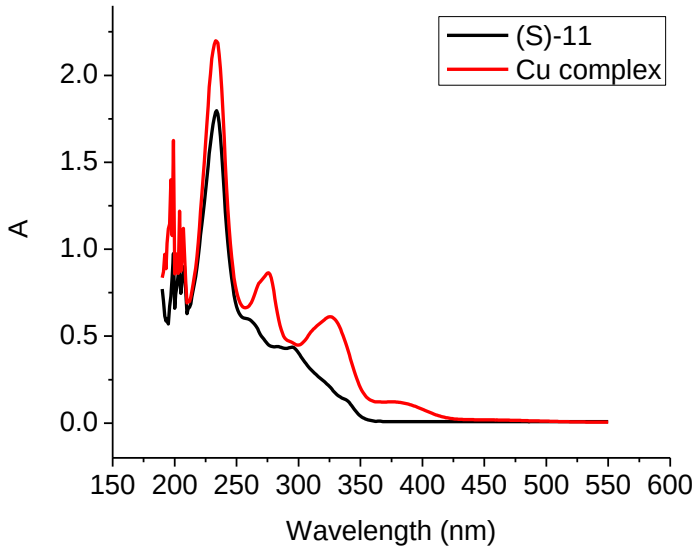

Figure AI-36. Fluorescence spectra of (S)-**7-11** and its copper complex (1×10^{-5} M in THF/H_2O 5:1). (λ_{exc} = 325 nm. slit =1.5/1.5 nm)

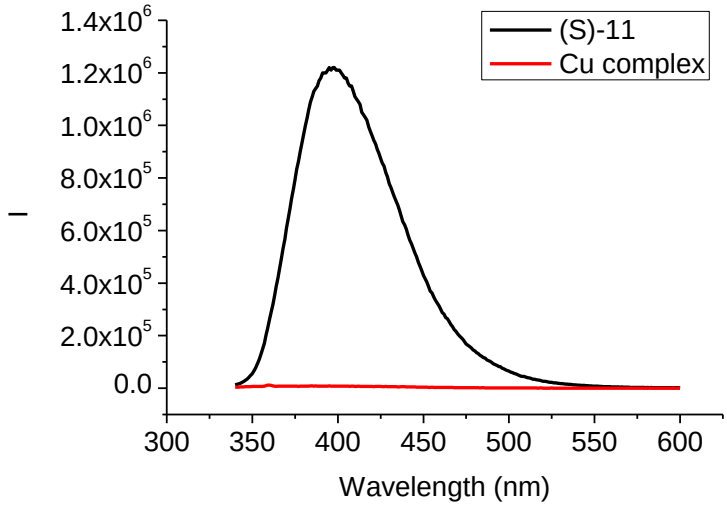

Figure AI-37. Fluorescence spectra of (S)-**7-11** $CuCl_2$ (1×10^{-5} M in THF/H_2O 5:1) in the presence of Ser (1×10^{-5} M, 5×10^{-5} M, 1×10^{-4} M). (λ_{exc} = 325 nm. slit =1.5/1.5 nm)

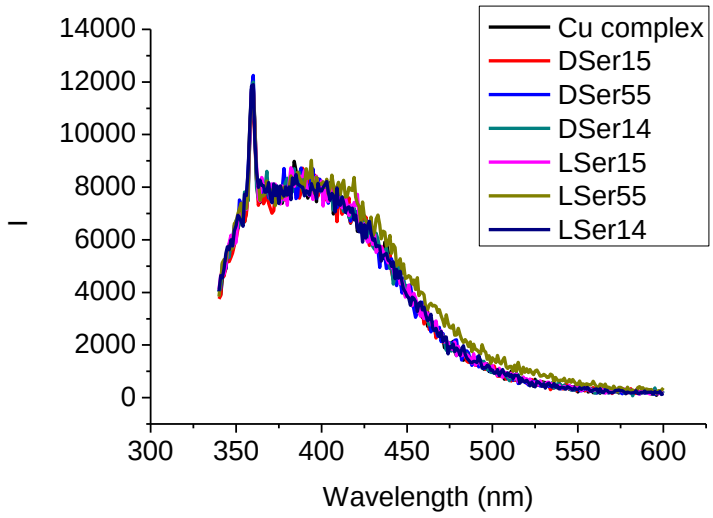

Figure AI-38. Fluorescence spectra of (S)-**7-11** $CuCl_2$ (1×10^{-5} M in THF/H_2O 5:1) in the presence of mandelic acid (1×10^{-4} M, 1×10^{-3} M, 1×10^{-2} M). (λ_{exc} = 325 nm. slit =1.5/1.5 nm)

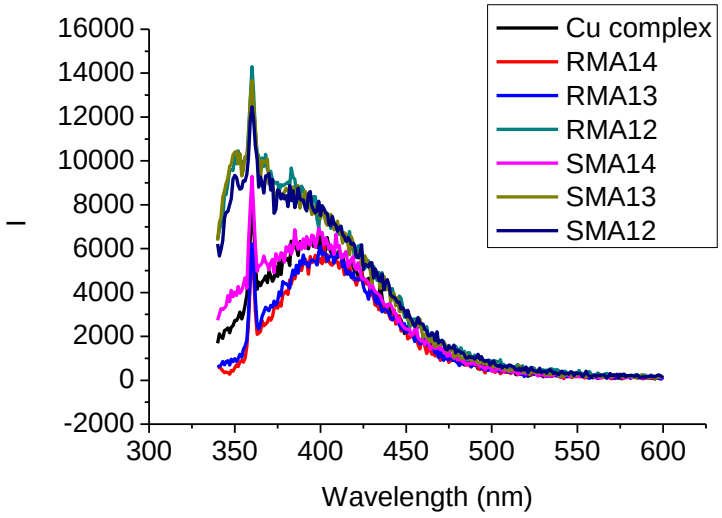

Figure AI-39. Fluorescence spectra of (S)-**7-11** $CuCl_2$ (1×10^{-5} M in THF/H_2O 5:1) in the presence of phenylalaninol (1×10^{-4} M, 1×10^{-3} M, 1×10^{-2} M). (λ_{exc} = 325 nm. slit =1.5/1.5 nm)

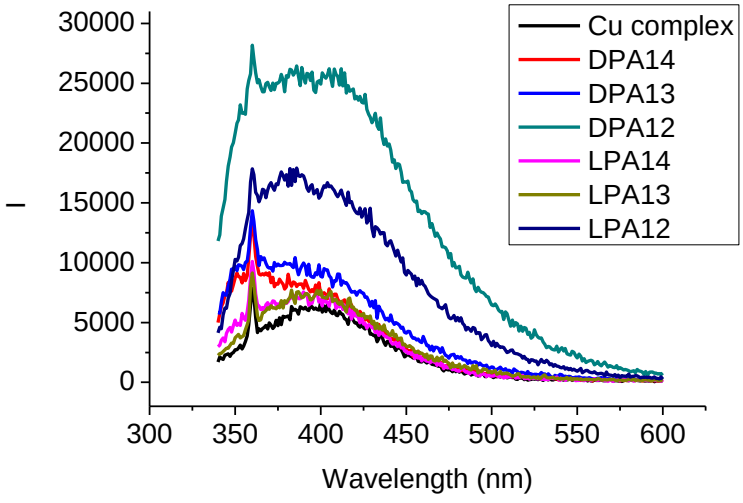

Figure AI-40. Fluorescence spectra of (S)-**7-11** $CuCl_2$ (1×10^{-5} M in THF/H_2O 5:1) in the presence of Alanine (1×10^{-4} M, 1×10^{-3} M, 1×10^{-2} M). (λ_{exc} = 325 nm. slit =1.5/1.5 nm)

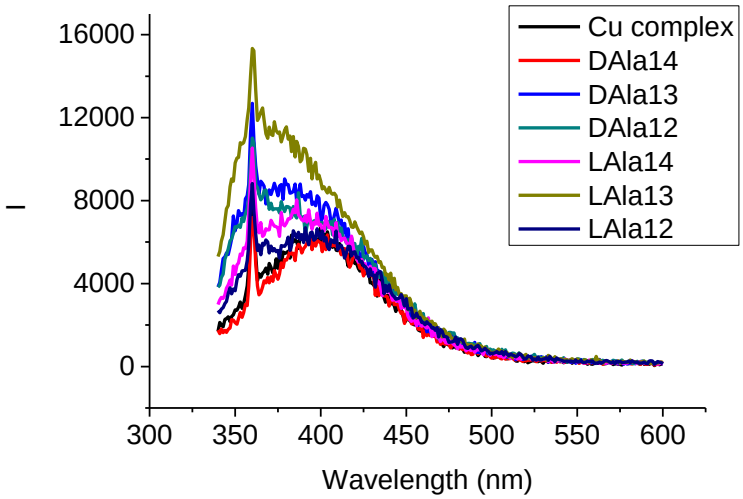

Figure AI-41. Fluorescence spectra of (S)-**7-11** $CuCl_2$ (1×10^{-5} M in THF : CH3OH : water = 1 : 16.6 : 12.6) in the presence of mandelic acid (1×10^{-4} M, 1×10^{-3} M, 1×10^{-2} M). (λ_{exc} = 325 nm. slit =1.5/1.5 nm)

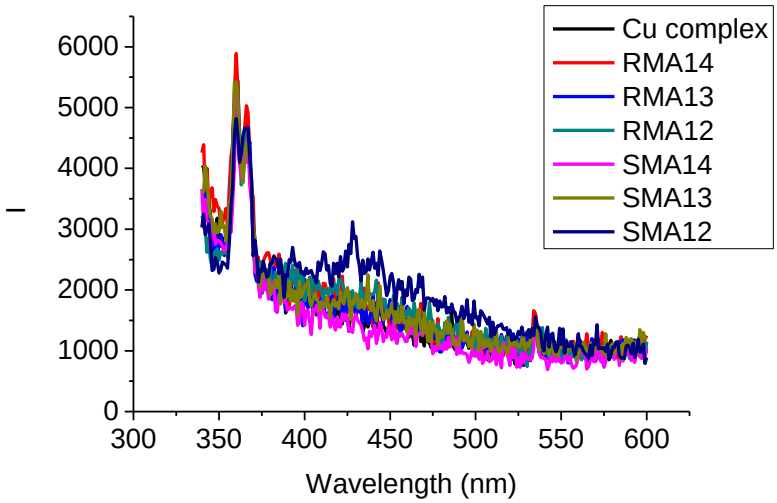

Figure AI-42. Fluorescence spectra of (S)-7-11 $CuCl_2$ (1×10^{-5} M in THF : CH3OH : water = 1 : 16.6 : 12.6) in the presence of phenylalaninol (1×10^{-4} M, 1×10^{-3} M, 1×10^{-2} M). (λ_{exc} = 325 nm. slit =1.5/1.5 nm)

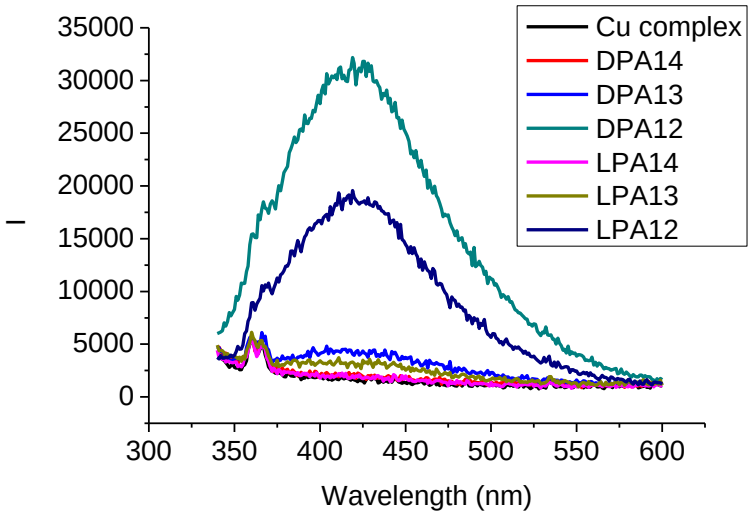

Figure AI-43. Fluorescence spectra of (S)-**7-11** $CuCl_2$ (1×10^{-5} M in THF : CH_3OH : water = 1 : 16.6 : 12.6) in the presence of Alanine (1×10^{-4} M, 1×10^{-3} M, 1×10^{-2} M). (λ_{exc} = 325 nm. slit =1.5/1.5 nm)

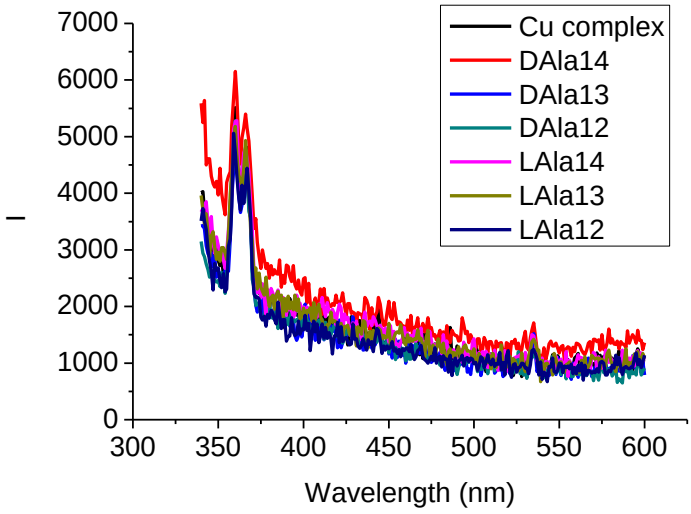

Figure AI-44. UV-Vis absorption spectra of (S)-**7-12** and its copper complex (1×10^{-5} M in THF/H_2O 5:1).

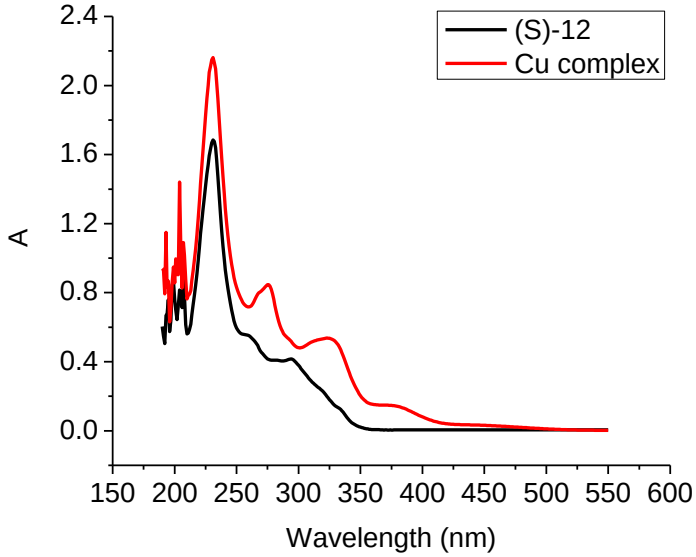

Figure I-45. Fluorescence spectra of (S)-**7-12** and its copper complex (1×10^{-5} M in THF/H_2O 5:1). (λ_{exc} = 325 nm. slit =1.5/1.5 nm)

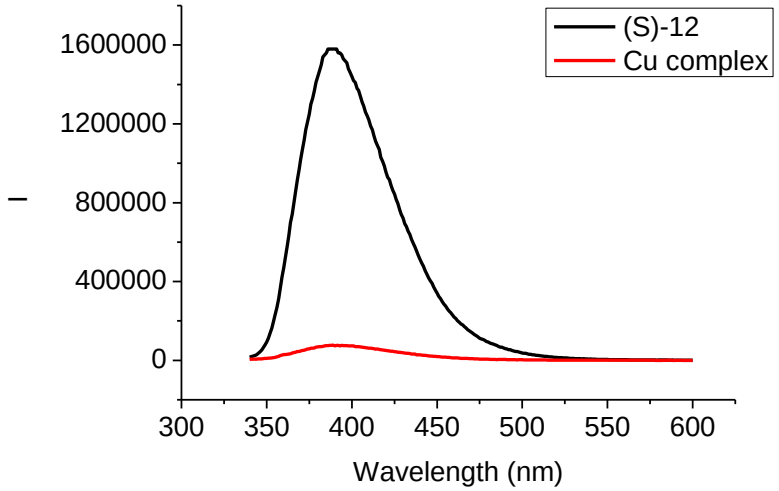

Figure AI-46. Fluorescence spectra of (S)-**7-12** $CuCl_2$ (1×10^{-5} M in THF/H_2O 5:1) in the presence of Ser (1×10^{-5} M, 5×10^{-5} M, 1×10^{-4} M). (λ_{exc} = 325 nm. slit =1.5/1.5 nm)

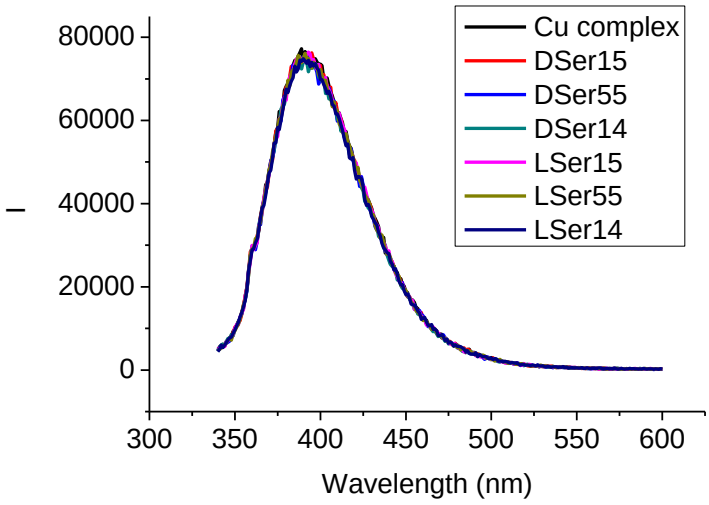

Figure AI-47. Fluorescence spectra of (S)-**7-12** $CuCl_2$ (1×10^{-5} M in THF/H_2O 5:1) in the presence of mandelic acid (1×10^{-4} M, 1×10^{-3} M, 1×10^{-2} M). (λ_{exc} = 325 nm. slit =1.5/1.5 nm)

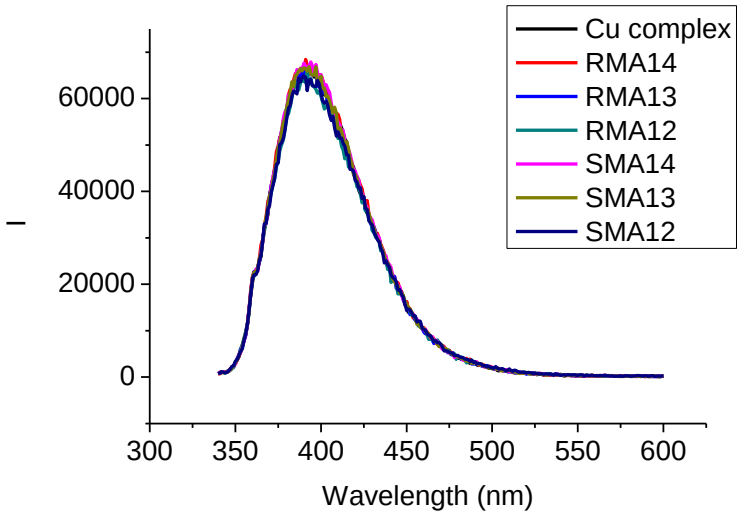

Figure AI-48. Fluorescence spectra of (S)-**7-12** $CuCl_2$ (1×10^{-5} M in THF/H_2O 5:1) in the presence of phenylalaninol (1×10^{-4} M, 1×10^{-3} M, 1×10^{-2} M). (λ_{exc} = 325 nm. slit =1.5/1.5

nm)

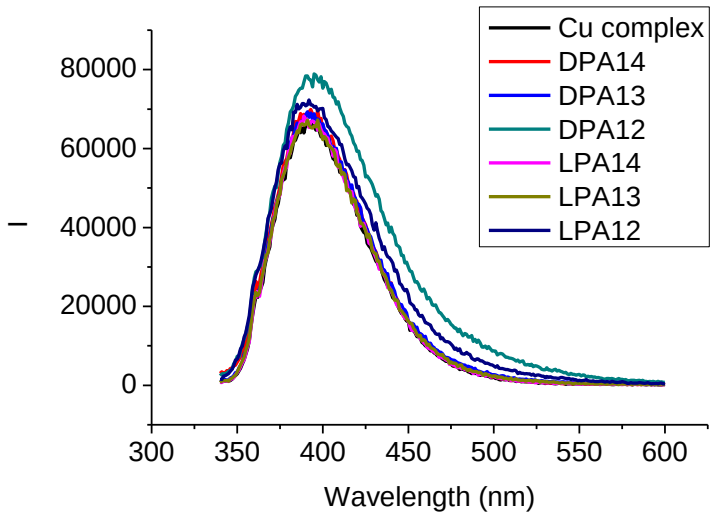

Figure AI-49. Fluorescence spectra of (S)-**7-12** $CuCl_2$ (1×10^{-5} M in THF/H_2O 5:1) in the presence of Alanine (1×10^{-4} M, 1×10^{-3} M, 1×10^{-2} M). (λ_{exc} = 325 nm. slit =1.5/1.5 nm)

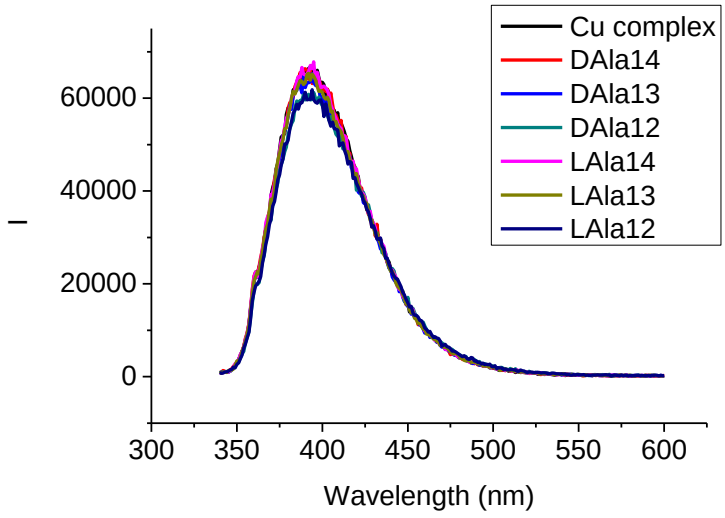

Figure AI-50. Fluorescence spectra of (S)-**7-12** $CuCl_2$ (1×10^{-5} M in CH_3OH : water = 1.2 : 1) in the presence of mandelic acid (1×10^{-4} M, 1×10^{-3} M, 1×10^{-2} M). (λ_{exc} = 325 nm.

slit =1.5/1.5 nm)

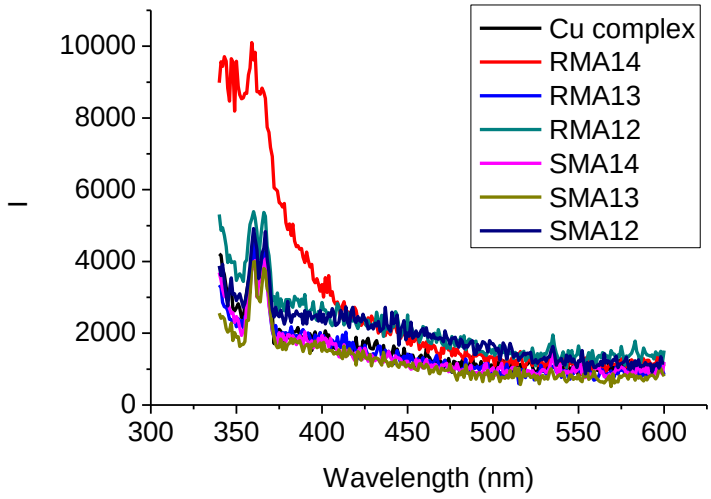

Figure AI-51. Fluorescence spectra of (S)-**7-12** $CuCl_2$ (1×10^{-5} M in CH_3OH : water = 1.2 : 1) in the presence of phenylalaninol (1×10^{-4} M, 1×10^{-3} M, 1×10^{-2} M). (λ_{exc} = 325 nm. slit =1.5/1.5 nm)

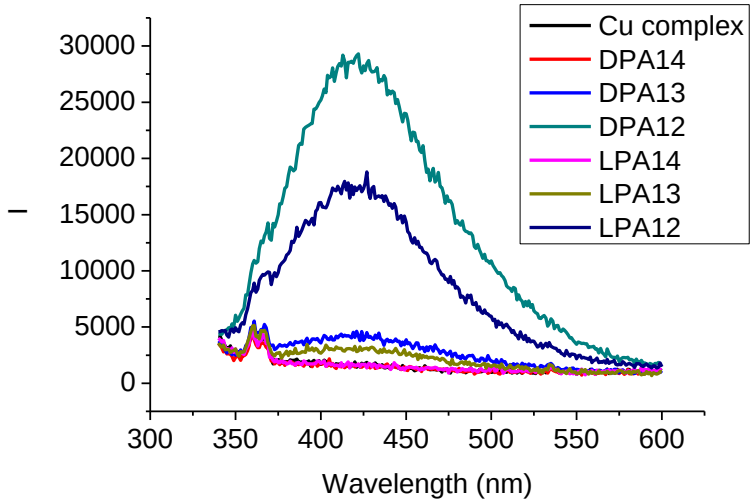

Figure AI-52. Fluorescence spectra of (S)-**7-12** $CuCl_2$ (1×10^{-5} M in CH_3OH : water = 1.2 : 1) in the presence of alanine (1×10^{-4} M, 1×10^{-3} M, 1×10^{-2} M). (λ_{exc} = 325 nm. slit

=1.5/1.5 nm)

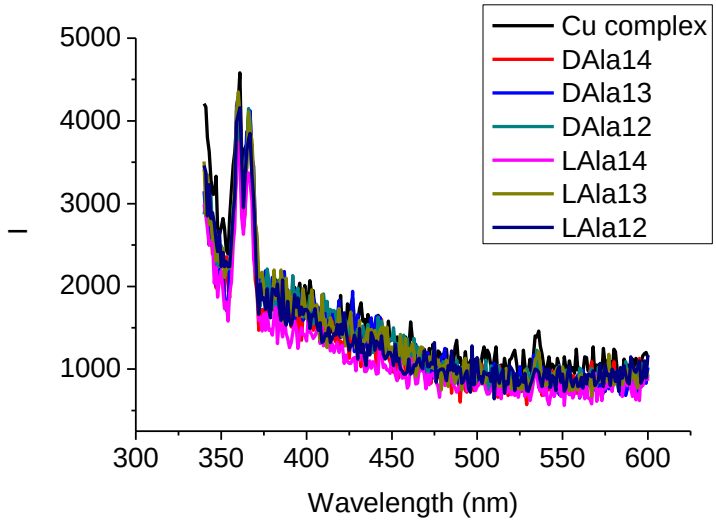

Figure AI-53. UV-Vis absorption spectra of (S)-**7-20** and its copper complex (1×10^{-5} M in THF/H_2O 5:1).

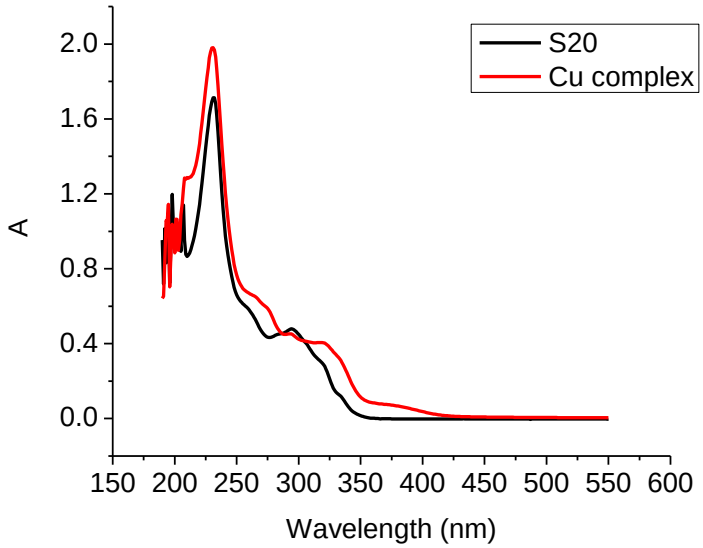

Figure AI-54. Fluorescence spectra of (S)-**7-20** and its copper complex (1×10^{-5} M in THF). (λ_{exc} = 290 nm. slit =1.5/1.5 nm)

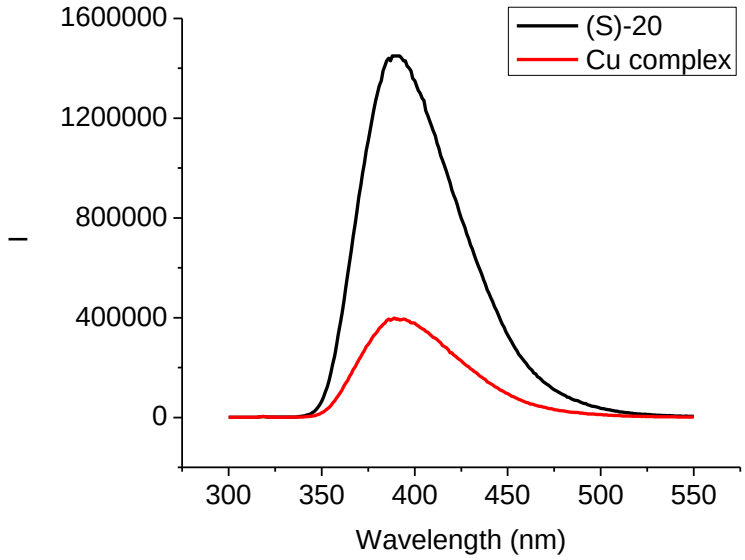

Figure AI-55. Fluorescence spectra of (S)-**7-20** $CuCl_2$ (1×10^{-5} M in THF/H_2O 5:1) in the absence and presence of D- or L-Ala, Ser and Arg (1×10^{-5} M, 5×10^{-5} M, 1×10^{-4} M). (λ_{exc} = 290 nm. slit =1.5/1.5 nm)

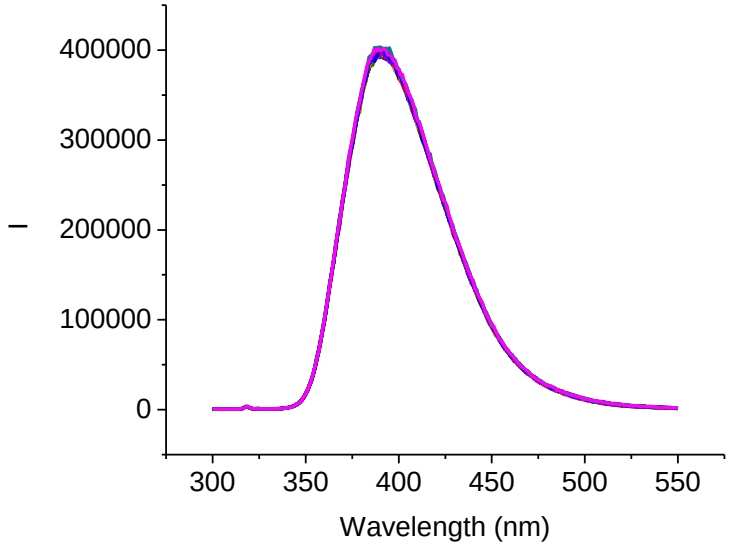

Figure AI-56. Fluorescence spectra of (S)-**7-20** $CuCl_2$ (1×10^{-5} M in DCM/hexane 2:3) in

the absence and presence of (R)- or (S)-leucinol and 2-amino-3-phenylpropanol (4.5×10^{-3} M). (λ_{exc} = 290 nm. slit =1.5/1.5 nm)

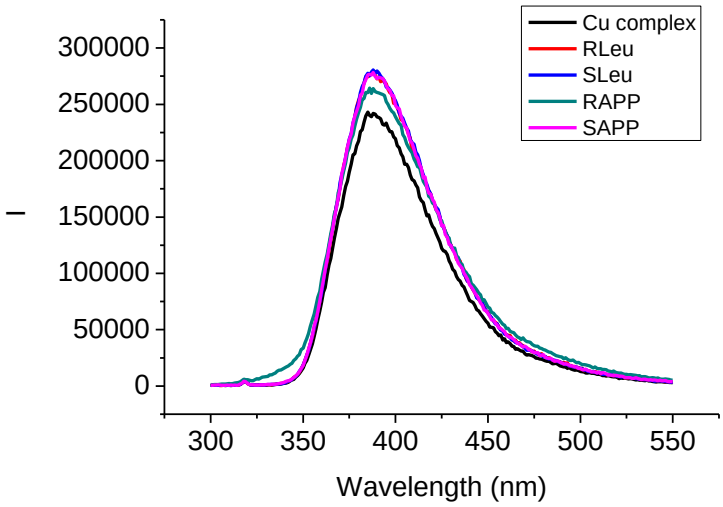

Figure AI-57. Fluorescence spectra of (S)-**7-20** $CuCl_2$ (5×10^{-7} M in DCM/hexane 2:3) in the absence and presence of (R)- or (S)-leucinol and 2-amino-3-phenylpropanol (5×10^{-4} M). (λ_{exc} = 290 nm. slit =1.5/1.5 nm)

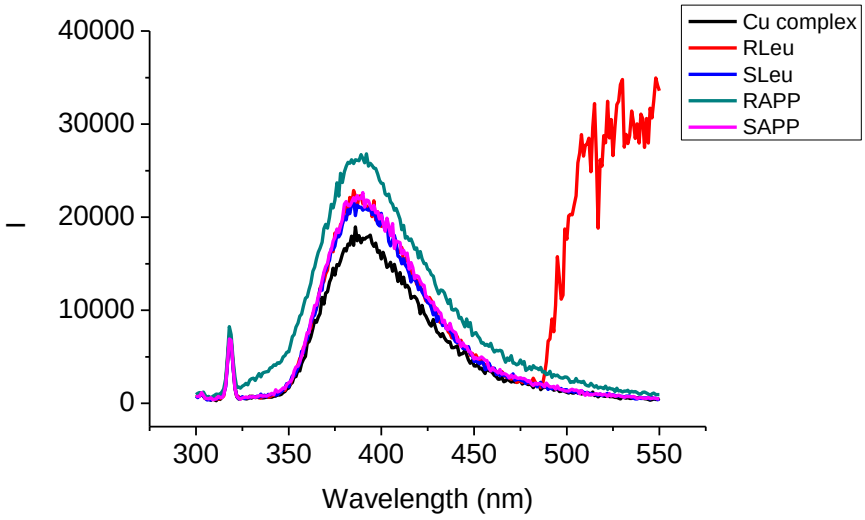

Figure AI-58. Fluorescence spectra of (S)-**7-20** and its copper complex (1×10^{-5} M in THF, THF/H_2O and methanol). (λ_{exc} = 290 nm. slit =1.5/1.5 nm)

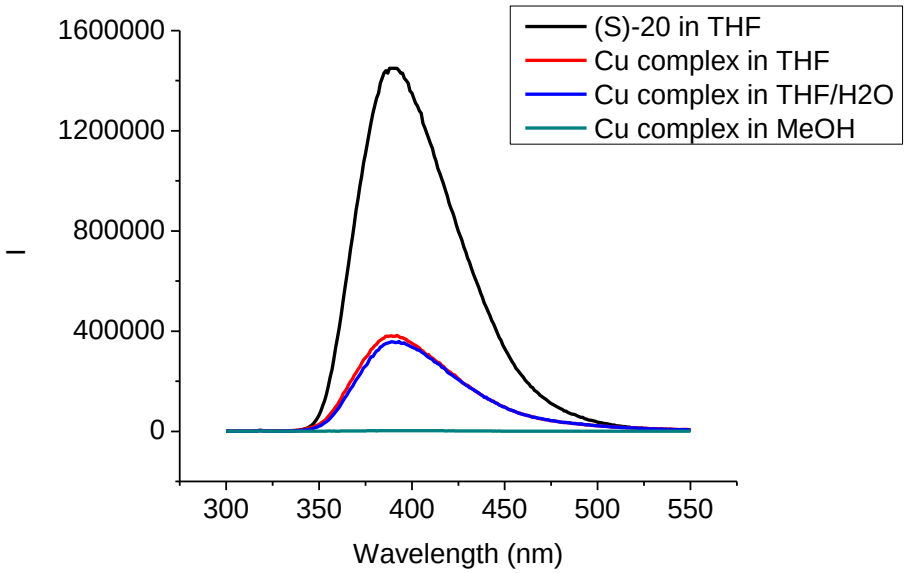

Figure AI-59. Fluorescence spectra of (S)-**7-20** $CuCl_2$ (1×10^{-5} M in THF) in the absence and presence of (R)- or (S)-mandelic acid [1×10^{-5} M in THF (0.1% methanol), 1×10^{-4} M (1% methanol), 1×10^{-3} M (10% methanol)]. (λ_{exc} = 290 nm. slit =1.5/1.5 nm)

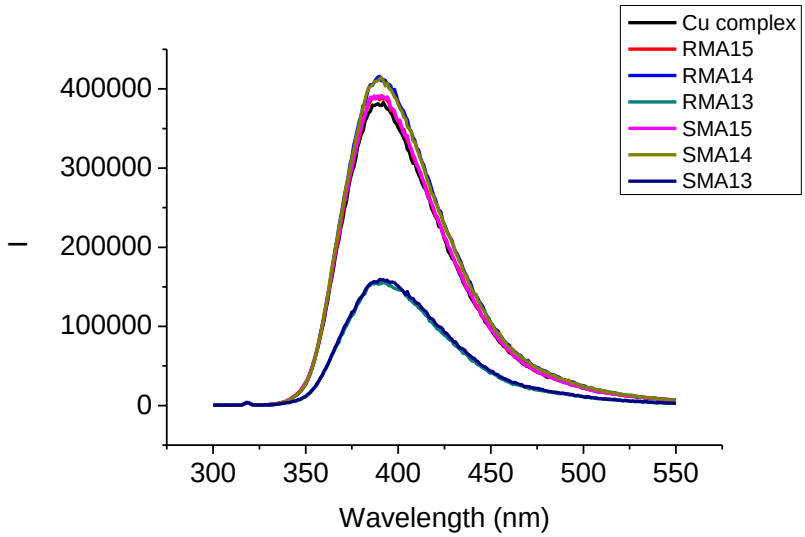

Figure AI-60. Fluorescence spectra of (S)-**7-20** $CuCl_2$ (1×10^{-5} M in MeOH) in the absence and presence of (R)- or (S)-mandelic acid [1×10^{-5} M, 1×10^{-4} M, 1×10^{-3} M]. (λ_{exc} = 290 nm. slit =1.5/1.5 nm)

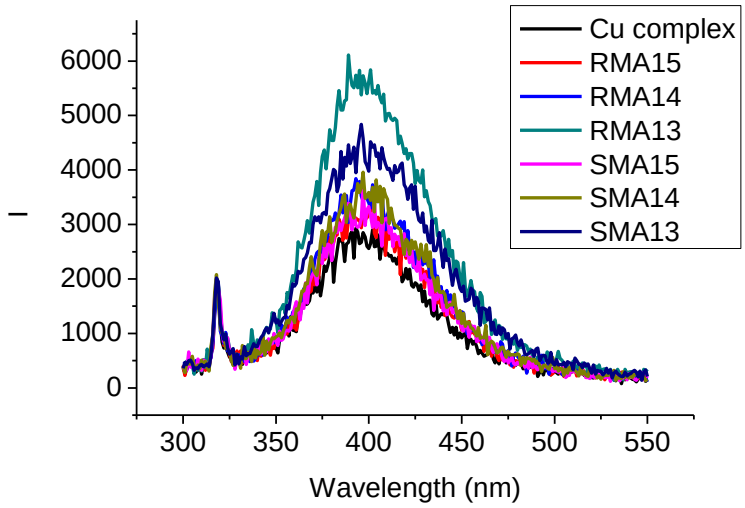

Figure AI-61. Fluorescence spectra of (S)-**7-20** $CuCl_2$ (1×10^{-5} M in THF) in the absence and presence of L-Histidine [1×10^{-5} M in THF (0.1% H_2O), 1×10^{-4} M in THF (1% H_2O),

1×10^{-3} M in THF (10% H_2O)]. (λ_{exc} = 290 nm. slit =1.5/1.5 nm)

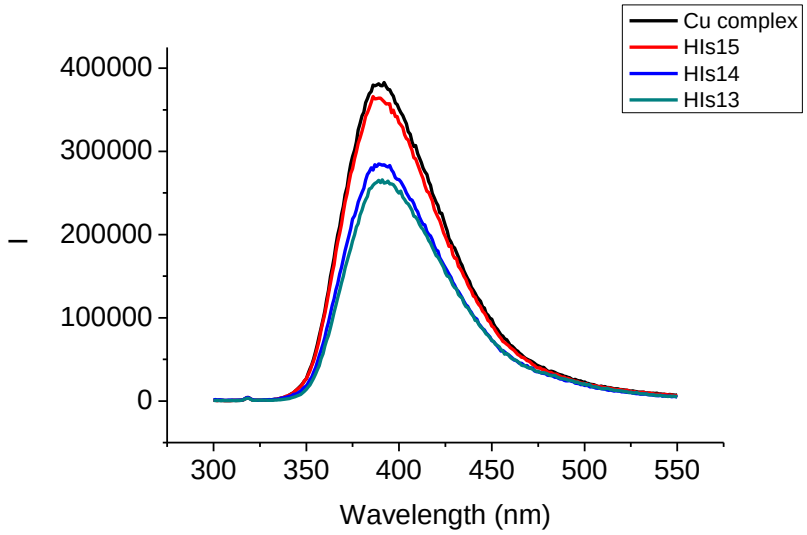

Figure AI-62. Fluorescence spectra of (S)-**7-20** $CuCl_2$ (1×10^{-5} M in MeOH) in the absence and presence of L-Histidine [1×10^{-5} M in MeOH (0.1% H_2O), 1×10^{-4} M in MeOH (1% H_2O), 1×10^{-3} M in MeOH (10% H_2O)]. (λ_{exc} = 290 nm. slit =1.5/1.5 nm)

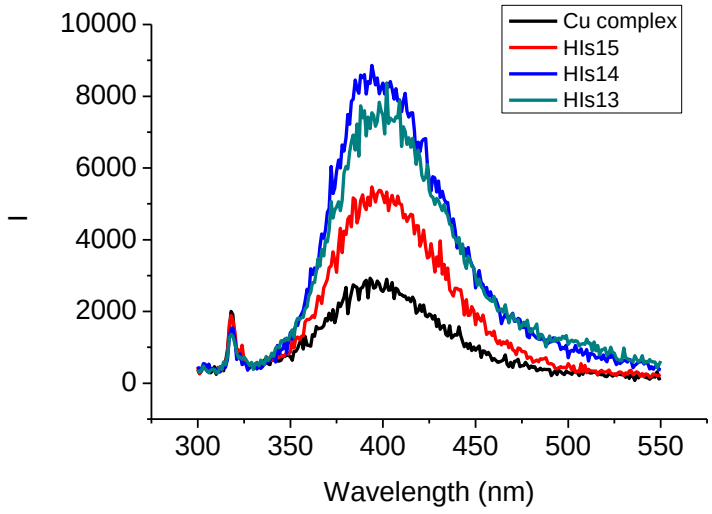

11. Interaction of (S)-7-9, (S)-7-13, (S)-7-14, (S)-7-15 and (S)-7-21 with substrates

Figure AI-63. Fluorescence spectra of (S)-**7-9** (1×10^{-5} M in THF/H_2O 5:1) in the absence and presence of D- or L-Alanine (1×10^{-4} M, 1×10^{-3} M, 1×10^{-2} M). (λ_{exc} = 325 nm. slit =3.0/3.0 nm)

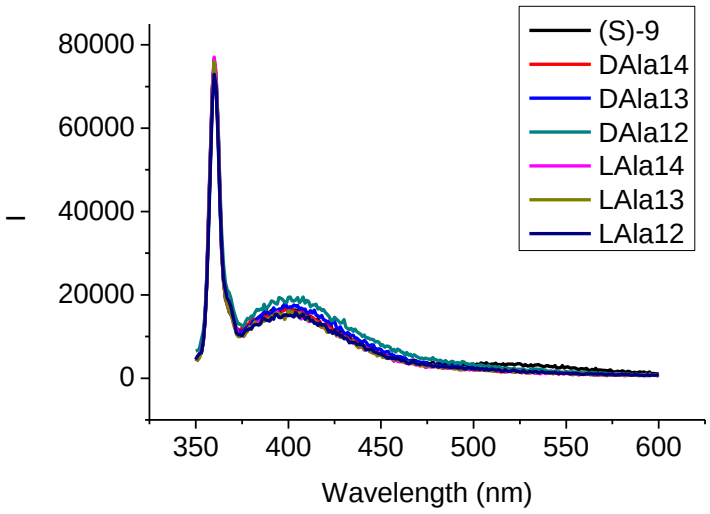

Figure AI-64. Fluorescence spectra of (S)-**7-9** (1×10^{-5} M in THF/H_2O 5:1) in the absence and presence of D- or L-Serine (1×10^{-4} M, 1×10^{-3} M, 1×10^{-2} M). (λ_{exc} = 325 nm. slit =3.0/3.0 nm)

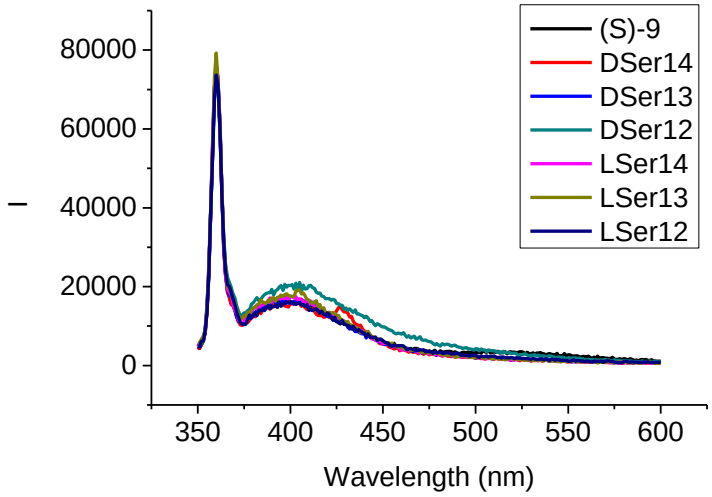

Figure AI-65. Fluorescence spectra of (S)-**7-9** (1×10^{-5} M in THF/H_2O 5:1) in the absence and presence of D- or L-Arginine (1×10^{-4} M, 1×10^{-3} M, 1×10^{-2} M). (λ_{exc} = 325 nm. slit =3.0/3.0 nm)

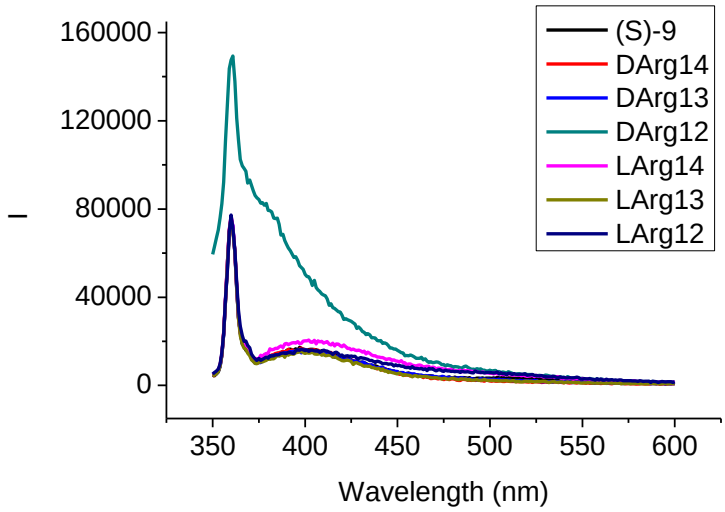

Figure AI-66. Fluorescence spectra of (S)-**7-13** (1×10^{-5} M in THF/H_2O 5:1) in the absence and presence of D- or L-Alanine (1×10^{-4} M, 1×10^{-3} M, 1×10^{-2} M). (λ_{exc} = 325 nm.

slit =3.0/3.0 nm)

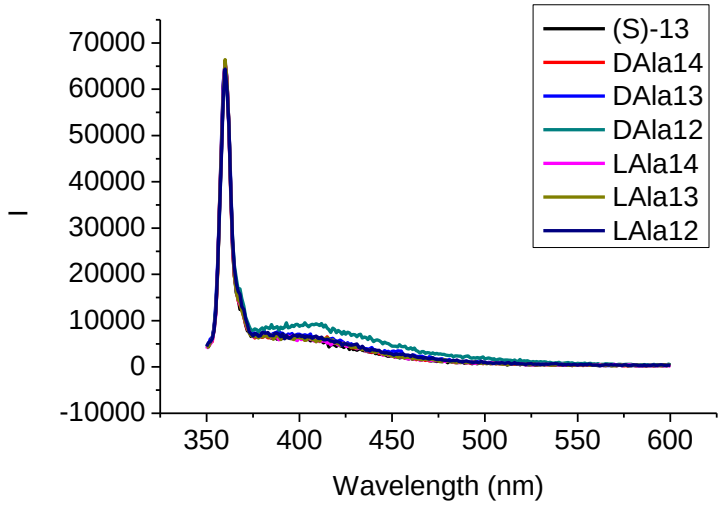

Figure AI-67. Fluorescence spectra of (S)-**7-13** (1×10^{-5} M in THF/H_2O 5:1) in the absence and presence of D- or L-Serine (1×10^{-4} M, 1×10^{-3} M, 1×10^{-2} M). (λ_{exc} = 325 nm. slit =3.0/3.0 nm)

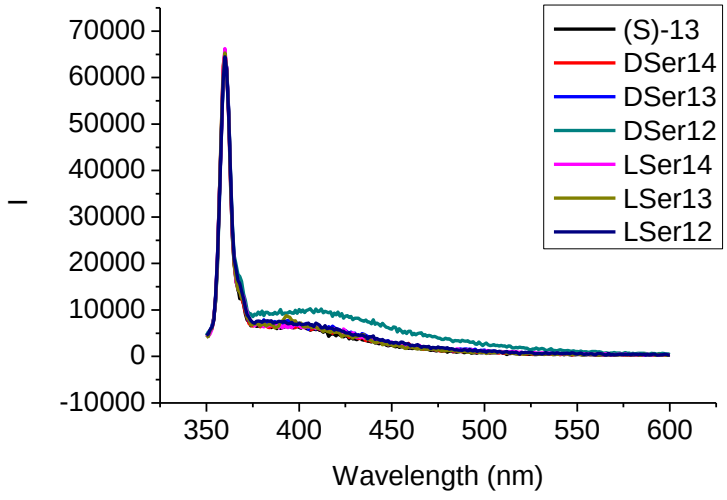

Figure AI-68. Fluorescence spectra of (S)-**7-13** (1×10^{-5} M in THF/H_2O 5:1) in the absence and presence of D- or L-Arginine (1×10^{-4} M, 1×10^{-3} M, 1×10^{-2} M). (λ_{exc} = 325

nm. slit =3.0/3.0 nm)

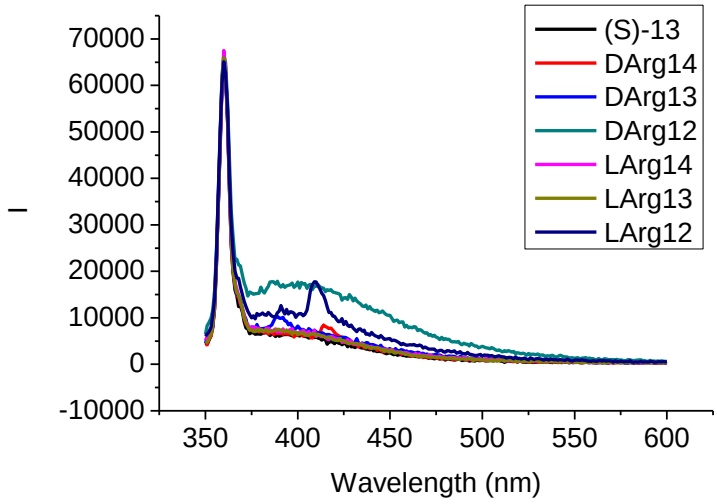

Figure AI-69. Fluorescence spectra of (S)-**7-14** (1×10^{-5} M in THF/H_2O 5:1) in the absence and presence of D- or L-Alanine (1×10^{-4} M, 1×10^{-3} M, 1×10^{-2} M). (λ_{exc} = 325 nm. slit =3.0/3.0 nm)

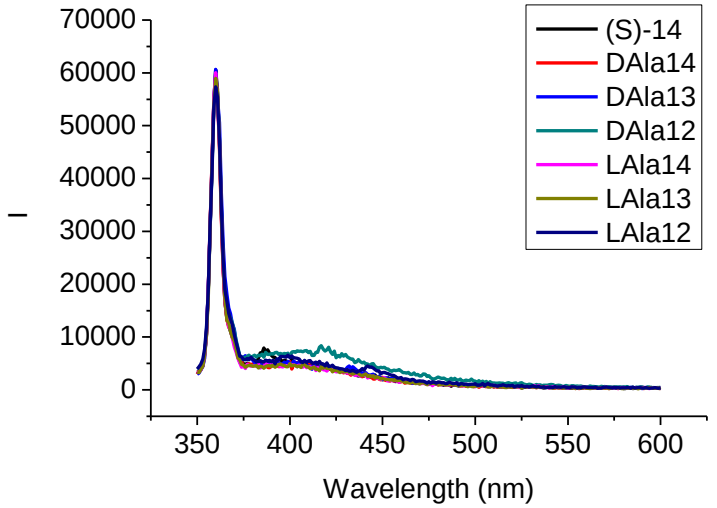

Figure AI-70. Fluorescence spectra of (S)-**7-14** (1×10^{-5} M in THF/H_2O 5:1) in the

absence and presence of D- or L-Serine (1×10^{-4} M, 1×10^{-3} M, 1×10^{-2} M). (λ_{exc} = 325 nm. slit =3.0/3.0 nm)

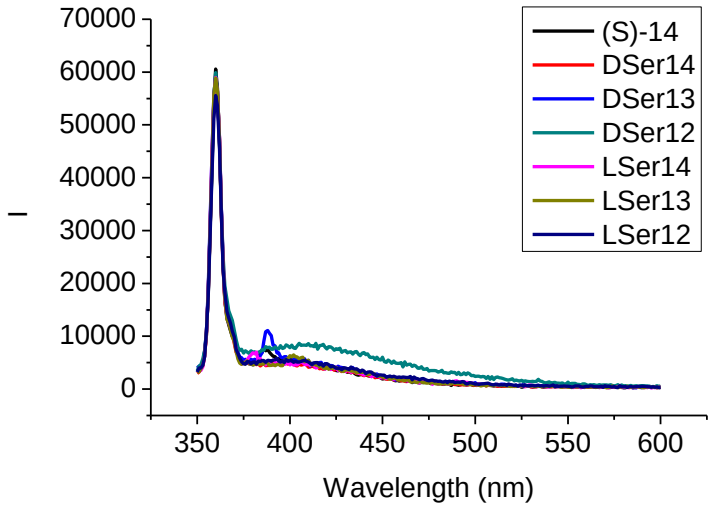

Figure AI-71. Fluorescence spectra of (S)-**7-14** (1×10^{-5} M in THF/H_2O 5:1) in the absence and presence of D- or L-Arginine (1×10^{-4} M, 1×10^{-3} M, 1×10^{-2} M). (λ_{exc} = 325 nm. slit =3.0/3.0 nm)

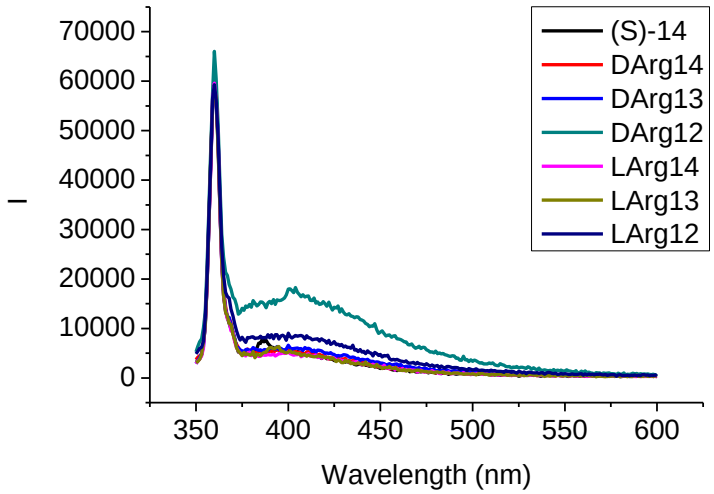

Figure AI-72. Fluorescence spectra of (S)-**7-15** (1×10^{-5} M in THF/H_2O 5:1) in the absence and presence of D- or L-Alanine (1×10^{-4} M, 1×10^{-3} M, 1×10^{-2} M). (λ_{exc} = 325 nm. slit =3.0/3.0 nm)

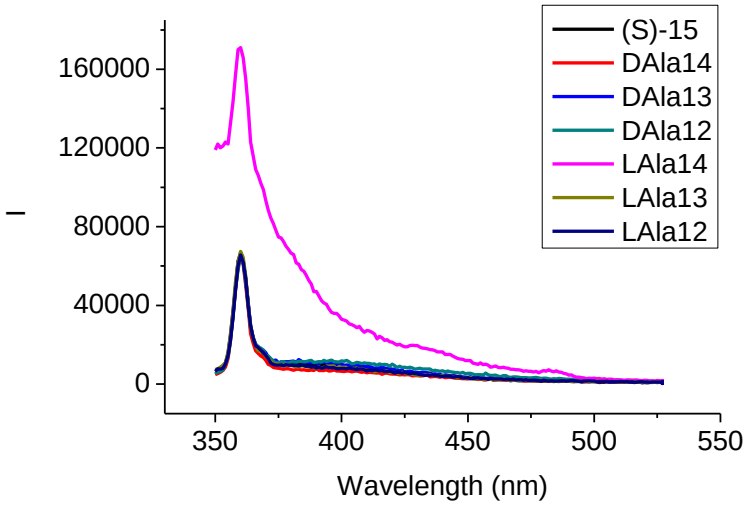

Figure AI-73. Fluorescence spectra of (S)-**7-15** (1×10^{-5} M in THF/H_2O 5:1) in the absence and presence of D- or L-Serine (1×10^{-4} M, 1×10^{-3} M, 1×10^{-2} M). (λ_{exc} = 325 nm. slit =3.0/3.0 nm)

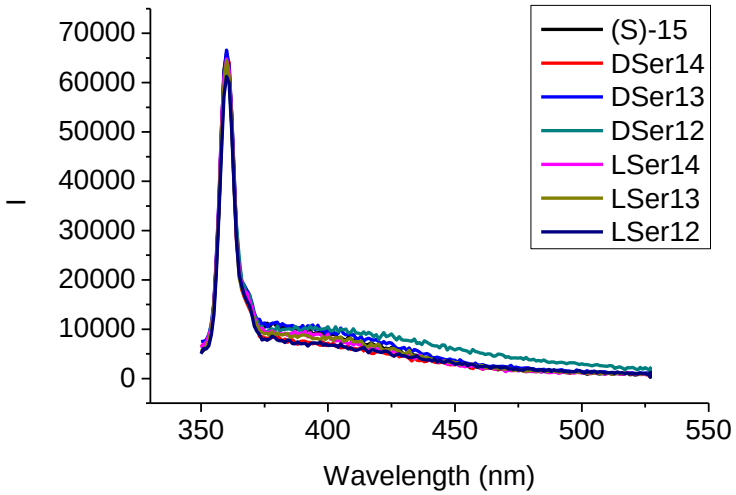

Figure AI-74. Fluorescence spectra of (S)-7-15 (1×10^{-5} M in THF/H_2O 5:1) in the absence and presence of D- or L-Arginine (1×10^{-4} M, 1×10^{-3} M, 1×10^{-2} M). (λ_{exc} = 325 nm. slit =3.0/3.0 nm)

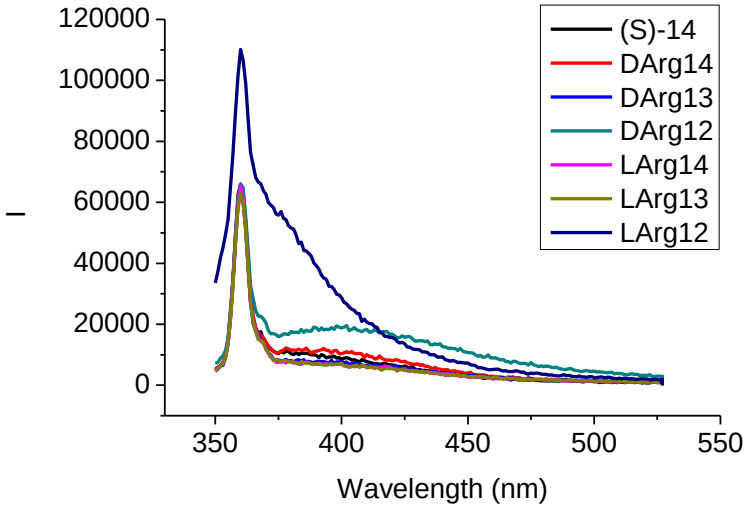

Figure AI-75. Fluorescence spectra of (S)-**7-21** (1×10^{-5} M in THF/H_2O 5:1) in the absence and presence of D- or L-Alanine (1×10^{-4} M, 1×10^{-3} M, 1×10^{-2} M). (λ_{exc} = 325 nm. slit =3.0/3.0 nm)

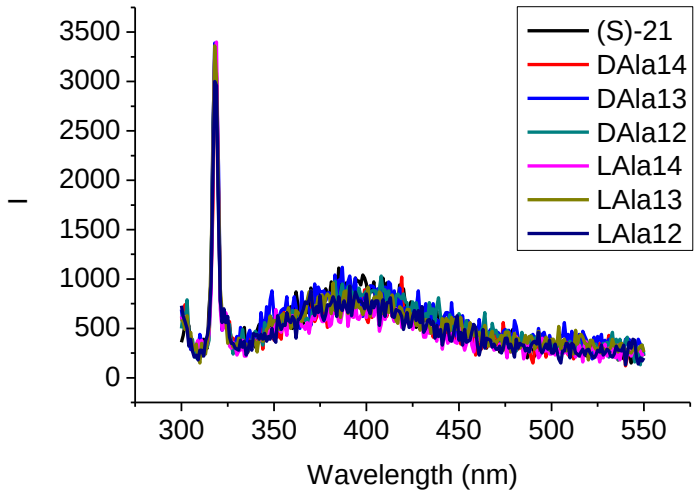

Figure AI-76. Fluorescence spectra of (S)-**7-21** (1×10^{-5} M in THF/H_2O 5:1) in the absence and presence of D- or L-Serine (1×10^{-4} M, 1×10^{-3} M, 1×10^{-2} M). (λ_{exc} = 325 nm. slit =3.0/3.0 nm)

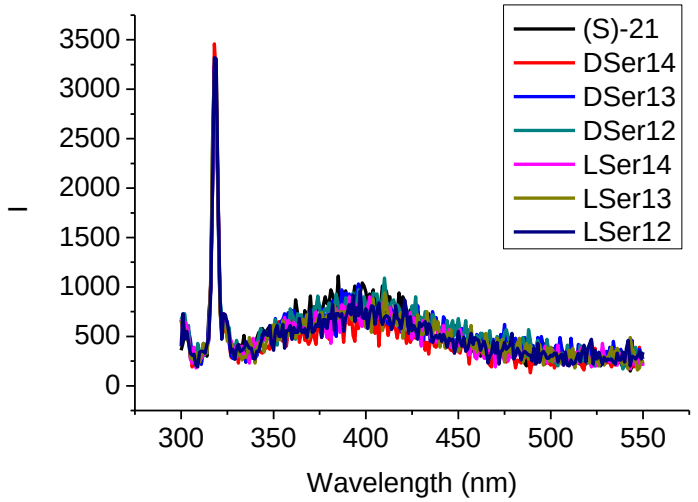

Figure AI-77. Fluorescence spectra of (S)-**7-21** (1×10^{-5} M in THF/H_2O 5:1) in the absence and presence of D- or L-Arginine (1×10^{-4} M, 1×10^{-3} M, 1×10^{-2} M). (λ_{exc} = 325 nm. slit =3.0/3.0 nm)

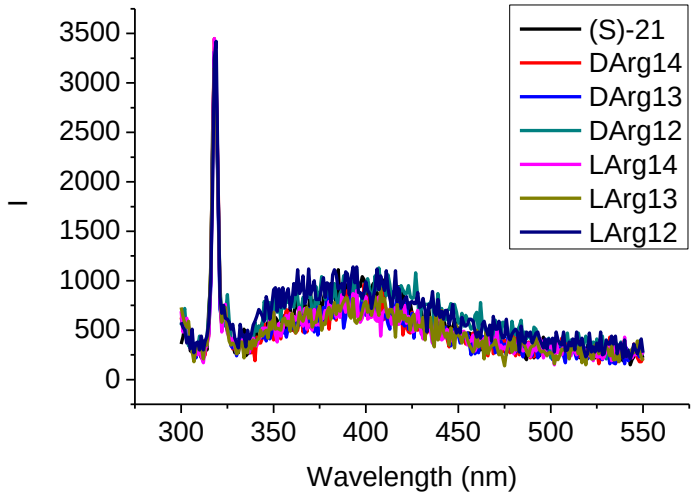

12. NMR spectra

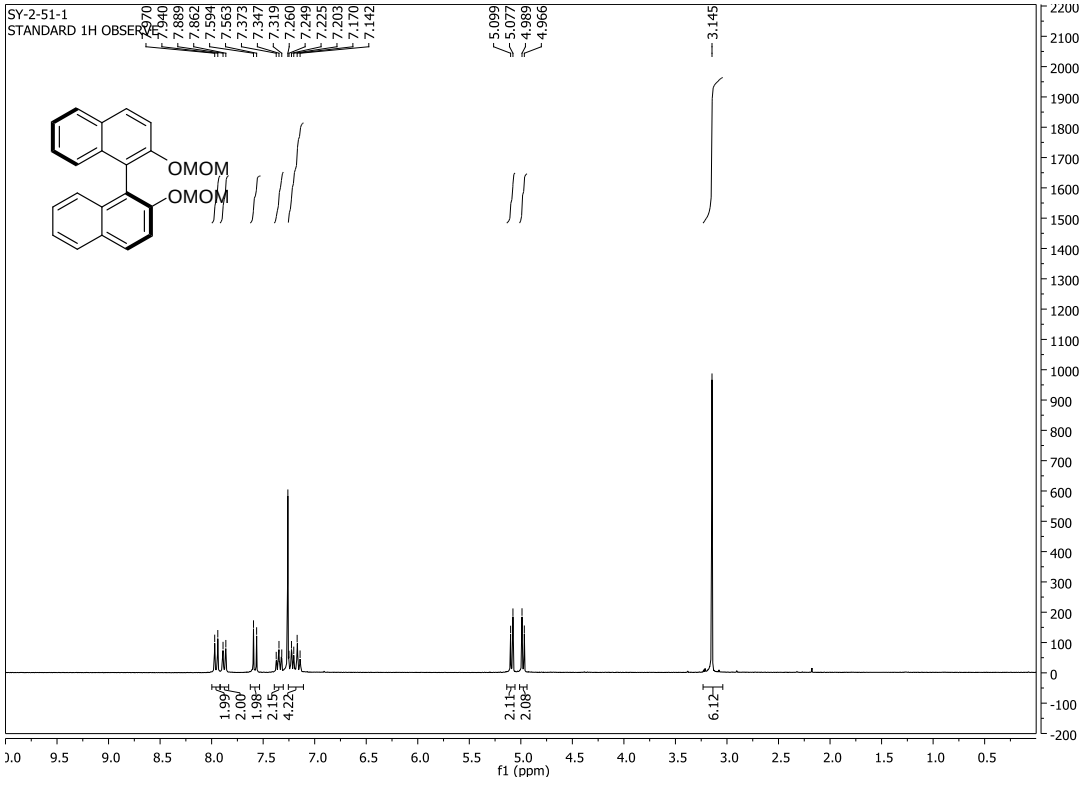

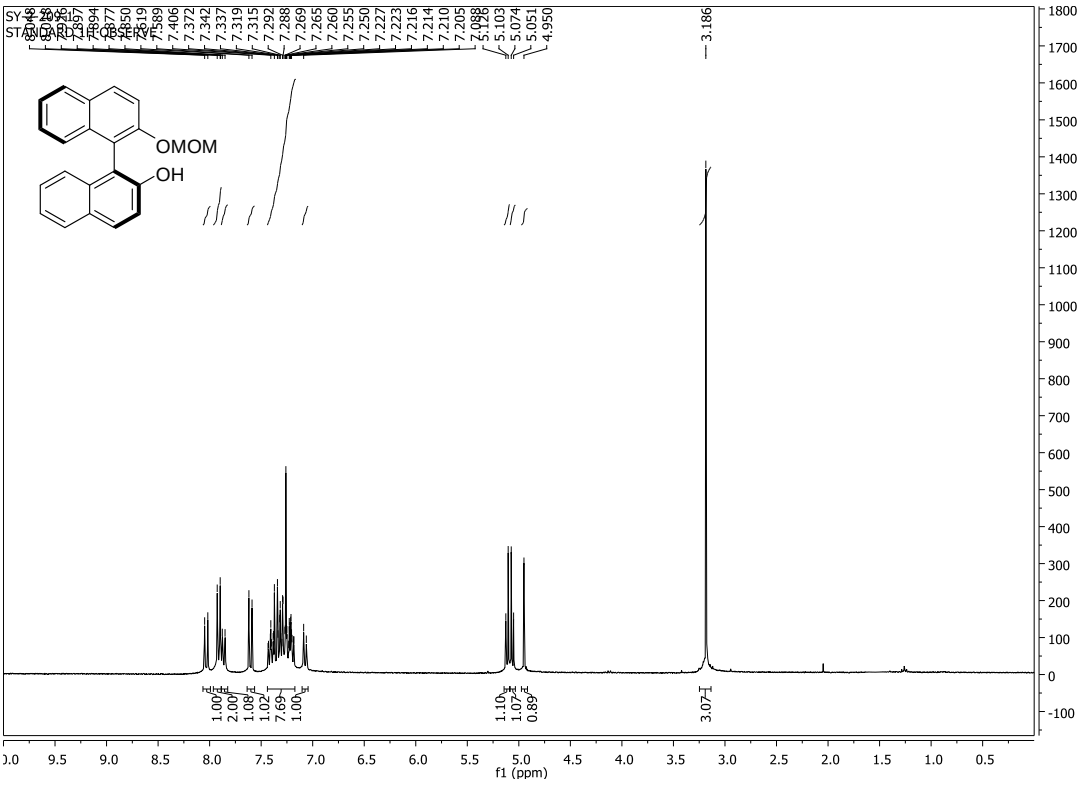
OMOM
OH
3.186
f1 (ppm)

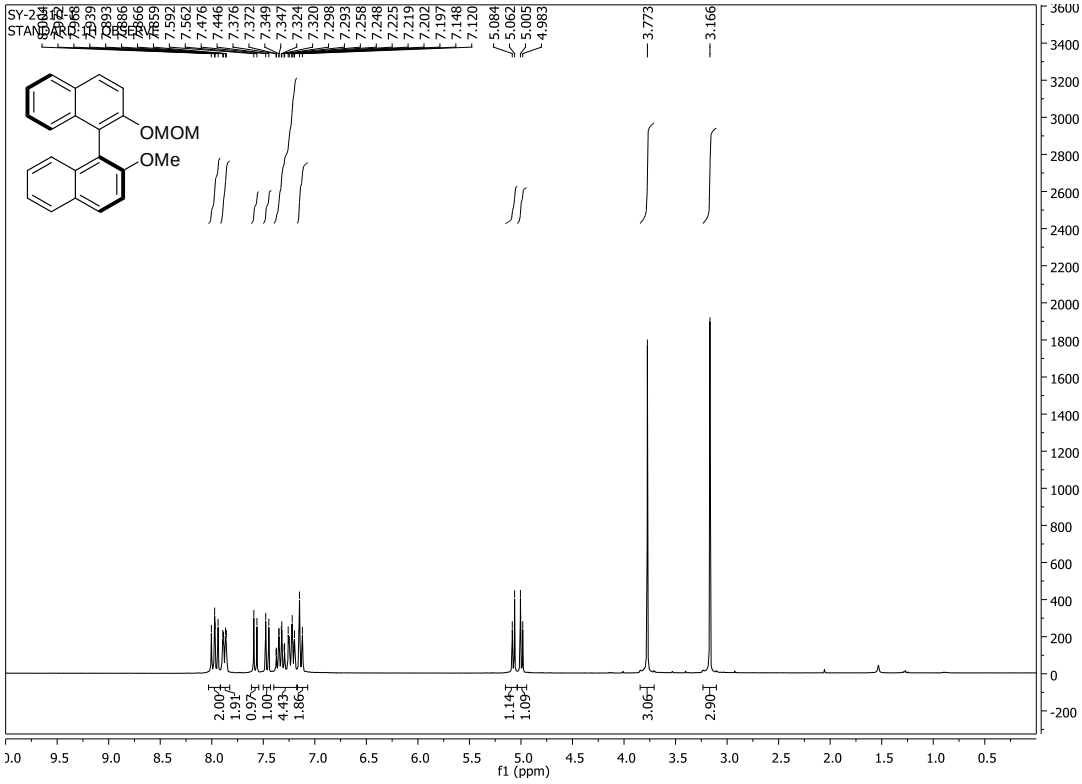
OMOM
OMe
3.773
3.166
f1 (ppm)

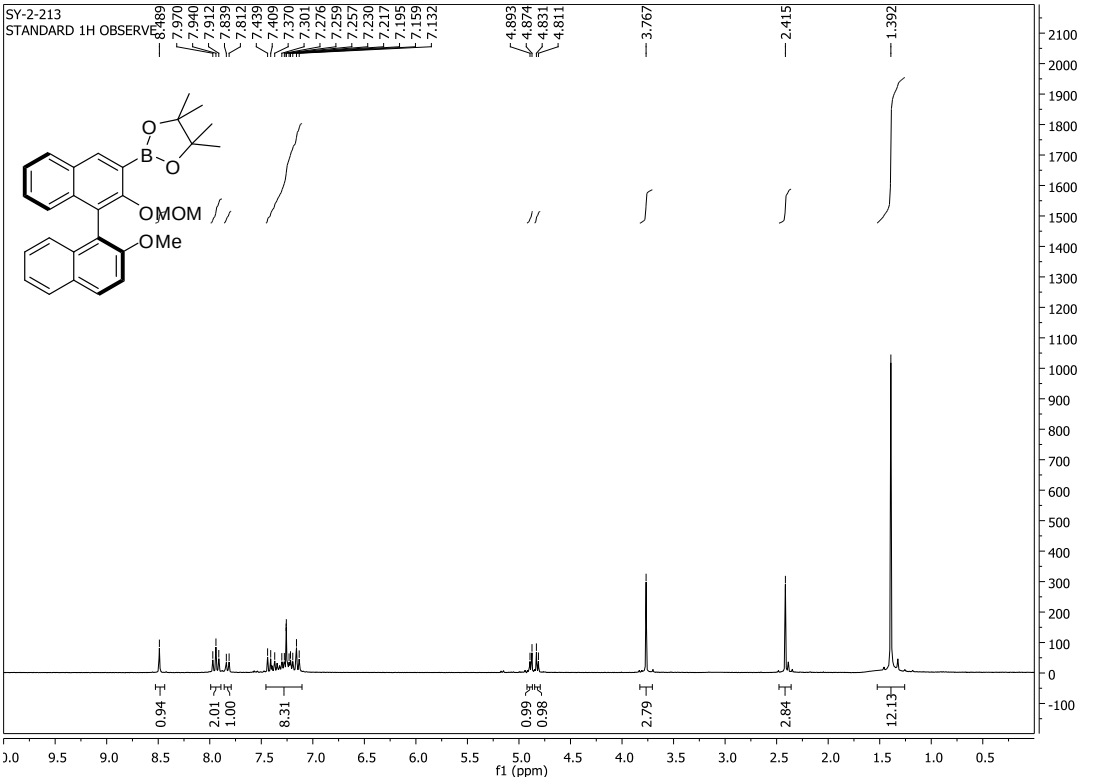
SY-2-213
STANDARD 1H OBSERVE
8.489
7.970
7.940
7.912
7.839
7.812
7.439
7.409
7.370
7.301
7.276
7.259
7.257
7.230
7.217
7.195
7.159
7.132
4.893
4.874
4.831
4.811
3.767
2.415
1.392
O
B
O
OMOM
OMe
0.94
2.01
1.00
8.31
0.99
0.98
2.79
2.84
12.13
f1 (ppm)

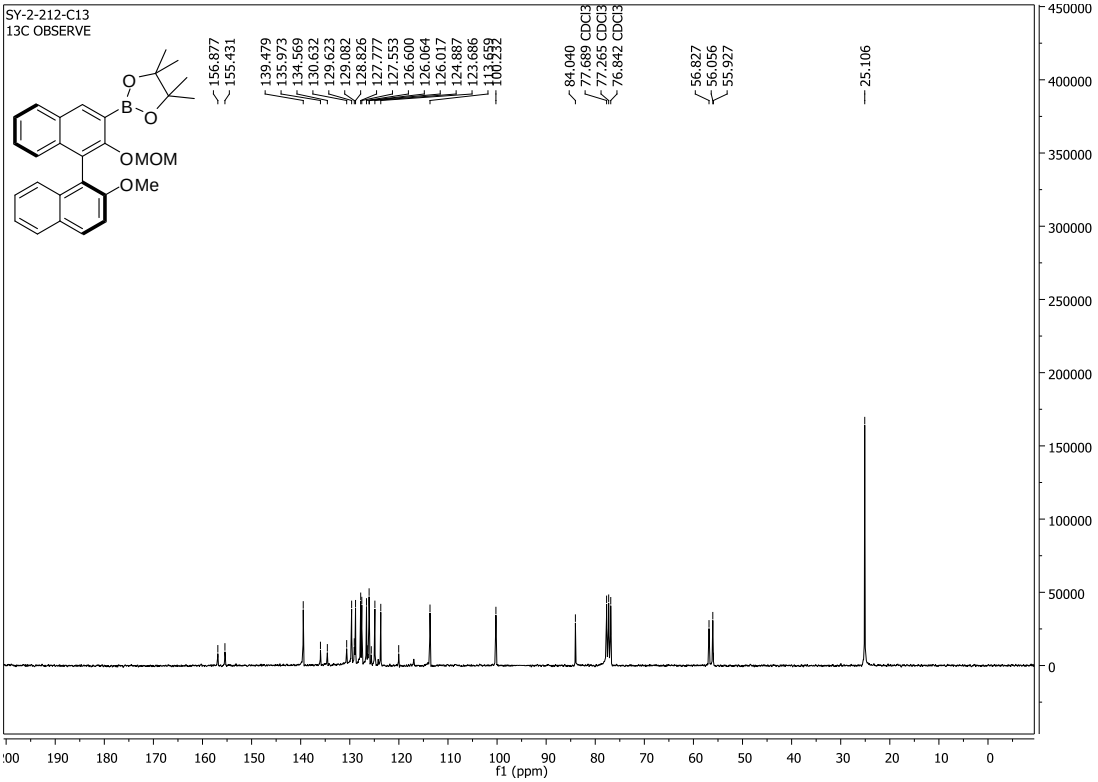
SY-2-212-C13
13C OBSERVE
156.877
155.431
139.479
135.973
134.569
130.632
129.623
129.082
128.826
127.777
127.553
126.600
126.064
126.017
124.887
123.686
84.040
77.689 CDCl3
77.265 CDCl3
76.842 CDCl3
56.827
56.056
55.927
25.106
O
B
O
OMOM
OMe
f1 (ppm)

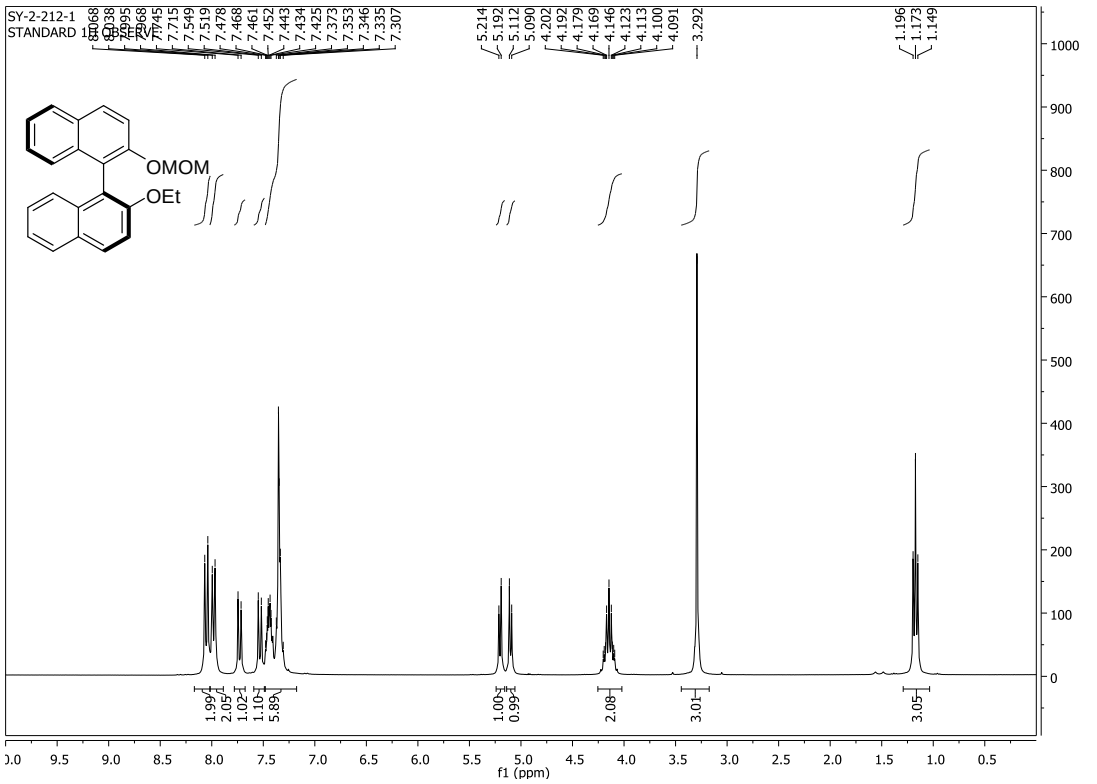
SY-2-212-1
STANDARD 1H OBSERVE
8.168
8.038
7.995
7.968
7.745
7.715
7.549
7.519
7.478
7.468
7.461
7.452
7.443
7.434
7.425
7.373
7.353
7.346
7.335
7.307
5.214
5.192
5.112
5.090
4.202
4.192
4.179
4.169
4.146
4.123
4.113
4.100
4.091
3.292
1.196
1.173
1.149
OMOM
OEt
1.99
2.05
1.02
1.10
5.89
1.00
0.99
2.08
3.01
3.05
f1 (ppm)

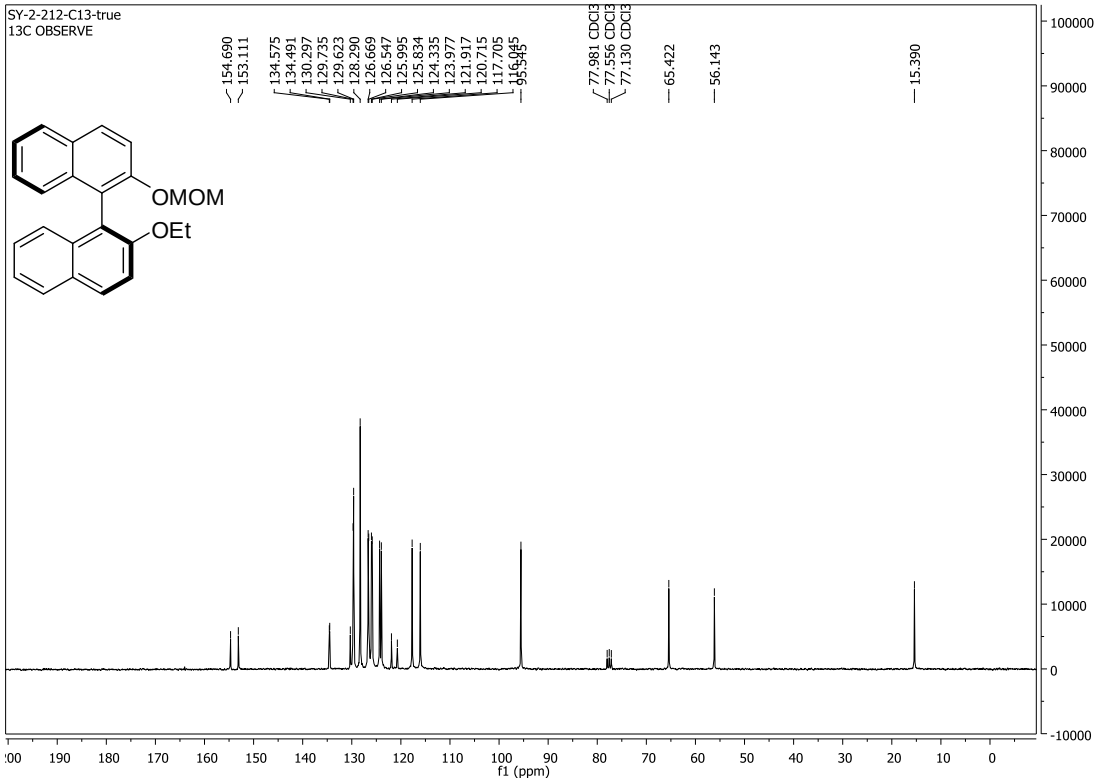
SY-2-212-C13-true
13C OBSERVE
154.690
153.111
134.575
134.491
130.297
129.735
129.623
128.290
126.669
126.547
125.995
125.834
124.335
123.977
121.917
120.715
117.705
116.045
95.545
77.981 CDCl3
77.556 CDCl3
77.130 CDCl3
65.422
56.143
15.390
OMOM
OEt
f1 (ppm)

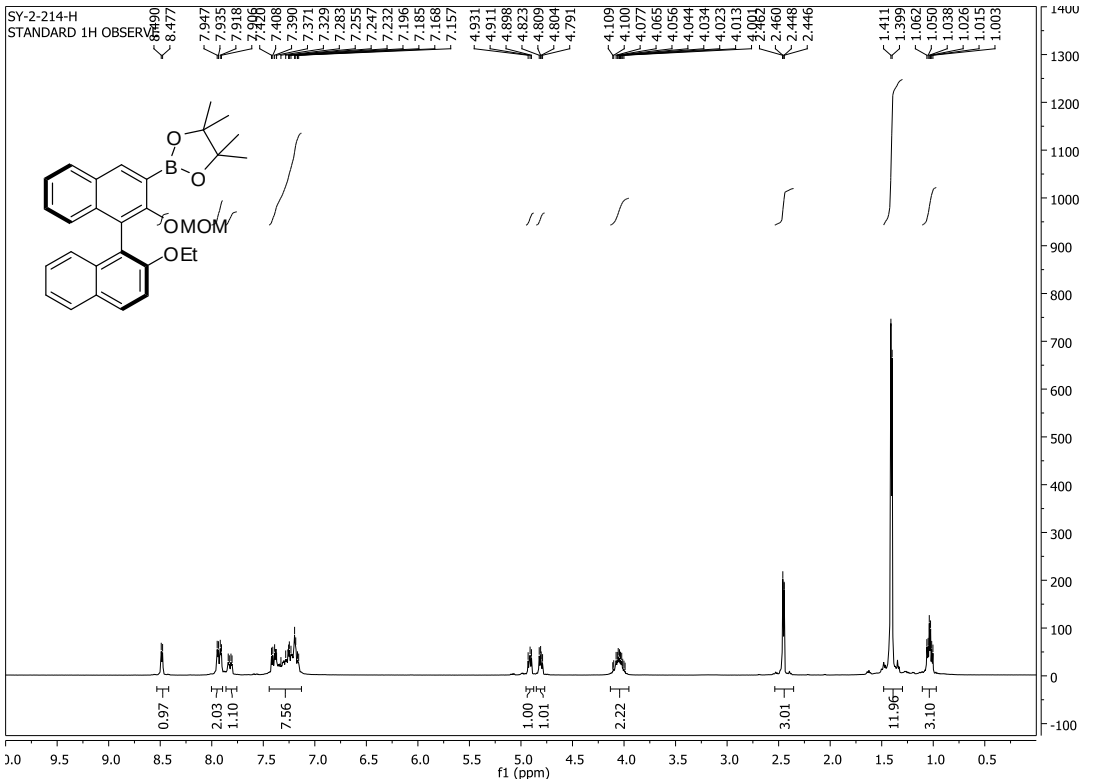
SY-2-214-H
STANDARD 1H OBSERVE
OMOM
OEt
f1 (ppm)

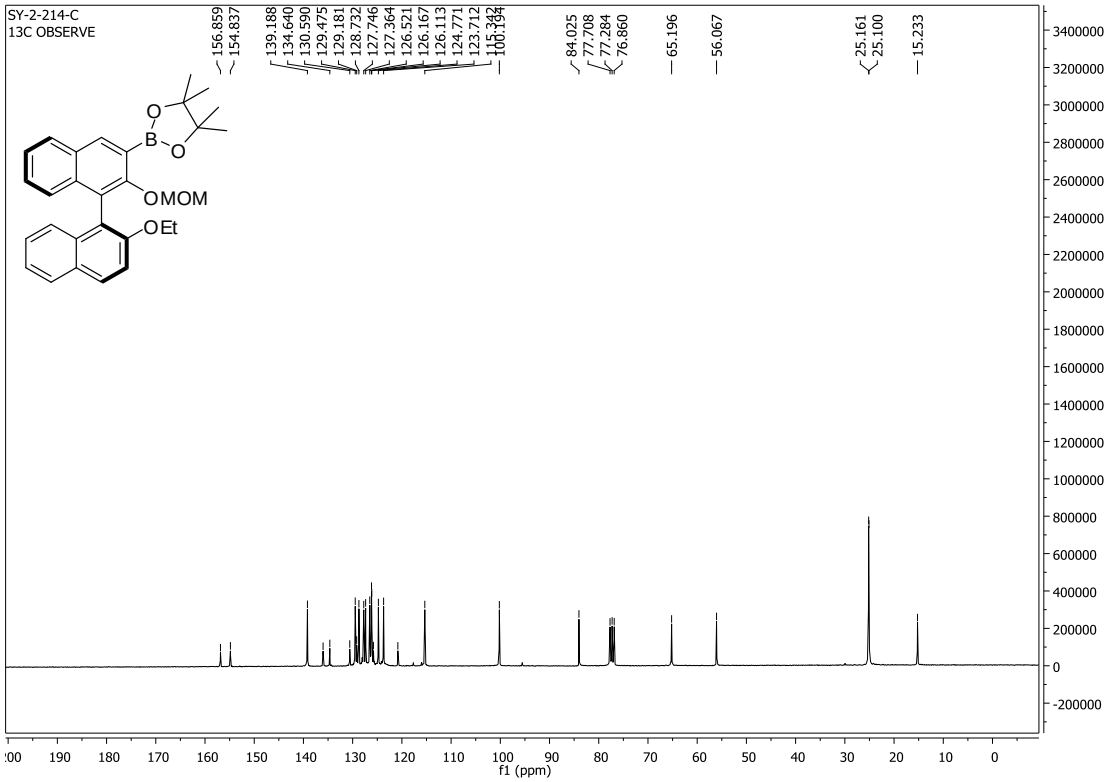
SY-2-214-C
13C OBSERVE
OMOM
OEt
f1 (ppm)

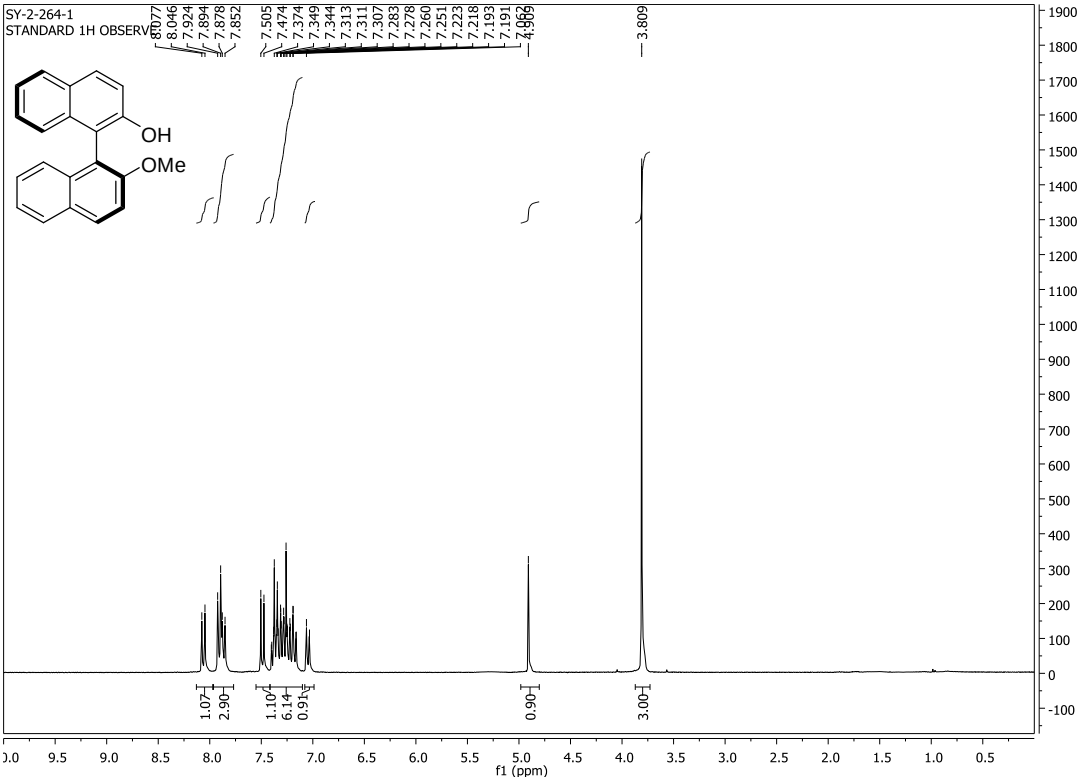
SY-2-264-1
STANDARD 1H OBSERV
OH
OMe
f1 (ppm)

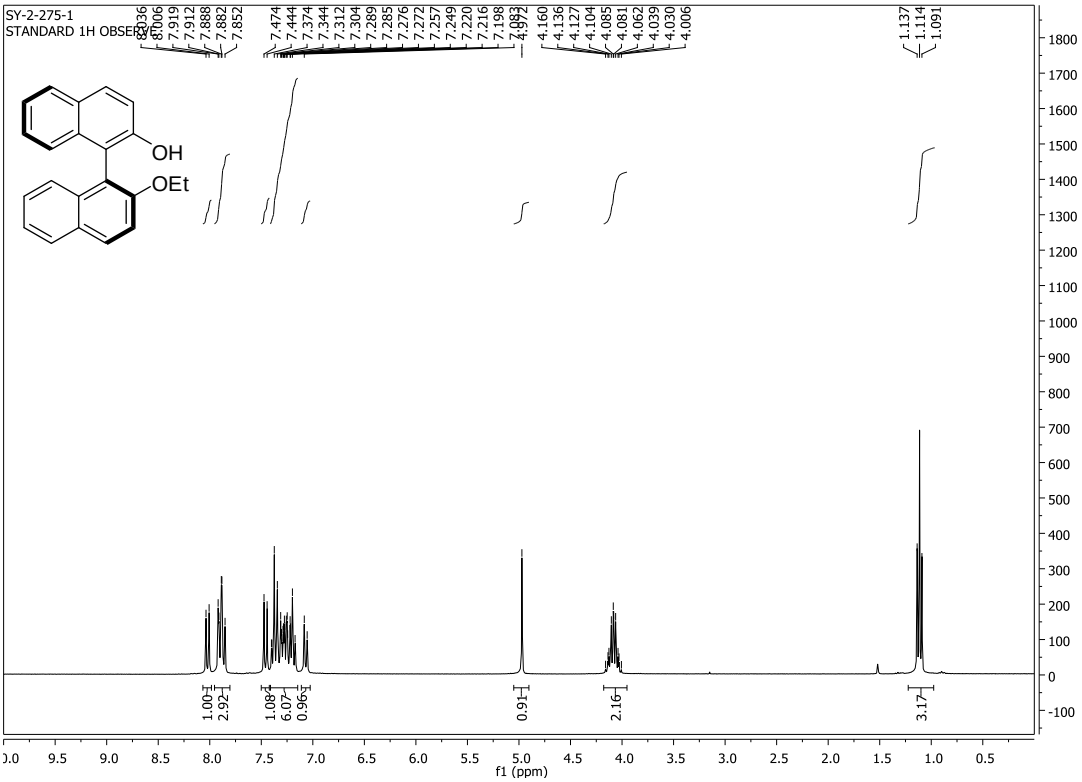
SY-2-275-1
STANDARD 1H OBSERV
OH
OEt
f1 (ppm)

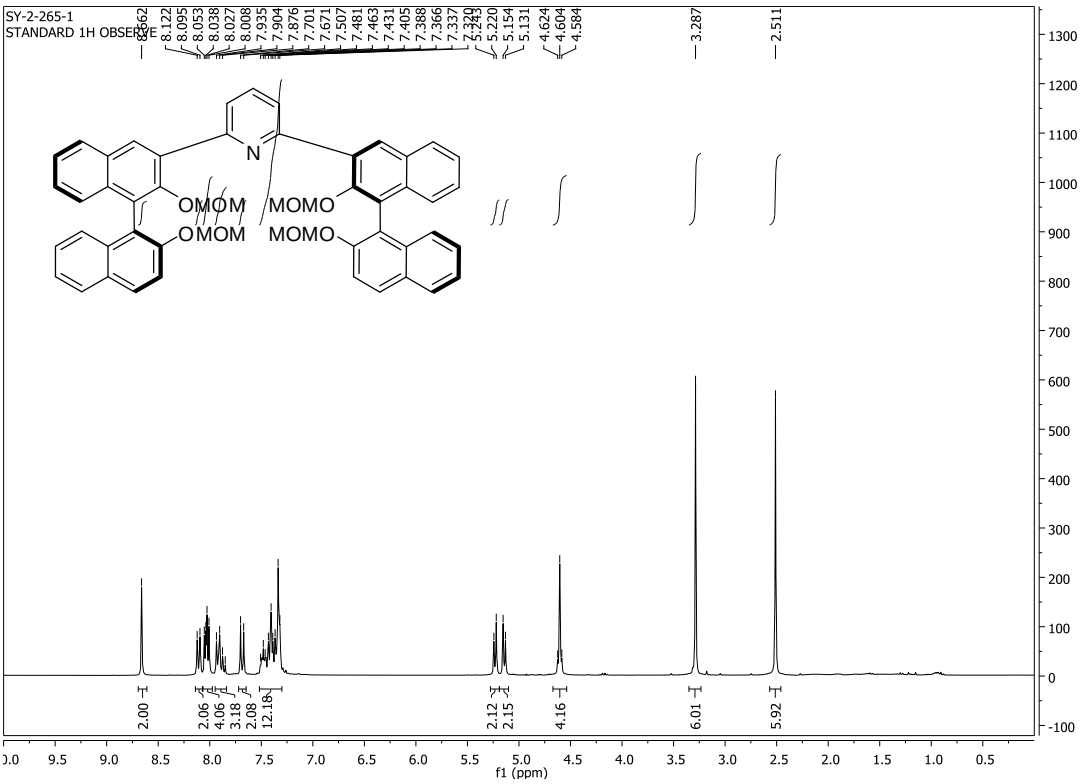
SY-2-265-1
STANDARD 1H OBSERVE
8.362
8.122
8.095
8.053
8.038
8.027
8.008
7.935
7.904
7.876
7.701
7.671
7.507
7.481
7.463
7.431
7.405
7.388
7.366
7.337
7.320
7.243
5.220
5.154
5.131
4.624
4.604
4.584
3.287
2.511
N
OMOM
MOMO
OMOM
MOMO
2.00
2.06
4.06
3.18
2.08
12.18
2.12
2.15
4.16
6.01
5.92
f1 (ppm)

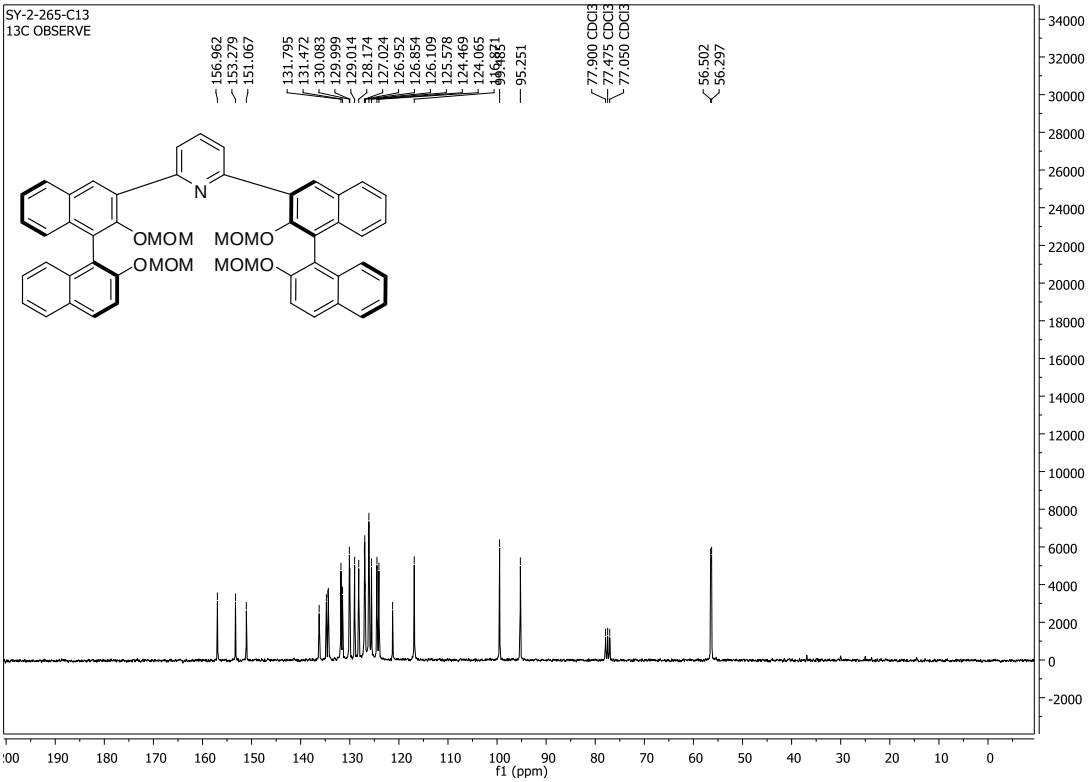
SY-2-265-C13
13C OBSERVE
156.962
153.279
151.067
131.795
131.472
130.083
129.999
129.014
128.174
127.024
126.952
126.854
126.109
125.578
124.469
124.065
99.485
95.251
77.900 CDCl3
77.475 CDCl3
77.050 CDCl3
56.502
56.297
N
OMOM
MOMO
OMOM
MOMO
f1 (ppm)

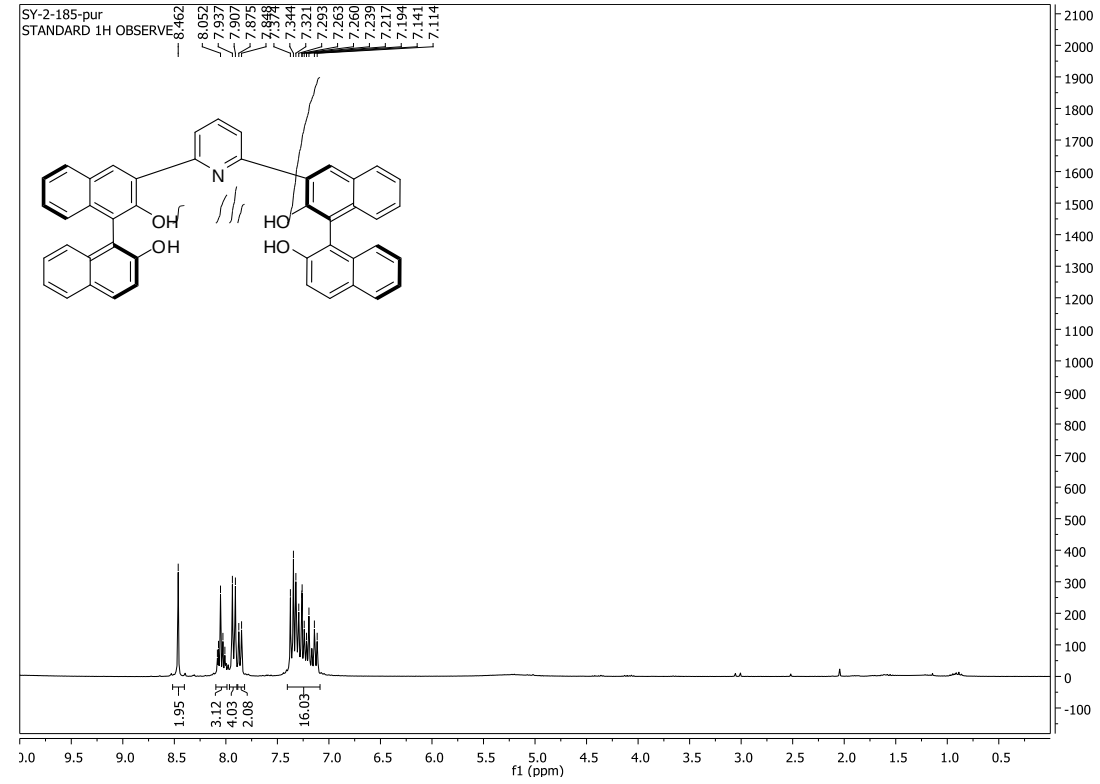
SY-2-185-pur
STANDARD 1H OBSERVE
8.462
8.052
7.937
7.907
7.875
7.344
7.321
7.293
7.263
7.260
7.239
7.217
7.194
7.141
7.114
N
OH
OH
HO
HO
1.95
3.12
4.03
2.08
16.03
f1 (ppm)

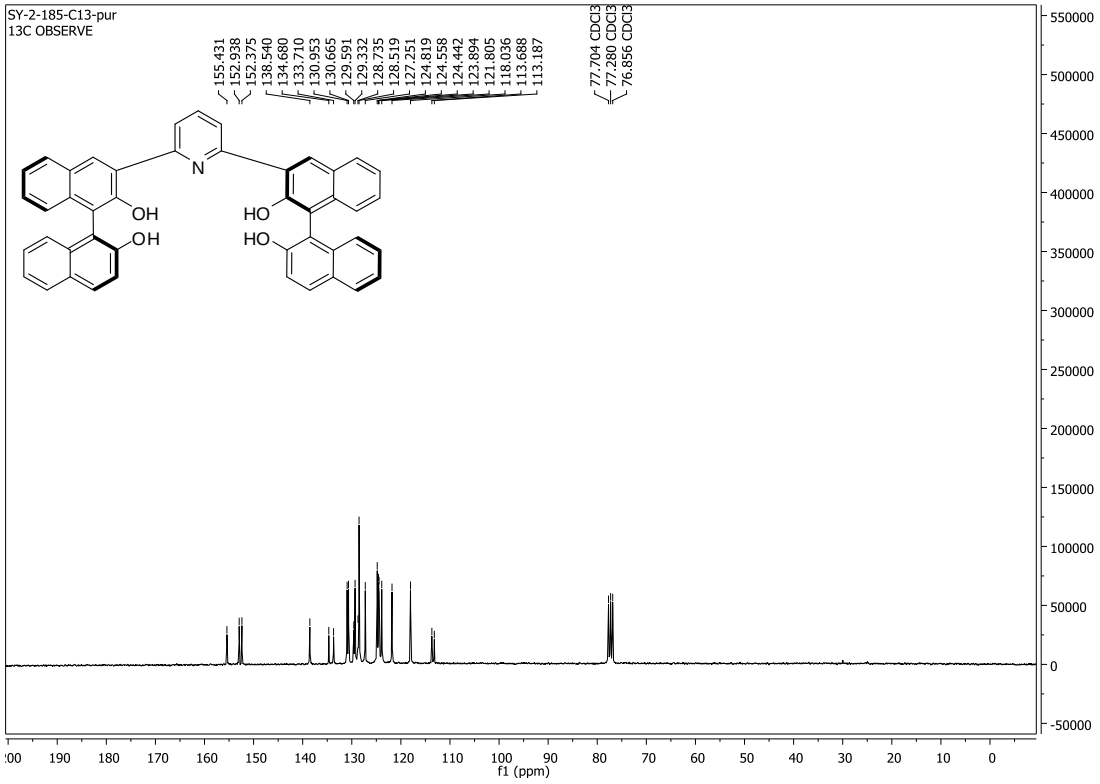
SY-2-185-C13-pur
13C OBSERVE
155.431
152.938
152.375
138.540
134.680
133.710
130.953
130.665
129.591
129.332
128.735
128.519
127.251
124.819
124.558
124.442
123.894
121.805
118.036
113.688
113.187
77.704 CDCl3
77.280 CDCl3
76.856 CDCl3
N
OH
OH
HO
HO
f1 (ppm)

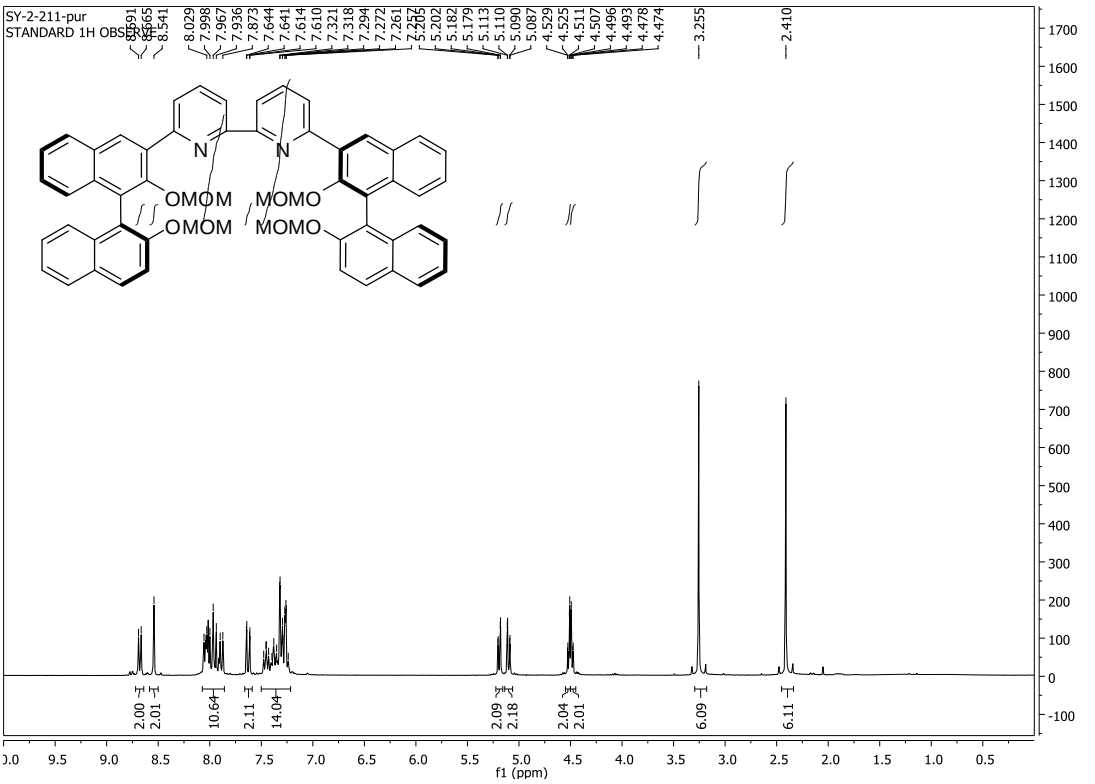
SY-2-211-pur
STANDARD 1H OBSERVE
8.591
8.565
8.541
8.029
7.998
7.967
7.936
7.873
7.644
7.641
7.614
7.610
7.321
7.318
7.294
7.272
7.261
7.257
7.205
5.202
5.182
5.179
5.113
5.110
5.090
5.087
4.529
4.525
4.511
4.507
4.496
4.493
4.478
4.474
3.255
2.410
N
N
OMOM
MOMO
OMOM
MOMO
2.00
2.01
10.64
2.11
14.04
2.09
2.18
2.04
2.01
6.09
6.11
f1 (ppm)

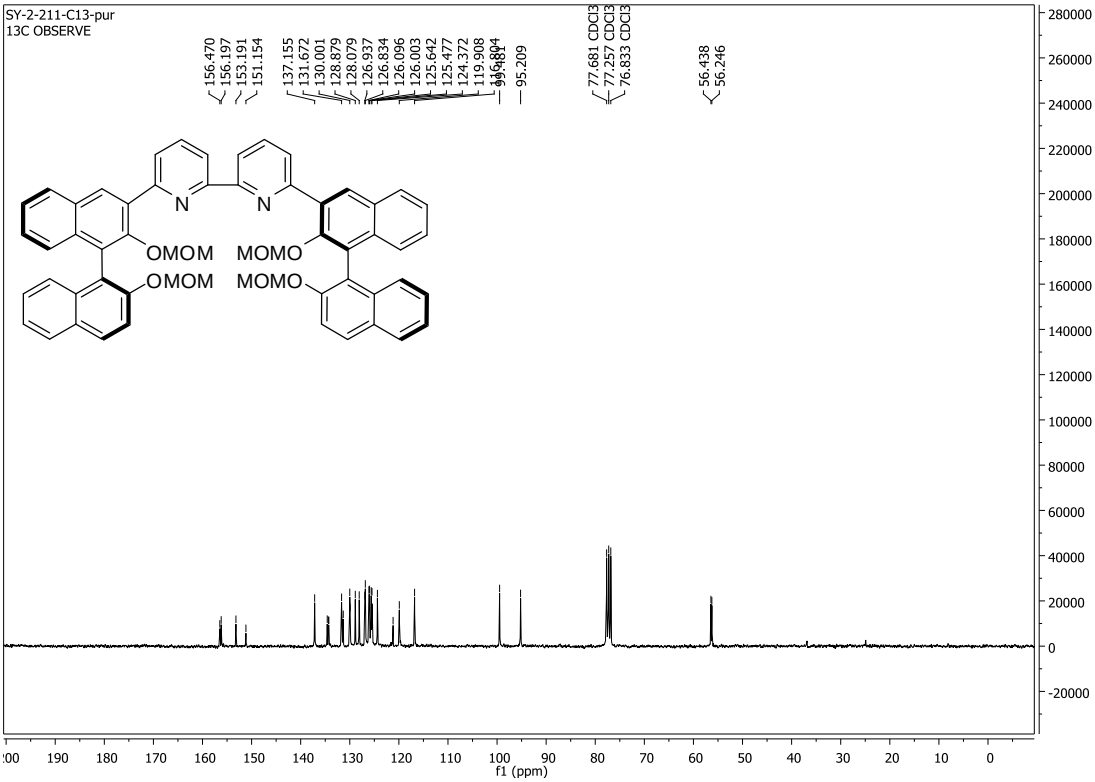
SY-2-211-C13-pur
13C OBSERVE
156.470
156.197
153.191
151.154
137.155
131.672
130.001
128.879
128.079
126.937
126.834
126.096
126.003
125.642
125.477
124.372
119.908
95.209
77.681 CDCl3
77.257 CDCl3
76.833 CDCl3
56.438
56.246
N
N
OMOM
MOMO
OMOM
MOMO
f1 (ppm)

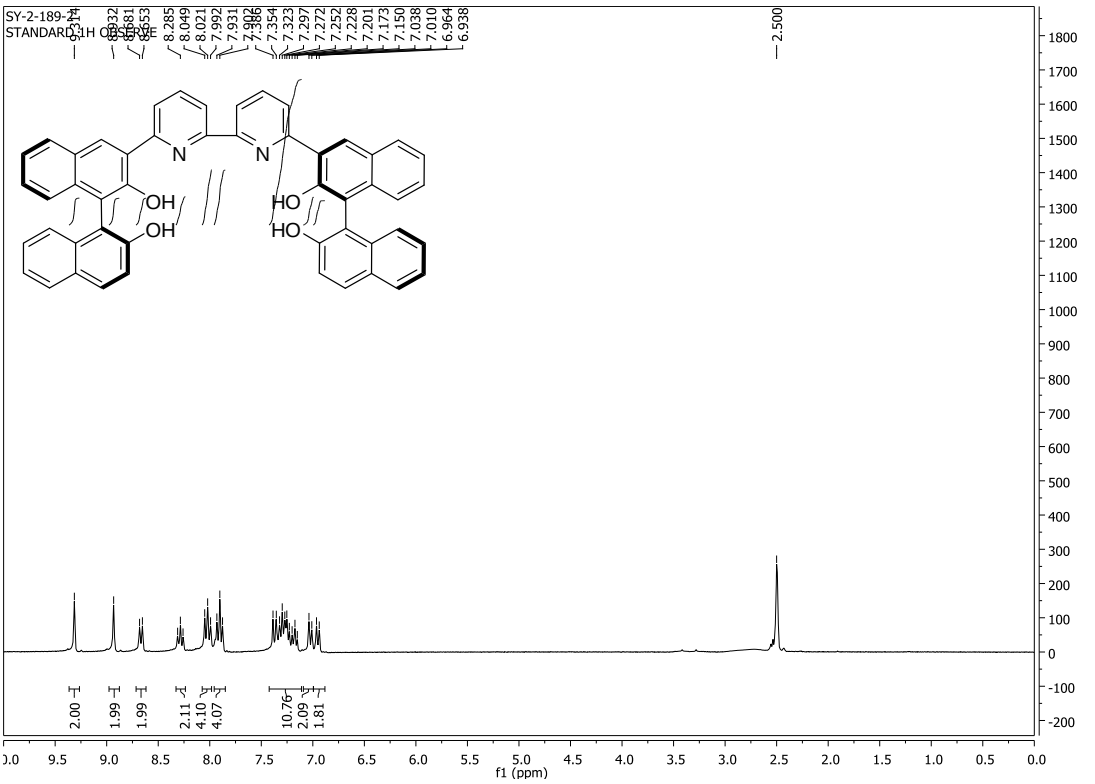
SY-2-189-1H
STANDARD 1H OBSERVE
9.314
8.932
8.681
8.553
8.285
8.049
8.021
7.992
7.931
7.902
7.386
7.354
7.323
7.297
7.272
7.252
7.228
7.201
7.173
7.150
7.038
7.010
6.964
6.938
2.500
N
N
OH
OH
HO
HO
2.00
1.99
1.99
2.11
4.10
4.07
10.76
2.09
1.81
f1 (ppm)

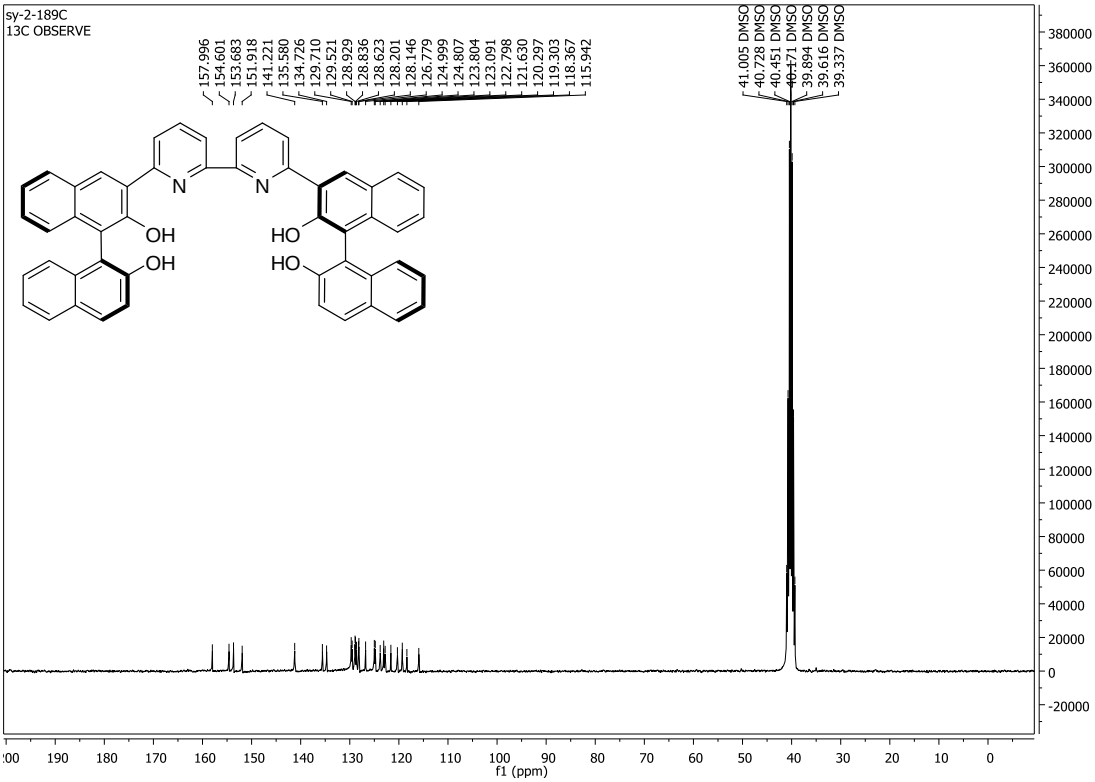
sy-2-189C
13C OBSERVE
157.996
154.601
153.683
151.918
141.221
135.580
134.726
129.710
129.521
128.929
128.836
128.623
128.201
128.146
126.779
124.999
124.807
123.804
123.091
122.798
121.630
120.297
119.303
118.367
115.942
41.005 DMSO
40.728 DMSO
40.451 DMSO
40.171 DMSO
39.894 DMSO
39.616 DMSO
39.337 DMSO
N
N
OH
OH
HO
HO
f1 (ppm)

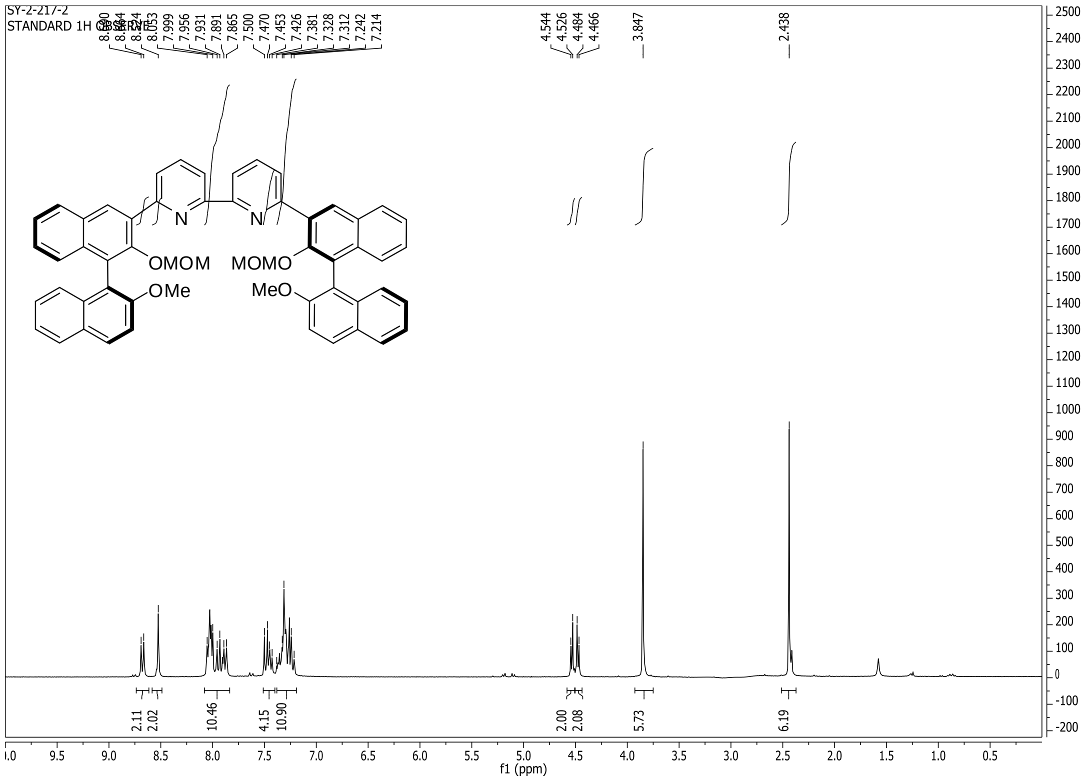
SY-2-217-2
STANDARD 1H OBSERVE
8.690
8.664
8.524
8.053
7.999
7.956
7.931
7.891
7.865
7.500
7.470
7.453
7.426
7.381
7.328
7.312
7.242
7.214
4.544
4.526
4.484
4.466
3.847
2.438
OMOM
MOMO
OMe
MeO
N
2.11
2.02
10.46
4.15
10.90
2.00
2.08
5.73
6.19
f1 (ppm)

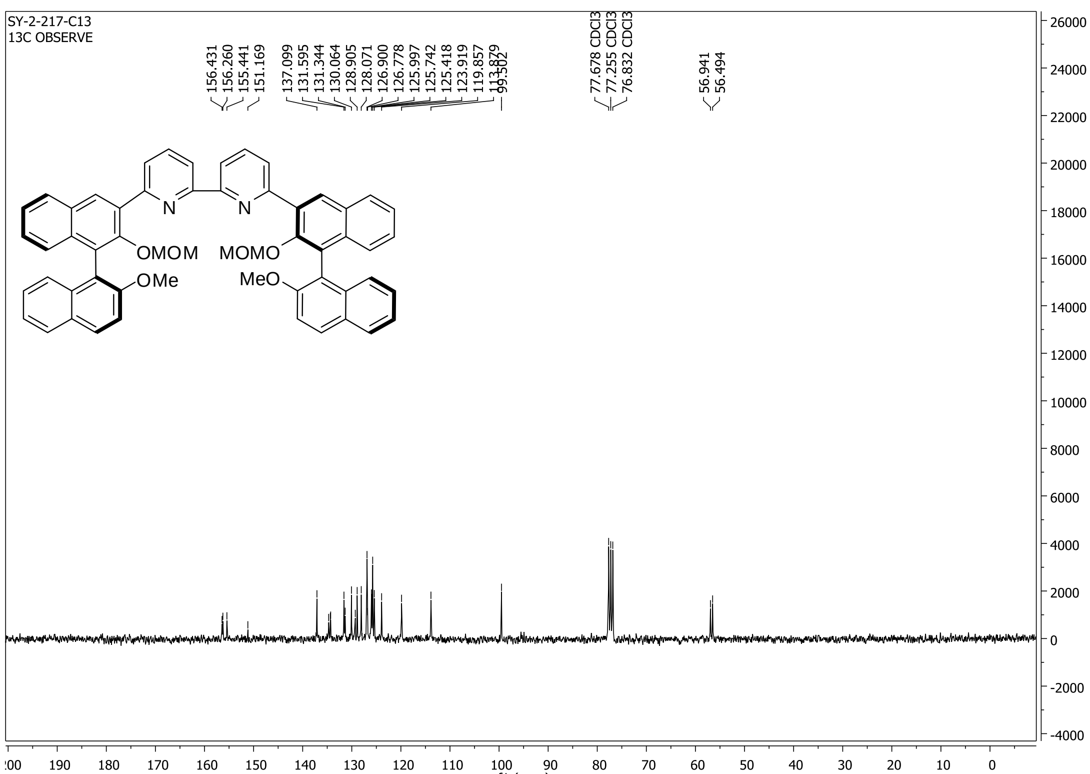
SY-2-217-C13
13C OBSERVE
156.431
156.260
155.441
151.169
137.099
131.595
131.344
130.064
128.905
128.071
126.900
126.778
125.997
125.742
125.418
123.919
119.857
113.829
99.302
77.678 CDCl3
77.255 CDCl3
76.832 CDCl3
56.941
56.494
OMOM
MOMO
OMe
MeO
N
f1 (ppm)

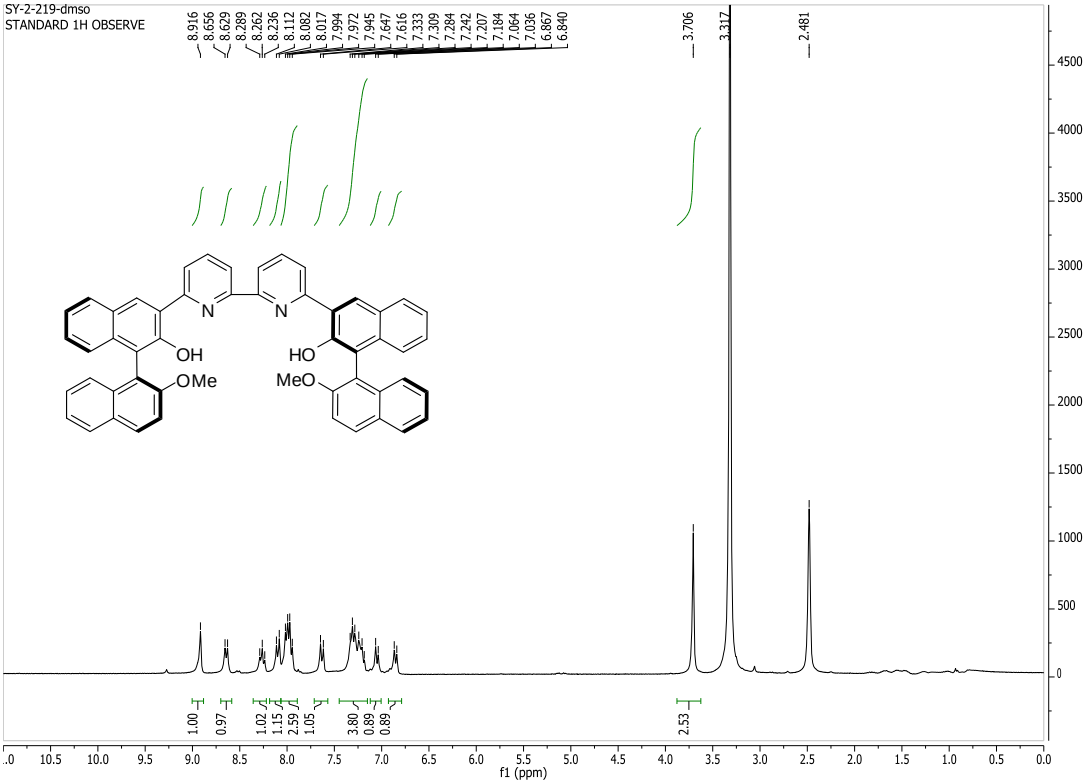
SY-2-219-dmso
STANDARD 1H OBSERVE
8.916
8.656
8.629
8.289
8.262
8.236
8.112
8.082
8.017
7.994
7.972
7.945
7.647
7.616
7.333
7.309
7.284
7.242
7.207
7.184
7.064
7.036
6.867
6.840
3.706
3.317
2.481
N
N
OH
OMe
HO
MeO
1.00
0.97
1.02
1.15
2.59
1.05
3.80
0.89
0.89
2.53
f1 (ppm)

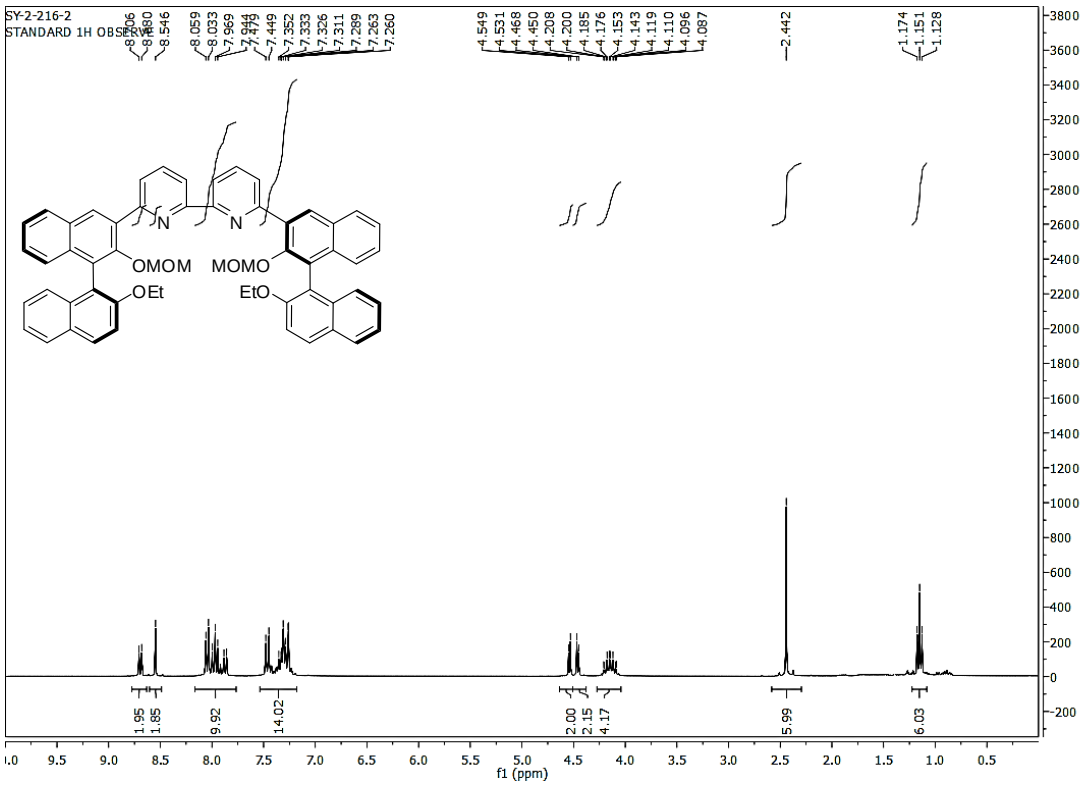
SY-2-216-2
STANDARD 1H OBSERVE
8.546
8.059
8.033
7.969
7.449
7.352
7.333
7.326
7.311
7.289
7.263
7.260
4.549
4.531
4.468
4.450
4.208
4.200
4.185
4.176
4.153
4.143
4.119
4.110
4.096
4.087
2.442
1.174
1.151
1.128
N
N
OMOM
OEt
MOMO
EtO
1.95
1.85
9.92
14.02
2.00
2.15
4.17
5.99
6.03
f1 (ppm)

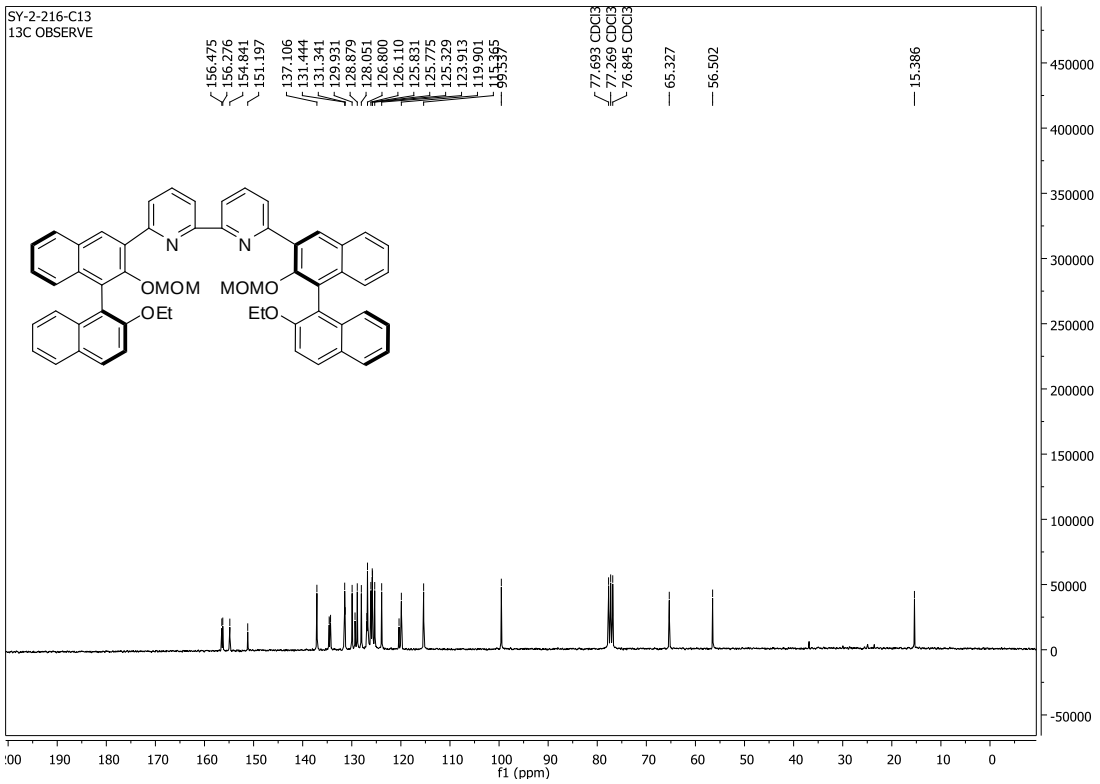
SY-2-216-C13
13C OBSERVE
156.475
156.276
154.841
151.197
137.106
131.444
131.341
129.931
128.879
128.051
126.800
126.110
125.831
125.775
125.329
123.913
119.901
99.537
77.693 CDCl3
77.269 CDCl3
76.845 CDCl3
65.327
56.502
15.386
OMOM
MOMO
OEt
EtO
N
N
f1 (ppm)

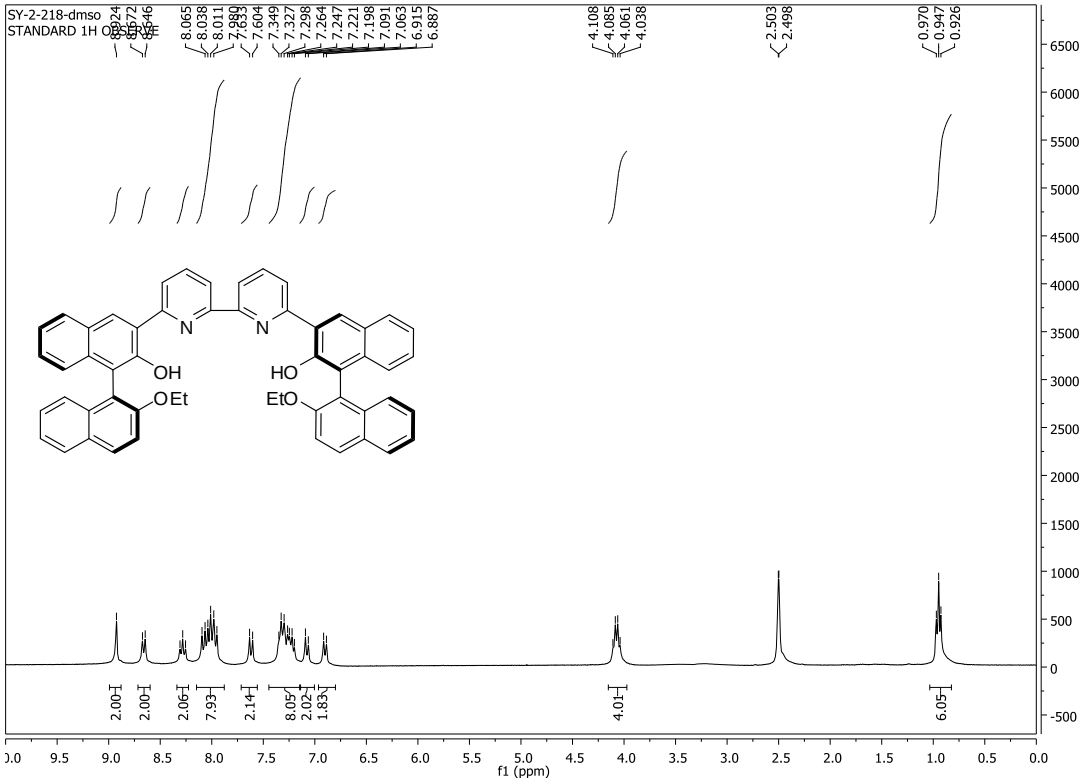
SY-2-218-dmso
STANDARD 1H OBSERVE
8.065
8.038
8.011
7.989
7.633
7.604
7.349
7.327
7.298
7.264
7.247
7.221
7.198
7.091
7.063
6.915
6.887
4.108
4.085
4.061
4.038
2.503
2.498
0.970
0.947
0.926
OH
HO
OEt
EtO
N
N
2.00
2.00
2.06
7.93
2.14
8.05
2.02
1.83
4.01
6.05
f1 (ppm)

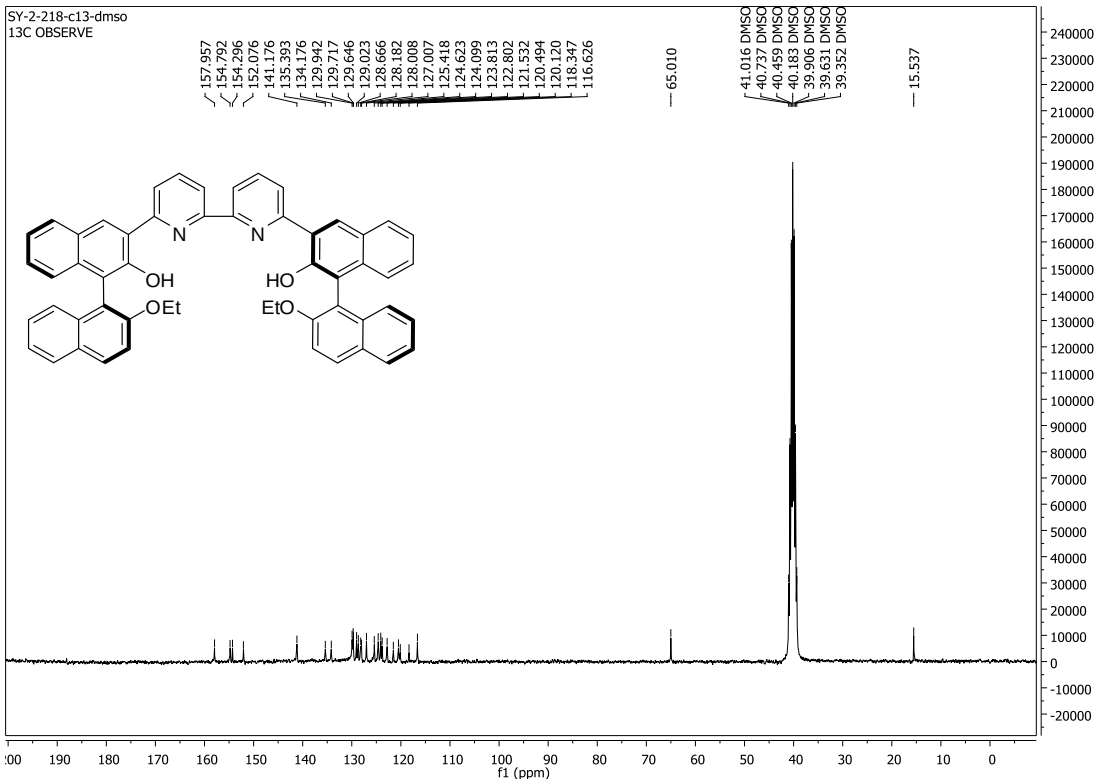
SY-2-218-c13-dmso
13C OBSERVE
157.957
154.792
154.296
152.076
141.176
135.393
134.176
129.942
129.717
129.646
129.023
128.666
128.182
128.008
127.007
125.418
124.623
124.099
123.813
122.802
121.532
120.494
120.120
118.347
116.626
65.010
41.016 DMSO
40.737 DMSO
40.459 DMSO
40.183 DMSO
39.906 DMSO
39.631 DMSO
39.352 DMSO
15.537
N
N
OH
OEt
HO
EtO
f1 (ppm)

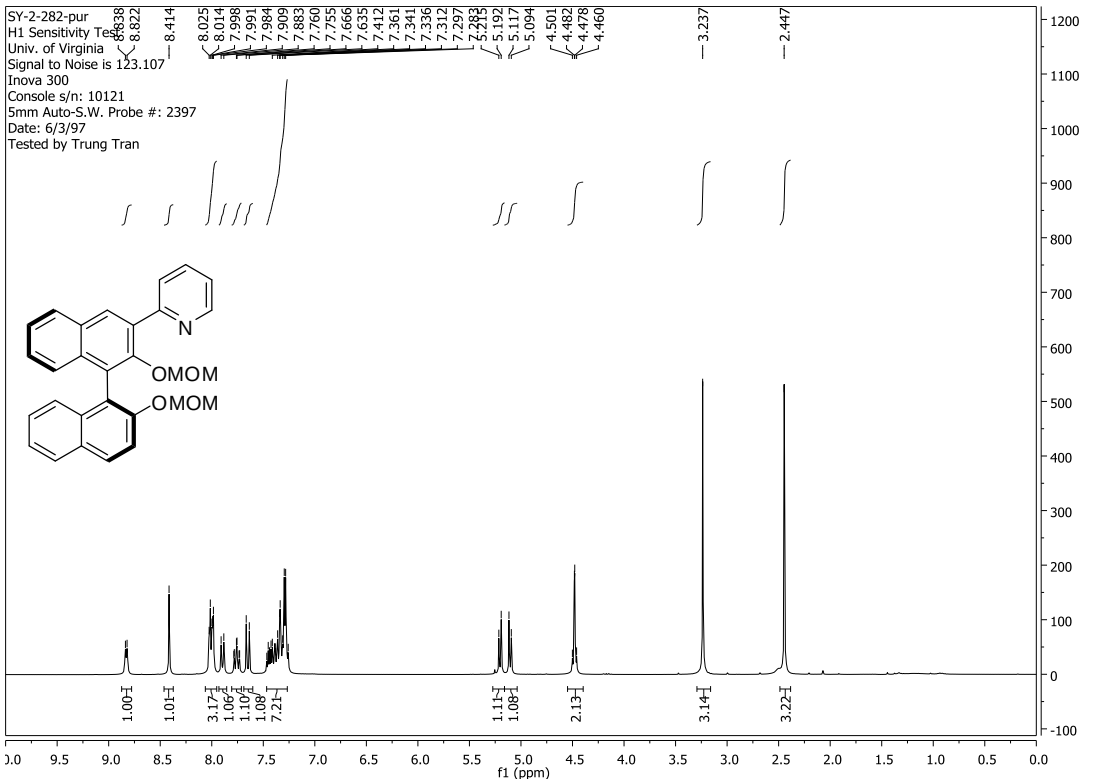
SY-2-282-pur
H1 Sensitivity Test
Univ. of Virginia
Signal to Noise is 123.107
Inova 300
Console s/n: 10121
5mm Auto-S.W. Probe #: 2397
Date: 6/3/97
Tested by Trung Tran
8.838
8.822
8.414
8.025
8.014
7.998
7.991
7.984
7.909
7.883
7.760
7.755
7.666
7.635
7.412
7.361
7.341
7.336
7.312
7.297
7.283
5.215
5.192
5.117
5.094
4.501
4.482
4.478
4.460
3.237
2.447
N
OMOM
OMOM
1.00
1.01
3.17
1.06
1.10
1.08
7.21
1.11
1.08
2.13
3.14
3.22
f1 (ppm)

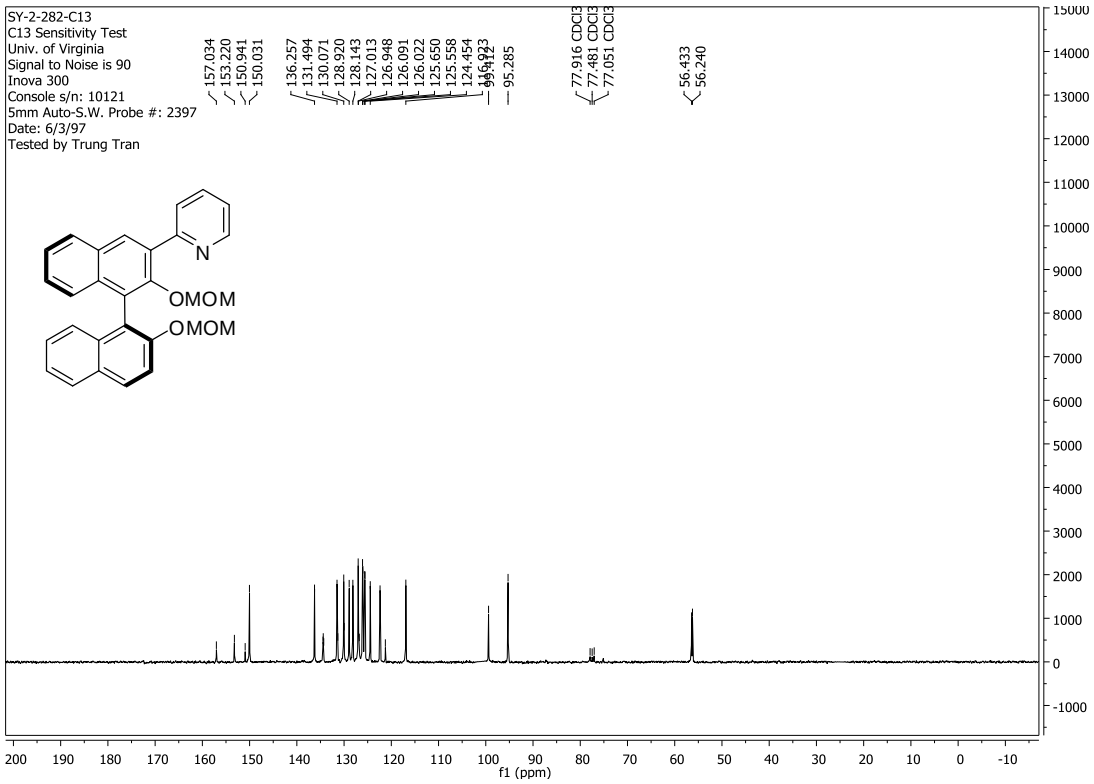
SY-2-282-C13
C13 Sensitivity Test
Univ. of Virginia
Signal to Noise is 90
Inova 300
Console s/n: 10121
5mm Auto-S.W. Probe #: 2397
Date: 6/3/97
Tested by Trung Tran
157.034
153.220
150.941
150.031
136.257
131.494
130.071
128.920
128.143
127.013
126.948
126.091
126.022
125.650
125.558
124.454
95.285
77.916 CDCl3
77.481 CDCl3
77.051 CDCl3
56.433
56.240
N
OMOM
OMOM
f1 (ppm)

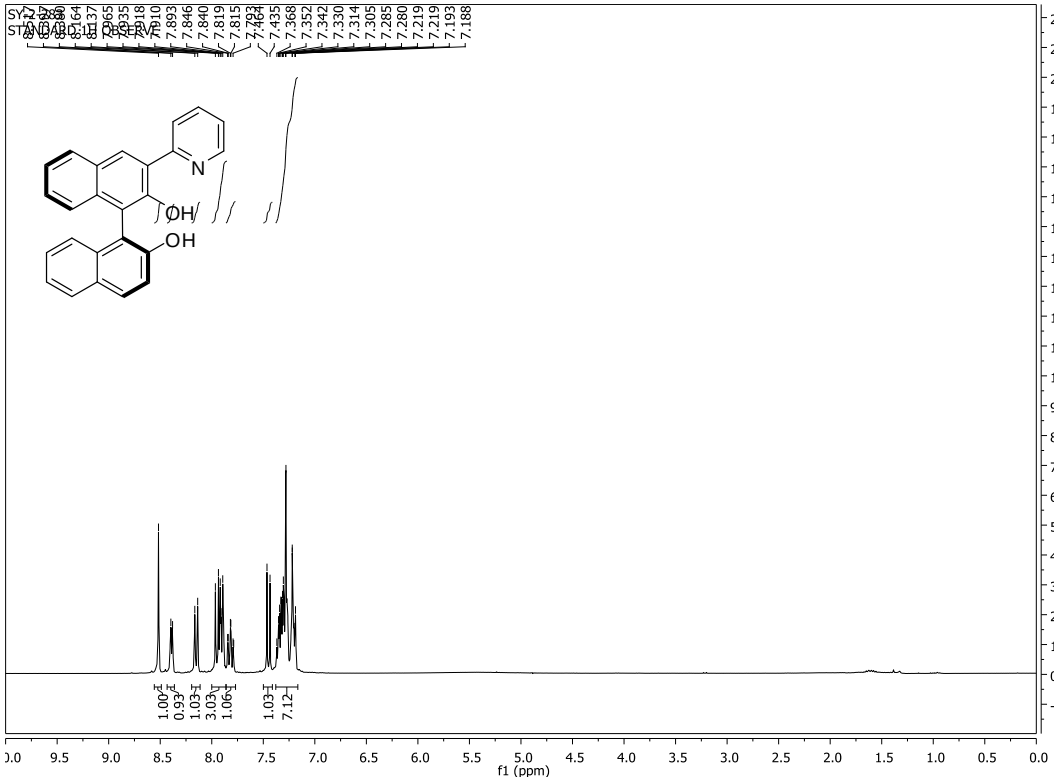
STANDARD: 1H OBSERVE
7.893
7.846
7.840
7.819
7.815
7.435
7.368
7.352
7.342
7.330
7.314
7.305
7.285
7.280
7.219
7.193
7.188
N
OH
OH
1.00
0.93
1.03
3.03
1.06
1.03
7.12
f1 (ppm)

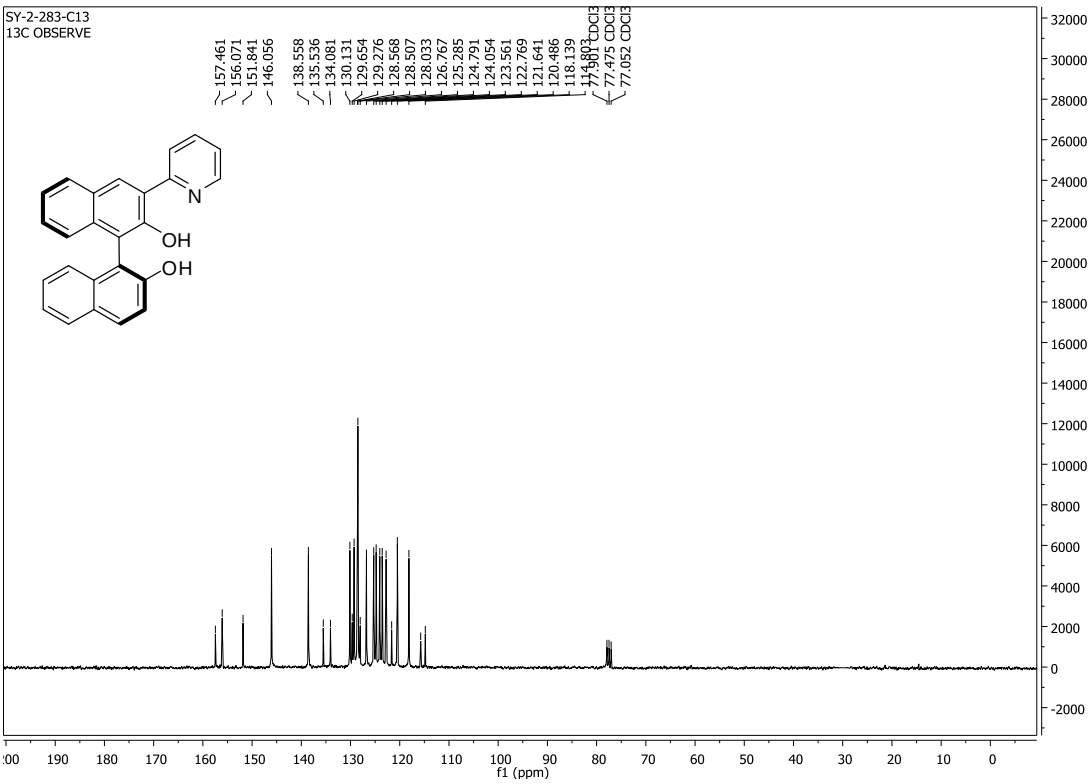
SY-2-283-C13
13C OBSERVE
157.461
156.071
151.841
146.056
138.558
135.536
134.081
130.131
129.654
129.276
128.568
128.507
128.033
126.767
125.285
124.791
124.054
123.561
122.769
121.641
120.486
118.139
77.580 CDCl3
77.475 CDCl3
77.052 CDCl3
N
OH
OH
f1 (ppm)

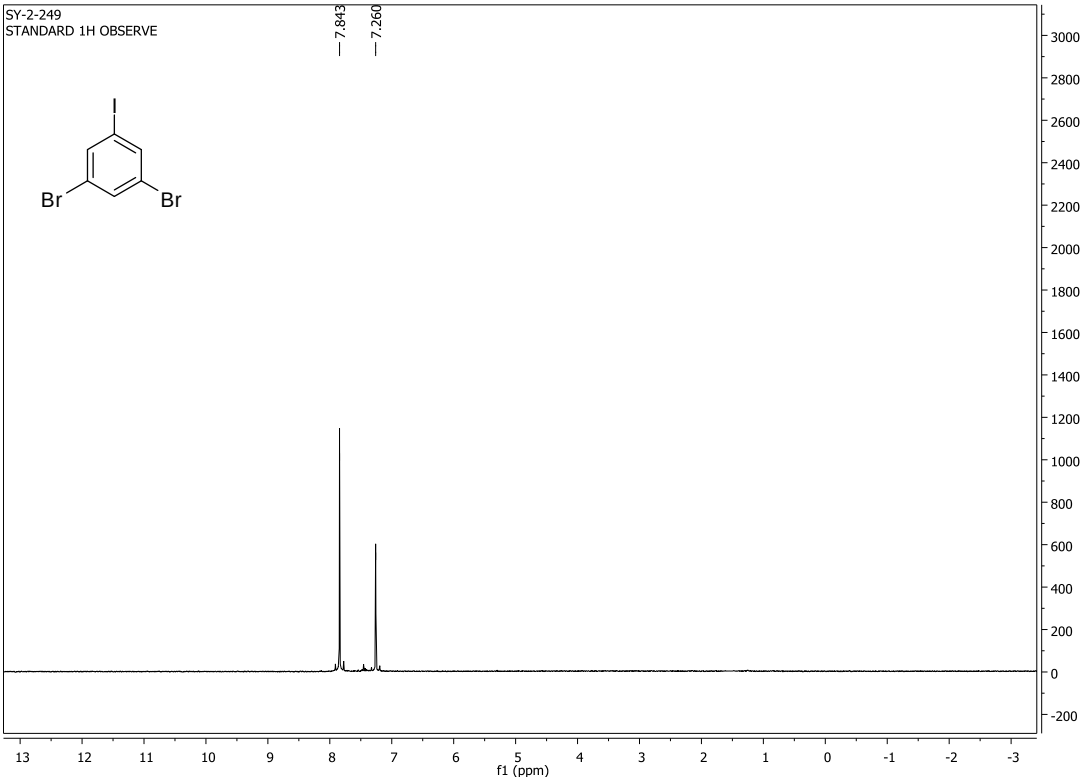
SY-2-249
STANDARD 1H OBSERVE
7.843
7.260
I
Br
Br
f1 (ppm)

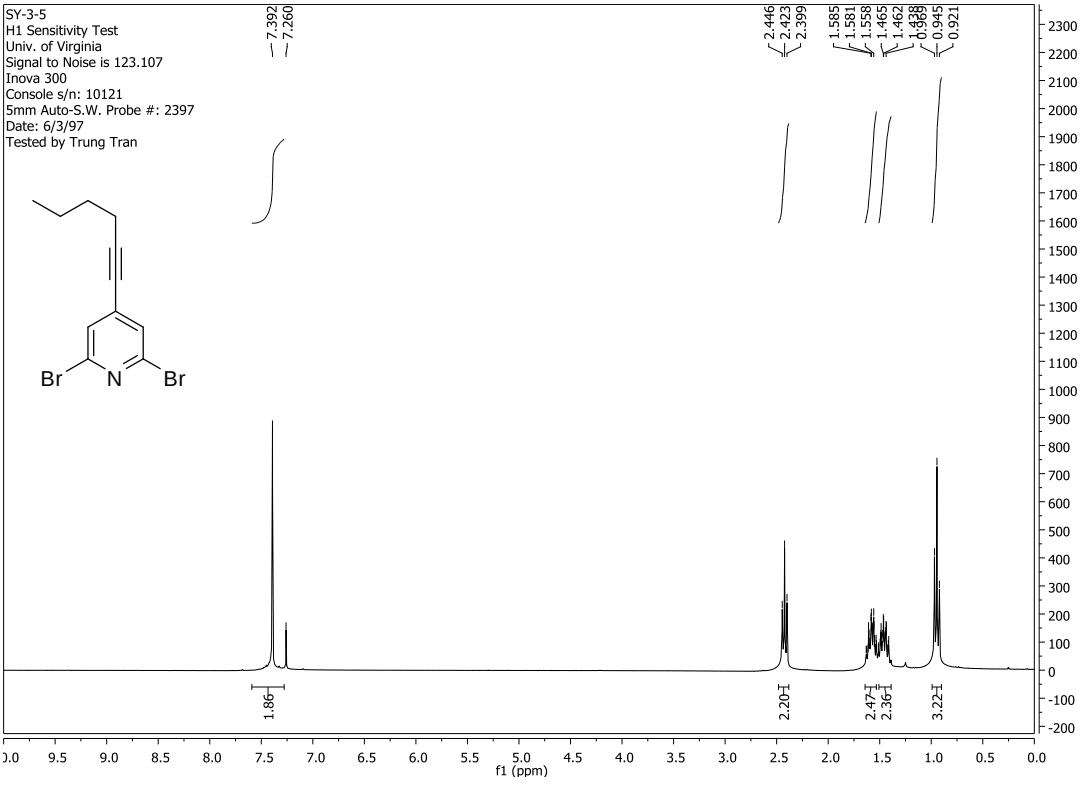
SY-3-5
H1 Sensitivity Test
Univ. of Virginia
Signal to Noise is 123.107
Inova 300
Console s/n: 10121
5mm Auto-S.W. Probe #: 2397
Date: 6/3/97
Tested by Trung Tran
7.392
7.260
2.446
2.423
2.399
1.585
1.581
1.558
1.465
1.462
0.969
0.945
0.921
Br
N
Br
1.86
2.20
2.47
2.36
3.22
f1 (ppm)

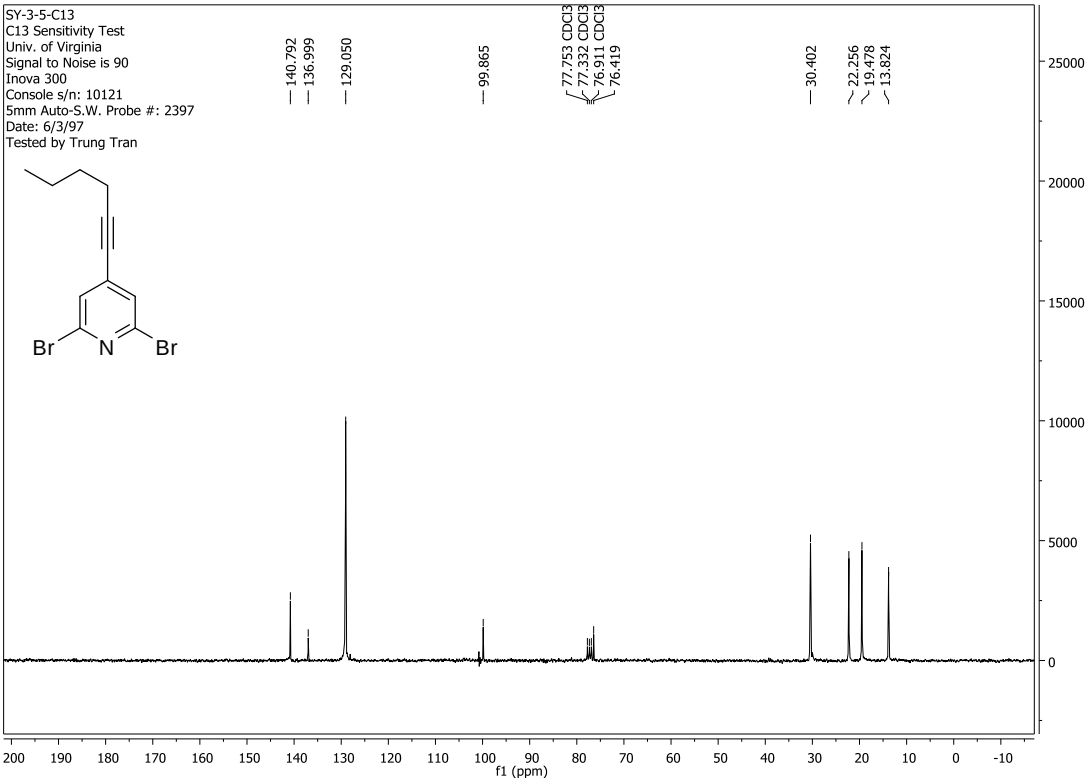
SY-3-5-C13
C13 Sensitivity Test
Univ. of Virginia
Signal to Noise is 90
Inova 300
Console s/n: 10121
5mm Auto-S.W. Probe #: 2397
Date: 6/3/97
Tested by Trung Tran
140.792
136.999
129.050
99.865
77.753 CDCl3
77.332 CDCl3
76.911 CDCl3
76.419
30.402
22.256
19.478
13.824
Br
N
Br
f1 (ppm)

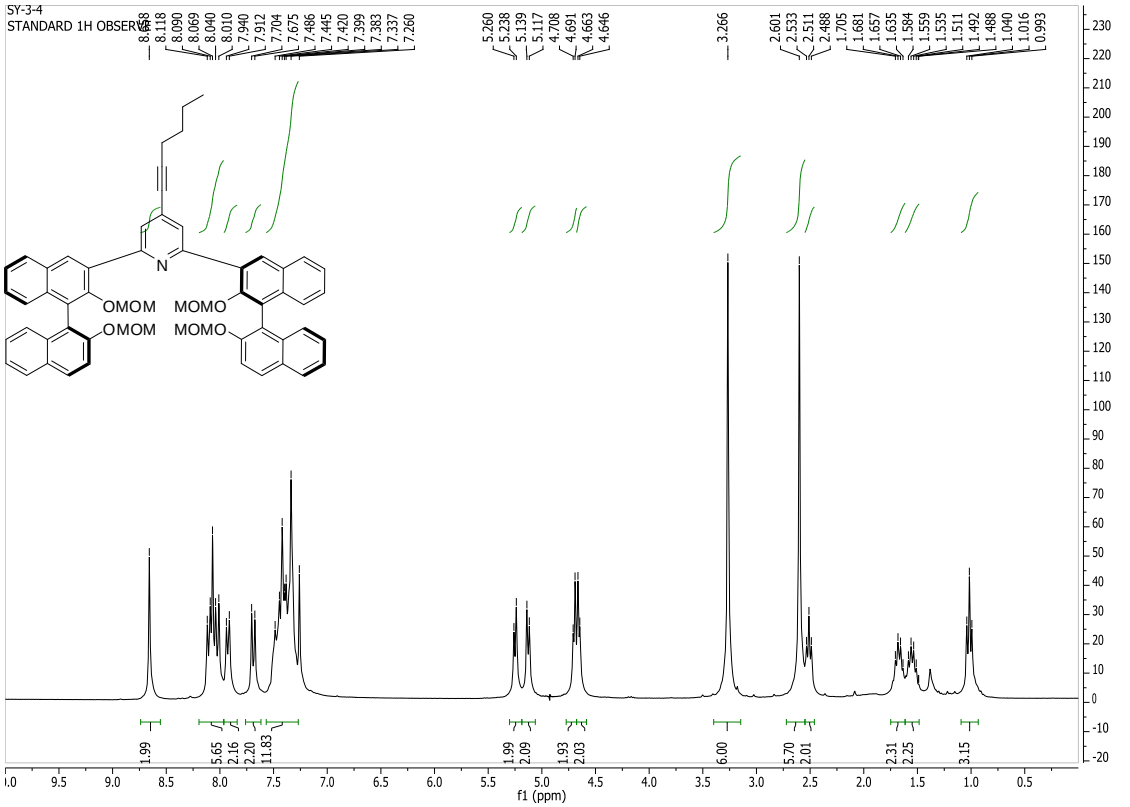
SY-3-4
STANDARD 1H OBSERVE
OMOM MOMO
OMOM MOMO
f1 (ppm)

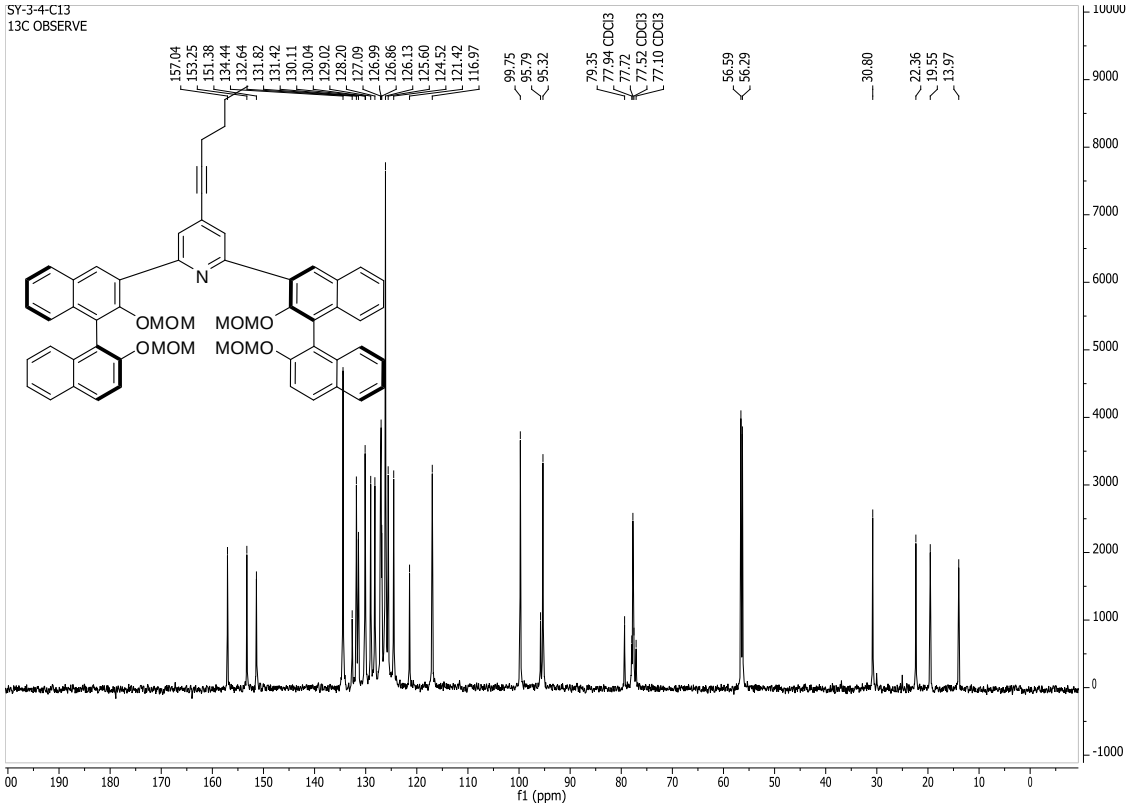
SY-3-4-C13
13C OBSERVE
OMOM MOMO
OMOM MOMO
f1 (ppm)

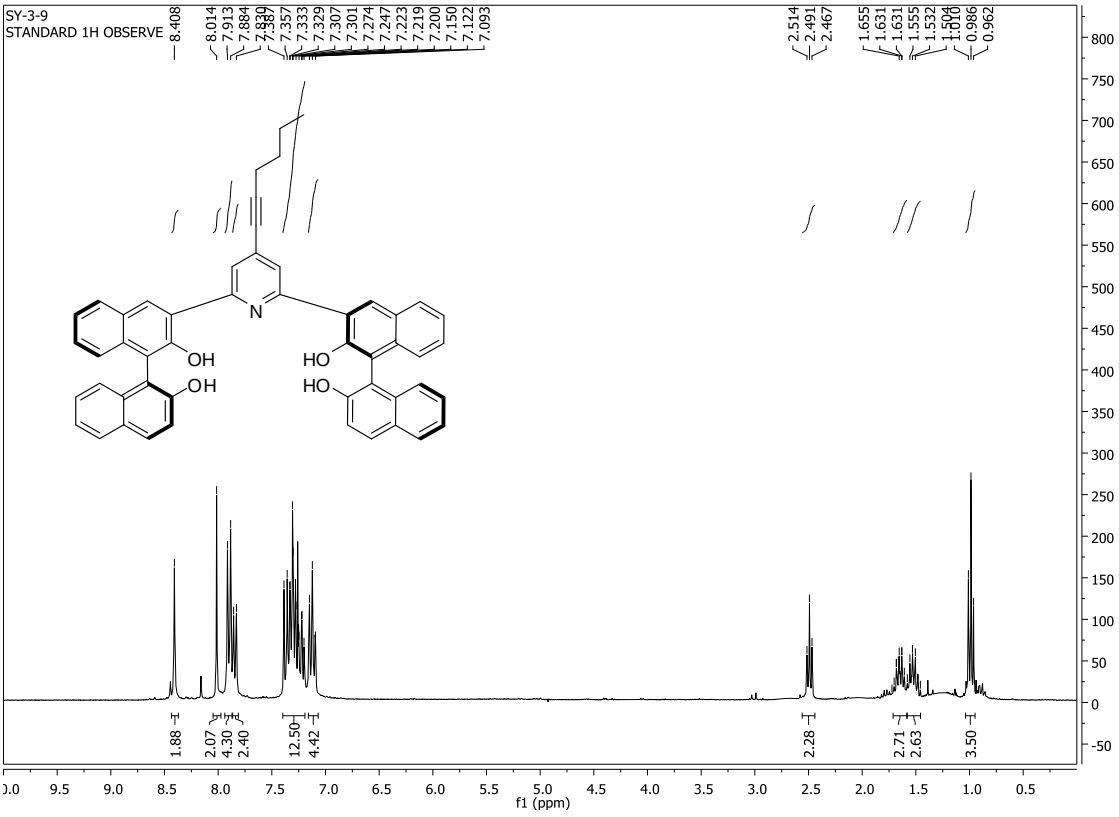
SY-3-9
STANDARD 1H OBSERVE
8.408
8.014
7.913
7.884
7.357
7.333
7.329
7.307
7.301
7.274
7.247
7.223
7.219
7.200
7.150
7.122
7.093
2.514
2.491
2.467
1.655
1.631
1.631
1.555
1.532
1.504
1.000
0.986
0.962
OH
OH
HO
HO
N
1.88
2.07
4.30
2.40
12.50
4.42
2.28
2.71
2.63
3.50
f1 (ppm)

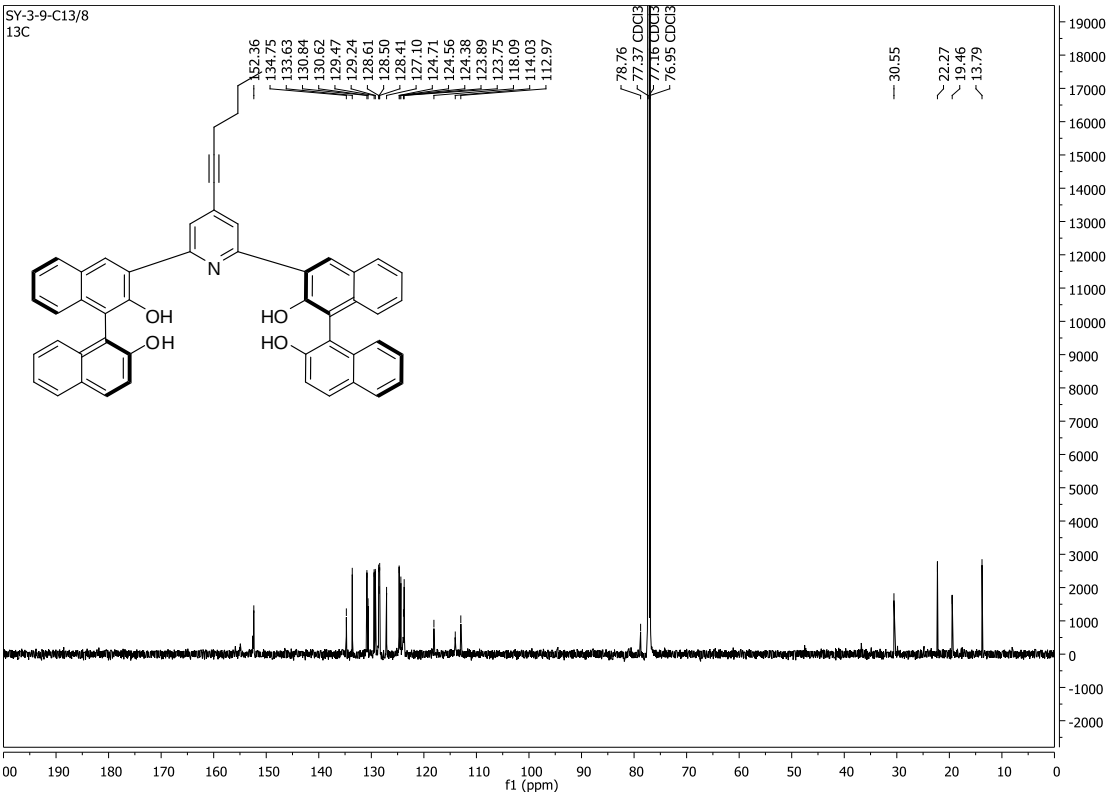
SY-3-9-C13/8
13C
152.36
134.75
133.63
130.84
130.62
129.47
129.24
128.61
128.50
128.41
127.10
124.71
124.56
124.38
123.89
123.75
118.09
114.03
112.97
78.76
77.37 CDCl3
77.16 CDCl3
76.95 CDCl3
30.55
22.27
19.46
13.79
OH
OH
HO
HO
N
f1 (ppm)

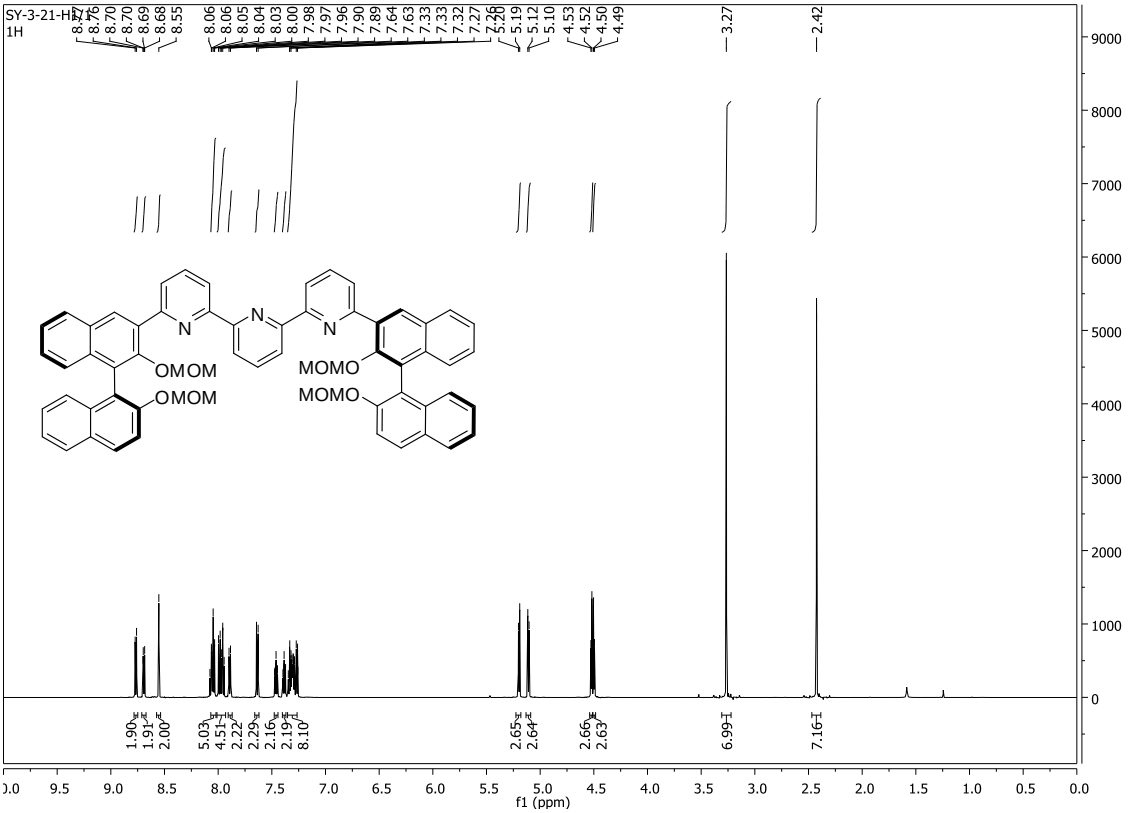
SY-3-21-H1
1H
8.77
8.76
8.70
8.69
8.68
8.55
8.06
8.06
8.05
8.04
8.03
8.00
7.98
7.97
7.96
7.90
7.89
7.64
7.63
7.33
7.32
7.27
7.26
5.20
5.19
5.12
5.10
4.53
4.52
4.50
4.49
3.27
2.42
OMOM
OMOM
MOMO
MOMO
1.90
1.91
2.00
5.03
4.51
2.22
2.29
2.16
2.19
8.10
2.65
2.64
2.66
2.63
6.99
7.16
f1 (ppm)

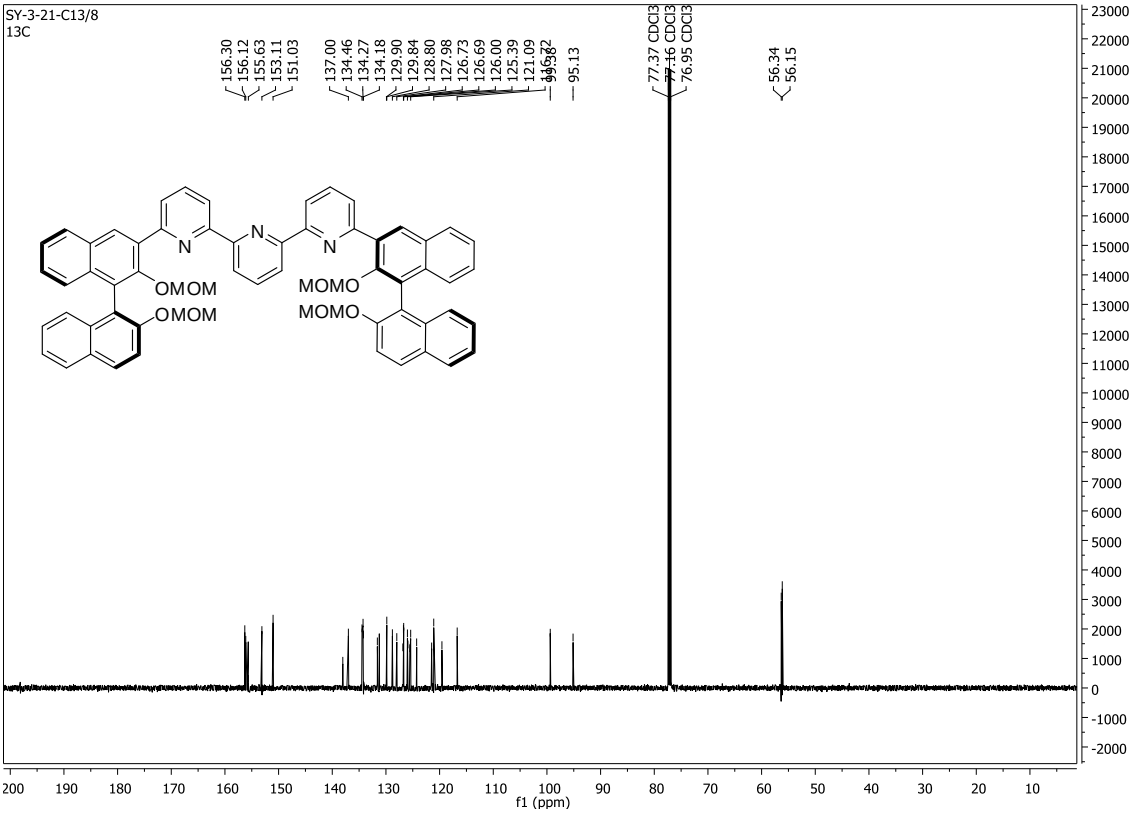
SY-3-21-C13/8
13C
156.30
156.12
155.63
153.11
151.03
137.00
134.46
134.27
134.18
129.90
129.84
128.80
127.98
126.73
126.69
126.00
125.39
121.09
95.13
77.37 CDCl3
77.16 CDCl3
76.95 CDCl3
56.34
56.15
OMOM
OMOM
MOMO
MOMO
f1 (ppm)

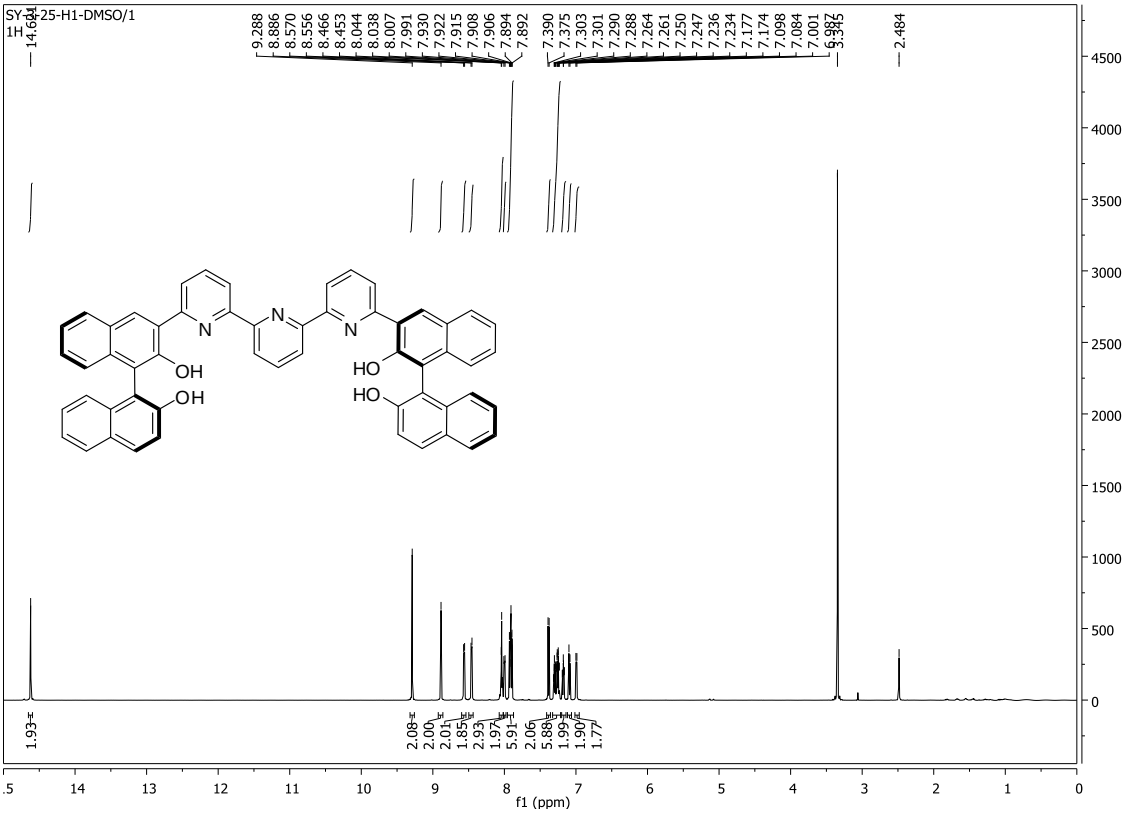
SY-3-25-H1-DMSO/1
1H
14.624
9.288
8.886
8.570
8.556
8.466
8.453
8.044
8.038
8.007
7.991
7.930
7.922
7.915
7.908
7.906
7.894
7.892
7.390
7.375
7.303
7.301
7.290
7.288
7.264
7.261
7.250
7.247
7.236
7.234
7.177
7.174
7.098
7.084
7.001
6.987
3.345
2.484
OH
OH
HO
HO
1.93
2.08
2.00
2.01
1.85
2.93
1.97
5.91
2.06
5.88
1.99
1.90
1.77
f1 (ppm)

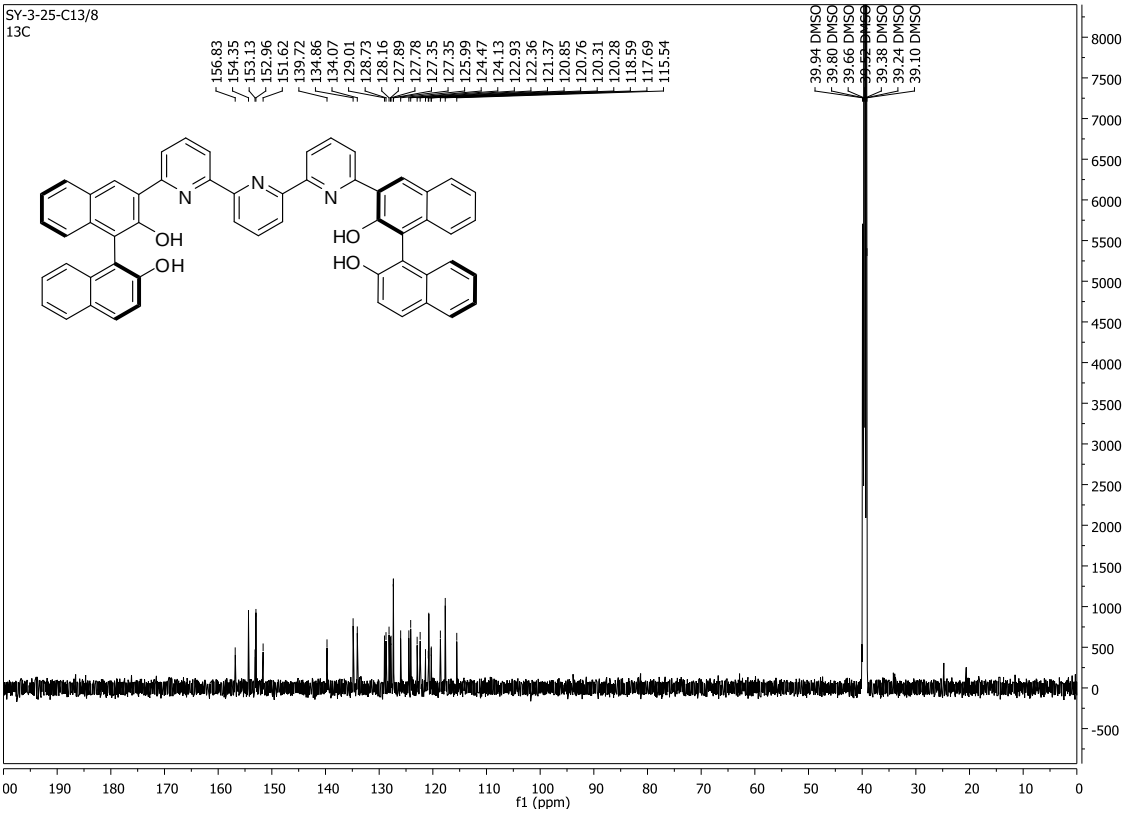
SY-3-25-C13/8
13C
156.83
154.35
153.13
152.96
151.62
139.72
134.86
134.07
129.01
128.73
128.16
127.89
127.78
127.35
127.35
125.99
124.47
124.13
122.93
122.36
121.37
120.85
120.76
120.31
120.28
118.59
117.69
115.54
39.94 DMSO
39.80 DMSO
39.66 DMSO
39.38 DMSO
39.24 DMSO
39.10 DMSO
OH
OH
HO
HO
f1 (ppm)

Appendix II. Indolizine-Terpyridine Compound

1. Preparation and Characterization of Compounds

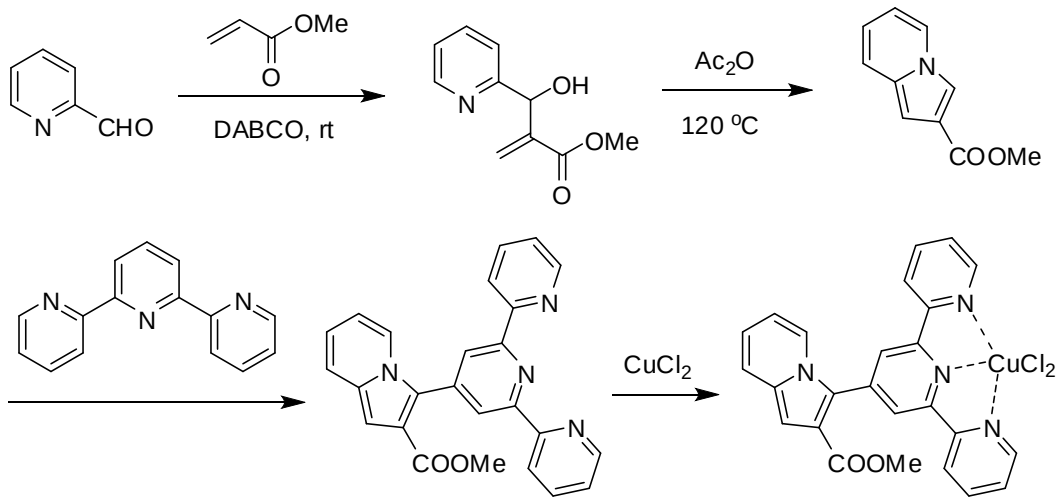

7-22 **7-23**

Preparation of methyl 2-(hydroxy(pyridin-2-yl)methyl)acrylate. A solution of methyl acrylate (2.50 g, 0.029 mol), DABCO (0.15 g, 1.34 mmol) and pyridine-2-carbalerhyde (2.95 g, 0.028 mmol) in $CHCl_3$ (2 mL) was allowed to stand at room temperature for 3 d. The solvent was evaporated and the crude product purified by flash chromatography on silica gel eluted with EtOAc to afford a colorless oil (5.08 g) in 94% yield. ^{1}H NMR (300 MHz, $CDCl_3$) δ 3.68 (s, 3H), 4.83 (s, br, 1H), 5.61 (d, J = 5.4 Hz, 1H), 5.90 (s, 1H), 6.33 (s, 1H), 7.15 (t, J = 6.0 Hz, 1H), 7.36 (d, J = 7.2 Hz, 1H), 7.55-7.60 (m, 1H), 8.48 (d, J = 4.8 Hz, 1H).

Preparation of methyl indolizine-2-carboxylate. The hydroxyl precursor methyl 2-(hydroxy(pyridin-2-yl)methyl)acrylate (1g, 5.2 mmol) was heated in Ac_2O (5 mL) at 110

^{o}C for 2 h. The cooled mixture was poured in to aq. NaHCO3-ice and stirred for 0.5 H. The mixture was then extracted with Et_2O (3x30 mL), washed with brine. The solvent was evaporated and the residue was purified by flash chromatography on silica eluted with hexane-EtOAc (3:1) to afford the desired product as yellowish crystal in 50% yield. ^{1}H NMR (300 MHz, $CDCl_3$) δ 3.88 (s, 3H), 6.52 (t, J = 6.6 Hz, 1H), 6.67 (t, J = 7.8 Hz, 1H), 6.81 (s, 1H), 7.35 (d, J = 9.3 Hz), 7.79 (s, 1H), 7.85 (d, J = 7.2 Hz, 1H).

Preparation of methyl 3-([2,2':6',2''-terpyridin]-4'-yl)indolizine-2-carboxylate. Under nitrogen, to a 10 mL flame-dried Schlenk flask was loaded methyl indolizine-2-carboxylate (43.8 mg, 0.25 mmol), 4'-chloro-2,2':6',2''-terpyridine (133.9 mg, 0.5 mmol), $Pd(OAc)_2$ (2.8 mg, 0.0125 mmol), tricyclohexylphosphine (0.025 mmol, 7 mg), Cs_2CO_3 (0.75 mmol, 244 mg), toluene (0.5 mL). The reaction mixture was stirred under reflux for overnight. After it cooled to room temperature, 10 mL water was added and the mixture was extracted with EtOAc (3 x 20 mL). The combined organic layer was washed with brine (20 mL) and dried over anhydrous Na_2SO_4. After evaporation of the solvent, the residue was purified by column chromatography on silica gel eluted with hexanes/ethyl acetate (2/1) to afford desired product as a yellow solid in 56% yield (60 mg). ^{1}H NMR (300 MHz, $CDCl_3$) δ 3.73 (s, 3H), 6.51 (t, J = 6.3 Hz, 1H), 6.73 (t, J = 7.8 Hz, 1H), 7.01 (s, 1H), 7.31 (t, J = 6.3 Hz, 2H), 7.42 (d, J = 9.0 Hz, 1H), 7.84-7.94 (m, 3H), 8.62-8.70 (m, 6H). ^{13}C NMR (75 MHz, $CDCl_3$) δ 51.7, 102.5, 113.1, 118.4, 119.1, 120.6, 121.5, 123.1, 124.2, 132.9, 137.1, 141.1, 149.4, 156.1, 156.2, 165.4. HRMS Calcd

for $C_{25}H_{19}N_4O_2$ (MH^+): 407.1508. Found: 407.1506. m.p. 225 ^{0}C.

Preparation of compound 7-23. **7-22** (53.2 mg, 0.13 mmol) and $CuCl_2 \cdot 2H_2O$ (26.6 mg, 0.16 mmol) in methanol (10 mL) at room temperature for about 0.5 h. The reaction was monitored by TLC. After the reaction was complete, the solution was concentrated and water (2 mL) was added to generate precipitate. The solid was collected through filtration, washed with water (1 mL) and methanol (several drops) and then dried under vacuum.

2. Fluorescent study

Figure AII-1. Fluorescence spectra of **7-22** and **7-23** [1×10^{-5} M in 25 mM HEPES (pH 7.46)]. (λ_{exc} = 360 nm, slit =2.0/2.0 nm)

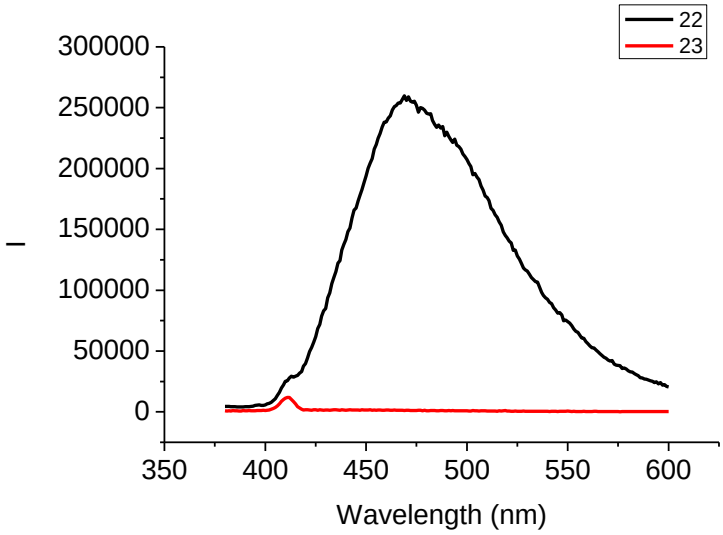

Figure AII-2. Fluorescence spectra of **7-23** [1×10^{-5} M in 25 mM HEPES (pH 7.46)] in the absence and presence of L-Histidine (1, 10, 50, 100, 250, 500 eq). (λ_{exc} = 360 nm, slit

=3.0/3.0 nm)

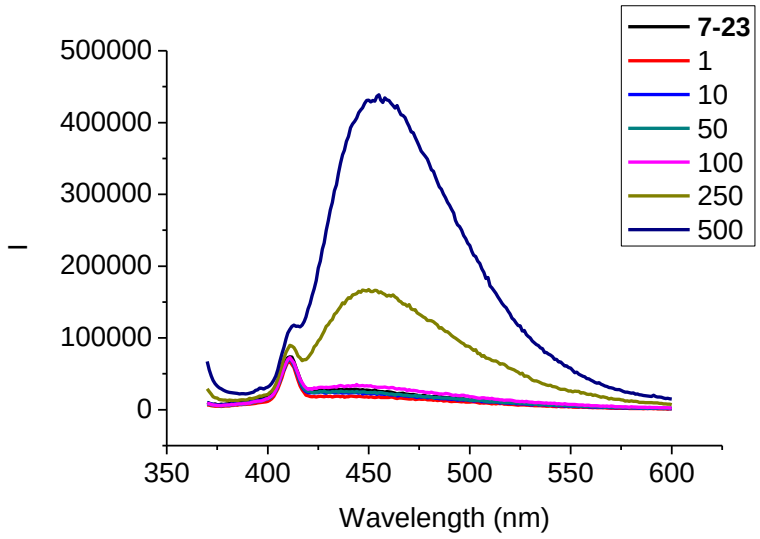

Figure AII-3. Fluorescence spectra of **7-23** [1×10^{-5} M in 25 mM HEPES (pH 7.46)] in the absence and presence of L-Cysteine (1, 10, 50, 100, 250, 500 eq). (λ_{exc} = 360 nm, slit =3.0/3.0 nm)

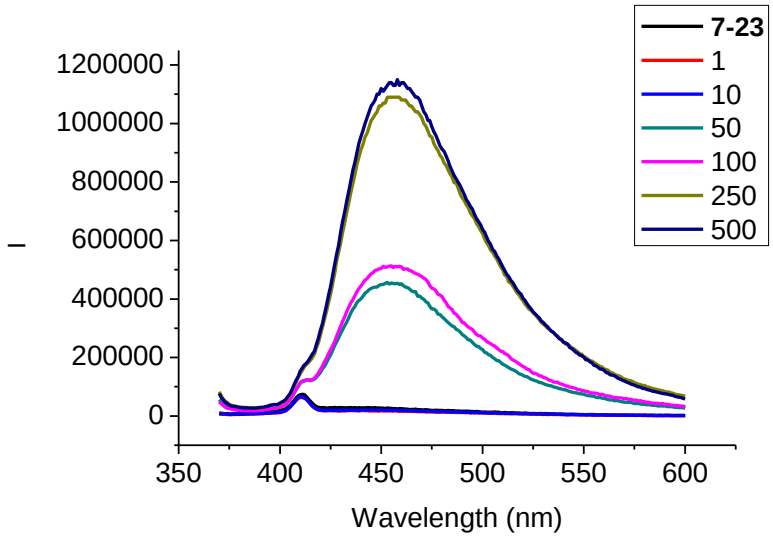

Figure AII-4. Fluorescence spectra of **7-23** [1×10^{-5} M in **degassed** 25 mM HEPES (pH

7.46)] in the absence and presence of L-Cysteine (1, 2, 3, 4, 5, 6, 7, 8, 9, 10 eq). (λ_{exc} = 360 nm, slit =3.0/3.0 nm)

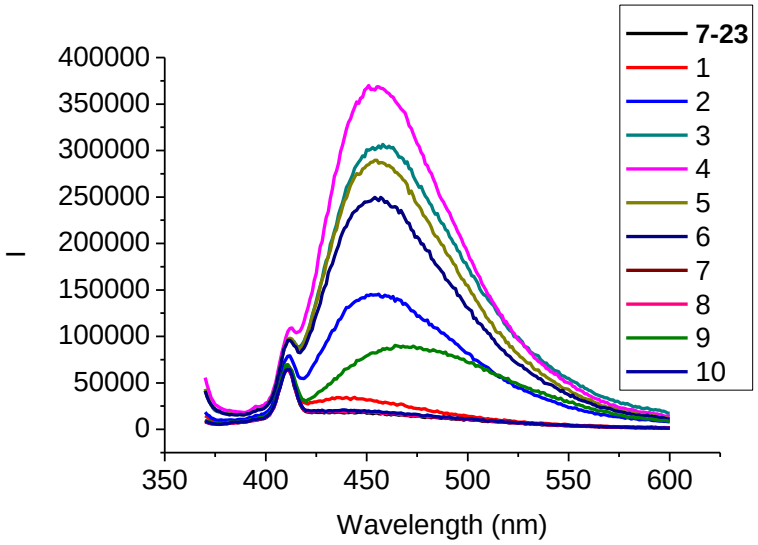

Figure AII-2. Fluorescence intensities of **7-22** (1×10^{-5} M in methanol) at 500 nm in the absence and presence of 1 eq of NaCl, KCl, $Cu(NO_3)_2\cdot2.5H_2O$, $Zn(NO_3)_2\cdot6H_2O$, $BaCl_2\cdot2H_2O$, $CaCl_2$, $MnCl_2\cdot4H_2O$, $SnCl_4\cdot5H_2O$, $Al(NO_3)_3$, $AgNO_3$, $NiCl_2$, $TbCl_3\cdot6H_2O$, $CoCl_2$, $CeCl_3\cdot7H_2O$, $La(NO_3)_3\cdot5H_2O$, $FeCl_3\cdot6H_2O$. (λ_{exc} = 360 nm, slit =3.0/3.0 nm)

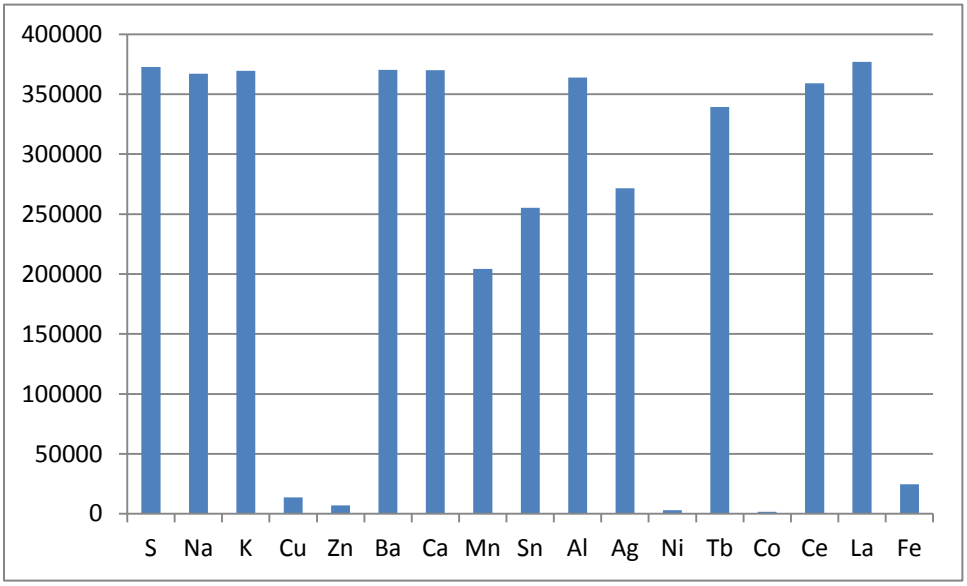

When **7-23** [1×10^{-5} M in 25 mM HEPES (pH 7.46)] was treated with 10 eq of various amino acids, including Cysteine, Valine, Proline, Histidine, Lysine, Alanine, Serine, Arginine, Glutamic acid, Aspartic acid, Glysine, Leucine, no change in fluorescence was observed half an hour after preparation. Cysteine showed fluorescence enhancement right after preparation but the fluorescence diminished quickly.

3. NMR spectra

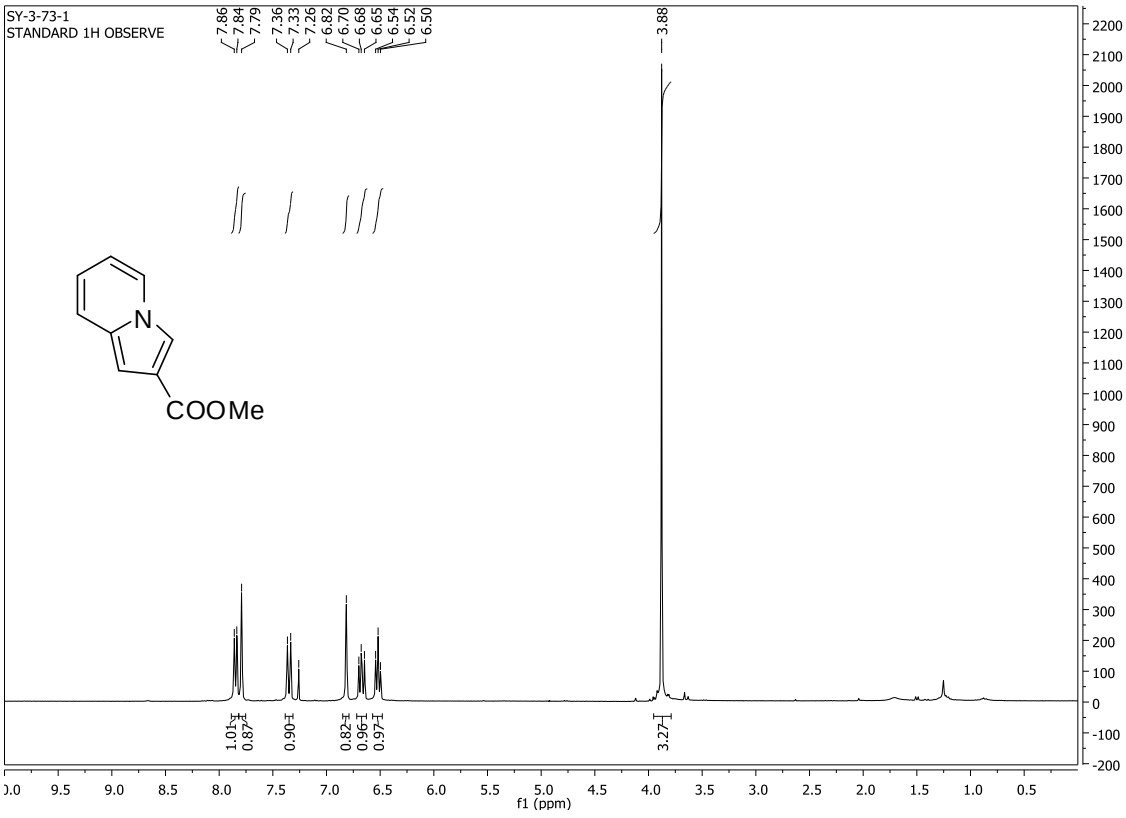

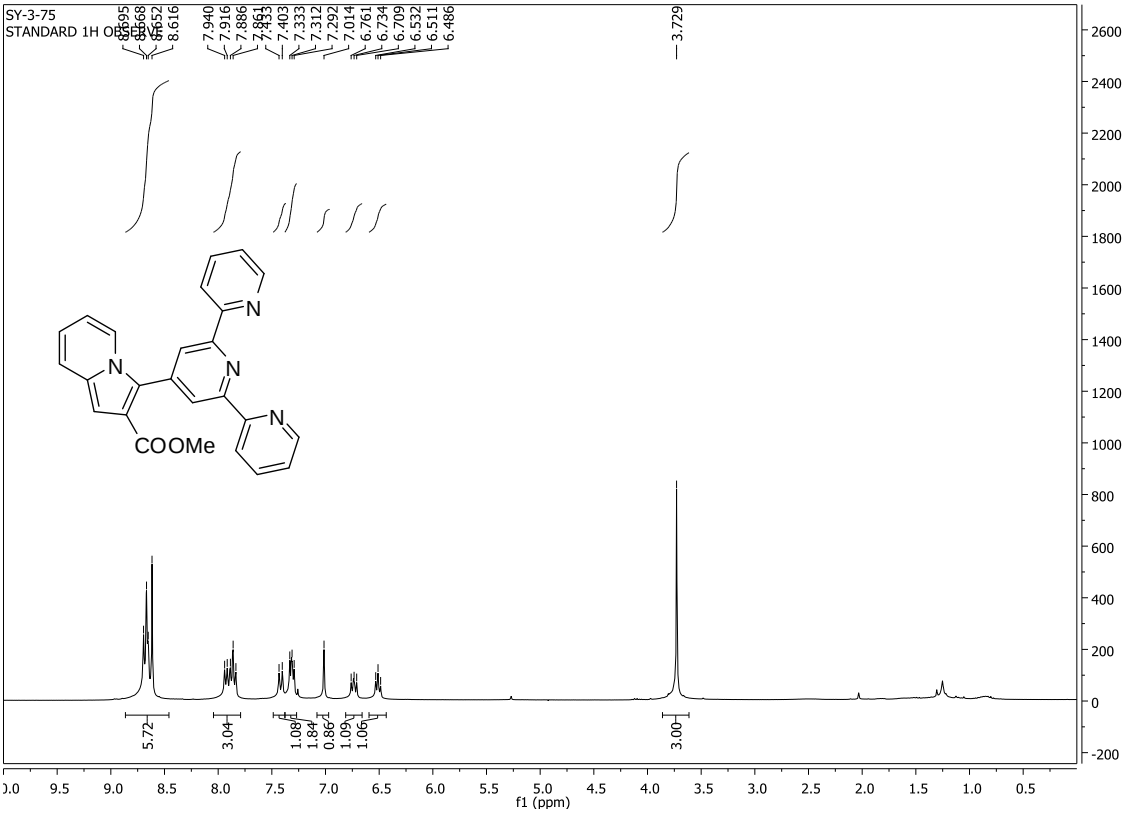
SY-3-75
STANDARD 1H OBSERVE
8.695
8.668
8.652
8.616
7.940
7.916
7.886
7.861
7.433
7.403
7.333
7.312
7.292
7.014
6.761
6.734
6.709
6.532
6.511
6.486
3.729
COOMe
5.72
3.04
1.08
1.84
0.86
1.09
1.06
3.00
f1 (ppm)

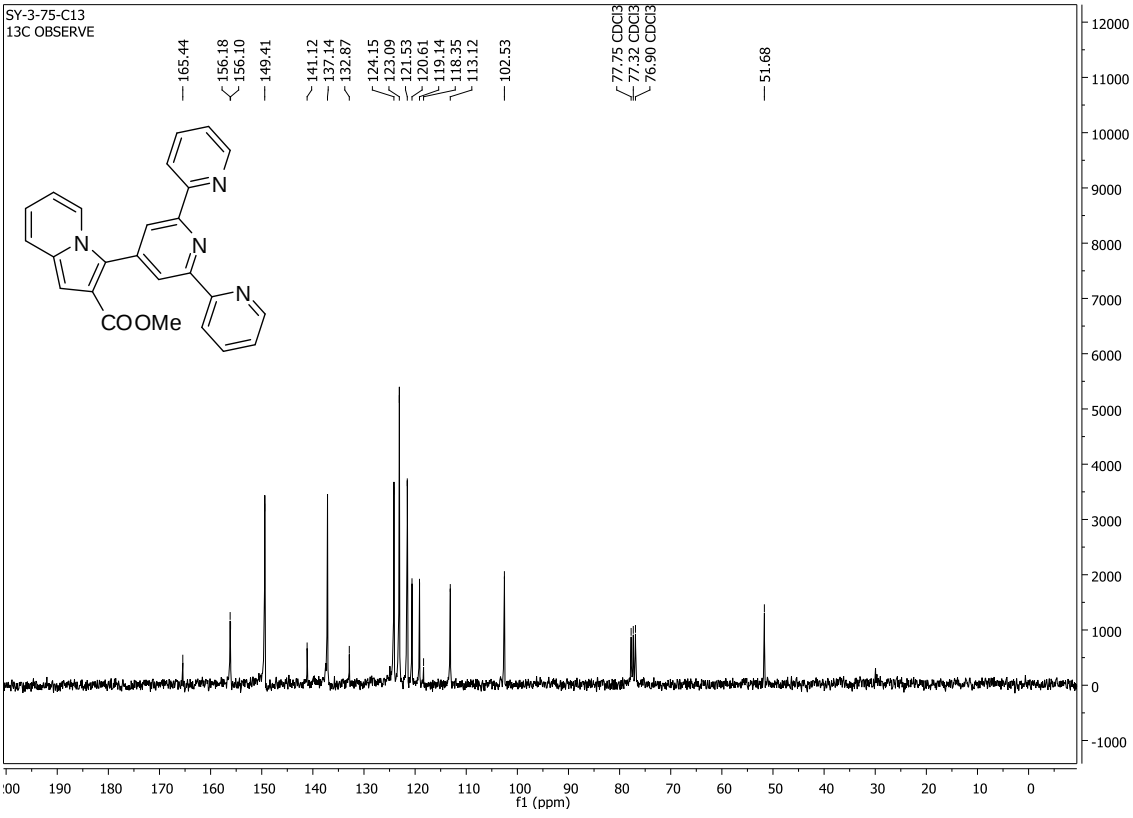
SY-3-75-C13
13C OBSERVE
165.44
156.18
156.10
149.41
141.12
137.14
132.87
124.15
123.09
121.53
120.61
119.14
118.35
113.12
102.53
77.75 CDCl3
77.32 CDCl3
76.90 CDCl3
51.68
COOMe
f1 (ppm)

Appendix III. Study of Aggregation-Induced Emission (AIE) in Fluorescence Sensing

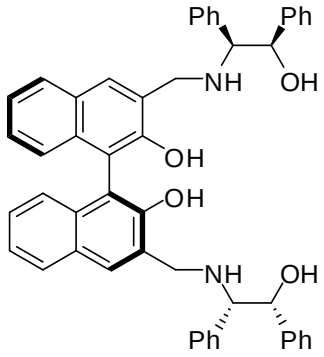

(S)-**7-24**

1. Study of the fluorescent properties

Figure AIII-1. Fluorescence spectra of (S)-**7-24** (2×10^{-4} M) in THF/H_2O (5/0, 4/1, 3/2, 2/3, 1/4, 0.1/4.9). (λ_{exc} = 341 nm, slit =2.0/2.0 nm)

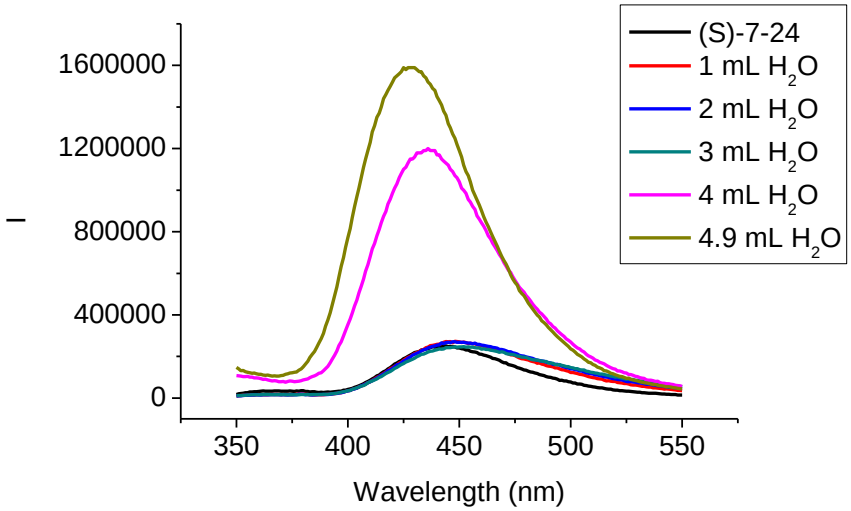

Figure AIII-2. Fluorescence spectra of (S)-**7-24** (2×10^{-4} M in THF/H_2O 0.1/4.9) in the presence of 1 eq $CuCl_2\cdot2H_2O$, $Zn(NO_3)_2\cdot6H_2O$, $FeCl_3\cdot6H_2O$. (λ_{exc} = 341 nm, slit =2.0/2.0 nm)

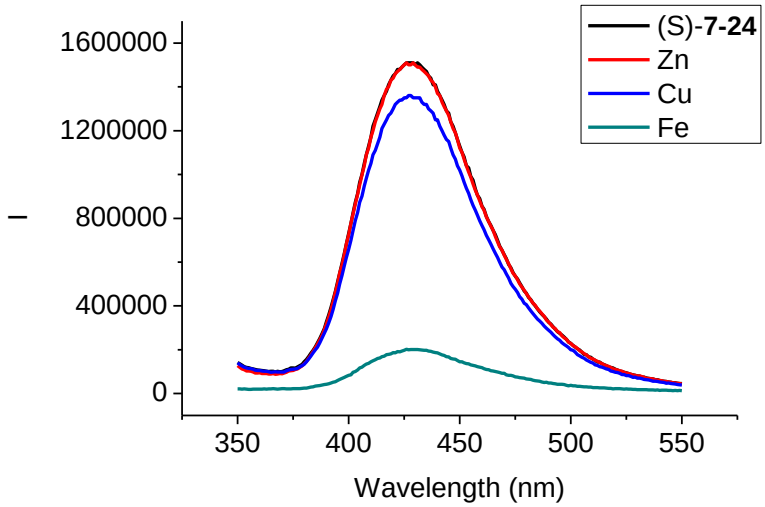

Figure AIII-3. Fluorescence spectra of (S)-**7-24** (1×10^{-4} M in THF/H_2O 0.05/4.95), (S)-**7-24** + 1 eq $FeCl_3\cdot6H_2O$ and (S)-**7-24** + 1 eq $FeCl_3\cdot6H_2O$ + Gly (1, 10, 100 eq) . (λ_{exc} = 341 nm, slit =2.0/2.0 nm)

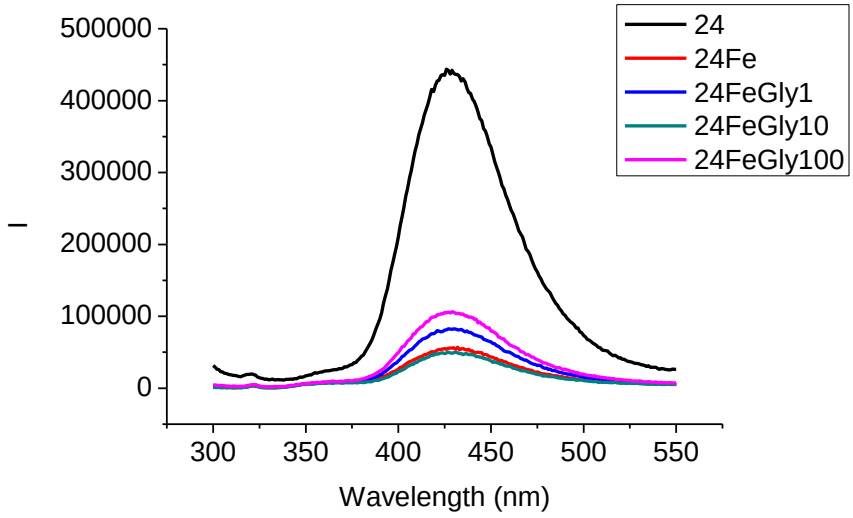

Figure AIII-4. Fluorescence spectra of (S)-**7-24** (1×10^{-4} M in THF/H_2O 0.05/4.95), (S)-**7-24** + 1 eq $FeCl_3\cdot6H_2O$ and (S)-**7-24** + 1 eq $FeCl_3\cdot6H_2O$ + 1eq Gly + NaOH (1, 10, 50 eq) . (λ_{exc} = 341 nm, slit =2.0/2.0 nm)

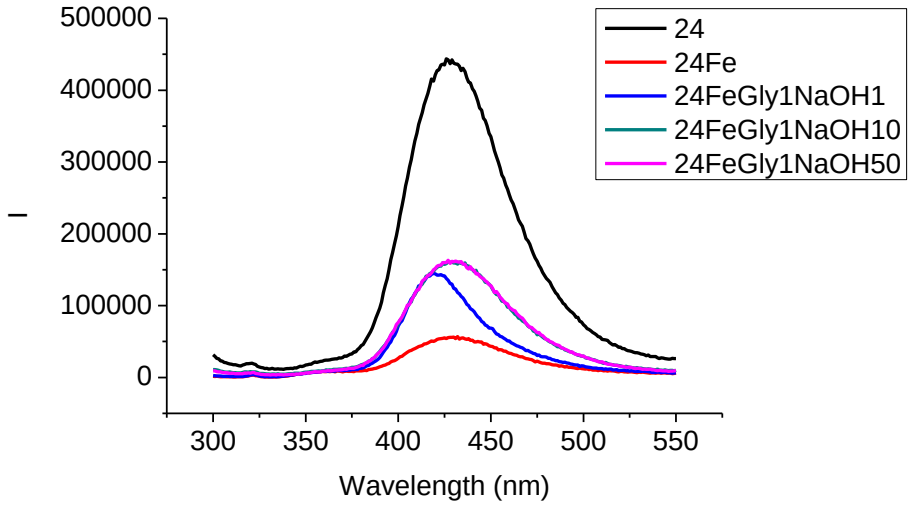

Figure AIII-3. Fluorescence spectra of (S)-**7-24** (1×10^{-4} M in THF/H_2O 0.05/4.95), (S)-**7-24** + 1 eq $FeCl_3\cdot6H_2O$ and (S)-**7-24** + 1 eq $FeCl_3\cdot6H_2O$ + 10 eq Gly + NaOH (10, 50, 100 eq) . (λ_{exc} = 341 nm, slit =2.0/2.0 nm)

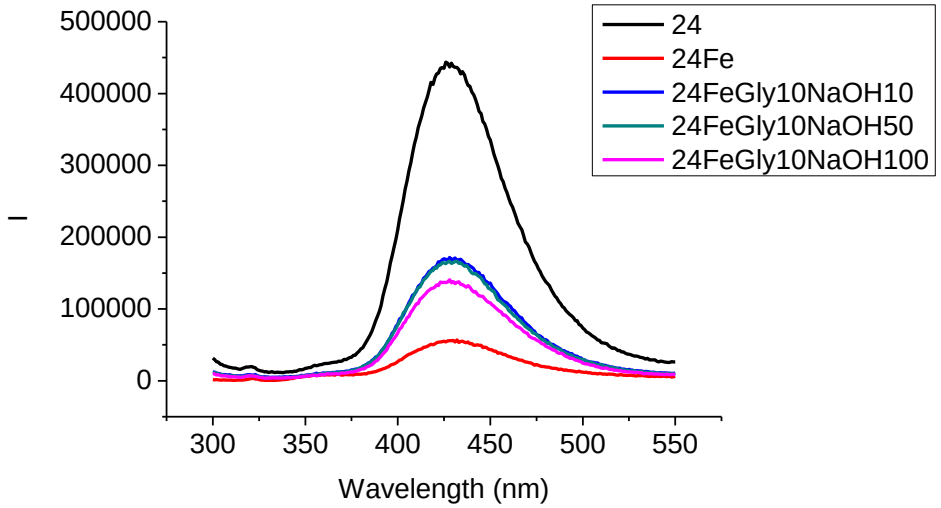

Appendix IV. Near-Infrared (NIR) Dyes

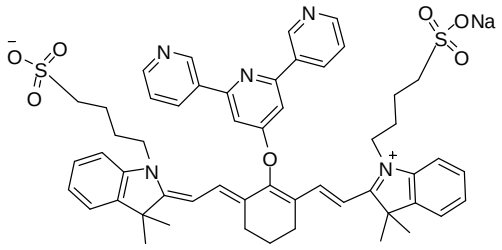

7-25

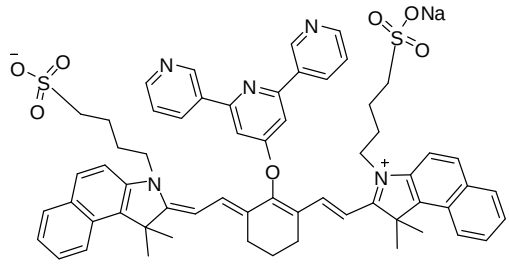

7-26

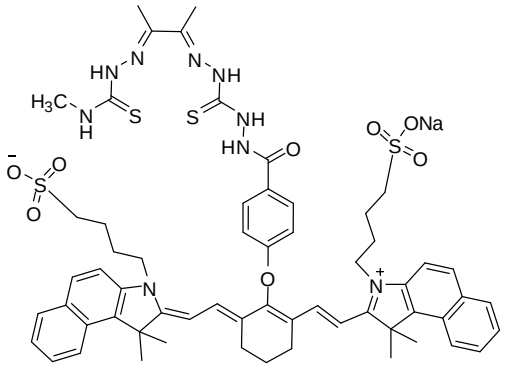

7-28

1. Synthesis and characterization of compounds

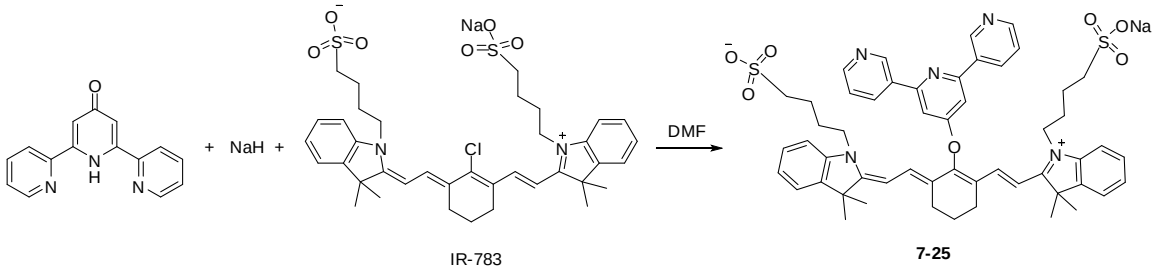

Preparation and characterization of compound 7-25. Under nitrogen, to a DMF (1.5 mL) solution of 6-bis(2-pyridyl)-4(1H)-pyridone (24.9 mg, 0.1 mmol) was added NaH (60% oil dispension, 4 mg, 0.1 mmol) at 0 ^{o}C. After 30 min, DMF solution (1 mL) of IR-783 (37.5 mg, 0.05 mmol) was added to the reaction mixture. After 18 h, the reaction was quenched with dry ice and the mixture as purified by preparative HPLC to afford 7-25 (25 mg) in 52% yield. ^{1}H NMR (300 MHz, $(CD_3)_2SO$) δ 1.26 (s, 12H), 1.73

(m, 8H), 2.00 (t, J = 6.3 Hz, 2H), 2.59 (t, 4H), 2.82 (t, J = 5.1 Hz, 4H), 4.14 (t, J = 7.5 Hz, 4H), 6.32 (d, J = 14.4 Hz, 2H), 7.14 (t, J = 7.2 Hz, 2H), 7.27-7.43 (m, 6H), 7.62 (t, J = 6.0 Hz, 2H), 7.77 (d, J = 14.4 Hz, 2H), 8.11 (t, J = 8.1 Hz, 2H), 8.23 (s, 2H), 8.72 (d, J = 7.2 Hz, 2H), 8.82 (d, J = 4.2 Hz, 2H).

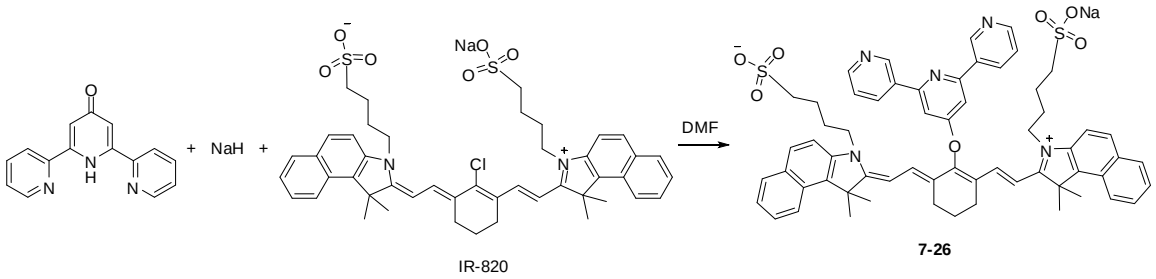

Preparation and characterization of compound 7-26. Under nitrogen, to a DMF (1.5 mL) solution of 6-bis(2-pyridyl)-4(1H)-pyridone (24.9 mg, 0.1 mmol) was added NaH (60% oil dispension, 4 mg, 0.1 mmol) at 0 ^{o}C. After 30 min, DMF solution (1 mL) of IR-820 (42.5 mg, 0.05 mmol) was added to the reaction mixture. After 18 h, the reaction was quenched with dry ice and the mixture as purified by preparative HPLC to afford **7-26** (15 mg) in 28% yield. ^{1}H NMR (300 MHz, $(CD_3)_2SO$) δ 1.54 (s, 12H), 1.75 (m, 8H), 2.01 (t, 2H), 2.52 (t, J = 6.9 Hz, 4H), 2.84 (t, 4H), 4.25 (t, 4H), 6.33 (d, J = 14.1 Hz, 2H), 7.38-7.50 (m, 4H), 7.64-7.72 (m, 4H), 7.85-8.00 (m, 8H), 8.15 (t, J = 7.8 Hz, 2H), 8.32 (s, 2H), 8.76 (d, J = 7.8 Hz, 2H), 8.87 (d, J = 4.2 Hz, 2H).

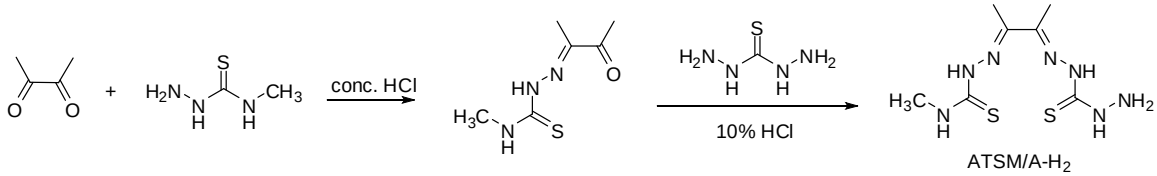

Preparation of (E)-N-methyl-2-(3-oxobutan-2-ylidene)hydrazinecarbothioamide. 2,3-Butanedione (2.08 mL, 24 mmol) and conc. HCl (1 mL) were added to 4-methyl-3-thiosemicarbazide (2.1 g, 20 mmol) in water (40 mL). The mixture was cooled in an ice

bath and stirred for 30 min. A bulky wihte solid settle out of solution and was filtered, washed with cold water and dried under vacuum. The product was isolated as a white solid in 65% yield.

Preparation and characterization of ATSM/A-H_2. Thiocarbohydrazide (530.8 mg, 5 mmol) was added to ethanol (30 mL) and the suspension stirred at 50 oC. A total of 1 eq of (E)-N-methyl-2-(3-oxobutan-2-ylidene)hydrazinecarbothioamide was added in portions over 2 h. After the final addition, 5 drops of 10% HCl was added and the reaction heated under reflux for 5 h. The mixture was allowed to cool to room temperature, and then the precipitate was collected by filtration, washed with ethanol (2x30 mL) and diethyl ether (5x30 mL), and then dried in vacuo to give the product in 76% yield. ^{1}H NMR (300 MHz, $(CD_3)_2SO$) δ 2.16 (s, 6H), 3.00 (d, J = 4.5 Hz, 3H), 4.94 (s, 2H), 8.34 (q, J = 3.9 Hz, 1H), 9.67 (s, 1H), 10.18 (s, 1H), 10.20 (s, 1H).

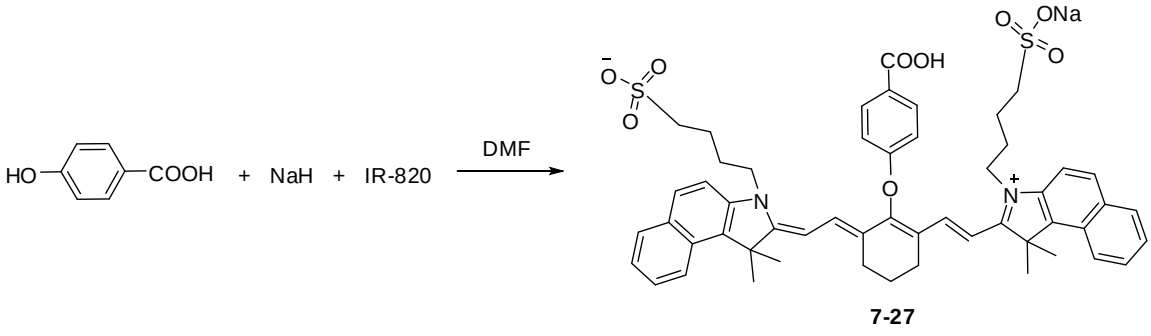

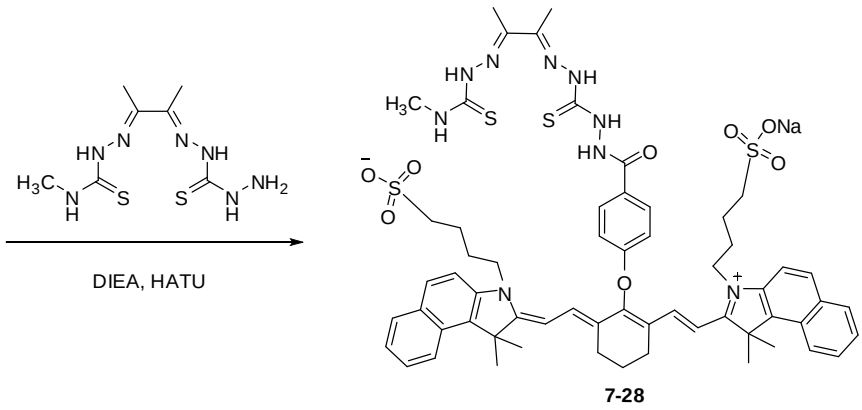

Preparation and characterization of compound 7-27. Under nitrogen, to an anhydrous DMF (1.5 mL) solution of 4-hydroxybenzoic acid (13.8 mg, 0.1 mmol) was added NaH (60% oil dispension, 8 mg, 0.2 mmol) at 0 ^{o}C. After 30 min, DMF solution (1 mL) of IR-820 (42.5 mg, 0.05 mmol) was added to the reaction mixture. After 18 h, the reaction was quenched with dry ice and the mixture as purified by preparative HPLC to afford 7-27 (17 mg) in 36% yield. ^{1}H NMR (300 MHz, $(CD_3)_2SO$) δ 1.55 (s, 12H), 1.73-1.97 (m, 10H), 2.53 (t, J = 6.0 Hz, 4H), 2.77 (t, 4H), 4.25 (t, 4H), 6.28 (d, J = 14.7 Hz, 2H), 7.33 (t, J = 6.9 Hz, 2H), 7.45 (t, J = 6.0 Hz, 2H), 7.58 (t, J = 7.8 Hz, 2H), 7.72 (d, J = 9.0 Hz, 2H), 7.86 (d, J = 14.4 Hz, 2H), 8.00-8.13 (m, 8H).

Preparation and characterization of compound 7-28. ATSM/A-H_2 (7 mg, 0.027 mmol) was suspended in the minimum amount of DMF. Compound **7-27** (17 mg, 0.018 mmol), diisopropylethylamine (3.5 mg, 0.027 mmol) and HATU (10.3 mg, 0.027 mmol) were added and the mixture was stirred at room temperature for overnight. After reaction diethylether (50 mL) was added and the corresponding precipitate was collected through filtration. The residue was purified by preparative HPLC to afford **7-28** (7.6 mg) in 35% yield. ^{1}H NMR (300 MHz, $(CD_3)_2SO$) δ 1.57 (s, 12H), 1.71-1.81 (m, 8H), 1.99 (s, 2H), 2.17 (s, 3H), 2.22 (s, 3H), 2.52 (t, J = 6.0 Hz, 4H), 2.78 (t, 4H), 3.00 (d, J = 4.2 Hz, 3H), 4.26 (t, 4H), 6.29 (d, J = 14.4 Hz, 2H), 7.38 (d, J = 8.7 Hz, 2H), 7.45 (t, J = 7.8 Hz, 2H), 7.58 (t, J = 7.5 Hz, 2H), 7.73 (d, J = 9.0 Hz, 2H), 7.90 (d, J = 14.4 Hz, 2H), 7.99-8.14 (m, 8H), 8.38 (d, J = 4.2 Hz, 1H), 10.11 (s, 1H), 10.20 (s, 1H), 10.56 (s, 1H), 10.61 (s, 1H).

2. Fluorescent study

Figure AIV-1. Excitation spectrum of (S)-**7-25** (1×10^{-5} M in H_2O). (λ_{emi} = 795 nm, slit

=5.0/5.0 nm)

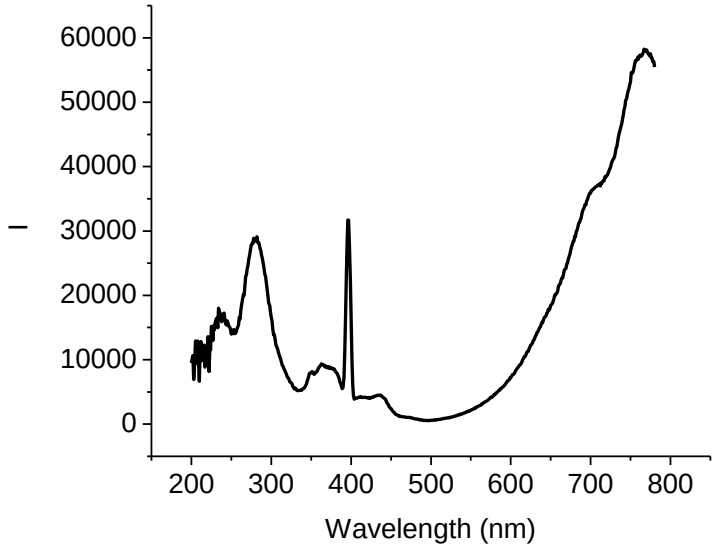

Figure AIV-2. Fluorescence spectra of (S)-**7-25** (1×10^{-5} M in H_2O) in the absence and presence of 1 eq $CuCl_2\cdot2H_2O$. (λ_{exc} = 280 nm, slit =5.0/5.0 nm)

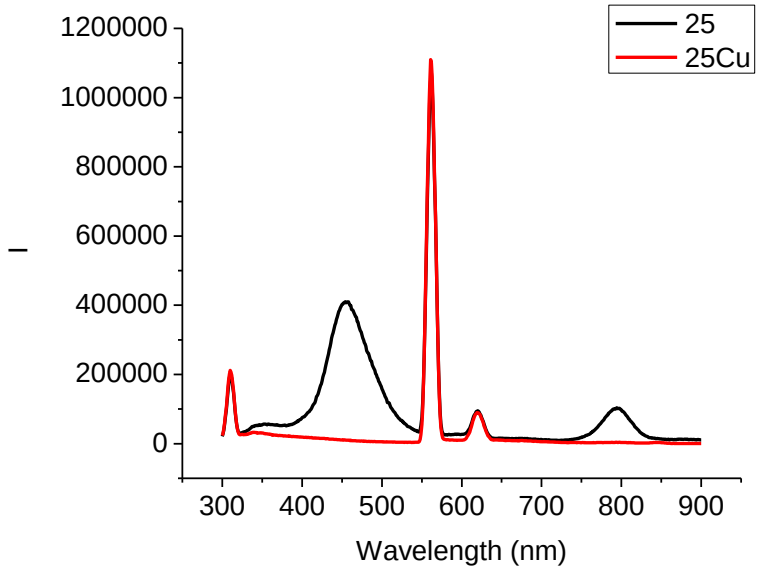

Figure AIV-3. Fluorescence spectra of (S)-**7-25** (1×10^{-5} M in H_2O) in the absence and

presence of 1 eq $CuCl_2 \cdot 2H_2O$. (λ_{exc} = 765 nm, slit =5.0/5.0 nm)

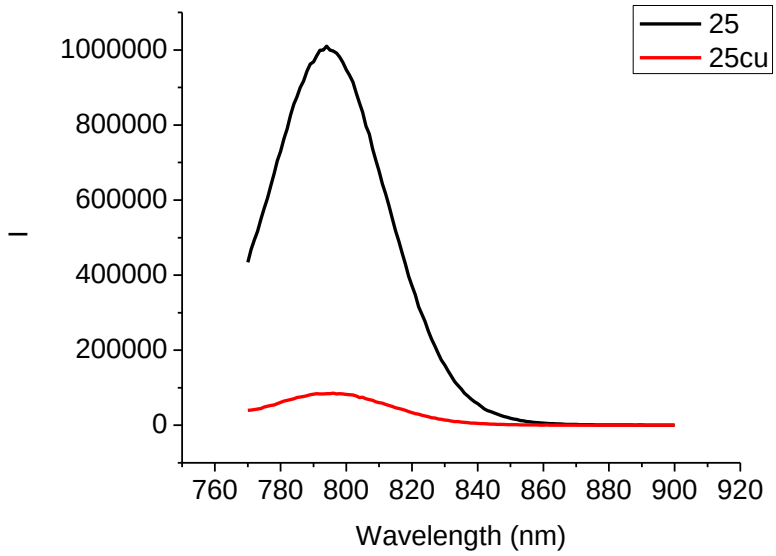

Figure AIV-4. Fluorescence spectra of (S)-**7-25** (1×10^{-5} M in H_2O) in the absence and presence of 1 eq $CuCl_2 \cdot 2H_2O$. (λ_{exc} = 700 nm, slit =5.0/5.0 nm)

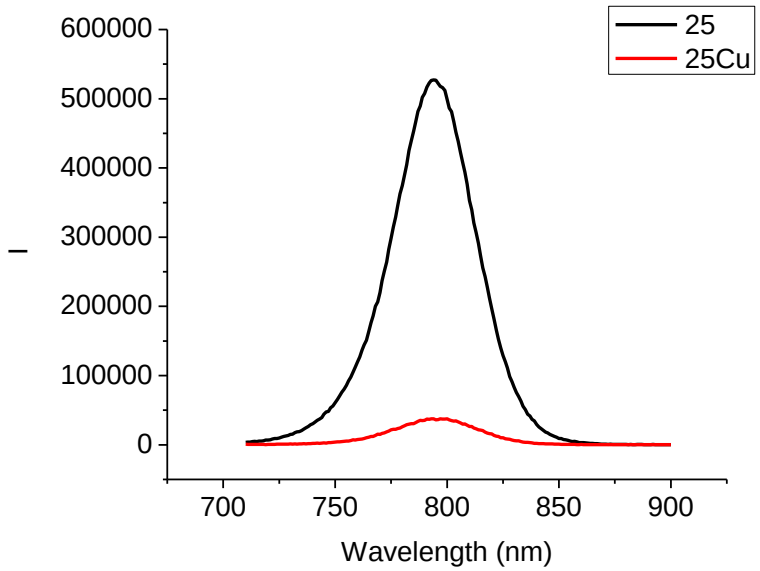

Figure AIV-5. Fluorescence titratoin of (S)-**7-25** + 1 eq $CuCl_2$ (1×10^{-5} M in 50 mM

HEPES) with L-Cysteine (1, 20, 40, 60, 80, 100, 150, 200 eq). (λ_{exc} = 700 nm, slit =5.0/5.0 nm)

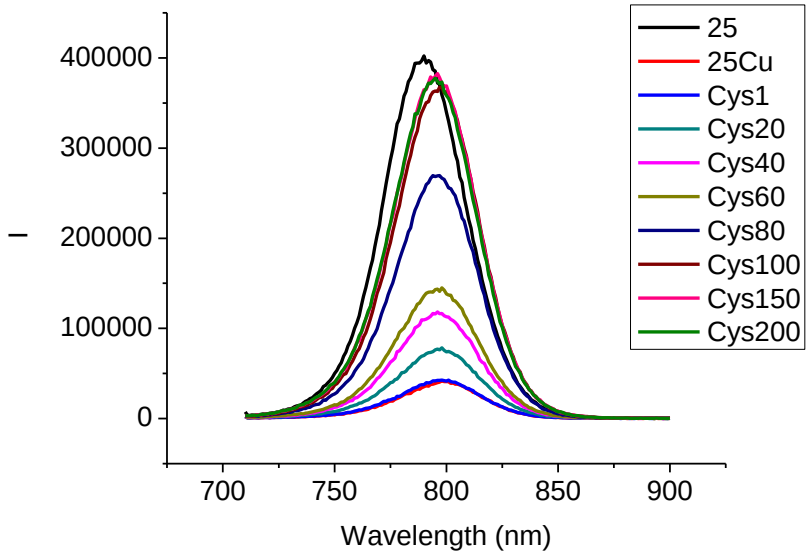

Figure AIV-6. Fluorescence titratoin of (S)-**7-25** + 1 eq $CuCl_2$ (1×10^{-5} M in 50 mM HEPES) with L-Histidine (10, 40, 80, 100, 150, 200, 250, 300, 350, 400, 450, 500 eq). (λ_{exc} = 700 nm, slit =5.0/5.0 nm)

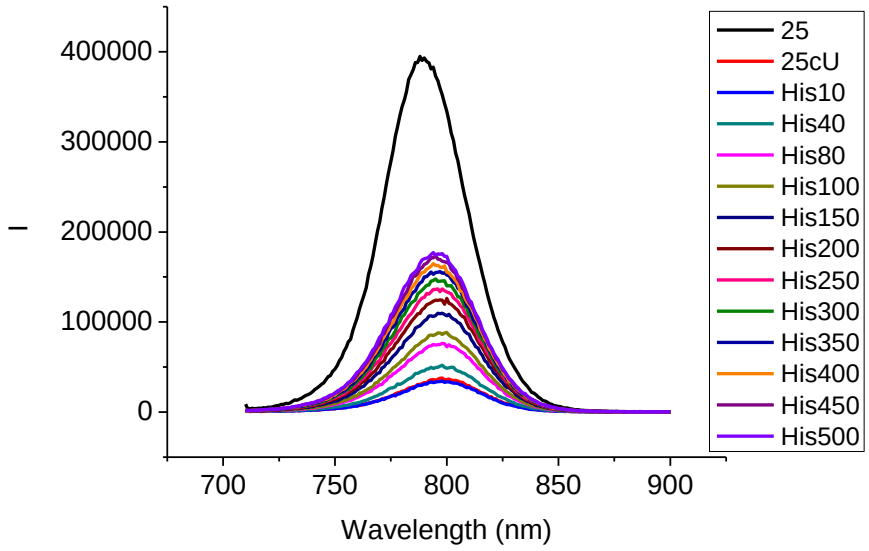

3. NMR spectra

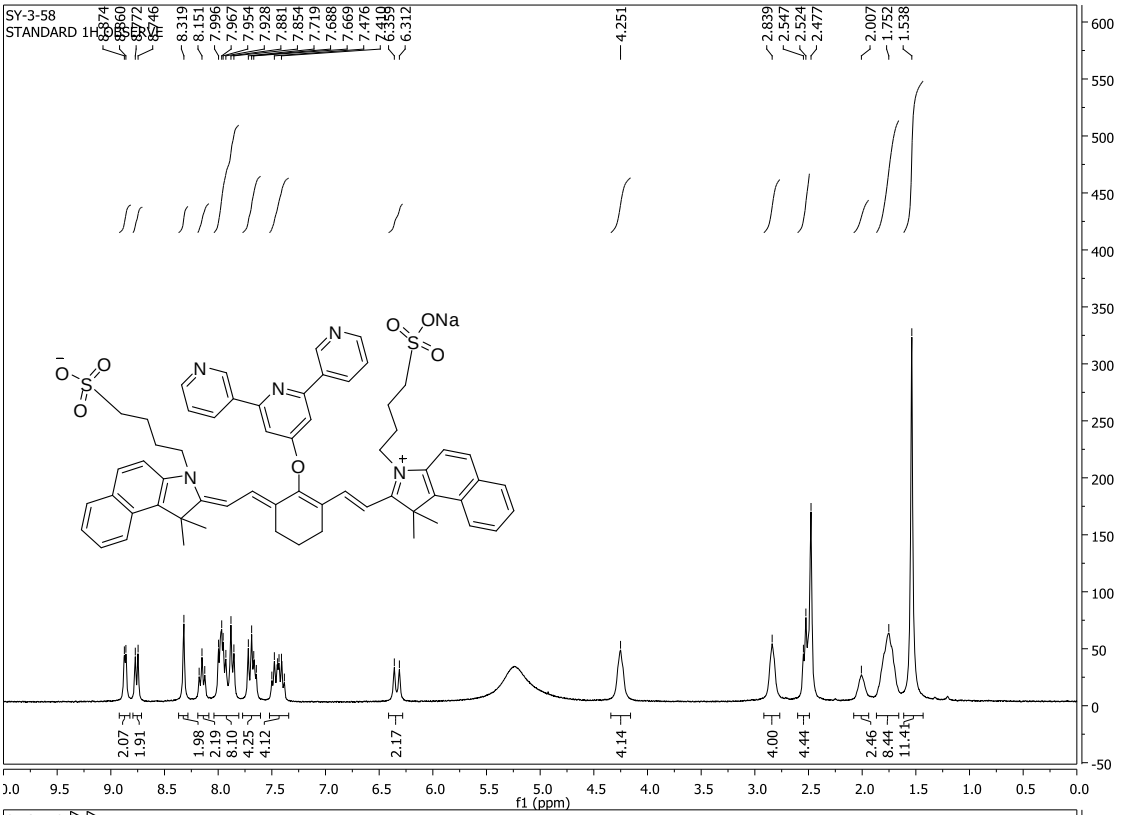

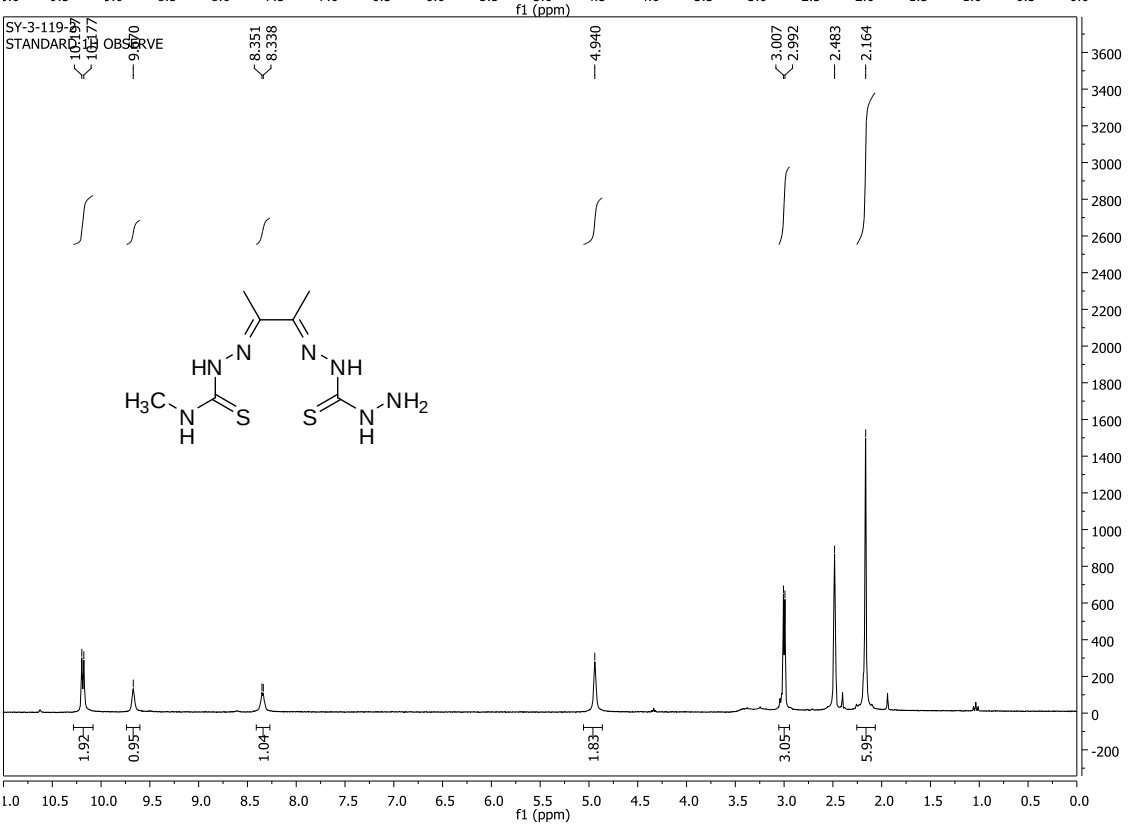

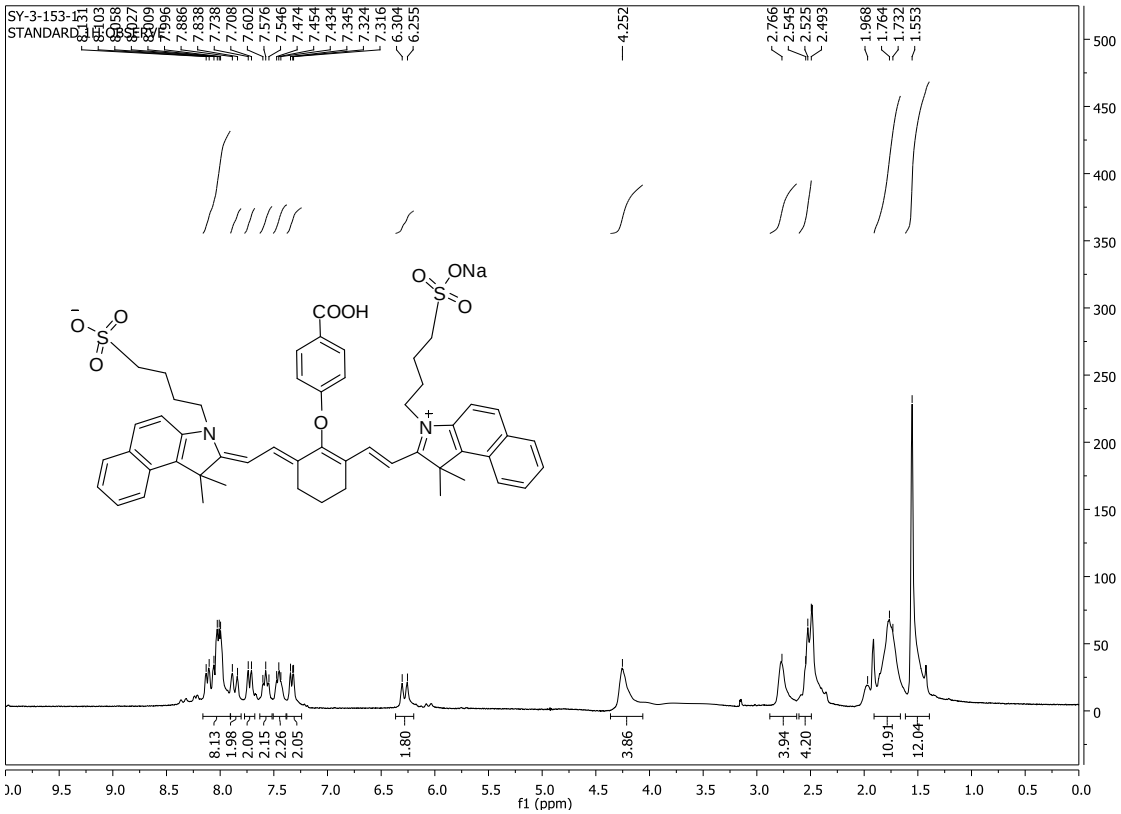
SY-3-153-1
STANDARD_1H_OBSERVE
8.131
8.103
8.058
8.027
8.009
7.996
7.886
7.838
7.738
7.708
7.602
7.576
7.546
7.474
7.454
7.434
7.345
7.324
7.316
6.304
6.255
4.252
2.766
2.545
2.525
2.493
1.968
1.764
1.732
1.553
COOH
ONa
8.13
1.98
2.00
2.15
2.26
2.05
1.80
3.86
3.94
4.20
10.91
12.04
f1 (ppm)

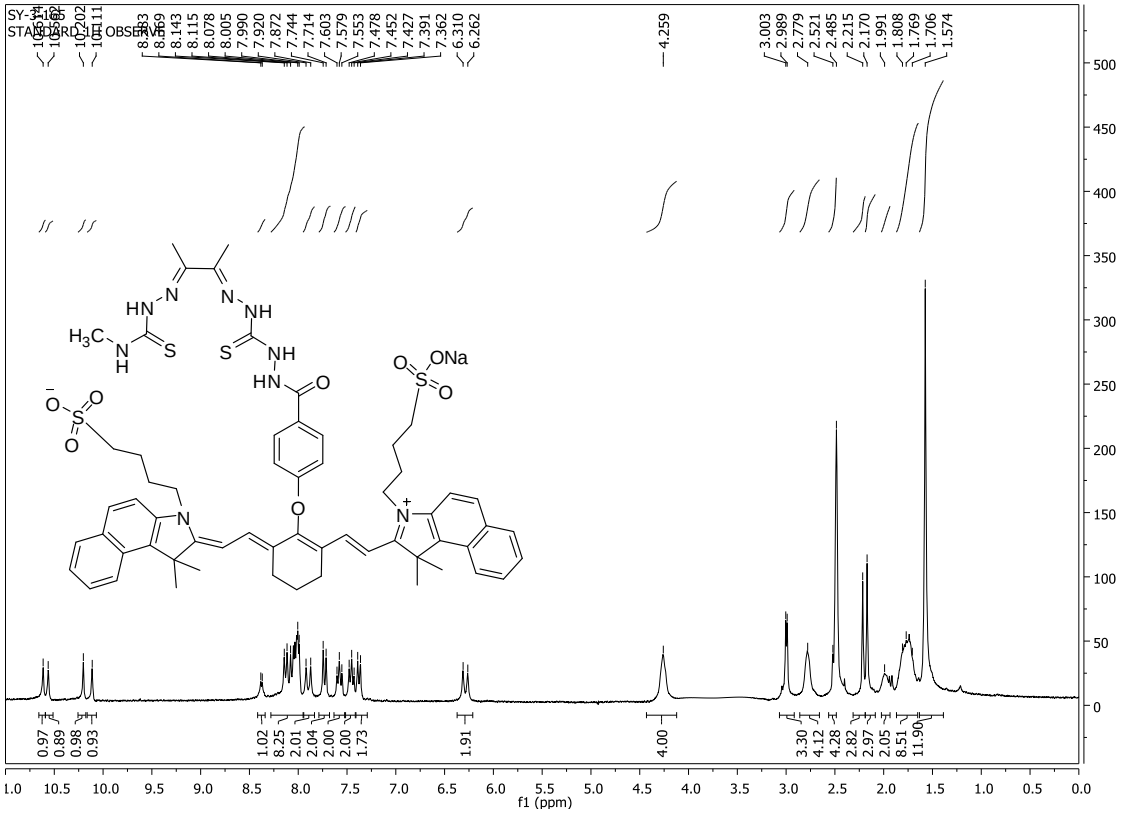
SY-3-168
STANDARD_1H_OBSERVE
8.183
8.169
8.143
8.115
8.078
8.005
7.990
7.920
7.872
7.744
7.714
7.603
7.579
7.553
7.478
7.452
7.427
7.391
7.362
6.310
6.262
4.259
3.003
2.989
2.779
2.521
2.485
2.215
2.170
1.991
1.808
1.769
1.706
1.574
ONa
0.97
0.89
0.98
0.93
1.02
8.25
2.01
2.04
2.00
2.00
1.73
1.91
4.00
3.30
4.12
4.28
2.82
2.97
2.05
8.51
11.90
f1 (ppm)

Appendix V. Derivatives of Binol-Amino Alcohol Sensors

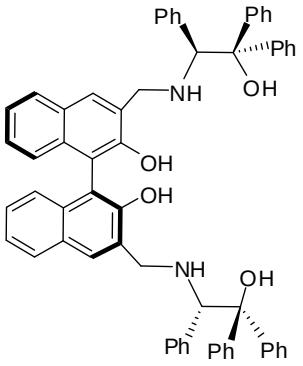

(*S*)-**7-35**

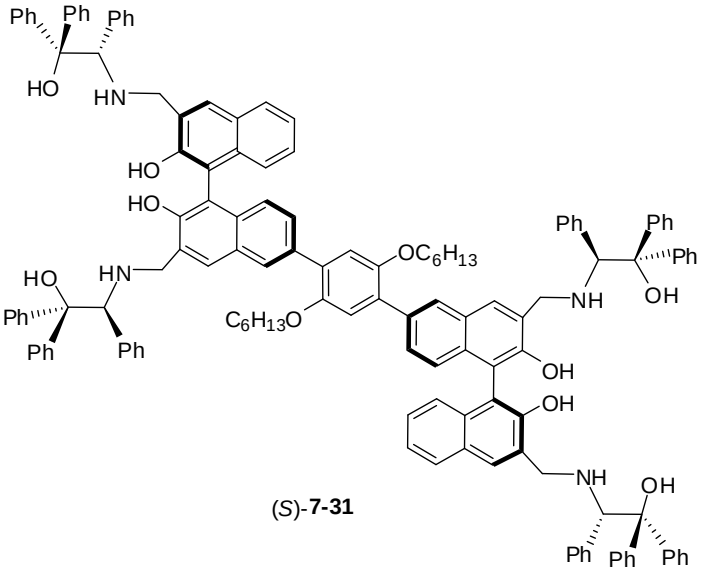

(*S*)-**7-31**

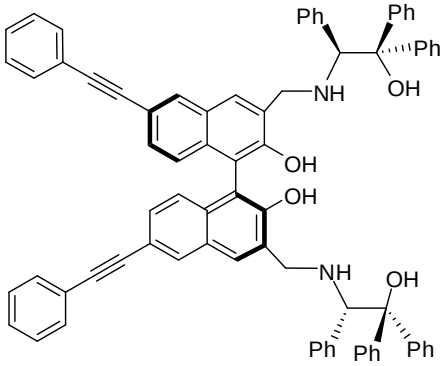

(*S*)-**7-32**

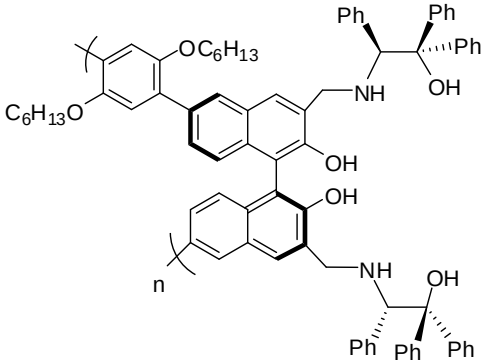

(*S*)-**7-33** **Mn=3330**
(*S*)-**7-34** **Mn=4496**

1. Preparation and Characterization of Compounds

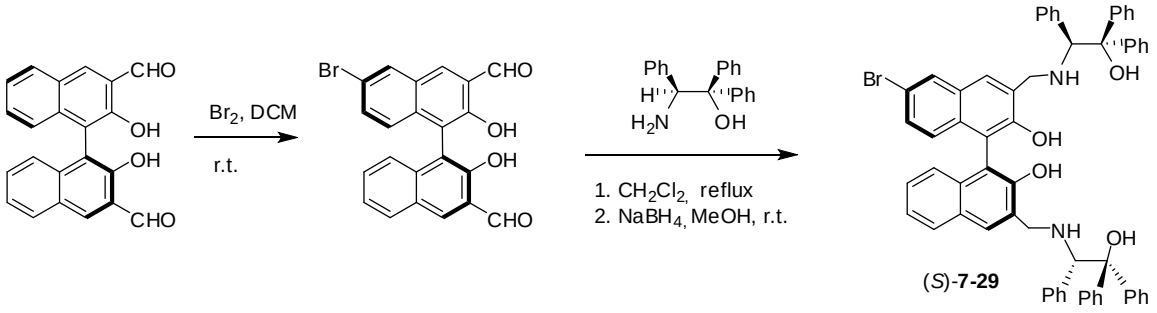

(*S*)-**7-29**

Preparation and characterization of (S)-6-bromo-2,2'-dihydroxy-1,1'-binaphthyl-3,3'-dicarbaldehyde. Under nitrogen, (S)-3, 3'-diformylBINOL (240 mg, 0.70 mmol) was dissolved in methylene chloride (20 mL). To the solution was added dropwise 0.13 mL (2.5 mmol) of bromine. The resulting solution was stirred overnight at room temperature. The remaining bromine was quenched by the addition of Na_2SO_3 aq. Then the aqueous layer was extracted with methylene chloride (2×10 mL). The combined methylene chloride layer was washed with brine (10 mL) and dried over anhydrous Na_2SO_4. After evaporation of the solvent, the residue was purified by column chromatography on silica gel eluted with dichloromethane/hexanes (3/2) to afford desired product as a yellow solid in 51% yield. ^{1}H NMR ($(CD_3)_2SO$, 300 MHz) δ 6.94 (d, J = 9.0 Hz, 1H), 6.98-7.01 (m, 1H), 7.42-7.45 (m, 2H), 7.53 (dt, J1 = 9.0 Hz, J2 = 2.1 Hz, 1H), 8.14-8.17 (m, 1H), 8.45 (s, 1H), 8.63 (s, 1H), 8.67 (s, 1H), 10.18 (d, J = 1.5 Hz, 1H), 10.21 (d, J = 1.5 Hz, 1H), 10.35 (d, J = 1.8 Hz, 1H), 10.37 (d, J = 1.8 Hz, 1H). ^{13}C NMR ($(CD_3)_2SO$, 75 MHz) δ 115.9, 117.1, 117.7, 123.9, 124.77, 124.83, 125.0, 127.3, 128.1, 129.3, 131.1, 132.5, 133.5, 135.5, 135.6, 136.0, 137.4, 137.5, 154.2, 154.6, 196.2, 197.0. HRMS Calcd for $C_{22}H_{14}BrO_4$ (MH^+): 421.0075, Found: 421.0075. HRMS Calcd for $C_{22}H_{13}BrO_4Na$ (MNa^+): 442.9895, Found: 442.9898. $[\alpha]_D$ = -190.17 (c = 0.31, DMSO).

Preparation and characterization of compound (S)-7-29. (1) Under nitrogen, (S)-6-bromo-2,2'-dihydroxy-1,1'-binaphthyl-3,3'-dicarbaldehyde (152 mg, 0.36 mmol) was dissolved in CH_2Cl_2 (15 mL) and combined with (S)-2-amino-1,1,2-triphenylenthanol (211 mg, 0.72 mmol). The reaction mixture was heated at reflux for overnight, and monitored by using ^{1}H NMR spectroscopy. When the reaction was complete, the solution was cooled to room temperature and dried over anhydrous Na_2SO_4. After filtration, the

filtrate was concentration under vacuum. The residue was passed through a silica gel column eluted with hexanes/ethyl acetate (8/1) to give the corresponding Schiff base. (2) The Schiff base was dissolved in methanol (15 mL) and cooled down to 0 °C. $NaBH_4$ (55 mg, 1.44 mmol) was added in small portions. The reaction temperature was maintained at 0 °C until the solution became colorless and transparent. Then it was allowed to proceed at room temperature for additional 30 min. Methanol was removed, and the residue was dissolved in ethyl acetate (25 mL) and washed with water (10 mL). The aqueous layer after separation was extracted with ethyl acetate (3x10 mL). The combined ethyl acetate layer was washed with brine (10 mL) and dried over anhydrous Na_2SO_4. After evaporation of the solvent, the residue was purified by flash column chromatography on silica gel eluted with hexanes/ethyl acetate (3/1) to afford (*S*)-**7-29** as a white solid in 43% yield. ^{1}H NMR ($CDCl_3$, 300 MHz) δ 3.31 (s, 1H), 3.53 (s, 1H), 3.73 (d, J = 14.1 Hz, 1H), 3.81 (d, J = 14.1 Hz, 1H), 4.08 (d, J = 6.3 Hz, 1H), 4.12 (d, J = 7.2 Hz, 1H), 4.57 (s, 1H), 4.63 (s, 1H), 6.88-7.51 (m, 37H), 7.76-7.79 (m, 1H), 7.89 (d, J = 1.8 Hz, 1H).

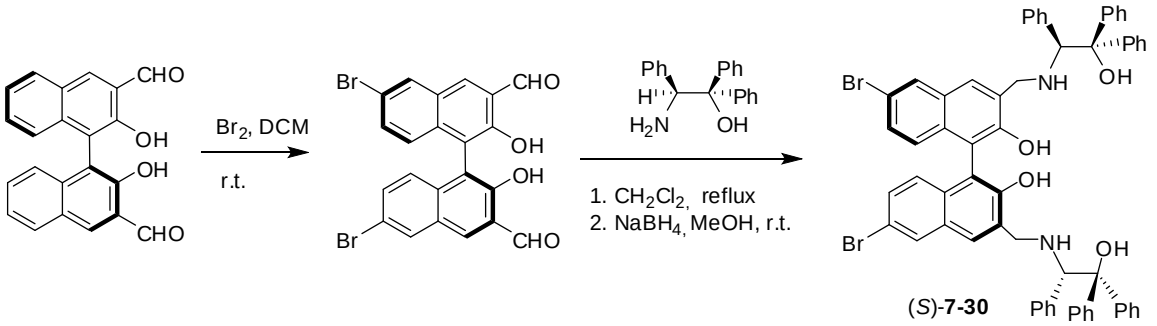

Preparation and characterization of (S)-6,6'-dibromo-2,2'-dihydroxy- 1,1'-binaphthyl-3,3'-dicarbaldehyde. Under nitrogen, (S)-3, 3'-diformylBINOL (120 mg, 0.35 mmol) was dissolved in methylene chloride (7 mL). To the solution was added dropwise 0.09 mL (1.75 mmol) of bromine. The resulting solution was stirred overnight

at room temperature. The remaining bromine was quenched by the addition of Na_2SO_3 aq. Then the aqueous layer was extracted with methylene chloride (2×10 mL). The combined methylene chloride layer was washed with brine (10 mL) and dried over anhydrous Na_2SO_4. After evaporation of the solvent, the residue was purified by column chromatography on silica gel eluted with dichloromethane/hexanes (3/2) to afford (*S*)-**7-3** as a yellow solid in 71% yield. ^{1}H NMR ($(CD_3)_2SO$, 300 MHz) δ 6.90 (d, J = 9.0 Hz, 2H), 7.52 (dd, J = 2.1, 9.0 Hz, 2H), 8.43 (s, 2H), 8.43 (s, 2H), 10.18 (S, 2H), 10.35 (s, 2H). ^{13}C NMR ($(CD_3)_2SO$, 75 MHz) δ 116.4, 117.7, 124.9, 127.1, 129.3, 132.5, 133.6, 135.6, 135.9, 154.7, 196.1. $[\alpha]_D$ = -143.4 (c = 0.30, DMSO).

Preparation and characterization of compound (S)-7-30. (1) Under nitrogen, (S)-6,6'-dibromo-2,2'-dihydroxy- 1,1'-binaphthyl-3,3'-dicarbaldehyde (298 mg, 0.60 mmol) was dissolved in CH_2Cl_2 (200 mL) and combined with (S)-2-amino-1,1,2-triphenylenthanol (345 mg, 1.20 mmol). The reaction mixture was heated at reflux for overnight, and monitored by using ^{1}H NMR spectroscopy. When the reaction was complete, the solution was cooled to room temperature and dried over anhydrous Na_2SO_4. After filtration, the filtrate was concentration under vacuum. The residue was passed through a silica gel column eluted with hexanes/ethyl acetate (8/1) to give the corresponding Schiff base. (2) The Schiff base was dissolved in anhydrous ethanol (60 mL) and cooled down to 0 °C. $NaBH_4$ (69 mg, 1.80 mmol) was added in small portions. The reaction temperature was maintained at 0 °C until the solution became colorless and transparent. Then it was allowed to proceed at room temperature for additional 30 min. Ethanol was removed, and the residue was dissolved in ethyl acetate (50 mL) and washed with water (15 mL). The aqueous layer after separation was extracted with ethyl acetate

(3x30 mL). The combined ethyl acetate layer was washed with brine (15 mL) and dried over anhydrous Na_2SO_4. After evaporation of the solvent, the residue was purified by flash column chromatography on silica gel eluted with hexanes/ethyl acetate (3/1) to afford (*S*)-**7-5** as a white silid in 72% yield. ^{1}H NMR ($CDCl_3$, 300 MHz) δ 3.30 (s, 2H), 3.79 (d, J = 13.8 Hz), 4.08 (d, J = 13.8 Hz), 4.60 (s, 2H), 6.99-7.36 (m, 34H), 7.48 (dd, J1 = 8.1 Hz, J2 = 1.5 Hz, 4H), 7.90 (d, J = 2.1 Hz). HRMS Calcd for $C_{62}H_{51}N_2O_4$ (MH^+): 1045.2216, Found: 1045.2211. $[\alpha]_D$ = -42.3 (c = 0.51, $CHCl_3$).

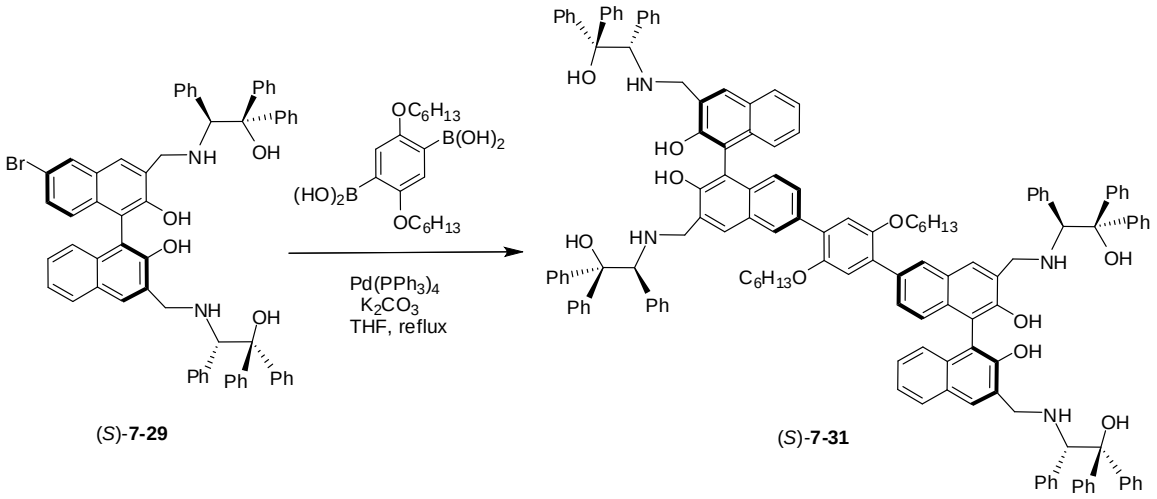

(*S*)-**7-29** (*S*)-**7-31**

Preparation and characterization of compound (S)-7-31. Under nitrogen, a mixture of (*S*)-**7-29** (281 mg, 0.29 mmol), 2,5-bis(hexyloxy)-1,4-phenylenediboronic acid (53 mg, 0.15 mmol), and $Pd(PPh_3)_4$ (17 mg, 0.015 mmol, 5 mol %) in THF(4.5 mL) and 2 M K_2CO_3 (4.5 mL) was heated at reflux for overnight. The organic layer was separated and then diluted with CH_2Cl_2 (20 mL). The solution was washed with 1 N HCl (10 mL) and brine (10 mL) and dried over anhydrous Na_2SO_4. After evaporation of the solvent, the residue was purified by flash column chromatography on silica gel eluted with CH_2Cl_2/methanol (100/1) to afford (S)-**7-31** as a light yellow solid in 60% yield. ^{1}H

NMR ($CDCl_3$, 300 MHz) δ 0.77 (t, J = 6.0 Hz, 6H), 1.16-1.31 (m, 12H), 1.62 (t, 6.6 Hz, 2H), 3.68-3.78 (m, 8H), 3.90 (t, J = 6.0 Hz, 4H), 4.09-4.16 (m, 4H), 4.65 (s, 4H), 6.95-7.83 (m, 78H), 8.07 (s, 2H). ^{13}C NMR ($CDCl_3$, 75 MHz) δ 14.2, 22.8, 25.9, 29.5, 31.6, 49.2, 67.7, 67.8, 69.8, 80.6, 114.5, 114.7, 116.7, 123.9, 124.5, 125.1, 126.0, 126.5, 126.9, 127.4, 127.7, 128.0, 128.3, 128.7, 128.9, 130.0, 130.1, 130.2, 130.7, 133.0, 133.97, 134.03, 137.05, 144.5, 145.0, 150.7, 152.8, 152.9. HRMS Calcd for $C_{142}H_{132}N_4O_{10}/2$ ($[M+2H]^{2+}$): 1026.4972, Found: 1026.4972.

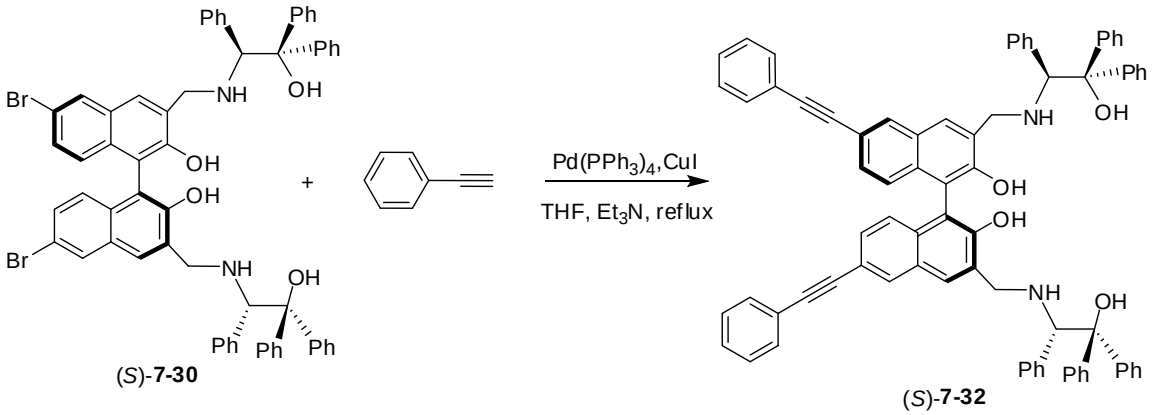

Preparation and characterization of compound (S)-7-32. Under nitrogen, to a 25 mL flame-dried Schlenk flask was loaded (S)-**7-30** (105 mg, 0.10 mmol), ethynylbenzene (44 μL, 0.40 mmol), triethylamine (1.5 mL), and THF (1.5 mL). The resulting solution was degassed for 30 min and then was combined with $Pd(PPh_3)_4$ (12 mg, 0.010 mmol) and CuI (2 mg, 0.010 mmol) in the dry box. After this reaction mixture was stirred at reflux for 24 h, it was filtered to remove the insoluble triethylamine hydrobromide salt. The salt was rinsed with diethyl ether until the filtrate was clear. After evaporation of the solvent, the residue was purified by flash column chromatography on silica gel eluted with hexane/ethyl acetate (3/1) to afford (S)-**7-32** as a white solid in 51% yield. ^1H NMR ($CDCl_3$, 300 MHz) δ 3.49 (s, 2H), 3.77 (d, J = 13.8 Hz, 2H), 4.08 (d, J = 13.8 Hz, 2H),

4.63 (s, 2H), 6.99-7.60 (m, 44H), 8.01 (s, 2H). ^{13}C NMR ($CDCl_3$, 75 MHz) δ 49.5, 67.9, 80.7, 89.6, 90.2, 115.2, 118.4, 123.6, 125.1, 126.0, 126.4, 126.7, 127.1, 127.5, 127.8, 128.2, 128.4, 128.5, 128.6, 128.8, 129.4, 129.5, 130.0, 131.9, 133.5, 139.9, 144.5, 144.8, 154.0. HRMS Calcd for $C_{78}H_{61}N_2O_4$ (MH^+): 1089.4631, Found: 1089.4611.

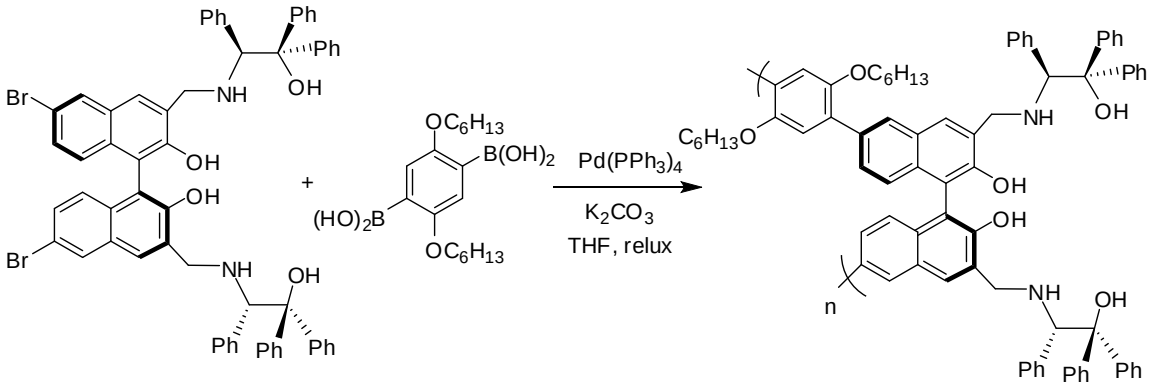

Preparation and characterization of compound (S)-7-33. Under nitrogen, a mixture of (*S*)-**7-30** (105 mg, 0.10 mmol), 2,5-bis(hexyloxy)-1,4-phenylenediboronic acid (37 mg, 0.10 mmol), and $Pd(PPh_3)_4$ (10 mg, 0.010 mmol, 10 mol %) in THF(2.0 mL) and 2 M K_2CO_3 (2.0 mL) was heated at reflux for 48 h. The organic layer was separated and then diluted with CH_2Cl_2 (20 mL). The solution was washed with 1 N HCl (10 mL) and brine (10 mL). After separation ,the solvent of the organic layer was removed to give a yellowish solid. The solid was redissoved in CH_2Cl_2 and precipitated out twice with MeOH. The solid, (*S*)-**7-33**, was isolated by centrifugation and was dried under vacuum at room temperature for 24 h. The yield was 67%. ^{1}H NMR ($CDCl_3$, 300 MHz) δ 0.71 (t, J = 6.0 Hz, 6H), 1.23-1.33 (m, 12H), 1.53-1.63 (m, 4H), 3.75-3.94 (m, 8H), 4.14 (d, J = 12.9 Hz, 2H), 4.64 (s, 2H), 6.84-7.78 (m, 38H), 8.04 (s, 2H). M_n = 3330. M_w/M_n = 1.40.

Preparation and characterization of compound (S)-7-34. Under nitrogen, a

mixture of (*S*)-**7-30** (105 mg, 0.10 mmol), 2,5-bis(hexyloxy)-1,4-phenylenediboronic acid (37 mg, 0.10 mmol), and $Pd(PPh_3)_4$ (10 mg, 0.010 mmol, 10 mol %) in THF(2.0 mL) and 2 M K_2CO_3 (2.0 mL) was heated at reflux for 60 h. The organic layer was separated and then diluted with CH_2Cl_2 (20 mL). The solution was washed with 1 N HCl (10 mL) and brine (10 mL). After separation, the solvent of the organic layer was removed to give a yellowish solid. The solid was redissoved in CH_2Cl_2 and precipitated out twice with MeOH. The solid, (*S*)-**7-34**, was isolated by centrifugation and was dried under vacuum at room temperature for 24 h. The yield was 85%. ^{1}H NMR ($CDCl_3$, 300 MHz) δ 0.70 (t, J = 6.0 Hz, 6H), 1.11-1.31 (m, 12H), 1.58 (t, J = 6.0 Hz, 4H), 3.74-3.94 (m, 8H), 4.14 (d, J = 10.8 Hz, 2H), 4.64 (s, 2H), 6.84-7.76 (m, 38H), 8.04 (s, 2H). M_n = 4496. M_w/M_n = 1.43.

2. Fluorescent study

Figure AV-1. Fluorescence spectra of (S)-**7-31**, (S)-**7-32**, (S)-**7-33** and (S)-**7-35** (5×10^{-6} M in benzene). (λ_{exc} = 334 nm for (S)-**7-31**, (S)-**7-33** and (S)-**7-35**, λ_{exc} = 314 nm for (S)-**7-32**, slit =2.0/2.0 nm)

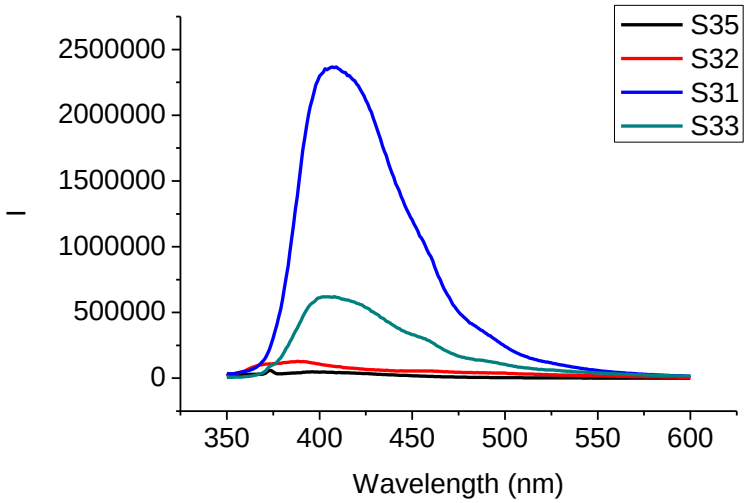

Figure AV-2. Fluorescence spectra of (S)-**7-35**, (S)-**7-31**, (S)-**7-32** (6×10^{-5} M) with/without mandelic acid ($3.0x10^{-3}$ M in benzene (0.4% DME)). (λ_{exc} = 334 nm for (S)-**7-31** and (S)-**7-35**, λ_{exc} = 314 nm for (S)-**7-32**, slit =2.5/2.5 nm)

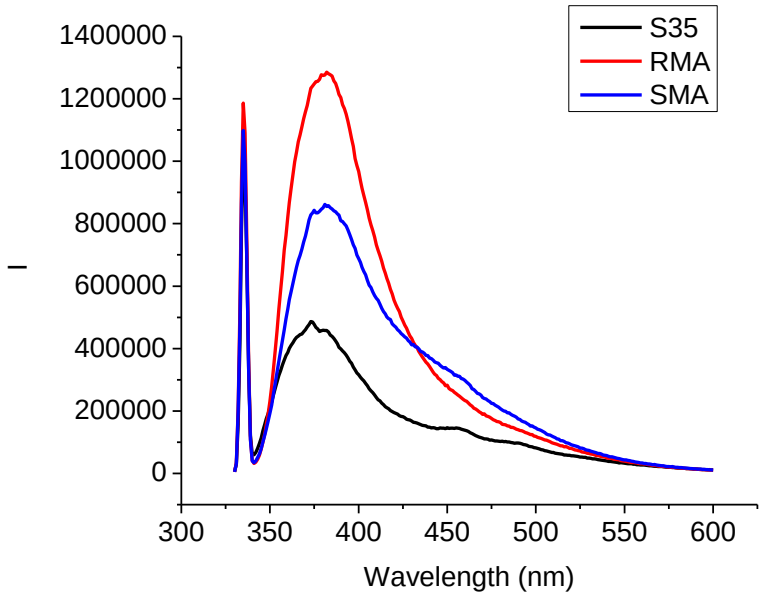

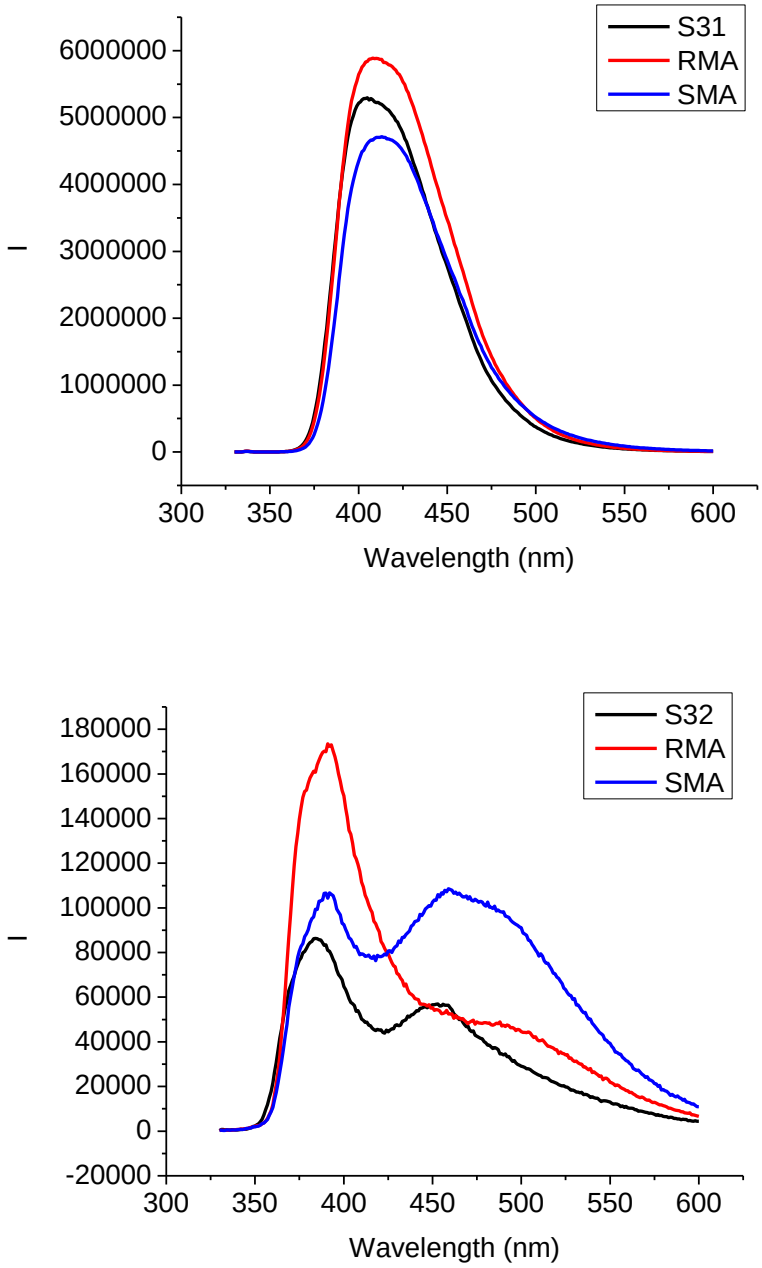

Figure AV-3. Fluorescence spectra of (S)-**7**-**35**, (S)-**7**-**31**, (S)-**7**-**32** (6×10^{-5} M) with/without phenyllactic acid ($3.0\text{x}10^{-3}$ M in benzene (0.4% DME)). (λ_{exc} = 334 nm for (S)-**7**-**31** and (S)-**7**-**35**, λ_{exc} = 314 nm for (S)-**7**-**32**, slit =2.5/2.5 nm)

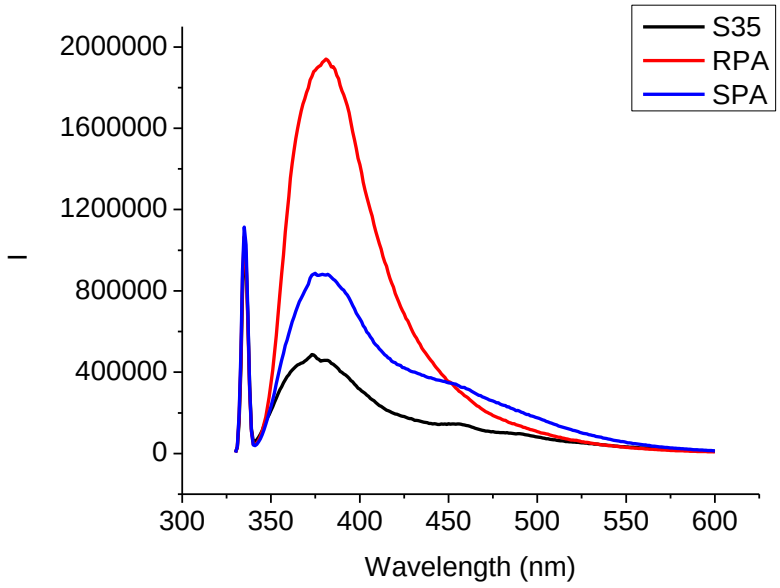
S35
RPA
SPA
2000000
1600000
1200000
800000
400000
0
I
300
350
400
450
500
550
600
Wavelength (nm)

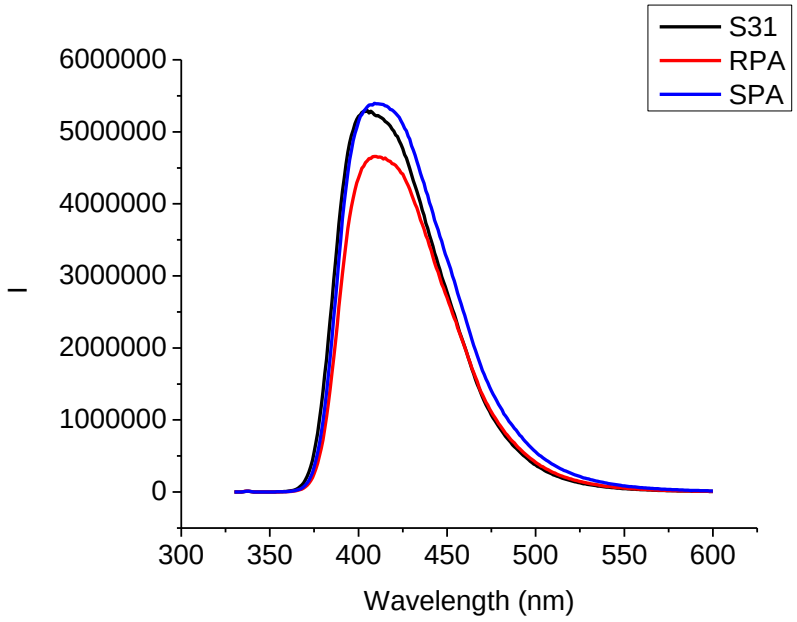
S31
RPA
SPA
6000000
5000000
4000000
3000000
2000000
1000000
0
I
300
350
400
450
500
550
600
Wavelength (nm)

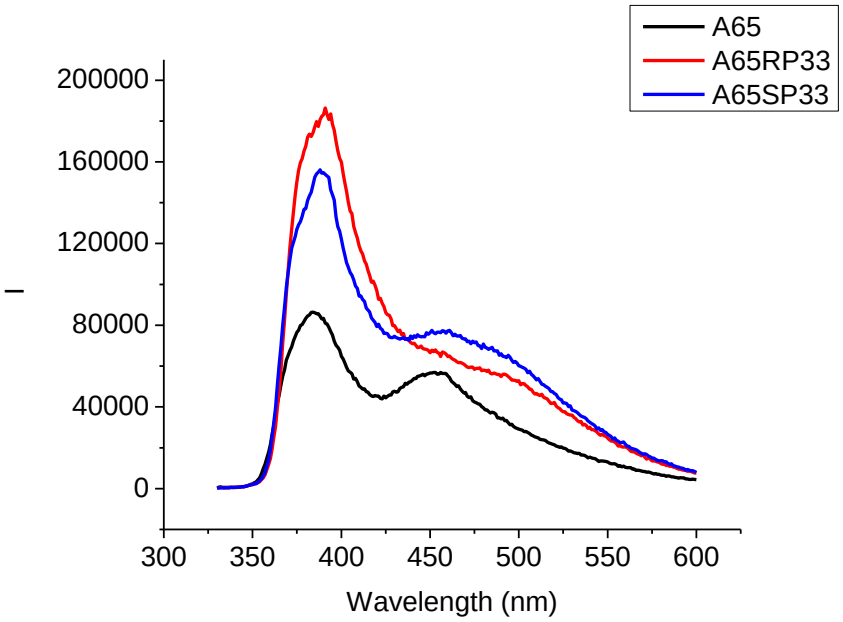

Figure AV-4. Fluorescence spectra of (S)-**7-31**, (S)-**7-32**, (S)-**7-33** and (S)-**7-34** (5×10^{-8} M) with/without mandelic ($1.0\text{x}10^{-3}$ M in CH_2Cl_2). (λ_{exc} = 336 nm for (S)-**7-31**, (S)-**7-33** and (S)-**7-34**, λ_{exc} = 313 nm for (S)-**7-32**, slit =4.0/4.0 nm)

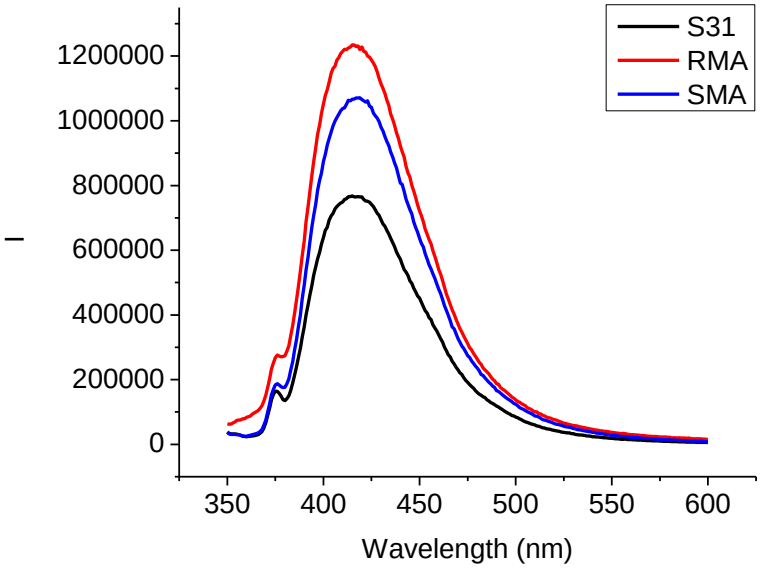

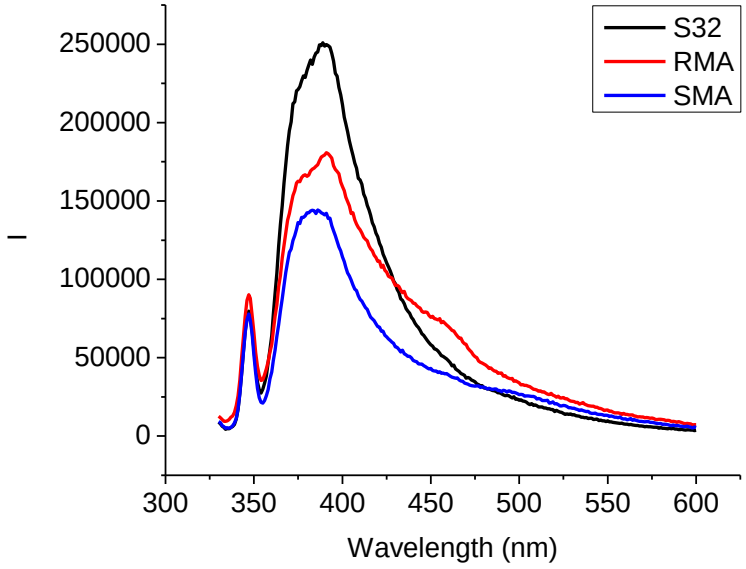
S32
RMA
SMA
I
250000
200000
150000
100000
50000
0
300
350
400
450
500
550
600
Wavelength (nm)

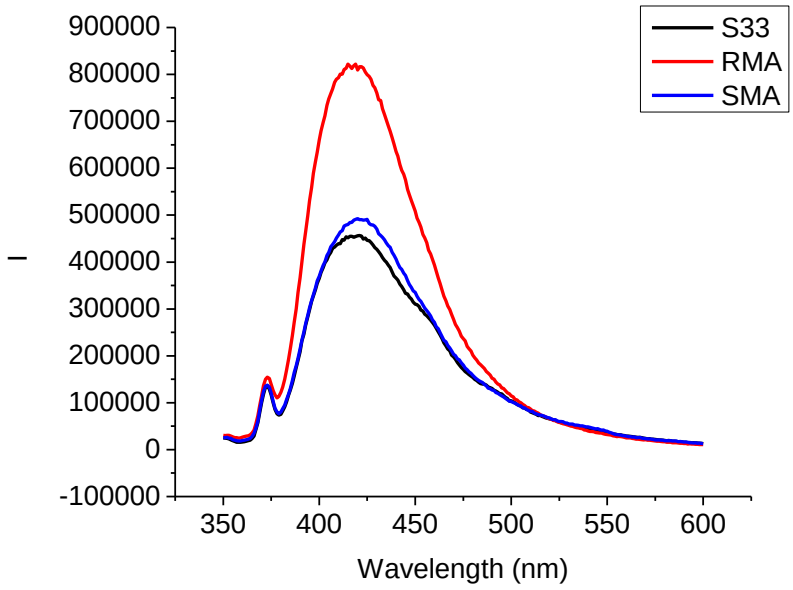
S33
RMA
SMA
I
900000
800000
700000
600000
500000
400000
300000
200000
100000
0
-100000
350
400
450
500
550
600
Wavelength (nm)

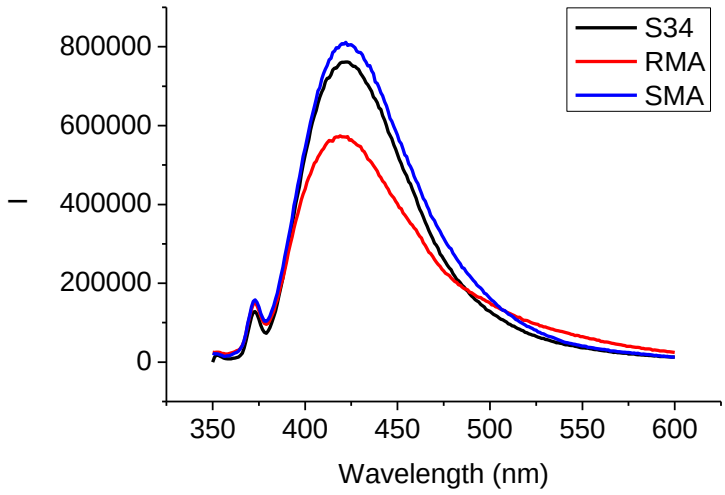

3. NMR spectra

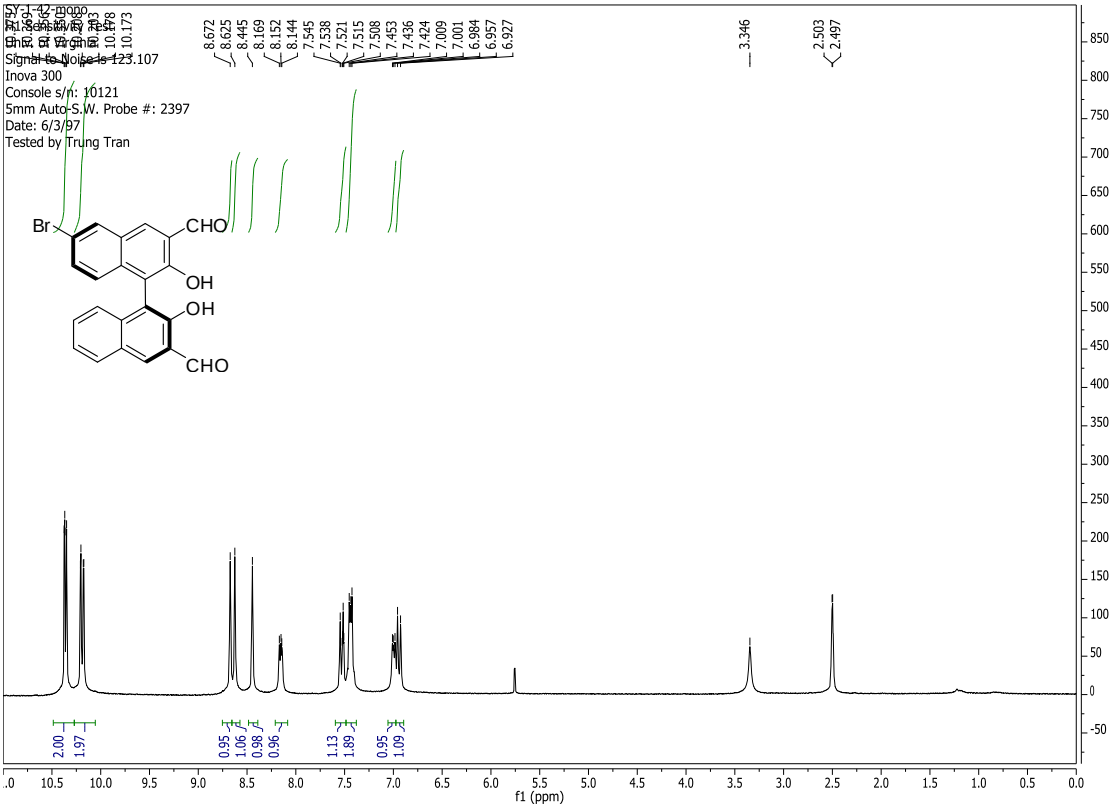

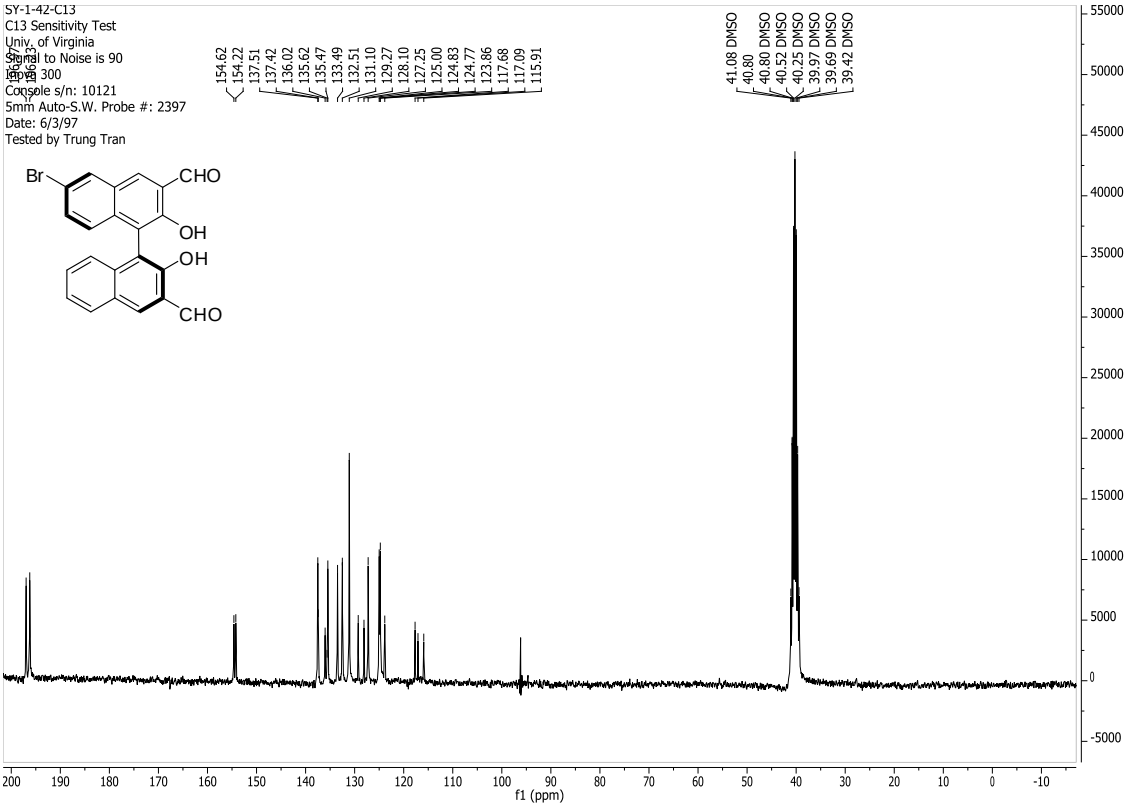
SY-1-42-C13
C13 Sensitivity Test
Univ. of Virginia
Signal to Noise is 90
Varian 300
Console s/n: 10121
5mm Auto-S.W. Probe #: 2397
Date: 6/3/97
Tested by Trung Tran
Br
CHO
OH
OH
CHO
f1 (ppm)

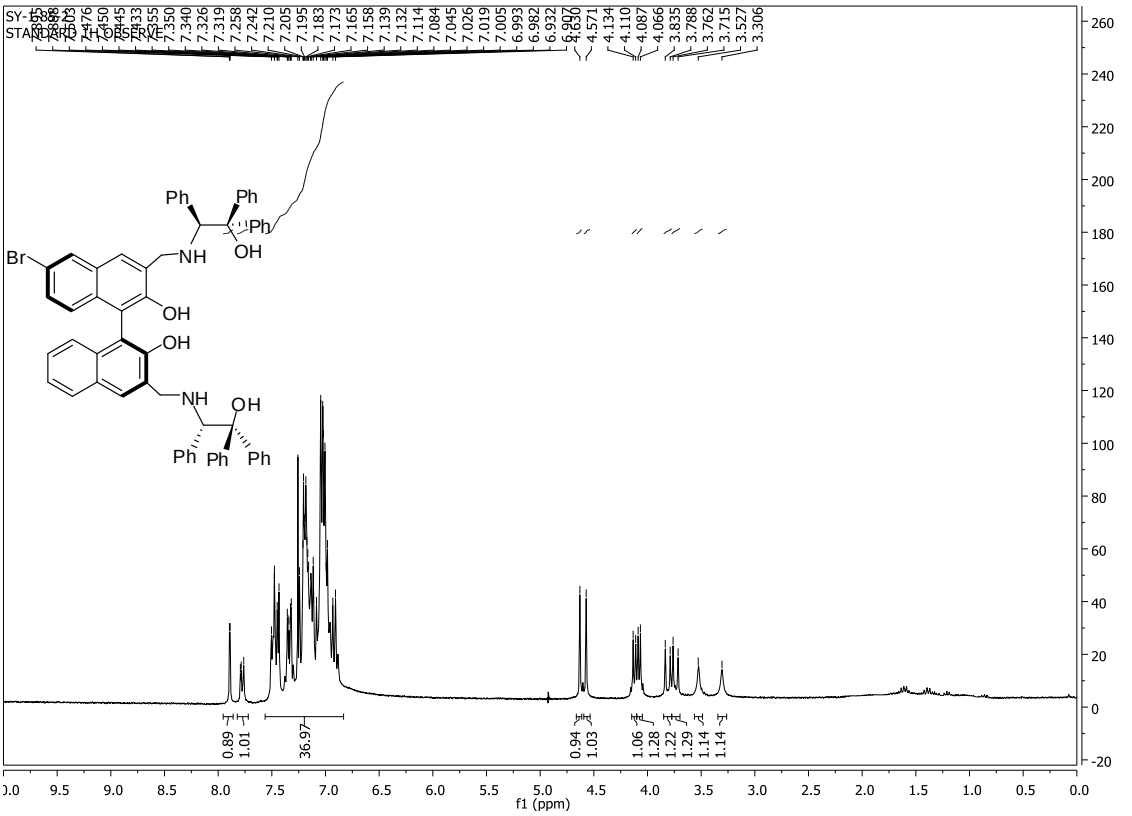
Ph
Ph
Ph
OH
NH
Br
OH
OH
NH
OH
Ph
Ph
Ph
f1 (ppm)

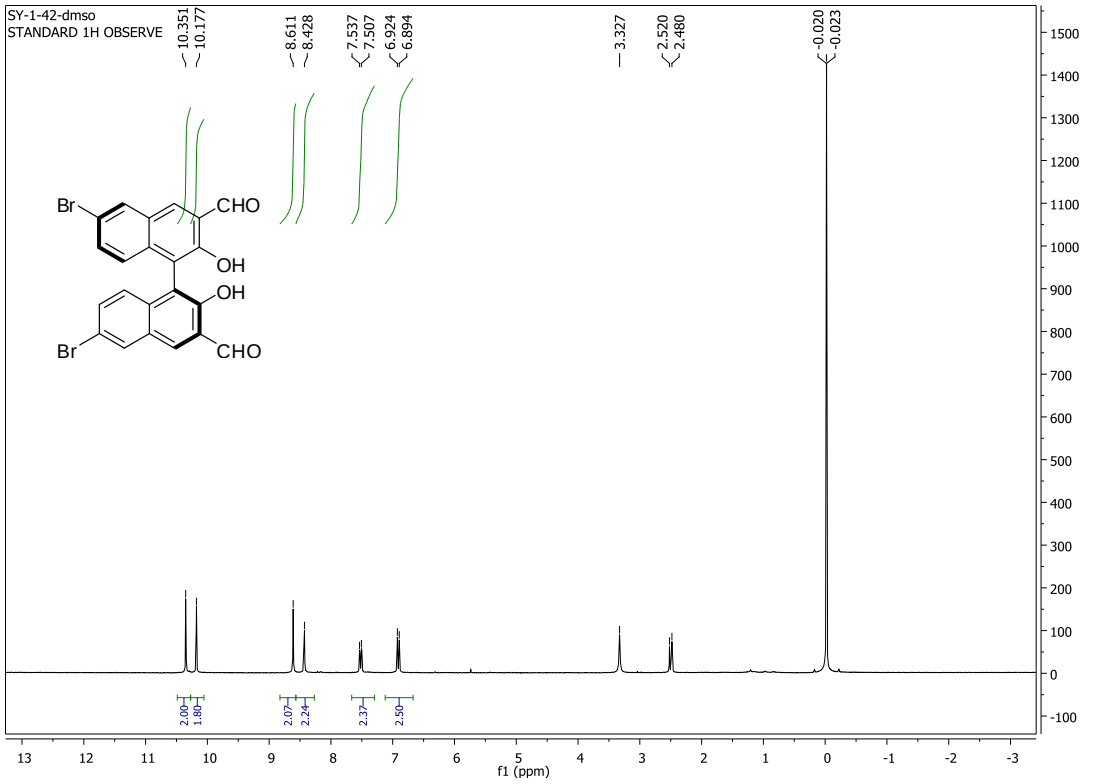
SY-1-42-dmso
STANDARD 1H OBSERVE
10.351
10.177
8.611
8.428
7.537
7.507
6.924
6.894
3.327
2.520
2.480
-0.020
-0.023
Br
CHO
OH
OH
Br
CHO
2.00
1.80
2.07
2.24
2.37
2.50
f1 (ppm)

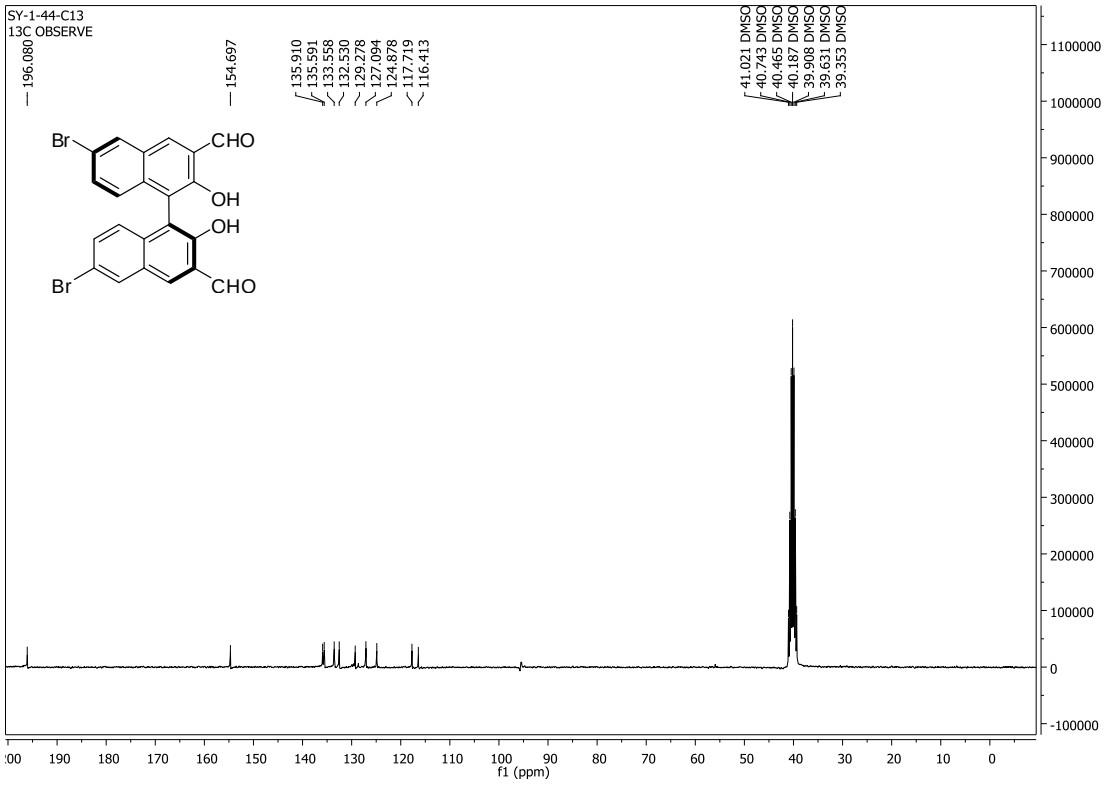
SY-1-44-C13
13C OBSERVE
196.080
154.697
135.910
135.591
133.558
132.530
129.278
127.094
124.878
117.719
116.413
41.021 DMSO
40.743 DMSO
40.465 DMSO
40.187 DMSO
39.908 DMSO
39.631 DMSO
39.353 DMSO
Br
CHO
OH
OH
Br
CHO
f1 (ppm)

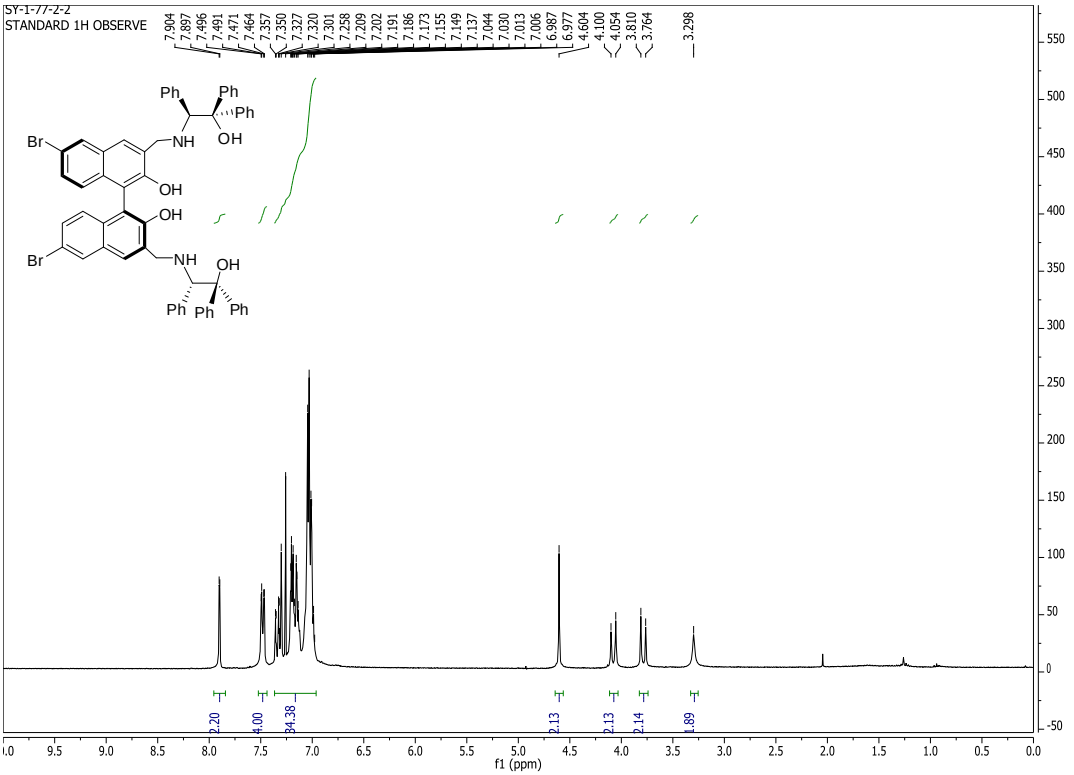
SY-1-77-2-2
STANDARD 1H OBSERVE
7.904
7.897
7.496
7.491
7.471
7.464
7.357
7.350
7.327
7.320
7.301
7.258
7.209
7.202
7.191
7.186
7.173
7.155
7.149
7.137
7.044
7.030
7.013
7.006
6.987
6.977
4.604
4.100
4.054
3.810
3.764
3.298
Ph
Ph
Ph
NH
OH
Br
OH
OH
Br
NH
OH
Ph
Ph
Ph
2.20
4.00
34.38
2.13
2.13
2.14
1.89
f1 (ppm)

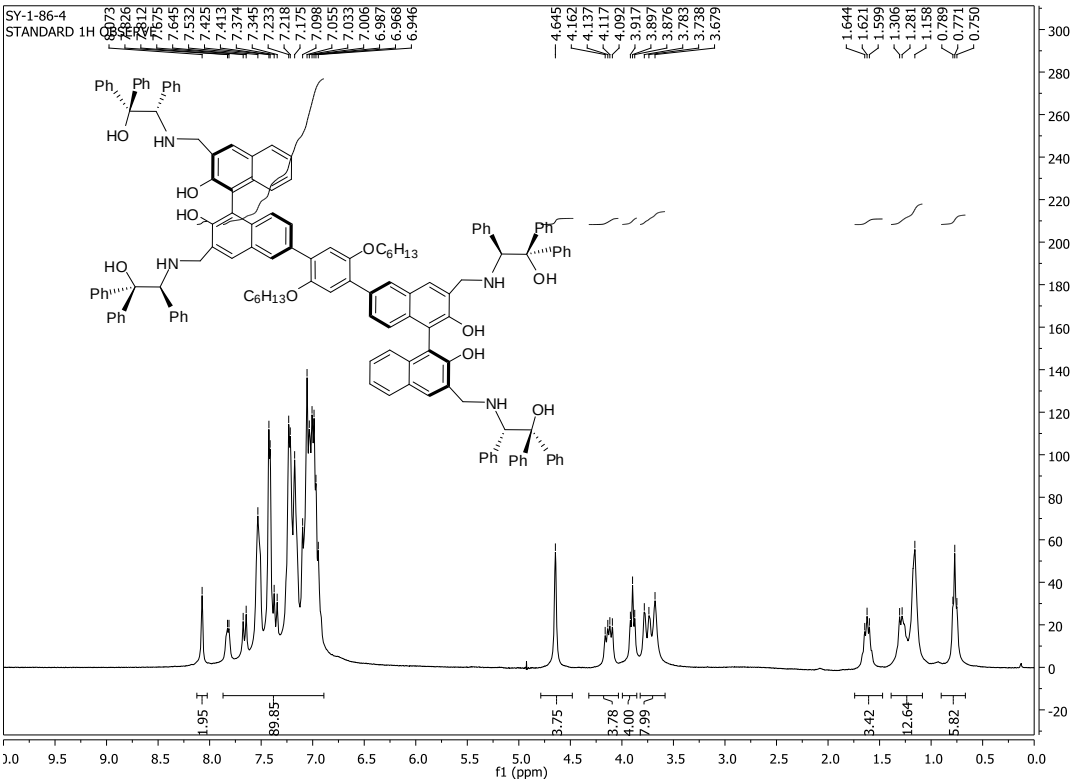
SY-1-86-4
STANDARD 1H OBSERVE
8.073
7.826
7.812
7.675
7.645
7.532
7.425
7.413
7.374
7.345
7.233
7.218
7.175
7.098
7.055
7.033
7.006
6.987
6.968
6.946
4.645
4.162
4.137
4.117
4.092
3.917
3.897
3.876
3.783
3.738
3.679
1.644
1.621
1.599
1.306
1.281
1.158
0.789
0.771
0.750
Ph
Ph
Ph
HO
HN
HO
HO
HO
HN
Ph
Ph
Ph
OC6H13
C6H13O
Ph
Ph
Ph
NH
OH
OH
OH
NH
OH
Ph
Ph
Ph
1.95
89.85
3.75
3.78
4.00
7.99
3.42
12.64
5.82
f1 (ppm)

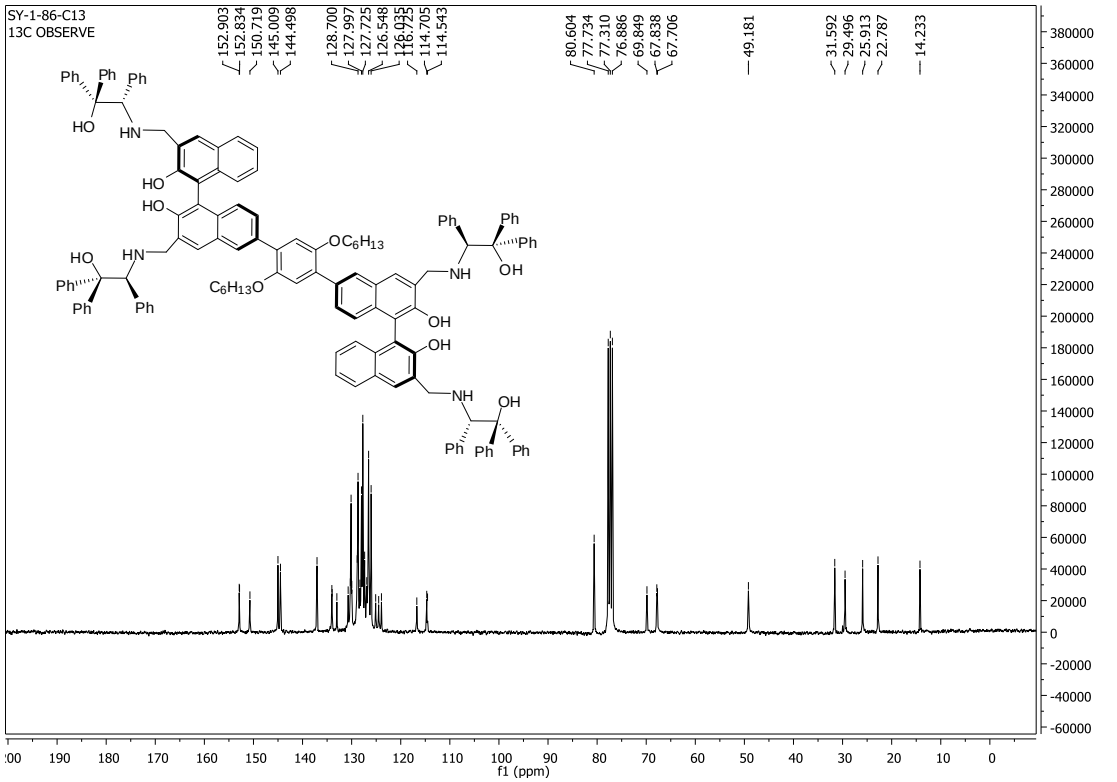
SY-1-86-C13
13C OBSERVE
f1 (ppm)

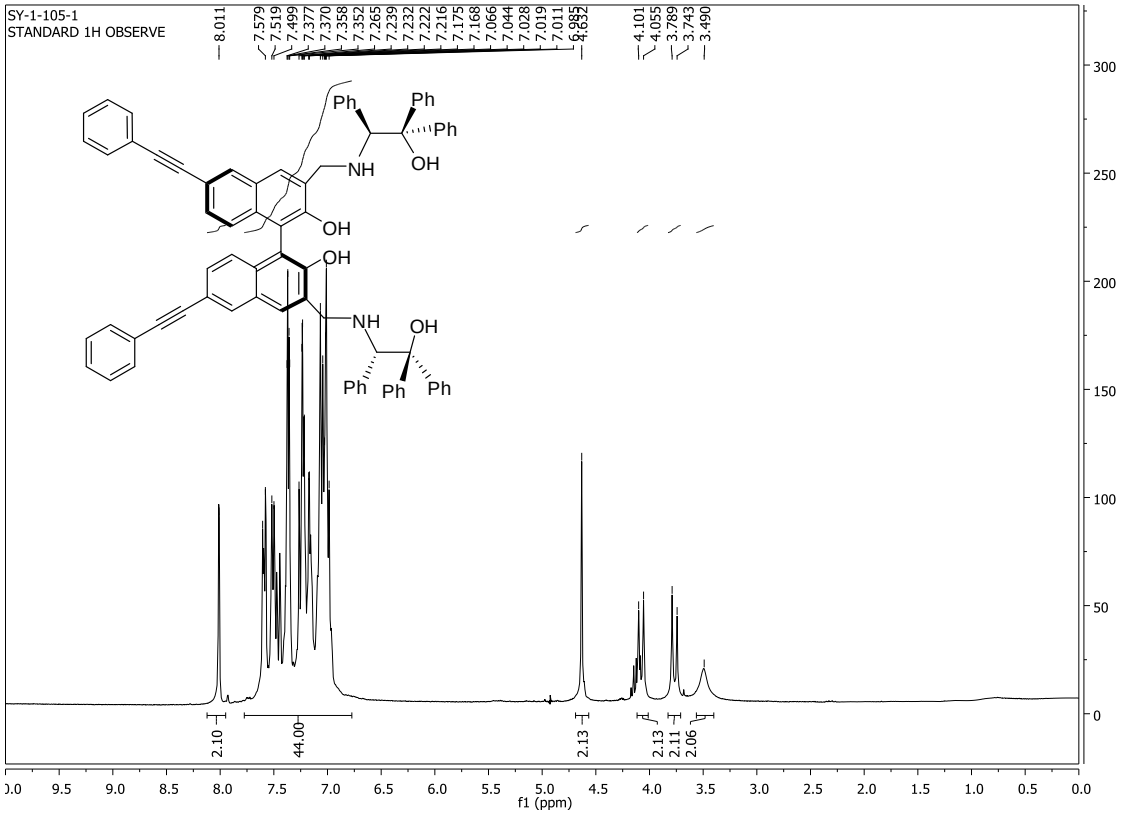
SY-1-105-1
STANDARD 1H OBSERVE
f1 (ppm)

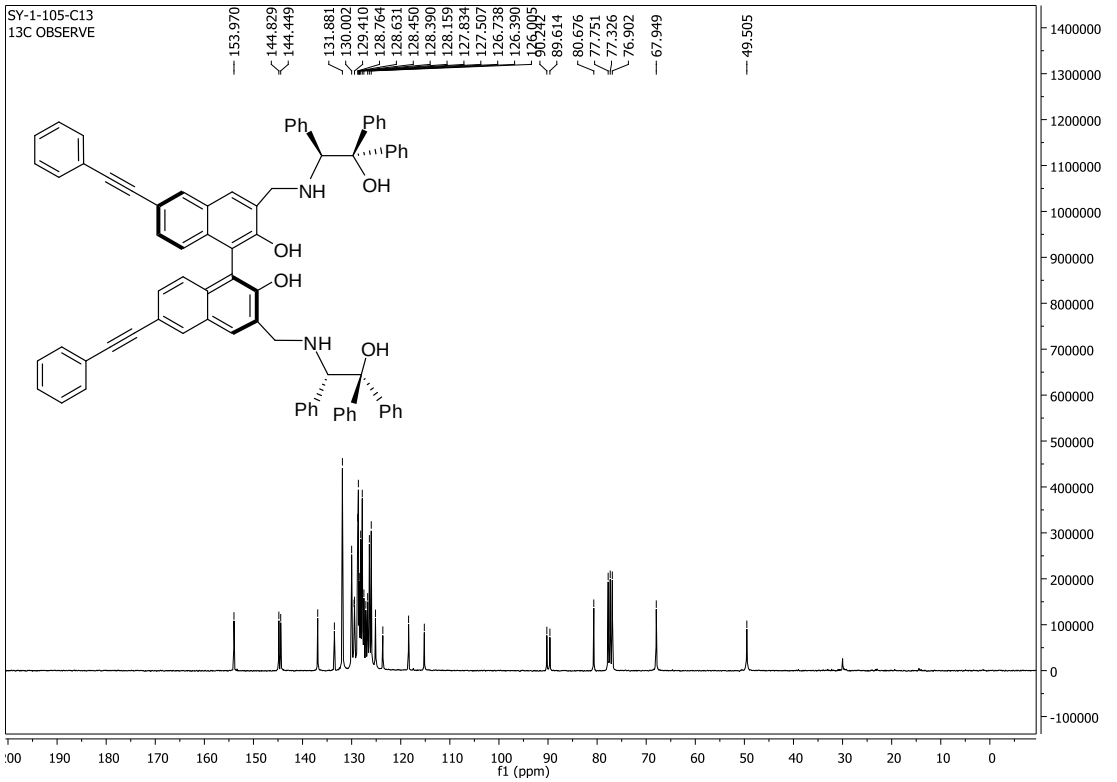
SY-1-105-C13
13C OBSERVE
f1 (ppm)

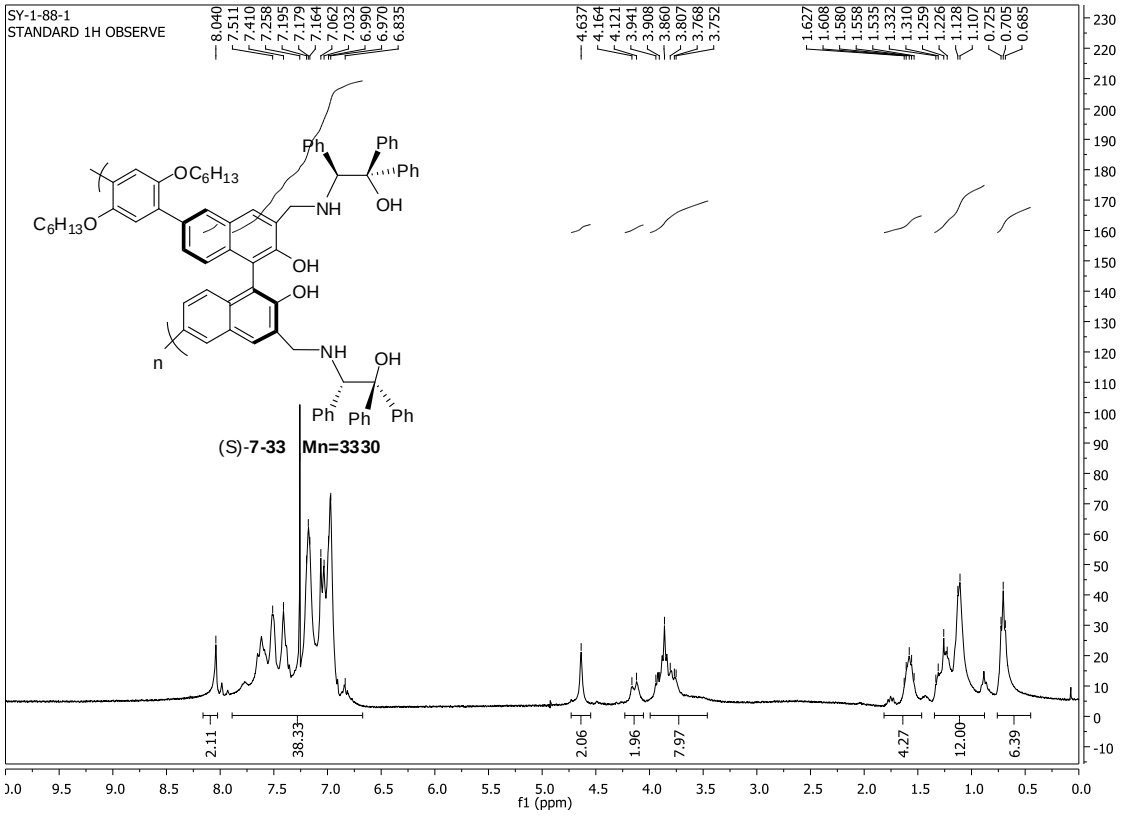
SY-1-88-1
STANDARD 1H OBSERVE
(S)-7-33 Mn=3330
f1 (ppm)

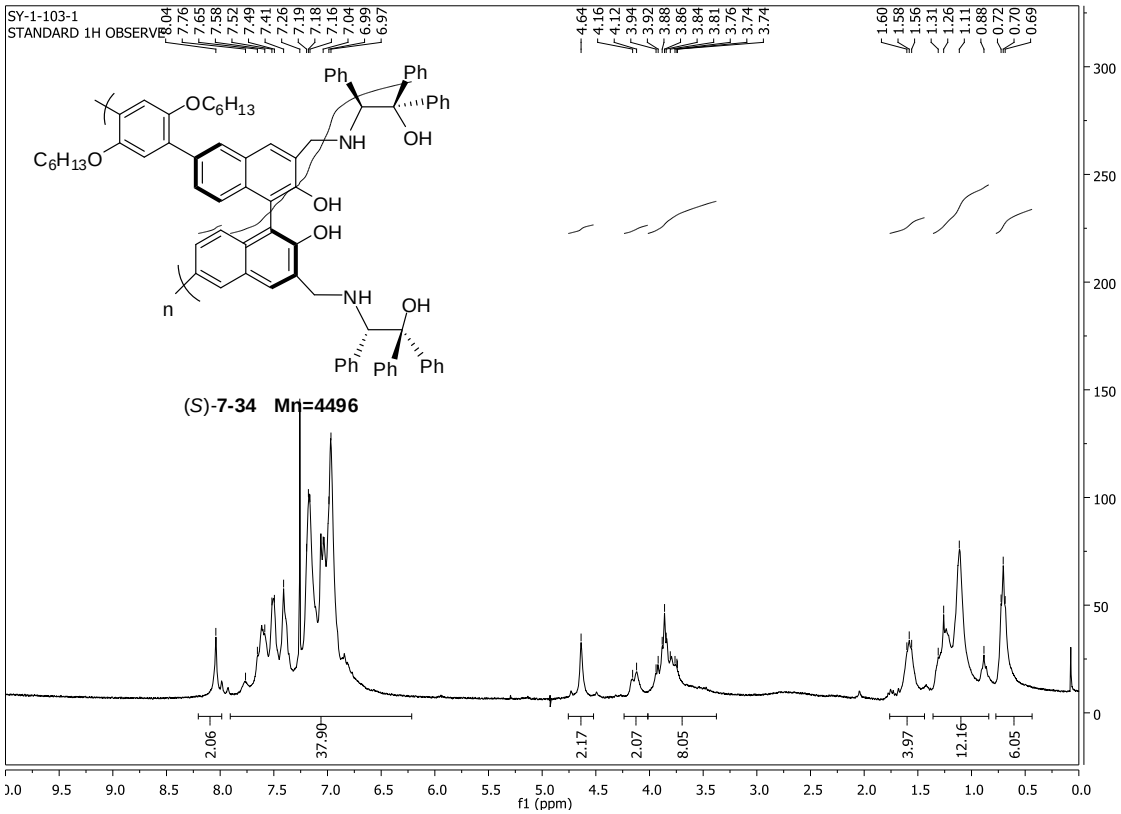
SY-1-103-1
STANDARD 1H OBSERVE
8.04 7.76 7.65 7.58 7.52 7.49 7.41 7.26 7.19 7.18 7.16 7.04 6.99 6.97
4.64 4.16 4.12 3.94 3.92 3.88 3.86 3.84 3.81 3.76 3.74 3.74
1.60 1.58 1.56 1.31 1.26 1.11 0.88 0.72 0.70 0.69
OC6H13
C6H13O
Ph
Ph
Ph
NH
OH
OH
OH
n
NH
OH
Ph
Ph
Ph
(S)-7-34 Mn=4496
2.06
37.90
2.17
2.07
8.05
3.97
12.16
6.05
f1 (ppm)